The geology of the hyperstheme Gabbro of Ardnamurchan point and implications for its evolution as an upper crustal basic magma chamber

Simon John Day

The Geology of the Hypersthene Gabbro of Ardnamurchan Point and implications for its evolution as an upper crustal basic magma chamber

VOLUME 2.

Simon John Day
B.A.(Oxon.), FGS

Department of Geological Sciences
University of Durham

Thesis submitted for the degree of
Doctor of Philosophy
University of Durham

September 1989

VOLUME II

CHAPTER 5.

METAMORPHISM ASSOCIATED WITH THE MARGINAL BORDER GROUP AND IMPLICATIONS FOR THE MASS AND HEAT FLUXES IN THE CONTACT AUREOLE AND IN THE BOUNDARY LAYER OF THE MBG MAGMA CHAMBER P.487

4. MAGMATIC PROCESSES IN THE MARGINAL BORDER GROUP MAGMA CHAMBER DURING M1 METAMORPHISM.

4.1. Theoretical models of magma chamber boundary layers and their application to the Marginal Border Group.

4.1.1. Introduction and the concept of a 'rigidus'.

The field and petrographic evidence presented in section 3.2 indicates that the Marginal Border Group was almost entirely liquid during M1 and then underwent rapid solidification during the quenching event (or events) at the end of M1. A plausible (although not certain) corollary of this is that the rocks of the contact zone suite, and the immediately adjacent mafic rocks, were present at, or close to, the wall of the M1 magma chamber immediately prior to the quenching event. They may therefore represent a more or less completely preserved example of a magma chamber boundary layer. If this is the case then the contact zone suite provides an opportunity to test theoretical models of magma chamber behaviour constructed on the basis of boundary layer theory, and to investigate ways in which these theories may have to be modified when applied to real magma chambers. In addition the compositions of the MBG rocks can be used to infer the petrogenetic effects and hence the geochemical 'signatures' of these processes.

As noted in Chapter 1, the application of fluid dynamics to magma chambers has led to the recognition of the importance of heat transfer and other processes in boundary layers in controlling the overall behaviour and evolution of magma chambers. A very general fluid dynamical definition of a boundary layer is that it is that part of a finite fluid body, such as a magma chamber, which is directly affected by the proximity of the margins or boundaries of the body. In stratified magma bodies these include the interfaces between discrete layers of magma, but in general the most important boundaries are the roof, walls and floor of the magma chamber. From the fluid dynamic point of view these can be divided into horizontal boundaries and more - or - less steeply inclined (including vertical) boundaries, the important difference between the two being that buoyancy instabilities at horizontal surfaces (for example dense layers produced by roof cooling) have to grow to a certain size (see Brandeis & Jaupart 1986; Marsh 1988) before producing fluid motion, whilst any difference in fluid densities at inclined walls will produce fluid motion. Studies of this

latter type are more relevant to the steep walls of the Hypersthene Gabbro found at outcrop, and it is upon these that the following discussion is concentrated.

The fluid dynamic models indicate that magma chamber walls will affect the adjacent magma in two main ways. The first of these results from the relative motion of the wall and the magma, which will be undergoing vigorous convection in magma bodies of any great size; see Marsh (1988) and Huppert & Sparks (1988a) for recent discussions of the minimum size of magma body in which convection can occur, which is in any event much smaller than the size of the MBG magma chamber. Within a certain distance from the contact the stationary wall rocks will exert a viscous drag force upon magma flowing past them, producing a viscous or **mechanical boundary layer**. The thickness of this slow - moving, relatively stagnant layer varies strongly with magma viscosity and the variation of viscosity with temperature (Spera et al. 1982): the latter is particularly significant in natural situations because of the strong thermal gradients in the associated thermal boundary layer (see below). Since these gradients are in general negative the result is typically a strong increase in viscosity toward the boundary of the magma chamber. Estimates of typical thicknesses of vertical mechanical boundary layers, when this effect is allowed for, range from a few metres or less in mafic magmas to more than a few hundred metres in felsic magmas (Spera et al. 1982). In the first instance, therefore, one should look for boundary layer phenomena in the MBG on a scale of a few metres to a few tens of metres, given the observed variation in rock compositions.

The second main boundary effect arises from the fact that the country rocks surrounding the magma chamber are normally significantly colder than the magma and will extract heat from it. The most general result of this is that a layer of magma adjacent to the contact will become significantly cooler than the rest of the magma, forming a **thermal boundary layer.** This layer, as a result of thermal contraction and partial crystallisation, will become denser and produce thermal convection in the rest of the chamber as it flows down the contact. Experiments with viscous fluids indicate that the downward flow will remain attached to the wall even if the contact dips outwards (see Turner & Campbell 1986; Huppert et al. 1986).

Magmas are extremely complex fluids, however, and a variety of other effects can arise as a result of their cooling (and the concommitant heating of the wall - rocks). These can be grouped under the headings of effects arising from magma crystallisation and those produced by wall - rock melting:

the various possibilities are reviewed by Turner & Campbell (1986) and McBirney et al. (1985). However, as has recently been emphasised by Huppert (1989) and Huppert & Sparks (1989), which, if any, of these effects actually occurs in a given situation depends on the heat fluxes on either side of the fluid/solid boundary (i.e. at the wall of the magma chamber itself) and the steady - state temperature at that boundary relative to the temperature (or temperatures, in the general case of rocks and magmas of different compositions) at which the magma(s) in the chamber and the wall rocks around it change from plastic or very high viscosity materials (solids) to low viscosity, fluid materials.

Before these various types of boundary can be considered it is necessary to consider the meaning of the transition from solid to fluid behaviour (on the timescale of the magma chamber) and the temperature at which it occurs. Most silicate rocks and magmas are non - eutectic and melt and crystallise over a temperature interval. At finite heating and cooling rates they will therefore melt or crystallise over extended periods of time. Eutectic materials will also show similar behaviour, because heat fluxes will also be finite and it will therefore take time for the latent heat absorbed (as melting proceeds) to be supplied, or the latent heat released (as crystallisation takes place) to be removed. Both processes can therefore only proceed at a finite rate.

Nevertheless, a distinct moment of transition from solid to fluid behaviour, occuring at a distinct rheological transition temperature (here termed a 'rigidus' temperature as a convenient shorthand), is as a first approximation a valid concept for rocks and magmas. This is because of the relatively narrow range of melt percentage present over which the material changes from an interlocking network of crystals with interstitial melt to a mobile melt with a high content of isolated crystals in suspension (Arzi 1978; Van der Molen & Paterson 1979). The experiments of these workers, together with the upper limit on the crystal contents of erupted lavas noted by Marsh (1981), suggest that this change occurs at a Rheological Critical Melt Percentage (R.C.M.P; Arzi 1978) of 20 – 50% and is marked by an abrubt change in effective viscosity, by several orders of magnitude, and the development of a high yield strength. The exact value of the R.C.M.P in any one instance depends to a certain extent on the crystal size distribution (greater scatter in the size distribution allows closer packing of suspended crystals and reduces the R.C.M.P) and crystal morphology (Ward & Whitmore 1950). It is therefore dependent on the crystallisation history of the material concerned. However, introducing a rate - of - cooling dependence effect of this sort into the thermal

equations described below would make them extremely intractable, as would attempting to allow for the possibility of intermittent brittle failure of the chill zone (see case (3), section 4.1.2). For the purpose of calculations, the transition is therefore treated here as occurring at a specific rigidus temperature T_r which is a constant for the composition of material concerned. As noted above, the viscosities of magmas increase markedly with crystal content for a given bulk composition, even above the rigidus, because of the combined effects of temperature, the suspended crystals and the changes in the composition of the remaining melt produced by partial crystallisation (Spera et al. 1982; Marsh 1988). Marsh (1988) reports the results of experimental work which indicates that convection at **horizontal** boundaries may be suppressed by as little as 20% crystallisation and the associated ten - fold increase in the viscosity of basaltic magmas, in which case the effective rigidus temperature would be much higher than that at the R.C.M.P. However, the results of calculations by Spera et al. (1982) indicate that buoyant flows at steeply - inclined thermal boundaries, such as the outer wall of the MBG, are much less sensitive to viscosity variations whilst the crystals in the magma are not actually interlocked (i.e. above the rigidus as defined above). In the discussion and calculations which follow the rigidus temperature of a magma will therefore be calculated as that at which it is 60% crystallised, unless stated otherwise. A similar definition is adopted by Huppert (1989) and Huppert & Sparks (1989).

4.1.2. Types of Magma Chamber Boundary Layer.

The various types of magma chamber thermal boundary layers, as defined by Huppert (1989) and Huppert & Sparks (1989). are described here in general terms; the question of when and if particular types are applicable to the margin of the Marginal Border Group is deferred until later. As noted above, it has been recognised that magma chamber behaviour is primarily controlled by the heat fluxes at the margins of the chamber. Three cases in particular were considered by Huppert (op cit.) and Huppert & Sparks (op cit.), who recognised that in general both the marginal temperature and the heat flux at the margin of any given magma body at any one time are fixed, but that the position of the margin is free to move through melting of the wall rocks or by crystallisation of the magma on the original wall: this is in contrast to the approach of previous workers, who fixed the position of the margin and the temperature, and allowed the heat flux to vary unrealistically. Huppert (op cit.)and Huppert & Sparks (op cit.) mainly deal with lava flows and dykes, but the same principles apply to magma chambers, the only difference being in the factors which control the

heat transfer coefficient defined below (see Huppert & Sparks (1989)). The three types of magma body margin defined by Huppert and Sparks are as follows:

1). In the case of first type of magma chamber boundary, the heat flux Q_c from the wall of the chamber into the country rocks, given by

$$-Q_c = k\frac{\partial T}{\partial x} \tag{4.1}$$

is greater than the heat flux $\mathbf{Q}_m$ from the interior of the magma chamber into the boundary layer. The quantities in (4.1) are as follows:

$k =$ thermal conductivity

$x =$ distance from the contact where distances into the wall rocks are negative and distances into the magma chamber positive

$\frac{\partial T}{\partial x} =$ temperature gradient in the wall rocks immediately adjacent to the contact

The temperature gradient in the wall rocks at any one time is governed by the history of the wall of the intrusion before that time, and hence by the age and temperature of the magma chamber, the thermal diffusivity of the country rocks, the amount of convective heat transfer and the amount of heat absorbed by metamorphic reactions: see Irvine (1970).

Q_m can be expressed as:

$$Q_m = -h(T_r - T_m) \tag{4.2}$$

where h is a heat transfer coefficient, T_r is the rigidus temperature defined above and T_m is the temperature in the interior of the magma chamber away from the boundary layer. (4.2) is valid provided that the wall of the magma chamber has a rigidus temperature below T_m (Huppert 1989) and is therefore applicable both to magma chambers lined with an initial chill zone produced by chilling of magma in the chamber and to those emplaced into rocks of the same or more fusible compositions, although not to those emplaced into refractory wall rocks or lined with adcumulates. As will be seen, this condition is satisfied for the Hypersthene Gabbro.

The imbalance between Q_c and Q_m in this situation leads to a thermal deficit at the boundary which in the absence of a phase change would lead to cooling of the boundary. In magma chambers, unless the magma is superheated, the result is instead solidification of magma on the boundary, with the

release of latent heat of crystallisation balancing the thermal deficit. Thus the boundary propagates into the magma chamber at a velocity a, given by

$$a = -\frac{Q_c - Q_m}{\rho L} \tag{4.3}$$

where ρ = density of material accreted onto the boundary and L = latent heat released during the process of solidification per unit mass of material solidified. It should be noted that for magmas, as described in 4.1.1, 'solidification' does not mean a complete phase change but rather the rheological transition defined in 4.1.1. This leads to a problem. If L is defined as the 'latent heat of congelation', the heat actually released as the cooling magma goes through the R.C.M.P, with the remainder of the latent heat of crystallisation going to increase Q_m and reduce Q_c, the right - hand side of (4.3) becomes an infinitesimally small number divided by an infinitesimally small number, and impossible to evaluate directly. For the purposes of calculating a, given values for the other quantities involved, it is easier to assume that all the latent heat of crystallisation is released at the boundary itself (e.g. Huppert 1989). However, the heat transfer coefficient h, which controls Q_m (equation (4.3)), is itself strongly dependent upon the rate of advective motion and heat transfer within the thermal boundary layer of the magma chamber. This depends on the viscosity of the magma in the boundary layer, and therefore upon the temperature variation within it, which depends on the distribution of latent heat release within the boundary layer. The full mathematical treatment of this situation is intractable and mathematical studies of it to date have employed various simplifications. These are discussed in section 4.1.3, below.

In geological terms, equation (4.3) describes the formation of a sidewall chill zone, which Huppert & Sparks (1989) show to be particularly likely to occur immediately after the initial emplacement of an intrusion when thermal gradients in the wall rocks are high, or the formation of sidewall cumulates. Which one of these two types of contact zone is produced in a given situation depends on whether the solidification process is purely one of in situ crystallisation or is slow enough to allow the separation of crystals and residual melts and hence the formation of sidewall cumulates. In this latter case, further complications are produced by the fact that the residual liquid will in general have a different density to both the accumulating crystals and the magma in the adjacent magma chamber boundary layer. It will therefore tend to migrate up or down the margin of the magma chamber, through the porous zone of the wall, according to the density differences produced by the compositional differences (Lowell 1985), in a form of compositional convection (Kerr & Tait 1986). Fig. 4.1A is a cartoon cross - section showing the general features of this type of boundary.

Fig. 4.1. Sketch Cross - sections of the three types of Magma Chamber wall Boundary Layer.

A: $Q_c > Q_m$: congelation cumulates or chill zone formed on wall.

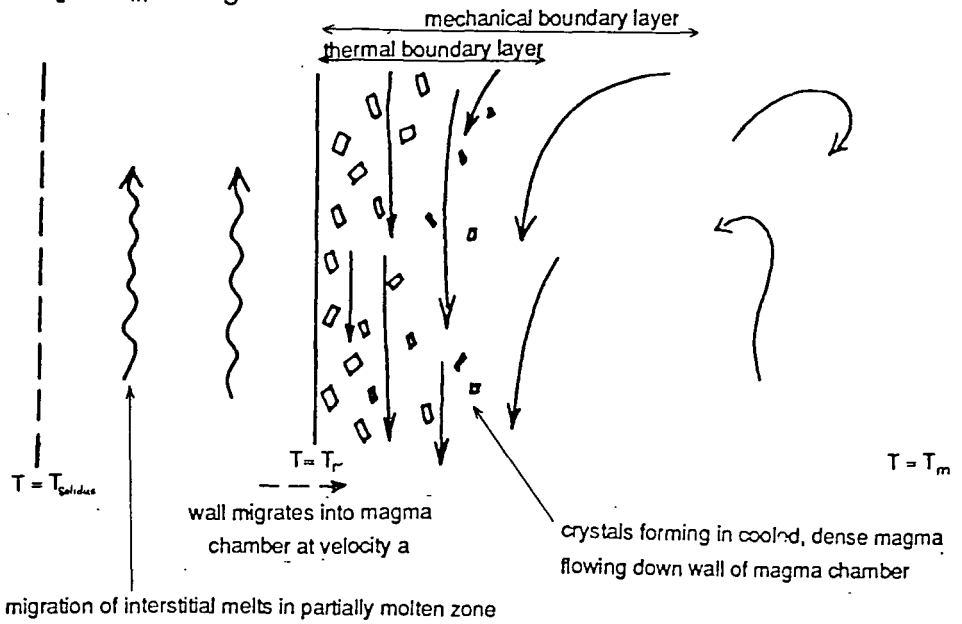

B: $Q_c < Q_m$: wall rock (country rock or chill zone) melting. Case of compositionally buoyant wall rock melts shown.

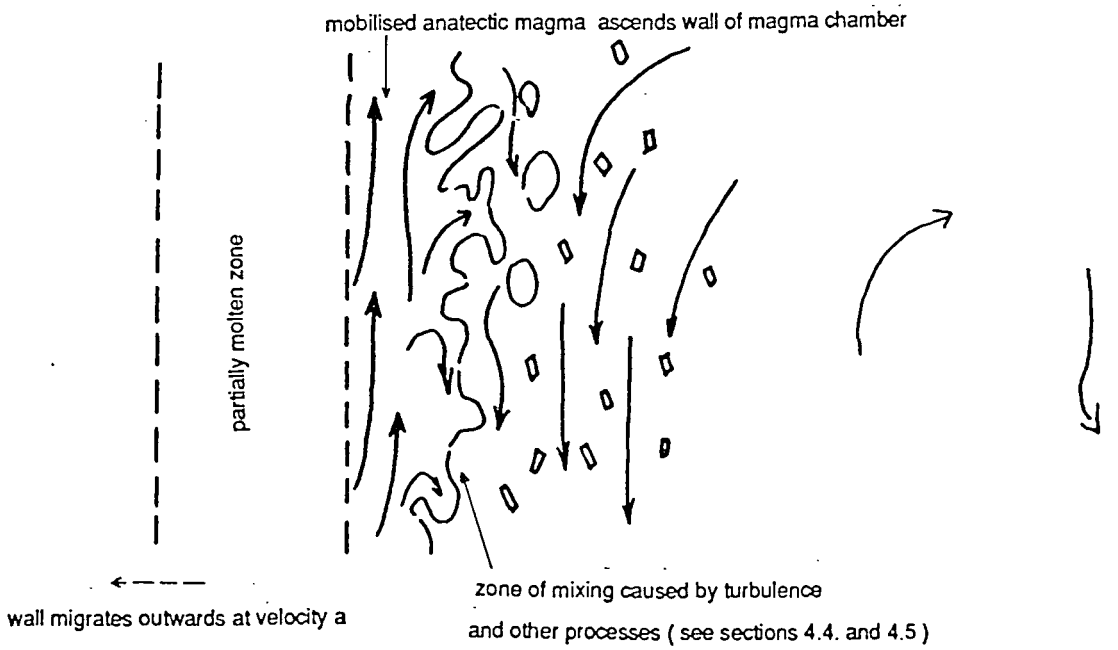

C,D: $Q_c \geqslant Q_m$ but T of mafic magma much higher than T of wall rocks. Simultaneous formation of wall rock melts and an unstable chill zone which forms and disintegrates cyclically.

C: Chill zone forms between ascending wall rock melt and descending cooled mafic magma.

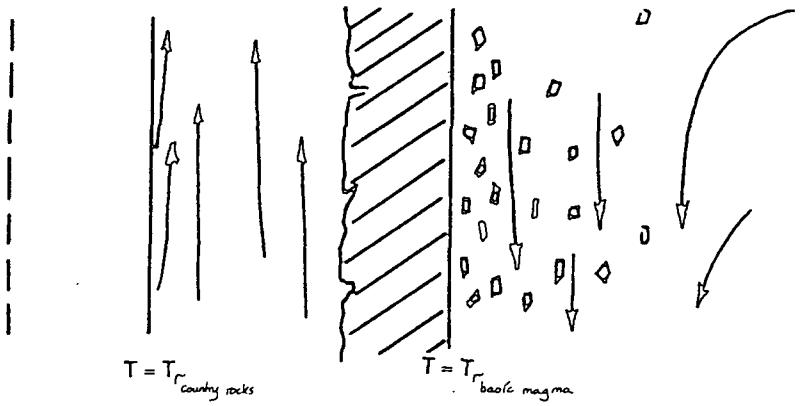

D: Old chill zone disintegrates and falls away into downward flow

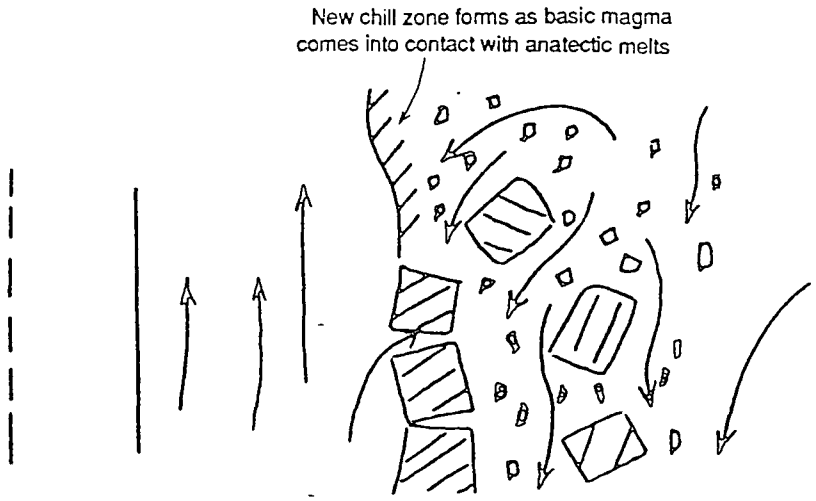

2). In a second type of boundary layer defined by Huppert (1989) Q_c is less than Q_m and T_r of the wall rocks is less than T_m (see above). In this case, although magma from the interior of the magma chamber is cooled as it passes through the boundary layer and undergoes partial crystallisation, it is never cooled below T_r and therefore never solidifies on the wall. The excess of Q_m over Q_c is absorbed by melting and mobilisation of the wall rocks at a rate which is given by (4.3). In the terms of this equation, a is now negative, and the margin of the magma chamber moves into the country rocks. The production of new magma at the boundary, particularly in the geologically very important case of melting of pre - existing country rocks with a different bulk composition to that of the magma in the interior of the chamber (and hence different temperature, viscosity and density) produces a variety of fluid dynamic complications which are discussed by Turner & Gustavson (1981), Spera et al. (1982), Turner & Campbell (1986), and Campbell & Turner (1987) amongst others. The most important possibilities can be summarised as follows: **(i)** The wall rock melt is sufficiently buoyant and abundant to flow up the wall of the magma chamber, in the opposite direction to the downflow of cooled ambient magma, and accumulate at its roof as a separate low - density anatectic melt layer. If the magma chamber is stratified as a whole the magma rising up the wall may be intercepted by a layer of low - density magma and mix with it; this situation will be considered further below. **(ii)** The wall rock melt is buoyant but is dragged down the wall by the downflowing cooled magma and is released into the interior of the magma chamber from the floor, in which case it is likely to mix with the magma in the interior of the chamber; this situation is most likely to occur when wall rock melting is slow (small a), the density difference betwen the wall rock melt and the ambient magma is small, and the melts are highly viscous (Spera et al. 1982). **(iii)** The wall rock melt is denser than the magma in the interior of the chamber and flows down the wall, ponding at its floor: this will in general only occur in replenished magma chambers in which evolved iron - rich sidewall cumulates are remelted by a fresh input of primitive magma. **(iv)** Turbulence in the boundary layer, or some other process, causes the wall - rock melt to mix with, and directly contaminate, the magma in the interior of the intrusion. This fourth possibility may, if the rate of mixing is low compared to the rate of melting at the wall, occur together with any one of the other three, producing a progressively eroded boundary - layer current. A situation of this sort is depicted in Fig. 4.1B. It should be noted that interstitial melt migration could take place in the partially molten zone between the solidus and the rigidus. However, in the most important case, that of the melting of felsic crustal rocks, this is unlikely to be an important process on the short timescale of upper crustal magma chambers (McKenzie 1985; see section 3.2.5.3 for textural evidence for the

limited scale of interstitial melt migration in the contact aureole of the Hypersthene Gabbro).

3). A third type of boundary layer occurs when the country rocks are fusible (i.e. have a low rigidus temperature) and the magmas in the interior of the magma chamber are both at high T_m and have a high T_r. In this case, Q_c may exceed Q_m, leading to the formation of a chill zone on the wall, but at the same time temperatures in the country rocks may exceed their T_r, producing a zone of mobile anatectic melt. Two rigidus boundaries are produced and initially migrate away from one another, but if the chill zone remains in place as it thickens, it will insulate the melted country rocks from the main magma chamber and they will cool and solidify. If on the other hand the presence of magmas on both sides causes the chill zone to break up, either as a result of drag forces from the moving magmas or under its own unsupported weight, the process may repeat itself cyclically, with successive chill zones growing and then breaking up and dispersing, allowing new chill zones to form and also causing the country rocks to continue to melt (Figs. 4.1C and 4.1D). The effect of a process of this sort is to increase the heat flux from the magma chamber, Q_m, by an amount given by:

$$\Delta Q_m = (C_p(T_r - T) + \Delta L) \times dM/dt \tag{4.4}$$

(where T is the mean temperature of the disrupted chilled material, C_p is its specific heat capacity, ΔL is the latent heat released as it cools from T_r to T, and dM/dt is the rate at which it breaks away from the wall of the chamber)

to the point where Q_m exceeds Q_c and the wall rocks continue to melt. The magnitude of this effect cannot be predicted theoretically because the processes inolved in the disruption of the chill zone are poorly understood (Huppert 1989).

Thermal modelling of magma chamber boundary of types (2) and (3) as defined above is made much more complicated by the presence of a third layer of mobile magma, the anatectic magma, between the wall rocks and the convecting magma in the interior of the magma chamber. In the case of a stably stratified horizontal boundary a multi - layered thermal model can be applied, with the motion of each boundary being described by a modified version of (4.3), as was done by Huppert & Sparks (1988a). However, when the boundary is inclined the thickness of the middle layer and the heat flow across it are also strongly dependent on the rate at which the anatectic magmas move up (or down) the magma chamber walls, or are mixed into the interior. This is itself dependent on

the temperature structure and viscosity of the boundary layer and the prediction of the behaviour and structure of the boundary layer becomes a very complex problem.

From a petrogenetic viewpoint (2) and (3) describe very important situations, those in which separate bodies of anatectic magma can be produced, or in which crustal contamination can occur, depending on the stability of the layer of anatectic magma at the boundary. At the same time, separation of the crystals formed in the descending thermal boundary current shown in Fig. 4.1B and 4.1C, once these currents reach the floor of the chamber and decelerate (Wager 1960; Irvine 1980, 1987), provides an efficient fractionation mechanism. On the large scale, boundary layers of types (2) and (3) above may be sites of thermally coupled assimilation and fractional crystallisation (AFC), although whether a geochemical AFC evolution trend is produced in the resulting magmas will depend on the magma - mixing processes in the magma chamber. In magma chambers with type (1) walls, the dominant process will be fractional crystallisation, without production of anatectic magmas or contamination of the magmas in the interior of the magma chamber.

4.1.3. The limitations of theoretical calculations regarding the behaviour of magma chamber boundary layers, and an outline of an alternative approach to the study of them.

Combining equations (4.2) and (4.3) gives an apparently simple expression for the overall thermal balance of a magma chamber boundary:

$$Q_c - h(T_r - T_m) = \rho L a \tag{4.5}$$

This apparent simplicity is due to the concealment of complex relationships between magma composition, magma viscosity and its variation with temperature, the buoyancy forces produced by cooling and crystallisation on the one hand and wall - rock melting on the other, thermal conductivities and heat capacities, the pattern of latent heat release in the boundary layer – in other words, all the factors which control advective and conductive heat transfer in the boundary layer – in the heat transfer coefficient h. In experiments on **constant - viscosity** fluids not affected by latent heat release, conducted at high Rayleigh numbers ($Ra \geq 10^6$), that is to say in turbulent flows, h has been found to be a constant for any given fluid and contact geometry at a given fluid and contact temperature but to vary considerably with the properties of the fluid (Huppert & Sparks 1988a, 1989). Although these experiments have been conducted on constant - viscosity, one - phase fluids

the normal procedure (e.g. Nilson et al. 1985) is to adapt the empirical equations produced, such as

$$h = \frac{L^{0.75} g \alpha \Delta T}{\kappa_T \nu^{0.583}} \tag{4.6}$$

where L = height of boundary under consideration, g = acceleration due to gravity, α = coefficient of thermal expansivity of the fluid, ΔT = temperature difference across boundary layer, κ_T = thermal diffusivity of the fluid, ν = fluid viscosity.

Equation (4.6) is obtained by combining an empirical expression for h at a vertical boundary layer in terms of boundary layer thickness and the Rayleigh Number of the convecting magma body, due to Kraussold (reproduced on p.541 of Eckert & Drake (1987)), and an expression for boundary layer thickness (Howard 1966) in a similar situation. The critical stage in adapting such equations to magmas is the insertion of a suitably weighted mean viscosity for the entire boundary layer. One problem with this procedure is that it corresponds to neglecting, to varying degrees, flow in the more viscous parts of the boundary layer (Nilson et al. 1985) which is the same as changing the rigidus temperature T_r: this affects h and, to an even greater degree, Q_m (see equation (4.3), above). Furthermore, there is no experimental evidence to suggest that this procedure is valid.

Although the effects of temperature - dependent viscosity on heat transfer coefficients have been studied by a number of workers, most of these studies are concerned with a horizontal layer heated from within and below, as well as cooled from above, such as the Earth's mantle (e.g. Richter et al. 1983), and are not applicable to the steep wall of a magma chamber in which convection is driven by buoyancy forces produced in the high - viscosity boundary layer. Spera et al. (1982) explicitly included viscosity variation in their magma chamber model, but to do this they had to assume a fixed boundary temperature and a fixed boundary position, whilst allowing the heat flux through the country rocks to vary freely with Q_m. Their results are nevertheless valuable in that they show that the inclusion of viscosity effects will produce factor - of - two variations in Q_m even with other variables kept constant and no allowance for latent heat release. Smith (1988) also considered the effects of temperature - dependent viscosity upon convective heat transfer in a horizontal, solidifying layer cooled from above, and found that the precise viscosity variation had a strong effect upon the rate of solidification of the layer. Smith's model is more realistic than that of Spera et al. in that he allowed the position of the top of the convecting layer to move as a result of the solidification, but he was obliged to fix the rate of movement, and by implication the heat flux Q_c through the roof of

the layer.

The practice of arbitrarily fixing Q_c at some constant value in these models has been criticised by Carrigan (1988), Marsh (1988) and, implicitly, by Huppert (1989), who point out that T_r, T_m, Q_c and Q_m are all constrained by the materials involved and the previous thermal state of the country rocks and that it is in fact the position of the boundary which is free to change. These authors are, however, then obliged to estimate h and hence Q_m by use of a constant - viscosity equation such as (4.5).

An alternative procedure to these purely theoretical analyses, which is attempted here for the first time, is to estimate variables such as Q_m, Q_c, h, a, T_m and T_r for a specific intrusion from the geology of that intrusion. As noted above, Q_c depends on the previous thermal history of the country rocks and will therefore change with time through the history of a magma chamber. It is therefore necessary to determine the values of these variables at a specific time in the evolution of the intrusion under investigation. This is possible in the case of the Marginal Border Group of the Hypersthene Gabbro because, as will be shown in Chapter 5, the quenching of the contact aureole and the solidification of at least the outer parts of the contact zone in any one sector of the contact occurred in an interval of time that was very short compared to the previous M1 phase of its thermal evolution. Within this period of time, the value of Q_c could not have changed greatly had the heat transfer mechanism in the country rocks not changed (see Chapter 5). It can therefore be taken as a constant when considering the period immediately prior to the onset of quenching. The other variables under consideration are not as time - dependent as Q_c and can also be taken to be constants during the same period. In addition to preserving the high - grade mineral assemblages of the M1 aureole, from which the value of Q_c at the end of M1 can be estimated (see Chapter 5), the abrubt quenching at the end of M1 may have, to a greater or lesser degree, preserved the boundary layer associated with this value of Q_c in the shape of the contact zone of the MBG. However, the solidification of these rocks necessarily implies that, during the quenching, the boundary layer was like the theoretical Type 1 boundary layer (section 4.1.2), as defined above, whilst the occurrences of wall rock melting and mobilisation (identified on the basis of field and petrographic evidence; section 3.2) imply that it previously bore a close resemblance to the theoretical Type 2 and 3 boundary layers defined in section 4.1.2, with Q_m greater than Q_c. One of the principal problems that will be dealt with in this chapter, and in Chapter 5, is the separation of phenomena characteristic of the

M1 boundary layer from the effects of crystallisation in the Type 1 boundary layer associated with the quenching event itself.

The quantititative value of this approach to the study of magma chamber boundary layers is dependent upon two factors. Firstly, the errors and assumptions involved in measurements of the various quantities of interest may be such as to make the results no more accurate than those of the theoretical models; estimation of these errors will therefore be of critical interest in what follows. Secondly, the behaviour of any one boundary layer will not be typical of them all, and in particular magmas of different compositions would be expected, from the theoretical studies, to show completely different responses to given heat fluxes in the country rocks. In general, magma chambers containing hotter and less viscous magmas would be expected to show type 2 or 3 boundary layer behaviour over a range of heat fluxes in the country rocks which extended to higher values (Huppert & Sparks 1989). This chapter and Chapter 5 should therefore, in part, be looked upon as an evaluation of methods of determining heat loss and boundary layer behaviour of the magma chambers represented by intrusions such as the MBG. The applicability of these methods to other intrusions will be considered in Chapter 8. A further purpose of the present chapter will, however, be to consider the behaviour of the MBG magma chamber during M1 in qualitative terms, in search of effects and phenomena which have not been included in theoretical models of magma chamber boundary layers.

4.2. The Felsic Rocks of the Marginal Border Group: Geochemistry, Petrogenesis and Physical Properties at the Time of Emplacement.

4.2.1. Overall Distribution of the Felsic Rocks.

As summarised in section 3.2.7, the felsic rocks of the Contact Zone of the MBG and the minor intrusions associated with it can be subdivided on their petrography and age relationships into M1 microgranodiorites and M2 felsites and microgranophyres (lumped together hereafter as 'felsites' except where stated otherwise and in the context of rock textures), which are mainly of subalkaline granitic to granodioritic composition; M1 microgranitoids with varied and anomalous mineralogies and compositions; and rheomorphic breccias. The overall distribution of these rocks around the periphery of the Hypersthene Gabbro is shown in Fig. 4.2. Several points are apparent from this map:

1). The M1 felsic rocks occur in a number of small, discrete areas immediately adjacent to the contact which, where exposure is sufficient, are seen to be elongated parallel to it.

2). The anomalous microgranitoid rocks, as noted in 3.2.7, are closely associated with pseudoscreens or downfaulted blocks of the country rocks which projected into the MBG magma chamber during M1.

3). In contrast, the M1 microgranodiorites and M2 felsites do not show a strong spatial association with those downfaulted blocks displaced along faults which are exposed close to the contact at the present level of exposure. These are those which intersect the wall of the magma chamber close to the present level of exposure. It should be noted that, except on the western margin where the relevant areas are submerged, the whole of the intrusion can be shown to be surrounded by concentric faults which intersect its margin at various depths below the present - day surface (see Chapter 7).

4). Although early M2 granitic vein networks occur in most sectors of the contact, the main outcrops of the M2 felsites are confined to the northern and extreme south - eastern sectors of the contact. The M1 microgranodiorites are much less abundant but appear to show a similar distribution.

Fig. 4.2. The distribution of M1 microgranodiorites, M2 felsites, M1 anomalous granitoids and rheomorphic breccias around the periphery of the Marginal Border Group.

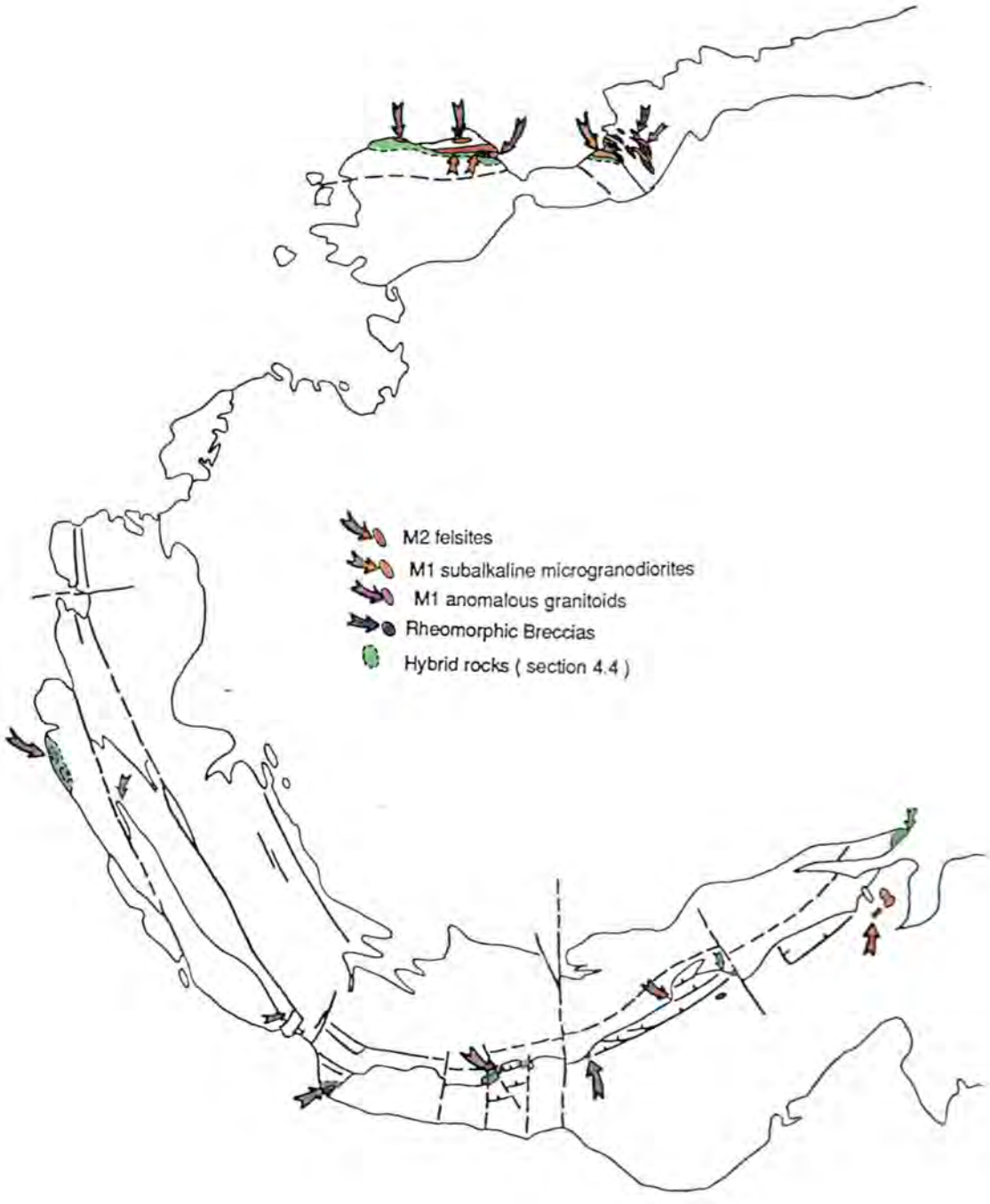

5). The M1 felsic rocks, which have liquid – liquid (lobate or, more commonly, chilled) contacts against the more mafic MBG rocks (section 3.2), do **not** show a strong association with irregular culminations in the wall of the intrusion which might have acted as traps for buoyant magmas flowing up the wall of the MBG magma chamber during M1. Similar felsic rocks in the contact zone of the Rhum ultrabasic complex (Greenwood 1987) are concentrated beneath sub - horizontal or inward - dipping segments of the roof of the complex, which Greenwood considers to have trapped buoyant magmas flowing up the wall of the magma chamber. A similar trapping mechanism could explain the occurrences of microgranitoid rocks south of the downfaulted blocks on Hill 210 (see Figs. 3.10 and 3.13) but does not appear to apply to the other occurences of M1 felsic rocks around the periphery of the MBG. This is particularly apparent at Glendrian Bay (section 3.2.2.1), where mafic and hybrid rocks locally overlie M1 felsic rocks with a pillowed contact between them. This contact, and the more common steeply inclined contacts between coexisting felsic and mafic magmas, must have been gravitationally unstable, given the difference between the densities of the felsic (section 4.2.5) and basic magmas (section 4.3.3). They must therefore have been preserved in situ by the rapid solidification of the contact zone at the end of M1.

4.2.2. M1 microgranodiorites and M2 felsites.

4.2.2.1. Geochemistry and mineralogy.

Important features of this suite of rocks are summarised in the series of compositional plots which make up Fig. 4.3. Overall, they are similar to the suites of relatively primitive, weakly fractionated subalkaline granodiorites and adamellitic granites which occur widely in the BTVP central complexes (Thompson 1982) and which are particularly common in the earlier stages of the histories of these complexes. Two such granitic rocks from other central complexes, SK69 from the Western Redhills Centre of Skye and M155 from Centre 1, Mull (see caption to Fig. 2.8 for data sources) are included in Figs. 4.4A and 4.4B to allow comparison of the trace and minor element geochemistry of these rocks. The only significant difference between the Ardnamurchan rocks and these two granites appears to be the lower abundance of Ba in the rocks from Ardnamurchan (particularly the two M1 rocks), which is also reflected in lower Ba/K, Ba/Na and Ba/Sr and hence does not appear to be the result of greater fractionation (also, see discussion of fractionation trends in the M2 felsites, below). The greater abundance of Rb in the Ardnamurchan samples may however be an analytical

Fig. 4.3. Geochemistry of the M1 microgranodiorites and M2 felsites. 1.

4.3.1 - 6: Major and trace element plots showing moderately good fractionation trends.
4.3.7: Plot of A/CNK vs. SiO2 showing the mainly subalkaline character of these rocks.
4.3.8 - 12: Minor and trace element plots showing wide scatter around fractionation trends. See text for discussion.

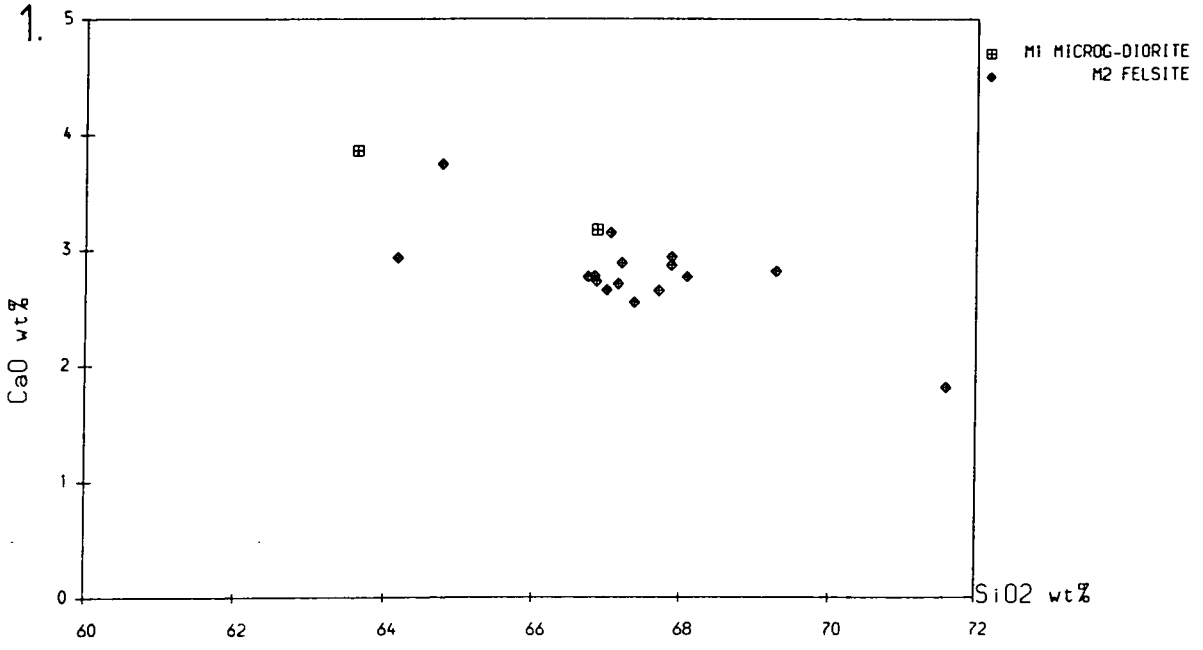

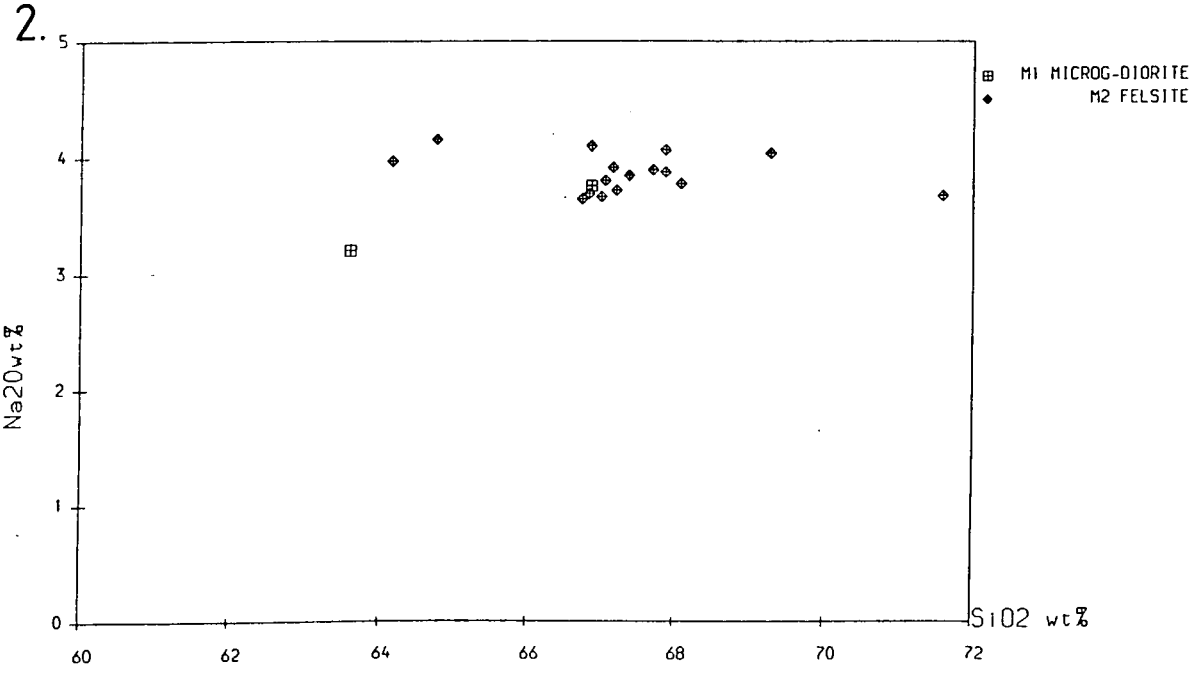

3.

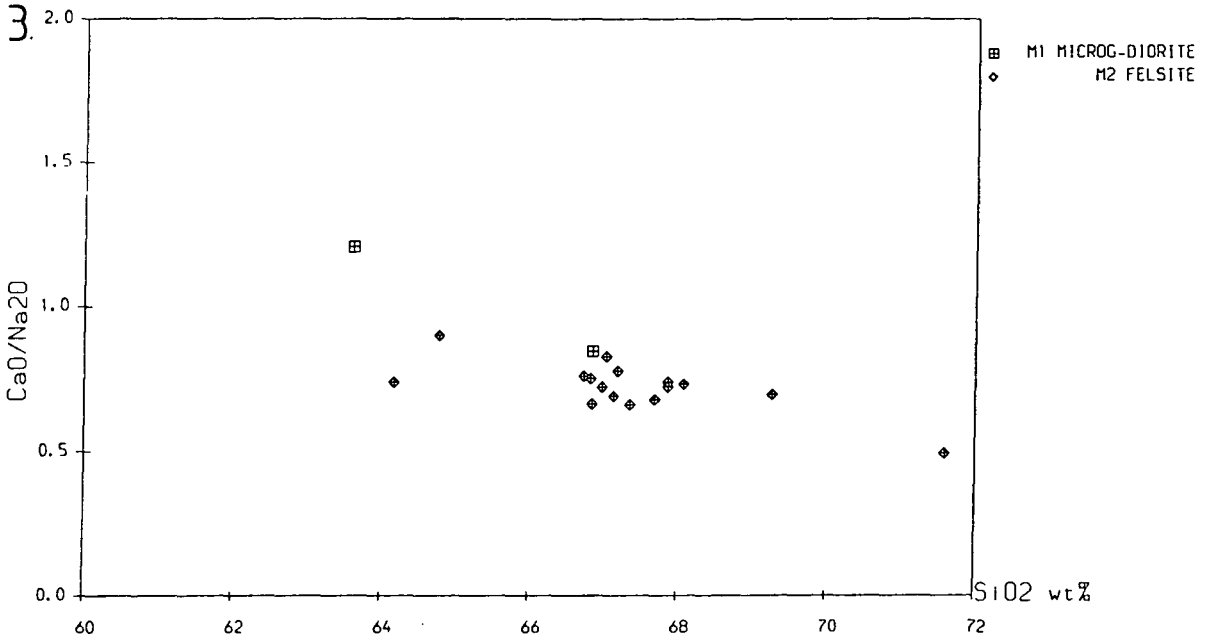
M1 MICROG-DIORITE
M2 FELSITE
CaO/Na2O
2.0
1.5
1.0
0.5
0.0
60
62
64
66
68
70
72
SiO2 wt%

4.

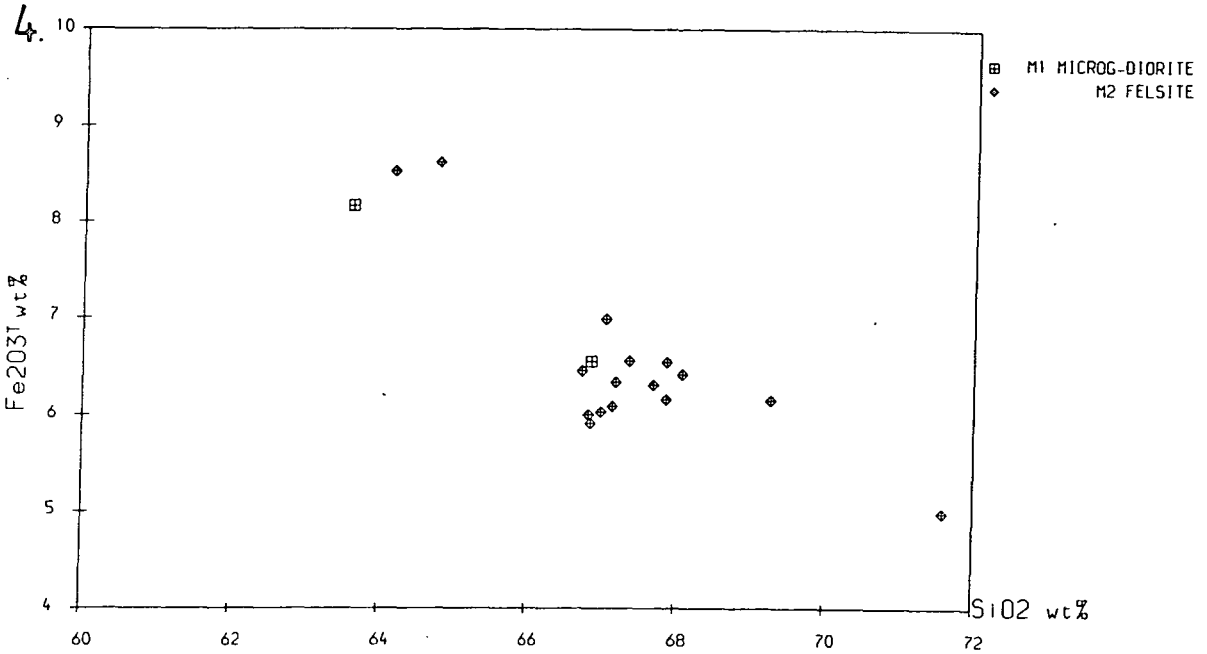
M1 MICROG-DIORITE
M2 FELSITE
Fe2O3T wt%
10
9
8
7
6
5
4
60
62
64
66
68
70
72
SiO2 wt%

5.

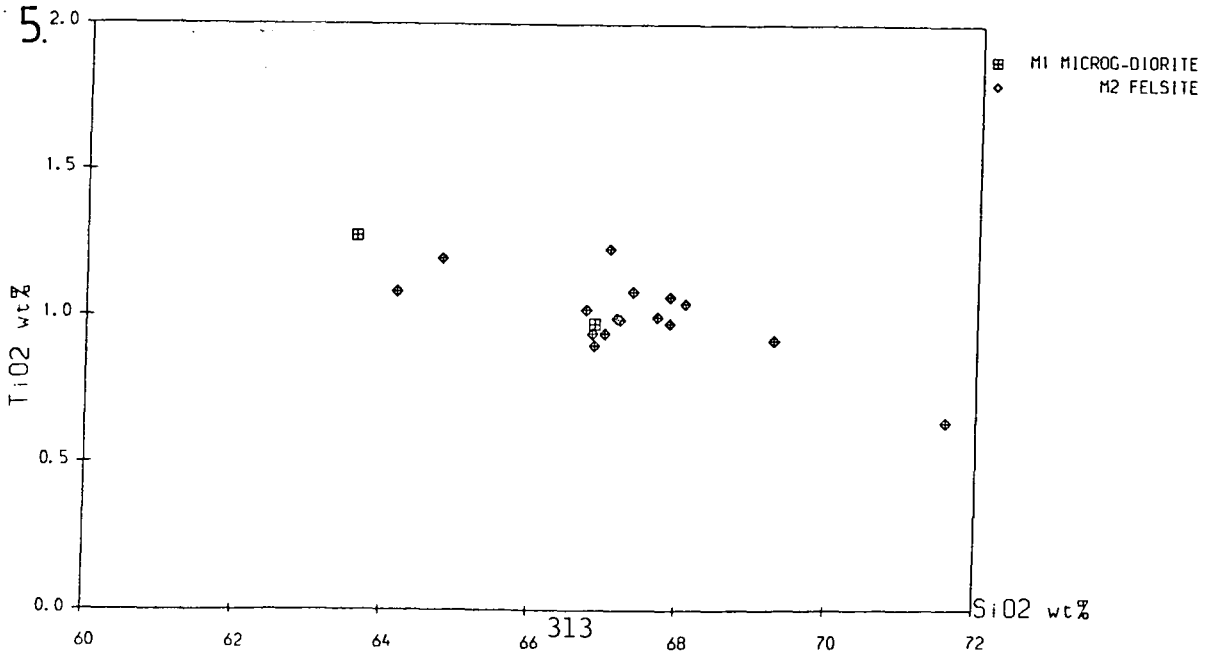
M1 MICROG-DIORITE
M2 FELSITE
TiO2 wt%
2.0
1.5
1.0
0.5
0.0
60
62
64
66
68
70
72
SiO2 wt%

6.

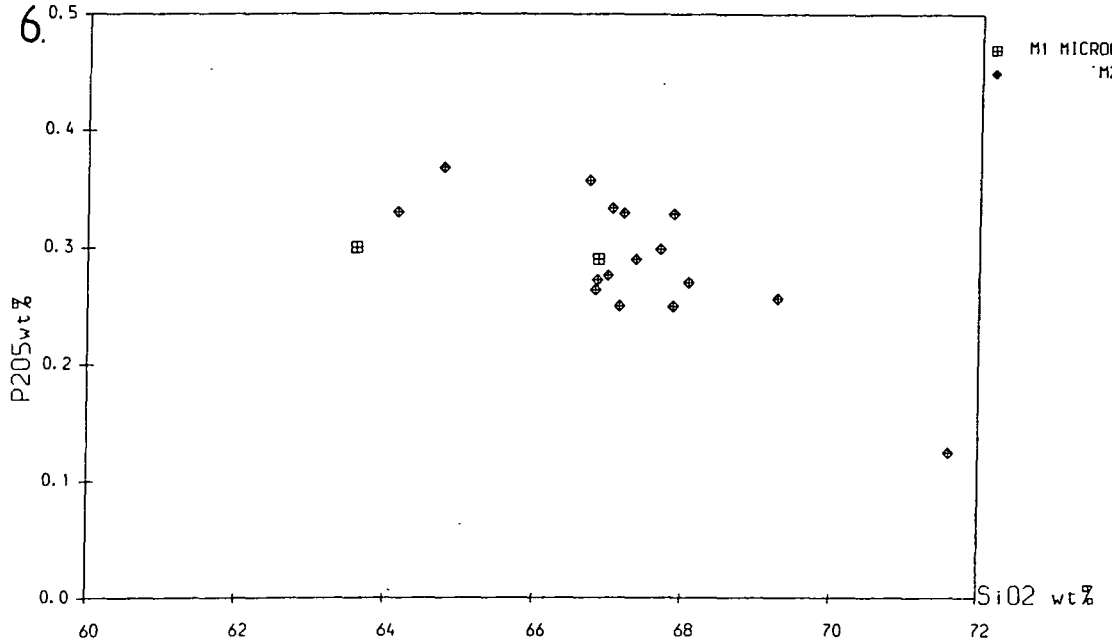
M1 MICROG-DIORITE
M2 FELSITE
P2O5wt%
0.0
0.1
0.2
0.3
0.4
0.5
60
62
64
66
68
70
72
SiO2 wt%

7.

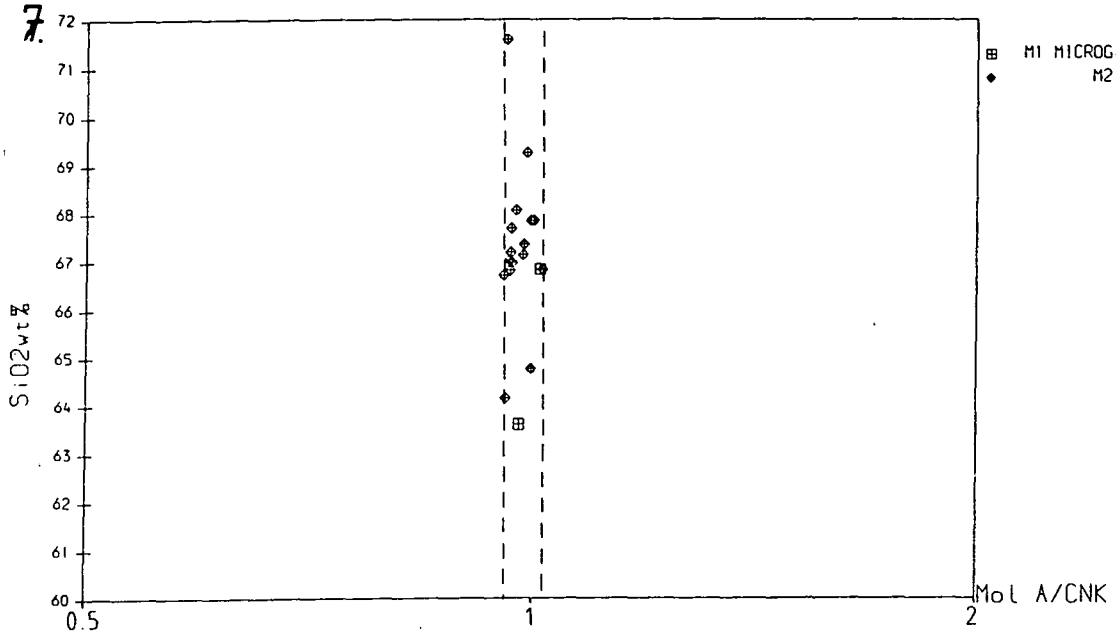
M1 MICROG-DIORITE
M2 FELSITE
SiO2wt%
60
61
62
63
64
65
66
67
68
69
70
71
72
0.5
1
2
Mol A/CNK

8.

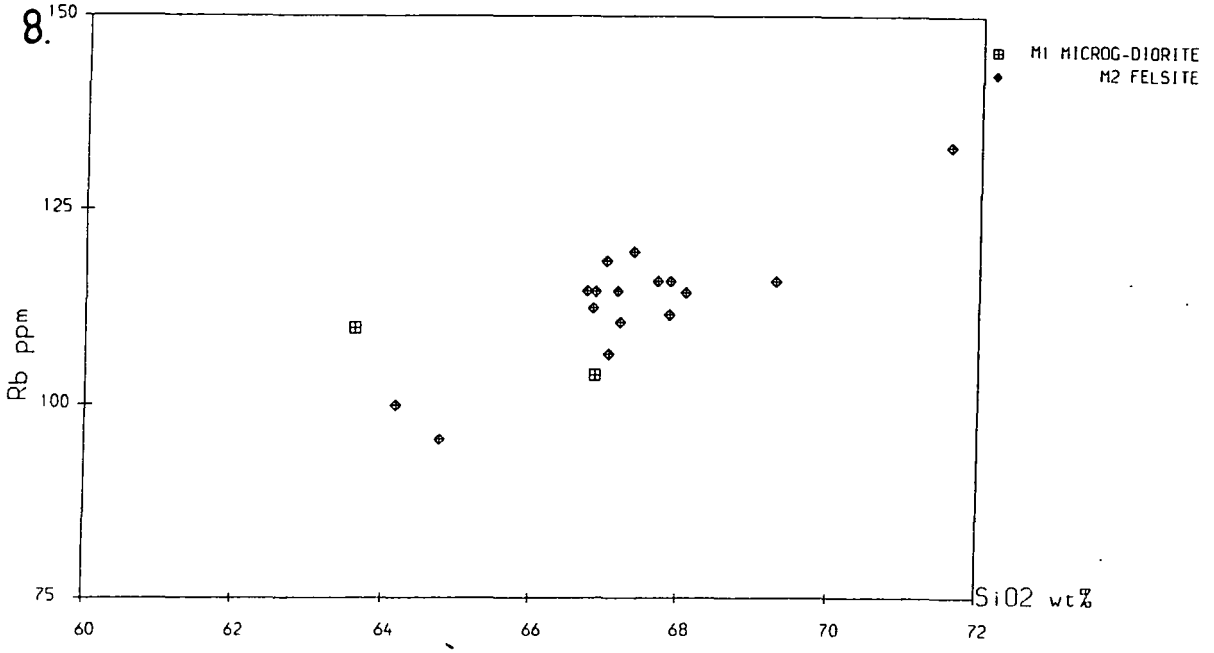
M1 MICROG-DIORITE
M2 FELSITE
Rb ppm
150
125
100
75
60
62
64
66
68
70
72
SiO2 wt%

9.

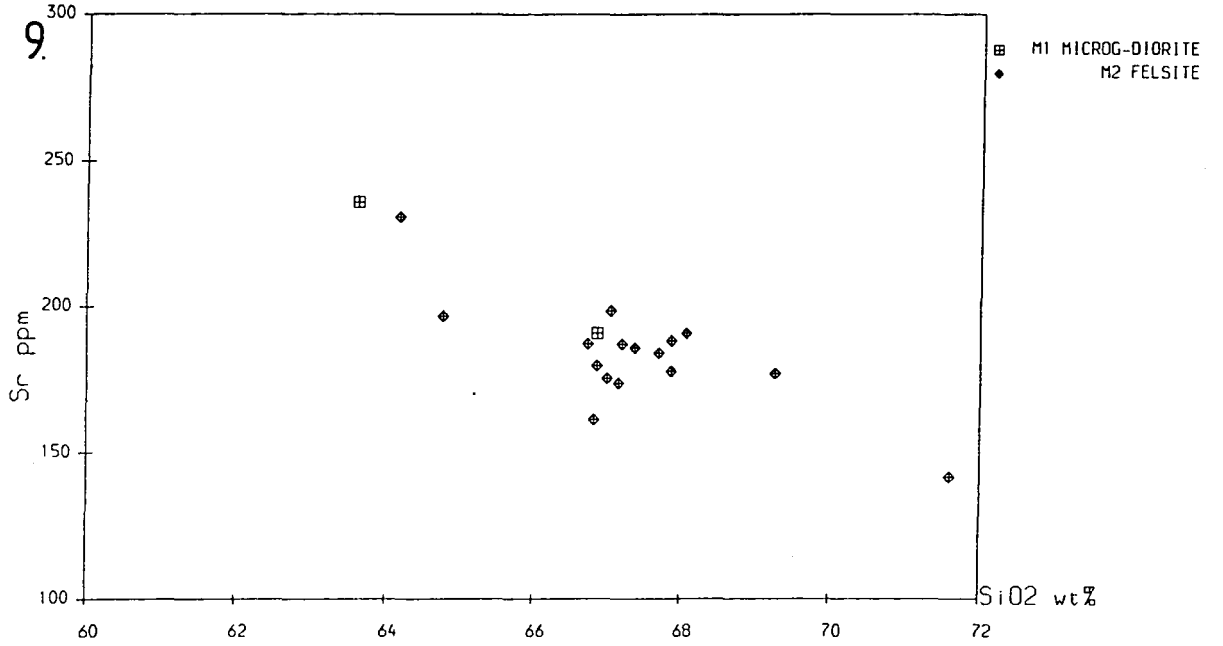
M1 MICROG-DIORITE
M2 FELSITE
Sr ppm
300
250
200
150
100
60
62
64
66
68
70
72
SiO2 wt%

10.

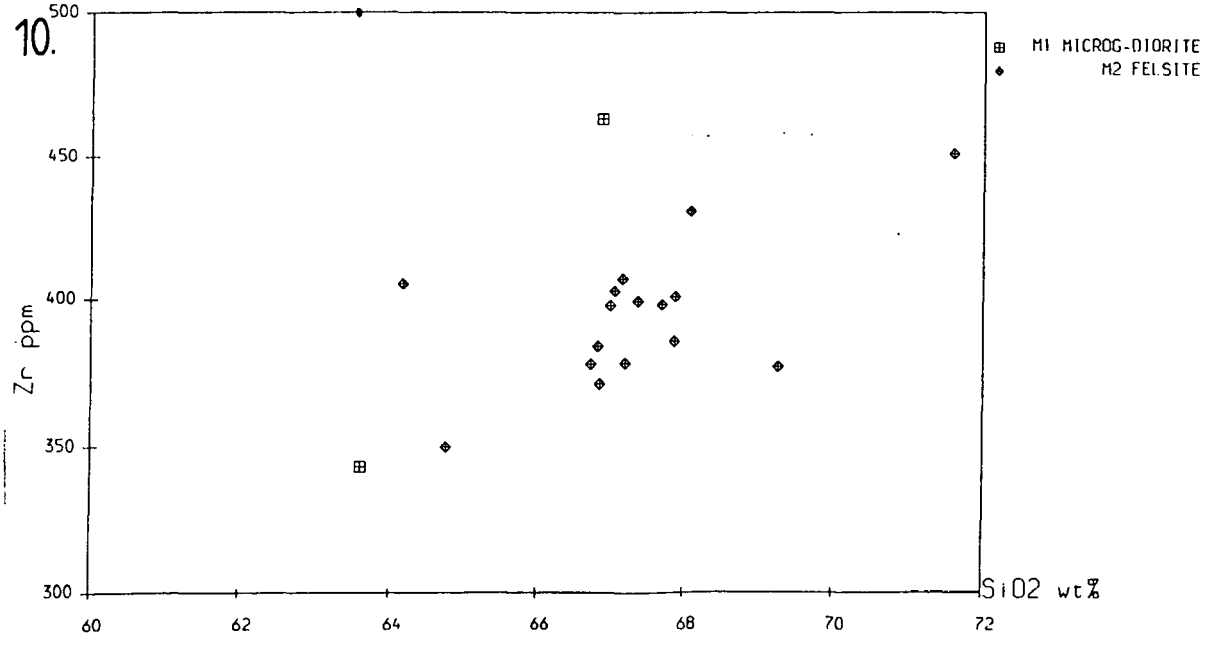
M1 MICROG-DIORITE
M2 FELSITE
Zr ppm
500
450
400
350
300
60
62
64
66
68
70
72
SiO2 wt%

11.

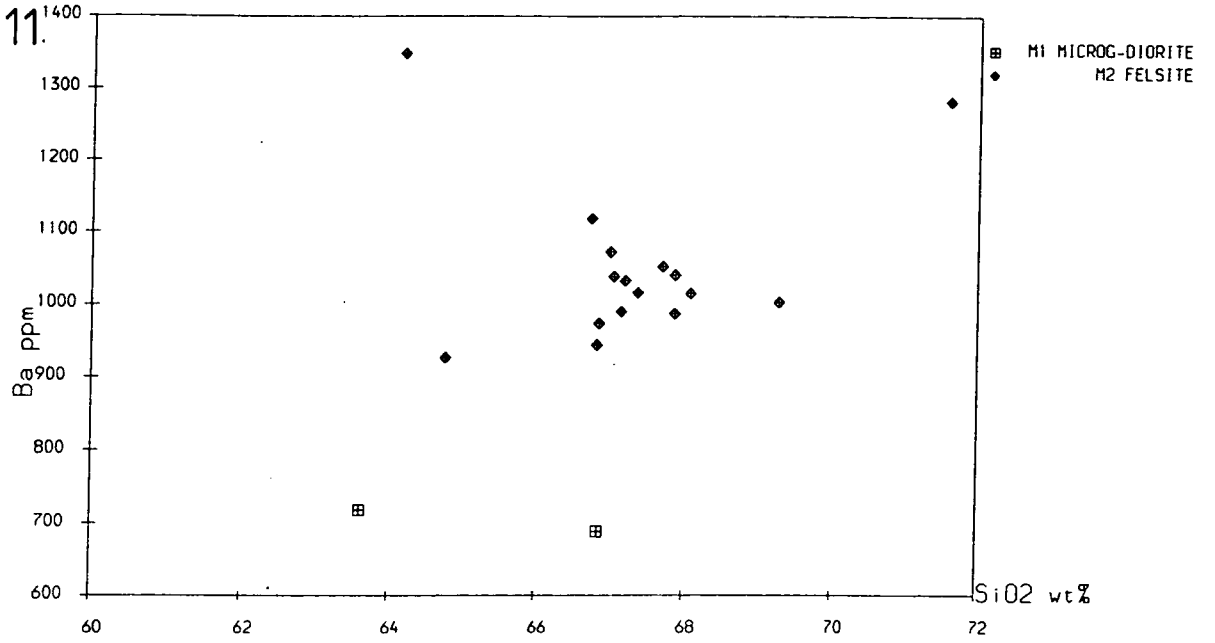
M1 MICROG-DIORITE
M2 FELSITE
Ba ppm
1400
1300
1200
1100
1000
900
800
700
600
SiO2 wt%
60
62
64
66
68
70
72

12.

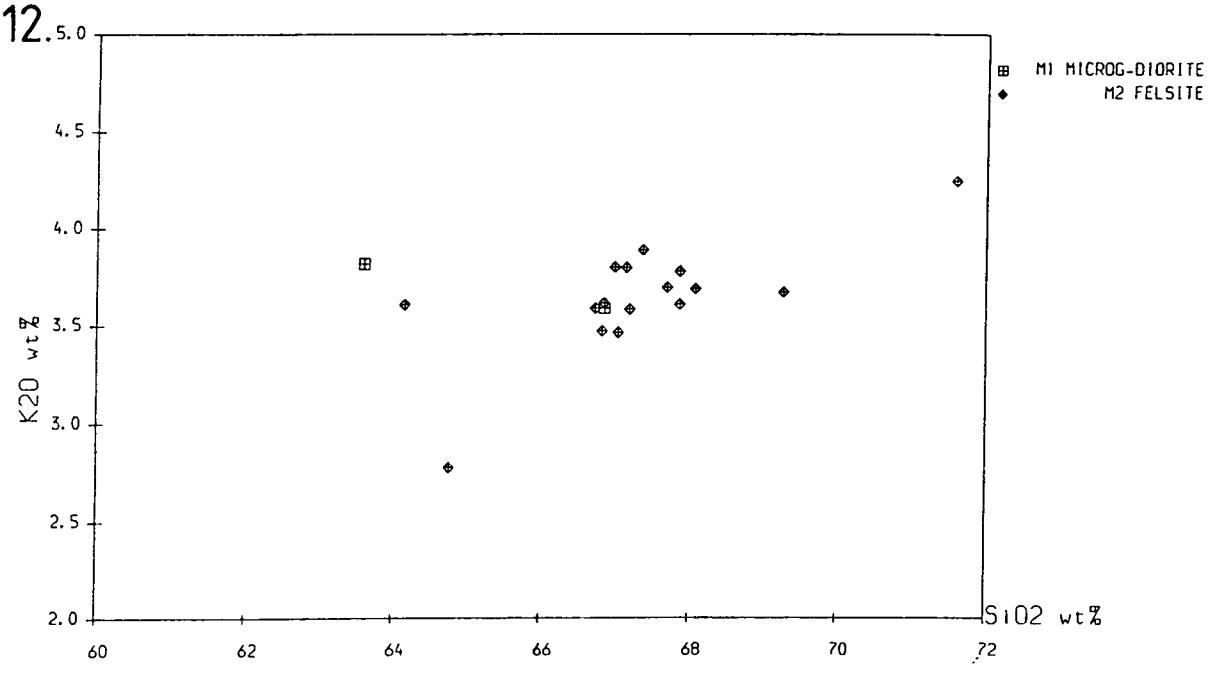
M1 MICROG-DIORITE
M2 FELSITE
K2O wt%
5.0
4.5
4.0
3.5
3.0
2.5
2.0
SiO2 wt%
60
62
64
66
68
70
72

artefact (see Appendix 1).

The most plausible overall model for the generation of these rocks appears to be by crystal fractionation from crustally contaminated basic magmas, as has been previously proposed by various workers (Thompson 1982 & references therein) for the majority of the BTVP granites. Two broadly tholeiitic rocks of M1 age from the MBG, an olivine - poor tholeiite (42D2) and a ferrodiorite (183B1), are included in Fig. 4.4A. These show the high La/Ta characteristic of crustal contamination in the BTVP (Thompson 1982; Thompson & Morrison 1987). Fractionation of similar contaminated tholeiitic magmas, involving the crystallisation of plagioclase and pyroxene(s) initially (to produce the Sr and HREE/LREE depletions apparent in 183B1) and subsequently of Ti-bearing oxides and apatite as well (to produce the Ti and P depletions in the felsic rocks, and also to suppress further LREE enrichment) could produce granitic rocks with the elemental abundances shown in Fig. 4.4. The details of this process, and the possibility of further crustal contamination, are considered further in section 4.3, in the context of the evolution of the basic and intermediate rocks of the MBG.

The alternative mechanisms for the genesis of the subalkaline rocks, by anatexis of pre - Tertiary country rocks or by mixing of melts of these rocks with basic magmas, can be excluded in a variety of ways (see Thompson 1982, 1983). Of these, the clearest and most generally applicable is shown in Fig. 4.5. On this chondrite - normalised La_N/Yb_N vs. La (ppm) plot the M1 and M2 subalkaline felsic rocks analysed for REEs plot in or close to the field occupied by several other BTVP 'primitive' granites. They lie well away from the fields occupied by the pre - Tertiary country rock groups, excluding the possibility that they are high - degree melts of these rocks, and from mixing lines between the country rocks and BTVP mafic rocks approximating to liquid compositions. It is however difficult, purely by geochemical arguments, to exclude the possibility that the BTVP granites are low - percentage partial melts, formed under low P_{H_2O}, of mafic Lewisian rocks: isotopic studies in other BTVP centres rule out this mechanism of felsic magma generation in these centres, however (Dickin 1981; Dickin et al. 1984).

Strong linear fractionation trends are apparent within the subalkaline microgranodiorite - felsite suite, as shown by plots 1 to 6 in Fig.4.3. As with the patterns of enrichment and depletion in Fig. 4.4, these can be explained in terms of fractionation of an intermediate plagioclase (c. An_{40}),

Fig. 4.4A: Chondrite - normalised plot comparing features of the chemistry of two M1 microgranodiorites with other "primitive" BTVP granitoids (see caption to Fig. 2.8 for data sources) and with contaminated basic (42D2) and intermediate (183B1) rocks of M1 age from the Marginal Border Group. The latter are comparable to the likely parent magmas of the subalkaline granitoids.

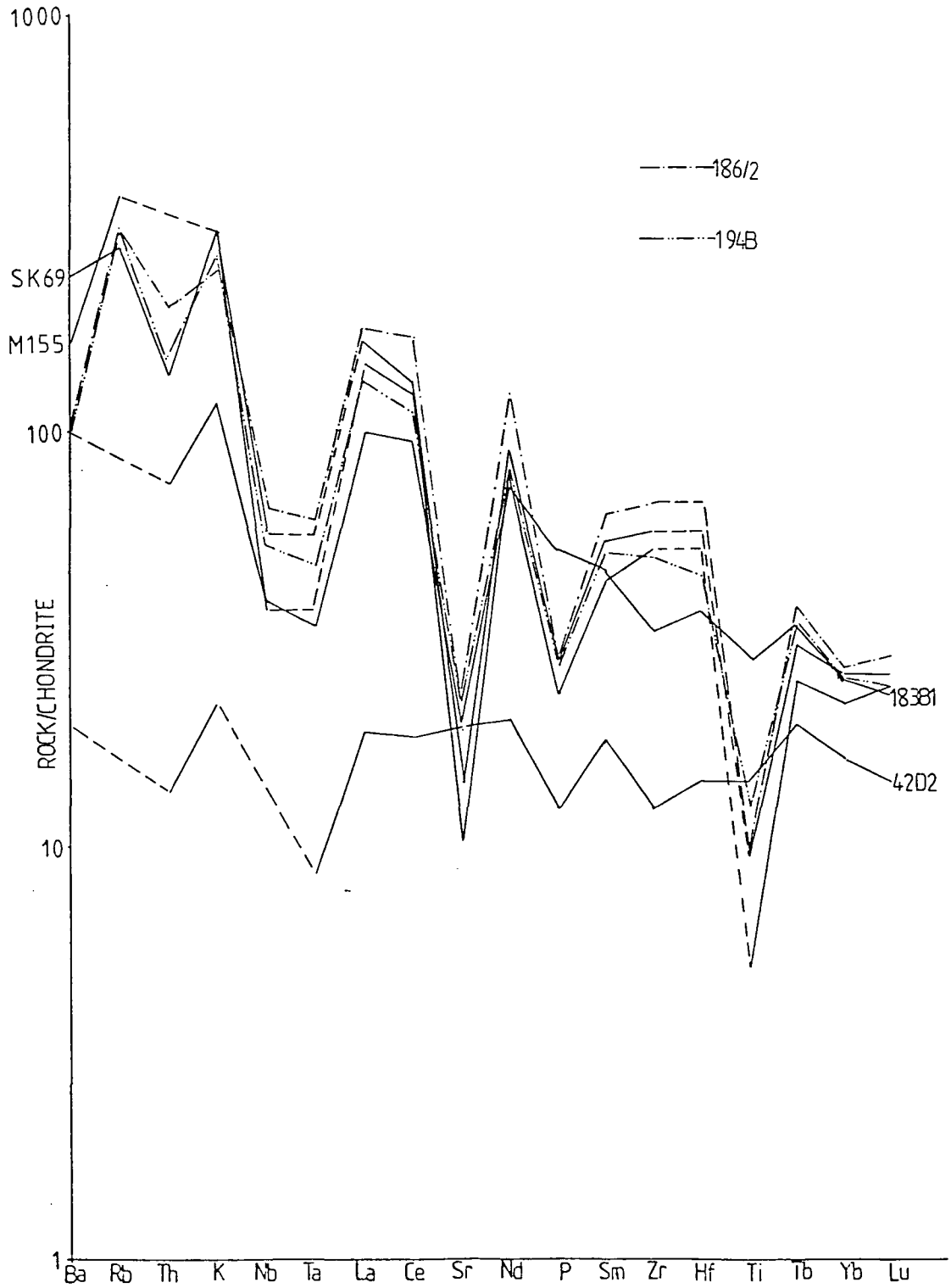

Fig.4.4B: Chondrite - normalised plot comparing features of the chemistry of two M2 felsites with that of Glamaig granite (Skye) sample SK69, a "primitive" BTVP granitoid.

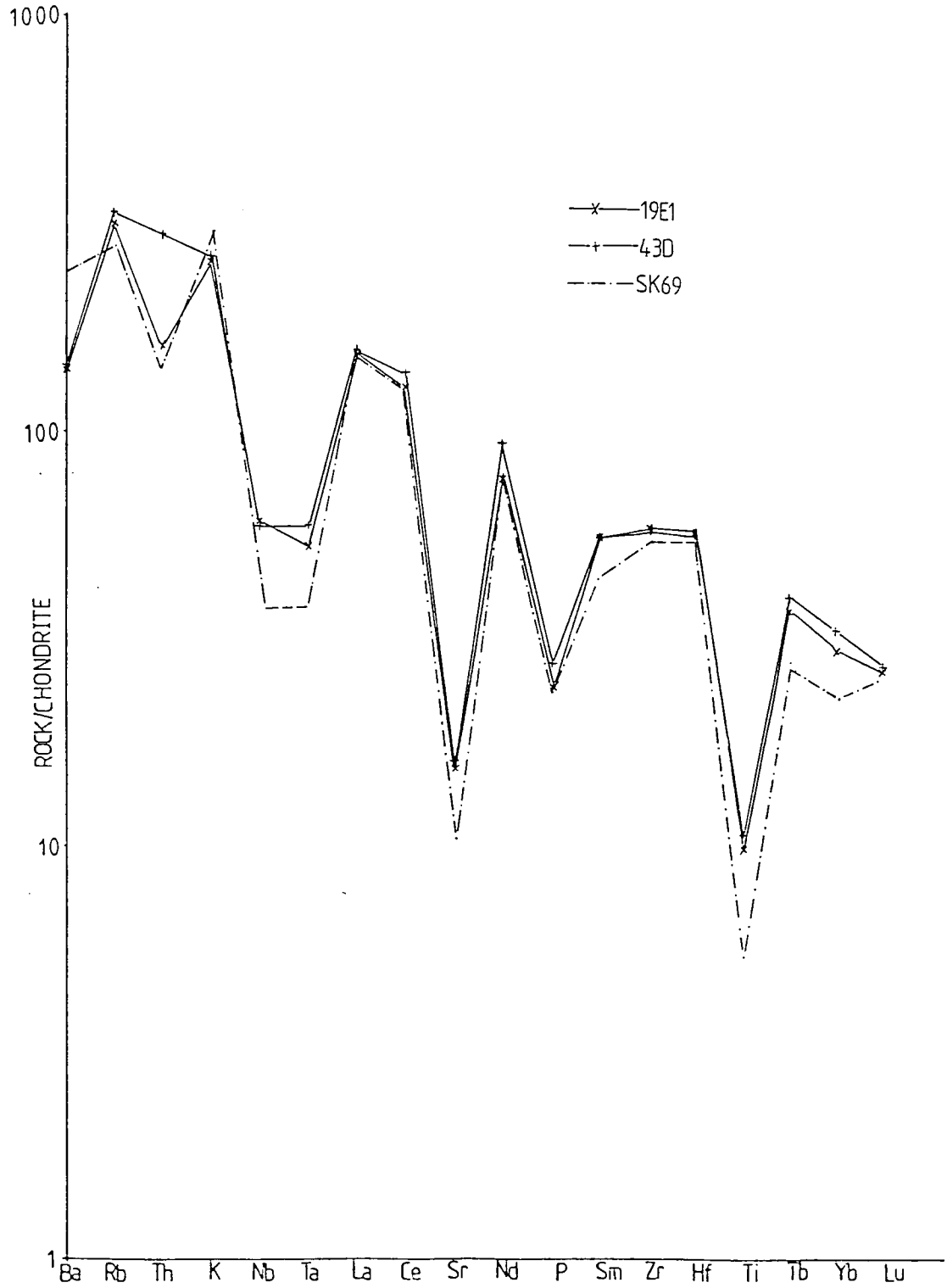

Fig. 4.5: La_N/Yb_N vs. La (ppm) plot showing that the MBG subalkaline granitoids cannot be be melts of any of the pre - Tertiary country rocks, nor mixtures of any of these rocks with basic to intermediate Tertiary magmas.

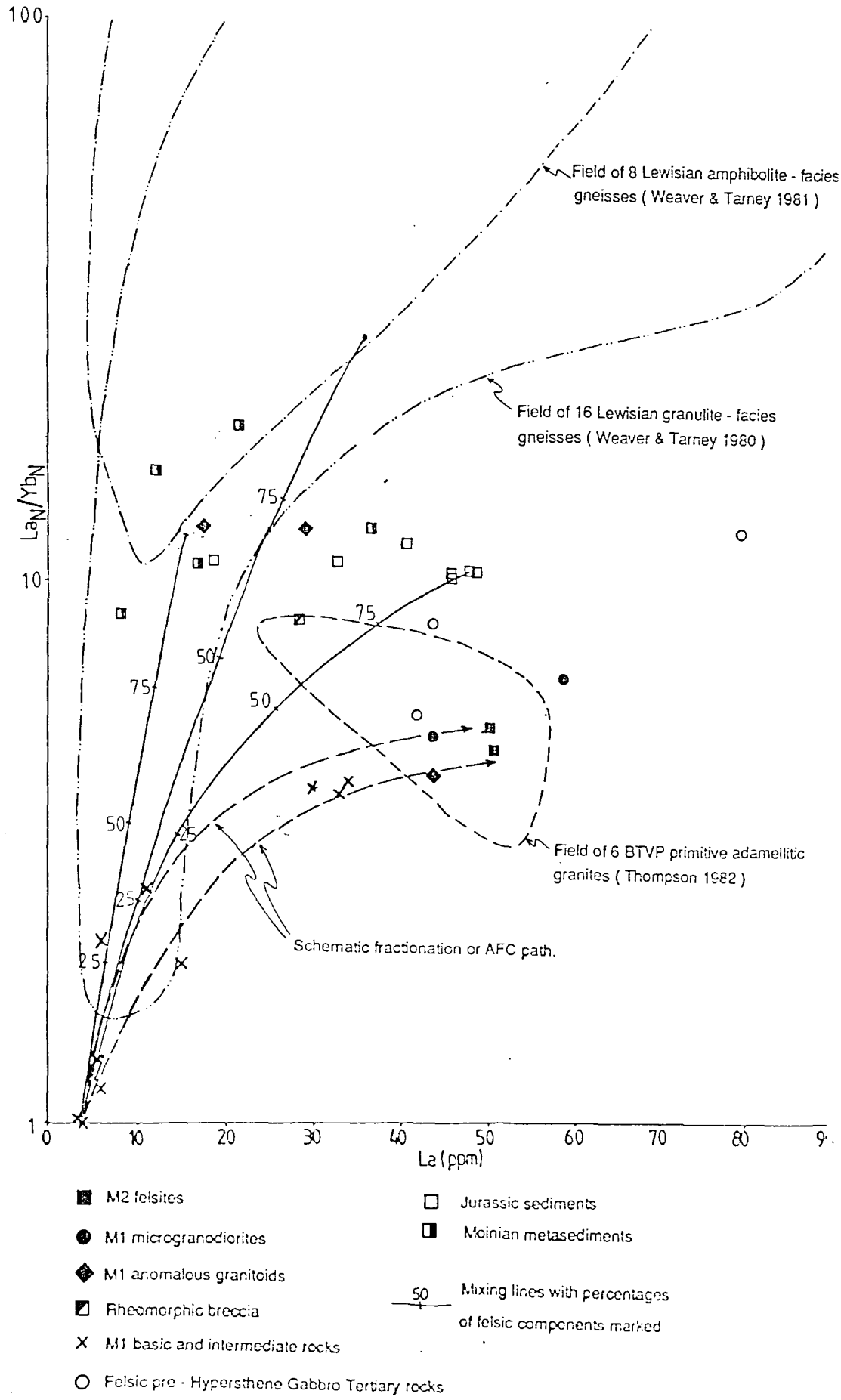

augite, Ti-magnetite and apatite in fairly constant proportions. Leaving aside the textural evidence which suggests a more complex history involving re - melting of porphyrocrysts (see section 4.2.2.2, below), these trends are consistent with fractionation of the porphyrocryst assemblage observed in the felsites (although apatite only occurs as small grains it is present as inclusions in some of the porphyrocrysts and appears to be an early - crystallising phase). However, a noticeable feature of these plots is the relatively large amount of scatter about the overall fractionation trends, particularly in plots of TiO_2, P_2O_5, Rb, Zr, Ba and K_2O against SiO_2. This could in part be due to the poor accuracy and precision of SiO_2 analyses by XRF (see Appendix 1; the predicted 2σ confidence limits, based on repeat analyses of separate splits of M2 felsite 19E6, are ± 1.7 wt%). However, the scatter is also apparent in plots not involving SiO_2, and estimated non - systematic errors in all other data presented in Figs. 4.3 and 4.6 are small compared to the scatter with the exception of XRF Ba data (2σ confidence limits $\pm$ 140ppm). ICP-AES data for Ba is much more precise and accurate ($2\sigma = \pm 8$ppm) and points analysed for Ba by ICP-AES are ringed as appropriate in the variation diagrams. The scatter apparent in Fig.4.6 can therefore be assumed to be a real feature of the rocks. It could be produced by a combination of varying degrees of fractional crystallisation with one or more of a variety of processes which are considered here in turn.

1). Hydrothermal Alteration. This would be expected to affect the alkali and alkali earth elements most (see, for example, Ferry (1985b)). In Fig.4.7, three of these elements, Rb, Ba and Sr, are plotted against Loss On Ignition, which is used here as a crude measure of the water content of the rocks and therefore of the intensity of alteration (note that the **absolute** range of $Fe_2O_3^T$ in the rocks plotted is less than 4 wt% and therefore can only produce a difference of 0.4wt% in the LOI). No variation in the abundances of these elements with LOI is apparent and it is therefore concluded that alteration did not have a significant effect upon the degree of variation in elemental abundances in these rocks.

2). Variations in the abundance and proportions of the observed porphyrocryst assemblage, caused by varying degrees of crystal - liquid separation or crystal accumulation, after formation of the magmas (i.e. after remelting, if the rocks represent remelts of pre - existing Tertiary granitoids, or after previous crystal fractionation if they are simple differentiates of basic magmas). The porphyrocrysts form from a few percent to as much as thirty percent of the rocks at outcrop and do not appear to vary greatly in the relative

Fig. 4.6: Geochemistry of the M1 microgranodiorites and M2 felsites.2. Trace element plots. Ringed samples are those analysed for Ba by ICP - AES. See text for discussion.

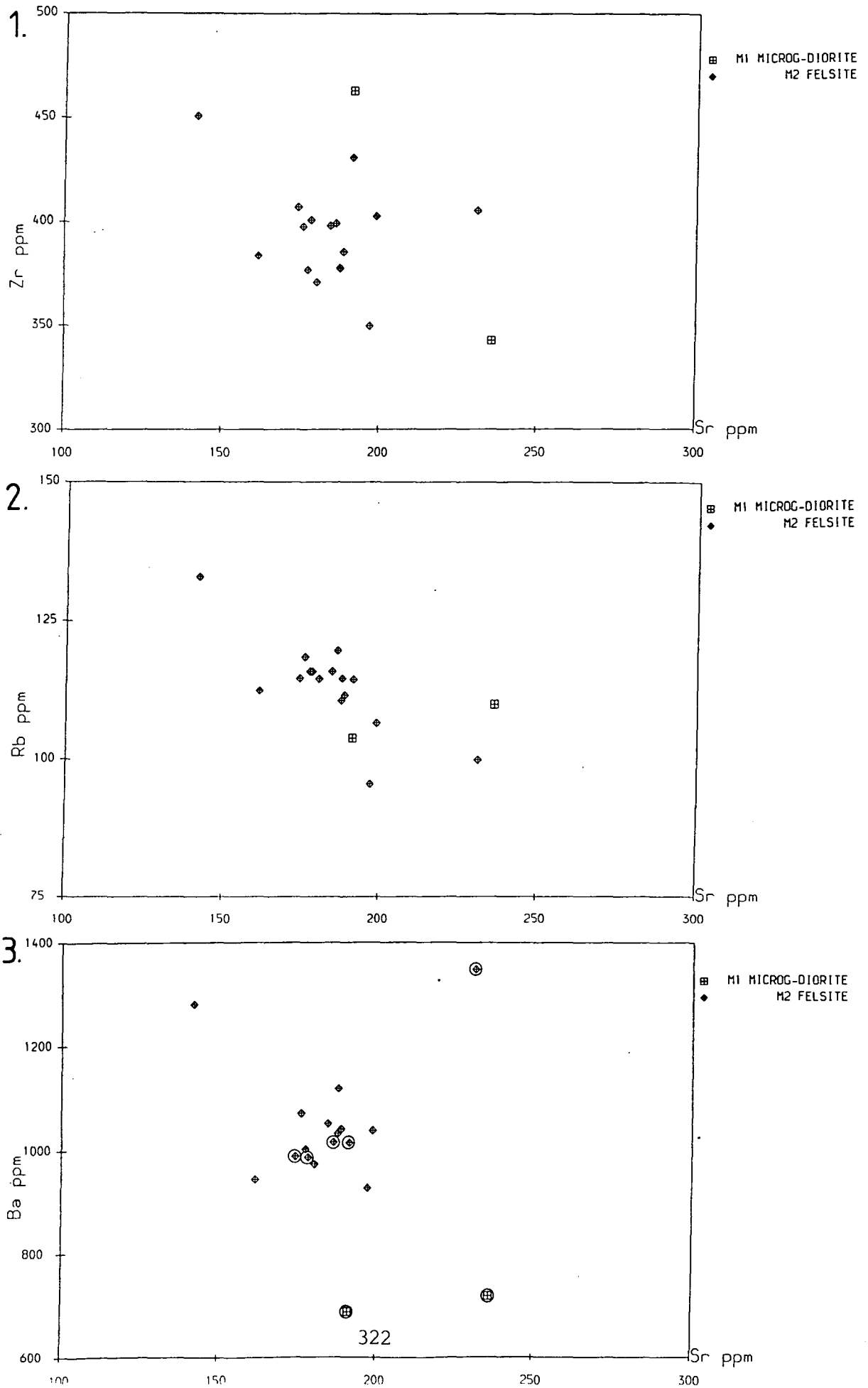

4.

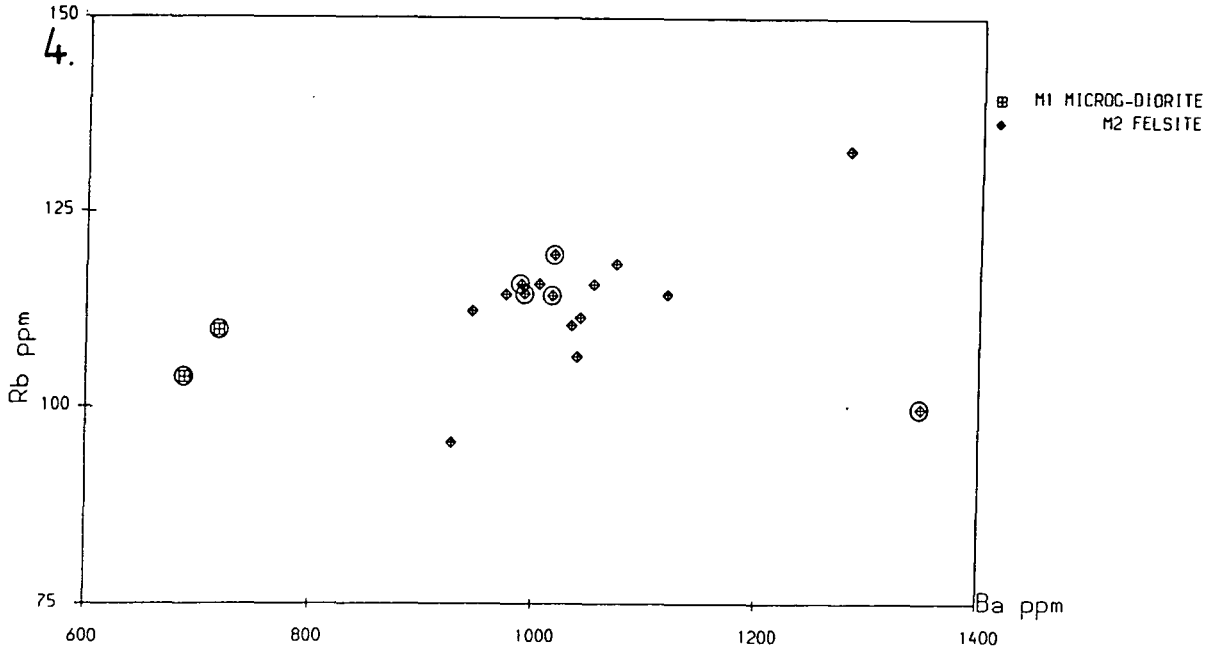
150
125
100
75
Rb ppm
600
800
1000
1200
1400
Ba ppm
M1 MICROG-DIORITE
M2 FELSITE

5.

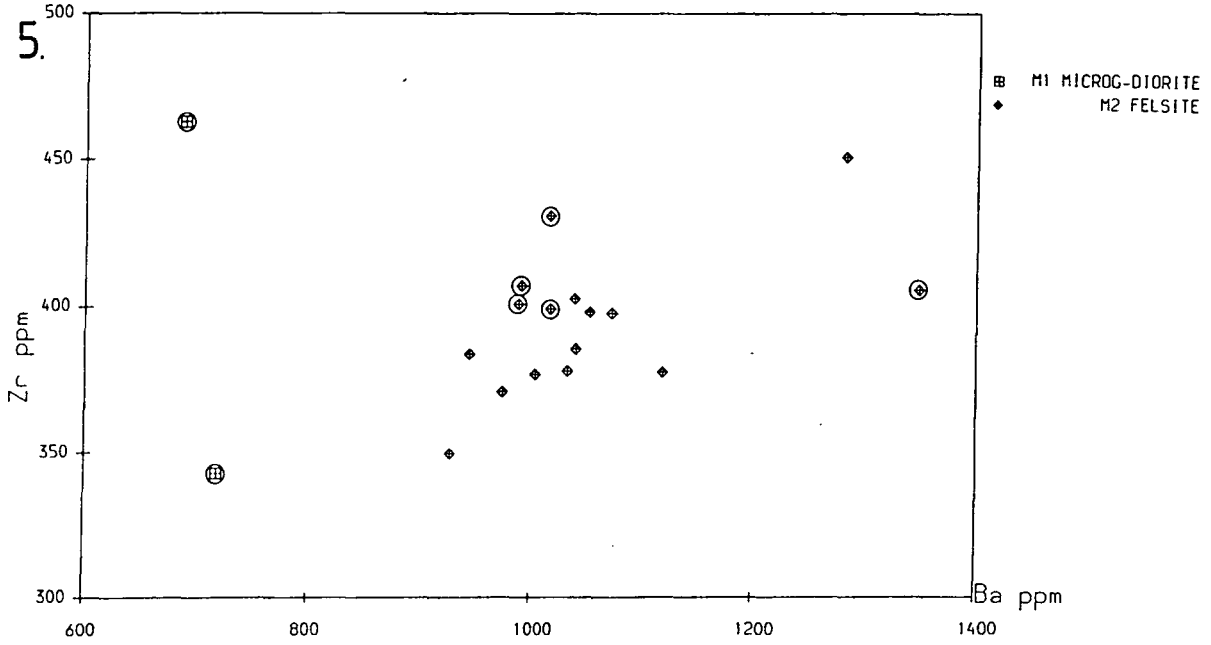
500
450
400
350
300
Zr ppm
600
800
1000
1200
1400
Ba ppm
M1 MICROG-DIORITE
M2 FELSITE

6.

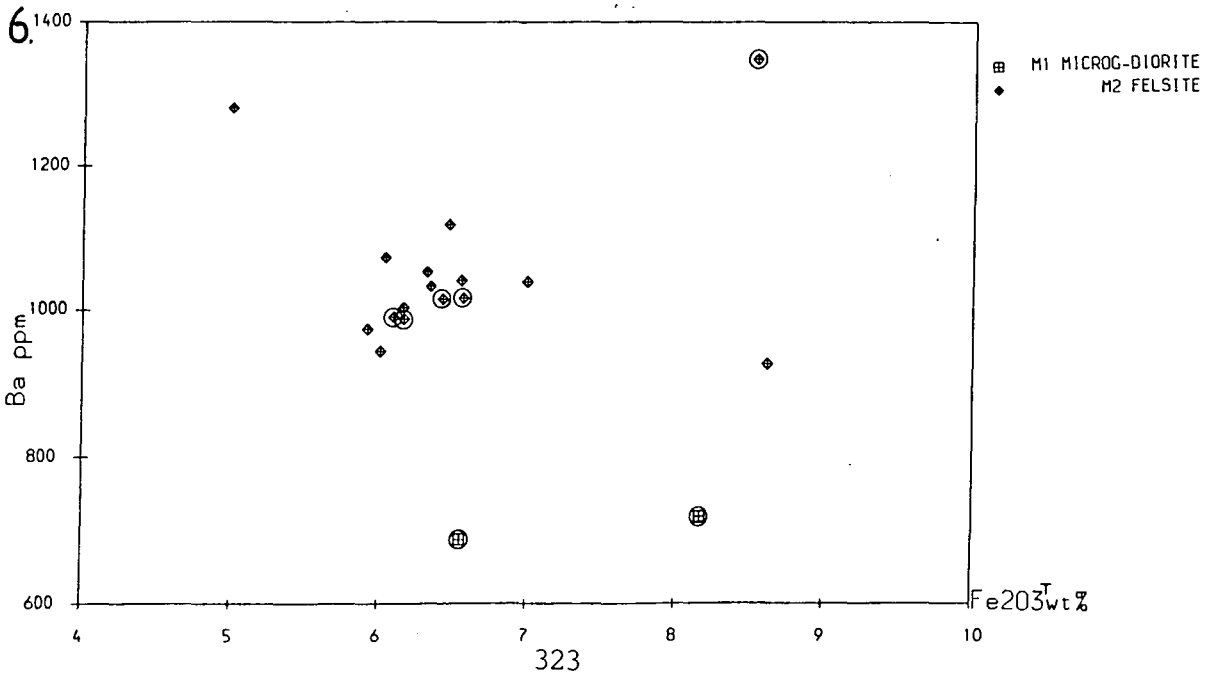
1400
1200
1000
800
600
Ba ppm
4
5
6
7
8
9
10
Fe203T wt%
M1 MICROG-DIORITE
M2 FELSITE

7

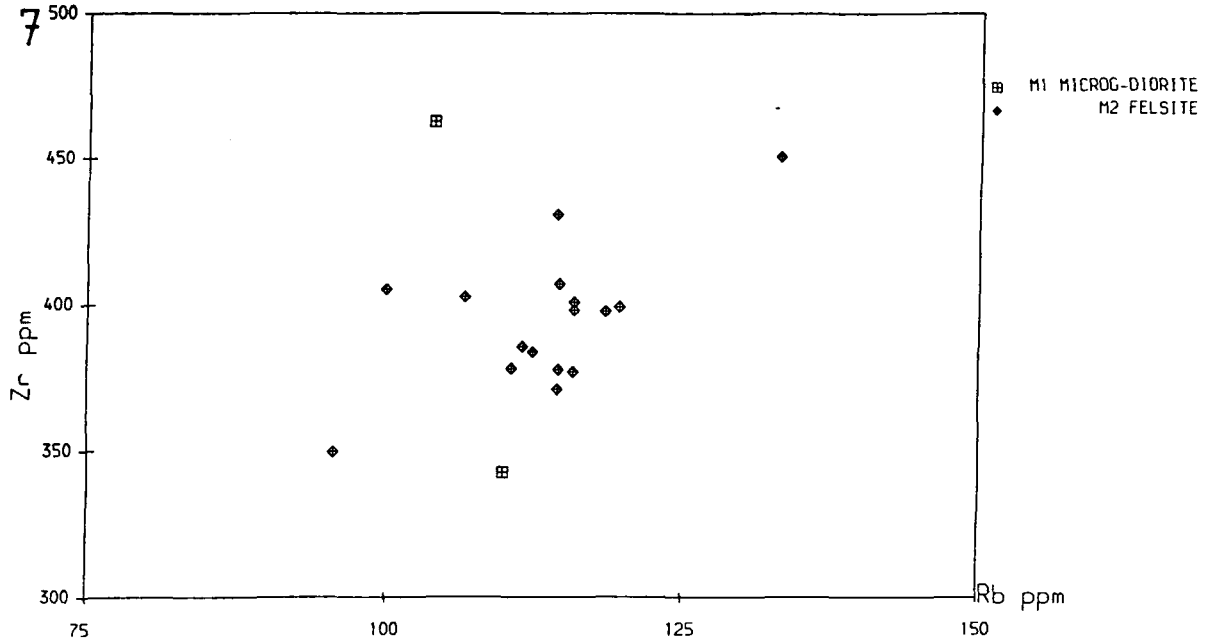
500
450
400
350
300
Zr ppm
75
100
125
150
Rb ppm
M1 MICROG-DIORITE
M2 FELSITE

8.

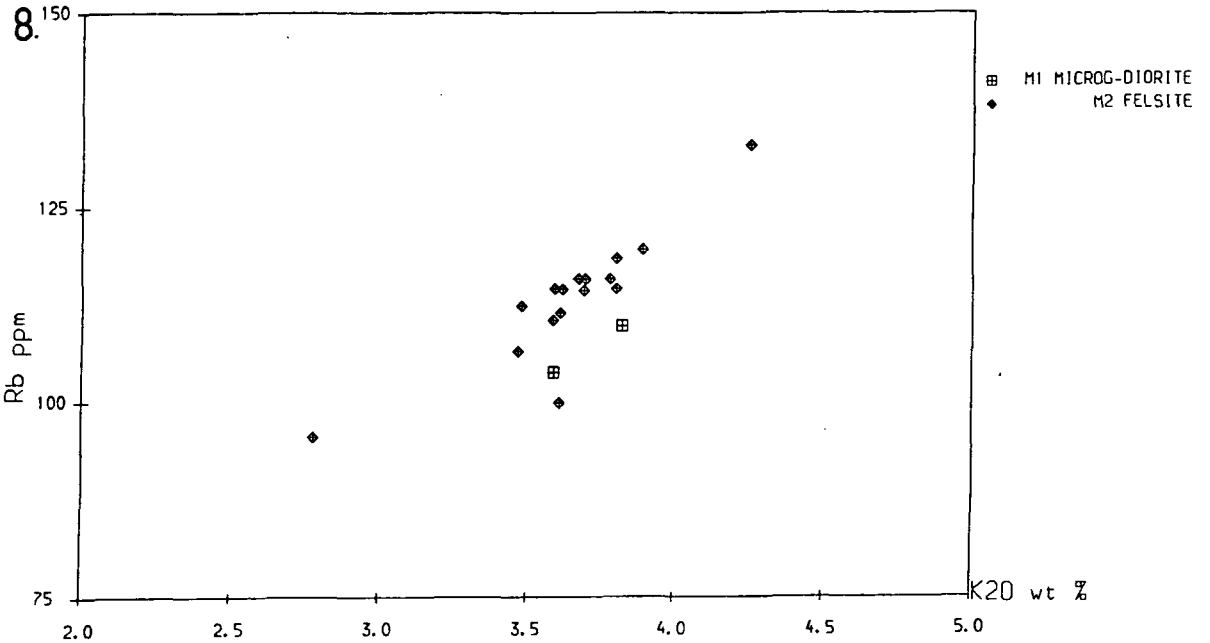
150
125
100
75
Rb ppm
2.0
2.5
3.0
3.5
4.0
4.5
5.0
K20 wt %
M1 MICROG-DIORITE
M2 FELSITE

9.

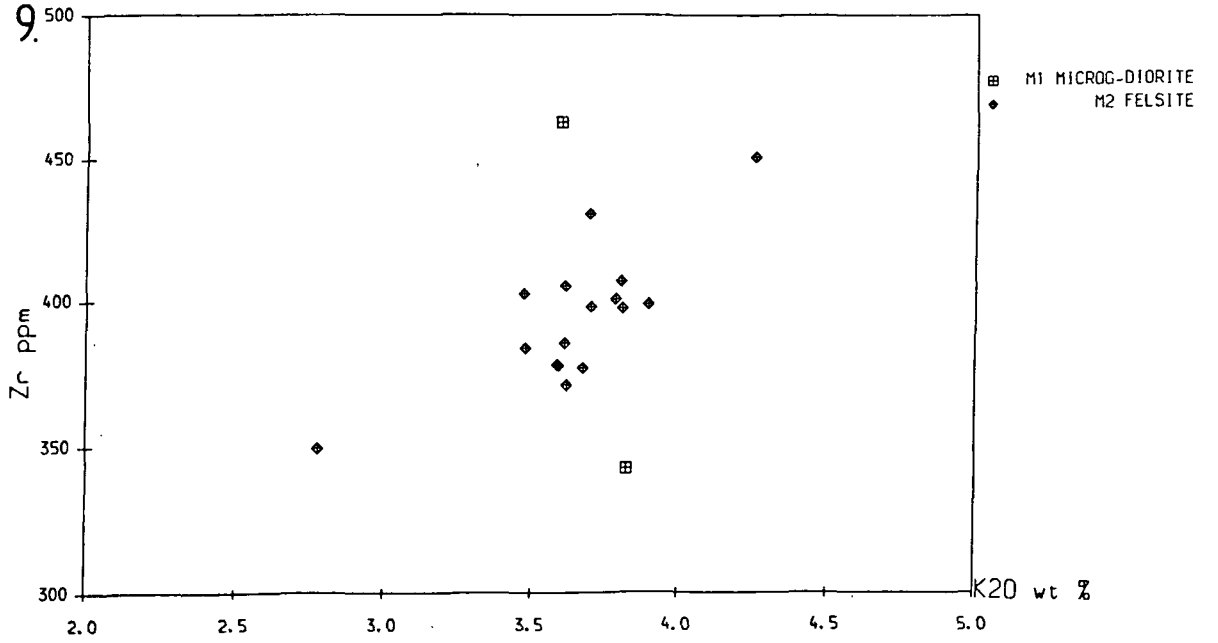
500
450
400
350
300
Zr ppm
2.0
2.5
3.0
3.5
4.0
4.5
5.0
K20 wt %
M1 MICROG-DIORITE
M2 FELSITE

Fig. 4.7: Plots showing lack of correlation between Loss - on - Ignition and the abundances of highly soluble elements, indicating that post - emplacement hydrothermal alteration has *not* greatly affected the bulk chemistry of the subalkaline granitoids.

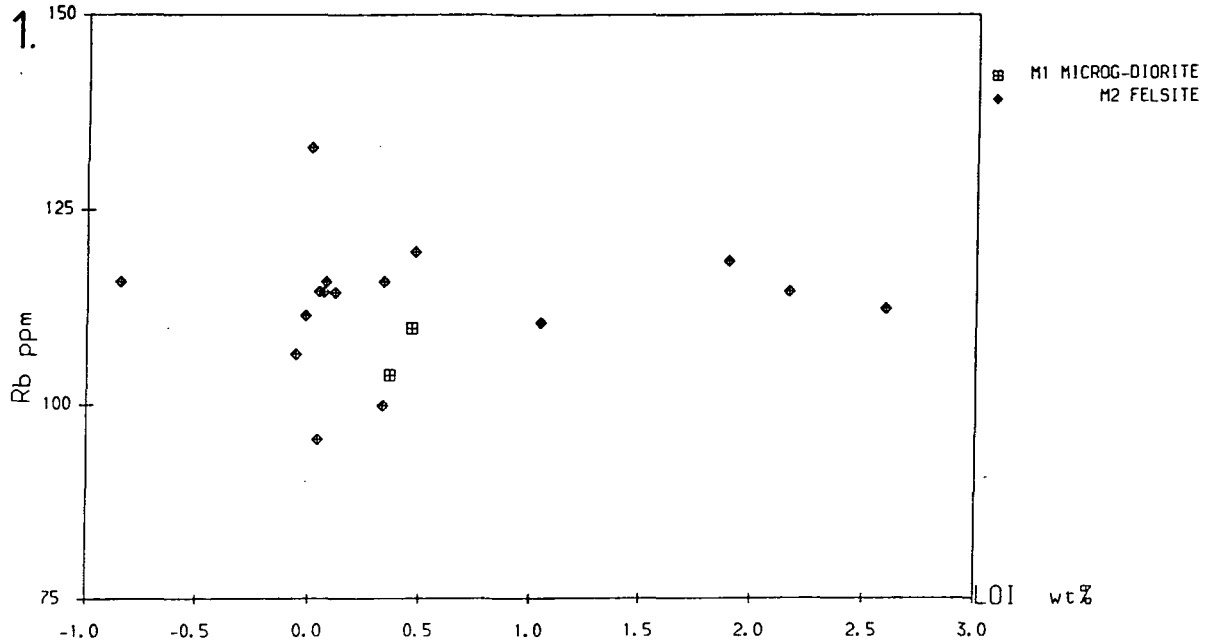

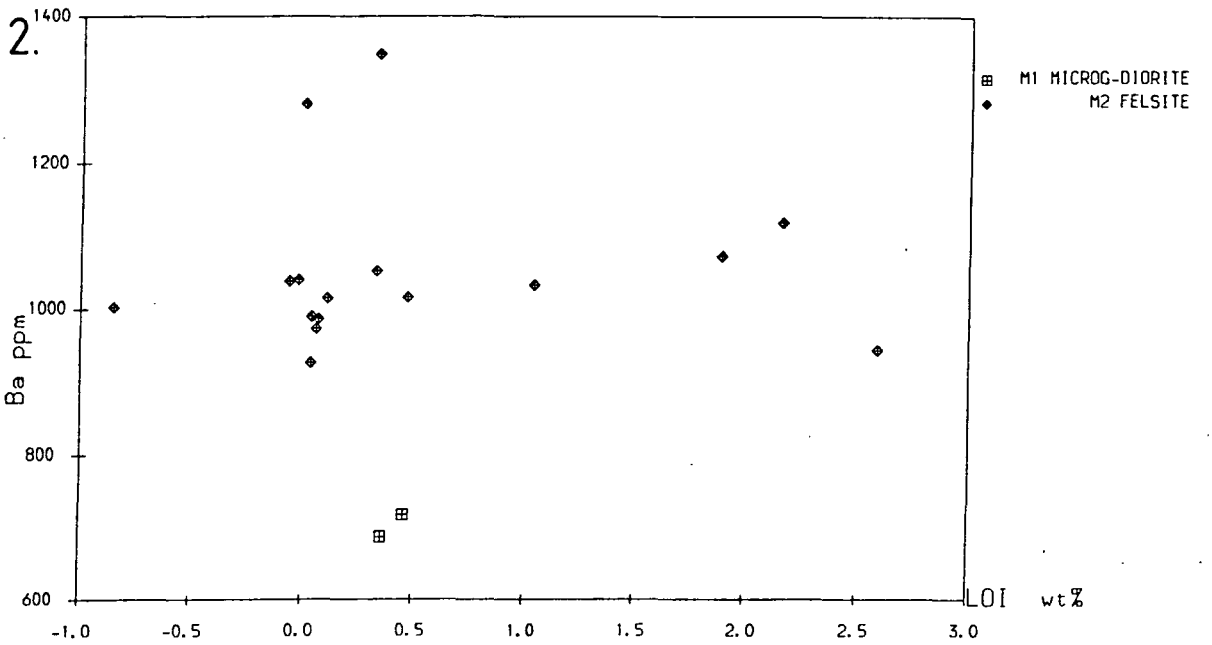

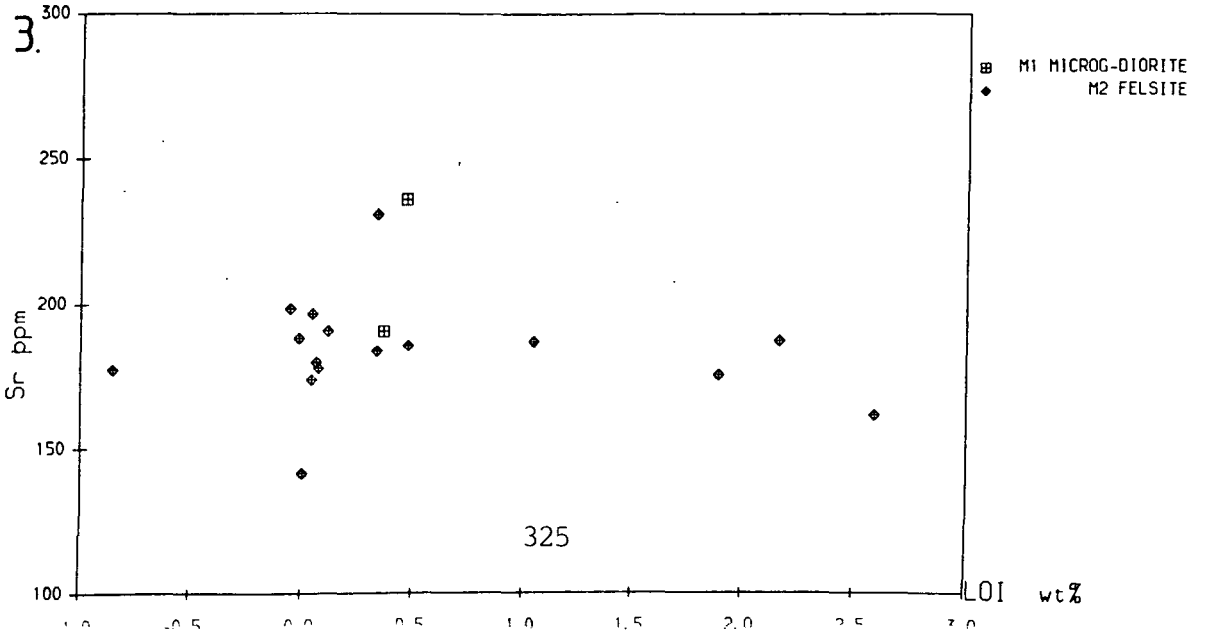

abundances of different minerals. Precise percentages of the different minerals, which would only be obtainable by point - counting of very large areas because of the low abundances of most of them, were not obtained during the course of this work. However, from visual inspection of the sections it is apparent that the dominant porphyrocryst phase throughout is unzoned to very weakly zoned (apart from quench rims) andesine plagioclase, and that the other porphyrocryst phases, augite and magnetite, form no more than 30% and 10% of the assemblage respectively, and usually rather less than this. Of the elements whose abundances show the greatest scatter in these rocks - Sr, Ba, K, Rb and Zr - only Sr is strongly compatible in andesine ($K_D \approx 10 - 20$; Drake & Weill (1975)). At the probable pre - quench temperatures of these magmas (c. 980 – 1060^oC; see section 4.2.5), Ba should be weakly incompatible, with a K_D between melt and feldspar of about 0.3 to 0.8 (Drake & Weill 1975); this is consistent with the weak negative correlation between Ba and Sr in Fig. 4.6.3. K and Rb should be largely incompatible, whilst Zr may subsititute to a limited extent into magnetite and augite under the conditions of formation of these magmas (Pearce & Norry (1979) suggest Zr distribution coefficents of 0.2 to 0.8 between intermediate to rhyolitic melts and these phases, giving an approximate bulk K_D of less than 0.2).

The variation in Zr abundances **cannot** be explained by zircon fractionation from, or accumulation in, the magmas which were quenched to produce these rocks. This is because, at the high pre - quench temperatures recorded by feldspar - melt equilibria in these rocks (see section 4.2.5), which are in the range 960 – 1120^oC, the magmas appear to have been undersaturated in zircon. The Zr concentrations at which they would have become saturated at their inferred temperature and measured composition, calculated by the method of E.B.Watson & Harrison (1983), are in the range 500 – 1670ppm. The higher values are more likely to be realistic because they are associated with the higher temperatures; the lower temperatures were calculated as a lower limit using an unrealistically high value of P_{H_2O} (see section 4.2.5). Thus the magmas which these rocks represent would either have been zircon - undersaturated (as is consistent with the observed lack of zircon microphenocrysts) or possibly just zircon - saturated, in which case zircon would only be a minor component of the zirconium budget in these rocks. The weakly incompatible nature of Zr in these rocks is confirmed by the negative correlation between Zr and Sr evident in Fig. 4.6.1.

It follows from these considerations that segregation or accumulation of the observed porphyrocryst assemblage would produce considerable variation in Sr abundances but not in ratios of the other elements under consideration. This is not what is observed (see plots of Ba vs. Zr and Rb vs. Zr in particular). The implication of these plots is that segregation or accumulation of the observed porphyrocryst assemblage cannot be the cause of the observed variation.

3). Mixing within the Contact Zone, between felsic and basic or intermediate magmas such as are also present in the Contact Zone (see section 4.3). Although fragments of **chilled** basic rocks are quite common in the M1 microgranodiorites and also occur occasionally in the M2 felsites (notably in sample 248, from the coarser M2 intrusions in the Glebe Hill area) these were easily separated out by hand - picking during sample preparation, whilst finer - scale heterogeneity was not observed in the groundmass of these rocks in thin section. Heterogenous mixing can therefore be excluded as a cause of the variation in these rocks.

The presence of chilled basic fragments in these felsic rocks implies a strong temperature contrast between the felsic and basic magmas in the contact zone, as discussed in section 3.2.7 (see also sections 4.2.5, 4.3.3 and 4.4 below). This would tend to inhibit complete or homogenous mixing between these two end - members. Furthermore, if basic magmas of the compositions present in the contact zone were involved in mixing, this would result in flat trends or trends with slight positive slopes in the plots of TiO_2 and P_2O_5 against SiO_2 (Figs. 4.3.5 and 4.3.6), rather than the observed negative correlations, or else produce a wide scatter, if fractional crystallisation of the felsic magmas was involved as well. Mixing (followed by complete homogenisation) between felsic magmas and Ti and P rich intermediate magmas is however less easily excluded by consideration of these two plots and is also physically more likely (see section 4.4). However, the heterogenous state of all rocks in the Contact Zone which can be shown on geochemical grounds to be hybrids of felsic and intermediate magmas indicates that in fact homogenous mixing did not occur. Mineralogical evidence relevant to the possibility of acid - basic/intermediate magma mixing is dealt with in the following section, although because most of the M1 basic and intermediate magmas are aphyric or nearly so, the absence of distinct populations of porphyrocrysts in the felsic rocks is not

secure evidence against an origin by magma - mixing.

4.) Thermochemical or thermogravitational diffusion (the Soret effect) has received much attention as a possible fractionation mechanism, particularly in silicic magma chambers (Hildreth 1981). However, the preservation of sharp boundaries betwen different rock types in the Contact Zone, and the lack of evidence for gradational, diffusion controlled, compositional gradients, implies that this process did not have a significant effect upon the MBG. This is as predicted by the theoretical calculations of Spera et al. (1982) and of Carrigan & Cygan (1986), which suggest that the timescale on which the process is likely to be significant is of the order of 10^6 years, far greater than the entire lifetime of the M1 magma chamber (see Chapter 5).

5). Varying amounts of contamination with rocks from the wall of the magma chamber after fractionation or remelting. This is difficult to exclude by geochemical arguments as the subalkaline granitoids are indeed crustally contaminated (Fig. 4.5). However, as is shown in section 4.3.2 below, in the context of crustal contamination of the basic rocks, much of this contamination (all of it in some of the felsic rocks) appears to have taken place as picritic to picrobasaltic parental magmas passed through the Lewisian crust beneath the Ardnamurchan central complex. There is no evidence at outcrop or in thin section for heterogenous mixing of magmas and diffuse refractory country rock inclusions are rare. Similar inclusions occur in large numbers in the anomalous granitoids and the one identified example of a subalkaline granitoid – anomalous microgranitoid hybrid rock (sample 183D1, see section 4.2.4). A small number of exotic xenoliths with sub - rounded margins and a larger number of angular fragments which correspond to the adjacent wall rock lithologies do occur. Only the former show any sign of reaction with the host subalkaline magmas (for example, in the case of a partially fused tridymite – wollastonite – diopside bearing quartzite xenolith in an M2 felsite at 44637032, which has a diffuse halo of apparently more quartz - rich felsite around it). These xenoliths are extremely useful in providing P – T constraints for the host magmas but occur far too infrequently for the assimilation of less refractory lithologies to explain the observed compositional variation.

6). Compositional variation reflecting remelting of heterogenous source rocks.

Plate 4.1. Granular, coarse - grained microdioritic polycrystalline inclusion or microxenolith in M2 felsite (sample 42F2). Note partial textural re - equilibration of inclusion, which shows several three - grain junctions with high interfacial angles and an overall granular texture. Euhedral grain surfaces against the host felsite suggest that near - equilibrium melting or overgrowth during the early stages of cooling has occurred (Donaldson 1985b). PPL, FOV 3.5mm.

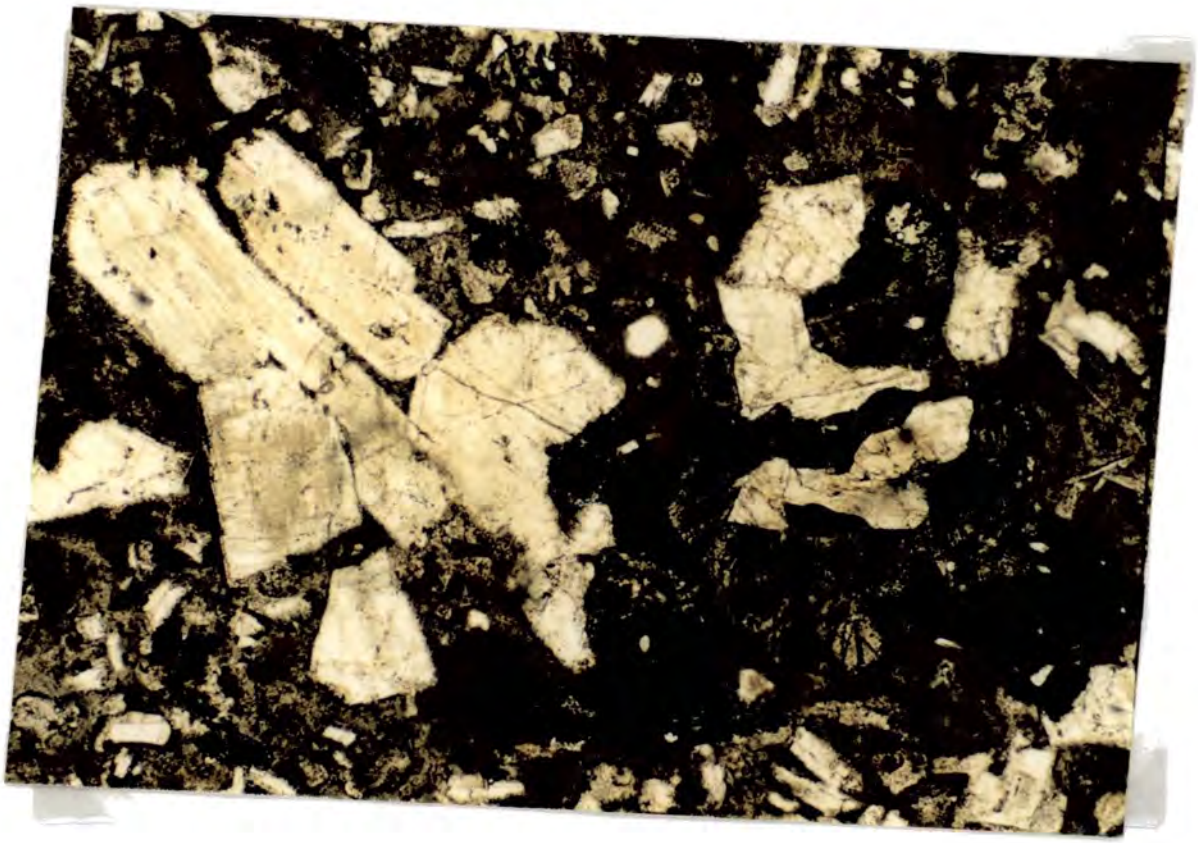

The presence of corroded microxenoliths and previously - deformed porphyrocrysts in the M2 felsites (and probably in the M1 microgranodiorites as well, although recrystallisation during and after quenching has made these latter difficult to interpret) suggests that part at least of these rocks were produced by remelting of pre - existing subalkaline Tertiary granitoids (see sections 3.2.3 and 3.2.6). A number of processes are likely to have operated during the formation of the latter which could explain the compositional scatter apparent in Fig. 4.6. The microxenoliths and glomerocrysts in particular frequently have equant, rather granular and moderately coarse - grained textures (Plate 4.1). These suggest a relatively low rate of cooling of these rocks, accompanied by supra- and sub-solidus recrystallisation and migration of interstitial melts with highly fractionated compositions. At the low temperatures at which such melt migration could occur (less than $950^{o}C$) Ba and Zr in particular cease to be incompatible elements.

The results of this are shown schematically in Fig. 4.9, for four pairs of elements:

(A) a strongly compatible element (e.g. Sr) and an incompatible element (e.g. Rb – see Fig. 4.6.2)

(B) an incompatible element and one which becomes compatible at lower temperatures, part - way through the crystallisation process (e.g. Ba or Zr – see 4.6.4 and 4.6.7)

(C) two elements which become compatible at different stages along the crystallisation path, such as Ba and Zr (4.6.6)

(D) two elements which remain incompatible throughout, producing a good positive correlation and only a little scatter caused by one of the elements becoming compatible in the last stages of crystallisation (e.g. K and Rb, Fig. 4.6.8).

No attempt is made here to model these pre - remelting processes numerically, for four reasons. Firstly, there are no definite liquid compositions amongst these rocks, since the remelting process, if it has occurred, will have obliterated much of the textural evidence for the former state of the rocks. Such evidence as does exist indicates that all the parental

Fig. 4.8: Schematic diagrams showing the effects of initial fractionation combined with various amounts of later interstitial melt movement and other late - stage crystallisation processes upon the bulk composition of granitoids.

4.8A

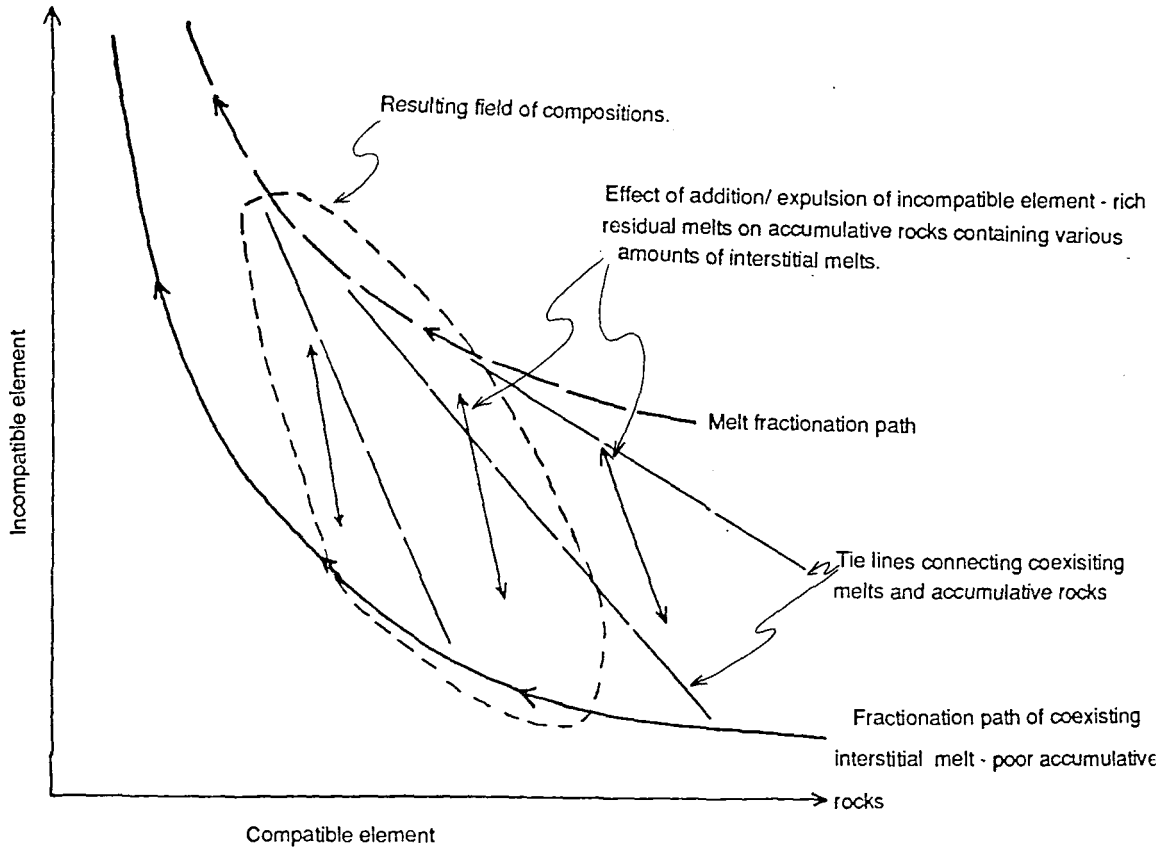

4.8B

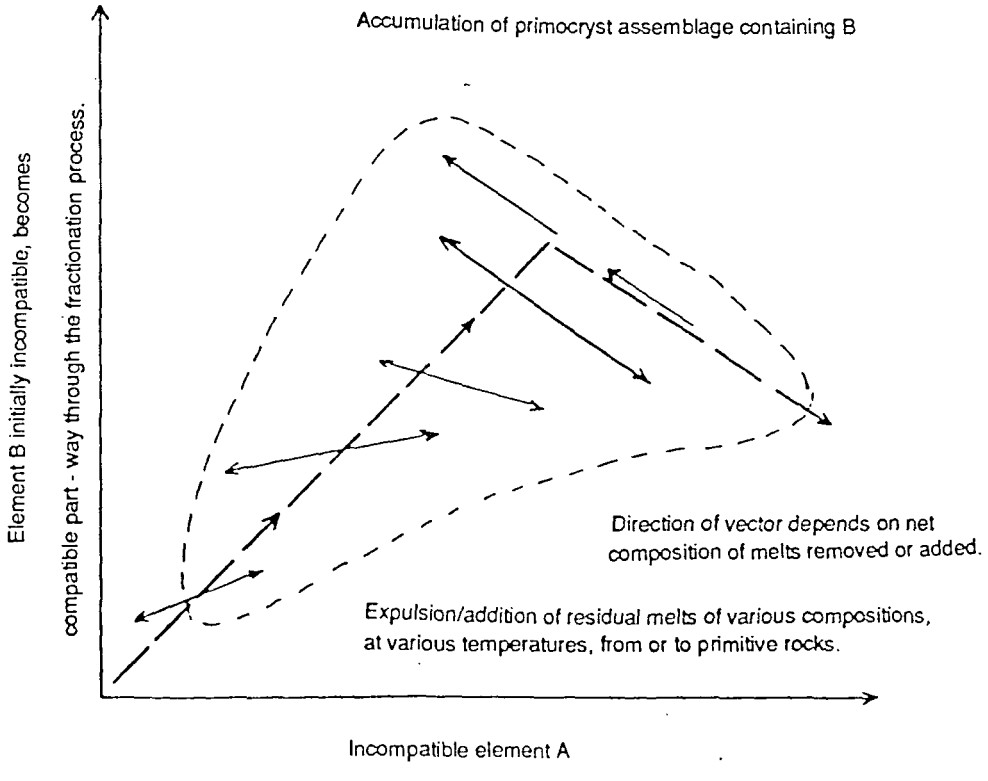

4.8C Two partially incompatible elements, which substitute into different phases which appear on the liquidus at different points along the fractionation path.

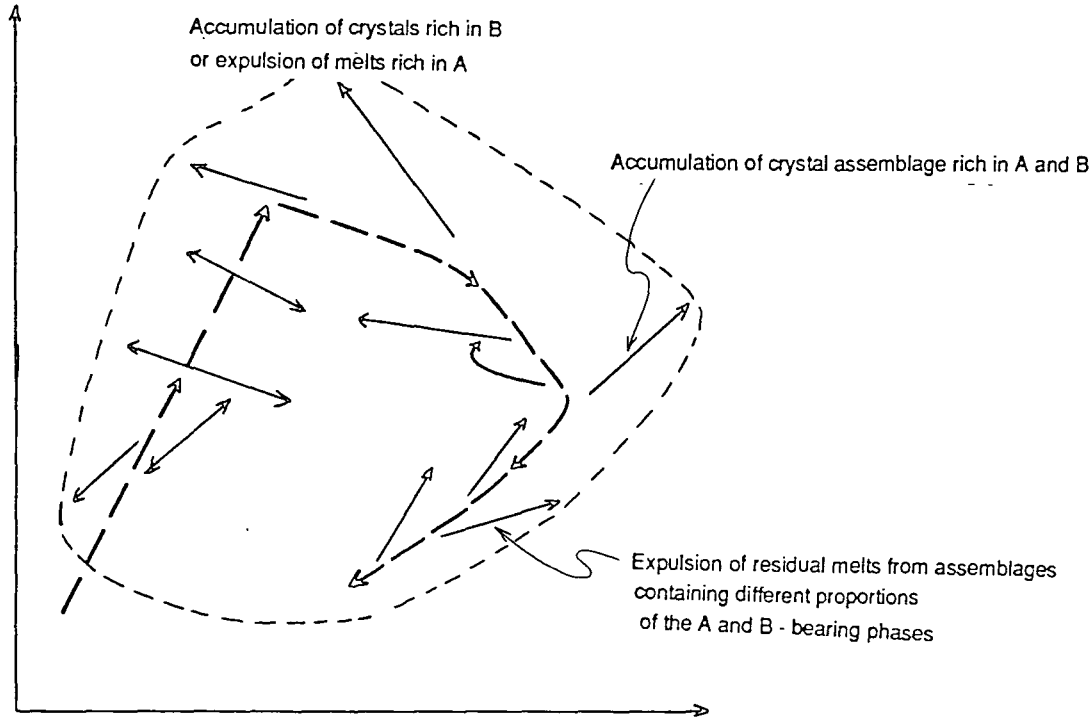

4.8D Two incompatible elements, one of which becomes slightly compatible in extremely fractionated magmas.

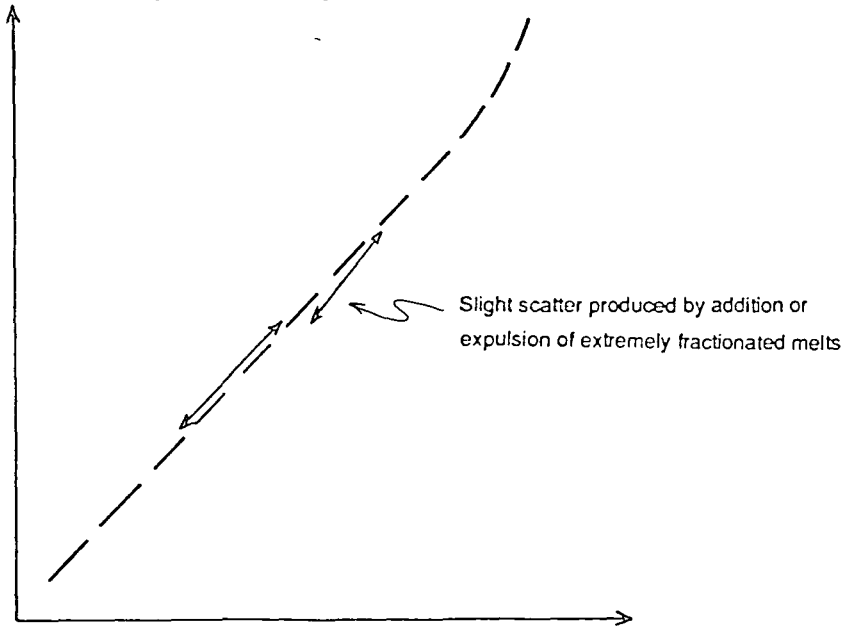

rocks were relatively coarse - grained and plutonic, and therefore unlikely to precisely match the compositions of the original magmas from which they formed, particularly in respect of the partly to completely incompatible trace elements which are the main subject of interest. Secondly, if these rocks, in their present state, were produced by remelting of pre - existing Tertiary rocks, there is no reason to suppose that they should form a cogenetic suite of rocks with a common basic parental magma and a common evolutionary path, involving both assimilation and fractional crystallisation. The effects of the mechanisms described here are therefore likely to be superimposed on those of varying fractionation paths. Thirdly, the rocks may have been affected by hydrothermal alteration between their first crystallisation and the subsequent reheating and remelting. Dehydration during reheating (see Chapter 5) would destroy any original correlation between elements affected by alteration and LOI. Finally, detailed calculations to evaluate the effects of interstitial melt migration in the parental subalkaline granitoids would require data on the abundances of late - crystallising phases and the concentrations of elements of interest in them which, in this model, has also been obliterated by the remelting. However, England (1988a) has modelled the effects of late - stage crystallisation and interstitial melt migration on abundances of Ba, Rb and Sr in the Tertiary North Arran Granite, which is composed of a single cogenetic suite of rocks, and has found that these processes can produce changes of the type and magnitude apparent in Fig.4.6.

If the microgranites and felsites are the products of remelting of earlier rocks, an additional factor in the variation in the elements shown in Fig. 4.6 could be mixing between melts derived from different intrusions, or from compositionally distinct parts of zoned bodies as they were mobilised and ascended the walls of the MBG magma chamber.

7). Varying fractionation paths, with differing ratios of fractionation to crustal contamination and different contaminant compositions. Since there are a wide variety of potential crustal contaminants in the area, with widely varying incompatible - element ratios (see Chapter 2), this process could produce much variablity in trace elements, whilst abundances of major components would be constrained to follow the same trends by phase equilibria constraints (Bowen 1928). This could account for the strong contrast between the major - element plots (Fig. 4.3.1 – 6) and the minor and trace - element plots. Further evidence for

the involvement of this process is apparent in Fig. 4.5, where those M1 and M2 subalkaline granitoid rocks analysed for REEs do not lie on a single fractionation trend. The negative correlation between La_N/Yb_N and La for the relatively primitive BTVP granitoids from outside Ardnamurchan which are plotted in this diagram can be explained in terms of varying amounts of contamination with a high SiO_2, high - alkalis but low - REE contaminant such as the normal, REE - poor Lewisian gneisses. The effect of a greater amount of contamination with such material would be to increase the La/Yb ratio of the magma whilst at the same time decreasing the amount of crystal fractionation needed to produce a residuum of granitic composition (and hence the degree of enrichment in incompatible elements) and possibly also decreasing the solubility of P_2O_5 in the melt, which would cause apatite to appear on the liquidus at higher temperatures and thus inhibit further enrichment in light REEs (c.f. Fig. 4.4, where there is very little increase in REE abundances between the intermediate - composition 183B1 and the felsic rocks). This suggests that the variation in the REE contents of the few M1 and M2 felsic rocks for which data are available could in part reflect different degrees of contamination and/or different contaminants in the parental basic magmas.

Of the seven possibilities discussed above, that of generation of the microgranodiorite and felsite magmas by remelting of a heterogenous suite of pre - existing Tertiary subalkaline granitoid rocks (process **(6)**) appears to be most able to produced the observed variation in trace element (and particularly incompatible trace element) ratios, particularly since various other processes (mixing between different felsic magmas after remelting and hydrothermal alteration prior to remelting) would also then be permitted by the data. With this in mind, a search was made amongst the exposed pre - Hypersthene Gabbro felsic rocks in Ardnamurchan for suitable compositions. As noted in Chapter 2, these rocks fall into two groups:

(1) Felsites associated with plateau basalt suite intrusions. These are more alkaline than the M1 and M2 rocks, their higher Zr contents being particularly distinctive. As noted above and discussed in section 4.2.5, below, the felsites at least were too hot at the time of emplacement and quenching to be Zr - saturated, making it unlikely that their source would contain residual zircon and thus reduce the Zr content of the magmas. Furthermore, fractionation of these rocks to produce the syn - MBG subalkaline magmas at temperatures at which zircon was stable would also have involved andesine plagioclase and therefore have strongly reduced the Sr content of the magmas: this effect

is not observed (see analyses in Appendix 2 and plot of Sr against SiO_2 in Fig. 4.11, below).

(2) Centre 1 granitic rocks. These are closer to the syn - Hypersthene Gabbro subalkaline felsic rocks in their overall composition, but the one sample analysed for REEs, 300/1, has markedly higher La_N/Yb_N, whilst having a similar La content to the M1 and M2 rocks (Fig. 4.5), suggesting that it has a significantly greater crustal component.

It therefore seems likely that the M1 and M2 subalkaline granitoid rocks were produced by remelting of a suite of relatively weakly contaminated (low La/Yb) Tertiary granitoids which are not exposed at the surface. The wide variation in the grain size of the microxenoliths (less than 0.2mm to more than 1mm), the wide variation in bulk compositions found at adjacent outcrops, and the restriction of large subalkaline granitoid bodies to the northern and south - eastern margins of the pluton suggests that the parental felsic intrusions were relatively small (no more than a kilometre or so across). If so, it is unlikely that they would produce a noticeable negative gravity or magnetic anomaly, since this would be superimposed on the flanks of the positive anomalies associated with the mafic plutons of Centre 2 (Barrett 1987; Harrison 1987) and would tend to be modelled as a slight change in the orientation of the outer contacts of the latter.

4.2.2.2 Mineralogy and textures of the porphyrocrysts in the M2 felsites.

This section will concentrate upon the porphyrocrysts and polycrystalline inclusions which occur in the finer - grained, devitrified glassy members of the M2 felsite suite. The porphyrocrysts and inclusions in the more coarsely crystalline, mainly micro - granophyric rocks of the M2 suite and the rare porphyrocrysts in the M1 microgranodiorites appear to differ from those in the very fine - grained and glassy rocks only in that they show more post - quench recrystallisation and hydrous alteration. For this reason they were studied less intensively.

As noted previously, the main components of the porphyrocryst and polycrystalline inclusion assemblage are andesine plagioclase, augite and opaques, in decreasing order of abundance; apatite is also present as inclusions in the feldspars.

Feldspar porphyrocrysts.

Four texturally distinct groups of feldspar porphyrocrysts occur in these rocks, in addition to the elongate quench feldspar crystals that occur in many, but by no means all of them.

1). This group includes those in the polycrystalline inclusions, which vary from compact, rather granular - textured bodies to clusters of corroded grains with intergranular quenched melt pockets, and a large proportion of the single - crystal grains. These crystals are typically 0.5 to 2mm long, but some of those in the polycrystalline inclusions are as small as 0.2mm long. They contain, at most, only a few rounded pockets filled with very fine grained granular aggregates of feldspar, pyroxene and opaques and rimmed by more sodic feldspar. These appear to represent devitrified melt inclusions. These grains and solid polycrystalline inclusions contain the best evidence for deformation prior to (or possibly during) incorporation of the porphyrocrysts into the magma which the host rocks represent, in the form of intragranular straining, subgrain formation and localised shearing and granulation (see Plates 3.27A and B). The presence of this textural evidence for pre - M1 initial crystallisation of these feldspars implies that the devitrified melt inclusions cannot have formed by trapping of melt during rapid crystal growth as the rock was quenched on intrusion at its present position. Possible mechanisms of formation of the melt pockets include infiltration of melt from the host or remelting of hydrous mineral grains formed within the feldspars during pre - M1 alteration of the parent rocks. When in contact with the devitrified groundmass, these feldspars have rounded, rarely slightly embayed margins which in some cases truncate the slight but complex internal zonation which is present in certain grains, suggesting either that the grains were brecciated during incorporation into the magma, or that extensive dissolution has taken place subsequently. Contacts against augites and opaques in the polycrystalline inclusions are typically straight and hypidiomorphic or granular, implying varying degrees of recrystallisation during slow cooling prior to incorporation in the felsites. In general these textures vary with grain size, with the coarser inclusions being more granular and containing more equant feldspars, although the most extreme granular textures are found in fine - grained deformed inclusions (Plate 3.27).

2). Sieve - textured feldspars, containing numerous rounded pockets of granular or devitrified material, are the next most common type of feldspar in most sections. Channels connecting the melt pockets to each other and to the surrounding groundmass (Plate 4.2) are rare but

Plate 4.2. Sieve - textured residual plagioclase porphyrocryst with irregular melt pockets and channels in the interior of the crystal. The exterior of the crystal is also corroded and irregular. Sample 42F2. XPL, FOV 1.5mm.

Plate 4.3. Residual plagioclase glomerocryst in M2 felsite (sample 42F2) showing a gradational transition from positive sieve texture (top left of field of view) to negative sieve texture (centre of field of view). XPL, FOV 3.5mm.

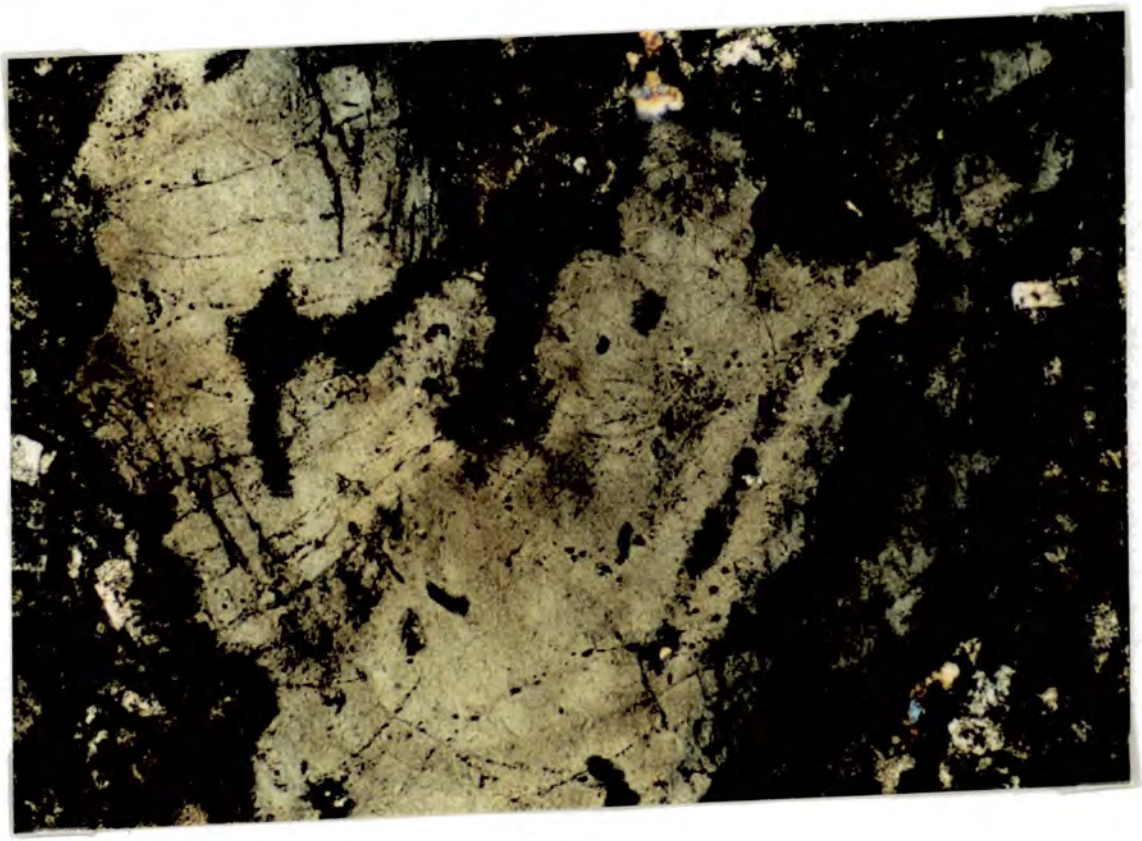

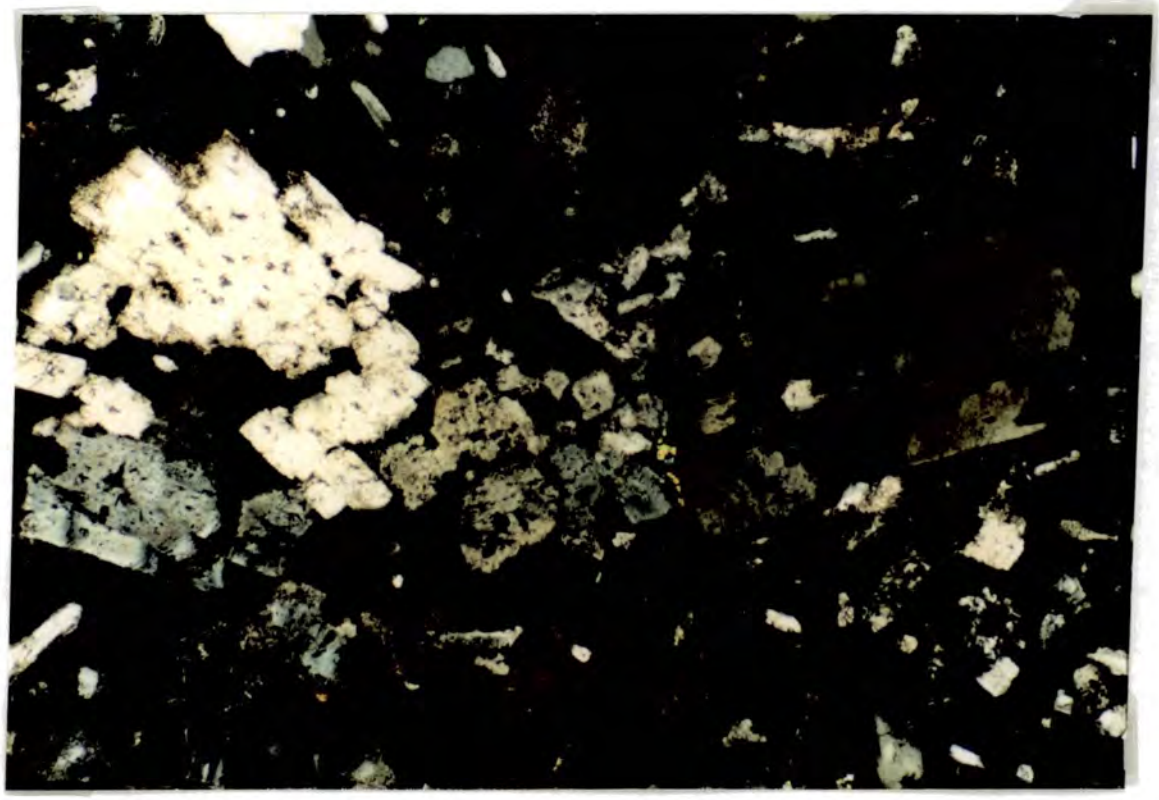

Plate 4.4. Negative sieve textured plagioclase glomerocryst with a continuous network of melt channels visible, even in two - dimensional section. This implies that many of the rounded residual subgrains in the interior of the crystal are entirely isolated. M2 (?) felsite, sample 250/1, Glebe Hill. XPL, FOV 3.5mm.

present in two dimensional sections. This implies that they are common in three dimensions but also that the crystals form physically continuous structures. As these channels increase in abundance, the crystals grade into negative sieve - textured grains (type (3), below). This transition only rarely occurs within single crystals or glomerocrysts (Plate 4.3): in general, individual crystals or polycrystalline inclusions show one or the other type of texture throughout. The spacing of the melt pockets or pores is typically less than 0.2mm, individual pores mostly being less than 0.1mm across. They are usually filled with very fine - grained granular feldspar - rich material rather than the pale brown devitrified glasses which form the groundmass. Similar granular material rims feldspar grains in some sections: probe analyses of this material (P42F2OG1 and OG2, Table 5.2, section 5.3.2.2) show it to be dominated by a sodic feldspar component and to contain 5 times more Ca than the devitrified glass around it. Relative to the adjacent feldspar, however, the granular material contains more Si, K, Ti and Fe, less Ca and Al, and does not have feldspar stoichiometry. It is not, therefore, simply recrystallised feldspar. The most likely explanation is that it is the product of feldspar nucleation on, and diffusion of feldspar components towards, pre - existing feldspars during devitrification, as it is not present in all sections and is too wide (100 – 200 microns) to reflect compositional zonation in the melt adjacent to dissolving feldspars prior to the quenching. as observed in experiments by Donaldson (1985a). These rims are only present in the sections with abundant quench feldspar crystals, suggesting that they only formed at relatively low cooling rates.

3). Negative sieve textured feldspars, as defined in 3.2.6. are characterised by an even higher content of quenched melt within the region occupied by the original feldspar crystal. This is defined by an optically continuous, or nearly continuous, cluster of rounded subgrains which together outline a single larger euhedral or subhedral grain. The subgrains are separated by a series of melt channels which are almost continuous in two dimensions, suggesting that at least some of the subgrains are isolated in three dimensions (Plate 4.4). The spacing of the melt channels is similar to that of the melt pockets in normal sieve - textured grains. This and the occurence of rare grains showing a gradation between the two textures suggests that feldspar types (1), (2) and (3) form a continuous series from grains melting only at their outer surfaces through those in which melting occurs within the grains, possibly at the sites of hydrous secondary mineral inclusions, to those in which the degree of melting has risen to

Plate 4.5A. Very fine - grained granular, negative sieve - textured (Type 4) plagioclase porphyrocrysts with opaque inclusions. Sample 43Q (M2 felsite, south of Duin Bhain). PPL, FOV 3.5mm.

Plate 4.5B. Detail of quench plagioclase overgrowths on granular subgrains within Type 4 feldspar porphyrocryst (Plate 4.5A). Sample 43Q. PPL, FOV 0.75mm.

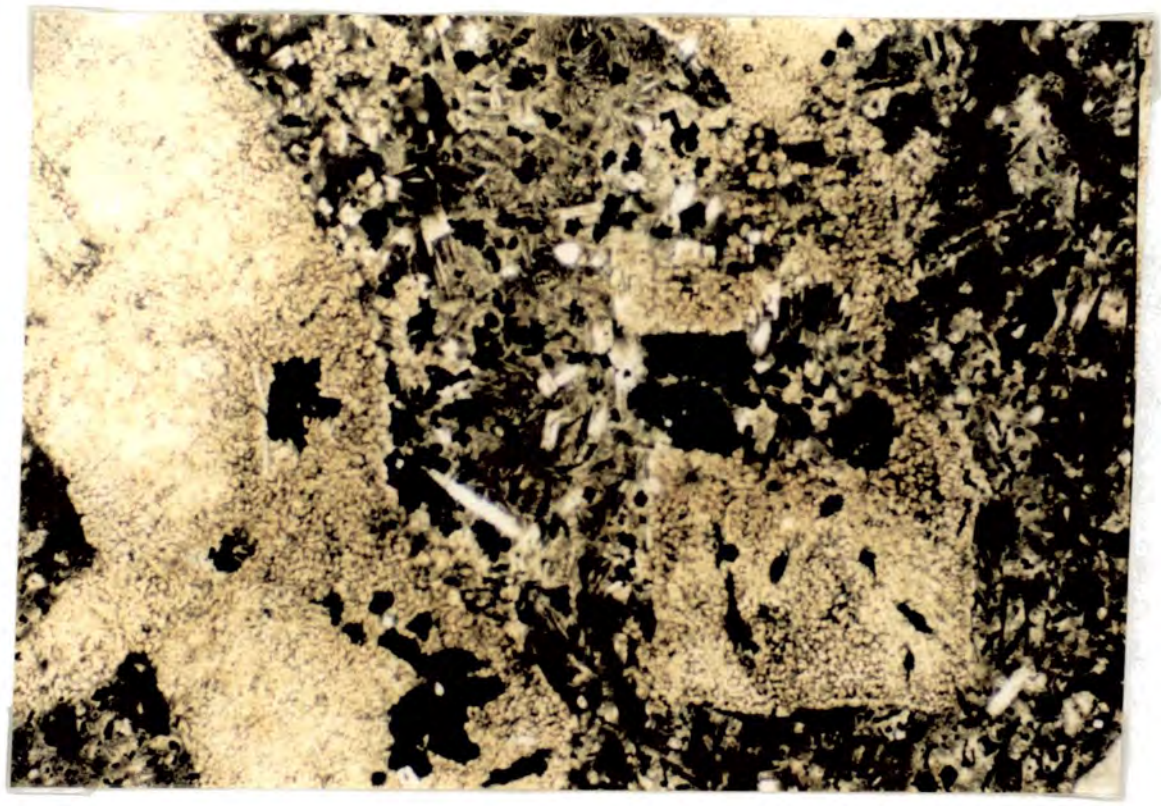

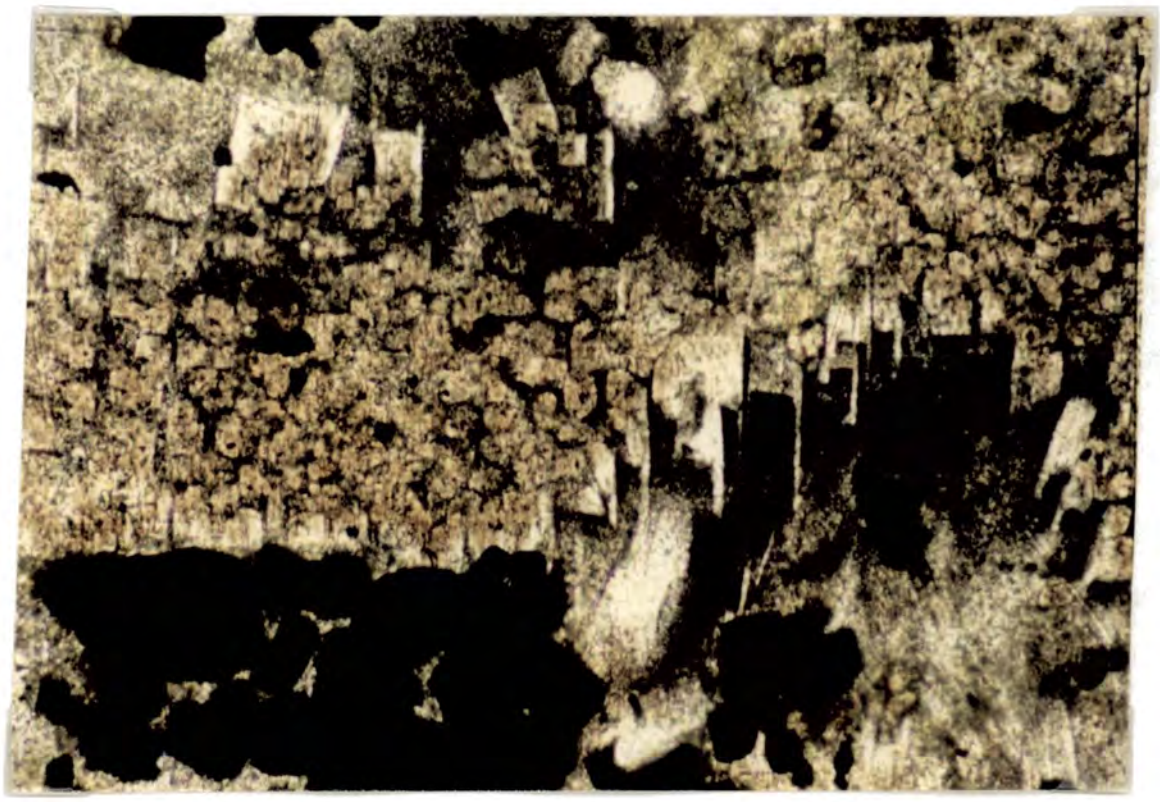

the stage at which the melt pockets interconnect.

4). A small number of sections of the finest - grained felsites from the Duin Bhain area contain subhedral to rounded pseudomorphs after large feldspars which are composed of very large numbers of very much smaller equant subgrains less than 30 microns across (Plate 4.5A). These subgrains are separated by quenched melt but are in optical continuity. They are usually pale brown and slightly turbid, but have clear quench feldspar overgrowths (Plate 4.5B). Owing to their small size it was not possible to analyse these subgrains using the electron microprobe, so it is not known whether or not they are compositionally distinct from feldspars of types (1) to (3) above. The pseudomorphed grains commonly enclose equant opaque grains and are never associated with augite or pseudomorphs after augite.

Electron probe microanalyses of grains of types (1) to (3) from different members of the M2 felsite suite show remarkable uniformity of composition between grains with different morphologies (Fig. 4.9). Most of the variation in M2 felsite feldspar porphyrocryst compositions within sections is formed by a patchy variation apparently unrelated to position within the grains or subgrains. This variation is interpreted as being due to patchy late M2 alteration associated with the formation of epidote in granular clusters of epidote, quartz, alkali feldspar and chlorite which patchily replace the groundmass. Epidote also occurs within a few feldspar grains. There is no obvious systematic compositional difference within individual sections between the different morphological groups of porphyrocrysts, implying that the textural differences between them are not related to composition. In contrast, there is a slight but distinct difference in feldspar composition between rocks, with the most calcic feldspars in the most evolved rock analysed, 250/1, being around 3% more sodic than those in the less evolved specimens 42F2 and 43K1.

Fig. 4.9 also indicates that the porphyrocryst feldspars are considerably more albite - rich than the majority of feldspars in the MBG basic rocks analysed: the exceptions are groundmass and secondary feldspar grains in the latter, which could not have been incorporated into the felsites by magma mixing. The results of geothermometric calculations presented in section 4.2.5 indicate that these feldspars would be in equilibrium with a dacitic host, of similar bulk composition to those in which they presently occur, at around $1000^{o}C$, the actual value being dependent upon water pressure. These values are typical of near - liquidus dacitic magmas at low confining pressures (

Fig. 4.9: All plagioclase analyses from M2 felsites and MBG basic rocks. The lack of Ca - rich plagioclases in the former and the much wider range of compositions in the latter indicates that the feldspar porphyrocrysts in the subalkaline granitoids are not xenocrysts from the latter.

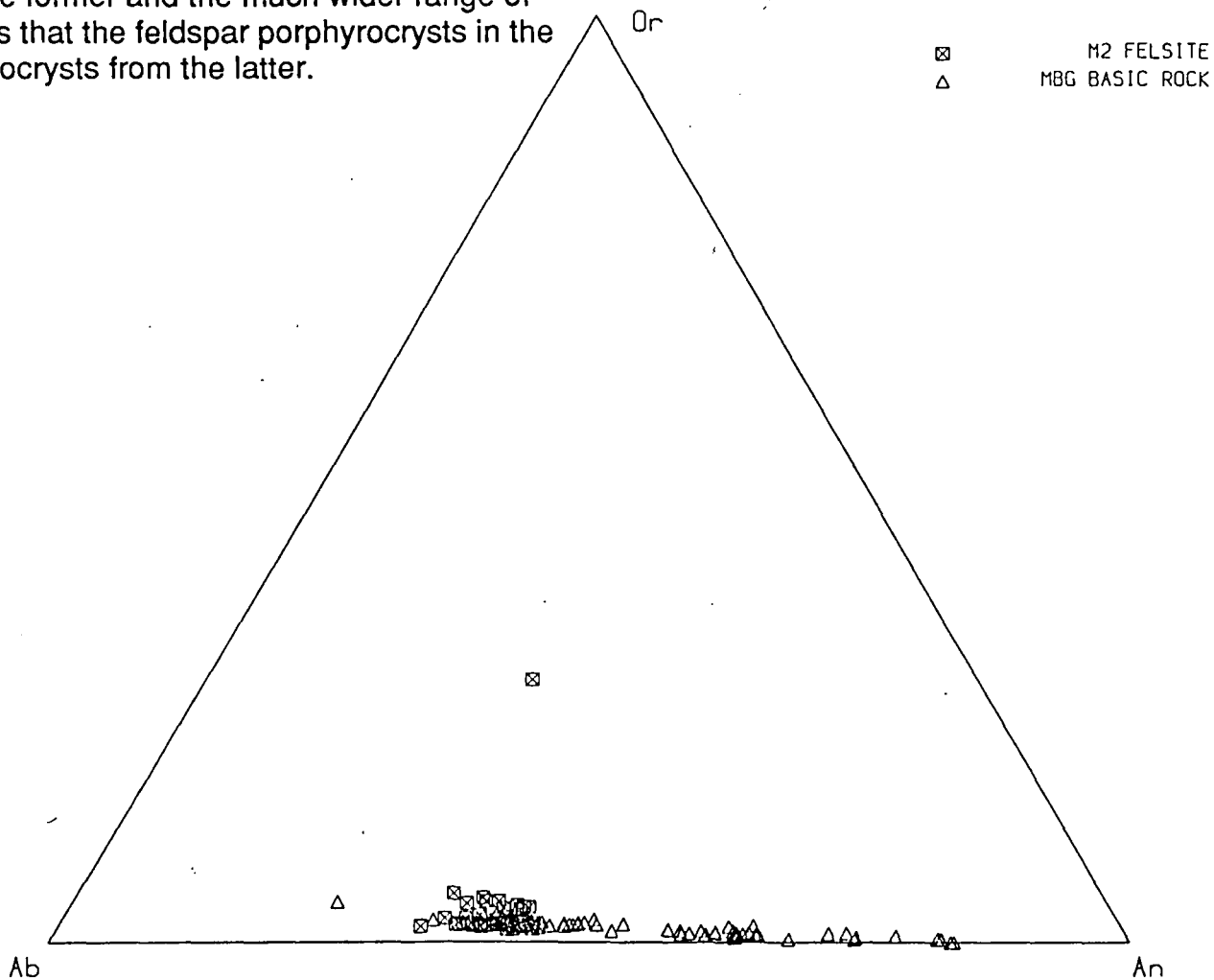

Wyllie et al. 1976; Thompson 1983; see section 4.2.5). The similarity of the temperatures obtained from geothermometry based on mineral **compositions** and those implied by the observed crystal assemblage and bulk composition in these rocks suggests that the plagioclases are unlikely to have formed as phenocrysts in a substantially more basic or felsic magma. Whether or not the basic magma involved in a hypothetical mixing process was aphyric (as is the case for the bulk of MBG basic rocks), this implies that magma mixing involving magmas of strongly contrasted compositions was not an important process in the formation of these rocks.

Pyroxene porphyrocrysts.

The main compositional features of the analysed pyroxenes are shown in Fig. 4.10, with pyroxenes from MBG basic rocks plotted for comparison. The difference in $(Mg/Mg + Fe^{2+})$ between the two groups is remarkably small. One reason for this may be the presence in the augite porphyrocysts of large numbers of magnetite inclusions (Plate 3.26; also Plate 4.6, below). These appear to replace the augites and if so would be expected to enrich the remaining pyroxene in magnesium relative to iron.

Two groups of isolated augite crystals occur in many of these rocks. One is composed of elongate prisms up to 2mm long and smaller needle - like crystals: these appear to be quench crystals. The second group are rounded to subhedral equant grains and stubby prisms, some of which are composed of optically continuous granular subgrains separated by thin quenched melt channels, in a texture which resembles the negative sieve texture in feldspars described above. Like the feldspar porphyrocrysts, these grains appear to be inherited from an earlier rock.

Augite is most common, however, in the polycrystalline inclusions. They commonly form a quarter to one - half of these, which therefore have a dioritic composition overall, in contrast to the broadly granodioritic composition of the rocks as a whole. This, however, is consistent with these inclusions being cognate in origin, if it is supposed that the parental rocks showed millimetre to centimetre scale heterogeneity such as occurs in the ferrobasaltic sills on the southern side of the intrusion and is picked out by metamorphism (section 3.2.5.5; Plate 3.59B). This heterogeneity is defined by local concentrations of low melting point components (especially alkali feldspar ± quartz). These were probably formed by segregation of residual melts during crystallisation into patches a

Fig. 4.10. Clinopyroxene analyses from the M2 felsites and MBG basic rocks. The lack of overlap between the two groups indicates that the augites in the former are not xenocrysts from the latter.

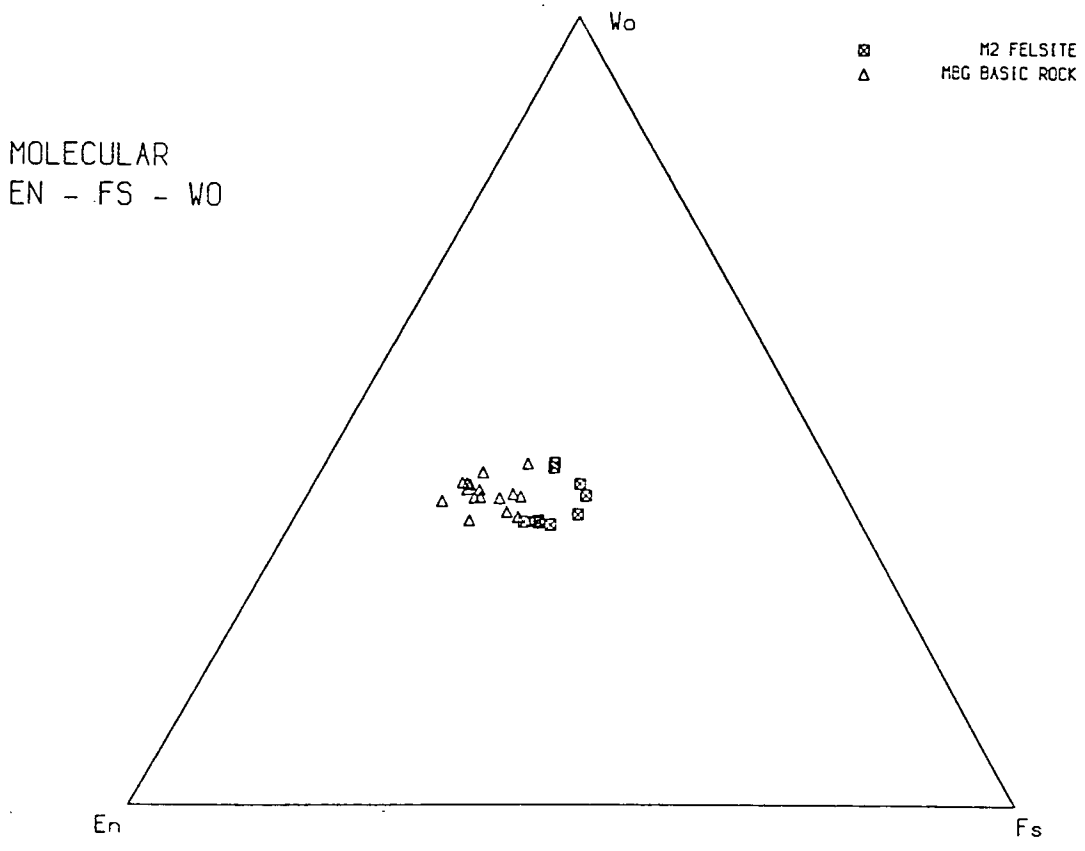

few millimetres across: the same microstructure is shown by the early M2 ferrogabbroic pods and veins within the MBG (Plate 3.10), in which the residual melt segregations are readily identified as areas of devitrified glass. In this case the melting process would be concentrated in, and cause preferential disaggregation of, the more fusible parts of the rock whilst the most refractory patches would be preferentially preserved. In the case of a rock of granodioritic bulk composition, the latter would be dioritic in composition, precisely as is observed.

The textures of the augites in the polycrystalline inclusions vary from sub - poikilitic to granular, with the former being more common in the finer - grained inclusions (Plate 4.6A) and the latter in the coarser inclusions (Plate 4.6B). As with the feldspars, this suggests that the coarser - grained parental rocks underwent recrystallisation at high temperatures, consistent with the inference of varying amounts of late - stage melt migration in the parent rocks which was made on the basis of geochemical data in section 4.2.2.1. A range of textures from finer - grained poikilitic to coarse granular occurs in different inclusions within the same thin section of some but not all of these rocks. Given that the polycrystalline inclusions are cognate in origin, as inferred in the discussion of the feldspars, above, this indicates that mixing of magmas derived from compositionally similar rocks with different textures and grain sizes took place in the source region of these magmas.

In contrast to the majority of the feldspar porphyrocrysts, however, some of the augite crystals in the polycrystalline inclusions have euhedral crystal faces against the quenched - melt groundmass. Donaldson (1985b) demonstrated that euhedral crystals could form during melting experiments and suggested that euhedral crystal morphologies formed in this way indicated that melting had taken place at near - equilibrium conditions.

Oxide Minerals.

Equant grains of opaque minerals, 0.2 to 0.5mm across, are a ubiquitous accessory phase in the porphyrocryst/polycrystalline aggregate assemblage in these rocks. In general they were originally titaniferous magnetites which have undergone lamellar and/or granular exsolution of ilmenite following quenching of the host magma. 43K1, an M2 felsite, contains equant, apparently primary grains of unexsolved ilmenite and magnetite, but probe analyses of these indicate, using the Ti - Fe exchange geothermometer of Buddington & Lindsley (1964), equilibration temperatures of

Plate 4.6A. Subpoikilitic augite in fine - grained doleritic - textured microdiorite inclusion in M2 felsite, south of Duin Bhain. Sample 43K1. PPL, FOV 1.5mm.

Plate 4.6B. Equant subhedral to granular augite grains in a coarser - grained, partly disaggregated polycrystalline dioritic inclusion in M2 felsite, Duin Bhain. Sample 43K1. XPL, FOV 1.5mm.

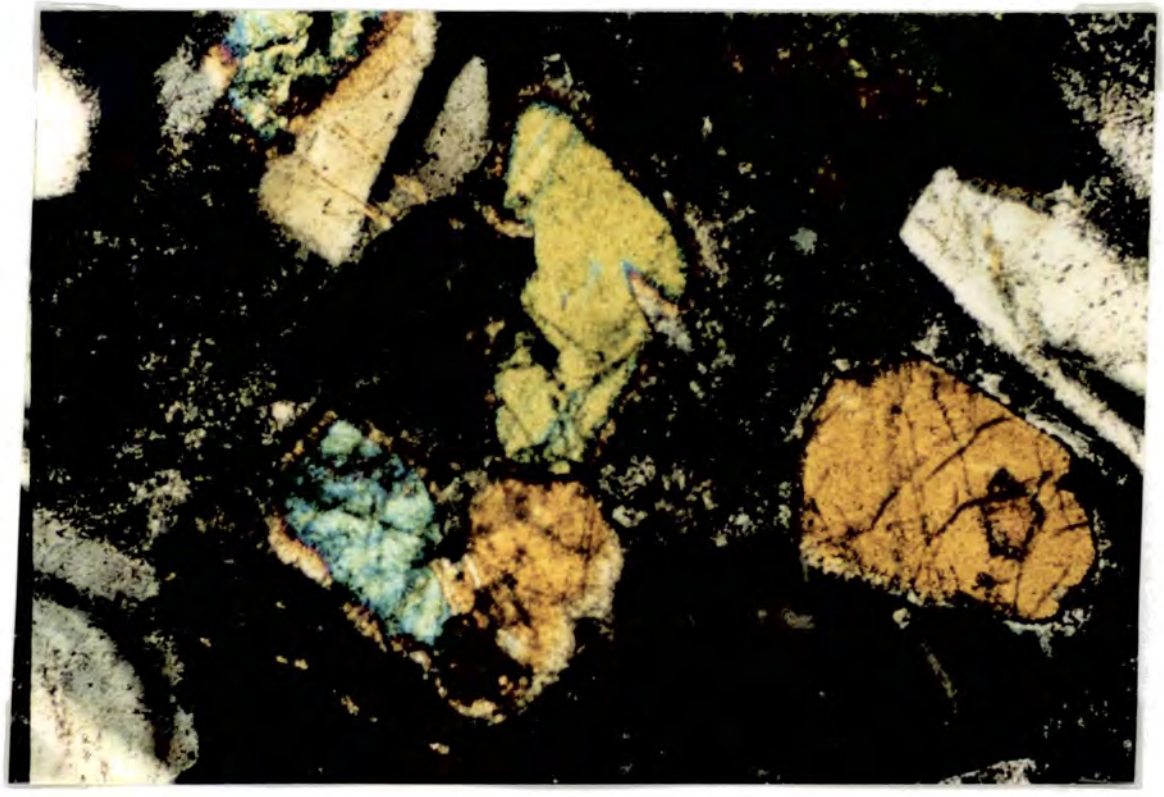

615 - 630°C and $\log f_{O_2} = -19.5 \pm 0.5$. This suggests that these grains have undergone granular recrystallisation rather than lamellar exsolution and record subsolidus alteration.

4.2.2.3. Summary of evidence for the origin of the subalkaline granitoids.

The M1 microgranodiorites and the M2 felsite intrusions appear to have been produced by remelting of pre - Hypersthene Gabbro Tertiary granitoid rocks as a result of reheating of earlier intrusions by the mafic magmas of the MBG magma chamber, rather than by crystal fractionation at the wall of the magma chamber. This occured during M1 high grade metamorphism at the level of origin of these felsic magmas: as noted in Chapter 3, the presence of the M2 felsite intrusions implies that M1 lasted longer at depth than it did at the present level of exposure. This conclusion is based on several lines of evidence, some of which were dealt with in section 3.2, which can be summarised as follows:

1). The felsic magmas which were quenched to form these rocks coexisted with hotter mafic magmas, and were not associated, at least at the present level of exposure, with cumulates of the appropriate (ferrogabbroic or ferrodioritic ?) composition to have formed from the dacitic magmas which these rocks represent.

2). Geochemical variations within the subalkaline granitoid suite cannot be explained in terms of fractionation of the observed porphyrocryst assemblage at the temperatures deduced for the magmas prior to quenching, nor by post - quench hydrothermal alteration or by mixing of felsic and basic magmas. These variations are best explained as the result of remelting, probably with mixing of magmas derived from different intrusions or distinct parts of texturally varied intrusions, of a suite of earlier Tertiary granitoid intrusions. Particularly significant features of the compositional variation in respect of this are (a) the partly compatible behaviour of elements (e.g. Ba and Zr) which are essentially incompatible at the temperatures recorded by the derived magmas immediately prior to quenching in their present position; (b) the variation in La/Yb vs. La in these rocks, which imply different histories of fractionation and crustal contamination for different samples within the suite; (c) the low La/Yb and subalkaline character of these rocks, which excludes an origin by melting of any of the pre - Tertiary country rocks. All of these features can be explained by the

remelting hypothesis, since the earlier suite of rocks could contain a number of intrusions with different compositional evolution paths and which had undergone various amounts of late - stage melt separation, involving residual melts of various compositions. They could also have undergone hydrothermal alteration prior to remelting, which could produce further variation in abundances of soluble elements.

3). The M2 felsites in particular contain corroded, compositionally uniform porphyrocrysts and polycrystalline inclusions. The mineral compositions of these are appropriate for the most refractory residual or restitic components of medium to coarse - grained (and microscopically heterogenous as a result of protracted crystallisation) granodioritic rocks. Textures in these inclusions indicate late - stage magmatic recrystallisation, consistent with the geochemical evidence for segregation of interstitial melts.

The protoliths of these rocks were not found at the surface, analysed pre - Hypersthene Gabbro granitoids being geochemically dissimilar from them. This suggests that the parent rocks must only be present at some depth (but at less than 3 – 5km; see Chapter 7).

4.2.3. Compositionally Anomalous Granitoid Rocks and Country Rock Xenoliths.

The rocks of broadly granitoid composition dealt with in this section are those identified as being compositionally and mineralogically distinct from normal, alkaline to mildly peraluminous British Tertiary Volcanic Province granitoids in Section 3.2. As noted in that section they exhibit a close spatial association with exposed or inferred downfaulted blocks or pseudoscreens of wall rocks. Field and petrographic evidence summarised in section 3.2.7 indicates that these were the main sites of high - degree partial melting and mobilisation during M1. The working hypothesis for the origin of these rocks, which will be examined further in this section, is therefore, that the anomalous microgranitoid rocks represent either (1) wall rock melts or (2) mixtures of wall - rock melts with mafic, intermediate or felsic Tertiary magmas produced by fractional crystallisation and contamination of mantle - derived magmas. One of the primary objectives of this section will be to determine which of these two alternatives applies to which, if any, of the anomalous microgranitoids. Another will be to investigate whether the country rock component in each granitoid is a mixture of the various compositionally distinct rock units described in Chapter 2 or whether it corresponds

to a particular lithology within the sequence.

The other type of country rock material which occurs within the MBG is the refractory material which makes up the various xenolith swarms found in the intrusion. The sites of origin of these xenoliths within the country rock sequence will also be considered in this section.

4.2.3.1. The Main types of Anomalous Granitoid Rocks within the Contact Zone.

These rocks are a volumetrically tiny component of the Contact Zone and it was only possible to collect a small number of samples. Heterogenous hybrid rocks with a wall - rock component are rather more common: these are dealt with in section 4.4. The analysed samples fall into two groups:

Group 1: Diopside Microgranites. These are all associated with the pseudoscreen of country rocks immediately south of Duin Bhain and with the diopside - quartzite xenolith swarm to the west of the pseudoscreen (section 3.2.3.1). Both of these are inferred to form part of a wedge - section downfaulted block of country rocks of which only the tip remains. The two analysed samples of diopside microgranite (42D1 and 42A4; see Appendix 2) originate from the outcrops south of Duin Bhain. The two are compositionally very much alike (see below). In thin section, both contain rounded, granular - textured relict quartzitic inclusions and numerous quench crystals of inverted tridymite: these indicate a very high silica activity. As noted in Chapter 3, they also contain large (up to 2mm long) euhedral to subhedral diopsidic clinopyroxene crystals with a faint pale green tint and, in some, vivid green rims which may indicate the presence of a significant amount of aegirine in the rims. The groundmass is composed of quench needles and skeletal grains of green clinopyroxene, inverted tridymite (commonly with several needles being replaced by a single micropoikilitic quartz grain), opaques and plagioclase, all set in microgranophyre or variolitic devitrified glass. The abundance of clinopyroxene and the possible presence of an aegirine component in the cpx both indicate that these rocks have a high Ca/Al ratio and low A/CNK. This was probably caused by a high ratio of carbonate to clay minerals in the parental sediment.

Similar but less extreme granitoids occur in association with a swarm of clinopyroxene - plagioclase - quartzite xenoliths on the western side of Gharblach Mhor (field location 143/1; Grid Ref. 416655). These granitoids contain prominent pyroxene needles (typically altered to green M2 hornblende

) and lack M2 biotite. This suggests a relatively Ca - rich, K - poor composition but it was not possible to collect suitable material for bulk analysis, the outcrops being intensely weathered and heavily jointed.

Group 2: Cordierite - Hypersthene Microgranitoids. The best example of this rock type is the hypersthene - phyric microgranitoid which occupies the wedge - shaped pocket between the downfaulted block on Hill 210 and the main wall of the Marginal Border Group (Fig. 3.13), and is exposed at field location 183D1. The petrography of this rock is described in Section 3.2.5.2. Microprobe analyses of the main porphyrocryst phases, orthopyroxene and plagioclase, and of groundmass K - feldspars, are presented in Fig. 4.11. Although only a few analyses are available, a number of conclusions can be drawn from these plots. Firstly, as is consistent with the presence of cordierite, the orthopyroxenes are very Ca - poor. These features indicate that the peraluminosity of the rock is a primary feature and not merely the product of M2 alteration. The feldspar compositions mainly record low - temperature alteration as the degree of solid solution between plagioclase and K - feldspar is very small: despite this, no discrete grains of Na - feldspar were found.

Related rocks on the southern margin of the intrusion include the felsic component of a heterogenous M1 sheet intrusion at An Acairseid which contains various mafic and granular quartzitic inclusions (field loc. 267/1; Grid Ref. 43626299) and granitic rocks within the MBG to the north - west of 267/1. The latter contain numerous rounded quartzite inclusions and lack the feldspar porphyrocrysts characteristic of the subalkaline microgranitoids, but it was not possible to sample them for analysis. Other occurences of similar rocks along the southern margin include an unchilled, irregular vein which cuts MBG basic rocks at the northern end of the Dubh Chreag gorge (see Fig. 3.14). This dates from the earliest part of M2 and is analogous to the unchilled heterogenous microgranodioritic veins which cut the MBG just east of Sanna Point (section 3.2.3). With the exception of the outcrops at 183D1, all of these rocks are intensely altered, with complete replacement of orthopyroxene by chlorite, partial replacement of early M2 biotite (also by chlorite), replacement of cordierite by pinitic aggregates, formation of turbid feldspars and complete recrystallisation of the groundmass to a granular matrix. The analysis of 267/1 in particular may therefore have been strongly affected by alteration.

4.2.3.2. Country Rock Xenoliths.

Fig. 4.11. Feldspar and orthopyroxene analyses from 183D1. See text for discussion.

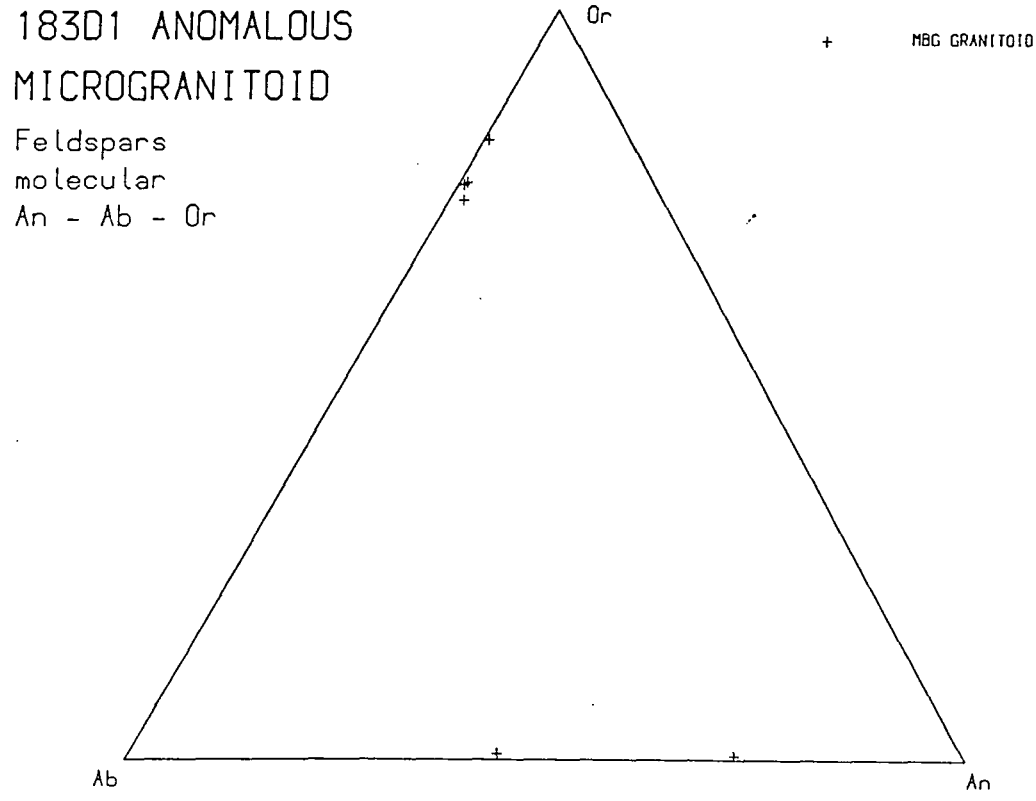

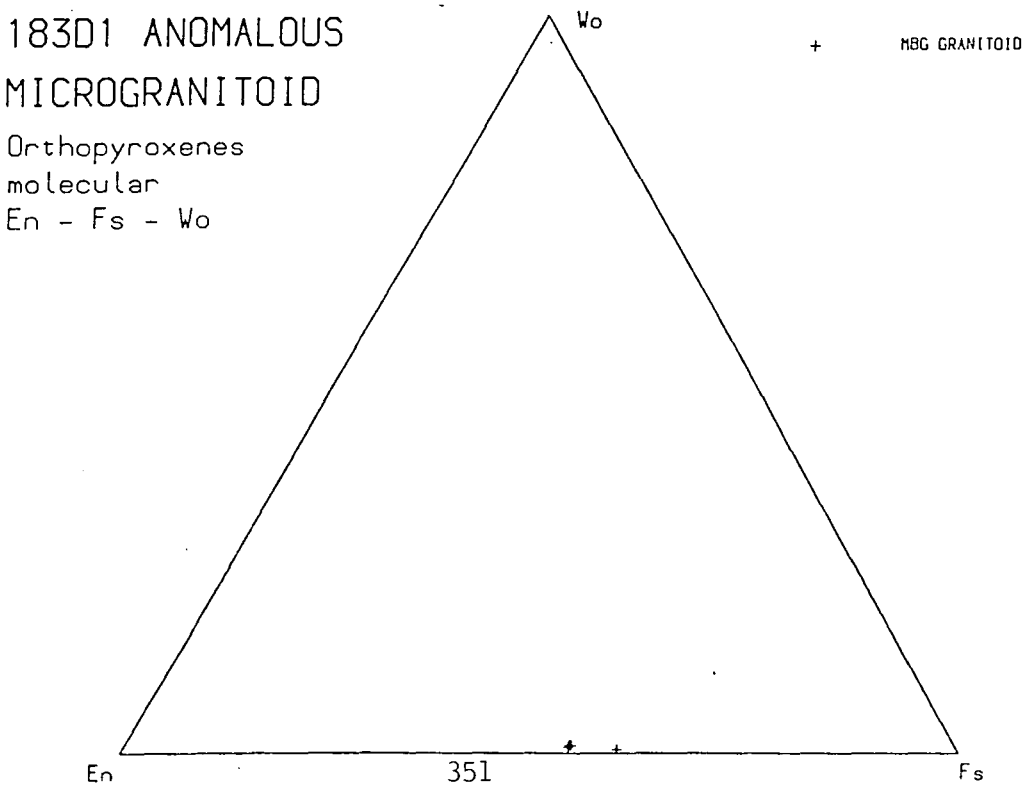

Plate 4.7. Orthopyroxene porphyrocryst in granular - poikiloblastic quartz + plagioclase + cordierite + opaques groundmass. Pelitic xenolith in MBG, north end of Gharblach Mhor. Note intense alteration of porphyrocryst rim and groundmass mafic minerals to M2 biotite and green hornblende, as well as to later chlorite. Sample 140/3. PPL, FOV 3.5mm.

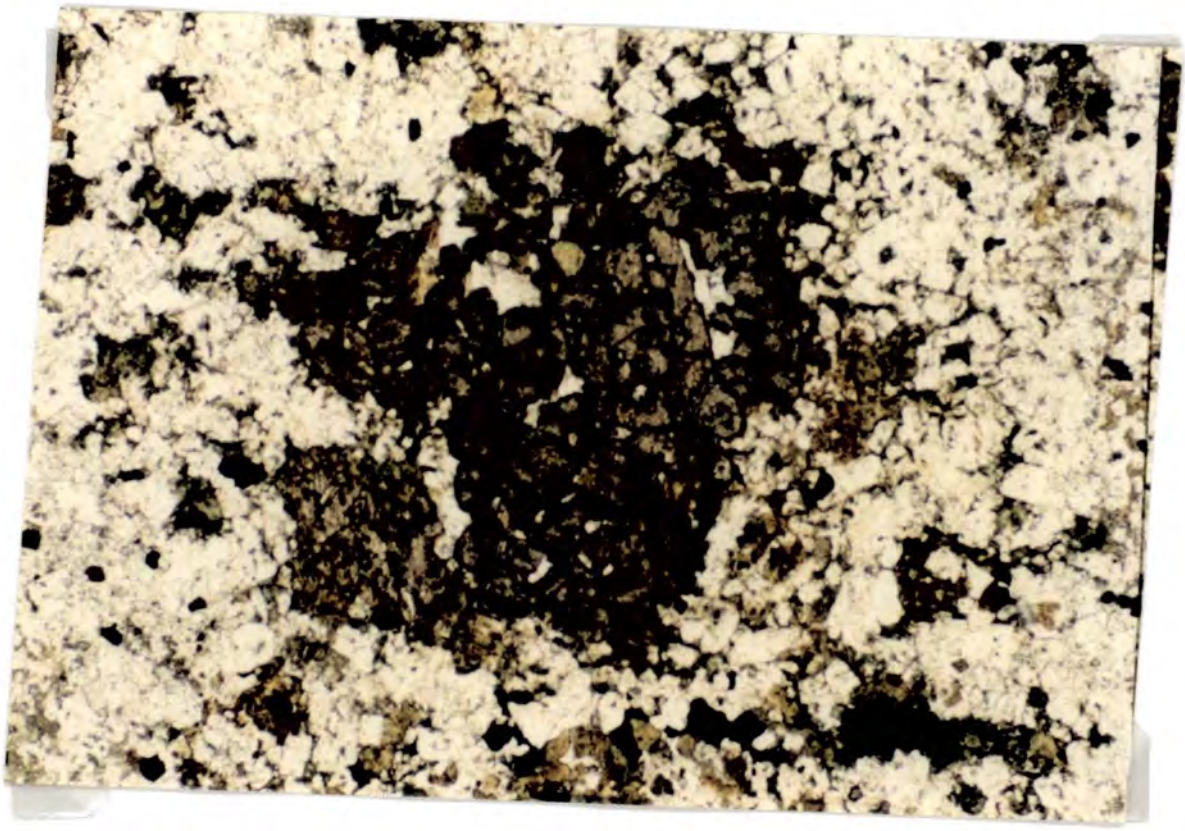

The sample of wall rock types represented by these xenoliths is strongly biased towards those of refractory, non - eutectic compositions and it is therefore not surprising that they fall into a number of very distinctive groups. As noted in Chapter 3, each of the swarms of xenoliths is dominated by xenoliths belonging to one of these lithological groups. The two most abundant xenolith types are:

1). Quartzites, composed of granular aggregates of residual quartz with minor amounts of other refractory phases and small amounts of interstitial granophyre or irregular quartz - feldspar intergrowth. The residual quartz grains adjacent to this interstitial material generally have syntaxial poikiloblastic overgrowths which replace tridymite needles in the intergrowths. The group can be divided into **(i)** a diopside- or augite- bearing subgroup (e.g. 20/1WR, which is from the xenolith swarm to the west of the Duin Bhain pseudoscreen (Grid Ref. 44587031), and sectioned but unanalysed xenoliths from swarms at Ardnamurchan Point (field location 101) and Gharblach Mhor (field loc. 143/1 ; these also contain residual plagioclase and seem to be more aluminous) and **(ii)** grey fine grained quartzitic xenoliths, the one sectioned and analysed sample of which (150/1, Grid Ref. 41966520) is intensely altered but appears to have contained an accessory mineral assemblage of hypersthene + cordierite (altered to chlorite + opaques and pinite respectively) + plagioclase + opaques.

(2) Aluminous rocks, with a low content of residual quartz (sometimes quartz - absent) and characterised by the assemblage opx + cordierite + opaques + plagioclase. The textures of these rocks vary widely. One, sample 140/3 which is from a xenolith swarm at the northern end of Gharblach Mhor (Grid Ref. 41466588), contains short subhedral plagioclase laths and large (up to 2mm across) ragged orthopyroxene porphyrocrysts, set in a poikilitic or poikiloblastic K - feldspar + quartz + cordierite + opaques groundmass (Plate 4.7). This texture, which is much coarser - grained than the normal granular hornfels textures found in the M1 contact aureole, suggests that partial melting occurred when the xenolith was incorporated into the MBG magma chamber during M1 and was followed by slow cooling during M2 (as is also found in the host rocks in this area (section 3.2.4)). The greater - than - normal degree of partial melting in this aluminous xenolith is explicable in terms of its relatively alkali - rich, fusible bulk composition (section 4.2.3.3, below). The other end of the spectrum of textures in the aluminous xenoliths is represented by sample 274/1 from the banded xenolith swarm on the eastern side of An Acairseid (section 3.2.5.2). This entirely lacks K - feldspar and quartz and has a granular hornfels texture, apart from the igneous

textured cordierite - norite veins which cut the banding.

4.2.3.3. Geochemistry and Petrogenesis of the Anomalous Granitoids and Country Rock Xenoliths. 1: General considerations.

Relevant features of the geochemistry of these rocks are presented in Fig. 4.12. The granitoids and xenoliths analysed are letttered individually in these diagrams as follows:

a 183D1 cord - opx microgranitoid

b 267/1 cord - opx (?) microgranitoid

c 42D1 diopside microgranite

d 42A4 diopside microgranite

e 274/1 aluminous xenolith

f 140/3 aluminous xenolith

g 150/1 quartzitic xenolith (opx - bearing ?)

h 20/1WR cpx - quartzite xenolith

Many aspects of these diagrams cannot be interpreted, owing to the small number of available samples of many of the numerous groups of rocks present, and the wide compositional variations that occur within as well as between the groups. However, they can be used to rule out or support various alternative models for the petrogenesis of the anomalous rocks and the xenoliths:

1) Do the anatectic components of the anomalous microgranitoids originate from the Moinian or the Mesozoic sequences, or from both ?

2) Is there a basic or intermediate magmatic component in the anomalous granitoids, despite the lack of outcrop or petrographic evidence for magma mixing between anatectic magmas derived from pre - Tertiary rocks and magmas from the interior of the MBG magma chamber ?

3) Could the anomalous granitoid have been produced by fractionation of strongly contaminated mafic melts ?

4) Has mixing occurred, between anatectic magmas derived from sedimentary rocks and the subalkaline granitic/granodioritic magmas also present at the wall of the MBG magma chamber, to produce the anomalous microgranitoids ?

5) Can particular lithologies within the country rock sequence be identified as parental to particular anomalous microgranitoids, or are the latter mixtures of various lithologies ?

6) From where in the country rock sequence do the various xenolith swarms originate, and have the xenolith compositions been modified by reaction with the enclosing magmas ?

Two of the potential mechanisms of formation in the above list can be eliminated immediately by inspection of the plots in Fig. 4.12. Plots of K_2O vs. SiO_2, Zr vs. SiO_2, Zr vs. CaO/Na_2O and K_2O vs. CaO indicate that the Moinian rocks have too low Zr/SiO_2 and $Zr/(CaO/Na_2O)$, and too high K_2O and K_2O/CaO at any given SiO_2 to be the sole source rocks of any of the anomalous microgranitoids. In addition, 42D1 and 42A4 both have CaO and CaO/Na_2O values which are too high, at their Zr and SiO_2 contents, for them to be mixtures of Moinian rocks and any of the other rocks plotted on these diagrams. Similarly, the Zr abundances of the peraluminous anomalous granitoids, 183D1 and 267/1, (Fig. 4.12.8) are such that they can only contain a significant Moinian component if they are mainly composed of high - Zr subalkaline Tertiary granitoid material. This is ruled out for 267/1 by its peraluminous character (although this could conceivably be a product of intense alteration rather than a primary feature), its high Cr content and inconsistencies between the proportions of subalkaline granitoid to Moinian material required to explain its the Zr, Ti and Al contents (note that these elements are generally considered to be inert during low - grade hydrothermal alteration and their relative abundances are unlikely to be affected by such alteration). 183D1, on the other hand, overlaps with the field of the subalkaline granitoid rocks in Fig. 4.12 and only plots between these rocks and the Moinian rocks in a few plots, in which it also plots between the subalkaline granitoids and the Mesozoic rocks. Its origin is discussed further below but there is no reason to infer the presence of a Moinian component in it.

Fig. 4.12 can also be used to rule out the presence of significant amounts of MgO - rich basic material, or of TiO_2 - rich intermediate material, mixed with anatectic material, in these rocks. The critical features of the anomalous granitoid rocks in this respect are their low MgO and high

Fig. 4.12. Variation diagrams illustrating various features of the geochemistry of the M1 anomalous granitoids and country rock xenoliths within the MBG. See text for discussion and key to individually labelled analyses. Dotted line encloses field of Moinian rocks analysed.

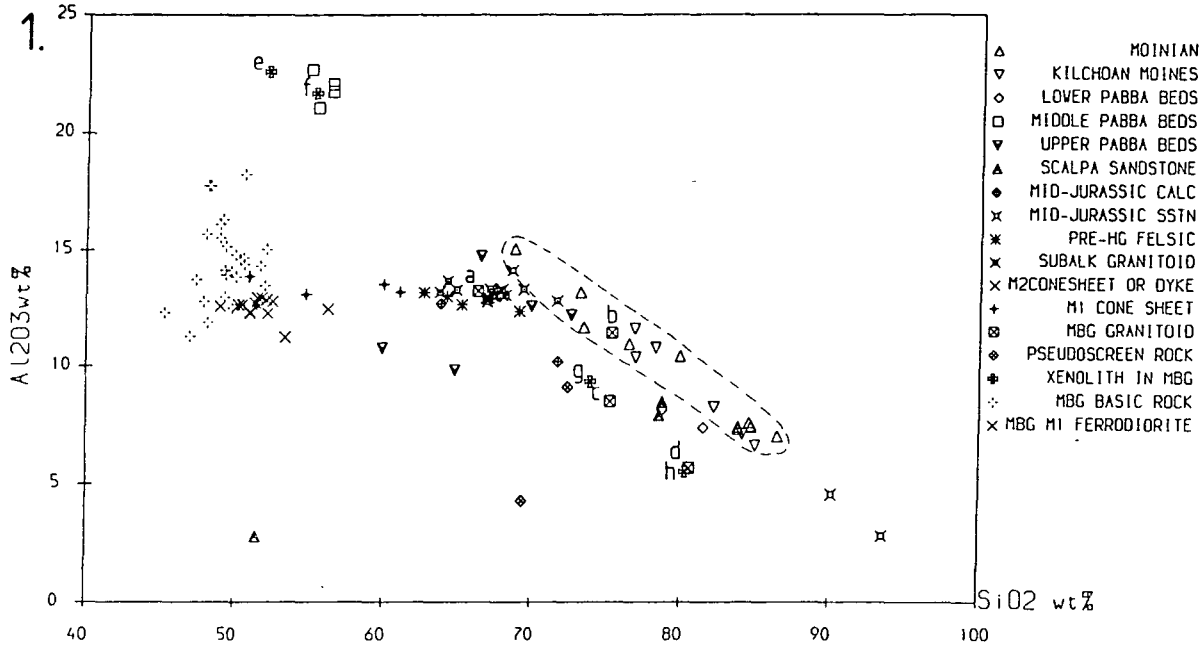

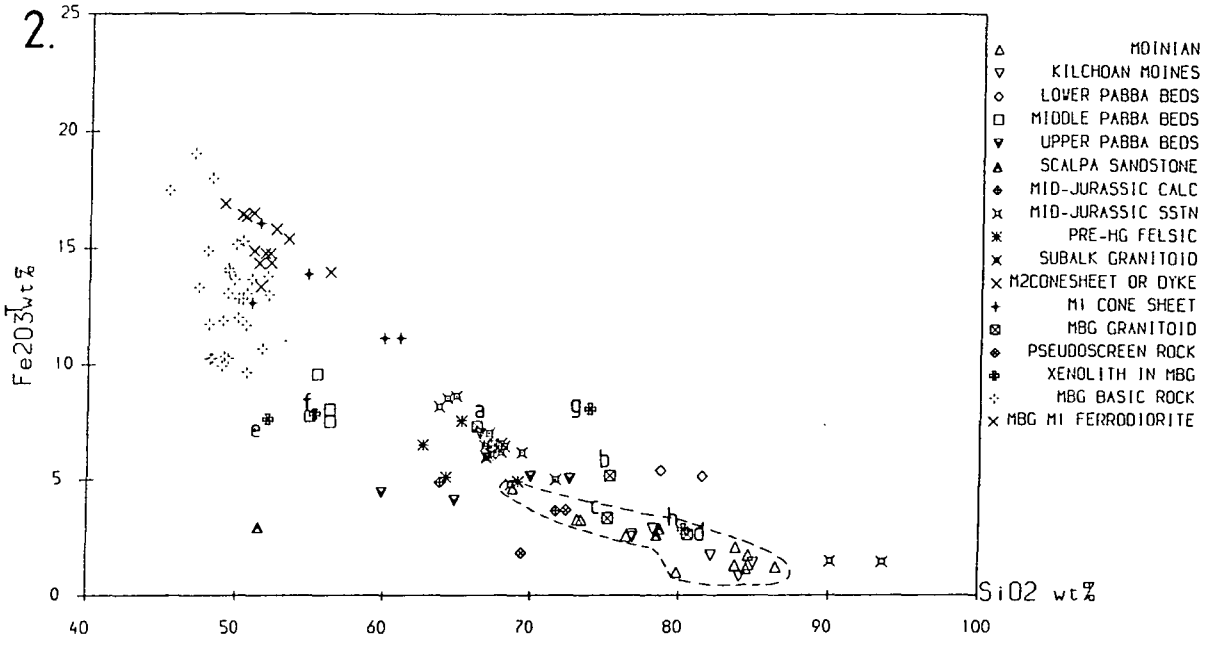

3.

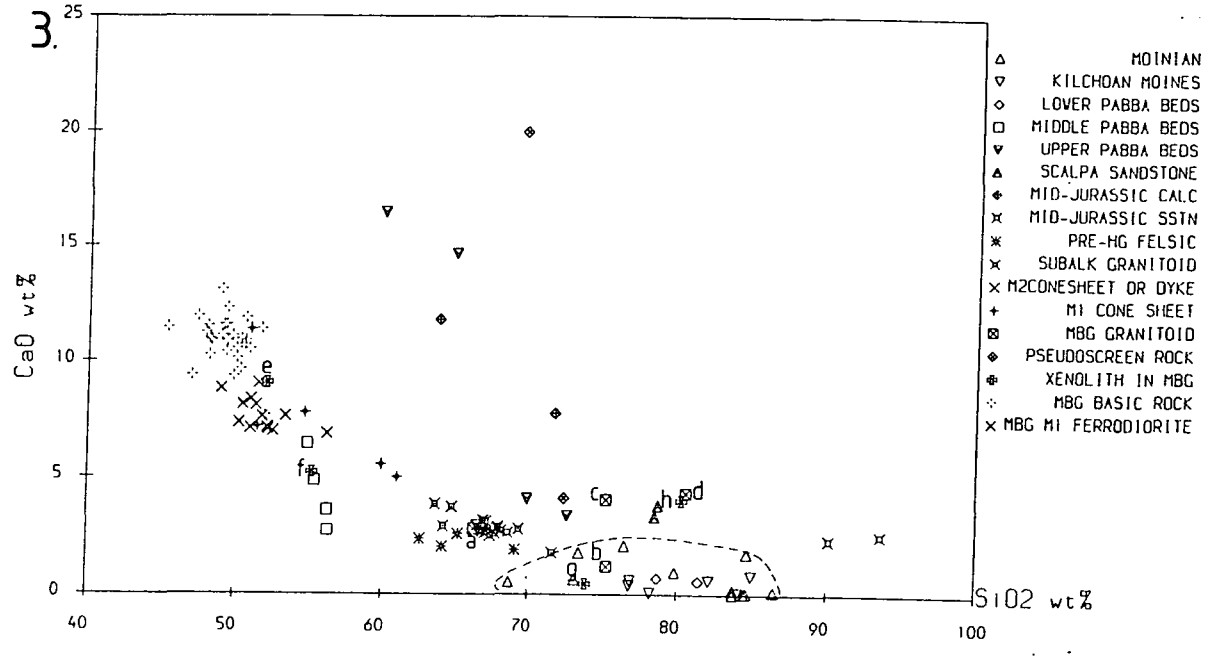
CaO wt%
SiO2 wt%
MOINIAN
KILCHOAN MOINES
LOWER PABBA BEDS
MIDDLE PABBA BEDS
UPPER PABBA BEDS
SCALPA SANDSTONE
MID-JURASSIC CALC
MID-JURASSIC SSTN
PRE-HG FELSIC
SUBALK GRANITOID
M2CONESHEET OR DYKE
M1 CONE SHEET
MBG GRANITOID
PSEUDOSCREEN ROCK
XENOLITH IN MBG
MBG BASIC ROCK
MBG M1 FERRODIORITE

4.

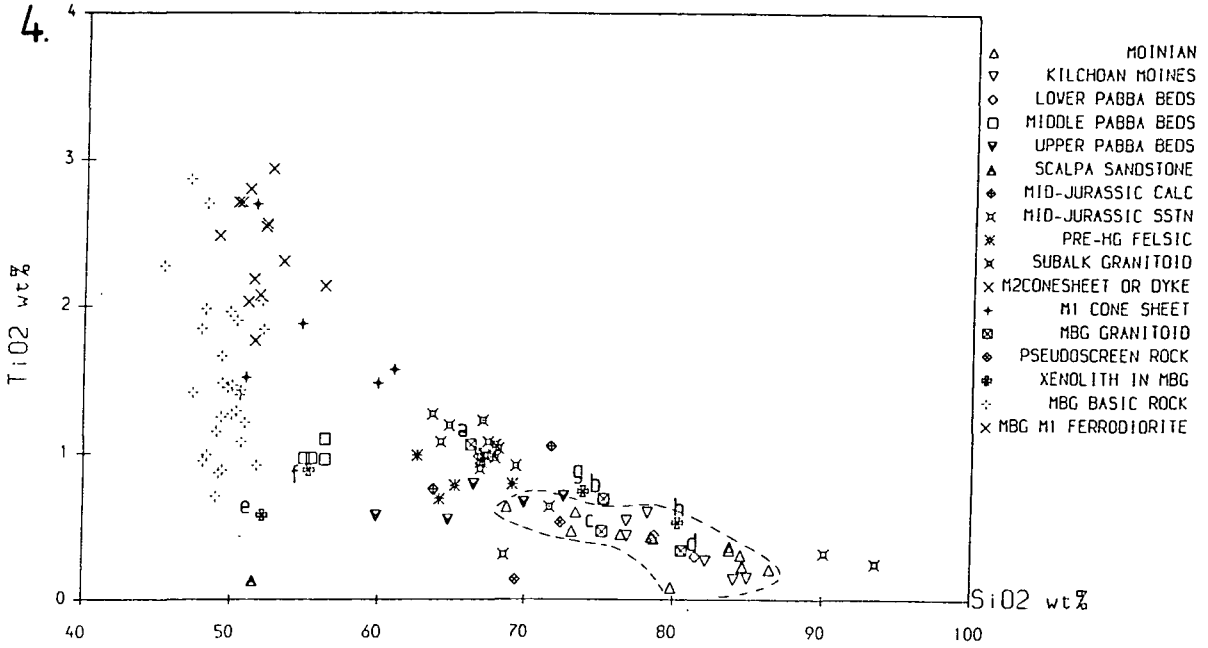
TiO2 wt%
SiO2 wt%
MOINIAN
KILCHOAN MOINES
LOWER PABBA BEDS
MIDDLE PABBA BEDS
UPPER PABBA BEDS
SCALPA SANDSTONE
MID-JURASSIC CALC
MID-JURASSIC SSTN
PRE-HG FELSIC
SUBALK GRANITOID
M2CONESHEET OR DYKE
M1 CONE SHEET
MBG GRANITOID
PSEUDOSCREEN ROCK
XENOLITH IN MBG
MBG BASIC ROCK
MBG M1 FERRODIORITE

5.

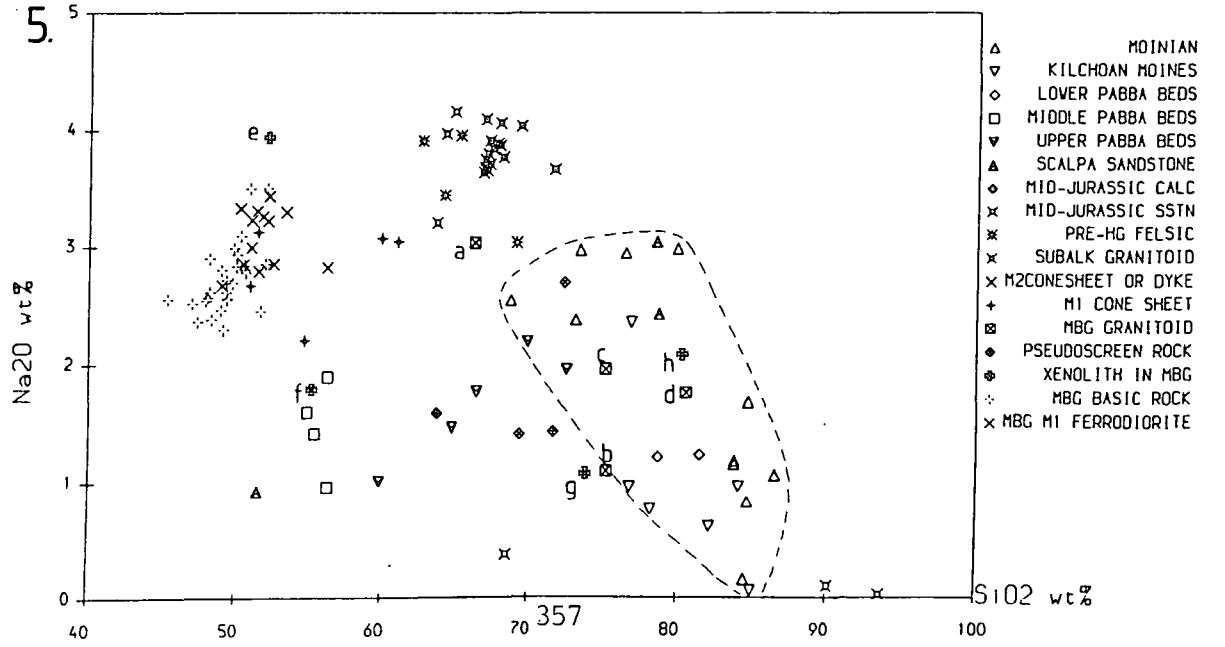
Na2O wt%
SiO2 wt%
MOINIAN
KILCHOAN MOINES
LOWER PABBA BEDS
MIDDLE PABBA BEDS
UPPER PABBA BEDS
SCALPA SANDSTONE
MID-JURASSIC CALC
MID-JURASSIC SSTN
PRE-HG FELSIC
SUBALK GRANITOID
M2CONESHEET OR DYKE
M1 CONE SHEET
MBG GRANITOID
PSEUDOSCREEN ROCK
XENOLITH IN MBG
MBG BASIC ROCK
MBG M1 FERRODIORITE

6.

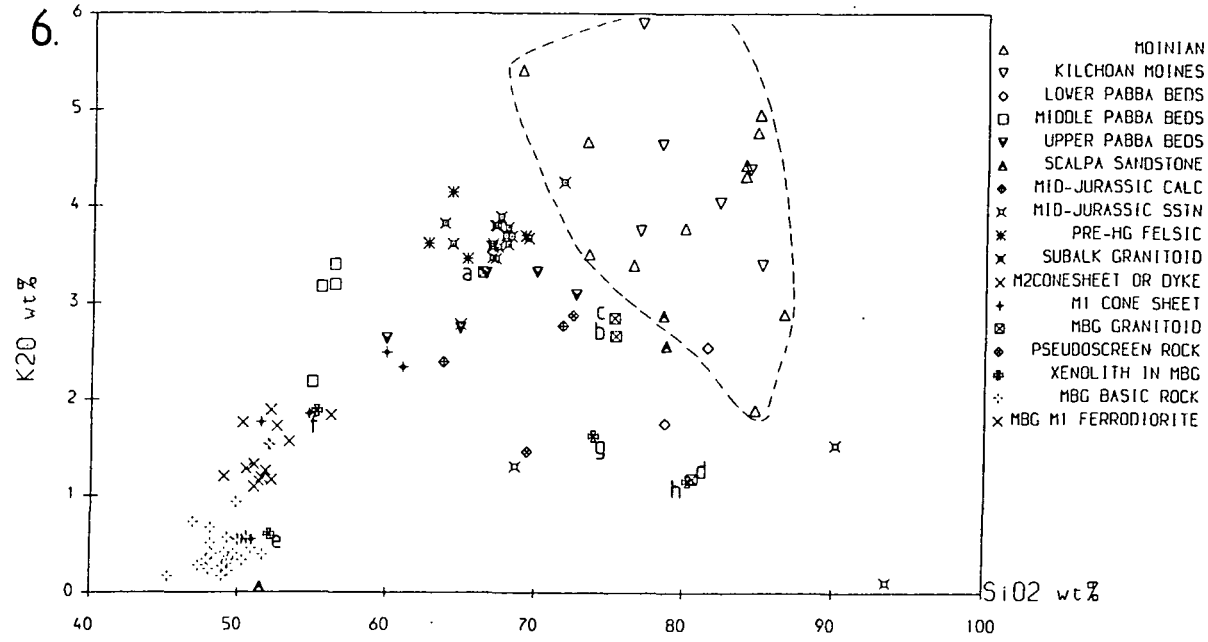
K20 wt%
SiO2 wt%
MOINIAN
KILCHOAN MOINES
LOWER PABBA BEDS
MIDDLE PABBA BEDS
UPPER PABBA BEDS
SCALPA SANDSTONE
MID-JURASSIC CALC
MID-JURASSIC SSTN
PRE-HG FELSIC
SUBALK GRANITOID
M2CONESHEET OR DYKE
M1 CONE SHEET
MBG GRANITOID
PSEUDOSCREEN ROCK
XENOLITH IN MBG
MBG BASIC ROCK
MBG M1 FERRODIORITE

7.

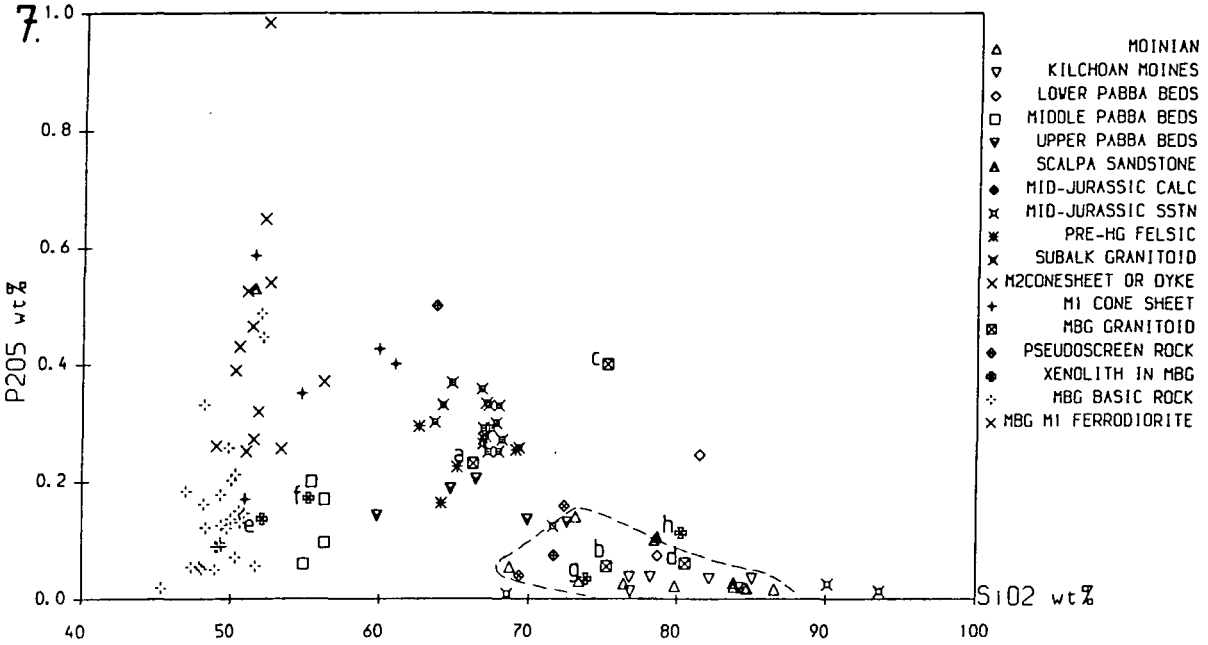
P205 wt%
SiO2 wt%
MOINIAN
KILCHOAN MOINES
LOWER PABBA BEDS
MIDDLE PABBA BEDS
UPPER PABBA BEDS
SCALPA SANDSTONE
MID-JURASSIC CALC
MID-JURASSIC SSTN
PRE-HG FELSIC
SUBALK GRANITOID
M2CONESHEET OR DYKE
M1 CONE SHEET
MBG GRANITOID
PSEUDOSCREEN ROCK
XENOLITH IN MBG
MBG BASIC ROCK
MBG M1 FERRODIORITE

8.

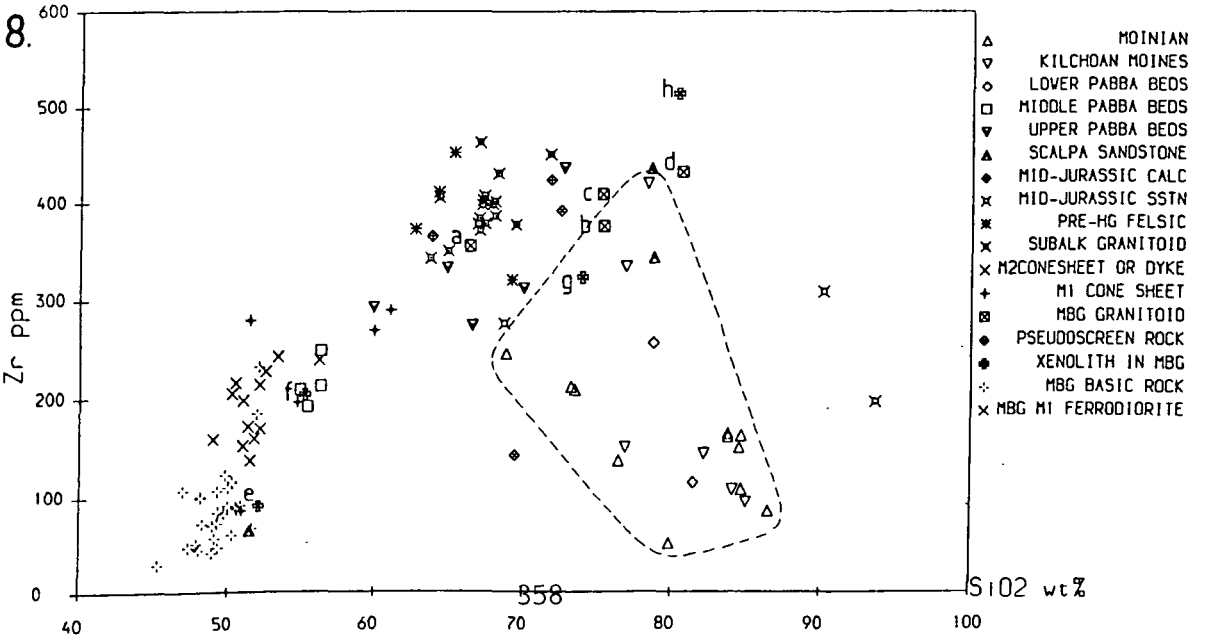
Zr ppm
SiO2 wt%
MOINIAN
KILCHOAN MOINES
LOWER PABBA BEDS
MIDDLE PABBA BEDS
UPPER PABBA BEDS
SCALPA SANDSTONE
MID-JURASSIC CALC
MID-JURASSIC SSTN
PRE-HG FELSIC
SUBALK GRANITOID
M2CONESHEET OR DYKE
M1 CONE SHEET
MBG GRANITOID
PSEUDOSCREEN ROCK
XENOLITH IN MBG
MBG BASIC ROCK
MBG M1 FERRODIORITE

9.

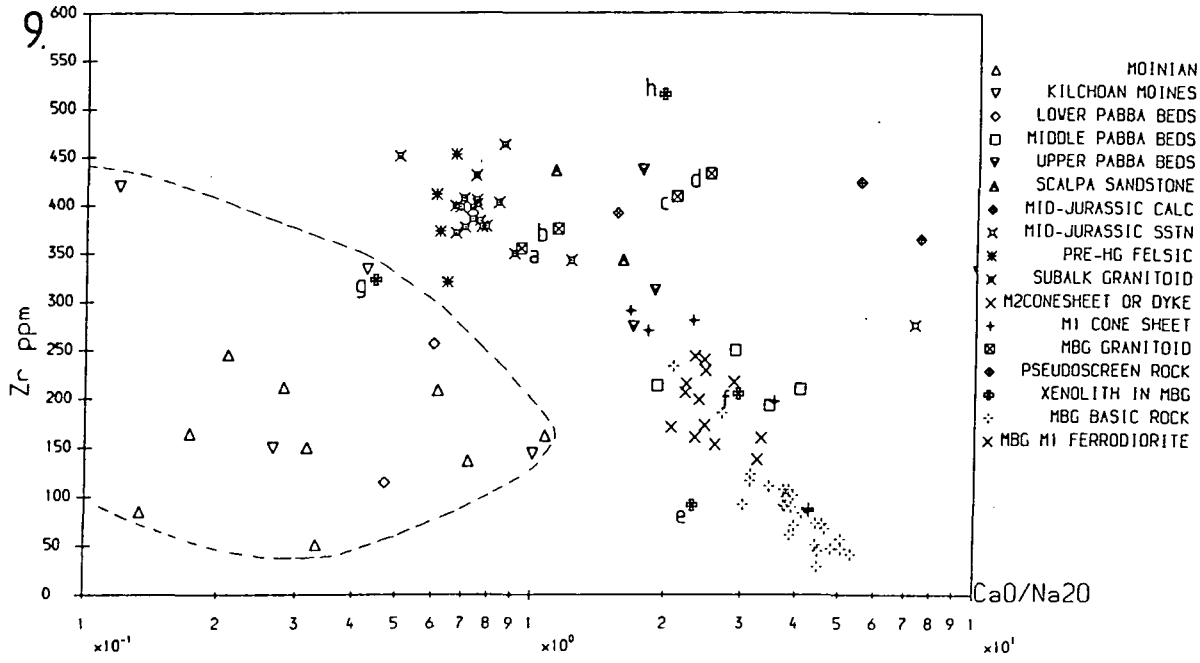
Zr ppm
CaO/Na2O
MOINIAN
KILCHOAN MOINES
LOWER PABBA BEDS
MIDDLE PABBA BEDS
UPPER PABBA BEDS
SCALPA SANDSTONE
MID-JURASSIC CALC
MID-JURASSIC SSTN
PRE-HG FELSIC
SUBALK GRANITOID
M2CONESHEET OR DYKE
M1 CONE SHEET
MBG GRANITOID
PSEUDOSCREEN ROCK
XENOLITH IN MBG
MBG BASIC ROCK
MBG M1 FERRODIORITE

10.

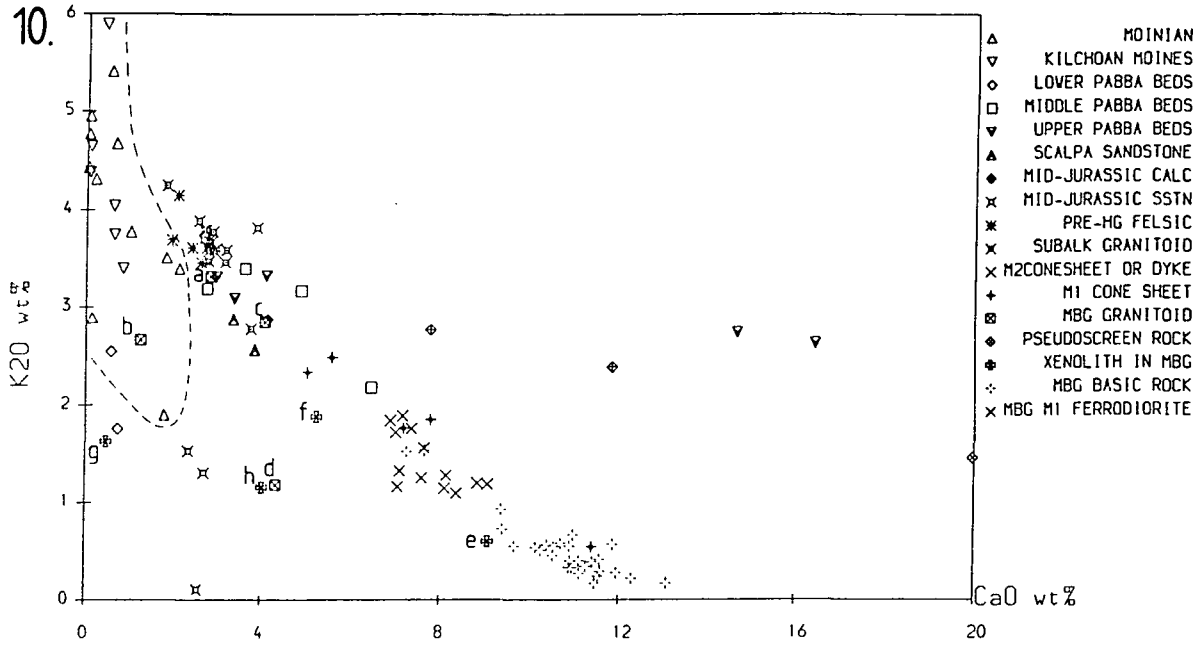
K2O wt%
CaO wt%
MOINIAN
KILCHOAN MOINES
LOWER PABBA BEDS
MIDDLE PABBA BEDS
UPPER PABBA BEDS
SCALPA SANDSTONE
MID-JURASSIC CALC
MID-JURASSIC SSTN
PRE-HG FELSIC
SUBALK GRANITOID
M2CONESHEET OR DYKE
M1 CONE SHEET
MBG GRANITOID
PSEUDOSCREEN ROCK
XENOLITH IN MBG
MBG BASIC ROCK
MBG M1 FERRODIORITE

11.

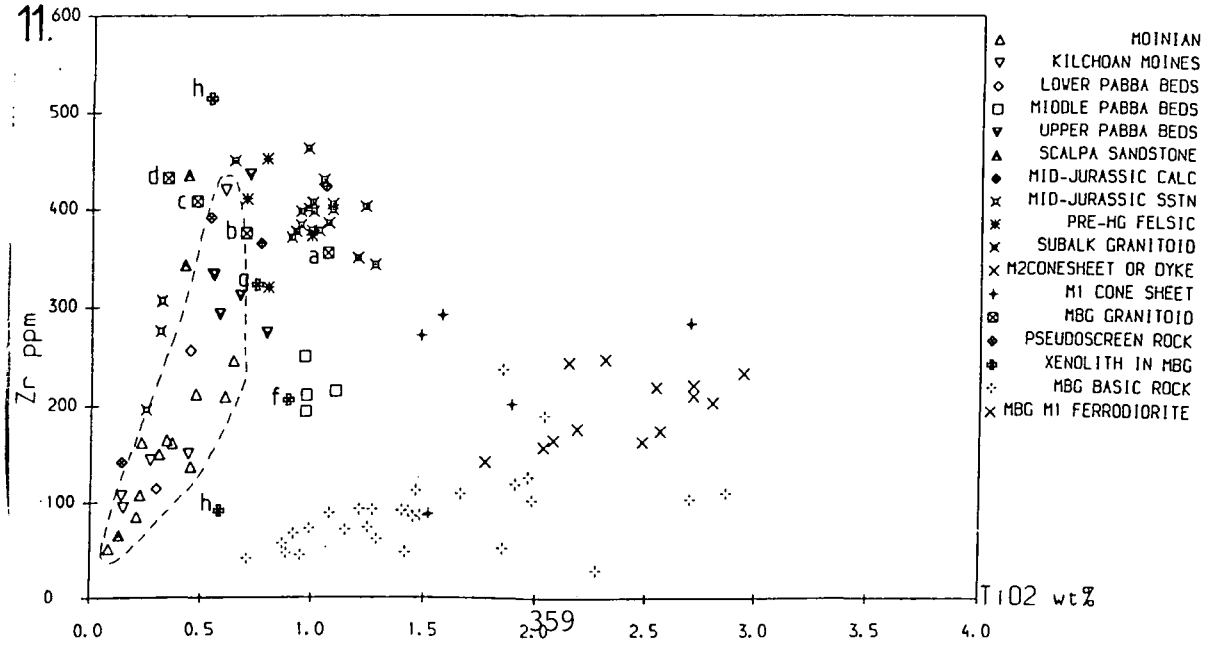
Zr ppm
TiO2 wt%
MOINIAN
KILCHOAN MOINES
LOWER PABBA BEDS
MIDDLE PABBA BEDS
UPPER PABBA BEDS
SCALPA SANDSTONE
MID-JURASSIC CALC
MID-JURASSIC SSTN
PRE-HG FELSIC
SUBALK GRANITOID
M2CONESHEET OR DYKE
M1 CONE SHEET
MBG GRANITOID
PSEUDOSCREEN ROCK
XENOLITH IN MBG
MBG BASIC ROCK
MBG M1 FERRODIORITE

12.

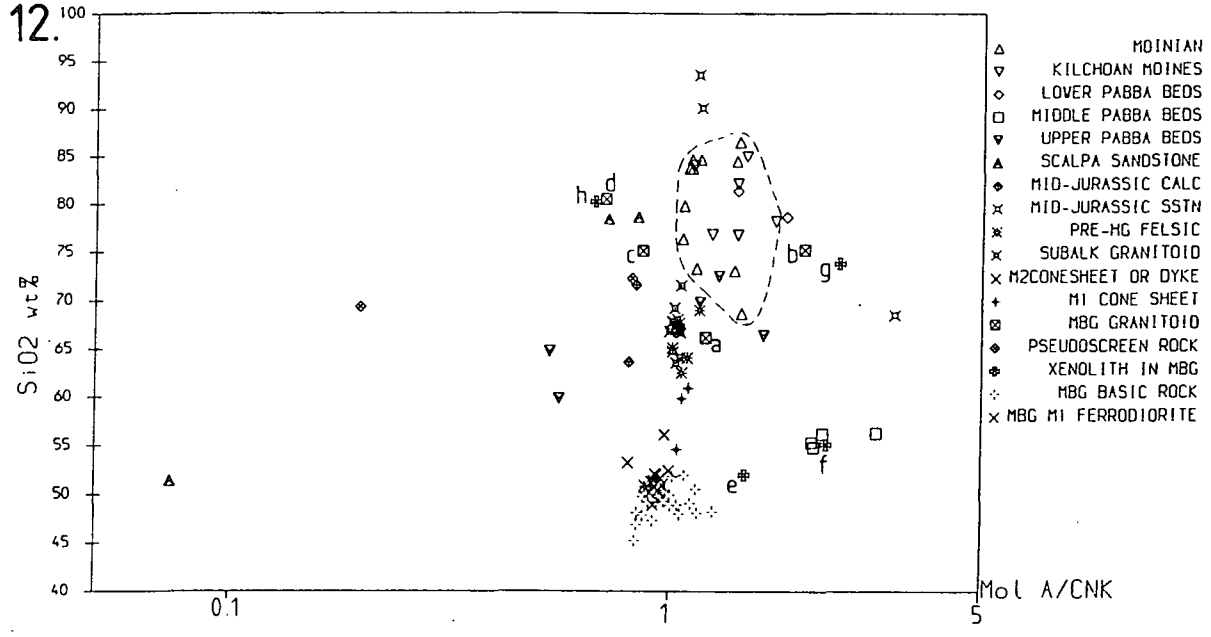
SiO2 wt%
100
95
90
85
80
75
70
65
60
55
50
45
40
0.1
1
5
Mol A/CNK
MOINIAN
KILCHOAN MOINES
LOWER PABBA BEDS
MIDDLE PABBA BEDS
UPPER PABBA BEDS
SCALPA SANDSTONE
MID-JURASSIC CALC
MID-JURASSIC SSTN
PRE-HG FELSIC
SUBALK GRANITOID
M2CONESHEET OR DYKE
M1 CONE SHEET
MBG GRANITOID
PSEUDOSCREEN ROCK
XENOLITH IN MBG
MBG BASIC ROCK
MBG M1 FERRODIORITE

13.

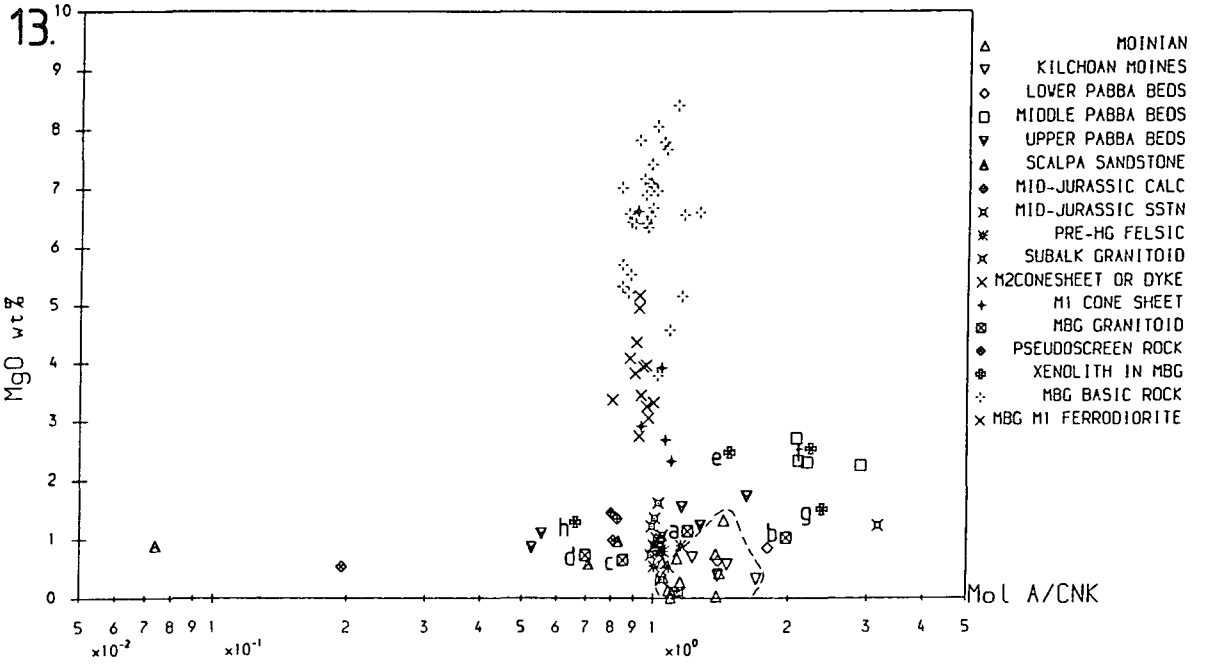
MgO wt%
10
9
8
7
6
5
4
3
2
1
0
5 6 7 8 9 1
×10⁻²
×10⁻¹
2 3 4 5 6 7 8 9 1
×10⁰
2 3 4 5
Mol A/CNK
MOINIAN
KILCHOAN MOINES
LOWER PABBA BEDS
MIDDLE PABBA BEDS
UPPER PABBA BEDS
SCALPA SANDSTONE
MID-JURASSIC CALC
MID-JURASSIC SSTN
PRE-HG FELSIC
SUBALK GRANITOID
M2CONESHEET OR DYKE
M1 CONE SHEET
MBG GRANITOID
PSEUDOSCREEN ROCK
XENOLITH IN MBG
MBG BASIC ROCK
MBG M1 FERRODIORITE

14.

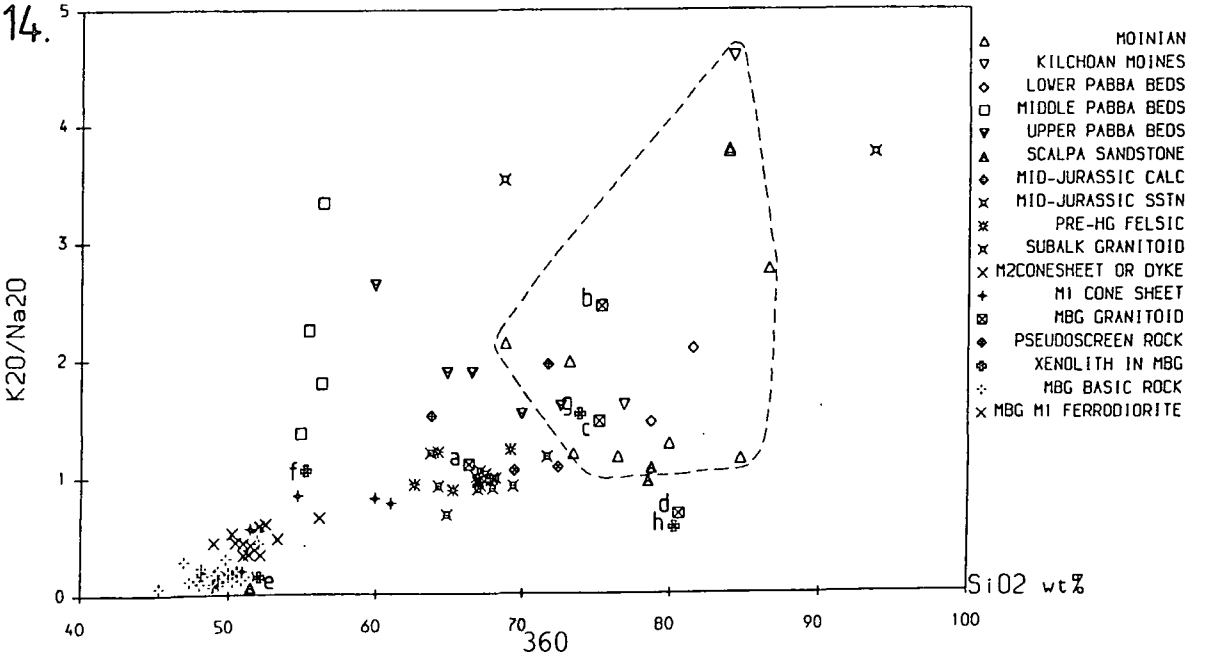
K2O/Na2O
5
4
3
2
1
0
40
50
60
70
80
90
100
360
SiO2 wt%
MOINIAN
KILCHOAN MOINES
LOWER PABBA BEDS
MIDDLE PABBA BEDS
UPPER PABBA BEDS
SCALPA SANDSTONE
MID-JURASSIC CALC
MID-JURASSIC SSTN
PRE-HG FELSIC
SUBALK GRANITOID
M2CONESHEET OR DYKE
M1 CONE SHEET
MBG GRANITOID
PSEUDOSCREEN ROCK
XENOLITH IN MBG
MBG BASIC ROCK
MBG M1 FERRODIORITE

15.

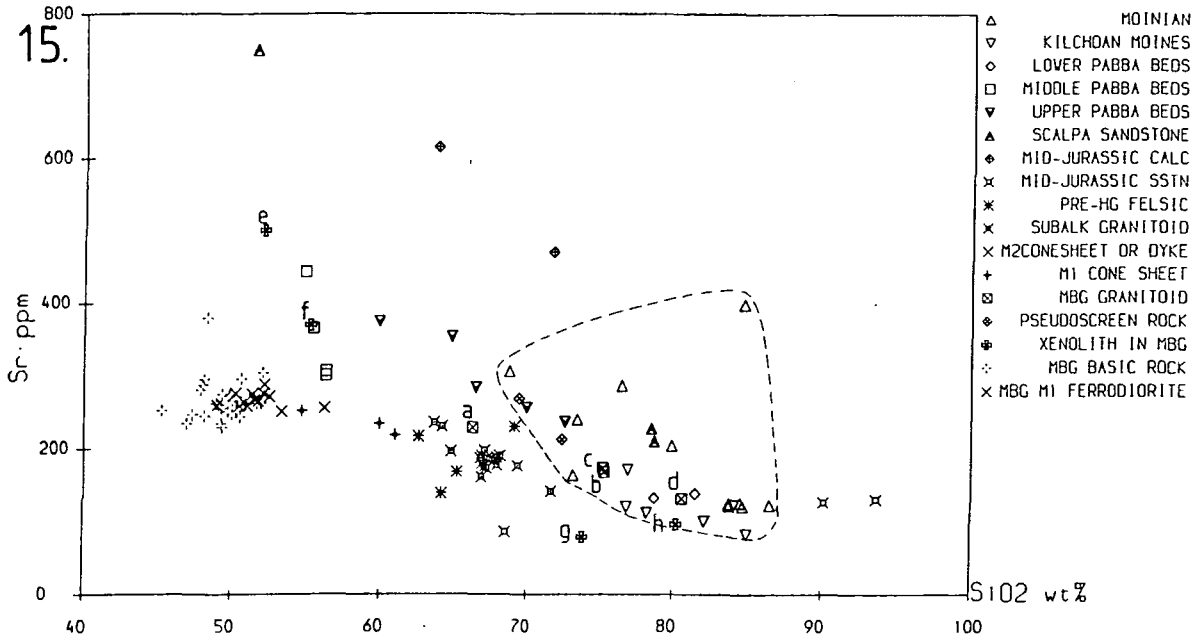
Sr ppm
SiO2 wt%
MOINIAN
KILCHOAN MOINES
LOWER PABBA BEDS
MIDDLE PABBA BEDS
UPPER PABBA BEDS
SCALPA SANDSTONE
MID-JURASSIC CALC
MID-JURASSIC SSTN
PRE-HG FELSIC
SUBALK GRANITOID
M2CONESHEET OR DYKE
M1 CONE SHEET
MBG GRANITOID
PSEUDOSCREEN ROCK
XENOLITH IN MBG
MBG BASIC ROCK
MBG M1 FERRODIORITE

16.

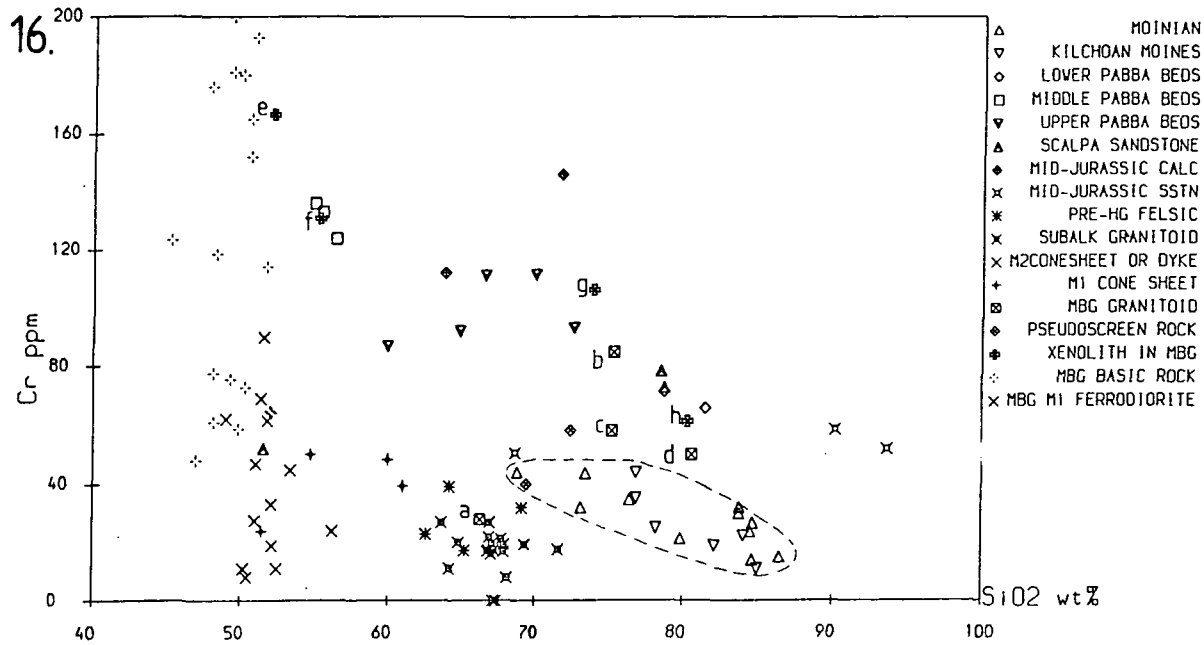
Cr ppm
SiO2 wt%
MOINIAN
KILCHOAN MOINES
LOWER PABBA BEDS
MIDDLE PABBA BEDS
UPPER PABBA BEDS
SCALPA SANDSTONE
MID-JURASSIC CALC
MID-JURASSIC SSTN
PRE-HG FELSIC
SUBALK GRANITOID
M2CONESHEET OR DYKE
M1 CONE SHEET
MBG GRANITOID
PSEUDOSCREEN ROCK
XENOLITH IN MBG
MBG BASIC ROCK
MBG M1 FERRODIORITE

17.

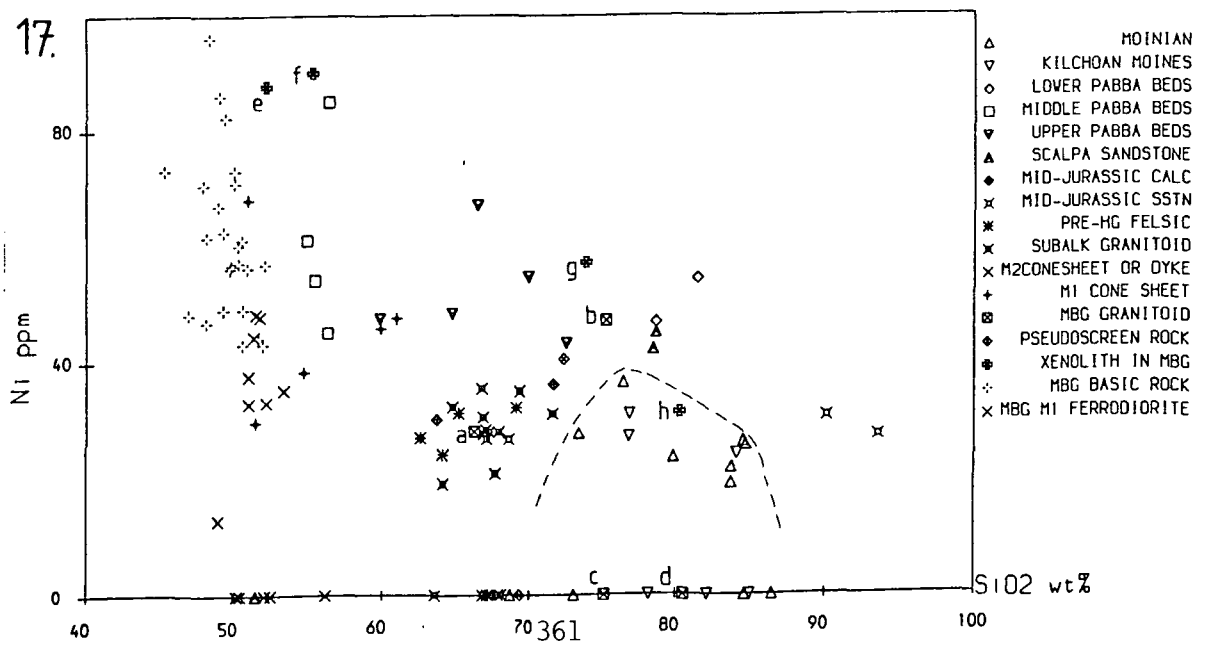
Ni ppm
SiO2 wt%
MOINIAN
KILCHOAN MOINES
LOWER PABBA BEDS
MIDDLE PABBA BEDS
UPPER PABBA BEDS
SCALPA SANDSTONE
MID-JURASSIC CALC
MID-JURASSIC SSTN
PRE-HG FELSIC
SUBALK GRANITOID
M2CONESHEET OR DYKE
M1 CONE SHEET
MBG GRANITOID
PSEUDOSCREEN ROCK
XENOLITH IN MBG
MBG BASIC ROCK
MBG M1 FERRODIORITE

Zr/TiO_2, which are similar to those of the sediments and subalkaline granitoids (see Figs. 4.12.13 and 4.12.11).

These arguments demonstrate that neither the Moinian sediments nor the basic to intermediate Tertiary magmas are suitable endmembers with which to generate the anomalous microgranitoids by a simple magma - mixing process. They do not, however, exclude the involvement of either rock type if the mixing or contamination process was followed by crystal fractionation. However, formation of these rocks by fractionation of a contaminated mafic magma seems an unlikely process for several reasons. Firstly, the peraluminous rocks could only be produced by fractional crystallisation of a subaluminous basic magma if amphibole was present in the fractionating assemblage (Ellis & Thompson 1986): there is no evidence to suggest that amphibole was a liquidus phase in these rocks, nor of the high P_{H_2O} needed to stabilise amphibole on the liquidus. Secondly, all are characterised by the presence of numerous refractory inclusions which correlate closely with the composition on the host magma: quartzite in the diopside microgranites; quartzite, orthopyroxene - quartz rock and magnetite - cordierite - hercynite rock in 183D1; quartzite in 267/1. These appear to be residual or restitic in origin: the retention of this material implies that separation of magmatic crystals is unlikely to have occurred. Finally, 267/1 and the diopside microgranites have certain compositional features inconsistent with an origin by crystal fractionation from mafic magma: high Cr (Fig. 4.12.16) and Sr, and Si contents, in 42D1 at least, which are probably in excess of the granitic minimum composition which represents the maximum possible silica content of a fractionated melt (see Appendix 1 for discussion of the uncertainties in the SiO_2 data).

4.2.3.4. Geochemistry and Petrogenesis of the Anomalous Granitoids and Country Rock Xenoliths. 2: Petrogenesis of each of the Granitoid Types and of the Xenoliths.

The other genetic models listed above seem to apply, to a greater or lesser extent, to particular anomalous granitoid compositions and it is therefore convenient to consider these in turn.

Origin of the Diopside Microgranites. The two diopside microgranite analyses both lie close to the analyses of silica - rich metacalcareous sandstones from the Middle Liassic Scalpa Sandstone in all the plots in Fig. 4.12. Given that further analyses of rocks from this unit would, by analogy with the other sedimentary units for which a larger number of analyses are available (e.g. the Upper

Pabba Beds), reveal more compositional variation, 42D1 and 42A4 probably lie entirely within the compositional field occupied by this unit. At the same time, the combination of high SiO_2 (c. 80%) with low Sr, low Al_2O_3 and relatively high CaO sets them apart from all the other samples analysed except for residual blocks of more Ca - rich, Si - poor refractory rocks which also originate from the Duin Bhain pseudoscreen ('pseudoscreen rocks' in Fig. 4.12). It is therefore concluded that the diopside microgranites are anatectic melts produced entirely by melting of Scalpa Sandstone, without involvement of other Mesozoic lithologies or of subalkaline granitoid magmas. This latter conclusion is supported by the position of these rocks in Fig. 4.5, where they plot in the high La/Yb, low La field ocupied by the Mesozoic country rocks. The conclusion that the diopside microgranites represent fused Scalpa Sandstone is also suggested by the structural and stratigraphic arguments for the original position of the rocks exposed in the pseudoscreen which were outlined in section 3.2.3.

Origins of the Peraluminous Granitoids. The two anomalous granitoids analysed differ in many respects and are dealt with separately here.

267/1 differs from each and every group of sediments plotted in Fig. 4.12 in its abundance of at least one element. However, it shows a marked tendency to plot either with the two analysed samples of the Lower Pabba Beds and the xenolith 140/3, or on a linear array along which the other three samples are also spread (for example, the plots of TiO_2, Zr and Cr vs. SiO_2). Inspection of the plots in Fig. 4.12 indicates that it shows no such consistent relationship with any of the other groups of Jurassic sediments, two of which, the Middle and Upper Pabba Beds, also form close clusters or linear arrays, according to the elements plotted in individual diagrams. The other units within the Jurassic sedimentary sequence are not represented by a sufficient number of analyses to form such arrays but mainly plot well away from 267/1.

The occurrence of such trends in the bulk chemical composition of sediments is explained by the petrographic observation that most clastic sediments are mixtures, in varying proportions, of a small number of detrital and authigenic components, each with its own characteristic composition (this forms the basis of the petrographic classification of clastic sediments: see, for example, Pettijohn et al. 1973; Folk 1974). In the case of the rocks analysed in the present work, these are: quartz, feldspar and quartzofeldspathic lithic clasts, which tend to be coarser than the other detrital grains and are therefore concentrated in the coarser - grained sediments; detrital heavy minerals, such as

zircon and Ti minerals which tend to be relatively fine - grained and are therefore concentrated in semi - pelitic rocks (see Chapter 2); clay minerals, which are rich in some or all of K, Mg and Al, and in transition metals (such as Fe, Cr, Ni); authigenic Fe minerals, phosphates, and organic material containing certain adsorbed transition elements; carbonates. 267/1 can be interpreted in these terms as a mixture of SiO_2 - rich sandstones such as the analysed Lower Pabba Beds samples, and a K, Al and Zr - rich, Na and Mg poor sediment which is also characterised by moderately high contents of Si, Fe, Cr, Ti, P and Ca. The general features of this mixture are those of a semipelite or siltstone, with significant quartz - rich detrital, fine - grained heavy mineral detrital, and clay - rich components. This sediment shows several characteristic features of the Jurassic sequence, in particular its contents of Ti, Ca and Cr, which are markedly higher than those of the Moinian rocks. It therefore seems most likely that 267/1 is the product of melting of siltstone and sandstone units within the lower Pabba Beds. According to Richey et al. (1930) the Pabba Beds in the Kilchoan Bay area contain a thick (30m+) basal siltstone/ shale sequence which passes up into a relatively thin (less than 10m) sandstone unit, below aluminous shales which were assigned in Chapter 2 to the Middle Pabba Beds. Whilst the thickness of the sandstone / siltstone units in the An Acairseid – Dubh Chreag area is very much greater than that of Richey et al.'s sandstone, there is no reason to suppose that less quartz - rich, semipelitic units are not present below the surface within the Lower Pabba Beds.

In contrast to the other anomalous granitoids, 183D1 shows some petrographic evidence for magma mixing, involving peraluminous magmas and porphyritic subalkaline magmas. This takes the form of abundant andesine plagioclase porphyrocrysts visible in thin section along with granular hornfels inclusions (see above and section 3.2.5.2). Similar large feldspar crystals are a minor component of the more Ca -rich Jurassic sandstones in Ardnamurchan but have not been found in sections of peraluminous rocks. Apart from its higher A/CNK 183D1 is compositionally quite similar to the subalkaline granitoids and distinct from the majority of analysed Jurassic sediments, including the rocks in the adjacent outcrops (see Fig. 4.12). This extends to the REE abundances of 183D1, which has low La/Yb (see Fig. 4.5 and Fig. 4.13) like the subalkaline granitoids and unlike any known Jurassic sediment. The adjacent Jurassic rocks are Al - rich, Si - poor pelites of the Middle Pabba Beds in the main wall of the intrusion and Ca - rich members of the Upper Pabba Beds in the downfaulted block to the north. Other members of the Upper Pabba Beds, which outcrop in other sectors of the contact, are broadly similar to 183D1 but have very much higher Cr and Ni contents.

Fig. 4.13. Chondrite - normalised element plot comparing 183D1 with subalkaline granitoid rocks associated with the MBG.

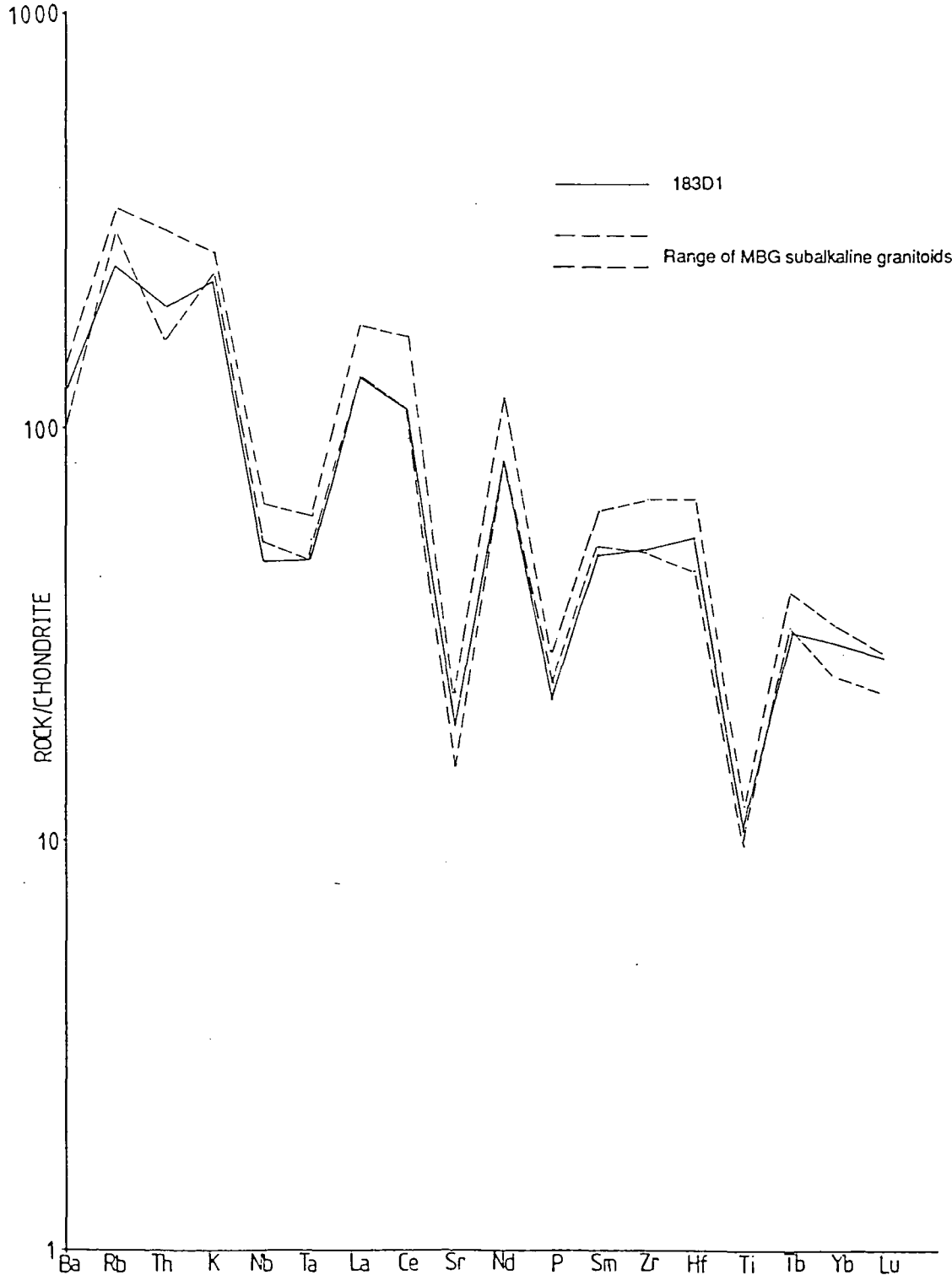

Furthermore, beds or nodules corresponding to the refractory Fe and Al rich inclusions which occur in 183D1 do not occur in the Upper Pabba Beds. Compositionally similar bodies, although with different mineral assemblages (cordierite + magnetite + plag ± Al-silicate(?)) as a result of different metamorphic conditions, do occur in medium - grade Middle Pabba Beds hornfelses at distances of a few hundred metres from the contact (see section 5.2). However, the Middle Pabba beds as a whole are too Al - rich and too refractory overall to be the other component of 183D1 (as well as having too - high contents of Ni and Cr; see Fig. 4.12.16 and .17). Consequently, it again seems necessary to postulate the presence of a micaceous (and hence peraluminous) siltstone unit in the wall of the MBG below the present level of exposure to account for the composition of this granitoid. As noted above, such rocks do occur in the Moinian sequence: however, they do not contain the observed Fe, Al - rich refractory inclusions. By elimination of these alternatives, the source of the sedimentary component of 183D1 is most likely to be part of the Lower Pabba Beds.

Origin of the Country Rock Xenoliths.

The four xenoliths analysed can be assigned to particular country rock units with a fair degree of confidence. They tend, however, to plot towards or beyond the refractory end of the range of compositions within each analysed group of rocks. One interpretation of this is that formation of the xenolith swarms has involved the separation of the most refractory lithologies from each country rock unit from the less refractory rocks. Possible mechanisms by which this could occur include physical separation by sinking of the denser (because still largely solid) xenoliths through the less dense anatectic melts and into the mafic magmas and/or assimilation of the less refractory material, following melting, in the mafic or hybrid rocks which enclose the xenoliths. The latter implies that the hosts to the xenolith swarms should be contaminated by the less - refractory material, with implications for the composition of the host rocks that are examined in sections 4.3 and 4.4.

Alternatively, the composition of the xenoliths could potentially have been modified by filter - pressing and explulsion of interstitial melts from the xenoliths. Although some melting and melt movement is implied by the cordierite - norite veins in 274/1 this may have involved particular fusible bands within these xenoliths rather than expulsion of low - degree partial melts from the whole of the rock. Pervasive melt movement in these xenoliths would be expected to either blur, or be obstructed by, the compositional banding observed at outcrop (Plate 3.39). Finally, filter pressing within

these xenoliths could only occur as part of a pervasive large - scale filter - pressing throughout the host rocks, after solidification of the latter. As will be seen in section 4.3, the compositions of the basic rocks show that this has not occurred. In addition, the composition of the xenoliths may have been modified by diffusive exchange between the xenoliths and their host magmas during M1, for example by selective loss of alkalis from the xenoliths to produce the observed alkali - poor refractory compositions. In the absence of a statistically significant number of analyses covering the xenoliths and the entire range of country rock compositions, it is not possible to exclude this using the chemical data. However, the preservation of the primary compositional banding in the xenoliths at An Acairseid (Plate 3.39) and the generally sharp xenolith margins, indicates that any such diffusive exchange process did not produce observable mineralogical effects. It is therefore assumed in the following discussion that any diffusive exchange which has occurred has not significantly modified the composition of the xenoliths.

274/1 and 140/3 (e and f in Fig. 4.12) have very distinctive low SiO_2 and high Al, A/CNK, Fe, Mg, Cr and Ni, features which are shared by the pelites of the Middle Pabba Beds and by no other analysed country rock lithology. Although 274/1 in particular is richer in Ca and poorer in alkalis, giving it a more refractory composition than even the analysed Middle Pabba Beds samples, these xenoliths are best explained as Middle Pabba Beds rocks. If this identification is correct, the xenoliths at 274 must have moved down from their original position since they now occur adjacent to outcrops of the uppermost Lower Pabba Beds. The position of 140/3 relative to the Middle Pabba Beds in the western wall of the MBG magma chamber is less certain but if the Port Min - Eilean nan Seachd Seisrichean fault is a normal fault (see section 3.2.4) then the occurrence at outcrop of the base of the Middle Pabba Beds on Druim na Cloise implies that 140/3 is also situated below its original position.

150/1. This xenolith has an analogous compositional relationship to the Lower Pabba Beds samples and to 267/1 as that of 274/1 to the Middle Pabba Beds. It has higher Fe and Ca and lower alkalis, and is therefore more refractory, but is otherwise similar to the Lower Pabba Beds rocks analysed. Its position relative to these is unclear, because the western wall of the MBG has not been preserved.

20/1WR. This xenolith (which includes a small amount of hybrid vein material) generally lies in the same compositional field as the Scalpa Sandstone and the diopside microgranites. Its occurrence in

the postulated westward extension of the downfaulted block which is also believed to form the Duin Bhain pseudoscreen also suggests that it is probably a relatively refractory component of the Scalpa Sandstone. The compositional similarities between this rock and the diopside microgranite 42A4 is surprising in view of the much lower degree of melting in the xenolith, and may be an artefact of the presence of the (silica - poor) veins, rather than reflecting markedly different peak temperatures between the two.

4.2.3.5 Conclusions: Implications of the petrogenesis of the Anomalous Granitoids and Xenoliths for processes at the wall of the MBG magma chamber.

Although they are volumetrically insignificant these rocks are important from the point of view of an understanding of the Marginal Border Group magma chamber in that they represent evidence for melting of country rocks at or near the present level of exposure towards the end of M1. The diopside microgranites in the Duin Bhain pseudoscreen appear to be more or less in the position in which they initially melted, as they are associated with refractory lithologies which also appear to be part of the Scalpa Sandstone. In contrast, the peraluminous microgranitoids which outcrop between An Acairseid and the western end of Druim na Gearr Leacainn are best interpreted as being wholly (267/1) or partly (183D1) derived from siltstones and possibly sandstones of the Lower Pabba beds, a few tens to a few hundreds of metres **below** their present position. Like the subalkaline granitoid magmas, the peraluminous magmas represented by these rocks apppear to have been migrating up the wall of the magma chamber towards the end of M1. None of the anomalous granitoids appears to have undergone post - melting fractionation and, apart from 183D1 which appears to contain a large subalkaline granitoid component, appear to be pure country rock magmas which have not been involved in magma mixing with normal Tertiary magmas. There is no Moinian component in any of these rocks.

The country rock xenoliths sampled correspond to particular rock units in the country rock sequence and appear to be composed of the more refractory lithologies from within those units. They appear to occur below the position of their parent rock units in the wall rock sequence, where this can be established, suggesting partial physical separation of fusible lithologies (which flowed upwards along the wall) and refractory lithologies (which sank, being largely solid and hence denser, quite apart from any compositional control on density) on melting and mobilisation of the former.

4.2.4. Rheomorphic Breccias.

The rheomorphic breccias which occur around the periphery of the Marginal Border Group differ from those which have been describd from around other intrusions in a number of important respects. Firstly, they occur in a number of discrete small intrusions, of the same age as the high - grade metamorphism associated with the intrusion around which they occur, rather than forming a semi - continuous sheath separating the country rocks from the intrusion. This latter setting is that in which the type examples of rheomorphic breccias occur, around mafic and ultramafic intrusions of the Monteregian province (Philpotts 1970), and around the Rhum complex, the other intrusive centre from which they have been described in detail in the British Tertiary Volcanic Province (Greenwood 1987). Secondly, there is no petrographic or field evidence to suggest mixing of basic or intermediate magmas from the interior of the MBG magma chamber with anatectic melts to form the rheomorphic breccias around the Hypersthene Gabbro. In contrast, shattered mafic pillows and other mafic rock fragments are important components of the Rhum 'intrusion breccias' (Greenwood 1987) whilst Philpotts (1970) considers that the matrix compositions in the Monteregian rheomorphic breccias show a continuous gradation from near - gabbroic rocks at their inner margin, through hybrid compositions, to anatectic rocks at their outer margins, implying a continuous mixing process involving crustal melts and mantle - derived magmas.

This section will consider, firstly, geochemical evidence for the origin of these rocks, and in particular whether or not the matrix contains magma from the earlier Tertiary granitic intrusions and/or a component from the interior of the MBG magma chamber. Secondly, the development of the unusual textures and structures in the quartzitic blocks within the breccias, described in section 3.2.2, will be considered.

4.2.4.1. Composition of the Rheomorphic Breccias.

The characteristic feature of all the rheomorphic breccia outcrops is the presence of rounded to subangular blocks of quartzitic, partially fused and quenched rock. These form between 15% and 60% of the rock by volume and range from almost pure metaquartzite, through 'sponge - textured' blocks with numerous rounded pockets of quenched melt, to blocks on the point of disaggregation, with numerous interconnected melt pockets and as little as 50% of the block composed of residual

quartz. The whole range of block compositions, with 0 to 50% quenched melt, are often present within a single outcrop. In addition to these, small numbers of very much smaller (less than 3mm across) refractory inclusions are present within some thin sections of rheomorphic breccia. These include diffuse fine - grained granular clinopyroxene - rich inclusions in the matrix of the breccias close to the contact with the MBG at Glendrian Bay, at Grid Ref. 45957028, and similar fine - grained aggregates of opaques + clinopyroxene ± plagioclase ± quartz, some with clinopyroxene - rich rims, which occur in the rheomorphic breccia intrusions on the eastern side of Hill 90 (Plate 4.8). These appear to represent the refractory remnants of, respectively, impure calcareous and ferriginous nodules. The quenched melt matrixes or groundmasses of almost all of the rheomorphic breccias in the Glendrian Bay area also contain anhedral feldspar porphyrocrysts which are choked with quartz (and, rarely, opaque and/or clinopyroxene) inclusions or intergrown with poikiloblastic or 'micropoikilitic' (Lofgren 1970) quartz grains (Plate 4.9). These bear a close resemblance to the feldspar grains within the quartz - rich residual blocks (Plates 3.16 and 3.17, section 3.2.3; also see below, section 4.2.4.2). Although they also bear some resemblance to the rare very fine - grained granular optically continuous feldspar aggregates which occur in some of the subalkaline M2 felsites (type 4 of section 4.2.2.2) the more common solid or sieve - textured plagioclase porphyrocrysts found in those rocks are entirely absent from the rheomorphic breccias, except in a thin section which cuts the breccia - M1 microgranodiorite contact (i.e. within a few millimetres of the contact).

The devitrified or microgranophyric groundmass of the rheomorphic breccias shows wide petrographic variation between samples, but this cannot be related to addition of a basic or intermediate igneous component. In all but one of the rheomorphic breccias sampled in the Glendrian Bay area the groundmass is almost entirely composed of intergrown quartz and alkali feldspar (discrete plagioclase grains may also be present but cannot be identified positively because of the extremely fine grain size of the intergrowths). The minor accessory minerals present in the matrix are pyroxene(s), now largely altered to green amphibole, opaques and zircon. Some grains of the latter contain distinct rounded residual cores. Apart from rare tridymite needles, now pseudomorphed by poikiloblastic quartz, no distinct quench phases are present in these rocks.

A very different matrix occurs in rheomorphic breccia outcrops on the north - western side of Hill 90 (field loc. 184, Grid Ref. 46087018). This contains no residual plagioclase or pyroxene at all,

Plate 4.8. Granular residual inclusion in rheomorphic breccia intrusion, east side of Hill 90, Glendrian Bay. Inclusion composed of opaques + clinopyroxene + plagioclase + quartz, probably derived from ferriginous or calcareous units in the parent sediemnts. Note presence of quartz - rich and augite + opaques - rich joint - like microveins which have been annealed by later metamorphism (either M2 or associated with the Great Eucrite to the south). PPL, FOV 3.5mm.

Plate 4.9. Very fine - grained negative sieve - textured plagioclase porphyrocryst in rheomorphic breccia matrix, sample 47C2. The feldspar is in extinction and is highlighted by the contrast with the interstitial - micropoikilitic feldspar with which the quartz is intergrown. Compare with Plate 4.5B. PPL, FOV 1.5mm.

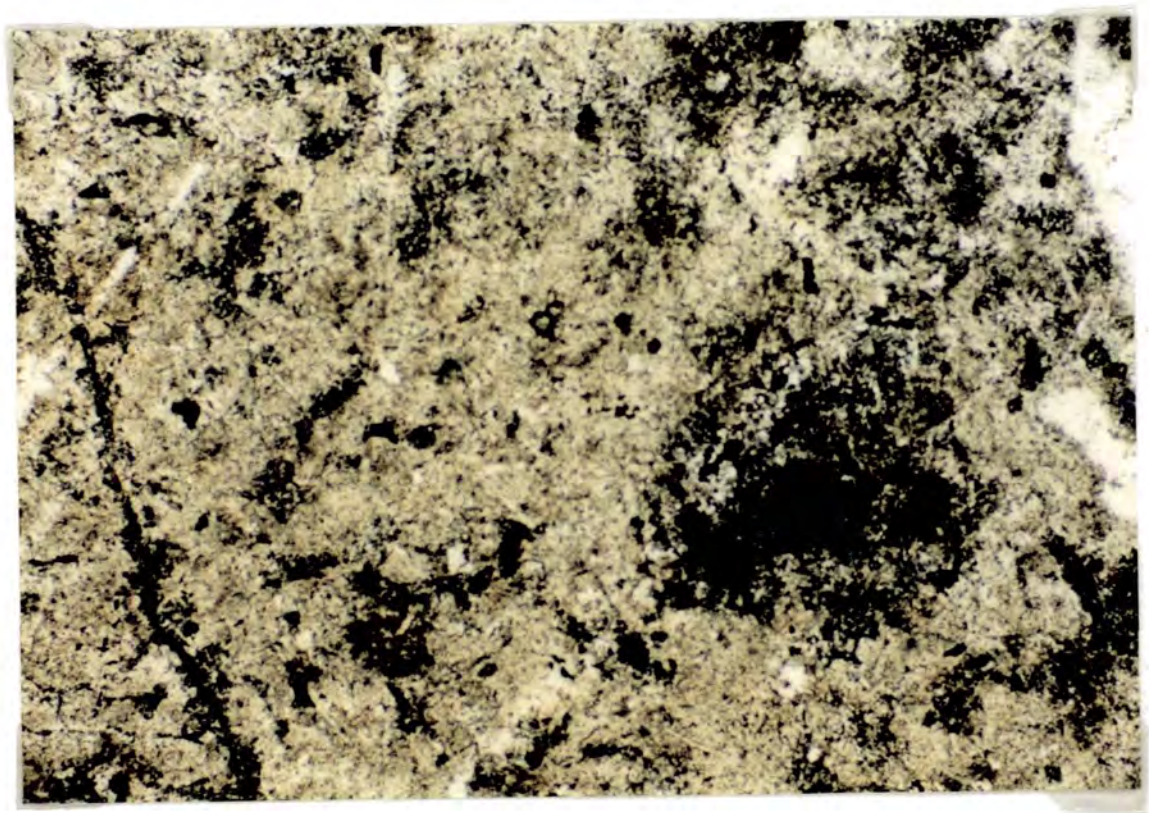

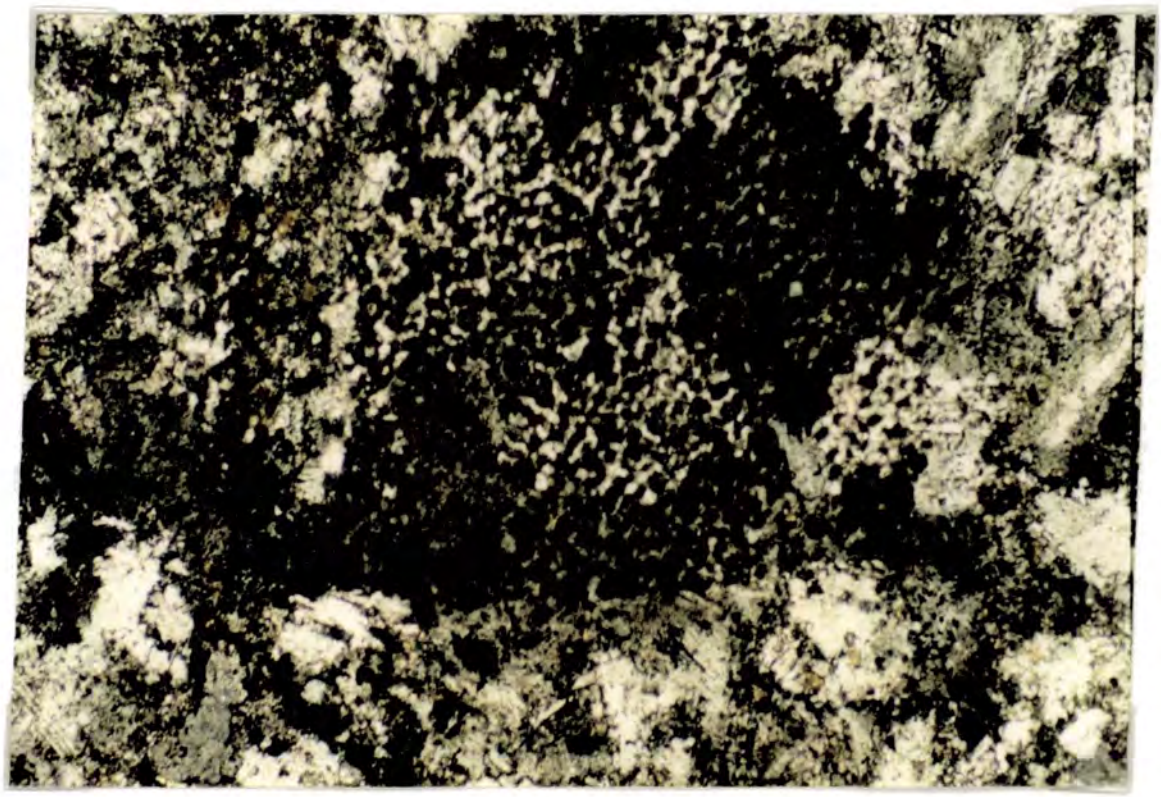

but contains prominent quench needles and hollow prisms of tridymite (inverted to quartz), calcic plagioclase and orthopyroxene. The latter is generally very Ca - poor, although slightly more Ca - rich rims are present on some of the grains (Fig. 4.14). The lack of clinopyroxene and abundance of quench tridymite, opx and calcic plagioclase in this rock point to a source rock for the matrix which is alkali - poor, silica and alumina rich, and has a low Ca/Al ratio relative to the other breccia matrixes in the Glendrian Bay area. The latter feature and the high silica activity point to a slightly calcareous pelitic or semipelitic source rock rather than to the presence of a basic igneous component in the matrix. Samples of this rock were not collected for bulk analysis but analyses of the residual devitrified glass which makes up the rest of the matrix are discussed in Chapter 5 (see Table 5.2). The high A/CNK of this material also points to a semipelitic source rock.

A second unusual rheomorphic breccia matrix is that in the outcrops at field location 240, at the south - eastern end of the Druim na Gearr Leacainn ridge (see section 3.2.5.3). The lack of quench tridymite, except as fringes around some of the melt pockets in the residual quartzite blocks, and the abundance of quench plagioclase point to a calc - pelitic or an anatectic - basic hybrid matrix composition. The former interpretation is supported by the occurrence of similar quenched melts in the pores of the sponge - textured blocks, but it was not possible to obtain probe analyses of this material owing to the relatively coarse grain size of the quench plagioclase crystals.

The petrographic evidence therefore suggests that the range in matrix compositions, although due solely to variation in the composition of the fusible component of the source rocks (with the possible exception of the breccia at loc. 240), is even greater than that apparent from the geochemical data presented in Fig. 4.15. The rheomorphic breccia samples in these plots are identified individually. as follows:

a: 47AW: Whole - rock sample, Glendrian Bay

b: 47AM: Matrix material hand picked from a split of 47AW

c: 47AR: Residual block material from a split of 47AW

d: 47U: Residual block - poor sample, Glendrian Bay

e: 267/3: Hydrothermally altered and recrystallised rheomorphic breccia, An Acairseid

Analyses b and d are of particular interest as samples of the matrix material, although they do contain a small amount of residual quartzitic material in the shape of rounded microclasts produced

Fig. 4.14. Probe analyses of quench crystals of plagioclase and orthopyroxene, 184.

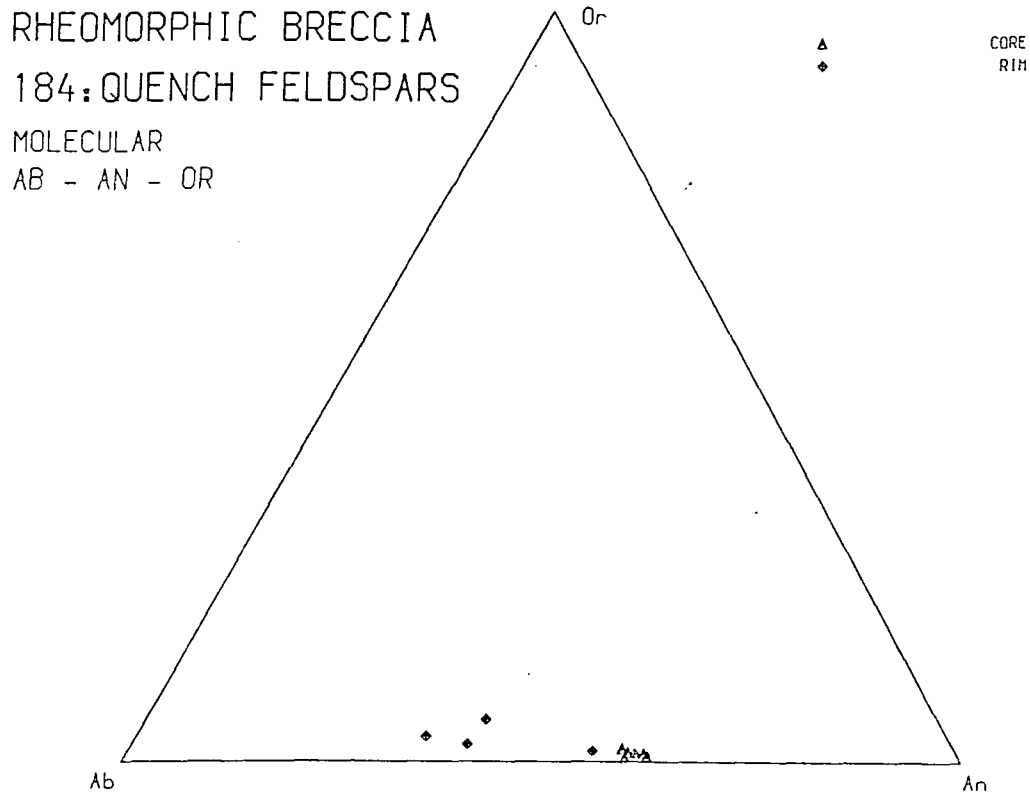

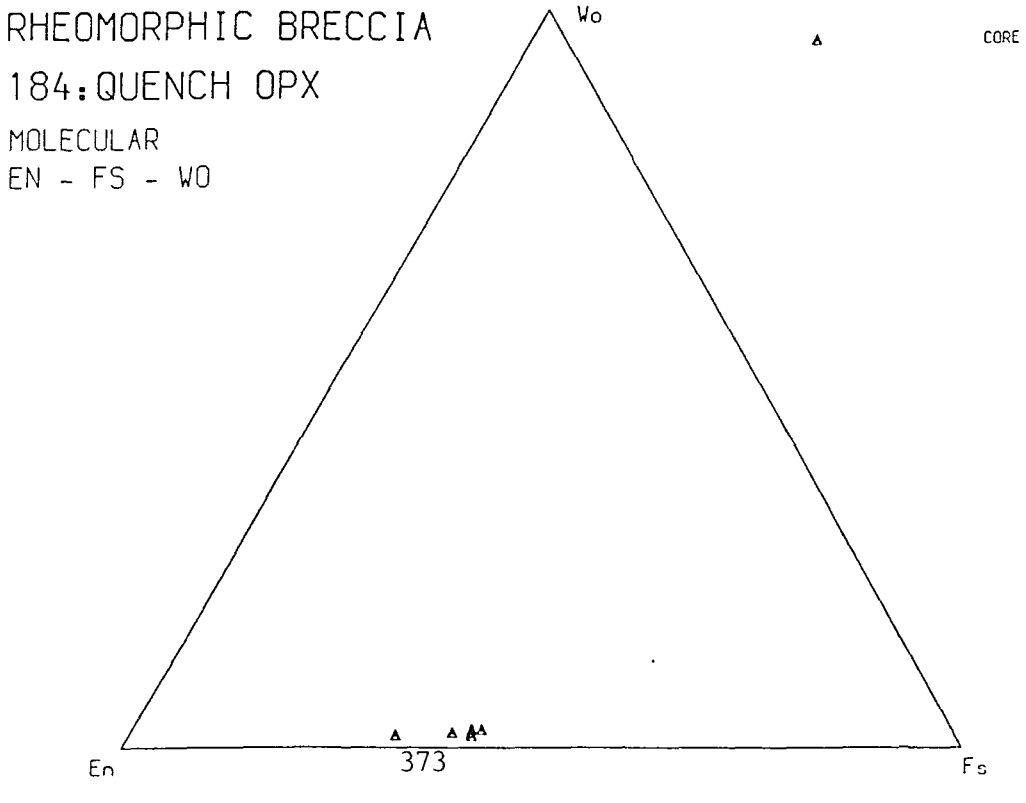

Fig. 4.15. Variation diagrams showing compositional features of the rheomorphic breccias used to determine the nature of the matrix and identify the protoliths of these rocks (see text for discussion). Individually labelled samples identified in text.

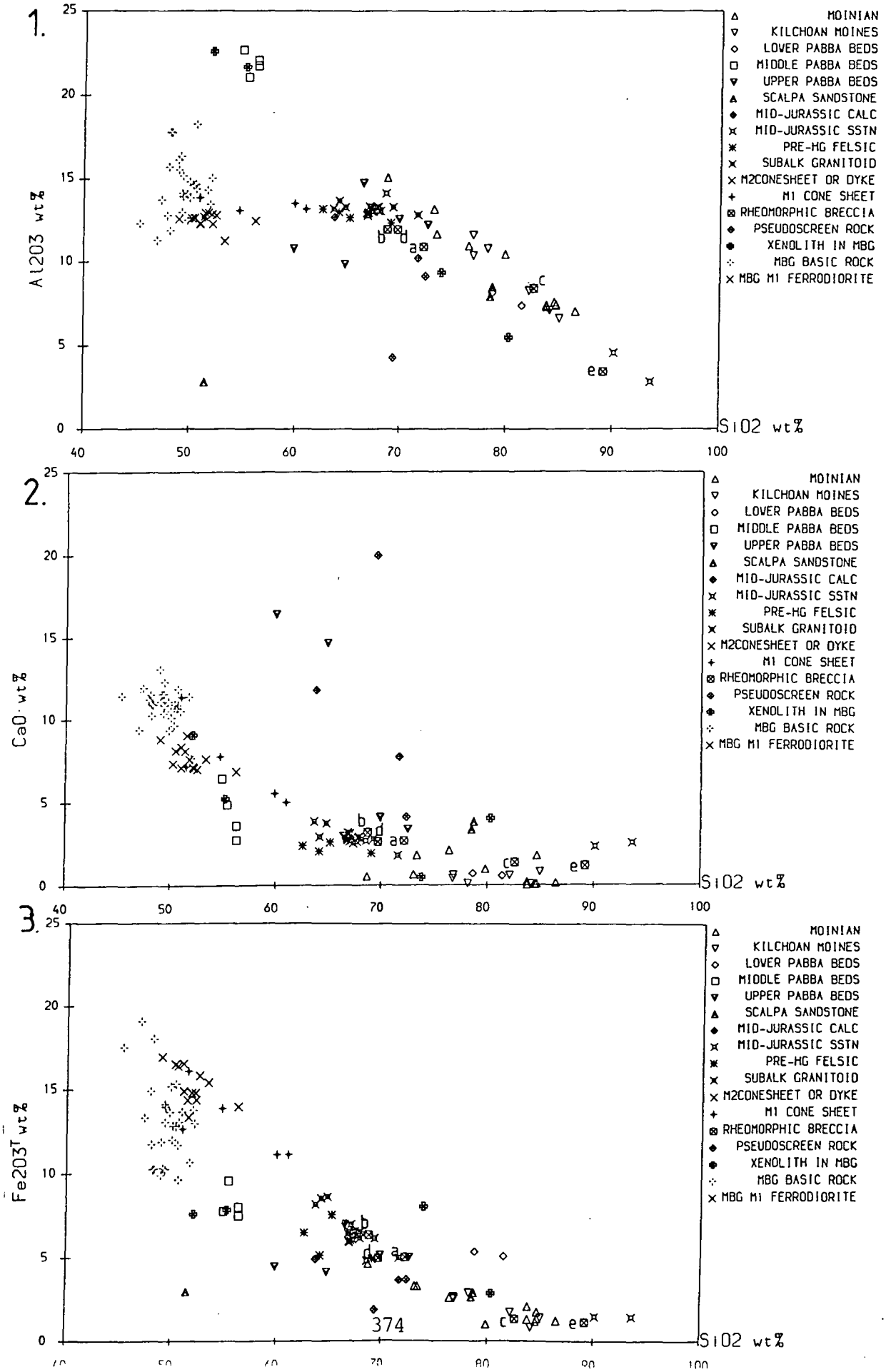

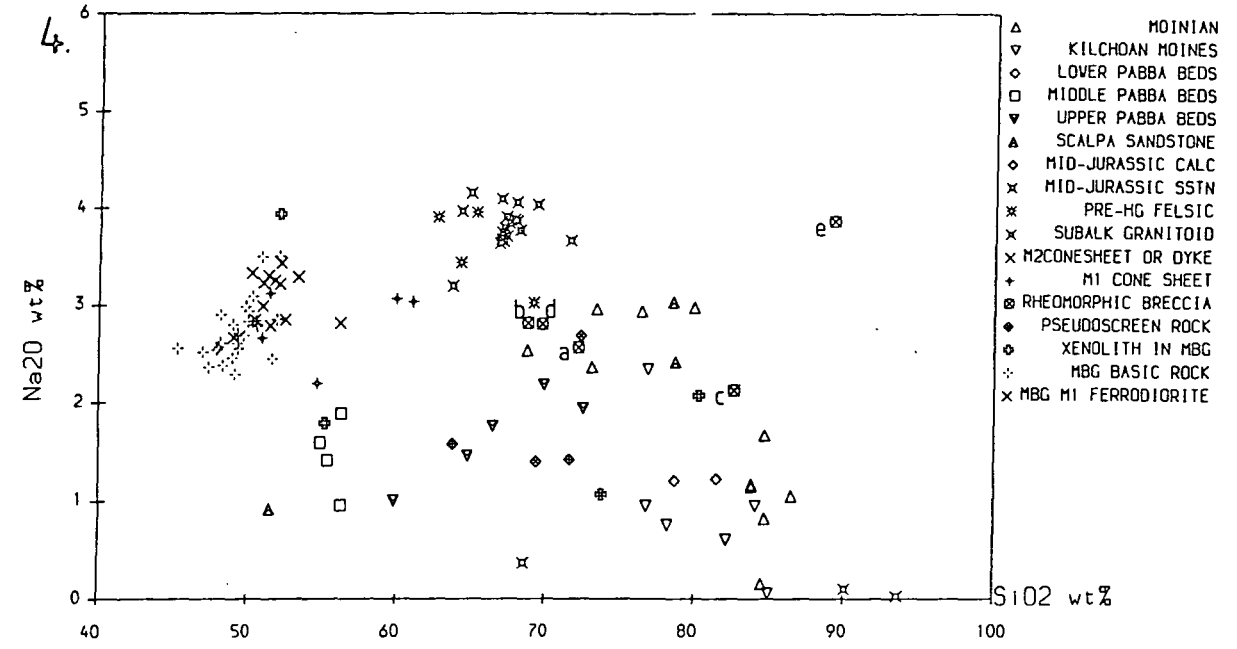
4.
Na2O wt%
SiO2 wt%
MOINIAN
KILCHOAN MOINES
LOWER PABBA BEDS
MIDDLE PABBA BEDS
UPPER PABBA BEDS
SCALPA SANDSTONE
MID-JURASSIC CALC
MID-JURASSIC SSTN
PRE-HG FELSIC
SUBALK GRANITOID
M2CONESHEET OR DYKE
M1 CONE SHEET
RHEOMORPHIC BRECCIA
PSEUDOSCREEN ROCK
XENOLITH IN MBG
MBG BASIC ROCK
MBG M1 FERRODIORITE

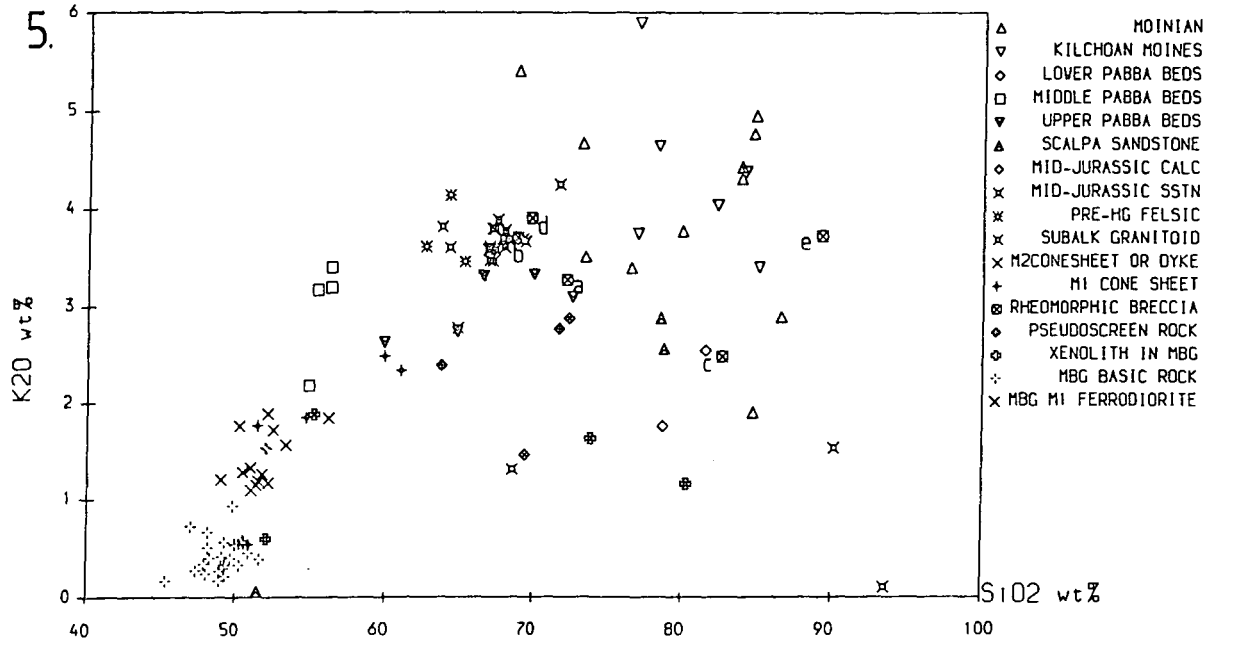
5.
K2O wt%
SiO2 wt%
MOINIAN
KILCHOAN MOINES
LOWER PABBA BEDS
MIDDLE PABBA BEDS
UPPER PABBA BEDS
SCALPA SANDSTONE
MID-JURASSIC CALC
MID-JURASSIC SSTN
PRE-HG FELSIC
SUBALK GRANITOID
M2CONESHEET OR DYKE
M1 CONE SHEET
RHEOMORPHIC BRECCIA
PSEUDOSCREEN ROCK
XENOLITH IN MBG
MBG BASIC ROCK
MBG M1 FERRODIORITE

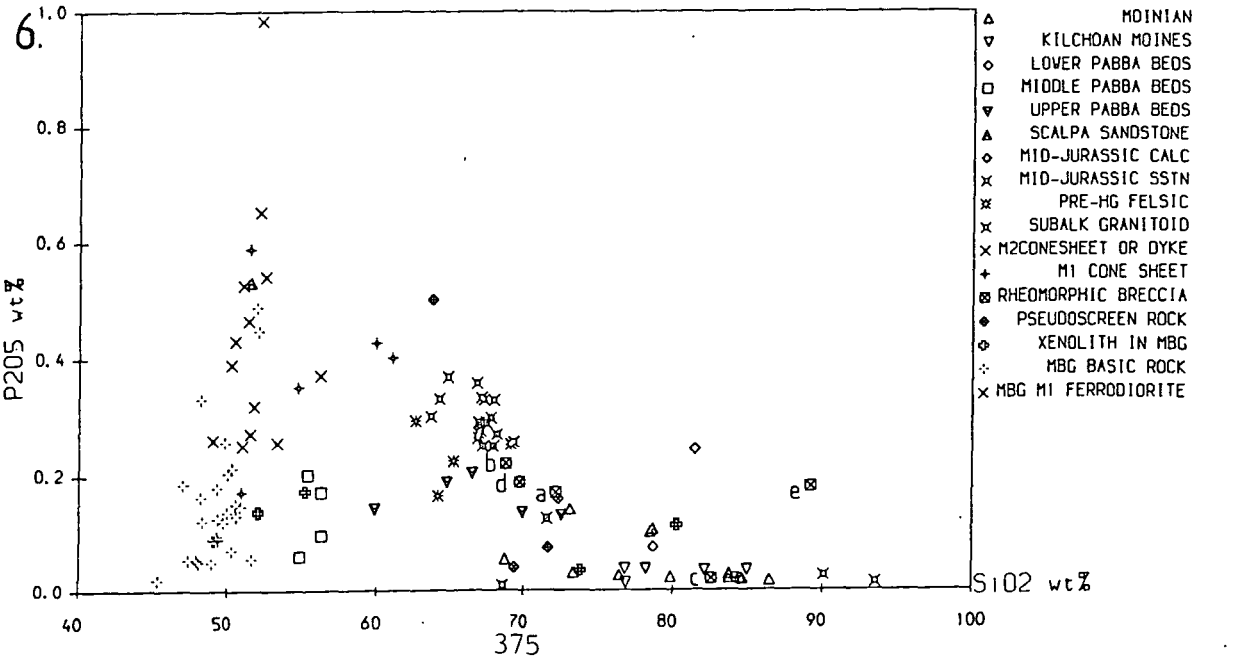
6.
P2O5 wt%
SiO2 wt%
MOINIAN
KILCHOAN MOINES
LOWER PABBA BEDS
MIDDLE PABBA BEDS
UPPER PABBA BEDS
SCALPA SANDSTONE
MID-JURASSIC CALC
MID-JURASSIC SSTN
PRE-HG FELSIC
SUBALK GRANITOID
M2CONESHEET OR DYKE
M1 CONE SHEET
RHEOMORPHIC BRECCIA
PSEUDOSCREEN ROCK
XENOLITH IN MBG
MBG BASIC ROCK
MBG M1 FERRODIORITE

7.

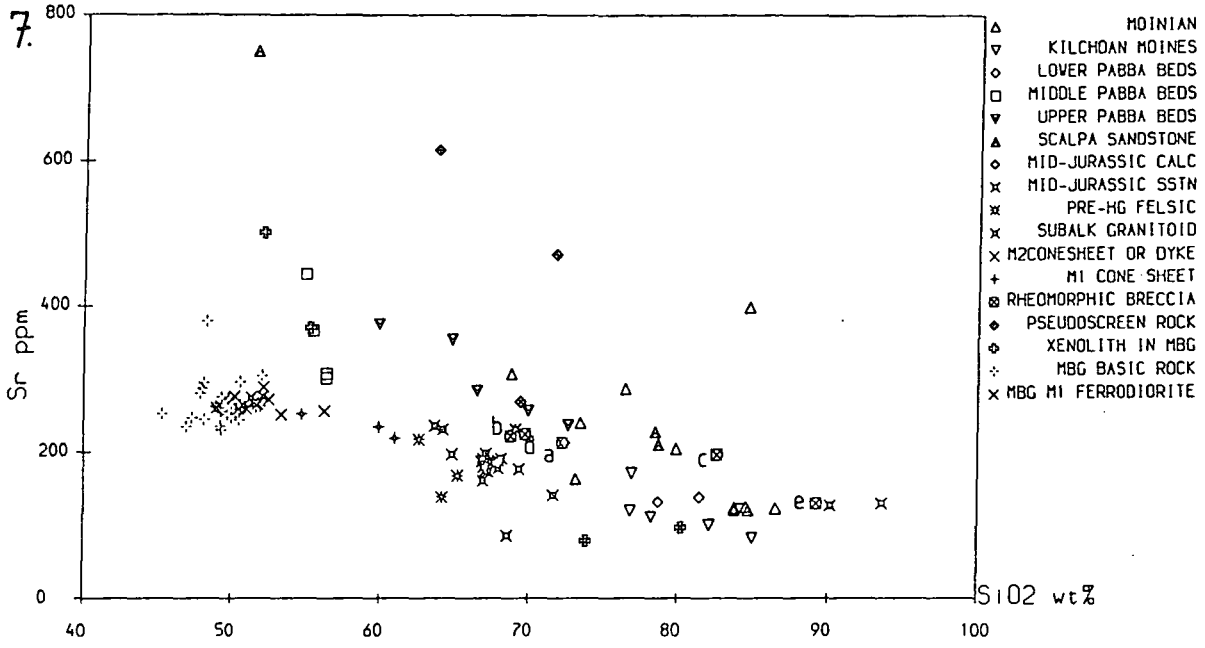
Sr ppm
800
600
400
200
0
40
50
60
70
80
90
100
SiO2 wt%
a
b
c
d
e
MOINIAN
KILCHOAN MOINES
LOWER PABBA BEDS
MIDDLE PABBA BEDS
UPPER PABBA BEDS
SCALPA SANDSTONE
MID-JURASSIC CALC
MID-JURASSIC SSTN
PRE-HG FELSIC
SUBALK GRANITOID
M2CONESHEET OR DYKE
M1 CONE SHEET
RHEOMORPHIC BRECCIA
PSEUDOSCREEN ROCK
XENOLITH IN MBG
MBG BASIC ROCK
MBG M1 FERRODIORITE

8.

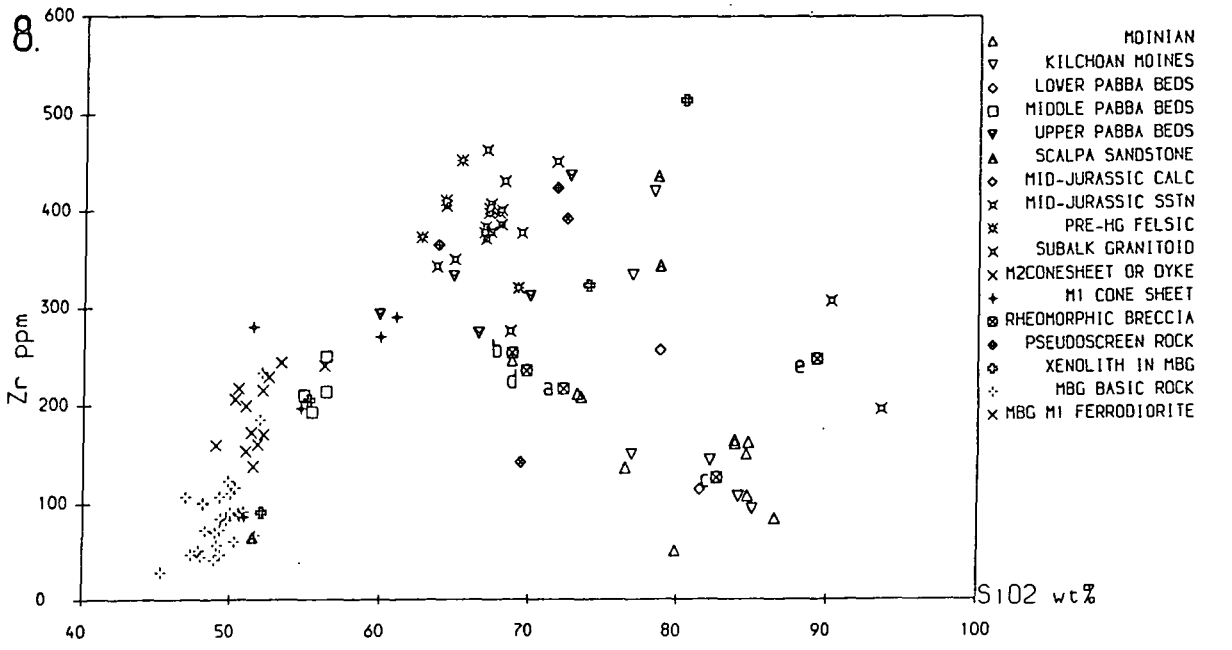
Zr ppm
600
500
400
300
200
100
0
40
50
60
70
80
90
100
SiO2 wt%
a
b
c
d
e
MOINIAN
KILCHOAN MOINES
LOWER PABBA BEDS
MIDDLE PABBA BEDS
UPPER PABBA BEDS
SCALPA SANDSTONE
MID-JURASSIC CALC
MID-JURASSIC SSTN
PRE-HG FELSIC
SUBALK GRANITOID
M2CONESHEET OR DYKE
M1 CONE SHEET
RHEOMORPHIC BRECCIA
PSEUDOSCREEN ROCK
XENOLITH IN MBG
MBG BASIC ROCK
MBG M1 FERRODIORITE

9.

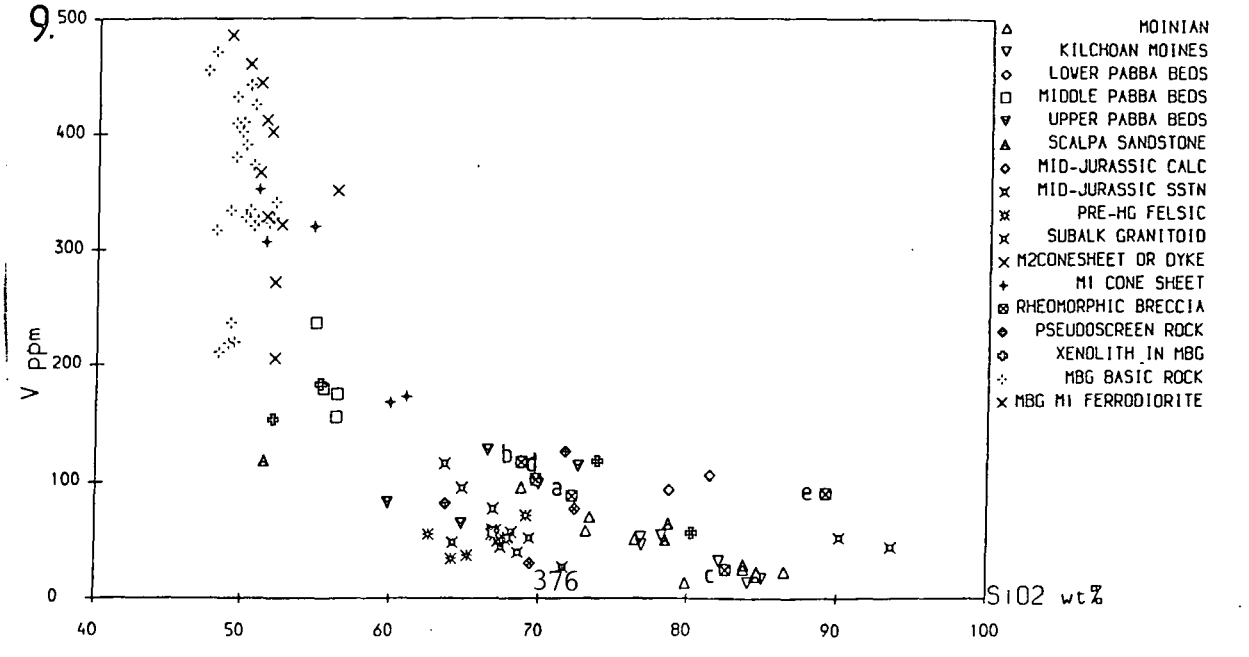
V ppm
500
400
300
200
100
0
40
50
60
70
80
90
100
SiO2 wt%
a
b
c
d
e
MOINIAN
KILCHOAN MOINES
LOWER PABBA BEDS
MIDDLE PABBA BEDS
UPPER PABBA BEDS
SCALPA SANDSTONE
MID-JURASSIC CALC
MID-JURASSIC SSTN
PRE-HG FELSIC
SUBALK GRANITOID
M2CONESHEET OR DYKE
M1 CONE SHEET
RHEOMORPHIC BRECCIA
PSEUDOSCREEN ROCK
XENOLITH IN MBG
MBG BASIC ROCK
MBG M1 FERRODIORITE

by disaggregation of sponge - textured quartzite blocks. Small residual fragments with other compositions (especially diopside - rich inclusions) may also be present in them in small numbers. Analyses a, b and c are all from the same rock (sample 47A: see Appendix 2), with 47AW being a whole rock mixture of the two components, matrix 47AM and residual blocks (47AR) which make up the rheomorphic breccias. These three samples plot in a straight line in Fig. 4.15, indicating that both the matrix and the refractory blocks are homogenous materials. It is also apparent from Fig. 4.15 that the quartzite blocks cannot simply be regarded as mixtures of matrix magma and pure quartz, since 47AR does not always plot on a line between the two. In particular, 47AR has much higher Sr, Al and Na and slightly higher K than a simple quartz - matrix mixture, due to the abundance of sodic feldspar in the sponge - textured blocks, and lower Fe, P and V, probably indicating a lower abundance of clay minerals and authigenic cement in the parental sediment. This confirms the petrographic observation that the quenched melts in the pockets within the sponge - textured blocks are compositionally distinct from the matrix melts, being poor in all components except quartz and feldspar. The quartzitic blocks and the matrix do not appear to be in equilibrium, since the matrix samples are too Si - poor to plot in the (quartz + liquid) field of the Qz - Or - Ab phase diagram, particularly when the presence of an An component in the feldspars is taken into account.

The matrix samples 47AM and 47U plot close to the field of the subalkaline granitoids in many of the plots which make up Fig. 4.15. However, they have lower Na and Zr contents, and greater abundances of Ca, Sr and V. In the case of plots of Na, Ca and Sr against silica they plot between the subalkaline granitoids and certain Jurassic country rock lithologies, suggesting that the rheomorphic breccias could be three - component mixtures of subalkaline granitoid magmas, quartzites similar to 47AR, and other Jurassic sediments. The three - component mixing model could also explain the REE data for 47AW, since it has lower La/Yb than the analysed Jurassic sediments (see Fig. 4.5, where it lies between them and the subalkaline granitoid samples). The uniform distribution, lithology and size of the residual blocks throughout the rheomorphic breccias in the Glendrian Bay area suggests, however, that these sediments must have been interbedded with the refractory quartzites and sandstones: if the refractory inclusions were accidental xenoliths a much more varied collection of inclusions would be expected. The only exposed sediments which occur interbedded with quartzitic sandstones in the Jurassic sequence are the semipelitic rocks of the Lower Pabba Beds: the compositions inferred for these in section 4.2.3 are too aluminous and Zr - rich to correspond to

the analysed matrix samples (see below). Furthermore, the plot of Zr vs. SiO_2 (Fig. 4.15.8) is inconsistent with a three component mixing model involving any known Jurassic lithologies, because the rheomorphic breccias have much lower Zr abundances than all other samples with comparable SiO_2 contents, apart from certain calc - silicate rocks which are far too Ca - rich (CaO= 20%+) to be suitable end - members. Similarly, in the plot of V vs. silica the only rocks with similar contents of silica which have higher V contents are far too Ca - rich to be important components of the rheomorphic breccias. It is therefore necessary to postulate the presence of a further group of compositionally distinct sedimentary rocks in the wall of the MBG magma chamber below the present level of exposure. In view of the petrographic evidence which suggests that the matrix is not a hybrid rock the composition of this material is deduced here on the assumption that the rheomorphic breccias are a two component material, the other component being the quartzitic blocks. It appears to be a slightly calcareous (and hence with elevated Ca and Sr contents), Zr and K - poor arkosic siltstone which was interbedded with quartz- and feldspar- rich arkosic sandstones which correspond to the sponge - textured quartzitic blocks. Compared to the Moinian rocks analysed, the samples from location 47 have lower K and Al, and higher Ca and Ca/Sr at any given SiO_2 content, due to a higher ratio of carbonate to micas and clay minerals in the fine - grained matrix or to a greater content of calcic feldspar (although the latter does not explain the higher Ca/Sr). In comparison to the analysed Jurassic rocks the rheomorphic breccias at Glendrian Bay have a combination of low Zr and only moderate Ca and Sr contents which is only found in much more Fe rich ferriginous sediments in the exposed Jurassic sequence, and a higher Na_2O/SiO_2 ratio which reflects the greater abundance of detrital plagioclase seen in thin section. Although geochemical analyses of Hebridean Triassic sediments are not available, these geochemical and mineralogical features would be expected to be a feature of the Triassic sandstone - siltstone sequence in the Hebrides, since this was deposited in an arid or semi - arid climate (Hudson 1983) which would favour preservation of detrital feldspar and reduce the rate of clay mineral formation. The exposed Triassic sequence in Mull (Lee & Bailey 1925) and in northern Mull and eastern Ardnamurchan (Richey et al. 1930) is composed of arkosic sandstones, conglomerates and cornstones. Work by Steel (1977) indicates that the Triassic sequences in the Hebrides tend to become thicker but finer - grained towards the centres of the basins from their south - eastern margins, so the sequence under the Glendrian Bay area would be expected to contain a siltstone rich Triassic unit since it lies closer to the centre of the Inner Hebrides basin (Fig. 2.1).

This conclusion does not apply to the rheomorphic breccia to the south of Glendrian Bay at Loc. 184, nor to the rheomorphic breccias at locations 240 and 267/3 on the southern margin of the intrusion. Assuming that these are also composed only of pre - Tertiary rocks, samples 184 and 240 appear to have been derived from an interbedded quartzose to impure sandstone / semipelitic or calc - pelitic sequence with the latter forming the rheomorphic breccia matrix on melting. Such rocks occur in both the Lower and, to a lesser extent, the Upper Pabba Beds: the lack of calc - silicate inclusions suggests that the former may be a more likely source but bulk - rock analyses are needed to examine this problem further. 267/3 is very strongly altered and recrystallised but it appears to have a silica - rich matrix which was probably, therefore, produced by melting of a quartzose sediment.

Although these identifications of the sources of the various rheomorphic breccia bodies are not conclusive, it is apparent that the breccias were produced by melting of the fusible components of bedded sedimentary units, which also contained relatively refractory arkosic sandstone and quartzite beds. These units are inferred to have been present below the present level of exposure: as with the anomalous microgranitoids, the rheomorphic breccias appear to have moved upwards from their original site of formation.

4.2.4.2. Development of Textures and Structures in the Rheomorphic Breccias.

This section is mainly concerned with the development of textures and structures characteristic of the rheomorphic breccias, in particular the 'sponge' texture that occurs in the partially melted blocks (Plates 3.15 to 3.17). and the development of the brecciation itself.

Sponge texture, as defined in section 3.2.2.2, is similar to the 'fingerprint' texture described from partially melted granitic and quartzofeldspathic xenoliths found in extrusive rocks (e.g. Hawkes 1929), which is attributed to the initial concentration of melting at quartz - feldspar grain boundaries.

The occurence of feldspar - rich patches at the centres of many of the melt pockets in sections from the quartz - rich blocks in the Glendrian Bay rheomorphic breccias suggests that melting in these was also concentrated around feldspar grains in the parent sandstones. This interpretation implies that these feldspar - rich patches represent the sites of original feldspar grains, now replaced by

Plate 4.10. Recrystallised melt pocket in 'sponge' textured residual quartzite block, rheomorphic breccia sample 47C2. The opaque and pyroxene grains at the left and top right of the field of view may have been derived from cement around the negative sieve - textured feldspar grain at centre right. Alternatively, the trail of opaque and pyroxene grains at upper right may represent an annealed M2 hydrothermal vein. PPL, FOV 1.5mm.

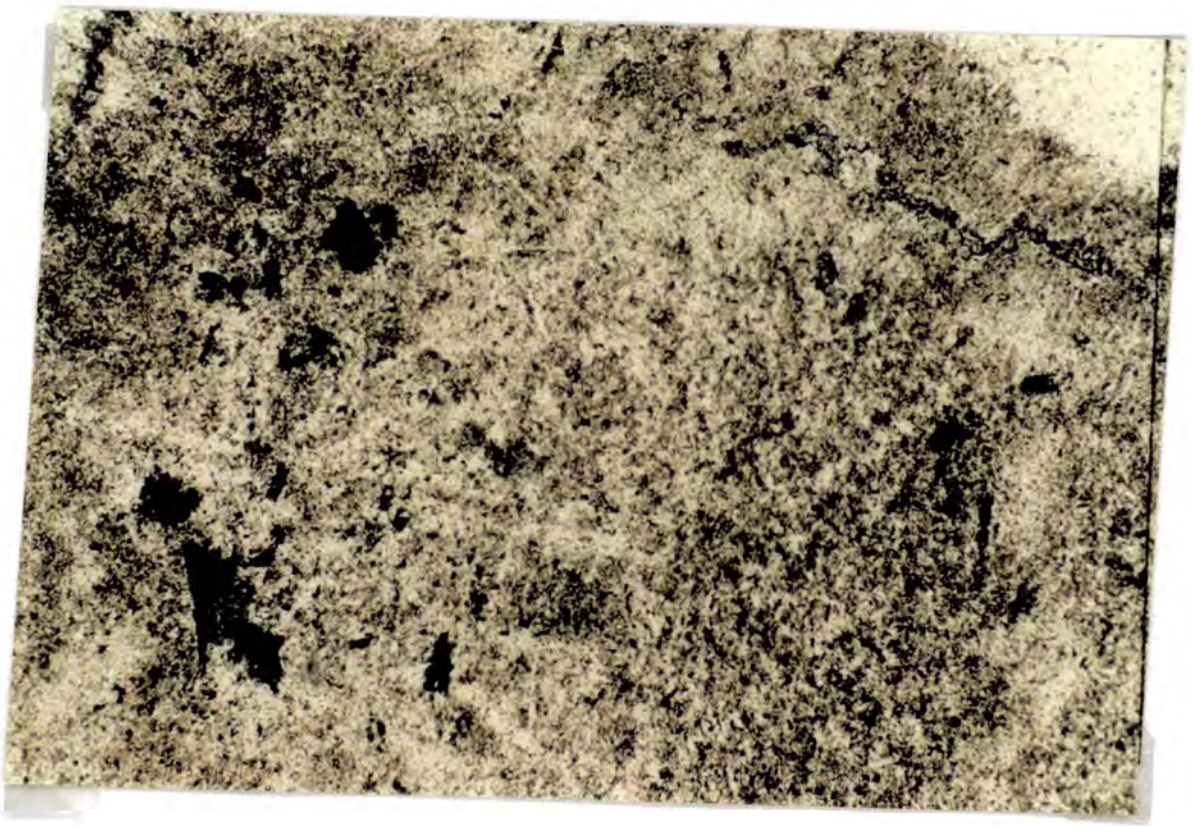

feldspar - rich quartz - feldspar intergrowths. Several other petrographic observations point to the same conclusion:

1). Individual feldspar patches are optically continuous although each is composed of a large number of small equant grains enclosed in poikilitic quartz grains. Some of the larger feldspars are divided into two crystallographic domains by a planar boundary which may represent a primary twin plane in the original crystal.

2). Trails of fine - grained granular opaque and/or clinopyroxene grains sometimes occur in the quenched melt between the feldspar - rich core and the outer edge of the melt pockets (Plate 4.10). These may be relicts of original carbonate, clay or iron oxyhydroxide cements between grains in the original sediment. If so, their preservation implies that the melts formed in the pockets were stagnant, even on the microscopic scale. Alternatively, they could simply have formed along post - M1 fractures which have subsequently been annealed.

3). The sharp margins and irregular outlines of the feldspar rich patches imply that they represent an earlier feature of the rocks rather than being a product of diffusion during the quenching of the melt pockets, which could in theory produce a feldspar - rich core zone as tridymite nucleated on the surrounding residual grains.

The intergrowth with quartz characteristic of these feldspar - rich patches bears a close resemblance to the micropoikilitic texture (Lofgren 1970) which is characteristic of advanced devitrification of felsic glasses under low - temperature hydrothermal conditions. However, it is also similar to the texture of the rare type 4 feldspars in the M2 felsites (Plate 4.2, section 4.2.2.2). The overgrowths of quench feldspar on the grains within the type 4 feldspar porphyrocrysts suggest that, had crystallisation proceeded further, the residuum between the growing feldspar grains would have approached the composition of quartz and eventually crystallised as such.

The interpretation of the feldspar - rich patches as relicts after detrital feldspar grains implies that the original grain size of the quartzitic blocks was of the same order as the size of the quenched melt pockets. This suggests an original grain size of the order of 0.5 to 2mm, with the smaller grain sizes being typical of the melt - rich blocks. In contrast the quartz grains in the host are rarely more

Plate 4.11. Randomly orientated, sutured quartz grains in residual quartzite block from rheomorphic breccia, Glendrian Bay area (sample 353). 1 – λ plate inserted to demonstrate lack of a preferred crystallographic orientation in the quartz grains. Also note the small size of the quartz grains relative to relict plagioclase crystal (large blue - tinted grain in centre of melt pocket) and to the melt pocket itself. XPL, FOV 3.5mm.

than 0.2mm across. They are equant and show random optic orientation (Plate 4.11), and there is little overall fabric in the blocks with the exception of a possible slight elongation or flattening of the quenched melt pockets. This suggests that the grain size of the quartz has not been reduced by deformation. The discrepancy between the original grain size of the rock, as inferred from the size of the melt pockets, and the present size of the quartz grains implies that intense grain size reduction has nevertheless taken place. A possible mechanism of static recrystallisation is suggested by the presence of inverted quench tridymite. Inversion of the primary quartz to tridymite during M1, followed by retrogressive inversion of tridymite to quartz during and after the quenching would involve two complete restructurings of the silica lattice: in contrast, the α-β quartz transition is not a reconstructive one (Deer et al. 1966) and would tend to produce only internal lattice strain, or subgrains with a preferred optic orientation. The tridymite - quartz inversion therefore occurred in both directions in this rock implying that the rheomorphic breccias were in the stability field of tridymite prior to the end - M1 quench. This suggests that tridymite growth during the quench was at least in part within the tridymite stability field, rather than being metastable.

As noted above and in Chapter 3, the uniformity of the residual inclusion assemblage in the rheomorphic breccias suggests that the quartzite and other blocks originate from the source region of the matrix rather than being accidental xenoliths caught up in it as it was intruded to higher levels. The differences in composition between the blocks and the matrix suggest that they formed an interbedded sequence of sandstones (the blocks) and siltstones (or semipelites in the cases of the occurrences at 184 and 240) which form the matrix. The sequence of events during disruption or brecciation of this sequence appear to have been as follows:

- Melting of the fusible siltstones

- Disruption of the arkosic sandstone beds

- Chaotic mixing, to produce the variety of quartzitic blocks seen at individual outcrops, and intrusion of the mobile mixture to the final position of the rheomorphic breccia intrusions.

Mobilisation of crustal melts is a key stage in the formation of intracrustal granites and is a poorly understood process, in part because it normally occurs at deep crustal levels where slow cooling

and recrystallisation obscure textural evidence. In contrast, although the rheomorphic breccias associated with the Hypersthene Gabbro have undergone post - quench devitrification and some recrystallisation of the quenched melt in particular, residual (or restite) and magmatic crystals can easily be distinguished on textural grounds, thereby avoiding the controversy over what is restite and what is not that arises in the case of plutonic rocks.

Two main processes can be identified as having operated in the rheomorphic breccias which would have contributed to disruption of the refractory quartz - rich beds, which is a necessary precondition for large - scale movement of the matrix melt. The first of these is dissolution of the quartzitic rocks in the matrix melt. As noted above, the matrix is almost certainly too Si - poor and Ca - rich to have been in equilibrium with quartz at the peak temperatures of metamorphism. It is difficult to be certain about this becuase of uncertainty about the oxidation state of the melt and the effects of Ca in feldspar upon the phase diagram, but well - developed rounding and corrosion of quartz microblocks and of the surfaces of the larger residual blocks is evident in thin section. This implies that the blocks have been preserved by the short duration of the melting event relative to the time required for a viscous melt such as the matrix to dissolve quartzitic inclusions with which it is not in equilibrium. The quartzitic blocks would not have survived in such numbers if the melting event which produced the rheomorphic breccias had lasted much longer, suggesting that the products of long - duration regional melting events can be distinguished from the products of short - duration, intrusion - related events such as those proposed by Huppert & Sparks (1988b) by considering whether melts and blocks of refractory lithologies from the source region have reached phase equilibrium. Dissolution may be an important mechanism for breaking up refractory beds under these circumstances because it will be concentrated at exposed surfaces such as those formed by cracks and faults and will tend to enlarge such dicontinuities, rather than being evenly spread over the entire surfaces of the refractory beds.

Mechanical processes of disruption of refractory beds will be particularly important if and when equilibrium has been reached between the refractory rocks and the intervening layers of melt. These melts will be orders of magnitude weaker than the refractory beds (Van der Molen & Paterson 1979), and as a result any external stresses will be concentrated in the latter. In the context of the rocks around the Hypersthene Gabbro these stresses would have been imposed by expansion and contraction of the MBG magma chamber (see Chapters 3 and 7). As a result the refractory

beds may have been alternately compressed (producing folding and possibly brittle shear failure: the latter is particularly likely to occur in partially melted refractory beds because the presence of melts will reduce the effective confining pressure) and extended, producing ductile boudinage or tensile brittle failure. Both of these latter would be particularly effective mechanisms for breaking up refractory beds. The lack of evidence for internal deformation within the quartzitic blocks and their overall subangular shapes suggests that brittle deformation must have been the dominant process involved in mechanical disruption of the more refractory beds in the source region of the rheomorphic breccias.

Considerable attention has been given to the role of thermal convection in producing isotropic granitic rocks from banded and foliated migmatitic rocks as partial melting proceeds (Wickham 1987; Sparks & Huppert 1988b). In the case of a bedded sequence, however, the strong dependence of the onset of convection upon the thickness of the fluid layer means that convection is more likely to be triggered by disruption of the refractory layers (which will cause a sudden increase in the thickness of the fluid layer) than to cause it. Thermal convection may however have been an important process in the chaotic mixing of the rheomorphic breccias implied by the juxtaposition of quartzitic blocks with a wide variety of grain sizes and degrees of melting (hence, different ratios of quartz to feldspar), which must have originated in different beds. It is, however, difficult to model the onset of convection in the case of the rheomorphic breccias because heating of the source rocks would probably have occurred from the side, given the evidence that the Marginal Border Group is steep - sided (see Chapter 3), under which circumstances the main control on the vigour of convection would have been the yield strength of the matrix magma, which is poorly known. Alternatively, the mixing may have been caused in part by forced convection associated with the emplacement of the rheomorphic breccia intrusions.

4.2.5. Estimates of the Conditions of Melting during the formation of the anomalous microgranitoids, M1 and M2 subalkaline granitoids and Rheomorphic Breccias.

The conditions of melting of the silica - rich and felsic rocks which gave rise to the magmas represented by these rocks are of considerable interest in connection with the magma chamber dynamics of the MBG magma chamber because, in conjunction with estimates of the temperatures of the mafic magmas in the interior of the MBG magma chamber (see section 4.3.3) they provide an estimate

of the temperature difference between the interior of the magma chamber and its wall rocks, and an upper limit upon the rigidus temperature of the wall rocks which were melted and mobilised to produce them. Unfortunately it is only possible to place constraints on the variables of interest – temperature, total pressure and partial pressure of water – by combining constraints from different rock types, although in some cases it is possible to use small xenoliths of one rock type in another, in which case thermal equilibrium between the two can be assumed. This procedure is justified in general terms by the age relationships described in Chapter 3, which indicate that all the rocks to be considered here were generated in a period spanning the latter part of M1 and the earliest part of M2 at the present level of exposure (but before the beginning of M2 at the depth of generation of the magmas concerned). It appears that all of these rocks were produced by melting at the walls of a magma chamber containing magmas of approximately uniform composition and temperature, at least at and below the present level of exposure (see section 4.3) and which was affected by the same heat loss mechanisms at the times and places at which melting occurred (see Chapter 5).

4.2.5.1. Temperature and pressure constraints from the quartz - tridymite inversion.

As noted in 4.2.4, there is evidence that the residual quartzitic blocks in the rheomorphic breccias inverted from quartz to tridymite as a result of heating during M1. Similar granular residual quartz textures occur in metasandstone residual blocks in the pseudoscreen at Duin Bhain and in the quartzite xenolith within an M2 felsite at field location 19 (see section 4.2.2.2), all of which also contain quench tridymite pseudomorphed by quartz. All of these rocks are therefore constrained to have formed at temperatures above the equilibrium quartz – tridymite inversion temperature. This inversion is, however, strongly pressure dependent (Tuttle & Bowen 1958) and additional pressure constraints are required before it can be applied.

4.2.5.2. Pressure - temperature constraints from phase assemblages in the subalkaline granitoids.

The residual assemblage in these rocks – plagioclase + augitic or salitic clinopyroxene + opaques, principally Ti - magnetite – is entirely anhydrous. Experiments by Thompson (1983) on the melting behaviour of BTVP granitoid rocks at 1kb P_{H_2O} and $P_{H_2O} = P_{total}$ indicate that biotite may persist at up to 900°C, and amphibole at up to 800°C, in granitic (sensu stricto) rocks under

these conditions, and that amphibole coexists with melt at over 1000°C in a rock of intermediate (monzonitic or quartz dioritic) composition. Furthermore, Thompson found that in two of his samples, a high - K granite and the monzonitic rock, hydrous phases (biotite and amphibole respectively) coexisted with melt at above the upper temperature limit of plagioclase + melt. The persistence of plagioclase and the complete absence of hydrous magmatic or residual phases from the M1 and M2 subalkaline granitoids therefore suggests that they were melted under conditions of P_{H_2O} much less than 1kb: the experiments of Wyllie et al. (1976) indicate that the stability field of plagioclase + granitoid melt expands greatly at low P_{H_2O}.

The actual water content of the magmas can be constrained by the following argument. Prior to melting the rocks in the MBG aureole were affected by thermal metamorphism as the aureole heated up. The resulting subsolidus metamorphism involved decomposition of all the hydrous phases present (principally biotite and muscovite; see section 3.2.5.5 in particular) well below the solidus (see Chapter 5) apart from cordierite, which only contains a very small amount of water. Consequently, when melting began the only water present in situ would have been in cordierite and an interstitial vapour phase, giving a total intrinsic water content of much less than 1%. As noted in Chapter 3, there is no evidence for an M1 fracture network along which water could have rapidly infiltrated the rock as melting proceeded, whilst evidence for wide variations in f_{O_2} during M1, to be presented in Chapter 5, indicates that very little fluid movement occurred at all during M1. The solubility of H_2O in felsic magmas is greater than 1% by weight even at low pressures (Wyllie et al. 1976) so it appears likely that the magmas were strongly water - undersaturated.

4.2.5.3. Plagioclase – Melt geothermometry.

The result of the previous section, that the magmas were strongly water - undersaturated and that P_{H_2O} was much less than 1kb, means that feldspar - melt geothermometry (Kudo & Weill 1970; Drake 1976) can be used to obtain fairly precise temperature estimates. The basic equation for this geothermometer is:

$$aT^2 - bT(20.31 + \ln(\frac{X_{NaO_{0.5}} X_{SiO_2}}{X_{CaO} X_{AlO_{1.5}}}) + \frac{X^{pl}_{An}}{X^{pl}_{Ab}}) + 12900(X_{CaO} + X_{AlO_{1.5}} - X_{NaO_{0.5}} - X_{SiO_2}) = 0 \quad (4.7)$$

T being the larger root of 4.7. The constants a and b are P_{H_2O} dependent and have to be experimentally determined: the values used below are taken from Kudo & Weill (1970) and Drake (1976

) for 0.5kb and 1 Atm respectively. The other quantities are the molar proportions of $NaO_{0.5}$, SiO_2, CaO and $AlO_{1.5}$ in the melt (normalised to sum to unity) and the molar proportions of anorthite and albite end - members in the coexisting feldspars. No allowance was made in the experiments on which this geothermometer is based for the effects of minor components (pricipally K and Fe^{3+}) in the feldspars.

Estimation of the various quantities in equation 4.7 posed certain problems which affect the accuracy of the results. The rocks for which melting temperature estimates were made are three M2 felsites, 250/1 (from the fine - grained felsite intrusion on Glebe Hill), 42F2 and 43K1 (both from the intrusions south of Duin Bhain). The groundmass of 42F2 is crowded with quench feldspar crystals, which are also present in 43K1 in smaller numbers, whilst that of 250/1 is too coarsely crystalline for rastered defocussed - beam microprobe analysis. Calculations using microprobe analyses of the residual devitrified glasses and analyses of relict feldspars from 42F2 gave unrealistically high temperatures due to the crystallisation of quench feldspars. It was therefore decided to estimate the composition of the melt which coexisted with the feldspars prior to quenching by using bulk rock analyses of 43K1, 250/1 and 42C (a sample from the same intrusion as 42F2, collected about 10m from the sample site of 42F2). These should be corrected for the effects of the residual plagioclase and pyroxene on X_{SiO_2}, $X_{NaO_{0.5}}$, $X_{AlO_{1.5}}$ and X_{CaO}. This leads to the problem of estimating the porphyrocryst contents of thse rocks. The porphyrocrysts are unevenly distibuted on scales of up to a few centimetres and point - counting of impractically large areas (20 – 50cm^2) would be necessary to obtain accurate estimates of porphyrocryst abundances. Accordingly, visual estimates of porphyrocryst abundances were made on the hand specimen scale and the calculations repeated using the uncorrected bulk rock analyses and analyses corrected for the following abundances of porphyrocrysts:

42F2	5% plagioclase	3% augite
250/1	5% plagioclase	3% augite
43K1	10% plagioclase	6% augite

The compositions of porphyrocrysts used were the median analyses from each rock, although which particular analysis was used would make little difference to the results as the range in porphyrocryst compositions is small (see section 4.2.2). Table 4 contains the results of the calculations for the full range of feldspar compositions analysed (with the exception of analyses which give non -

stoichiometric results or low totals) and for various estimated melt compositions and values of P_{H_2O}. It indicates that the errors potentially introduced by the groundmass composition recalculation procedure are small compared to other errors ($\pm 55^{o}C$ (3σ confidence limits) due to errors in the experimental calibration (Drake 1976) and $160^{o}C$ per kilobar of uncertainty in P_{H_2O}) as the difference between the results obtained using the raw analysis of 43K1 and the corrected analysis is only some $40^{o}C$. The error introduced by errors in the estimated porphyrocryst abundances is therefore likely to be $20^{o}C$ or less since even at the few - percent abundance level visual estimates of porphyrocryst abundances are unlikely to be out by more than a factor of two.

Equation 4.7 assumes that the analysed feldspar is in equilibrium with the melt. As noted in 4.2.2.2, the analysed feldspars show a range in compositions from about An_{35} to An_{42} in 42F2, An_{37} to An_{44} in 43K1 and An_{34} to An_{42} in 250/1. There is no systematic core - to - rim zonation pattern in the majority of grains. This latter feature suggests that much of the variation may be due to post - quench Ca loss to the hydrothermal epidote which occurs in small amounts replacing quench glass in these samples, in which case the most Ca - rich analyses (which give the highest temperatures) are in general those most likely to represent the feldspar in equilibrium with the M1 melts.

The development of sieve textures in the feldspar porphyrocrysts may indicate disequilibrium between the feldspars and the enclosing melts, in which case the temperatures obtained should be regarded as underestimates. This conclusion is supported by the preservation of slight zonation within certain of the feldspar porphyrocrysts. However, Johannes (1983) considers that equilibrium between feldspar and melt in experimental charges at $1000^{o}C$ or more is reached within a few hours for feldspars less calcic than the equilibrium composition. Furthermore, Johannes (1983) considers that the rate of equilibration is controlled by surface processes and is therefore largely independent of grain size. The duration of melting events around the MBG magma chamber is uncertain because the precise geometry of the region of melting is unknown. However, given the low values of Q_m deduced in Chapter 5 (which are only slightly sensitive to the temperatures deduced here) the time taken to produce a significant volume of melt ($10^3 - 10^4$ m^3, judging by the size of the M2 felsite intrusions), by conductive heating of a downfaulted block wall of the intrusion will be of the order of years at least. Order of magnitude estimates obtained from the rule of thumb that the time taken for a body to achieve thermal equilibrium during conductive heating from its exterior is proportional to the square of its smallest dimension (Jaeger 1957, 1959) suggest that the larger

downfaulted blocks will take some tens of years to melt. More precise estimates are not attempted here because of the porblem of allowing for the effect of removal of melts (i.e. ablation) from the surface of the block on its thermal history (in physical terms, this constitutes a two - dimensional moving - boundary problem in which the position of the boundary and its motion are dependent upon the previous history of heat flow (a Stefan problem): such problems are in general only soluble by numerical simulation). However, the rule - of - thumb estimate used here suggests that, although the sieve textures of the feldspars may record initial disequilibrium, the highest - Ca feldspars in the rocks analysed have compositions which are close to being in equilibrium with the melt and therefore give realistic temperature estimates for the felsites immediately prior to quenching.

The results of the feldspar geothermometry calculations are presented in Table 4. Assuming that the most calcic feldspars and the recalculated melt compositions give the most accurate temperature estimates, the higher temperature values are more likely to be close to the true values. For P_{H_2O} = 0.5kb these are in the range 990 – 1050°C, whilst at 1 Atm. pressure they rise to 1070 – 1120°C. The data of Kudo & Weill (1970) suggest that the water pressure correction to the geothermometer is approximately linear, allowing estimation of temperatures at intermediate pressures by interpolation. As noted above, P_{H_2O} was probably much less than P_{total} in the felsitic magmas: however, given the uncertainty in its actual value the calculations presented below will be repeated for various water pressures and hence feldspar - melt temperatures.

4.2.5.4. Geological Constraints on the lower value of P_{total}.

In addition to mineralogical constraints on P_{total}, indirect arguments based upon estimates of the amount of cover over the MBG magma chamber and the original height of the roof of the chamber above the present level of exposure can be used to place a lower limit on the pressure at which melting occured in its wall rocks. This can only ever be a lower limit for many of the granitoid rocks considered in this section because they have been emplaced up to several hundred metres (and possibly a few kilometres in the case of the subalkaline granitoids) above the sites at which they initially formed. The M2 felsites in particular may have been intruded very rapidly and without further re - equilibration. Three lines of evidence suggest that this lower limit is of the order of 0.2 to 0.3 kilobars:

Table 4.1. Uncorrected and Corrected groundmass or Quenched Melt Compositions for Feldspar - Melt Geothermometry.

Bracketed values are corrected for porphyrocryst contents. See text for discussion of correction procedure.

Sample	X_{SiO_2}	$X_{AlO_{1.5}}$	X_{CaO}	$X_{NaO_{0.5}}$
42F2	0.7263	0.1641	0.0316	0.0780
....	(.7375)	(.1617)	(.0231)	(.0776)
250/1	0.7483	0.1575	0.0203	0.0740
....	(.7611)	(.1545)	(.0112)	(.0733)
43K1	0.7173	0.1680	0.0360	0.0787
....	(.7400)	(.1635)	(.0184)	(.0780)

Table 4.2. Pre - Quench Temperatures (°C) of M2 felsites Calculated using feldspar - melt geothermometers of Drake (1976) (1 atm.) and Kudo & Weill (1970)

First two columns are temperatures calculated using uncorrected groundmass data, second two are temperatures calculated using corrected groundmass data (see Table 4.1).

Sample	1 Atm.	0.5kb	1 Atm.	0.5kb
42F2	—	—	—	—
Max.	1053	964	1077	995
Min.	1011	906	1035	939
250/1	—	—	—	—
Max.	1067	986	1117	1043
Min.	1027	923	1077	1001
43K1	—	—	—	—
Max.	1058	974	1096	1019
Min.	1030	935	1067	980

1). With the single exception of the M2 vent at Glas Eilean (Richey et al. 1930) there is no evidence of syn - MBG explosive brecciation or volcanicity such as is normally associated with felsic magmatism at very shallow depths, although as noted above the anatectic felsic magmas associated with the MBG may have been unusually dry and hence less prone to degassing and vesiculation.

2). As far as can be identified from the mapping, the observed M1 and M2 isograds, which occur at up to 700m from the contact, are steeply inclined and sub - parallel with the contact. This suggests that they formed at a steep angle (30° or more ?) to the palaeosurface, implying that the latter was further from the rocks in which the isograds occur than the contact of the MBG and therefore had less effect upon the direction of heat flow, which should be approximately normal to the isograds, given that the latter approximate to isotherms (see Chapter 5).

3). The development of radially directed thrusts around the MBG (sections 3.2.2.2, 3.2.3.4 and 3.2.5.4; see also Chapter 7) implies that the magma chamber was able to exert an excess hydrostatic pressure upon its wall rocks greater than the shear failure strength of the latter. The development of this excess pressure requires the presence of a thick, rigid roof above the intrusion and / or the presence of a column of dense magma above the present level of exposure with an excess weight, above that of the country rocks above the wall of the intrusion at the same level, which exceeds the shear failure strength of the latter. In this case an influx of magma into the chamber would cause shear failure of the wall rather than eject magma in a surface eruption, which would occur without deformation of the wall rocks if the overlying column of magma was shorter. In practice both of these factors are likely to be significant. The wall rock yield strength (a few to several hundred bars ?(values obtained by Van der Molen & Paterson (1979) for fine grained granite at c. 700°C)) and the other factors involved are poorly constrained (see Chapter 7) but it seems unlikely that less than a kilometre or so of cover could have the necessary weight and/or strength. Similarly, the presence of the system of M1 and M2 concentric and radial faults described in Chapter 3 requires the roof of the intrusion to behave as a coherent, relatively rigid body rather than brecciating in a chaotic fashion: given the 6 to 8 kilometre diameter of the MBG magma chamber, this suggests a roof a few kilometres rather than a few hundred metres thick.

It seems probable, therefore, that P_{total} was more than a few hundred bars and is more likely to have been above 0.5kb, which is equivalent to about 2km of low - density sedimentary and volcaniclastic cover above the MBG magma chamber at the present level of exposure. The arguments on which this conclusion is based are not strong, however, as they rely on poorly understood aspects of the mechanical or structural behaviour of very large shallow magma chambers.

An upper limit on the pressure of formation of these rocks is provided by the geophysical evidence(Bott & Tuson 1963; Barrett 1987; Harrison 1987) which suggests that the base of the Ardnamurchan intrusive complex is no more than 3 to 5 kilometres below the surface. Given the geological evidence that the M1 and M2 granitoids discussed in this section all formed at the wall of the Hypersthene gabbro this places the maximum possible pressure of formation of the subalkaline granitoids at about 2kb; the rocks with protoliths in the Mesozoic succession must have formed at shallower depths than this (see Chapter 2 for the estimate of the thickness of the Mesozoic sequence on which this is based).

4.2.5.5. Synthesis of the constraints on the Temperature and Pressure of formation of the MBG granitoids.

The available temperature and pressure constraints on the formation of the granitoids associated with the MBG are summarised in Fig. 4.16. It should be noted that because the only tridymite occurences in the subalkaline granitoids are in metasedimentary xenoliths enclosed within them they could have originally formed at slightly higher pressures.

The likely melting temperatures can be summarised for two extreme cases, one with P_{H_2O} close to zero and the other with P_{H_2O} equal to P_{total}. As noted above the granitoid magmas were probably strongly water - undersaturated and the former case is more likely to be closer to the true values:

1) Low P_{H_2O}: T = 1070 - 1120°C, P_{total} 0.2 - 1 to 1.3kb.

2) $P_{H_2O} = P_{total}$: T = 990 - 1050°C, P_{total} 0.2 - 0.5 to 0.75kb.

These temperatures are much higher than the liquidus temperatures predicted by the empirical

Fig. 4.16. Pressure and temperature constraints on the conditions of formation of anatectic magmas at the wall of the MBG magma chamber during M1.

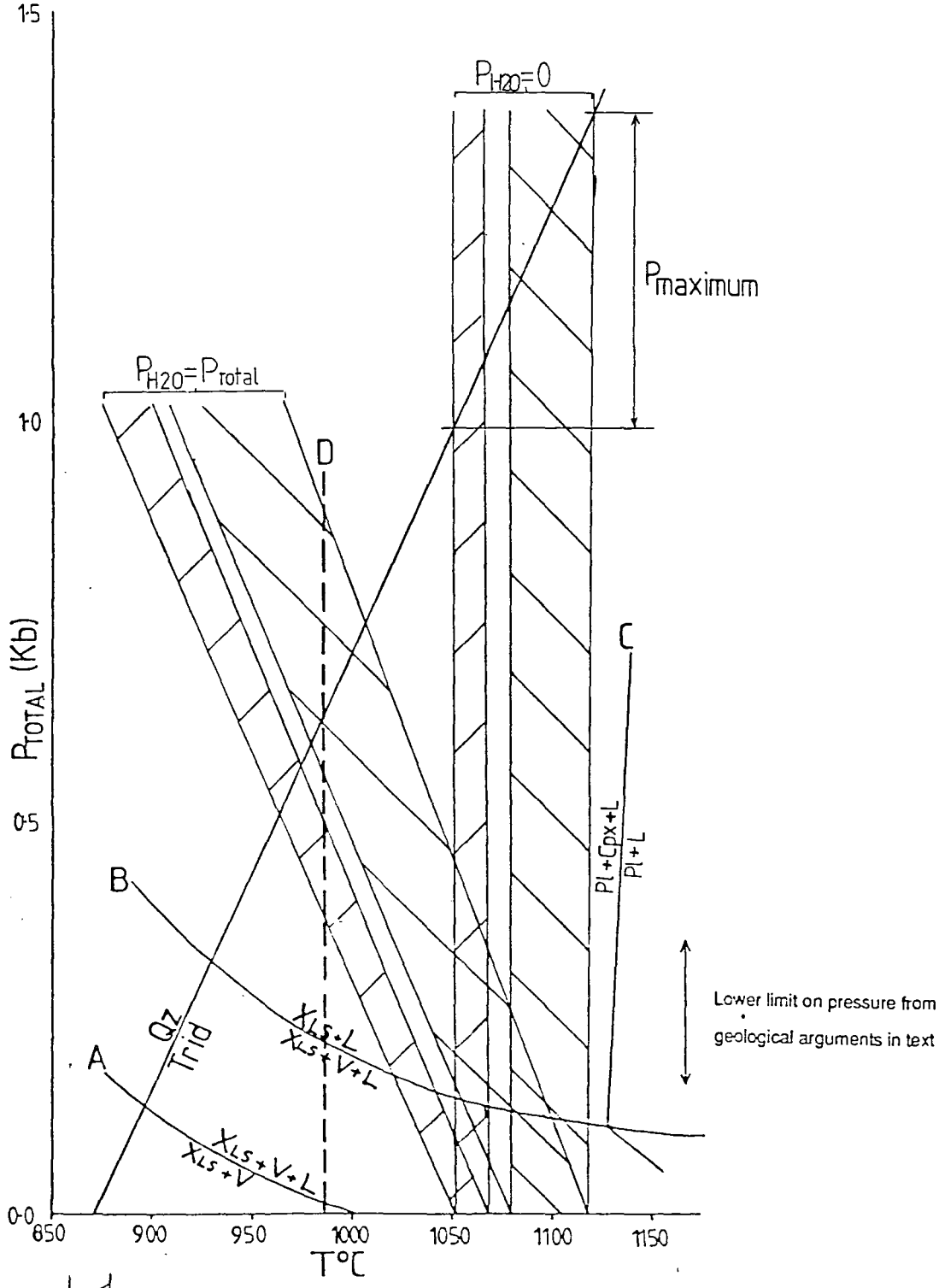

relationship between MgO content and liquidus temperature proposed by Sparks & Marshall (1986) for low - MgO magmas. The latter, however, is based upon data from Thompson (1983) which as noted above was collected at P_{H_2O} = 1kb and upon ilmenite - magnetite phenocryst geothermometry from lavas of unknown but probably non - zero P_{H_2O} at the time of phenocryst growth. The evidence given above for low P_{H_2O} in the M2 felsites indicates that these magmas would be expected to have higher liquidus temperatures than predicted by the Sparks & Marshall MgO - geothermometer, and the discrepancy does not seem to invalidate either method.

The densities of the felsic magmas under these conditions are considered in section 4.3.3 along with those of the more mafic MBG magmas.

4.2.6. Implications of the petrogenesis of the felsic rocks for the behaviour of the MBG magma chamber at the end of M1.

The results of the geochemical and mineralogical studies of the felsic rock types associated with the MBG which have been presented in this section can be summarised as follows:

1). None of the felsic rocks were produced by crystal fractionation within the MBG magma chamber. Instead, they were produced by melting of pre - existing fusible lithologies in the wall of the intrusion.

2). The rocks sampled are unrelated to the rocks which presently outcrop adjacent to them in the main wall of the intrusion. With one exception, the felsic magmas appear to have either flowed up the wall of the magma chamber or have been intruded upwards as separate small intrusions after having been generated by melting at depth. The exception to this rule is formed by the diopside microgranites south of Duin Bhain. These occur with rocks from the same unit (the Scalpa Sandstone) as their likely protoliths, in a pseudoscreen which forms the tip of a downfaulted block (section 3.2.3.2), and some metres below the probable position of the Scalpa Sandstone in the main wall of the MBG in the Duin Bhain area.

The other felsic rocks analysed can be assigned, with varying degrees of confidence and

precision, to particular wall rock lithological units which occur or are believed to occur below the present level of exposure. The subalkaline granitoid rocks appear to have been produced by partial remelting, without separation of residual crystals, of earlier Tertiary granodioritic to adamellitic intrusions. The peraluminous microgranitoids on the southern side of the intrusion appear to be melted siltstones from the Lower Pabba Beds (267/1) or mixtures of these with subalkaline granitoid magmas (183D1). Finally, the rheomorphic breccia intrusions at Glendrian Bay appear to correspond to a largely fused sequence of interbedded fusible siltstones and refractory arkosic sandstones, the latter corresponding to the residual quartz - rich blocks which are a characteristic feature of the rheomorphic breccias. This does not correspond to any of the exposed Jurassic or Moinian lithological units and is best interpreted as part of a Triassic sequence below the Jurassic sequence in north - west Ardnamurchan.

The upward movement of the anatectic felsic magmas is as would be expected, given that crystal - poor felsic magmas are generally of lower density than mafic magmas even though the latter are generally at higher temperatures (Murase & McBirney 1973; see also section 4.3.3, below).

3). The xenolith swarms also appear to correspond to particular wall rock units. **Where the relative positions of xenoliths and source rocks can be determined, the xenoliths appear to occur below the latter, suggesting that they sank in the magma chamber.** In some cases they correspond to the refractory component of otherwise fusible rock units, suggesting that physical separation of xenoliths and felsic magmas has taken place, either as a result of density differences or of assimilation of fusible components into the basic or hybrid magmas which host the xenoliths.

4). Wall - rock melting probably occurred at a total pressure of less than 1 – 1.3 kb, under strongly water - deficient conditions, at peak temperatures of 1070 – 1120°C. It is possible but unlikely that $P_{H_2O} \approx P_{total}$, in which case P_{total} was probably around 0.5kb and the felsic magmas may have formed at temperatures of as little as 990°C.

Conclusion (1) implies that, prior to the sudden cooling of the wall rocks at the end of M1, the wall of the MBG magma chamber was a site of active country - rock melting at the sites of generation of the felsic magmas. This latter qualification is necessary because of the age relationships of the M2

felsites, which were generated by wall - rock melting at depth and then intruded to higher levels at which the quenching had already taken place. As note in Chapter 3, this is possible if the M1/M2 transition was diachronous and propagated down the wall of the magma chamber with time. In terms of the classification of magma chamber boundary layers outlined in section 4.1, conclusion (1) implies that **the M1 magma chamber had a type 2 or type 3 boundary layer.**

Conclusions (2) and (3), however, together with the observations discussed in Chapter 3 to the effect that visible evidence of in situ high - degree wall - rock melting and large - scale anatectic magma mobilisation during M1 only occurs in and around the downfaulted blocks in the wall of the intrusion, indicate that the wall - rock melting process was in fact more complex. In part the lack of wall - rock melting in the main wall of the intrusion at the present level of exposure could be explained by the fact that many of the rocks exposed at the present outcrop of the contact have refractory compositions. However, the lateral uniformity and known structure of the Jurasic sequence means that the fusible siltstones of the Lower Pabba Beds can be predicted to occur in the wall of the MBG at depths of a few tens to a few hundreds of metres below the present level of exposure along both the northern and southern margins of the intrusion. Despite this, granitoid rocks derived from the Lower Pabba Beds only occur in the section of the contact zone between An Acairseid and the Dubh Chreag gorge. In view of the association of large - scale country rock melting with downfaulted blocks at the present level of exposure it is of interest to note that this is the only section of the contact in which a major M1-age set of the concentric inward - dipping normal faults associated with downfaulted block formation is predicted to intersect the wall of the MBG at a similar depth to the occurrence of the Lower Pabba Beds in the wall (see Fig. 3.13). It therefore appears that the melting which produced magmas such as 267/1 and the peraluminous component of 183D1 also occured in the tip of a dowfaulted block where it projected into the M1 magma chamber. The depths and distributions of the source rocks of the rheomorphic breccias and the subalkaline granitoids are not well enough constrained for similar reasoning to be applied to see if the model also applies to them.

Although the geometry of the main, southernmost concentric normal fault on Druim na Gearr Leacainn (Fig. 3.11) is such as to indicate that Scalpa sandstone should be present close to the tip of its hanging wall block, diopside granites do not occur on its northern side, as would be predicted on the downfaulted block melting model.. This can, however, be explained away by the uncertainty

in the age of movement on this fault, which is only constrained to have been earlier than the later stages of M2 (section 3.2.5.1). Hybrid rocks with a component derived from the more northerly blocks, which are known to have been displaced by M1 fault movements, are present on the north side of the downfaulted blocks (see section 4.4.1.1, below).

The distribution of wall rock xenoliths in monolithological swarms within the magma chamber also supports the idea of anatectic magma generation being confined to the projecting tips of the downfaulted blocks. Each of the country rock units has its own characteristic rock types (for example, quartzites and ferriginous nodules in the Lower Pabba Beds, and quartzites and calc - silicate rocks in the Scalpa Sandstone). Consequently, melting and mobilisation of the tip of a downfaulted block would produce a low - density felsic magma containing residual blocks composed of whichever refractory lithology was present. Such mixtures – essentially rheomorphic breccias – form the western end of the Duin Bhain pseudoscreen and also occur on the southwestern side of the downfaulted block on Hill 210, just north of Loc 183 (see section 3.2.5.2, especially Fig. 3.12). Assuming that they were initially associated with felsic anatecticmagmas, the subsequent behaviour of the refractory blocks appears to have been density - dependent. Thus the partially melted (and therefore low - density, quite apart from any compositional effects) quartzite blocks in the rheomorphic breccia intrusions appear to have remained in suspension. In contrast the refractory pelitic and semi - pelitic rocks which form the swarm at An Acairseid (Loc 274) and xenoliths 150/1 and 140/3 appear to have become separated from any felsic magmas which may have originally enclosed them. The mechanism of this process of separation is considered further in section 4.5.

The association of high - degree partial melting and anatectic magma generation with the formation of the downfaulted blocks during M1 is easily explained in terms of the heat flow into and out of that part of the block which projected into the magma chamber after its formation. This situation is depicted schematically in Fig. 4.17. In qualitative terms, two factors will contribute to heating and melt formation within the projecting tip of the fault block:

1). The area exposed to the magma in the magma chamber is increased by the area of the fault surface between the tip of the block and the intersection of the fault with the wall of the magma chamber in the footwall of the fault.

Fig. 4.17. Cartoon cross - sections showing simplified thermal evolution of a downfaulted block projecting into a magma chamber, ignoring effects of melting in the block upon heat flow.

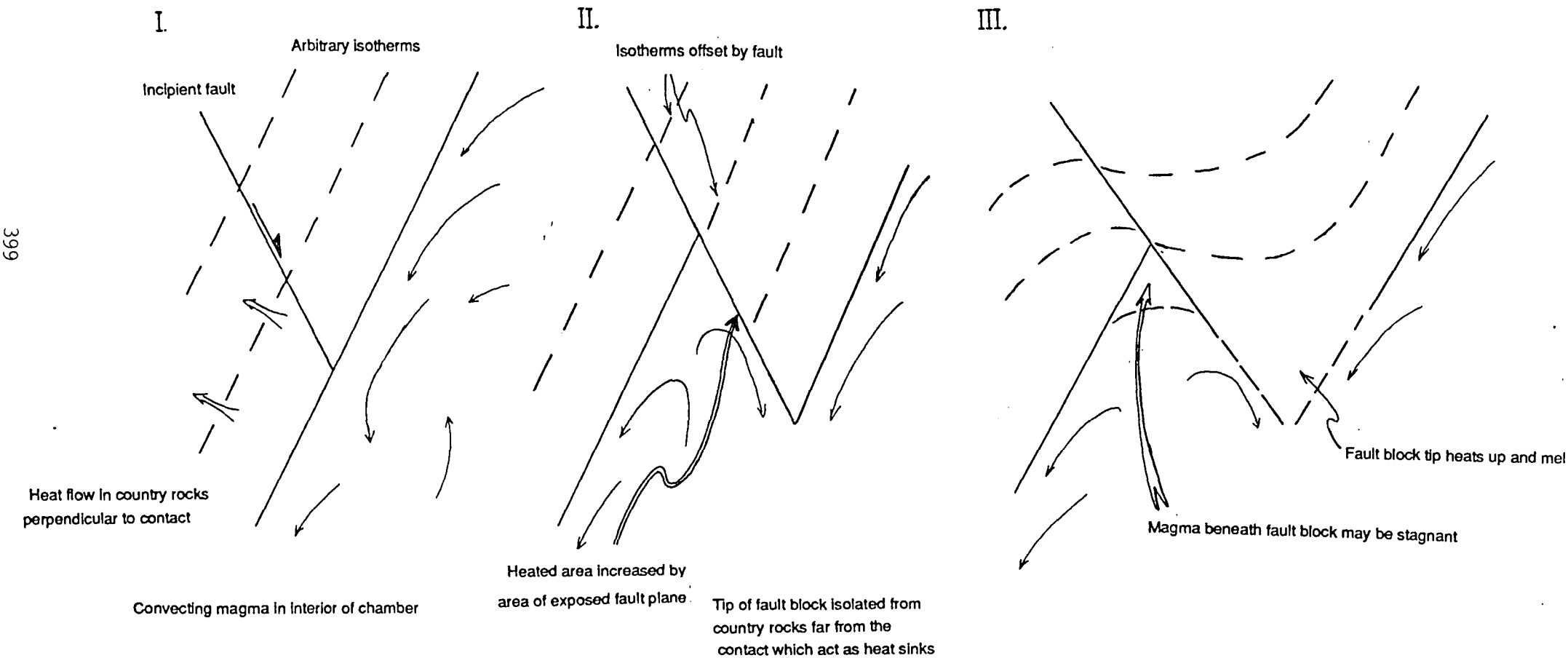

2). Heat flow out of the projecting tip of the downfaulted block may be reduced if the inward - dipping fault makes an acute angle with the wall of the magma chamber as it is then partially isolated from the cooler rocks away from the intrusion.

The isotherms sketched in in Fig. 4.17 are only schematic and do not take account of two additional factors which may change heat flow into and within the downfaulted block . The first of these is the latent heat absorbtion which will occur if some or all of the blocks in the downfaulted block are fusible. This will tend to reduce the rate of temperature increase in those parts of the block which are melting. In effect, the melting reactions act as a thermal buffer. A similar effect in the case of regional metamorphism has been modelled by Zen (1988) and discussed in terms of the likely melting reactions by Vielzeuf & Holloway (1988). Numerical modelling by Zen (1988) suggested that large - scale melting could reduce the peak temperature of regional metamorphism by up to 100°C. An upper limit is placed on the temperature difference ΔT which can be produced by this thermal buffering effect by:

$$\Delta T = \frac{L}{C_p} - \Delta T_m \tag{4.8}$$

where L is the latent heat of melting, C_p the heat capacity (assumed constant) and ΔT_m the temperature interval over which melting takes place. This limit will be most closely approached in the case of thick fusible beds affected by rapid heating by a very much hotter magma, when heat flow from adjacent refractory beds (which will be hotter as a result of not being thermally buffered) is reduced to a minimum. In such a situation, the thermal buffering effect could produce a large body of mobile, high percentage partial melt in the downfaulted block substantially cooler than the main wall of the magma chamber if the latter was dominated by refractory rocks. Conversely, if the downfaulted block was composed of refractory rocks which did not show large degrees of melting (and therefore have a large thermal buffering effect) until very high temperatures were reached, melts could be produced in downfaulted blocks at higher temperatures than the temperature of the main wall of the magma chamber if the rigidus temperature of the wall rocks exceeded that of the magma in the magma chamber. This would account for the occurrence in downfaulted blocks projecting in the MBG of high percentage partial melting of normally refractory rocks, for example the melting of Middle Pabba Beds lithologies recorded in rocks within the downfaulted block on Hill 210 (section 3.2.5.3).

The second additional factor is the effect of the irregular deformation of the wall upon the magma

chamber boundary layer itself. All numerical and analogue experiments upon magma chamber boundary layers to date have used a model magma chamber which does not deform its walls in an irregular fashion: the only studies of chambers with deformable walls have been carried out in connection with diapirs, whose walls deform in a ductile fashion (e.g Marsh 1982). In general terms the deformation would be expected to disrupt the downward flow of cooled magma at the wall of the magma chamber and bring hot magma from the interior of the chamber into direct contact with the wall. Further discussion of potential effects of this sort is deferred to section 4.5, after evidence relating to the flow of magma in the M1 boundary layer has been discussed.

No attempt is made here to model the complex two - dimensional moving - boundary heat flow problem which melting of such a downfaulted block represents. However, the control exerted by the formation of the downfaulted blocks upon wall - rock melting around the Hypersthene Gabbro has one very important implication. If appreciable volumes of wall - rock, anatectic magmas were only produced when the heat flux into the country rocks was reduced and the effective heat flux from the magma was increased, by the effects described above, then it follows that **at the main wall of the intrusion $Q_c \approx Q_m$ for the period in the life of the MBG magma chamber, just prior to the end of M1, which is recorded by the contact zone suite of the MBG.** It should be noted that Q_m cannot have been appreciably less than Q_c at this time because otherwise M1 cumulates would have formed on the main wall of the intrusion and the felsic rocks would not occur directly against the contact where they have been preserved above their initial site of formation (as is observed, for example in the case of the M1 microgranodiorites at Glendrian Bay and the anomalous granitoids on Hill 210). The small but finite rate of melting, averaged over the entire wall of the intrusion, which resulted from melting in the downfaulted blocks, suggests however that Q_c was slightly less than Q_m when averaged over the wall of the intrusion. In theory this difference can be obtained from equation (4.3). However, the rate of magma production due to melting of downfaulted blocks is unknown (largely because the frequency of formation of such blocks is very poorly known) and the difference between the two heat fluxes cannot be obtained from studies of the contact zone. An alternative method of constraining the difference between Q_c and Q_m, using the width of the M1 aureole, is followed in Chapter 5 (section 5.2).

As was suggested in section 3.2.7 on the basis of field evidence, the causal association of anatectic magma and xenolith swarm formation with the formation of downfaulted blocks by concentric normal

faulting implies that, when $Q_c \approx Q_m$, **the rate at which material is mobilised from the wall of a magma chamber, either as anatectic magmas or as residual blocks,** and made available for intrusion as separate bodies of magma or for contamination of the magmas in the interior of the magma chamber, **is controlled by the rate of deformation of the rocks around the magma chamber.** Furthermore, if the downfaulting produced by this deformation was episodic, as implied by the alternation of the inward - directed downfaulting with outward - directed reverse faulting and thrusting (Chapter 3, especially section 3.2.5.4) and by the high strain rates indicated by cataclasis on the faults concerned, then mobilisation of wall rock magmas would also be an episodic process. This would produce discrete and compositionally distinctive xenolith swarms and batches of anatectic magma, whose composition was controlled by the composition of the wall rocks present in the hanging wall of whichever part of the concentric fault system was active at the time of their formation, just above the intersection of the active fault(s) with the wall or the intrusion. This is precisely the pattern of spatial distribution of these rocks which is observed in the contact zone of the Marginal Border Group at the present day. The frequency with which a similar situation might arise in other magma chambers is considered in subsequent chapters.

4.3. Homogenous Basic and Intermediate Rocks of the Marginal Border Group.

The rocks dealt with in this section are those basic and intermediate rocks within the MBG and the associated minor intrusions which do not show mesoscopic (i.e. outcrop or hand - specimen scale) or textural evidence of incomplete magma mixing. It should be noted that the classification of MBG rocks into heterogenous hybrid and homogenous rocks was made on the basis of this evidence. It does not exclude the possibility of magma - mixing, followed by macroscopic homogenisation, during the evolution of the magmas represented by the homogenous rocks. The purpose of distinguishing the two groups of rocks on petrographic grounds was to separate those rocks which have been affected by incomplete magma mixing at the wall of the MBG magma chamber(the heterogenous hybrid rocks to be dealt with in section 4.4) from those which have not.

The basic and intermediate rocks within the MBG and in the associated M1 and M2 minor intrusions are of particular interest as potential products of the processes which operated within the MBG magma chamber. The principal purposes behind the study of these rocks were to investigate the effects of the processes of wall - rock melting and magma mixing, as recorded in the contact zone, upon the geochemistry of the magmas in the interior of the magma chamber, and to determine their physical properties (particularly temperatures) for the purposes of modelling the MBG M1 boundary layer. The issue of the geochemical relationships of the various groups of small intrusions emplaced in the MBG and the adjacent country rocks between early M1 and late M2, to the MBG magmas, will also be considered in this section.

4.3.1. General Geochemistry of the Basic and Intermediate Rocks.

The main features of the basic and intermediate MBG rocks and of the Groups 1 and 2 cone sheets are summarised in Fig. 4.18. The porphyritic rocks of the later M2 minor intrusions present special problems of interpretation and are dealt with in a later section (4.3.4). Overall, the rocks show a tholeiitic fractionation trend with initial Fe and Ti enrichment followed by Fe and Ti depletion, although strictly, since they are of distinct ages within the life of the MBG, they should be considered to form a series of overlapping parallel trends. The fractionating crystal assemblages which produce these trends can be summarised as follows in sequence from high - MgO to low - MgO rocks:

Fig. 4.18. Geochemistry of the homogenous basic and intermediate rocks of the MBG and rocks from the associated minor intrusions. of M1 to mid - M2 age. Subalkaline granitoid compositions plotted to complete tholeiitic fractionation trend (see text)

Generalised tholeiitic fractionation trend, marked to highlight homogenous hybrid nature of many of the rocks plotted: ——→

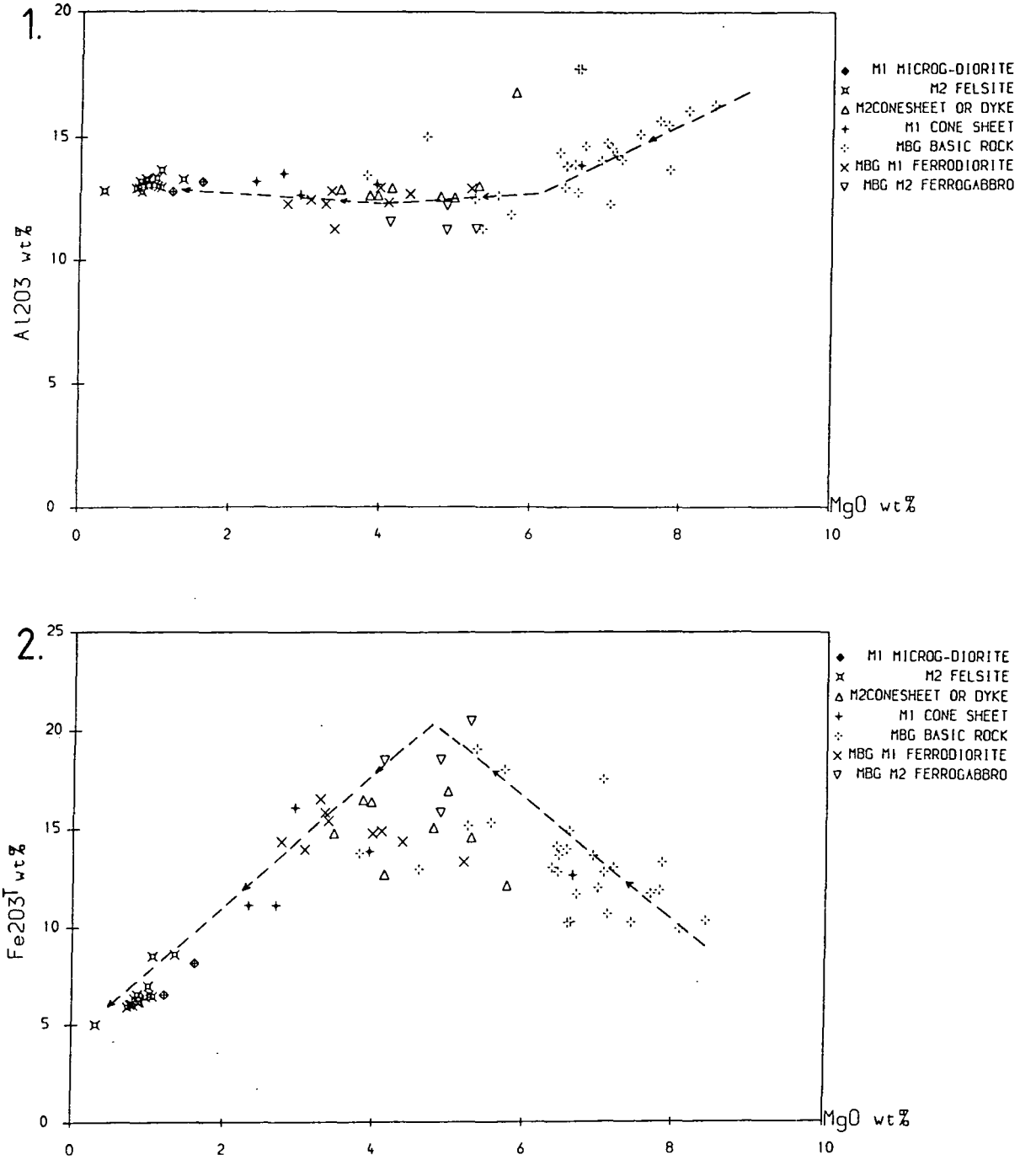

3.

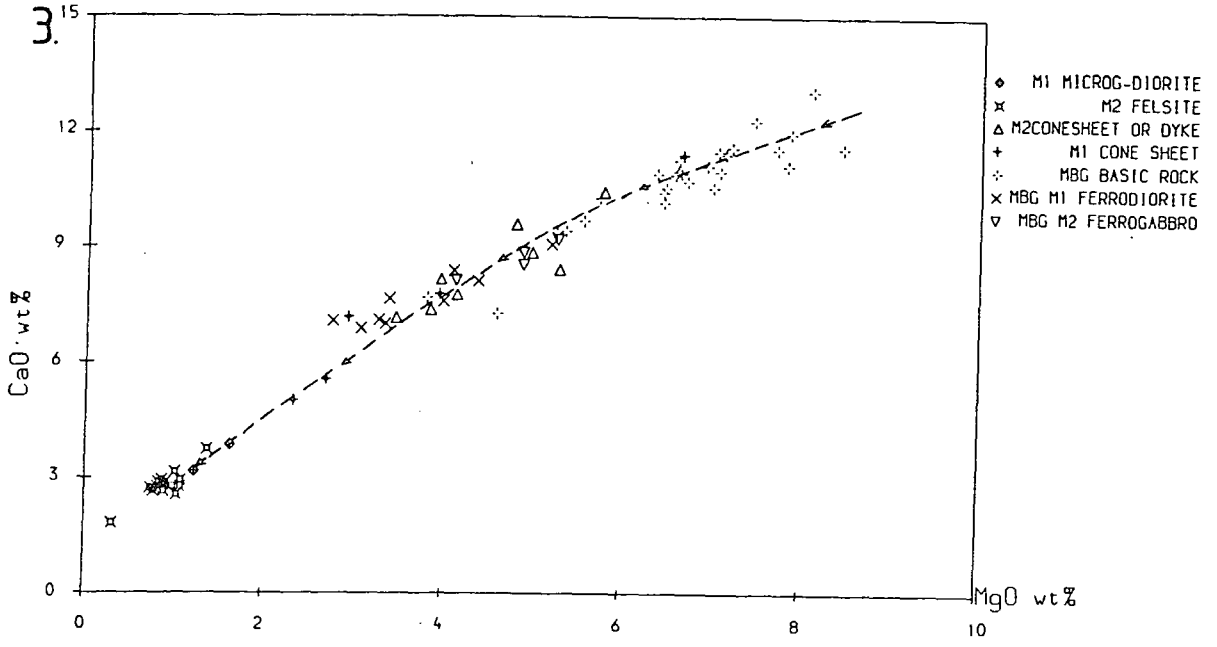
CaO wt%
MgO wt%
0
2
4
6
8
10
3
6
9
12
15
M1 MICROG-DIORITE
M2 FELSITE
M2CONESHEET OR DYKE
M1 CONE SHEET
MBG BASIC ROCK
MBG M1 FERRODIORITE
MBG M2 FERROGABBRO

4.

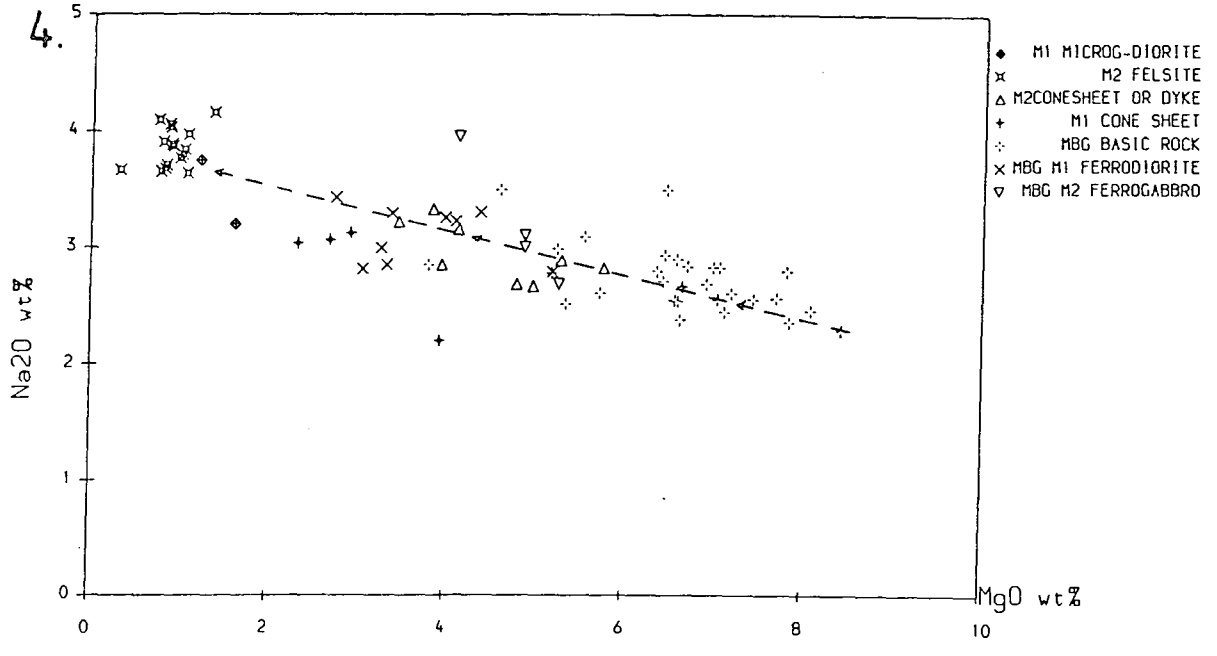
Na2O wt%
MgO wt%
0
1
2
3
4
5
6
8
10
M1 MICROG-DIORITE
M2 FELSITE
M2CONESHEET OR DYKE
M1 CONE SHEET
MBG BASIC ROCK
MBG M1 FERRODIORITE
MBG M2 FERROGABBRO

5.

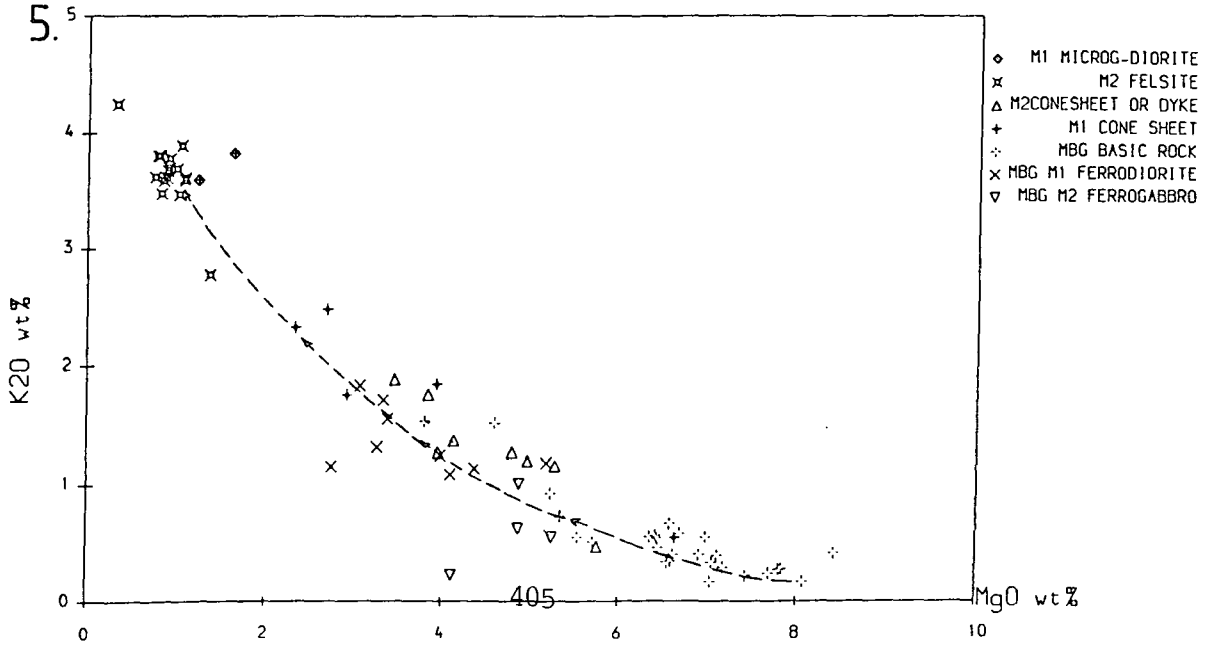
K2O wt%
MgO wt%
0
1
2
3
4
5
6
8
10
M1 MICROG-DIORITE
M2 FELSITE
M2CONESHEET OR DYKE
M1 CONE SHEET
MBG BASIC ROCK
MBG M1 FERRODIORITE
MBG M2 FERROGABBRO

6.

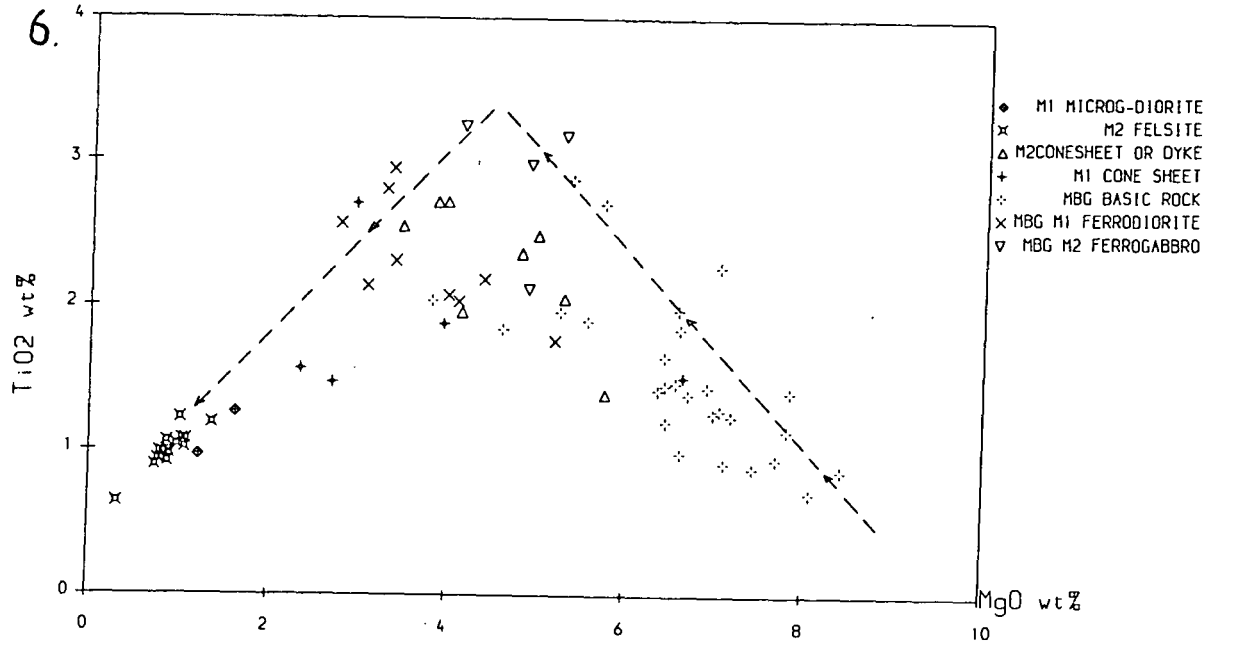
TiO2 wt%
MgO wt%
0
1
2
3
4
0
2
4
6
8
10
M1 MICROG-DIORITE
M2 FELSITE
M2CONESHEET OR DYKE
M1 CONE SHEET
MBG BASIC ROCK
MBG M1 FERRODIORITE
MBG M2 FERROGABBRO

7.

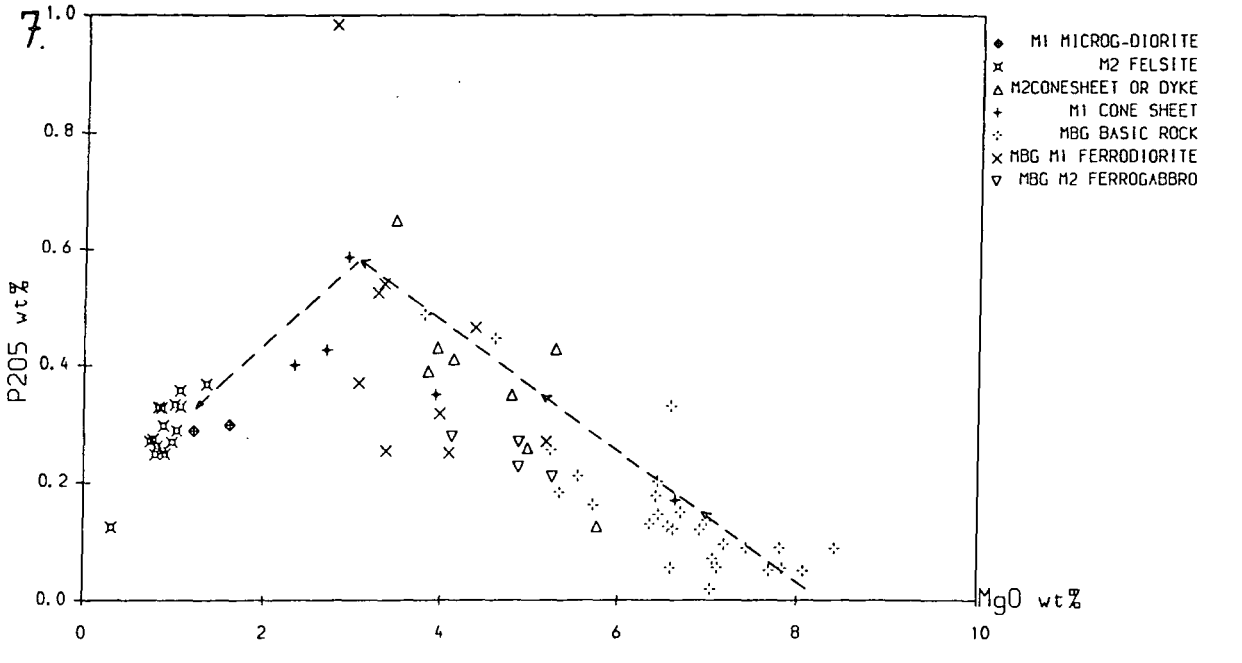
P2O5 wt%
MgO wt%
0.0
0.2
0.4
0.6
0.8
1.0
0
2
4
6
8
10
M1 MICROG-DIORITE
M2 FELSITE
M2CONESHEET OR DYKE
M1 CONE SHEET
MBG BASIC ROCK
MBG M1 FERRODIORITE
MBG M2 FERROGABBRO

8.

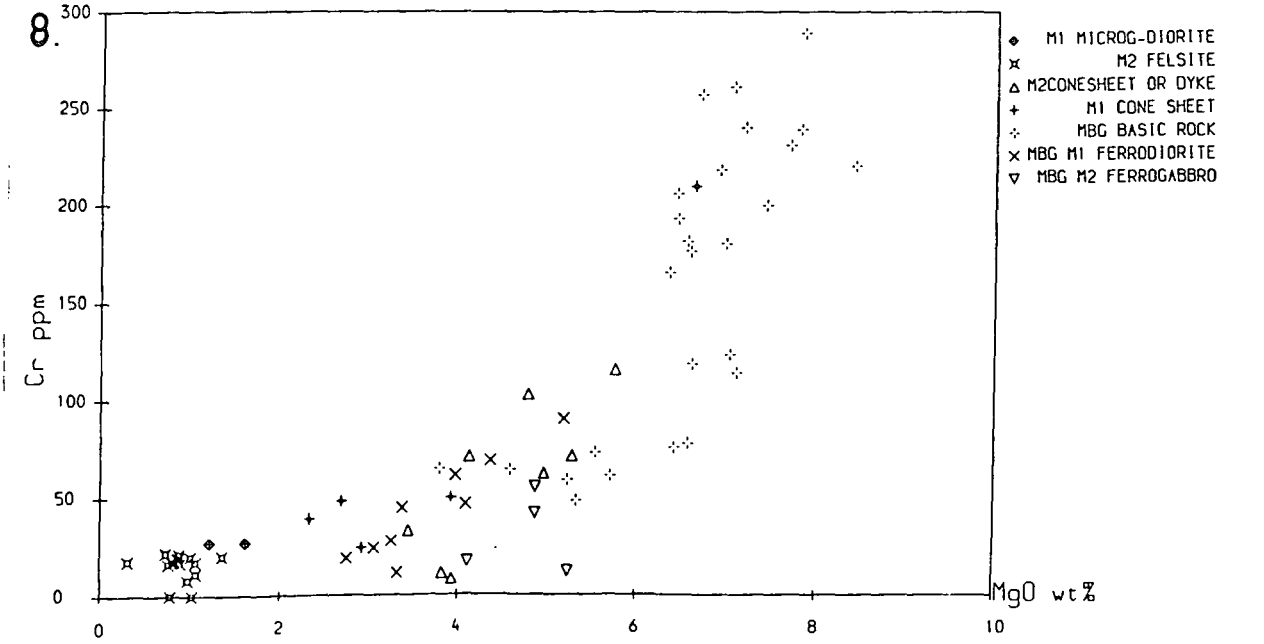
Cr ppm
MgO wt%
0
50
100
150
200
250
300
0
2
4
6
8
10
M1 MICROG-DIORITE
M2 FELSITE
M2CONESHEET OR DYKE
M1 CONE SHEET
MBG BASIC ROCK
MBG M1 FERRODIORITE
MBG M2 FERROGABBRO

9.

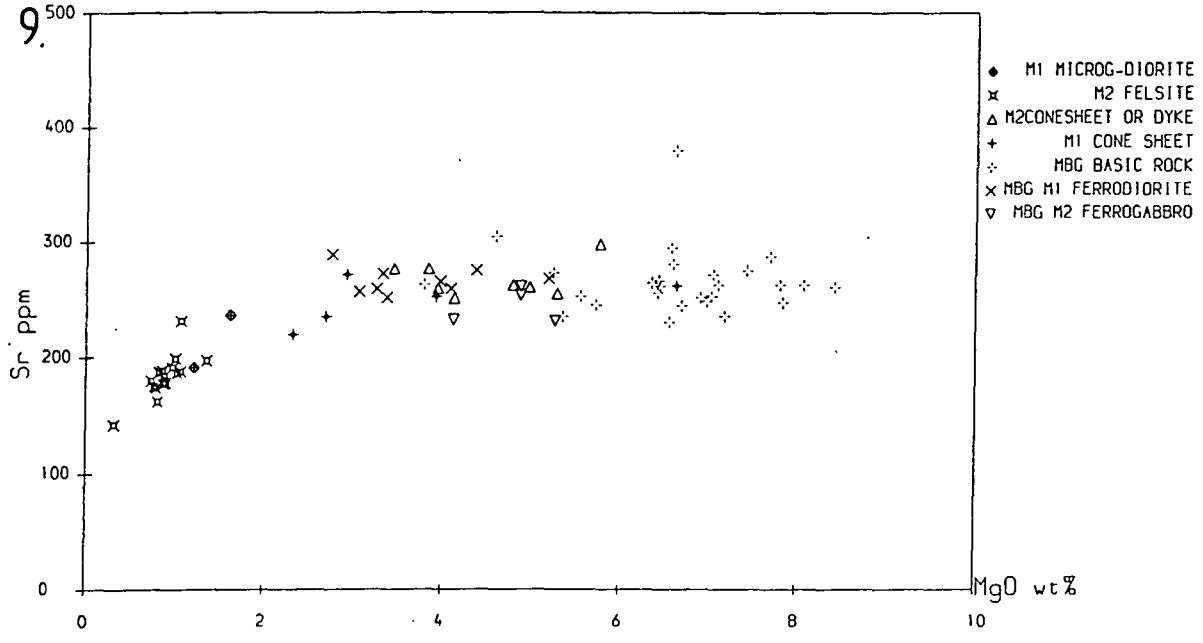
Sr ppm
500
400
300
200
100
0
0
2
4
6
8
10
MgO wt%
M1 MICROG-DIORITE
M2 FELSITE
M2CONESHEET OR DYKE
M1 CONE SHEET
MBG BASIC ROCK
MBG M1 FERRODIORITE
MBG M2 FERROGABBRO

10.

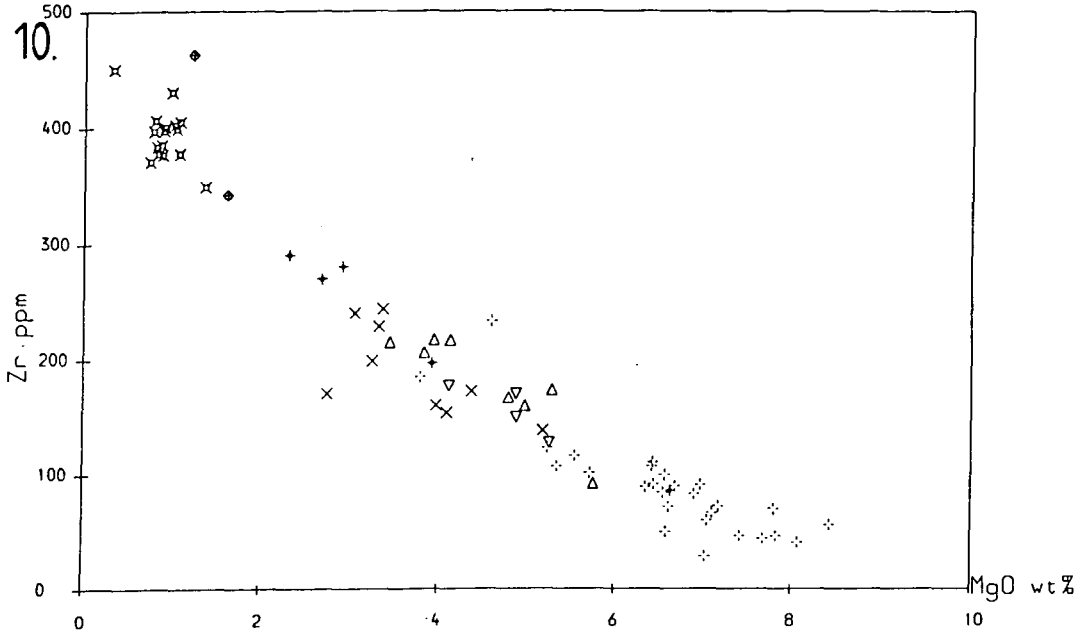
Zr ppm
500
400
300
200
100
0
0
2
4
6
8
10
MgO wt%

1). 6 – 8% MgO: plagioclase + olivine (note falling Al_2O_3 and CaO, uniform Sr with decreasing MgO). The decrease in CaO with fractionation may suggest the involvement of clinopyroxene in the production of the fractionation trend. This 'cryptic fractionation' is a common feature of tholeiitic suites such as Mid - Ocean Ridge Basalts (Thompson 1987). Possible causes of such trends are discussed in section 6.2.1 in the context of the Inner Series gabbronorite suite rocks, which also show 'cryptic fractionation' of clinopyroxene.

2). At $\approx$ 6% MgO, augite joins the fractionating assemblage, producing an increase in the Ca content of the fractionating assemblage and a decreas in its Al content, relative to its MgO content (note the resultant kinks in the trends of CaO and Al_2O_3 in Figs. 4.18.3 and 4.18.1 respectively).

3). The appearance of FeTi oxides (or Ti - magnetite alone) in the fractionating assemblage at 4.5 – 5% MgO is marked by sharp inflections in the plots of $Fe_2O_3^T$ (Fig. 4.18.2) and TiO_2 (Fig. 4.18.6) vs. MgO.

4). The final change in the fractionating assemblage apparent in these plots is the appearance of apatite in equilibrium with magmas with about 3% MgO (Fig. 4.18.7).

The plots which make up Fig. 4.18 show varying amounts of scatter about this overall fractionation trend which can be attributed to a number of causes. These vary between plots and are discussed here in turn:

1). A small number of samples from within the MBG are plagioclase - phyric and these lie off the main trend in the plots of Al_2O_3, Sr and, in some cases, CaO or Na_2O as well. They appear to contain accumulative feldspar rather than simply being liquid compositions which have undergone two - stage cooling histories. In general, however, the rocks lie close to the main fractionation trend, which appears to approximate to a liquid line of descent in these plots.

2). Those plots with inflections resulting from a change in the fractionating crystal assemblage partway along the fractionation trend (particularly plots involving Fe, Ti and P (4.18.2, 4.18.6 and 4.18.7 respectively)) contain a large number of samples with compositions lying in the

triangular field beneath the fractionation trend. This is a characteristic feature of suites of rocks affected by magma mixing between end - members which lie on opposite sides of the inflection in the main fractionation trend. The limits of the compositional range of magmas which are involved in this mixing are defined by the vertices of the triangular field in each plot. Considering only those magmas of M1 age for the moment, it is apparent from Figs. 4.18.2, .6 and .7 that the extreme end members are a ferrodioritic magma with 2.5 – 3% MgO and a low - Ti tholeiite with at least 8% MgO, and that a range of end member magmas between the two including extremely Ti and Fe - rich ferrogabbroic compositions were also involved. The upper limit on the MgO content of the magmas involved in mixing is rather poorly constrained because it coincides with the highest - MgO M1 magmas analysed. However, the boundaries of the field of analyses in Fig. 4.18.2 and 4.18.6 converge on a point with MgO just above 8%, suggesting that this is indeed the highest MgO content of any magma involved in the mixing, rather than just an artefact of the data set. The field of compositions in Fig. 4.18.7 does not show similar convergence at high MgO, because of the much greater error in P_2O_5 determinations, relative to the errors in Ti or Fe determinations at the low P_2O_5 concentrations found in the MgO rich rocks (see Appendix 1).

Turning to the later magmas, the M2 ferrogabbros mainly lie close to the tholeiitic fractionation trends in Figs. 4.18.2, .6 and .7, implying that they can be considered as simple residual melts remaining after about 70% partial crystallisation of tholeiitic magmas broadly equivalent to the rocks in which they occur. This suggests that these rocks represent residual melts extracted from the surrounding rocks during the relatively slow cooling of the Marginal Border Group rocks at the beginning of M2, prior to the quenching recorded by the interstitial devitrified glasses and microgranophyres present in some of these ferrogabbros (see Chapter 3, especially section 3.2.2). However, some of the ferrogabbroic rocks are themselves depleted in certain incompatible elements, (for example K (Fig. 4.18.5) but not Zr (Fig. 4.18.10)) suggesting that they themselves may have had residual melts expelled from them. The fact that they are depleted in K but not Zr suggests, however, that this may simply be an effect of later hydrothermal alteration. In contrast, the M2 (Group 2) cone sheet samples plotted in Fig. 4.18 plot below the fractionation trend in the Ti, Fe and P plots and appear, like many of the M1 magmas, to be homogenous hybrid rocks produced by complete mixing of magmas of contrasted compositions.

3). As was mentioned in (2) above, some of the rocks within the MBG itself may in fact not be true liquid compositions, being residua remaining after extraction of evolved interstitial melts. However, the fields occupied by the rocks within the MBG, which includes both quench - textured samples from homogenous pillows in the contact zone and coarser - grained rocks from further within the intrusion, shows complete overlap with the compositional fields of the M1 and M2 cone sheets. The latter intrusions are too small to have been affected by late - stage melt expulsion. The compositional overlap between the two groups of rocks therefore implies that any late - stage melt expulsion which may have occurred within the MBG produced shifts in the compositions of the parent rocks which were small compared to the compositional variations already present in them. This implies that the M2 ferrogabbroic veins and pods must only represent a small fraction of the partially crystallised rocks from which they were extracted, including those immediately adjacent to ferrogabbro vein outcrops (for example, samples 100/2, 193/2 and 102/2; see Appendix 2). The observation made in section 3.2, that the veins and pods form a large proportion of the contact zone in some sectors of the contact (particularly at Ardnamurchan Point and at Corrachadh Mhor; see section 3.2.4) therefore implies that these residual melts migrated some distance (tens of metres or more) between the rocks from which they formed and the places in which they eventually crystallised. Detailed discussion of late - stage melt migration in the MBG, in particular its timing relative to crystallisation of the basic rocks, is deferred to Chapter 5 as it has to be considered in the context of the cooling of the MBG which took place during M2.

4). Analytical errors. The abundances of P_2O_5 and Zr in the more mafic rocks, and of Cr in the more evolved rocks, are close to the detection limits of these elements by ICP - AES and XRF analysis methods (see Appendix 1). As a result they are likely to be affected by random and sample - specific errors due to counting statistic effects and incomplete background and interference corrections. However, subsequent arguments do not depend on the scatter about the trends in these plots, although use is made of the overall trends in the abundances of these elements which are apparent from these diagrams.

A further possible cause of scatter in these plots, particularly plots of incompatible elements against MgO, is variation in the amount of crustal contamination independent of the degree of fractionation of the rocks and hence their MgO contents. The pattern of contamination in these rocks is considered

further in section 4.3.2.

The **lack** of scatter about the fractionation trend in certain plots in Fig. 4.18, notably plots of CaO, Al_2O_3 and Sr vs. MgO (apart from the rare plagioclase - accumulative samples) and also Zr vs. MgO, strongly suggests that the basic and intermediate rocks all form a cogenetic suite with a relatively uniform parental magma composition, with uniform elemental abundances and ratios at a given MgO content. The good negative correlation of Zr (a relatively incompatible element) against MgO in particular implies a constant degree of partial melting in a relatively homogenous mantle source, since Zr abundances in the MBG magmas at a given MgO content are very uniform. It should be noted, however, that none of these elements are very highly concentrated in most components of the crust of North - West Scotland (see Chapter 2) relative to their abundances in basaltic or even picritic melts, and as a result their abundances at any one MgO content are not sensitive to small differences in the amounts or timing of crustal contamination.

The distribution of M1 samples within the MBG shows a fairly strong systematic variation with distance from the contact. The less MgO - rich samples (including a number of samples which were initially classified in the field as basic rocks and are plotted as such in Fig. 4.18 and subsequent diagrams) tend to occur within the contact zone, either as homogenous inclusions within hybrid rocks where the contact zone suite defined in section 3.2.7 is well developed, or as more continuous outcrops within a few metres of the contact where it is not. More primitive compositions also occur in the contact zone, mainly as pillows, and all the samples collected away from the contact in the interior of the intrusion have MgO $\geq$ 6% except on the western margin where more evolved rocks are more abundant. Although sampling was not intensive enough to make estimates of relative areas of outcrop, it is apparent that the homogenous part of the MBG at the present level of exposure is dominated by rocks with $\geq$ 6% MgO. The mixing trends apparent in Figs. 4.18.2, 4.18.6 and 4.18.7 indicate, however, that many of these rocks contain a significant component (of the order of 10 - 30%) of more evolved material.

A final significant feature of the plots in Fig. 4.18 concerns the positions of the M2 cone sheets relative to the M1 rocks in these plots. They occupy a field within the field of M1 rocks and below the tholeiitic fractionation trend in Figs. 4.18.2, .6 and .7. This last feature implies that they too are composed of homogenous mixtures of MgO - rich and MgO - poor magmas and that, therefore, the

MBG magma chamber still contained a wide range of magma compositions later in M2, comparable to that present at the end of M1 and the earliest part of M2 when the MBG rocks were solidified. Similarly, the M1 cone sheets mainly plot within the field of the basic and intermediate rocks within the MBG, although some have lower MgO contents and are more evolved than any of the homogenous basic to intermediate rocks within the MBG. These extremely MgO - poor M1 cone sheets are best interpreted as magmas tapped from the heterogenous hybrid magmas present at the wall of the MBG magma chamber towards the end of M1 (see section 4.4) or as evidence for the presence of evolved tholeiitic andesite to dacite magmas in the MBG magma chamber earlier in M1 than the period represented by the MBG rocks. There is however no evidence for secular change in the range of magma compositions present in the MBG magma chamber during the period from the latter part of M1 through to the end of Group 2 cone sheet emplacement, partway through M2.

When compared to other, better known suites of British Tertiary basic magmas, the MBG tholeiites show a close resemblance to the other tholeiitic magma suites, such as the Preshal Mhor magma type (Skye) and the Non - Porphyritic Central magmas of Mull. They appear, however, to have been even more depleted in incompatible elements than these suites prior to crustal contamination. This feature is illustrated by Fig. 3.19, which shows the chondrite - normalised trace - element patterns of three fine - grained basic rocks from the MBG. All three were collected from rocks with pillowed chilled contacts against hybrid or felsic rocks and are therefore certain to correspond to liquid compositions, apart from the few percent of plagioclase phenocrysts which occur in all three. All three show evidence of crustal contamination with calc - alkaline rocks in the shape of high La_N/Ta_N, in the range 2 to 5: BTVP magmas without isotopic evidence of crustal contamination all have La_N/Ta_N in the range 0.6 – 2.0 (Thompson & Morrison 1988). They are also characterised by a very strong depletion of Ta relative to Zr, Hf, Ti and the HREE. This is not a consequence of crustal contamination as all the potential contaminants have Ta_N/Yb_N greater than 1 (see Chapter 2) and crustal contamination will therefore tend to raise the Ta/Yb ratio of contaminated relative to uncontaminated magmas with initial $Ta_N/Yb_N \leq 1$. This suggests that the parental, uncontaminated magmas of the MBG tholeiite suite must have had a strongly incompatible - element depleted chondrite - normalised 'spiderdiagram' similar to that of depleted Mid - Ocean Ridge Basalts.

4.3.2. The Nature of Crustal Contamination in the Homogenous Marginal Border

Fig. 4.19. Chondrite - normalised element plot for three M1 chilled basalt/dolerite samples from the northern margin of the MBG. Note variation in La/Ta ratio (see section 4.3.2).

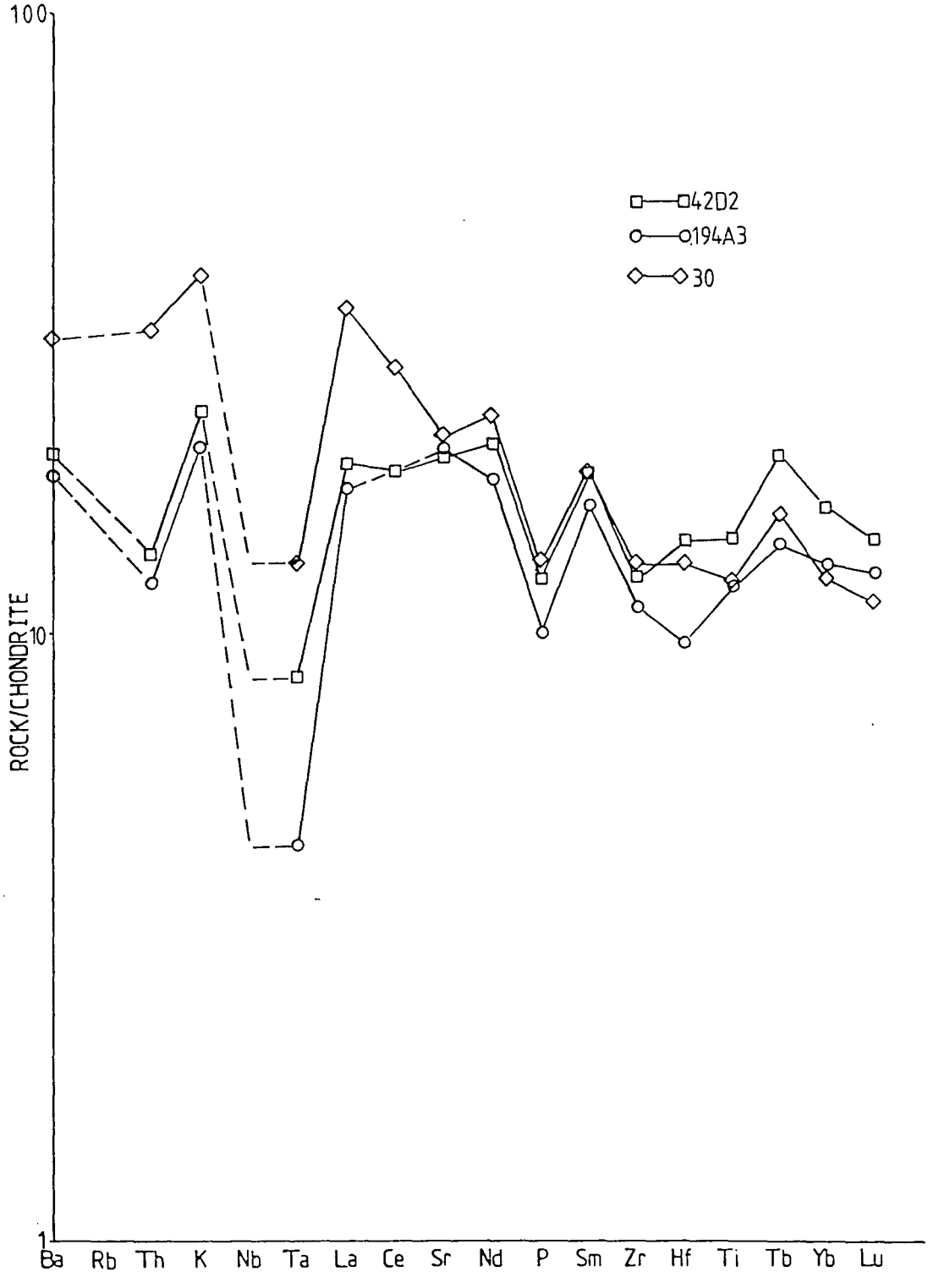

Group Rocks: Contamination Within or Beneath the MBG Magma Chamber ?

As was shown in Chapter 2, the various crustal rock units which are exposed at the surface in Ardnamurchan or inferred to lie beneath it have a variety of characterisitic compositional features. This means that, by identifying the source(s) of the crustal contaminants in the mafic magmas, it should be possible to identify where in the crust this contamination took place. In particular, it should be possible to distinguish contamination occurring at high crustal levels, above the Moine thrust plane and probably within the MBG magma chamber, from contamination which occurred as the magmas passed through the Lewisian Gneiss complex, either in conduits feeding the Ardnamurchan central complex or in deep, mid - to lower - crustal magma chambers (Fig. 2.9).

4.3.2.1. Assimilation before, during or after fractional crystallisation ?

As a preliminary stage in the identification of the crustal contaminants in the MBG magmas it is necessary to determine whether the contamination took place before, during or after the fractional crystallisation which produced the wide compositional variations shown in Fig. 4.18. In particular, it is essential to establish whether the assimilation took place independently of fractional crystallisation or whether the two occurred together in a coupled assimilation - fractional crystallisation (AFC) process, becuse trends pointing towards spurious end - member compositions can result from the latter (De Paolo 1981).

As noted in Chapter 1, previous workers have been divided in their interpretations of the geochemistry of the Ardnamurchan cone sheets, a large proportion of which are formed by the Groups 1 and 2 cone sheets of chapter 3: as was shown in section 4.3.1, these two groups are essentially equivalent to MBG basic to intermediate rocks. Holland & Brown (1972) considered that all the cone sheets in Ardnamurchan lay on identical tholeiitic fractionation trends, although they recognised that they could not exclude the possibility of small amounts of crustal contamination in addition to fractional crystallisation and the statistical correlation method used to interpret their data could not have distinguished fractional crystallisation from an AFC process. In contrast, Thompson (1982) considered that the rocks lay on an AFC trend or trends, albeit ones in which greater rates of assimilation relative to the rate of fractional crystallisation occurred in the most magnesian, primitive and hottest magmas.

Problems of this sort can be resolved by plotting an index of contamination (ideally an isotopic ratio, but ratios of two incompatible elements which differ greatly between crust and mantle – for example the ratio of a large ion lithophile element such as K or Rb to a high field strength element such as P – can also be used) against an index of fractional crystallisation, such as MgO content. The results for homogenous basic and intermediate rocks from the MBG and associated minor intrusions are shown in Fig. 4.20. In 4.20.1 and 4.20.2, there is no correlation between K_2O/P_2O_5 or Ba/P_2O_5 (both sensitive indicators of crustal contamination because K and Ba are both greatly enriched in most calc - alkaline rocks relative to their abundances in tholeiitic magmas whilst P is not) and MgO, except when MgO falls below 3% and the rocks become sufficently evolved for apatite to begin to crystallise out (see Fig. 4.18.7). Similarly, in the smaller data set plotted in Fig. 4.20.3, there is no correlation between La_N/Ta_N and MgO, although the high La/Ta ratio indicates that much crustal contamination has taken place. Only in plots of Zr/P_2O_5 (Fig. 4.20.4) and K_2O/Zr (Fig. 4.20.5) are correlations with MgO evident at MgO $\geq$ 3%. If real, these particular correlations are more likely to reflect substitution of Zr into augite and Ti - magnetite than contamination, given the lack of correlation in the much more contamination - sensitive plots in Fig. 4.20.1 – 3. However, the positive blank Zr value, which was not correctly allowed for during processing of XRF data, means that the correlation in 4.20.4 and 4.20.5 may in fact be an analytical artefact, at least in part.

Fig. 4.20 therefore indicates that contamination of the MBG rocks was not coupled to fractional crystallisation in an AFC process. The lack of any correlation, positive or negative, between La_N/Ta_N and MgO which is apparent in Fig. 4.20.3 suggests in addition that the assimilation occurred prior to fractionation of the rocks to their present compositions, because La and Ta abundances both increase markedly with fractionation and as a result the La/Ta ratios of the felsic magmas would be much less sensitive to crustal contamination than those of the mafic magmas: post - fractionation contamination would therefore tend to produce a negative correlation between La/Ta and MgO, which is not observed.

4.3.2.2. Identification of the Contaminant Lithologies. Fig. 4.21 is the most important chemical plot used in this work to identify the sources of crustal contamination in the MBG basic and intermediate rocks. In this plot of chondrite - normalised Th/Hf against chondrite - normalised Hf/Sm ratio the Lewisian rocks analysed by Weaver & Tarney (1980, 1981) divide into two groups, low Th/Hf granulite - facies gneisses and high Th/Hf amphibolite - facies gneisses. Hf/Sm ratio in

Fig. 4.20. Incompatible - element - ratio plots for the MBG basic to intermediate rocks showing much variation in these ratios but no systematic variation (only in rocks with MgO content above 3% MgO in case of plots involving P2O5; see
text) in 4.20.1 - 3, indicating that contamination was not coupled to fractional crystallisation. Cause of variations in 4.20.4 and 4.20.5 discussed in text.

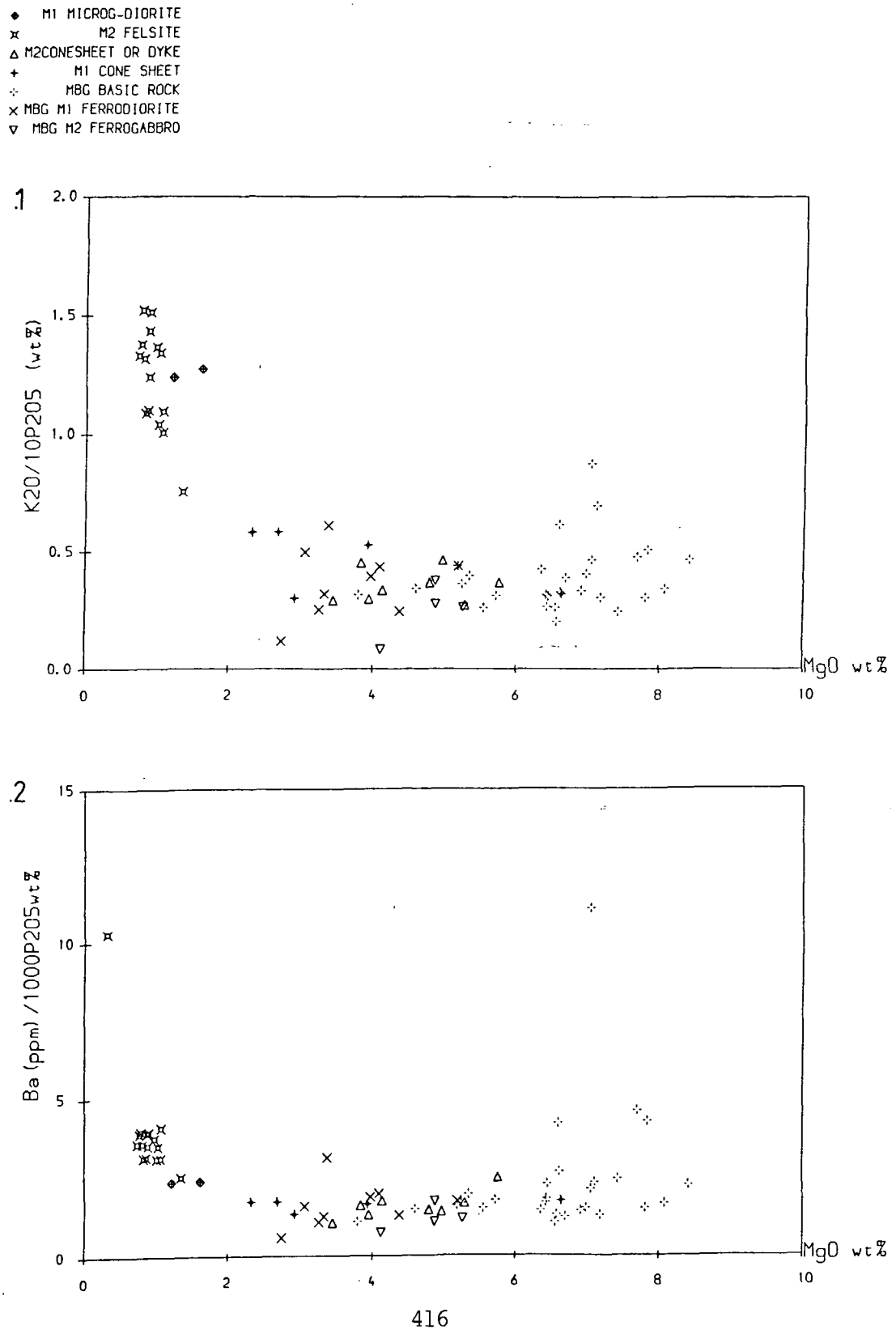

4.20.3

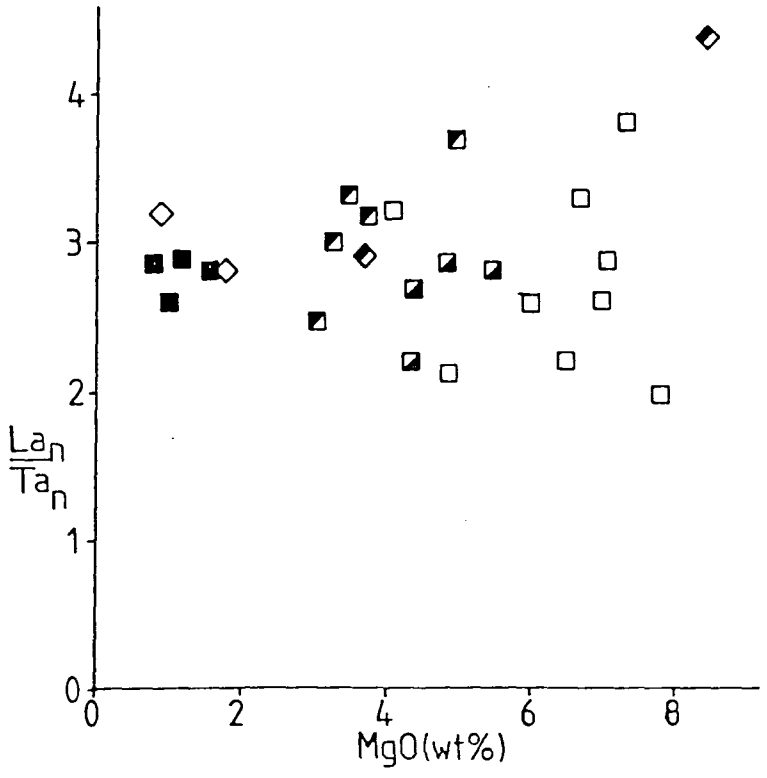

- MBG subalkaline granitoids.
- M1 intermediate rocks
- Hybrid rocks
- M1 basic rocks
- Felsic pre - Hypersthene Gabbro Tertiary rocks
- Basic pre - Hypersthene Gabbro Tertiary rocks

.4

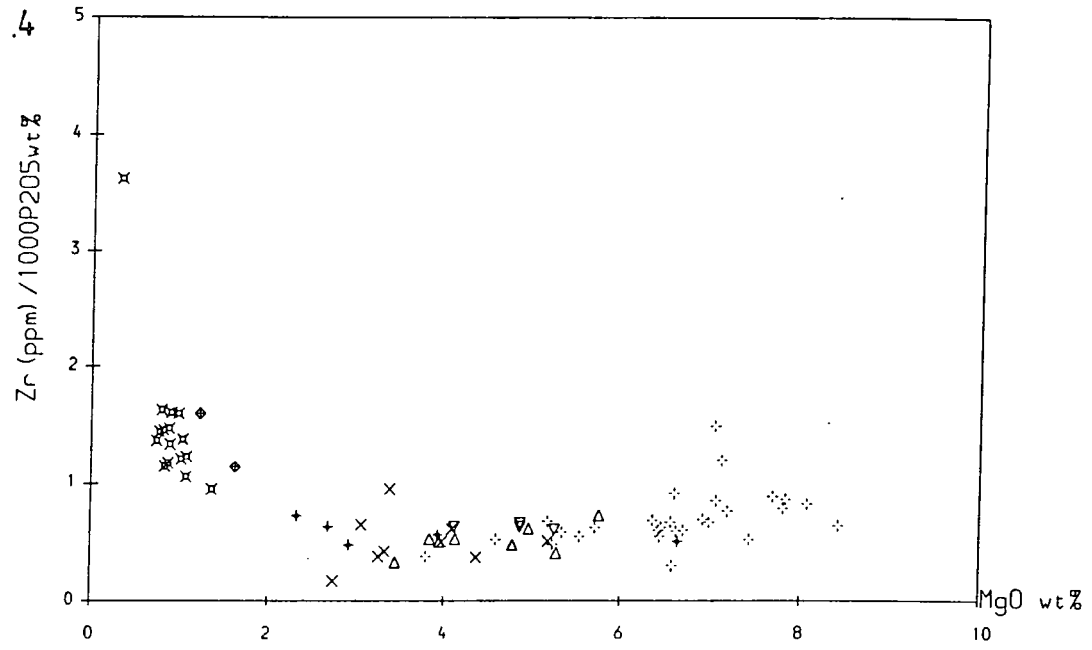

◇ M1 MICROG-DIORITE
✳ M2 FELSITE
△ M2CONESHEET OR DYKE
+ M1 CONE SHEET
⁘ MBG BASIC ROCK
× MBG M1 FERRODIORITE
▽ MBG M2 FERROGABBRO

.5

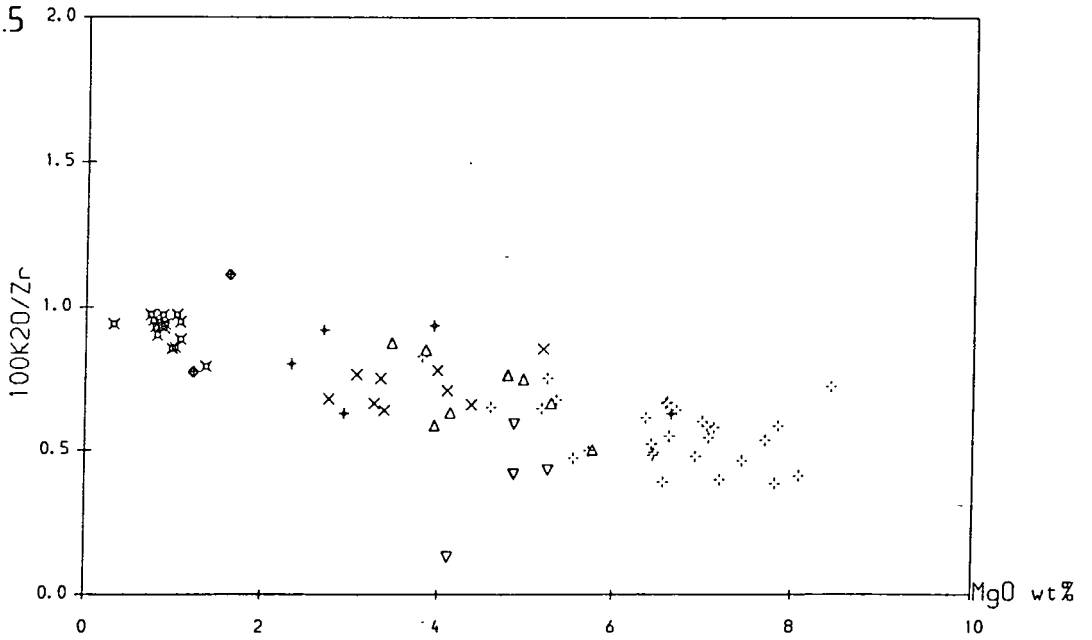

◇ M1 MICROG-DIORITE
✳ M2 FELSITE
△ M2CONESHEET OR DYKE
+ M1 CONE SHEET
⁘ MBG BASIC ROCK
× MBG M1 FERRODIORITE
▽ MBG M2 FERROGABBRO

Fig. 4.21. Plot of chondrite - normalised Th/Hf vs. Hf/Sm used to identify the crustal contaminants present in the Tertiary Igneous rocks analysed by INAA during the course of this work.

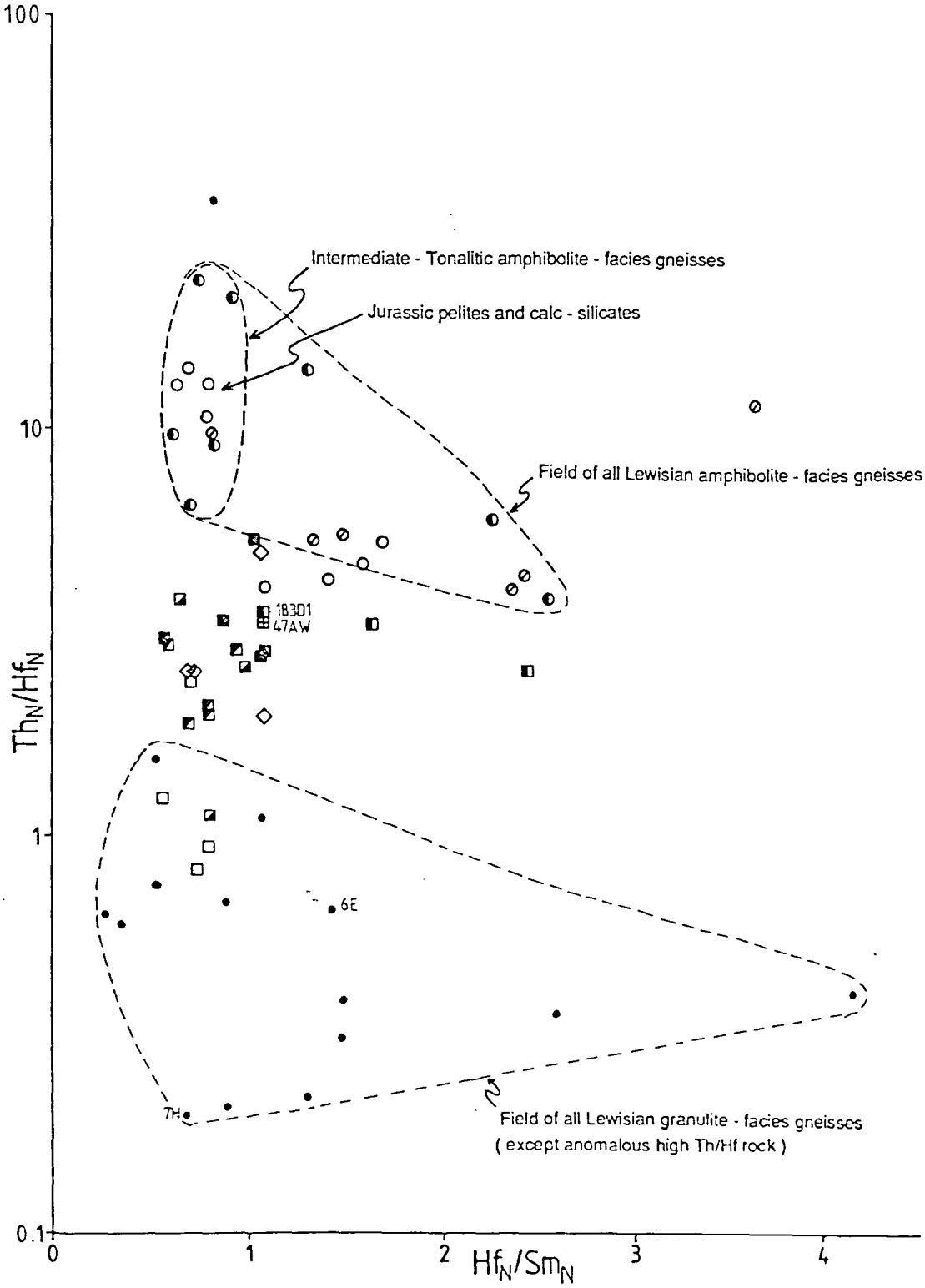

the gneisses varies with bulk rock composition, with basic, intermediate and tonalitic gneisses all having $Hf_N/Sm_N \leq 1$ and almost all the granitic gneisses having $Hf_N/Sm_N \geq 1$. The exceptions to this rule are the REE - enriched (and also Hf and Zr rich) granulite - facies granitic rocks 6E and 7H (Weaver & Tarney 1980). However, within the limited data set of Weaver & Tarney (1980, 1981) it appears that all the more evolved granitic gneisses of the amphibolite - facies Lewisian gneiss complex have high Hf/Sm. Tarney et al. (1979) contains data for Zr_N/Sm_N in four Lewisian granitic rocks from Coll and Tiree. Values of this ratio, which should be similar to Hf_N/Sm_N, are in the range 0.6 to ≥ 3 in these rocks, but the Zr and Sm rich rocks have Zr_N/Sm_N greater than 2.0. These Zr, (and presumably Hf) and Sm rich rocks would tend to dominate the Hf and Sm budgets of the granitic rocks, causing the average Hf_N/Sm_N ratio to be greater than 1. The Moinian and Mesozoic sediments largely overlap with the field of amphibolite - facies gneisses, although they do tend to have lower Th/Hf, particularly when the anomalous microgranitoid (except 183D1) and rheomorphic breccia samples are included in the field of Mesozoic rock compositions, it having been shown in sections 4.2.3 and 4.2.4 that these are anatectic melts of Mesozoic country rocks. The composition of the uncontaminated parental magmas could not be directly determined because no uncontaminated rocks were found, but the inference made in 4.3.1 to the effect that they were incompatible - element depleted tholeiitic magmas suggests pre - contamination ratios of $Hf_N/Sm_N \approx 0.8 - 0.9$ and $Th_N/Hf_N \approx 0.5 - 0.7$.

Apart from the anomalous granitoids and the rheomorphic breccia all of the Tertiary igneous rocks in this diagram fall into two groups. These have, respectively, high Hf_N/Sm_N (> 0.9;mostly ≥ 1.0) and values of 0.9 or less, close to the inferred values for uncontaminated rocks. However, they can also mainly be distinguished by their major element geochemistry, field relationships and petrography, as follows:

Group A. This is composed of most (but not all) of the subalkaline granitoids and pre - Hypersthene Gabbro felsic rocks, one hybrid rock and a highly fractionated dioritic rock (sample 183A). These have $Hf_N/Sm_N \geq 0.9$. Possible causes of this include contamination with high Hf/Sm sediments (the probable cause in the case of the hybrid rock, 42A2, which is a hybrid of basic magma and diopside microgranite derived from Scalpa Sandstone; see section 4.4), or contamination with felsic Lewisian rocks, or, in the case of the subalkaline granitoids, late - stage accumulation of zircon relative to REE - rich minerals in their parent rocks (section 4.2.2).

Group B. This includes almost all the basic to intermediate Tertiary rocks in Fig. 4.21, including two pre - Hypersthene Gabbro intermediate rocks which had slightly less incompatible - element depleted parental magmas (section 2.4.1) and also a few felsic and hybrid rocks. These rocks form an array in Fig. 4.21, showing wide variation in Th/Hf but approximately constant Hf/Sm (Hf_N/Sm_N 0.6 – 0.9). The causes of the wide variation in the latter are discussed further below but the key point to be drawn from Fig. 4.21 is that these rocks cannot have been greatly contaminated with high Hf/Sm rocks, including almost all of the fusible Moinian and Mesozoic sediments and most of the Lewisian granitic gneisses (including all of the high Th/Hf amphibolite - facies granitic gneisses). It is difficult to place a precise upper limit upon the amounts of high Hf/Sm contaminants that could be present in these rocks because, as was shown in section 4.3.1, contamination probably took place prior to much fractional crystallisation. However, a magma with initial Hf and Sm contents typical of the basic rocks in Fig. 4.19 ($Hf_N \approx 12$ and $Hf_N/Sm_N \approx 0.8$) could not be contaminated with, for example, material with $Hf_N/Sm_N = 2$ and 10ppm Hf ($Hf_N = 50$) and still have $Hf_N/Sm_N \leq 0.9$ if the proportion of contaminant rose above about 5% of the mixture. If these magmas have themselves been affected by post - contamination fractional crystallisation, with a consequent increase in Hf and Sm contents, the maximum permitted proportion of high Hf/Sm contaminant is even smaller.

The only Jurassic rocks with low Hf/Sm plotted in Fig. 4.21 are Middle Pabba Beds pelites and a high - Ca calc - silicate rock from within the Scalpa sandstone. The high - Al, peraluminous character of the former and the extremely high Ca content of the latter (sample 199) make them unsuitable contaminants becuse of the effects they would have on other features of the chemisty of these rocks. The coherent decreases with fractionation of Ca and Al in Fig. 4.18 is inconsistent with contamination of the basic rocks with either of these rock types unless the contamination occured in an AFC process in which the major - element composition of the rocks was very strongly buffered by fractional crystallisation of plagioclase and augite (Bowen 1922). As was shown above in Fig. 4.20, these rocks were not contaminated in an AFC process and the uniform Hf/Sm of these rocks cannot therefore be a product of contamination with these lithologies, which are in any case only a small part of the Jurassic sequence as a whole.

More plausible explanations for some or all of the variation in Th/Hf at near - constant Hf/Sm shown by these rocks are as follows:

1). Fractional crystallisation involving partition of Hf into augite and Ti - magnetite.

2). Contamination with high Th/Hf, low Hf/Sm intermediate to tonalitic Lewisian amphibolite facies gneisses. These gneisses all have high Th/Hf but low and very uniform Hf/Sm: they form the cluster of points at the low end of the Hf/Sm range in the field of amphibolite - facies gneisses in Fig. 4.21.

Fig. 4.22.1 shows Th_N/Hf_N vs. MgO, the latter being used here as an index of fractional crystallisation, for those MBG and earlier Tertiary rocks from Ardnamurchan with $Hf_N/Sm_N \leq 0.9$. There is possibly a weak overall negative correlation betwen the two. If present, this suggests, in view of the lack of correlation between other crustal contamination indicators and MgO (Fig. 4.19.3 in particular), that significant fractionation of Hf into augite and, in the case of rocks with MgO $\leq$ 5% or containing a low - MgO component, magnetite may have taken place. The amount of scatter about the trend is much greater in Fig. 4.22.1 than in 4.20.4 (K_2O vs. Zr), which probably reflects the much smaller variation in K/Zr ratio within the crustal contaminant suite than in Th/Hf (however, see discussion of analytical errors in section 4.3.2.1 and below). This difference, if real, arises from the observation (Weaver & Tarney 1980, 1981) that K/Zr ratios in amphibolite - and granulite - facies gneisses are similar whereas Th/Hf differs greatly because of the Th - depleted character of the granulite facies rocks (section 2.1). The variation in Th/Hf at constant MgO is as great as the variation with MgO which suggests that differences in the amount of crustal contamination, the composition of the contaminant and also the Th and Hf abundances in the parental magma (which affects the sensitivity of its Th/Hf ratio to crustal contamination) are at least as important in controlling the Th/Hf ratio of these rocks as the substitution of Hf into pyroxene and/or opaques.

Figs. 4.22.2 and 4.22.3 present further evidence for the involvement of Lewisian amphibolite - facies gneisses in contamination of the low - Hf/Sm rocks, and also for the involvement of a granulite - facies component. In non - calc - alkaline, non - Benioff - zone related suites of basic rocks Ta behaves much more like Th than like Hf (Thompson et al. 1984): hence varying degrees of mantle melting or of fractional crystallisation will change Th/Hf much more than Th/Ta and will therefore produce trends with the same general direction in Fig. 4.22.2 as the diagrammatic vector B. The steep slope of the Th_N/Ta_N vs Th_N/Hf_N array defined by the basic and intermediate rocks in Fig. 4.22.2 therefore implies that these rocks have been contaminated with varying amounts of a

Fig. 4.22. Plots of MBG and other Tertiary rocks from Ardnamurchan with Hf /Sm < 0.9 (those with negligible crustal contamination above the Moine Thrust Zone) showing inheritance of variation in contamination which occurred below the Moine Thrust Zone. Vectors A -- D discussed in text.

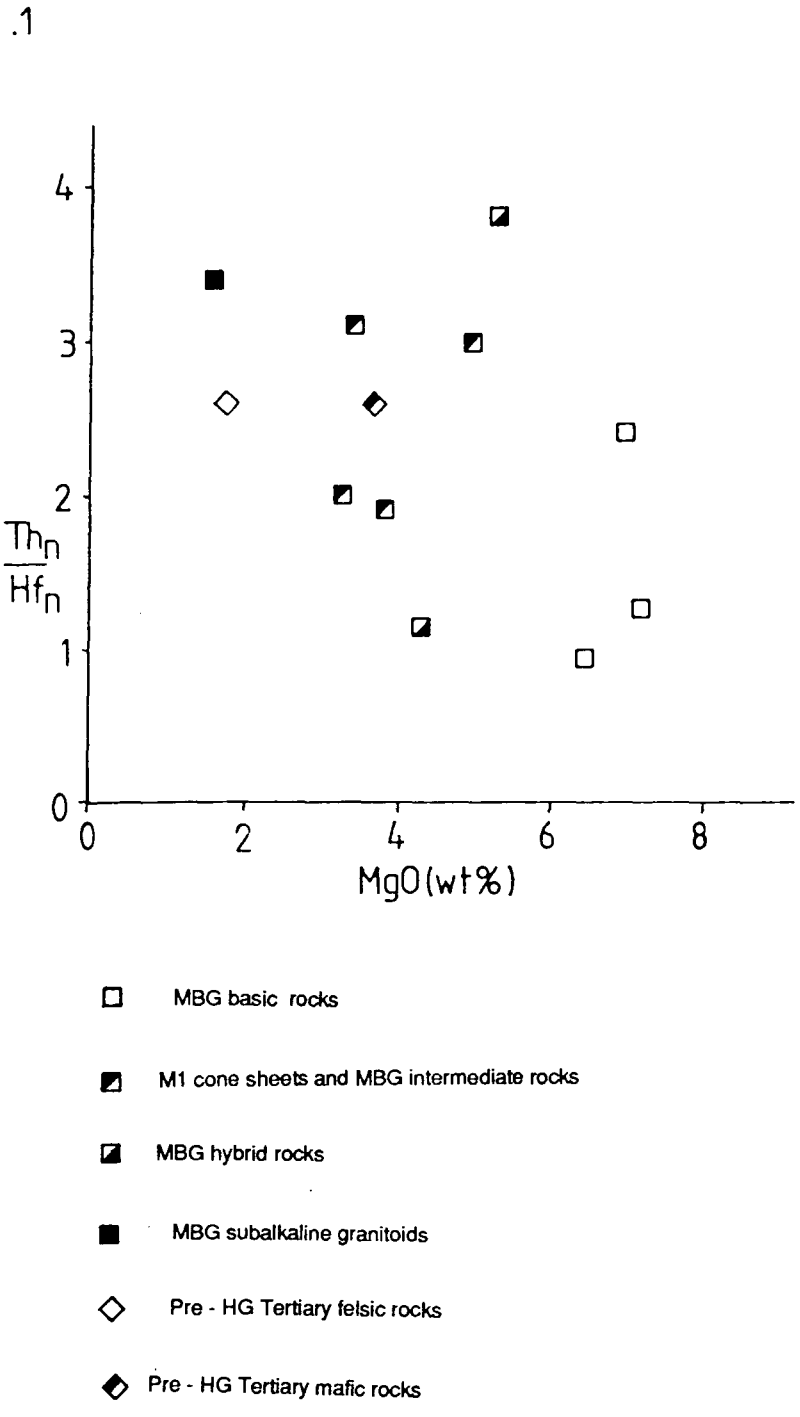

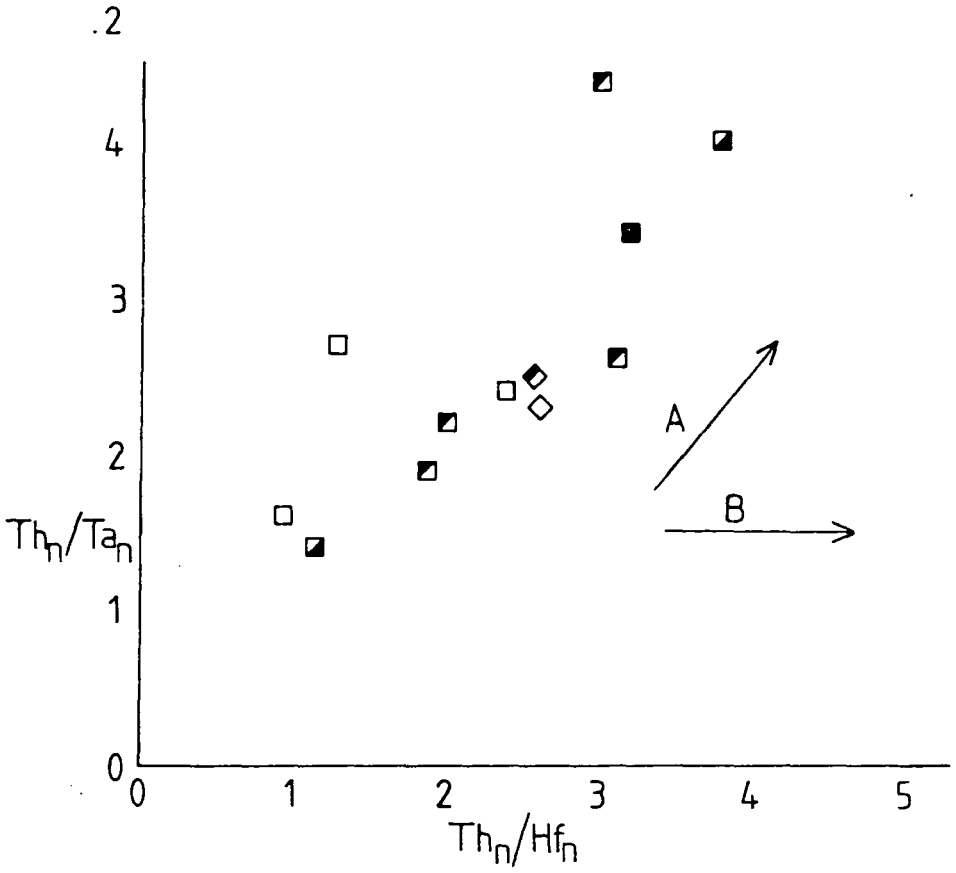
.2
4
3
2
1
0
0
1
2
3
4
5
Th_n/Ta_n
Th_n/Hf_n
A
B

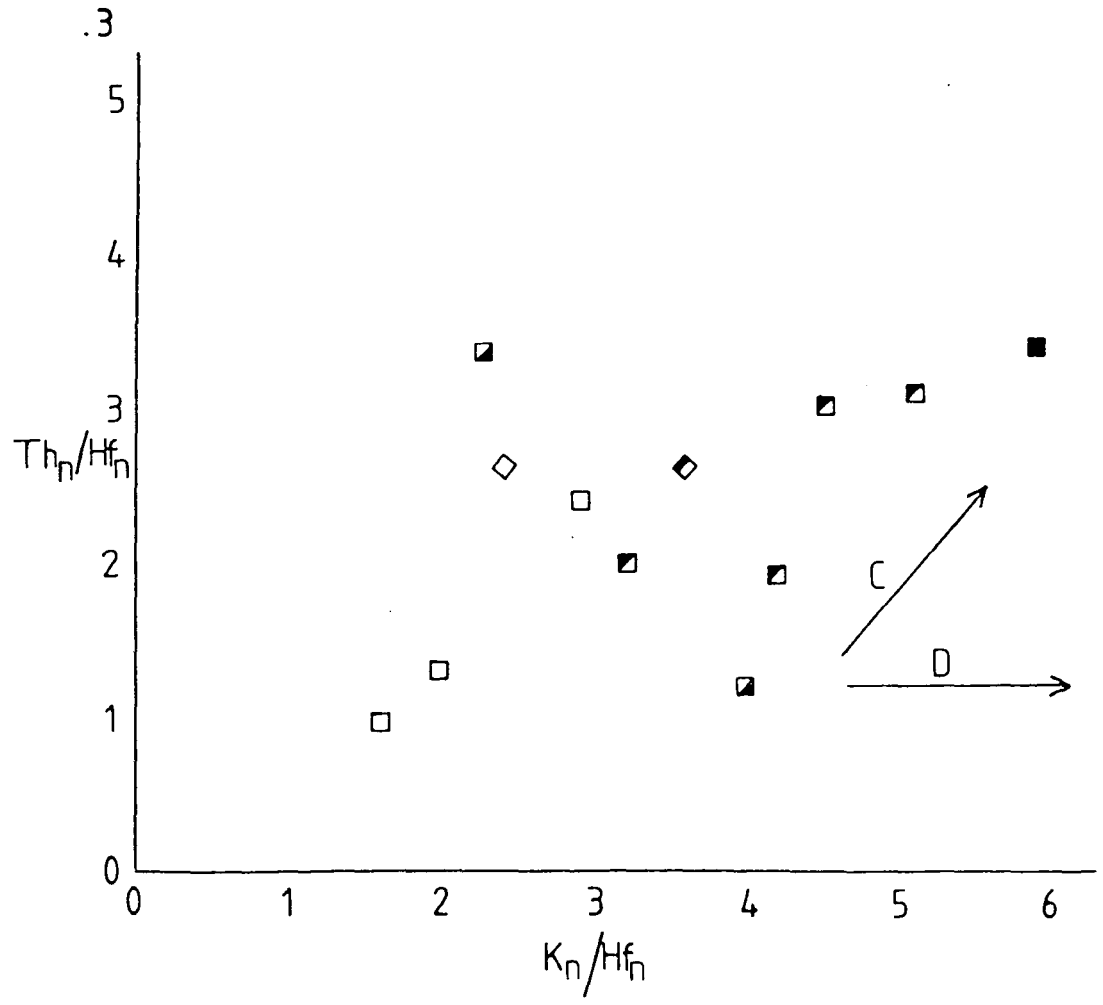
.3
5
4
3
2
1
0
0
1
2
3
4
5
6
Th_n/Hf_n
K_n/Hf_n
C
D

high Th/Ta material such as amphibolite facies Lewisian gneisses. This trend cannot have been produced by contamination with Lewisian granulite - facies gneisses because these rocks are Th - depleted and contamination involving them would produce very little movement from the position of uncontaminated tholeiites in this diagram ($Th_N/Ta_N \approx 1$, $Th_N/Hf_N < 1$; see Fig. 4.19 and section 4.3.1).

Conversely, K and Th correlate extremely well in all uncontaminated basic and intermediate rocks in the BTVP (Thompson et al 1982, Thompson & Morrison 1988) and also in the amphibolite - facies gneisses: the diagrammatic vector C in Fig. 4.22.3 has a slope of 1 and represents the effects of lower degrees of primary partial melting or of derivation from a less - depleted mantle source, fractional crystallisation of basic assemblages, and of contamination with evolved, intermediate to felsic Lewisian amphibolite - facies gneisses. The rocks plotted, however, are scattered about a trend with a slope of approximately 0.5, suggesting contamination with varying proportions of low Th/K granulite facies gneisses (vector D) and normal Th/K amphibolite - facies gneisses.

Errors in the INAA data on which these plots are based are of the order of 15 – 20% (2 Relative Standard Deviations), based on replicate analyses of AGV - 1 and SOIL - 5 (see Appendix 1). Both of these standards have higher Th abundances than the unknown samples plotted in these diagrams but most errors in INAA analysis are proportional to the abundances of the elements concerned in the unknowns (see Appendix 1) and these errors can be considered typical for the samples plotted in Fig. 4.22: single analyses of Th, Ta, Hf and La poor reference materials (notably BOB - 1 and SKB; see Appendix 1) lie within 20% or less of their recommended values. The overall trends in Fig. 4.22 can therefore be considered to be real but the scatter in Fig. 4.22.3 in particular may be due to analytical error rather than indicating real variation in the ratio of granulite - facies gneiss to amphibolite - facies gneiss contaminants. The low slope of the array of data points in this plot can , however, only be explained in terms of a mixture of granulite - facies and amphibolite - facies Lewisian contaminants.

The conclusions which follow from these data can be summarised as follows:

1). The majority of those basic and intermediate rocks in, or associated with, the MBG which were analysed for REEs, Th, Ta and Hf were contaminated with both amphibolite - and granulite

- facies intermediate to tonalitic Lewisian gneisses. They were not, however, contaminated to any great degree by high Hf/Sm rocks, including both Moinian and Mesozoic sedimentary rocks and Lewisian granitic rocks.

2). The majority of the observed contamination took place prior to the crystal fractionation which produced the observed range of compositions. The contamination is independent of the degree of fractional crystallisation and was not produced in an AFC process.

3). A small proportion of the contact zone suite rocks, mainly granitic and heterogenous hybrid rocks but also one homogenous dioritic rock, have $Hf_N/Sm_N \geq 0.9$. This is probably due to contamination with high Hf/Sm material in the less evolved rocks but may have been caused by late - stage zircon accumulation in the rocks which were subsequently remelted to form the M1 and M2 subalkaline granitoids.

As noted in Chapter 2 the observed gravity and magnetic anomalies associated with the Ardnamurchan central complex as a whole suggest that its base is fairly close to the Moine Thrust Zone, suggesting that the Hypersthene Gabbro itself is mainly or entirely enclosed within the Moinian and younger rocks above the MTZ. **The inference that most of the MBG rocks are mainly contaminated with Lewisian contaminants therefore implies that contamination of the parental magmas of the homogenous basic and intermediate rocks mainly occurred before they entered the MBG magma chamber rather than taking place within it.** The contamination appears to have taken place as the magmas passed through conduits in the Lewisian gneiss complex, or in deeper - level intrusions within it. It also seems to have preceded the fractional crystallisation which produced the observed compositional variations in Fig. 4.18.

This last conclusion permits (but does not prove) the following explanation for the strong contrast in the style of contamination of the MBG and related basic and intermediate rocks and the contamination patterns shown by the majority of the BTVP basic rocks which have been investigated by Thompson and co - workers (Thompson et al. 1982, 1986; Dickin et al. 1984). These workers showed that the principal contaminants in the various suites of rocks from Mull and Skye which were studied by them were the lowest - melting - temperature components of the Lewisian Gneiss complex, in particular the various granitic gneisses and granitic rocks (section 2.1). In contrast

to the case of the MBG rocks, the volumetrically dominant Lewisian lithologies, the intermediate to tonalitic gneisses, were considered to be unimportant as contaminants. This observation was explained by the hypothesis that the parent magmas to the Mull and Skye suites were too cool and evolved to assimilate these relatively refractory rocks, which make up by far the largest part of the Lewisian complex. This constraint on the compositional range of potential contaminants would no longer apply if the parental magmas to the MBG basic and intermediate rocks were, at the time of contamination, picrites or picritic basalts rather than basalts. Such magmas are able to assimilate a greater range of contaminants for a number of reasons:

1). They are hotter, have greater heat capacities (Murase & McBirney 1973), release a greater amount of latent heat during a given percentage of crystallisation and crystallise over a much larger temperature range whilst olivine (± minor chrome spinel) is the only major liquidus phase (Sparks 1986) and are therefore able to release more heat, and raise wall rocks to higher temperatures, before cooling below their rigidus temperature, at which point further melting of the wall rocks is inhibited by the formation of an insulating chill zone and mixing of crustal melts with the interstitial residual melt becomes a much slower process.

2). They have lower viscosities and will therefore be more prone to turbulent flow in magma conduits (Huppert & Sparks 1985). Heat transfer from fluids flowing in conduits to the conduit walls is much more efficient when the flow is turbulent than when it is laminar, and the formation of chill zones on the conduit walls is inhibited (Huppert 1989 and P.M.Bruce pers. comm.). Both of these factors act to increase the temperatures reached in the wall rocks, whilst the latter will allow crustal melts to mix freely with the magmas in the interior of the conduit.

Magnesium - rich, high - temperature magmas will therefore be able to assimilate both fusible granitic and more refractory intermediate rocks, and will therefore not show the pattern of selective assimilation of the most fusible lithologies shown by basaltic magmas. The dominant contaminant of magnesian magmas will in general be whichever lithology is volumetrically dominant in the crust through which they pass. In the case of the crust of North - West Scotland this is the intermediate to tonalitic 'grey gneisses' of the Lewisian complex.

The pattern of contamination shown by the MBG and associated rocks therefore implies that they

were derived from picrobasaltic to picritic tholeiite parent magmas which assimilated Lewisian gneisses before, or in the earliest stages of, the extensive crystal fractionation which produced the observed range of basic to intermediate homogenous MBG magma compositions. It also implies the presence of ultrabasic cumulates within the crust beneath Ardnamurchan, either within the lower parts of the Ardnamurchan central complex or at sufficiently deep crustal levels to not produce a detectable gravity anomaly.

4.3.2.3. Implications of the Crustal Contamination patterns for Convection in the MBG Magma Chamber.

As is apparent from Figs. 4.20.3, 4.21 and 4.22, the amount and/or composition of the crustal contaminants in the MBG and associated rocks shows significant variations. Similarly, the three samples plotted in 4.19 show significant differences in La/Ta resulting from crustal contamination despite being of similar major element composition and uniform low Hf/Sm. **The inheritance of incompatible element ratio heterogeneities due to crustal contamination which occurred BEFORE the magmas entered the MBG magma chamber implies that convection within the MBG magma chamber did not homogenise the various magmas which entered it with varying compositional signatures arising from previous crustal contamination.**

Fig. 4.23 provides further constraints on the scale of the heterogeneity within the MBG magma chamber. In these plots M1 basic and intermediate rocks are plotted according to whether they come from the northern, western or southern sides of the intrusion. Within each of these areas considerable variation is present at any given MgO content but the compositional fields defined by samples from each area overlap in all the plots with the possible exceptions of Figs. 4.23.1 and 4.23.2 ($Fe_2O_3^T$ and TiO_2 vs. MgO respectively). Abundances of these two elements are lower in crustal rocks than in basic to intermediate tholeiitic magmas and they will therefore be much less sensitive to crustal contamination than, for example K_2O, which shows no similar variation between the three areas. The variation in Fe and Ti must therefore be due to some other factor. Enrichment of the rocks on the western margin of the intrusion in FeTi oxides by early accumulation or late stage melt expulsion is unlikely to be the correct explanation becuse this would also cause them to have lower contents of incompatible elements such as K and higher contents of other elements which also substitute strongly into FeTi oxides, such as Cr, than rocks from the other sectors of the intrusion.

Fig. 4.23. Geochemical data for M1 rocks divided up according to whether they occur on the northern, western or southern margins of the intrusion. See text for discussion.

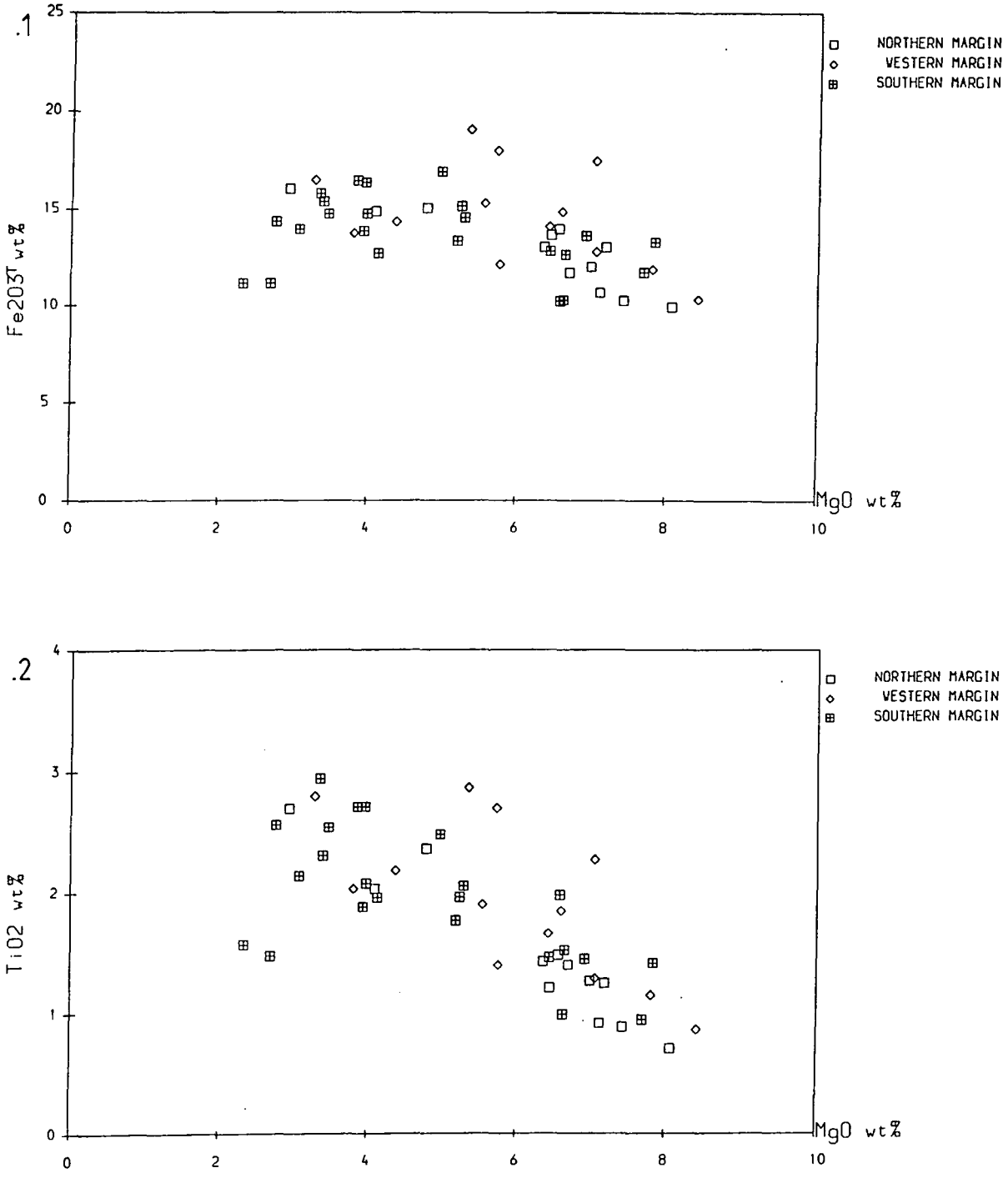

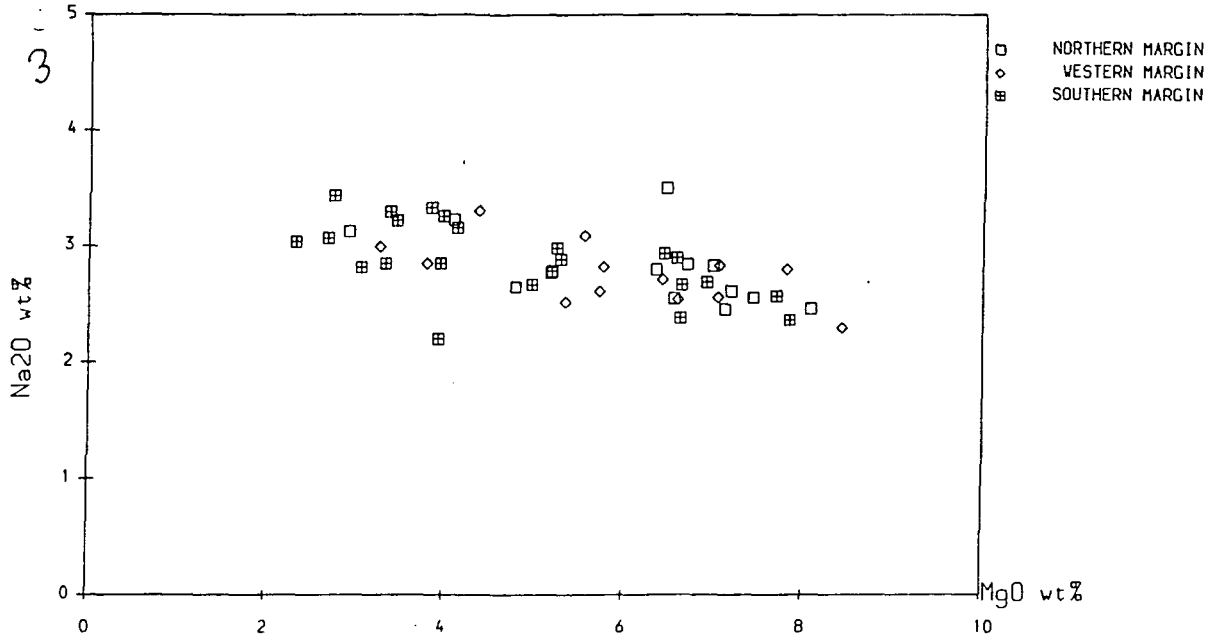
3
Na2O wt%
MgO wt%
NORTHERN MARGIN
WESTERN MARGIN
SOUTHERN MARGIN

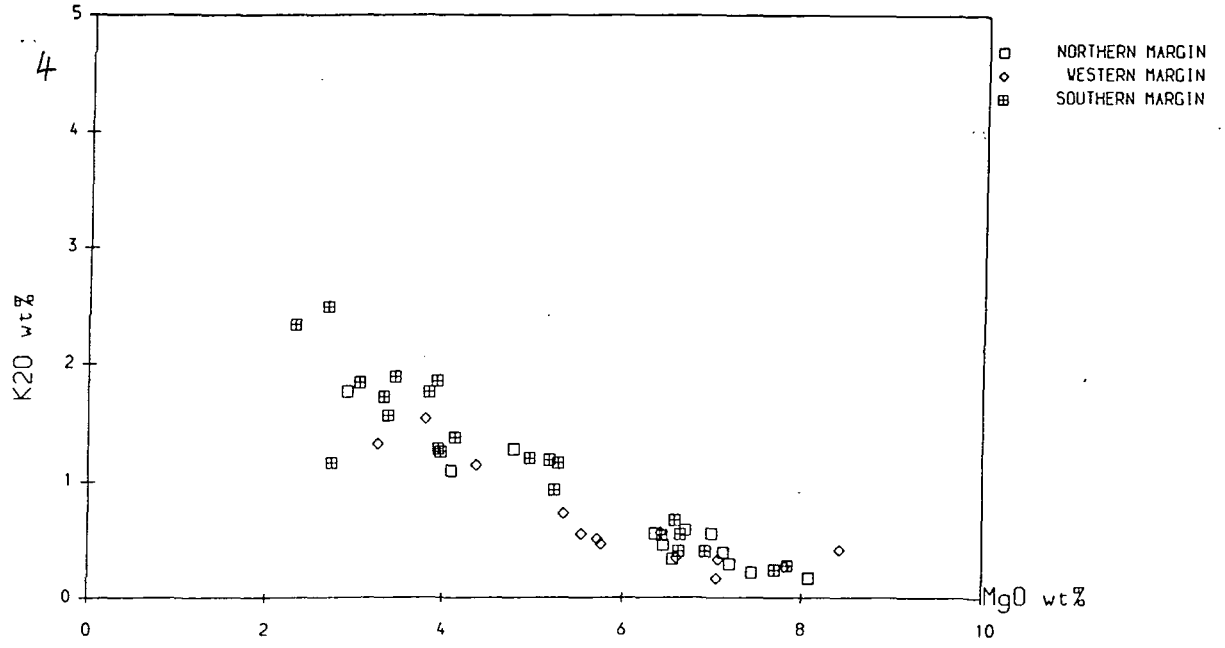
4
K2O wt%
MgO wt%
NORTHERN MARGIN
WESTERN MARGIN
SOUTHERN MARGIN

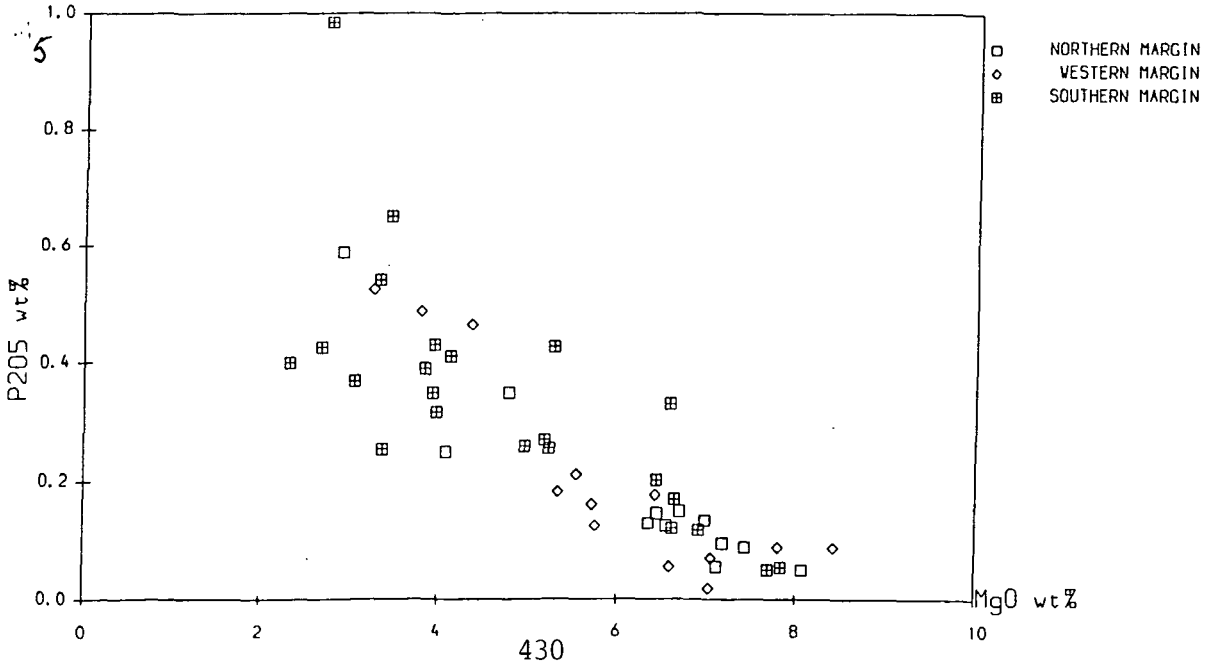
5
P2O5 wt%
MgO wt%
NORTHERN MARGIN
WESTERN MARGIN
SOUTHERN MARGIN

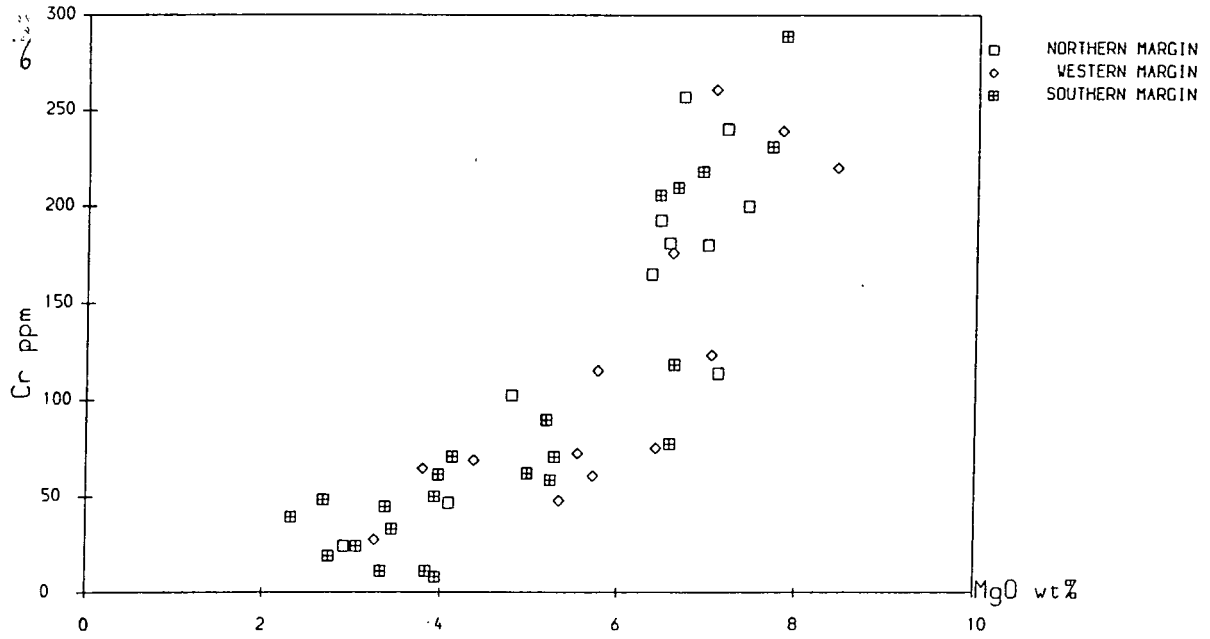
Cr ppm
300
250
200
150
100
50
0
0
2
4
6
8
10
MgO wt%
NORTHERN MARGIN
WESTERN MARGIN
SOUTHERN MARGIN

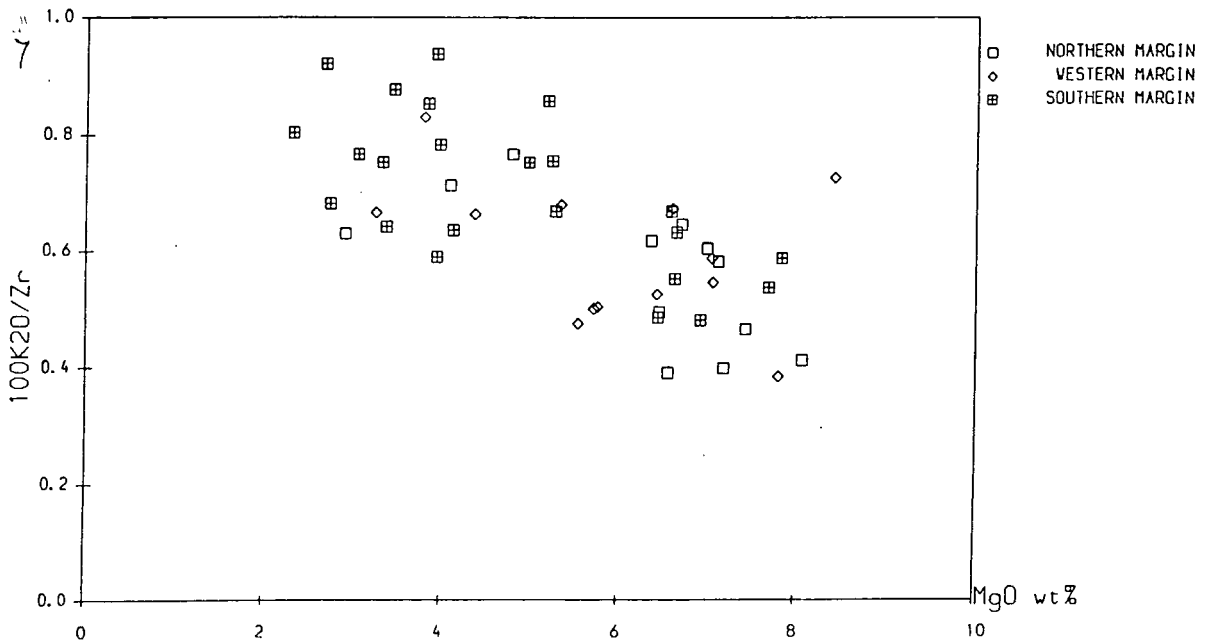
100K20/Zr
1.0
0.8
0.6
0.4
0.2
0.0
0
2
4
6
8
10
MgO wt%
NORTHERN MARGIN
WESTERN MARGIN
SOUTHERN MARGIN

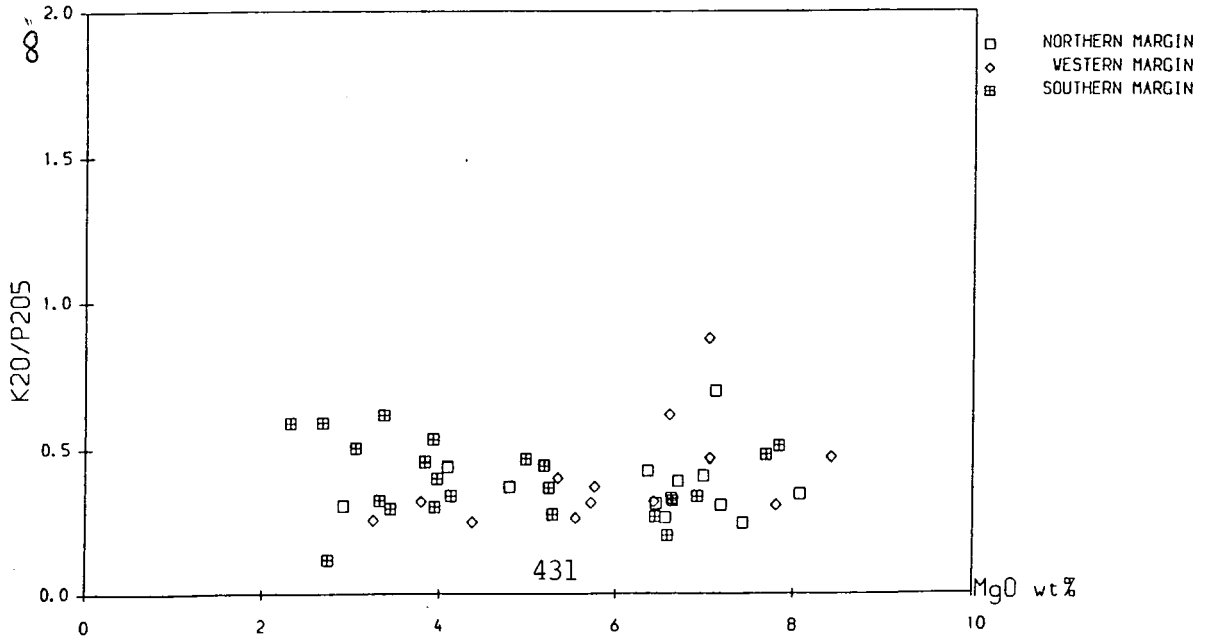
K20/P205
2.0
1.5
1.0
0.5
0.0
0
2
4
6
8
10
MgO wt%
NORTHERN MARGIN
WESTERN MARGIN
SOUTHERN MARGIN

These depletions and enrichments are not observed (see Figs. 4.23.4 and 4.23.6 respectively). One explanation of the variation between sectors of the MBG intrusion is that the rocks on the western side of the intrusion contain smaller amounts of low Ti and Fe material formed by mixing of the extreme low - and high - MgO endmembers involved in the mixing process documented in Fig. 4.18 (section 4.3.1, above), and a higher proportion of Fe and Ti rich ferrogabbroic magma formed by simple fractionation of the tholeiitic basic magmas. The most important conclusion to be draw from Fig. 4.23, however, is that the heterogeneity in earlier crustal contamination is developed on a scale much smaller than that of the size of the areas distinguished in Fig. 4.23, each of which represents between 10% and 25% of the margin of the intrusion at the present level of exposure. This is because the variation in elements and element ratios affected by contamination is much greater within each area than the overall differences between them.

The preservation of isotopic heterogeneities within layered intrusions, resulting either from differential contamination of stratified layers within the magma chambers represented by the intrusions or from variations in the isotopic composition of the input to the chambers, has been documented from the Eastern Layered Series of the Rhum complex (Palacz & Tait 1985; Young et al. 1988) and from the Fongen - Hyllingen intrusion (Wilson & Engell - Sorenson, 1986). However, in the case of the MBG, the evidence for extensive mixing between magmas of differing MgO contents (e.g. plots of $Fe_2O_3^T$ and TiO_2 vs. MgO, Fig. 4.18), implies that the magma chamber was not entirely stably stratified, although the pattern of distribution of the intermediate rocks in the MBG suggests that some form of 'leaky stratification' with only slow transfer of material between layers was present (see below, sections 4.3.3 and 4.4.1.2).

In principle the variation in La/Ta and other incompatible - element ratios at constant MgO could also have been produced by this mixing, provided that a range of Mg - rich end members with MgO $\gg$ 8% (and therefore high contents of Cr as well) and MgO - dependent variation in incompatible - element ratios was present. However, as shown in section 4.3.1 the most magnesian rock involved in the mixing must have had an MgO content of little more than 8% and there is no evidence for the involvement of high - Cr magmas in the mixing process either (Fig. 4.18.). There is a factor - of - two variation in La/Ta in rocks with 6 – 8% MgO, close to the the Mg - rich end - member in the mixing process and the amount of variation in La/Ta at any given MgO in the M1 rocks in Fig. 4.20.3 actually decreases with falling MgO content. Although the decrease may not be statistically

significant, there is no sign that the variation increases in the range 4 – 6% MgO as would be expected if the variation in La/Ta was produced by the magma - mixing apparent in Fig. 4.18. This is as would be expected if the magma mixing was taking place in the MBG magma chamber whilst, as shown above, the generation of La/Ta variation by crustal contamination in these rocks preceded their entry into the MBG magma chamber.

4.3.3. Temperatures of the basic and intermediate magmas within the MBG magma chamber during M1 and estimated density differences between the basic, intermediate and subalkaline granitoid magmas.

The best estimate for the temperatures of the intermediate and basic magmas, most of which are aphyric, of the MBG is provided by the correlation between liquidus temperature and MgO content of basaltic to intermediate rocks evident in the results of numerous melting and crystallisation experiments. This relationship was first quantified for basic magmas at 1 atmosphere pressure by Thompson (1973), whose plot of MgO content of natural rock samples against their 1 Atm. liquidus temperature constitutes an empirical geothermometer for dry magmas at low pressure. Above about 4% MgO, the range of liquidus temperatures at a given value of MgO for the wide range of magma compositions considered by Thompson is only about 30°C, suggesting that the geothermometer is accurate to within ±15°C provided certain assumptions are satisfied (see below) and a correction for the pressure - dependence of the liquidus is made. Fujii & Kushiro (1977) obtained a value of $+3.7°C\ kb^{-1}$ for this at high pressures, whilst the parameterisation of a large data set by McKenzie & Bickle (1988) yielded a value of $10 - 20°C\ kb^{-1}$. However, at the low pressure of emplacement of the Hypersthene Gabbro ($\leq$ 1.0 – 1.3kb, section 4.2.5) the pressure correction will be no greater than the error in the geothermometer at 1 Atm., so it only needs to be approximate. A value of $10°C\ kb^{-1}$ is used here.

Below about 4% MgO larger variations in liquidus T with MgO content are apparent in Thompson's data set. However it was noted that much of this variation involved alkalic and potassic magmas and tholeiitic magmas continued to lie on a well - defined trend, albeit one which showed significant departure from linearity below about 6% MgO. The following equation is an approximate fit to Thompson's data in the range 3% – 10% MgO and also passes through the data points used to construct the liquidus T - MgO relationship employed by Sparks & Marshall (1986): it is therefore

likely to underestimate the liquidus temperatures of dry magmas with less than 3% MgO since the latter workers used data from experiments on granitic magmas at $P_{H_2O} = 1$ kb (Thompson 1983).

$$T_{liquidus} = 1240 - 12(10 - X) - 2(10 - X)^2 \qquad (4.9)$$

where the liquidus temperature is in degrees centigrade and X is the MgO content of the magma in weight percent.

Equation (4.9) is valid provided that the magmas concerned were at their liquidus temperature and were dry. Apart from a few feldspar - phyric samples the M1 MBG magmas are aphyric and show no variation attributable to phenocryst accumulation (section 4.3.1). This suggests that the magmas in the interior of the magma chamber were close to their liquidus temperatures, whilst the presence of sparse phenocrysts implies that they were not actually superheated. Hydrous magmatic phases and evidence of vesiculation are absent, implying that the magmas were H_2O undersaturated. Low values of f_{O_2} and therefore low water activities are also indicated by the tholeiitic fractionation trend apparent in Fig. 4.18. Although the MBG magmas are unlikely to have been completely dry it would appear that the error produced by neglecting the effect of dissolved volatiles is small.

The range in M1 MBG magma liquidus temperatures obtained by this method is 1050 - 1200°C at P =1Atm.. However, at the present level of exposure homogenous MBG rocks with MgO $\leq$ 6% are mostly confined to the contact zone, particularly on the northern and southern margins of the MBG. The temperature data from the wall rocks and anatectic magmas used in subsequent thermal modelling also come from these two sections of the wall of the MBG, so for the purposes of this work it is appropriate to treat the interior temperature of the magma chamber, T_m in equation 4.2, as being in the range of liquidus temperatures of magmas with 6 - 8% MgO. According to equation (4.8) these are 1160 - 1200°C at 1 Atm. (1170 - 1210°C at 1Kb).

Liquidus densities of the MBG magmas were calculated from their compositions using the partial molar volume and partial molar expansivity data of Bottinga & Weill (1970) and Nelson & Carmichael (1979): where data were given in both works for the same components the weighted data (see Nelson & Carmichael (1979) p. 121) of the latter were used. The effects of minor components (notably Ba, Sr and V) and the unknown volatile content of the magmas could not be allowed for because of lack of data, but a temperature correction, using equation (4.9) to estimate the temperature, was made. The results of the density calculations are presented in Fig. 4.24.

Fig. 4.24. Variation of calculated liquidus densities with MgO content for MBG rocks. See text for method of calculation.

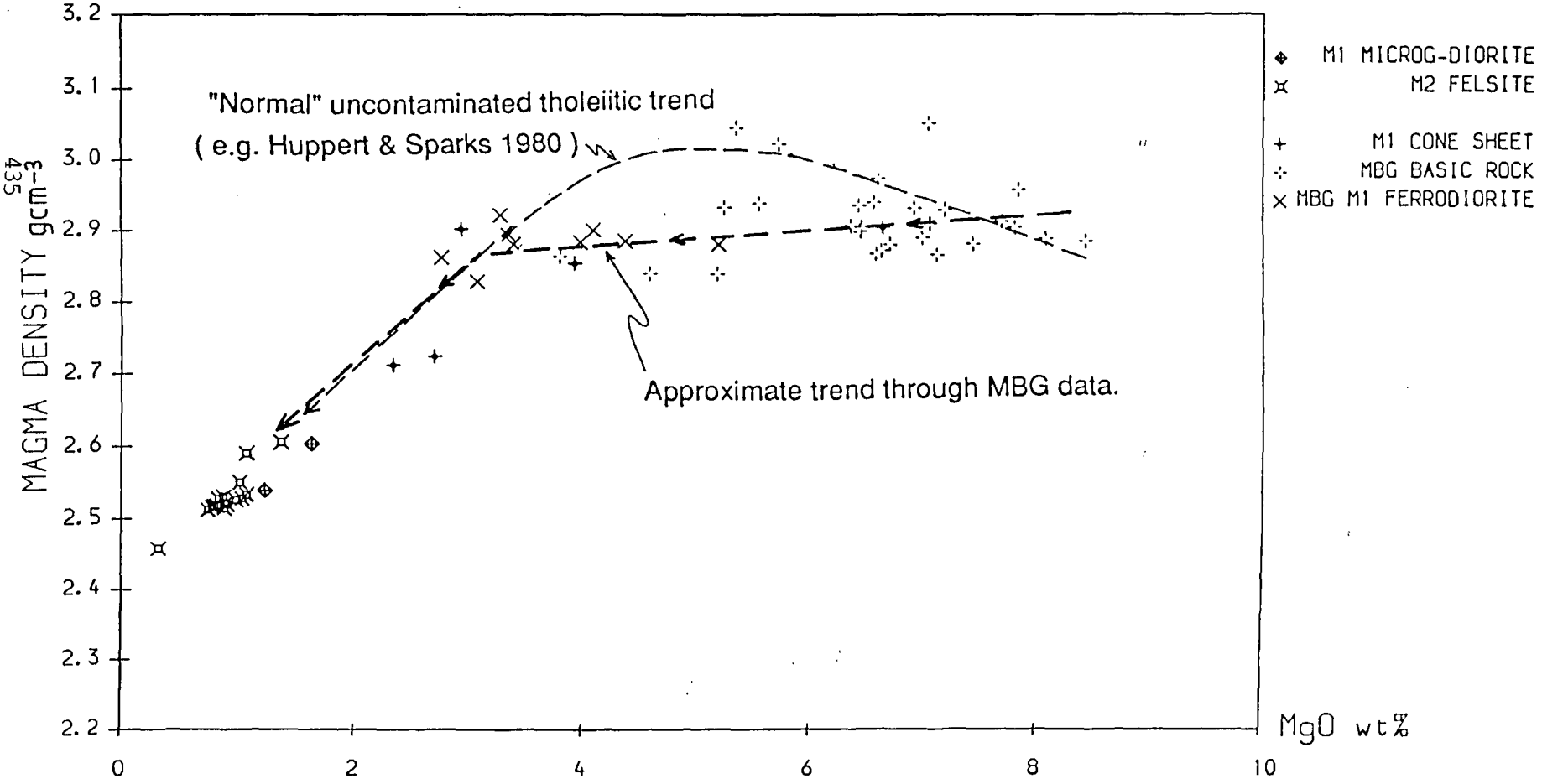

The calculated densities, around 2.9gcm^{-3} for magmas in the range 3 – 8% MgO , are likely to be slight overestimates because of the omission of the unknown, but probably low, water content of the magma from the calculations. Michael (1988) found that H_2O contents in fresh Mid Ocean Ridge basalts were as low as 0.01% ; these are likely to be rather lower than those of the MBG magma chamber magmas because of the effects of crustal contamination. The data of Nelson & Carmichael indicate that dissolved water reduces the liquidus density of basic to intermediate magmas by about 0.1gcm^{-3} per weight percent of dissolved water present; thus even if the water contents of the MBG magmas were ten times those of MORBs the effect on density would be small. H_2O behaves incompatibly in tholeiitic magmas so the effects of dissolved water would be greatest in the MgO - poor magmas.

There is little sign in Fig. 4.24 of the density maximum associated with tholeiitic magmas by most workers (e.g. Huppert & Sparks 1980, although Robins et al. (1987) deduced a continuous density decrease with fractionation from patterns of cryptic variation in the tholeiitic cumulates of the Honingsvag intrusive suite in northern Norway). The slight decrease in average magma density with fractionation apparent in Fig. 4.24 is probably caused by two factors. The first of these is the previous crustal contamination (section 4.3.2), which would have increased the ratio of relatively incompatible ($K_D < 1$) low - partial - molar - density components such as Si, Na and K (enriched in the crust relative to picritic or picrobasaltic magmas) to high - partial - molar - density incompatible components such as Fe and Ti. The effect of this would be to decrease the density of the residual melt relative to the density of the fractionating crystal assemblage plagioclase ± augite and thereby reduce or even reverse the density increase produced by fractionation of this assemblage. Campbell et al. (1978) found experimentally that the density of magmas is strongly dependent on their contents of low partial molar density components, H_2O in particular but also K, Na, Si and Al. The second factor tending to reduce the **calculated** liquidus densities, and which probably also produces much of the variation in calculated density at constant MgO in Fig. 4.24, is the fact that many of the rocks plotted have lower Fe and Ti contents than rocks with comparable MgO contents lying on the tholeiitic fractionation trend as a result of the mixing between MgO - poor and relatively high - MgO magmas shown to have occurred in section 4.3.1. Many of these homogenous hybrid magmas are likely to have been subliquidus immediately after mixing because of the convex - up geometry of liquidus surfaces in silicate systems (Bowen 1928), which would tend to increase their true densities over their calculated liquidus densities, unless they were reheated

after mixing took place or any crystals formed separated out. The occurrence of reheating, which would be expected to occur in compositionally stratified magma bodies, and/or efficient phenocryst separation, is indicated by the fact that almost all of the MBG magmas are aphyric.

Overall, Fig. 4.24 indicates that M1 MBG magmas with compositions between 3% and 8% MgO, the range of compositions inferred to be involved in mixing on the basis of the plots of $Fe_2O_3^T$, TiO_2 and P_2O_5 against MgO in Fig. 4.18, would all have had much the same density, within $\pm 0.05 gcm^{-3}$, although the effect of increasing H_2O content with fractionation would be to produce an overall slight decrease in density. This suggests that the MBG magma chamber would have been just stably stratified, with a continuous upward decrease in MgO content. This inference is consistent with the structure of the radial fault system in the An Acairseid area, which suggests that the rocks to the northwest of these faults were downthrown relative to those to the southeast (section 3.3.2). This implies that the MBG rocks on the western side of the Hypersthene Gabbro originate from a higher structural level than those on at least the southern margin of the intrusion. This is consistent with normal stratification of the MBG magma chamber, with more evolved magma compositions present towards its roof, because Fig. 4.23, above, indicates that the rocks on the western margin of the intrusion have, on the whole, more evolved compositions.

Stratification of this sort is normally considered to inhibit mixing of magmas within magma chambers (for example, Campbell & Turner 1986), which makes the homogenous hybrid character of the majority of the MBG basic and intermediate rocks and the occurence of rocks of widely differing MgO contents of the same age (end - M1/ earliest M2) at the same level of exposure somewhat surprising. However, the partial molar thermal expansivity data of Nelson & Carmichael (1979) suggest that mafic magma densities change with temperature at rates of the order of $-5.10^{-4} gcm^{-3}K^{-1}$, the negative sign indicating that densities decrease with increasing temperature. Any crystallisation which might occur would increase the effective thermal expansivity: the data of Murase & McBirney (1973) on the one basalt sample investigated by them which crystallised significantly at the high cooling rates employed in their experiments indicate that the effective thermal expansivity of basic magmas in the liquidus to rigidus temperature interval may be as much as $-10^{-3} gcm^{-3}K^{-1}$. Hence the density difference between MgO - rich and MgO - poor magmas in the MBG magma chamber could, quite possibly, be removed by cooling of the MgO - poor magma through less than 50°C. This is less than the liquidus - to - rigidus temperature interval for such magmas (section 4.5, below).

It follows that cooling at the steep wall of the magma chamber would produce a density current of cool, dense magma capable of penetrating otherwise stable interfaces between stratified layers, a possibility which is examined further in section 4.5.

The calculated liquidus densities of the M1 microgranodiorites and M2 felsites are also shown in Fig. 4.24. These are much less likely to be precise for a number of reasons, the effects of some of which will, however, tend to cancel out:

1). The densities were calculated assuming a temperature of about 970°C , given by (4.9), which as noted above tends to underestimate liquidus temperatures of low - MgO magmas. This temperature is much lower than the 1070 – 1120°C (at $P_{H_2O} = 0$) estimate of section 4.2.5 and will increase the calculated densities of the felsic magmas over the true value.

2). The calculation procedure used in this section neglects the effect of dissolved water on magma density. Although, as noted in section 4.2.5, the felsic magmas were H_2O - poor, they are unlikely to have been completely dry and as a result the densities will again be slight overestimates, although conversely the presence of water will reduce the error due to the temperature used ((1) above), as it will reduce the magma temperature indicated by the feldspar - melt geothermometer (section 4.2.5).

3). Although crystal - poor, the subalkaline granitoids do contain up to about 20% porphyrocrysts (rarely, even more): the effect of these will be to increase the density of the magmas over their calculated liquidus values, cancelling out some or all of the density decreases produced by (1) and (2) above.

Although the calculated density of the subalkaline magmas plotted in Fig. 4.24 is therefore unlikely to be as close to the true values as the calculated densities of the mafic magmas, the key fact is that they were almost certainly very much less dense than the mafic magmas at the time at which both were present at the wall of the MBG magma chamber, as is consistent with the inference, made in section 4.2, that the M1 microgranodiorites flowed up the wall of the magma chamber.

4.3.4. Relationships of the MBG basic rocks to the later M2 minor intrusions.

As was shown in Chapter 3, several groups of strongly plagioclase - phyric minor intrusions, emplaced during the latter part of M2, are associated with the Hypersthene Gabbro. These include the porphyritic dolerites emplaced within the Marginal Border Group, particularly along the western sector of its outcrop between Ardnamurchan Point and An Acairseid (section 3.2.4) and the Group 3 cone sheets which occur in the country rocks to the south of the MBG (section 3.2.5). A particular problem associated with these rocks is the question of whether the groundmass component is equivalent to batches of magma of essentially the same composition as the aphyric or near - aphyric rocks of the MBG, or whether they represent different magma batches equivalent, perhaps, to the Inner Series magmas or to later intrusions within Centre 2 of the Ardnamurchan complex.

Investigation of this problem using whole - rock analyses of these rocks requires some care because the very high contents of plagioclase phenocrysts in these rocks, which form 20 – 50% of the rocks by volume, will inevitably displace them from the trends formed by the aphyric rocks on simple element - element plots. One way of avoiding this is to divide the abundances of both of the components to be plotted by the abundance of another (MgO, for example) which does not substitute into plagioclase. Provided that the same is true of the other components involved as well, the values of the ratios plotted will be independent of the abundance of plagioclase phenocrysts and will instead reflect compositional features of the groundmass.

Three such plots are shown in Fig. 4.25. These indicate that both groups of late - M2 minor intrusions are similar to the earlier MBG magmas in several aspects of their history. Fig. 4.25.1 indicates a uniform $TiO_2/Fe_2O_3^T$ ratio in the rocks, which suggests that the porphyritic rocks belong to a TiO_2 - poor tholeiite magma suite similar to the MBG rocks, rather than a TiO_2 - rich suite such as the pre - Hypersthene Gabbro plateau basalts of Chapter 2, and have a similar compositional range in terms of TiO_2/MgO and $Fe_2O_3^T/MgO$ ratios, both of which increase markedly with fractionation. Figs. 4.25.2 and 4.25.3 are both complicated by variation in P_2O_5 with apatite fractionation at low MgO contents but demonstrate the same conclusion. The uniform Zr/P_2O_5 at high MgO indicates that the uniform value of $TiO_2/Fe_2O_3^T$ in 4.25.1 is not merely the result of control by a Ti and Fe rich phase with constant Ti/Fe (e.g. Ti - magnetite), whilst the lack of systematic variation in K_2O/P_2O_5 at high MgO in 4.25.3 suggests that, like the MBG magmas, the porphyritic magmas were not affected by AFC processes.

Fig. 4.25. Ratio - ratio plots showing similarity of the ultraporphyritic M2 dolerites to the near - aphyric MBG magmas.

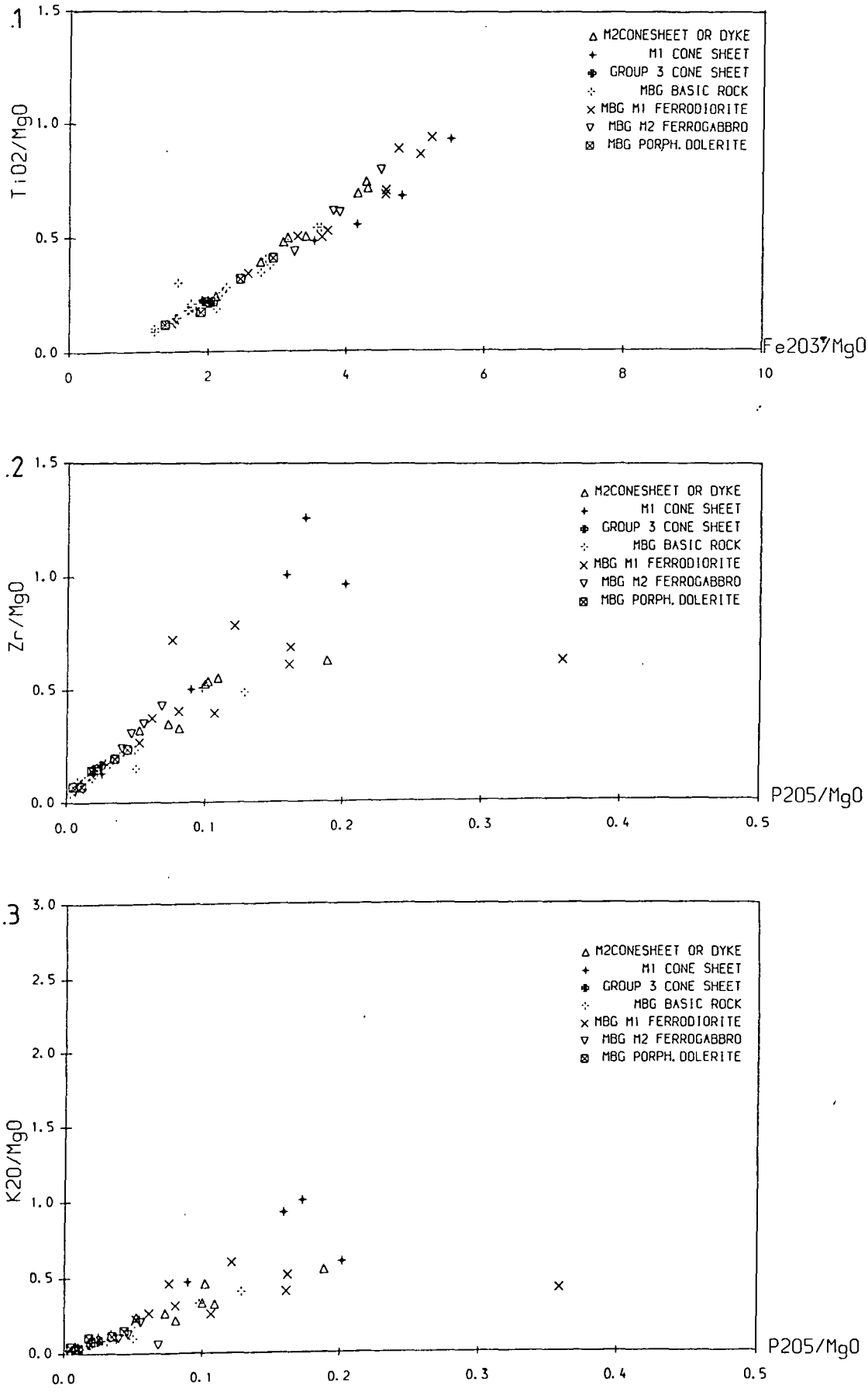

These plots therefore indicate that the late - M2 porphyritic dolerites represent a suite of rocks with a similar compositional evolution history to the MBG basic rocks. This is not, of course, the same thing as asserting that they were derived from the same batch of magma, as similar magmas may have been present throughout the evolution of the Hypersthene Gabbro. This question is considered further in Chapter 6.

4.3.5 Conclusions on the Petrogenesis of the MBG Homogenous Basic and Intermediate rocks and Implications for the behaviour of the MBG Magma Chamber.

The rocks dealt with in this section include all the basic and intermediate rocks of M1 and M2 age within or associated with the MBG except the heterogenous hybrid rocks in the contact zone of the intrusion, which are discussed in section 4.4. Of these rocks, the basic and intermediate rocks of M1 age within the MBG, the M2 ferrogabbroic pods and veins, and the Groups 1 and 2 cone sheets all form a single suite of rocks, characterised by broadly tholeiitic compositions with a range of MgO contents from 3% to 8% . Most of the rocks within these limits do not, however, lie exactly on a tholeiitic fractionation trend, but are instead homogenous mixtures of various MgO - poor, magnetite - saturated magmas and more MgO - rich magmas without magnetite on the liquidus. The principal exceptions to this rule are the M2 ferrogabbro veins and pods which lie close to the tholeiitic fractionation trend and are close to simple fractionated tholeiitic liquids. The Group 3 cone sheets and M2 porphyritic dolerite sheets within the MBG have groundmass compositions corresponding to similar tholeiitic liquids but are difficult to interpret because of their high accumulative plagioclase contents.

The MBG rocks analysed for REEs, Th, Hf and Ta were mainly contaminated by both granulite - facies and amphibolite - facies Lewisian gneiss complex rocks of intermediate to tonalitic composition during their ascent through the crust. This contamination took place prior to the entry of these rocks into the MBG magma chamber. Contamination with the high Hf/Sm sedimentary rocks and Tertiary subalkaline granitoids which make up the bulk of the wall of the intrusion at and below the present level of exposure can only have been minor in most of these rocks, although some rocks close to the contact show evidence for contamination with high Hf/Sm material. The contamination with Lewisian crustal material did not take place in a coupled assimilation and fractional crystallisation process and almost certainly occurred prior to the fractionation which produced the observed range

of basic to intermediate compositions. The Lewisian rocks involved in contamination of the MBG magmas are the volumetrically dominant component of the Lewisian complex and have relatively refractory compositions. This is in strong contrast to the principal Lewisian contaminants in the basalts of Skye and Mull, which are the volumetrically minor low - melting - temperature granitic gneisses and granites and suggests that the parental magmas to the MBG rocks were picritic or picrobasaltic in composition. Such magmas are characterised by high temperatures and able to melt, and be contaminated by, a wide range of wall - rock compositions.

Although this contamination occurred prior to entry of the low Hf/Sm MBG magmas into the MBG magma chamber, the low Hf/Sm MBG basic rocks show substantial variations in incompatible - element ratios sensitive to crustal contamination (such as La/Ta). These variations reflect differences in the amounts of contaminant present or differences in the composition of the contaminant or of the parental ultrabasic magma at the time of contamination. They must have been preserved, at least partially, throughout the residence period of these magmas in the magma chamber. The alternative interpretation, that they reflect temporal variation in the composition of a homogenous magma body, seems unlikely because of the random nature of the trace - element - ratio variations with respect to major element compositions, the small scale on which the heterogeneity occurs and the evidence for mixing of different magma compositions present in the magma chamber at any one time provided by the major - element data.

The combination of major - element evidence of magma mixing and trace element ratio evidence for incomplete homogenisation suggests that mixing of magmas occurred within the MBG magma chamber during the period represented by these rocks (mainly late M1 and early M2) but was an inefficient process. More precisely, the rate at which trace - element - ratio heterogeneity was created in the magma chamber by input of fresh batches of compositionally varied magma was sufficient to maintain a noticeable level of heterogeneity within the magma chamber and therefore similar to, or greater than, the rate of compositional homogenisation by mixing. The alternative interpretation, that the range of compositions was generated by secular variation in the composition of a homogenous (with respect to incompatible element ratios) magma chamber is inconsistent with the evidence from rocks of various ages (including M1 cone sheets, end - M1/earliest M2 rocks in the MBG itself, and later M2 cone sheets) which indicates that a wide range of magma compositions with 3 – 8% MgO was present at all times from late M1 to early or mid - M2 and that there was no

change in this range of compositions.

The cooler and more evolved MgO - poor MBG magmas mainly occur close to the contact at the present level of exposure, particularly on the northern and southern margins of the intrusion. The interior of the magma chamber at the present level of exposure on these margins was dominated by crystal - poor magmas with 6 – 8% MgO and probable temperatures in the range 1160 – 1210°C. The western margin of the MBG, which was at a structurally higher level prior to late M2 (syn - Inner Series) faulting in the An Acairseid area, contains rather more evolved rocks.

This latter observation is consistent with calculated magma densities which suggest that the MBG magma chamber was marginally stably stratified with a continuous upward decrease in MgO content but an overall liquidus density variation of no more than about $0.1 gcm^{-3}$. Cooling through as little as 20°C at the wall of the intrusion would be sufficient to eliminate this density difference and cause more evolved magmas to flow down the wall of the magma chamber, as is consistent with the occurrence of more evolved rocks close to the contact. Experiments by Goldman & Jaluria (1986) on buoyant flows in a stratified air body adjacent to a steep boundary indicate that, even at a higher Reynolds number (ratio of inertia to buoyancy forces) than is likely to occur in a magma body, the boundary current came to an abrubt halt when it reached a layer with the same density as the material in the flow and that rapid mixing of the two occurred. An analogous situation would arise in the case of a current or pulse of cooled dense magma descending the wall of a magma chamber when it reached a layer which was of the same density or still denser (because of the difference in compositions), in which case mixing of compositionally distinct magmas would occur as indicated by the data in Fig. 4.18. Alternatively, if the density increase produced by cooling were sufficiently great, the cooled intermediate magma might sink all the way to the floor of the magma chamber. This suggests that sidewall cooling can produce mixing of a nearly unstable stratified magma body at a rate that is a complex function of the density variation in the magma body, the properties of the magma (such as thermal expansivity, viscosity and temperature - dependence of viscosity) which determine flow flux at a given rate of cooling and the heat flux out of the magma chamber interior, Q_m.

Given the evidence presented above which indicates that a wide variety of magma compositions were entering the MBG magma chamber and thus maintaining the incompatible - trace - element -

ratio heterogeneity, the possibility of partial mixing as the magmas entered the chamber also arises. The input of magmas into stratified magma chambers has been extensively studied by Turner and co - workers (see review in Turner & Campbell (1986)). Analogue experiments by these workers indicate that magma inputs through narrow pipes or dyke - like conduits (note that the geophysical evidence (see Chapters 2 and 7) requires all the feeders to the Ardnamurchan central complex to be small dykes or plugs) produce a plume of magma which rises to a layer in the chamber with the same or a lower density as the magma in the plume. The magma in the plume then mixes with that layer if it has the same density, or spreads out to form a new layer at the interface between a denser and the less dense layer. The experiments conducted by Turner & co - workers mainly dealt with turbulent plumes in which extensive entrainment and mixing also occurred as the plumes ascended through magmas of greater density. Experiments by Goldman & Jaluria (1986) on axisymmetric laminar plumes away from walls indicate that inputs of buoyant magma under a laminar flow regime will behave in a similar fashion except that entrainment of denser magmas in the rising plume will be much reduced. Unfortunately, it is not possible to distinguish between these two cases using the geochemical data.

In contrast to the complex variation in mafic magma densities, the subalkaline granitoid magmas had much lower (by around $0.3 gcm^{-3}$) densities than the basic to intermediate magmas at all magmatic temperatures and must have flowed up the wall of the intrusion, as is consistent with the inference made in section 4.2 that the sources of these rocks lay well below the present level of exposure.

4.4. Heterogenous Hybrid Rocks in the Marginal Border Group.

The subjects of this section are the compositionally and texturally heterogenous rocks which form most of the contact zone of the MBG and are characterised in the field by a diffuse decimetre - to centimetre - scale mottling. Field and petrographic evidence summarised in section 3.2.7 indicates that they were formed by incomplete mixing of at least two compositionally distinct magmas, generally a felsic magma and a basic or intermediate magma, and that mixing may have occurred in more than one distinct event. The aims of this section are to determine, using geochemical data, the number, origins and physical properties of the magma compositions involved in the mixing process and to use the results, in conjunction with field observations, to investigate the mechanisms of heterogenous hybrid magma formation.

4.4.1. Geochemistry of the Heterogenous Hybrid Rocks.

4.4.1.1 Compositions of and Compositional Variation in the End - Member Magmas.

Various aspects of the geochemistry of these rocks are depicted in the series of element - element plots which make up Fig. 4.26.1 – 8. The first four plots are of element pairs which show kinked or 'dog - leg' fractionation trends in tholeiitic suites of rocks (section 4.3.1). In these plots the heterogenous hybrid rocks of the MBG form triangular fields, one side of each of which is formed by the homogenous basic to intermediate Marginal Border Group rocks (discussed in section 4.3). There is some compositional overlap between texturally heterogenous and texturally homogenous MBG rocks, reflecting the role of complete magma mixing between basic and intermediate magmas in the formation of the homogenous rocks (section 4.3.1). However, a large area in the centre of the triangular hybrid field in each of these plots is occupied only by heterogenous hybrid rocks. The third corner of the triangular field of hybrid rocks is occupied by a number of overlapping groups of rocks from the walls and contact zone of the MBG. The compositional variation in the heterogenous hybrid rocks is largely due to the involvement of some of these groups of rocks. They include both the subalkaline granitoids associated with the MBG (the M1 microgranodiorites and M2 felsites), the anomalous granitoids and rheomorphic breccias, and a wide variety of Tertiary and pre - Tertiary country rocks. It is not possible to exclude any of these rock types as potential end - members in the formation of the hybrid rocks because of the broad field of compositions of the

Fig. 4.26. Important features of the geochemistry of the MBG heterogenous hybrid rocks.

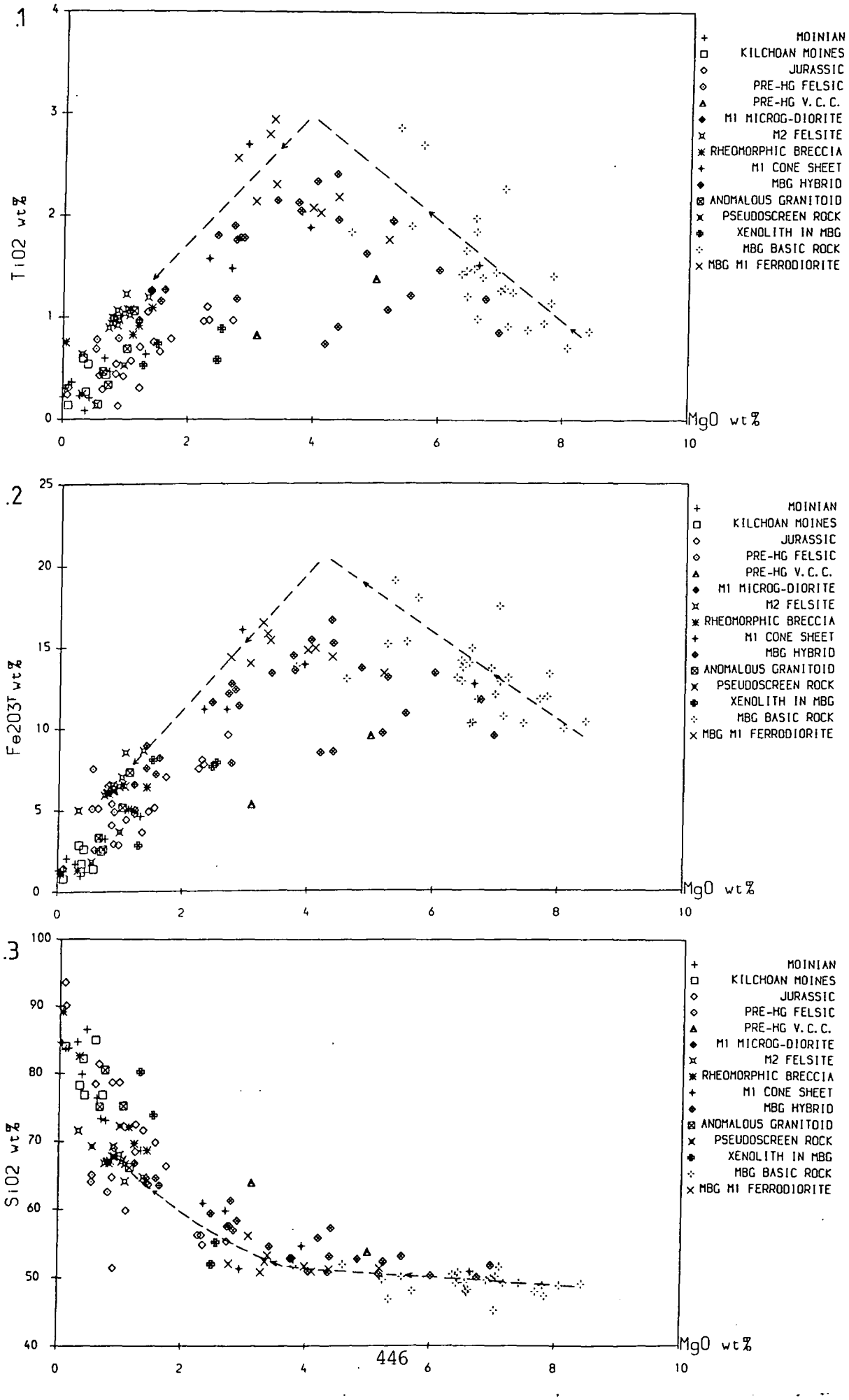

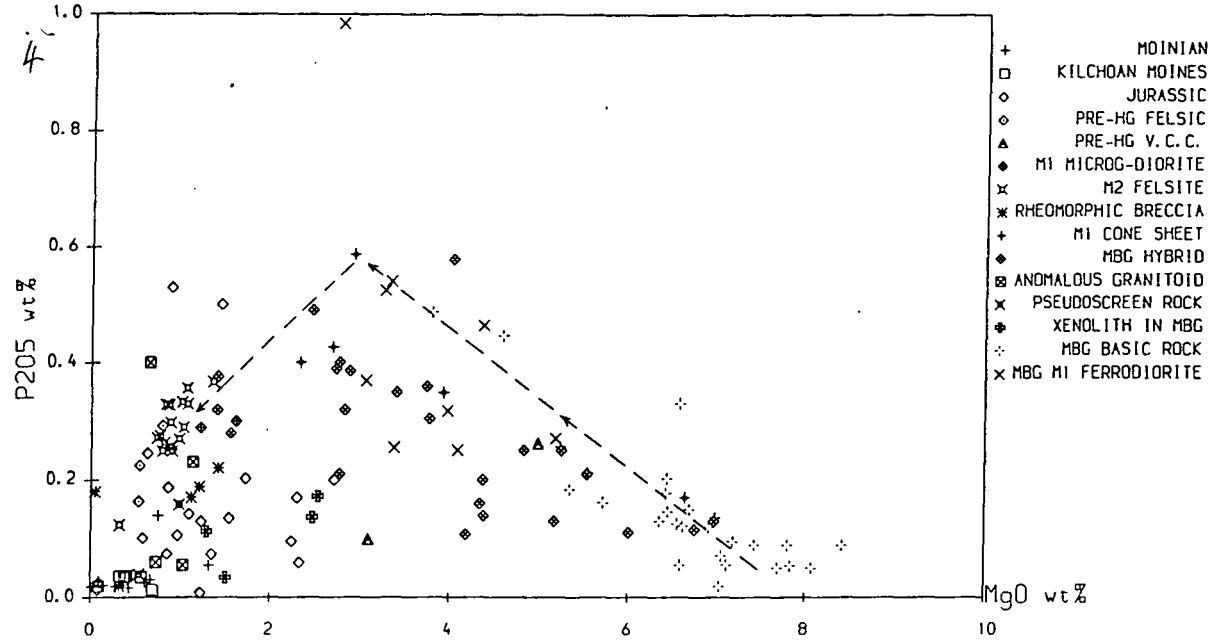
4
P2O5 wt%
MgO wt%
MOINIAN
KILCHOAN MOINES
JURASSIC
PRE-HG FELSIC
PRE-HG V.C.C.
M1 MICROG-DIORITE
M2 FELSITE
RHEOMORPHIC BRECCIA
M1 CONE SHEET
MBG HYBRID
ANOMALOUS GRANITOID
PSEUDOSCREEN ROCK
XENOLITH IN MBG
MBG BASIC ROCK
MBG M1 FERRODIORITE

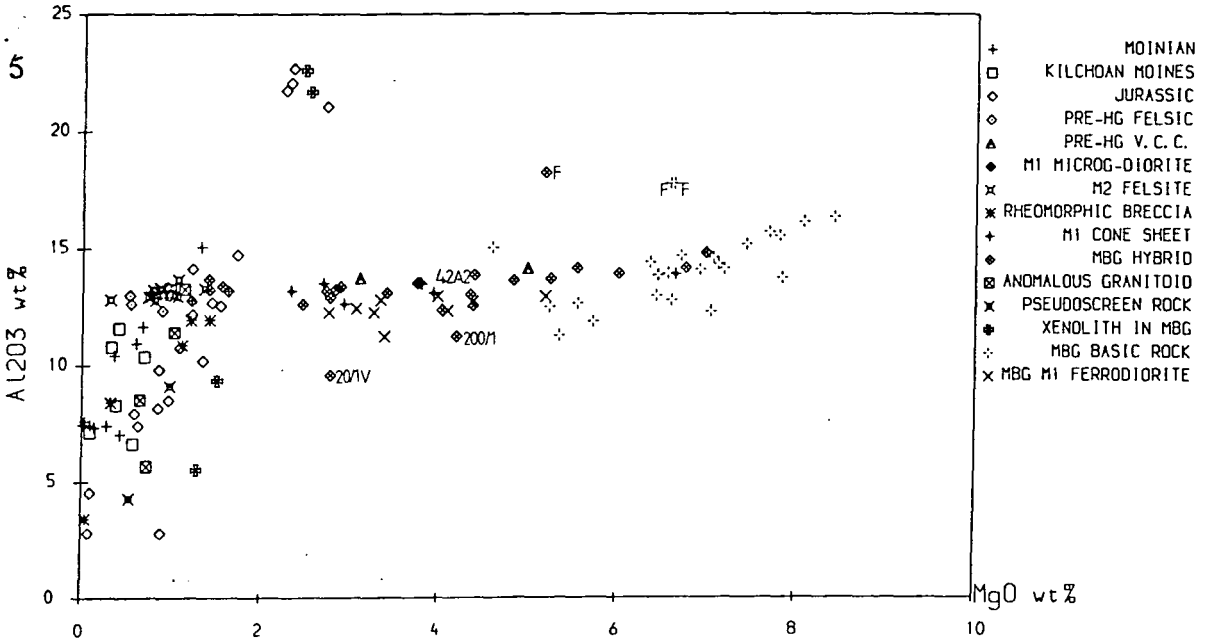
5
Al2O3 wt%
MgO wt%
F
42A2
200/1
20/1V
MOINIAN
KILCHOAN MOINES
JURASSIC
PRE-HG FELSIC
PRE-HG V.C.C.
M1 MICROG-DIORITE
M2 FELSITE
RHEOMORPHIC BRECCIA
M1 CONE SHEET
MBG HYBRID
ANOMALOUS GRANITOID
PSEUDOSCREEN ROCK
XENOLITH IN MBG
MBG BASIC ROCK
MBG M1 FERRODIORITE

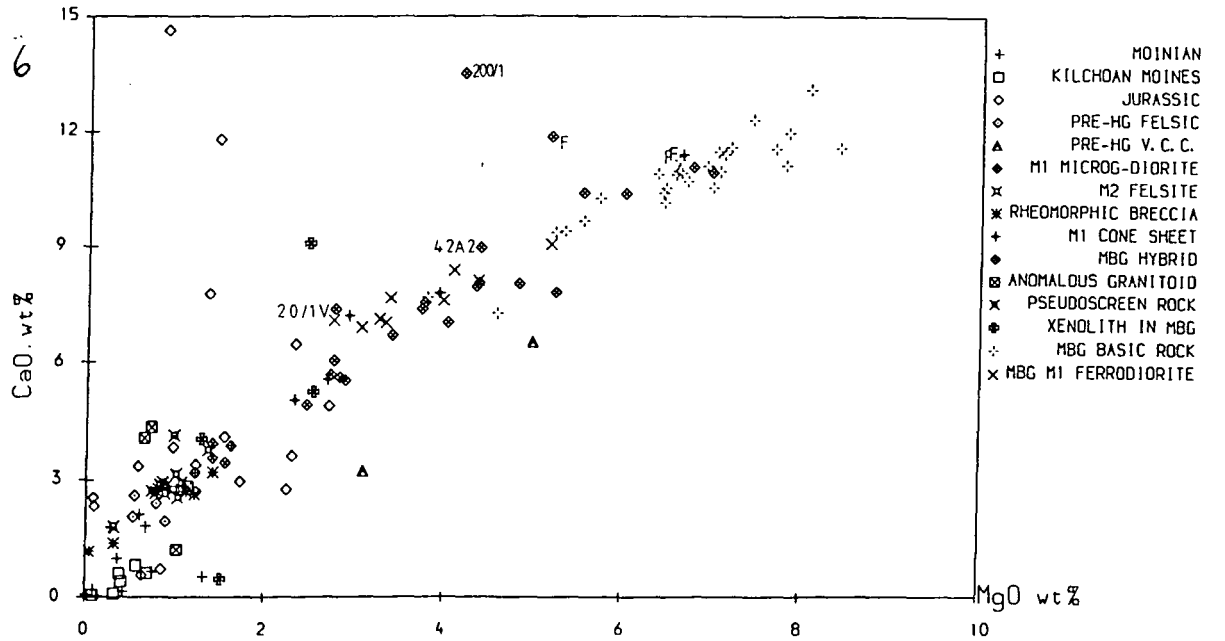
6
CaO wt%
MgO wt%
200/1
F
42A2
20/1V
MOINIAN
KILCHOAN MOINES
JURASSIC
PRE-HG FELSIC
PRE-HG V.C.C.
M1 MICROG-DIORITE
M2 FELSITE
RHEOMORPHIC BRECCIA
M1 CONE SHEET
MBG HYBRID
ANOMALOUS GRANITOID
PSEUDOSCREEN ROCK
XENOLITH IN MBG
MBG BASIC ROCK
MBG M1 FERRODIORITE

.7

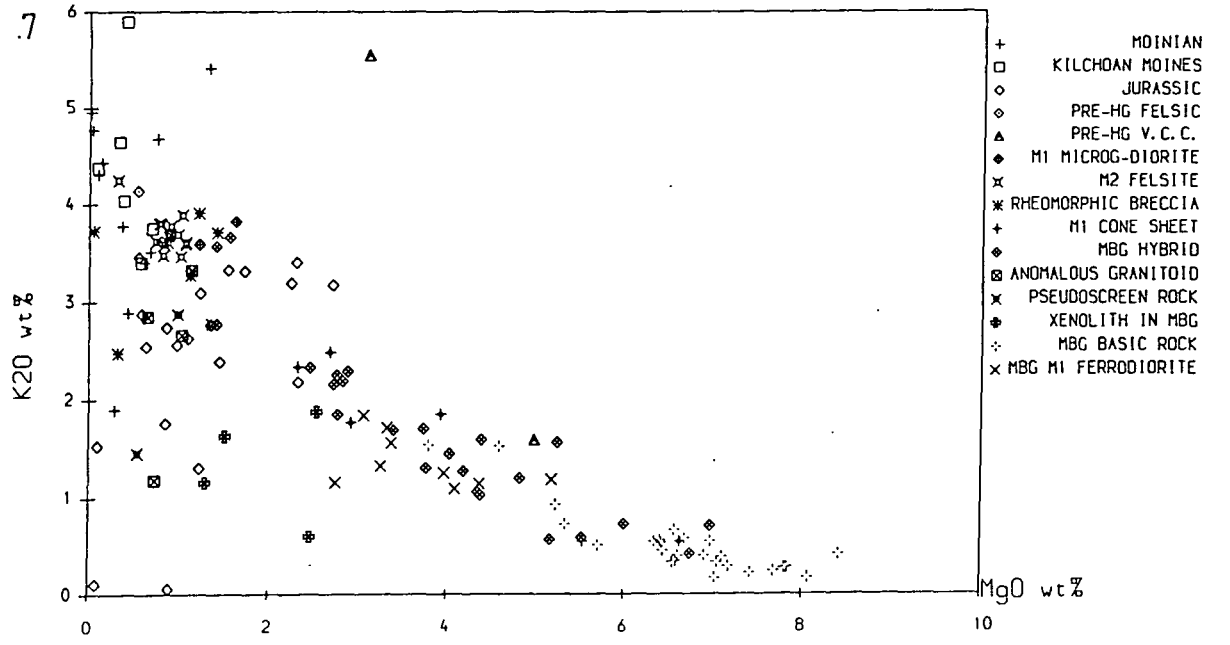
K20 wt%
MgO wt%
0
1
2
3
4
5
6
0
2
4
6
8
10
MOINIAN
KILCHOAN MOINES
JURASSIC
PRE-HG FELSIC
PRE-HG V.C.C.
M1 MICROG-DIORITE
M2 FELSITE
RHEOMORPHIC BRECCIA
M1 CONE SHEET
MBG HYBRID
ANOMALOUS GRANITOID
PSEUDOSCREEN ROCK
XENOLITH IN MBG
MBG BASIC ROCK
MBG M1 FERRODIORITE

.8

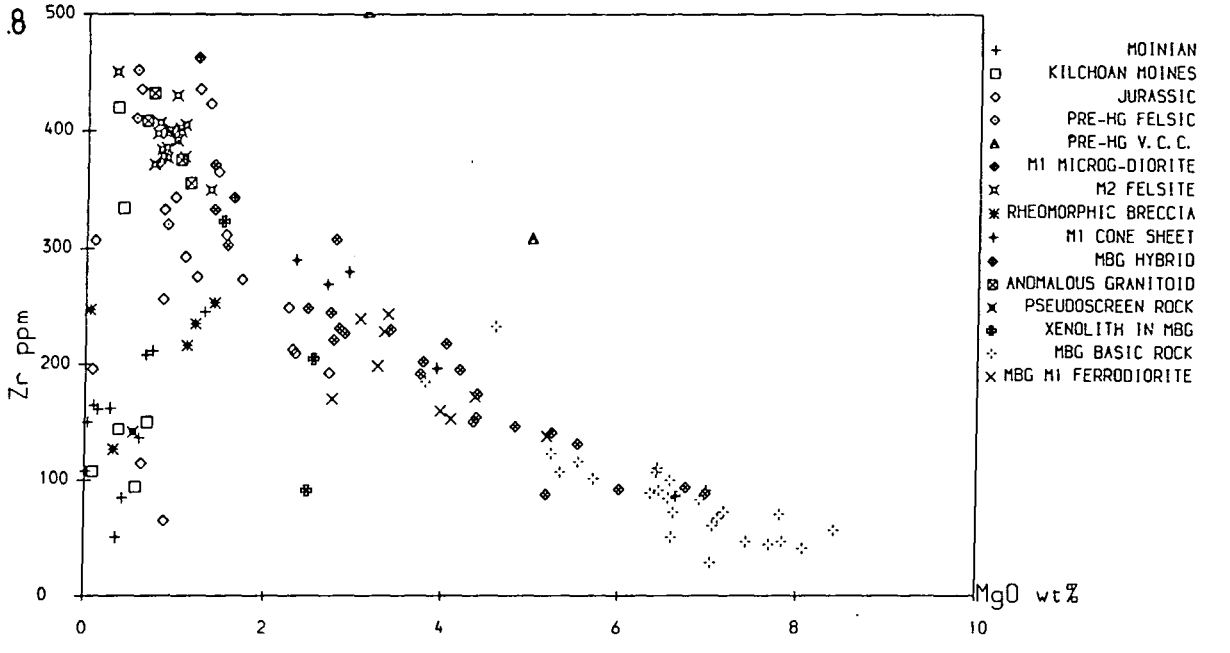
Zr ppm
MgO wt%
0
100
200
300
400
500
0
2
4
6
8
10
MOINIAN
KILCHOAN MOINES
JURASSIC
PRE-HG FELSIC
PRE-HG V.C.C.
M1 MICROG-DIORITE
M2 FELSITE
RHEOMORPHIC BRECCIA
M1 CONE SHEET
MBG HYBRID
ANOMALOUS GRANITOID
PSEUDOSCREEN ROCK
XENOLITH IN MBG
MBG BASIC ROCK
MBG M1 FERRODIORITE

latter in these diagrams, although in Fig. 4.26.1 and Fig. 4.26.4 no hybrid composition lies below a line connecting the most basic MBG rocks to the relatively Ti - and P - rich subalkaline granitoids and country rock lithologies, suggesting that the Ti - and P - poor country rock lithologies were at most a volumetrically minor component in the mixing process.

More positive information on the compositions of the felsic end - members involved in the mixing process can be gained from Fig. 4.26.5 – 8. In these the near - aphyric homogenous basic and intermediate rocks and almost all the heterogenous hybrid rocks form a single elongate linear field. This lies at a high angle to a second elongate compositional field which contains the MBG granitoids and country rocks. The three homogenous basic rocks plotting off the main array in Fig. 4.26.5 are all plagioclase - phyric and originate from the Glebe Hill area: the presence of strained plagioclase porphyrocrysts and microxenoliths in other rocks from this area suggests that these rocks are feldspar - accumulative (section 3.2.6.1). The source of the felsic component in the vast majority of the hybrid rocks must plot where the two fields intersect in this diagram. Rocks plotting at the intersections of the two elongate fields in these plots invariably include the subalkaline granitoids and the essentially similar pre - Hypersthene Gabbro felsic rocks which were sampled outside the intrusion. A number of country rock lithologies also plot in this area, notably the matrix component of the rheomorphic breccia and various siltstone lithologies within the Jurassic sequence. However, two major country rock units can be ruled out as significant components of most of the hybrid rocks on the basis of the plots in Fig. 4.26. These are the Middle Pabba Beds, which are too Al - rich (Fig. 4.26.5), and the Moinian rocks, which are almost all too Zr - poor (Fig. 4.26.8). Ca - rich rocks within the Jurassic sequence cannot have been a significant component of the heterogenous hybrid rocks which lie on the main trend but were involved in the generation of the Ca - rich and Al - poor hybrid rocks which lie off the main array in Fig. 4.26.6: these are discussed further below.

In general, however, the heterogenous hybrids are mixtures of basic to intermediate magmas with a small range of rock compositions which are characterised by low fusion temperatures: Tertiary subalkaline felsic rocks and various Mesozoic siltstone to impure sandstone units. This restricted range of MgO - poor endmember compositions in the hybrid rocks suggests that the pattern of hybrid formation seen at outcrop, where hybrids only appear to form by mixing of mafic magmas and pre - existing felsic magmas (section 3.2) rather than by direct assimilation of solid wall rocks, is a general feature of the M1 MBG magma chamber.

Figs. 4.26.5 – 8 cannot, however, be used to distinguish which of the fusible rock types which plot at the intersection of the two arrays were involved in the formation of any given hybrid rock. The simplest way to distinguish the Tertiary subalkaline granitoid rocks from all the pre - Tertiary country rocks is by the generally higher REE contents and consistently lower La/Yb of the former, as was shown in section 4.2.2.1. The same technique can in principle be used to identify the felsic components of the hybrid rocks, with results shown in Fig. 4.27. The main problem in the interpretation of this diagram is that the hybrid rocks are dominated by a basic to intermediate component which itself shows considerable variation in La/Yb at given La contents as a result of the varying degrees of previous crustal contamination, as was shown in section 4.3.2. However, the hybrid rocks show even greater variation in Fig. 4.27, implying that their formation must have involved a variety of felsic components. In the case of relatively high - La, low - La/Yb hybrids such as 42B, the felsic component must have been dominated by subalkaline granitoid magma, whilst in the case of high La/Yb, low La samples such as 33B1 and 33B2 it must have been mainly composed of La - poor, high La/Yb magma produced by anatexis of pre - Tertiary country rocks such as the rheomorphic breccia 47AW or 185/2, which is an Upper Pabba Beds siltstone.

The wide range in the compositions of the potential end - members, together with the evidence for multi - stage (and therefore, potentially, three - component) mixing, means that in general two component mixing mass - balance calculations on the heterogenous hybrid rocks are not worthwhile. However, in the case of the extreme compositions noted above it is possible to place additional constraints on the REE compositions of the mafic end - members using mass - balance constraints. 33B2 lies close to mixing lines connecting MBG basic rocks with various La/Yb ratios to the high La/Yb pre - Tertiary country rocks. However, its MgO content (6.97%) is close to the maximum value in the homogenous MBG basic rocks (about 8% ; see section 4.3.1), implying that the proportion of the country rock component, with 0.5 – 2% MgO, must be small, and certainly less than 20% . The mixing lines plotted on Fig. 4.27 have percentages of the felsic component marked on them and indicate that the basic component of 33B2 must have been a high La/Yb magma, one which had been strongly contaminated prior to fractional crystallisation and entry into the MBG magma chamber (for example, sample 30), rather than a low La/Yb basic magma such as that represented by 42D2. In contrast, hybrids such as sample 33B1, which was collected less than 10m from 33B2 (Grid Ref. 44357043; see Map 3) in a continuous outcrop of heterogenous hybrid rocks, and sample 18, which was collected from outcrops 80m west of location 33B, have much lower La/Yb

Fig. 4.27. La /Yb vs. La (ppm) plot of hybrid rocks and various possible end - members involved in production of the hybrid rocks by magma - mixing. See text for discussion of named samples.

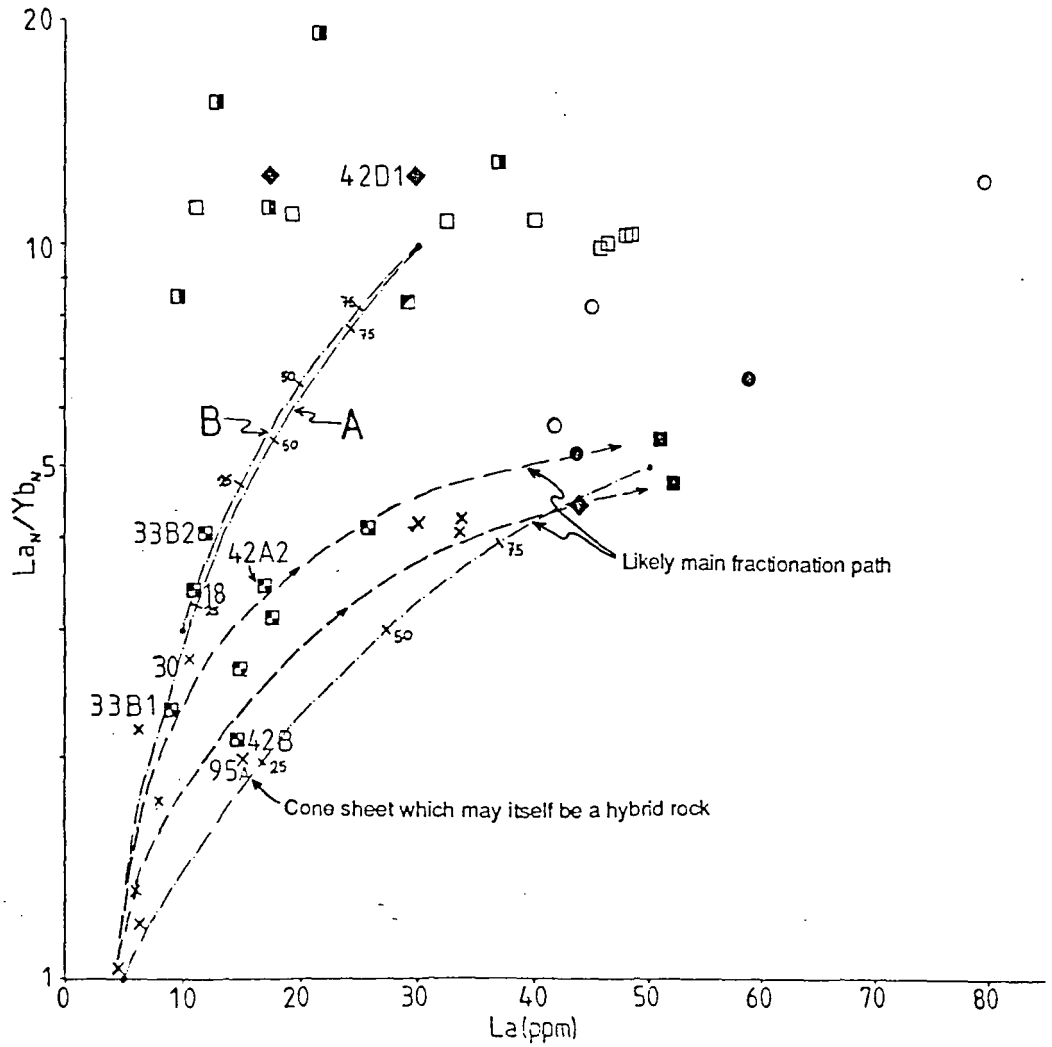

Key

- Heterogenous hybrid rocks
- M1 microgranodiorites
- M2 felsites
- M1 anomalous granitoids
- Rheomorphic breccia
- M1 basic and intermediate rocks
- Felsic pre - Hypersthene Gabbro Tertiary rocks
- Jurassic sediments
- Moinian metasediments
- Mixing lines with proportion of felsic component

and lower MgO and cannot have been generated by mixing of the same combination of high La/Yb, low La magmas. 33B1, for example, has slightly lower MgO and SiO_2 than 33B2, higher Ti and V (suggesting a more evolved mafic component), and very much lower K_2O and La/Yb. These differences can be explained in various ways, by supposing that 33B1 is a mixture of (1) a doleritic magma with slightly lower La/Yb and a subalkaline granitoid magma, (2) a similar doleritic magma and an intermediate magma, (3) a low La/Yb doleritic magma and a less K_2O and SiO_2 rich country rock or (4) some combination of these involved in a multistage mixing process. It is clear from Fig. 4.27, however, that 33B1 and 33B2 cannot be cogenetic and must have been juxtaposed by large - scale (of hundreds of metres ?) magma movements after their formation.

With a few exceptions it is not possible to identify the position of the source of the felsic component of individual hybrid rocks in the same way as the positions of the sources of the anomalous granitoids can be determined (section 4.2.3). The exceptions are the anomalously high CaO and/or low Al_2O_3 hybrid rocks which lie off the main trends in Figs. 4.26.5 and .6. Two of these, 20/1V and 42A4, are associated with, respectively, the xenolith swarm to the west of the Duin Bhain pseudoscreen (Grid Ref. 44587031) and with the pseudoscreen itself (Grid Ref. 44967023); see Map 3. 20/1V is the host to the xenolith swarm and appears to be a mixture of basic magma and diopside granitoid magma similar to the more fusible rocks of the pseudoscreen. 42A4 is a more normal mottled hybrid rock which occurs just south - west of the pillowed and veined contact at the south - western end of the pseudoscreen (Fig. 3.6) and can be modelled as a mixture of a low La/Yb basic magma and a La - rich diopside microgranite such as 42D1 (see Fig. 4.27) although possibly one with a slightly higher CaO content. The third anomalous hybrid, 200/1, is a heterogenous augite - diorite (locally pyroxenitic) which occurs adjacent to the downfaulted block on Druim na Gearr Leacainn at 47686384, in a position analogous to that of 183D1 in relation to the downfaulted block on Hill 210 (see section 3.2.5.1, in particular Figs. 3.10 and 3.11). The wall - rock - derived component of this rock has to be a very Ca - rich, moderately Fe and Mg rich impure calc - silicate rock bearing a close resemblance to samples 67/1 and 81/3 (see Appendix 2), which form part of the Middle Jurassic succession in the downfaulted block. This suggests that 200/1 formed by mixing of basic magma with anatectic melts formed by fusion of Middle Jurassic rocks within the downfaulted block. If this interpretation is correct, 200/1 represents the only case of hybrid formation involving fusion of a relatively refractory wall rock lithology. As noted in section 3.2.5.3, high degree partial melting of refractory lithologies at the present level of exposure only took place in downfaulted blocks.

The origins and distribution of these anomalous hybrid rocks has been dealt with at some length because, like the anomalous granitoids examined in section 4.2.3, their association with downfaulted blocks is indicative of the control exerted by deformation of the wall of the MBG magma chamber upon melting and mobilisation of wall rocks during the latter stages of M1.

4.4.1.2. Large - scale magma movements associated with the formation of the heterogenous hybrid rocks.

The extreme local variation in the compositions of the end - members involved in the formation of these rocks discussed in the previous section suggests that large - scale mixing of previously formed heterogenous hybrid magmas took place within the contact zone of the MBG magma chamber. Further evidence for this comes from Fig. 4.28.1 – 4. Only M1 MBG and related samples from the northern margin of the MBG (the Glendrian Bay and Duin Bhain - Sanna Point sectors) are plotted in these diagrams. In contrast to the MBG as a whole, which contains a continuous range of compositions from 8% MgO to 3% MgO (Fig. 4.18), most homogenous MBG magmas on the northern margin of the intrusion have 6 – 8% MgO and there is a marked compositional gap between these and the very rare M1 ferrodioritic rocks (some M2 rocks from the northern margin of the intrusion are also plotted in Fig. 4.28 to give a better indication of the normal compositional range of these rocks). Nevertheless, it is apparent that many of the heterogenous hybrid rocks on the northern margin of the intrusion contain a large proportion of basic to intermediate components, with 3 – 6% MgO, that lie on the tholeiitic fractionation trend.

The discrepancy between the low abundance of homogenous intermediate rocks at the present level of exposure and the high proportion of the heterogenous hybrid rocks with a high content of such material, can be explained in terms of two models:

1). Cooling at the wall of the magma chamber, together with the formation of hybrid magmas by mixing of ferrodioritic and anatectic magmas, produced a density current of ferrodioritic and ferrodioritic - felsic hybrid magmas flowing down the wall of the intrusion. Mixing of this density current with hybrid and basic magmas of the same density at deeper levels in the magma chamber would produce the observed mixture of heterogenous hybrid rocks with different end - member components. The rarity of hybrid rocks with compositions plotting in the middle of the

Fig. 4.28. M1samples from the MBG on the northern margin of the intrusion, indicating the much greater abundance of high - Ti and - Fe material as components of heterogenous hybrid rocks than as pure samples at the present level of exposure.

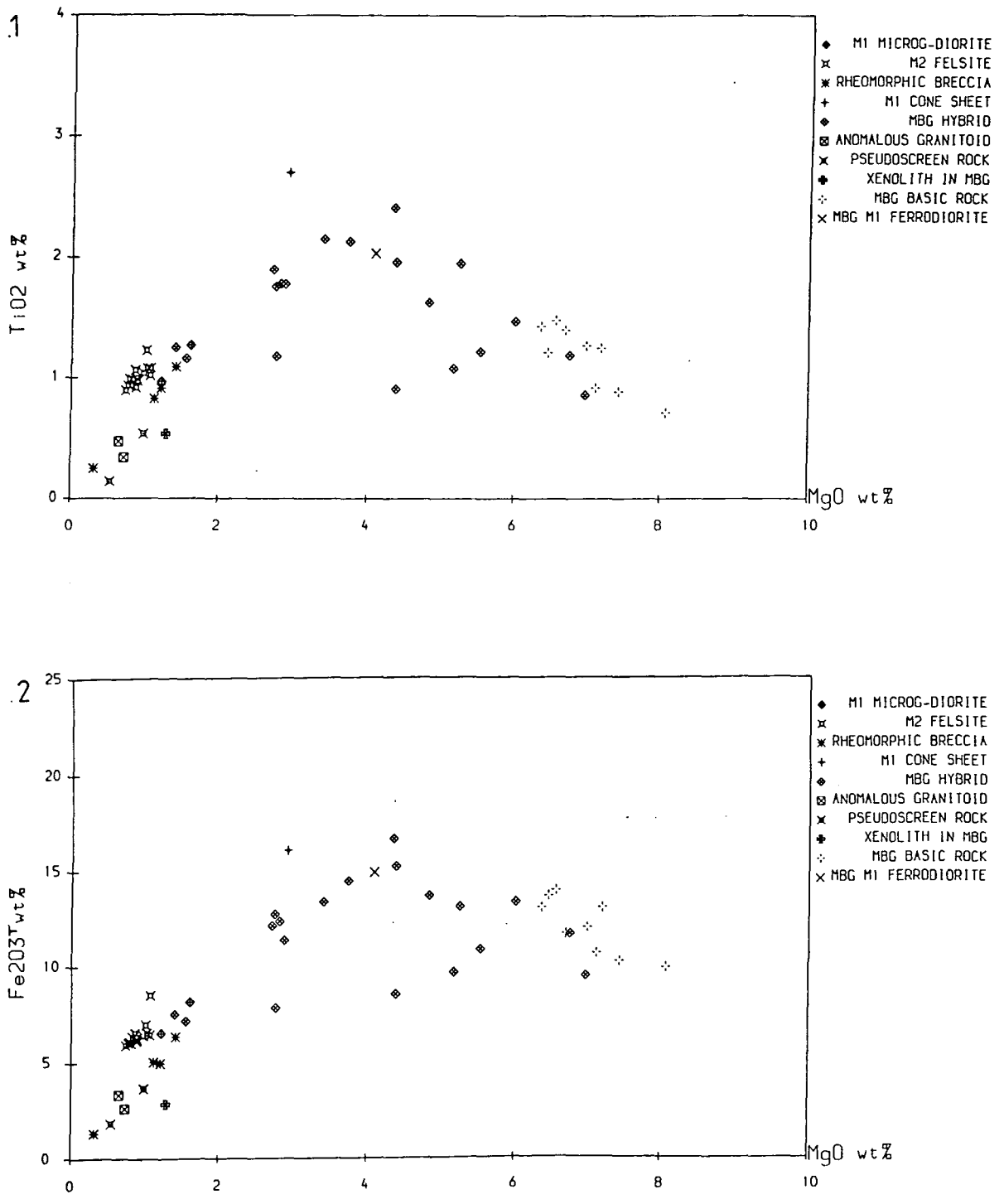

3

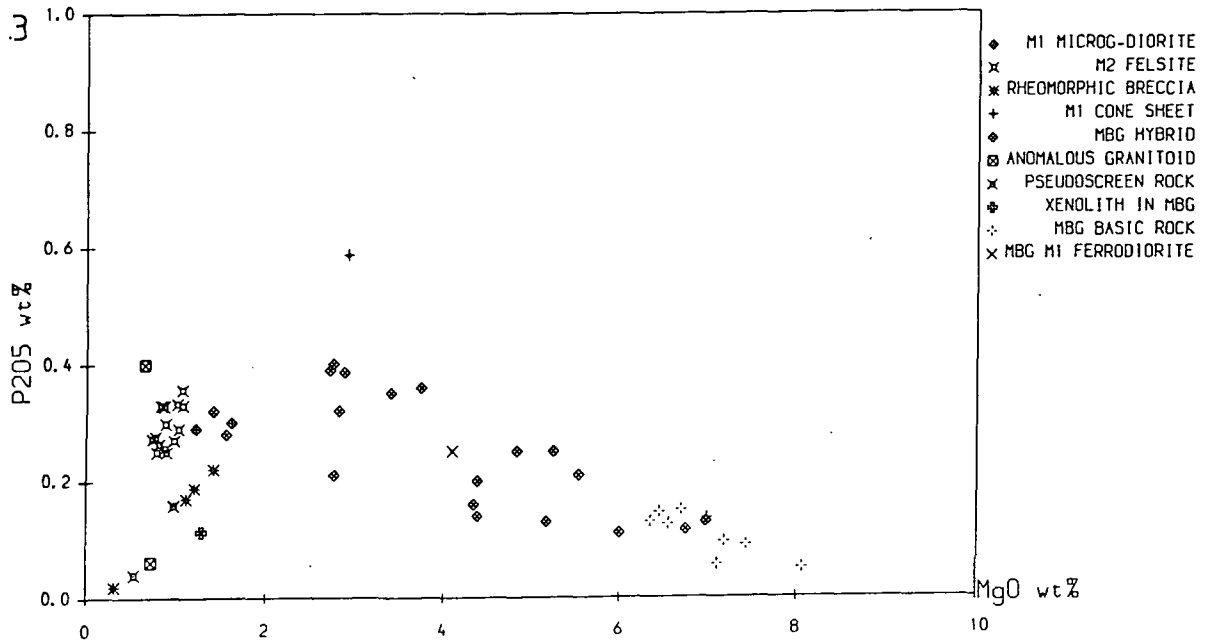
P2O5 wt%
1.0
0.8
0.6
0.4
0.2
0.0
0
2
4
6
8
10
MgO wt%
M1 MICROG-DIORITE
M2 FELSITE
RHEOMORPHIC BRECCIA
M1 CONE SHEET
MBG HYBRID
ANOMALOUS GRANITOID
PSEUDOSCREEN ROCK
XENOLITH IN MBG
MBG BASIC ROCK
MBG M1 FERRODIORITE

4

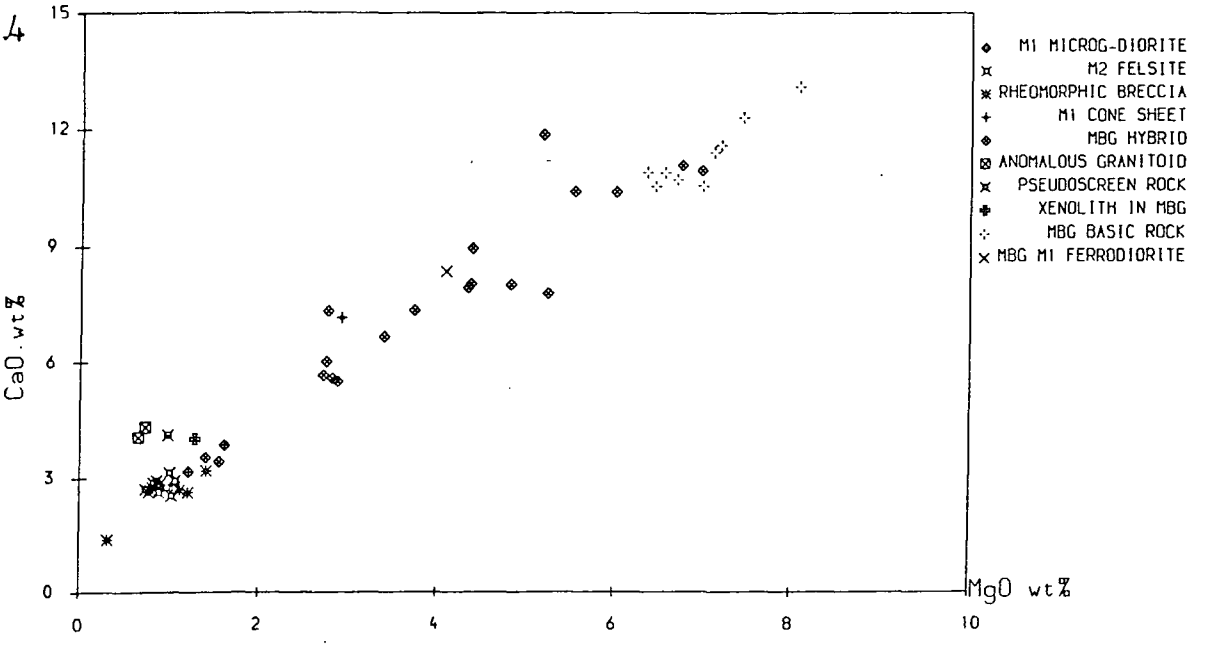
CaO wt%
15
12
9
6
3
0
0
2
4
6
8
10
MgO wt%
M1 MICROG-DIORITE
M2 FELSITE
RHEOMORPHIC BRECCIA
M1 CONE SHEET
MBG HYBRID
ANOMALOUS GRANITOID
PSEUDOSCREEN ROCK
XENOLITH IN MBG
MBG BASIC ROCK
MBG M1 FERRODIORITE

hybrid fields in Fig. 4.28 suggests, however, that mixing at this later stage was rarely on a fine enough scale to produce samples (typically of volumes in the range 100 - 300cm^3) composed of three widely different end - member components which would plot in this central area.

2). Cooling and hybrid magma formation produced a stagnant, high - crystallinity contact zone with a high viscosity relative to the rest of the magma chamber. Such high - viscosity zones may become isolated from convection in the interior of the magma chamber (Marsh 1988). Subsequent influxes of basic magma into the base of the magma chamber elevated the stratified layers within the magma chamber in a manner analogous to the floating - off of evolved low - density magmas postulated to explain transgressive reversals of cryptic zonation found in certain cumulate sequences (Wilson & Engell - Sorenson 1986; Young et al. 1988). This would juxtapose the stagnant hybrids in the contact zone with hotter and more MgO - rich magmas, resulting in reheating and remobilisation of the hybrids in the contact zone which would allow the formation of the basic pillows which occur within the hybrid rocks and also the formation of those hybrid rocks which contain a large component of relatively MgO - rich magma.

This second model is essentially similar to the cyclic cooling - and - crystallisation / reheating - and - remobilisation model developed to account for the three - component felsic/ basic/ ultrabasic hybrid rocks and intrusion breccias at the margin of the Rhum complex (Greenwood 1987). However, the Rhum breccias contain a large number of chilled and subsequently hornfelsed basaltic, doleritic and gabbroic blocks. Greenwood (1987) considers these to be fragments of pillows and minor basic intrusions emplaced before and during the period of stagnation of the marginal zone and subsequently veined and broken up during remelting and remobilisation of the felsic to intermediate hybrid hosts. Similar brecciated basic hornfelses of M1 age are not present in the hybrid rocks at the contact zone of the MBG, in contrast to the M1 and M2 subalkaline and anomalous granitoids, which contain chilled and brecciated basic pillow fragments and, in the case of the outcrops at Glendrian Bay, backveined hornfelsed dolerite sheets (sections 3.2.3.1 and 3.2.2.1). The latter are the only rocks to suggest that reheating of rocks previously solidified at the margin of the MBG took place during M1. These observations suggest that, prior to the end of M1 when the contact zone as a whole solidified, the heterogenous hybrid rocks never cooled to temperatures (below around 1050 – 1150°C, depending on composition (Wood 1978; also see below, section 4.5)) below which the crystal contents of the most mafic parts of the mottled hybrid rocks rose to values (60 – 70% ; Arzi

Plate 4.12. Chilled basic pillow with large segment of the margin spalled of and separated from the rest of the pillow by a granitoid vein. Field location 42D, south of Duin Bhain. Grid reference 44997026.

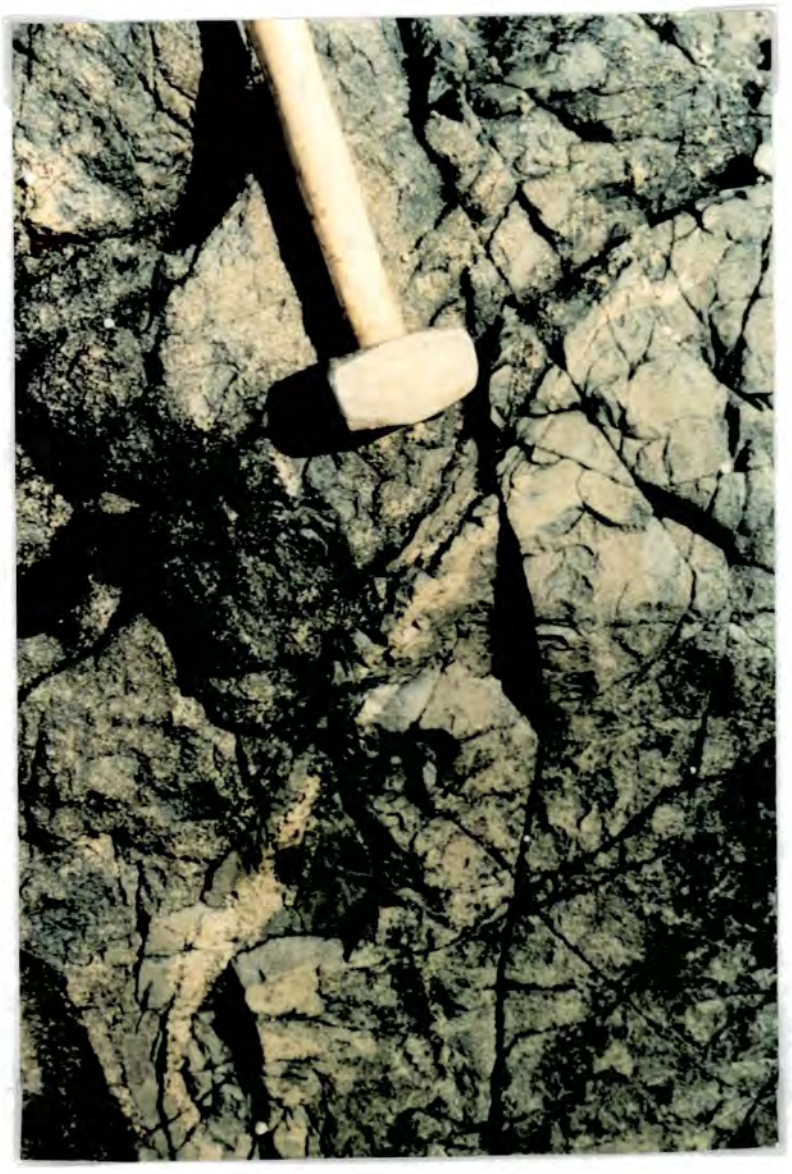

1978, Van der Molen & Paterson 1979) at which the more mafic material became rigid and could be veined and brecciated by more fusible components of the hybrid rocks on reheating. One possible exception to this rule is provided by the heterogenous and pillowed rocks at the extreme south - eastern corner of the MBG outcrop, at the eastern end of the Abhainn Chro Bheinn gorge (Grid Ref. 48116494 ; see section 3.2.6.1). However, as noted in 3.2.6.1 the age of the granitic veining in these rocks is uncertain as it postdates metamorphism which is apparently of M2 age.

Granitoid veins do occur within the hybrid rocks but do not appear to be associated with remobilisation during M1. They are of two types:

1). Veins cutting mafic pillow margins (Plate 3.23) and separating spalled segments of the outer crusts of chilled mafic pillows from the pillow interiors (Plate 4.12). The gradation of the former into hybrid rocks in the pillow interior and the geometry of the latter suggest that, rather than forming during reheating, these veins fill fractures formed by differential thermal stressing of the pillows as they cooled from the outside inwards after being injected into cooler but still mobile heterogenous hybrid magmas.

2). Large, laterally continuous vein complexes, such as those in Grid Square 441704 (section 3.2.3 and Map 3). These veins postdate the consolidation of **all** of the heterogenous hybrid rocks which they cut and are therefore considered to be earliest M2 in age, although relatively coarse - grained. Although grain - size variation producing textural heterogeneity is present, the two samples from the vein complex in 441704 are compositionally almost identical. They are compositionally similar to the subalkaline granitoids, plotting close to them in Fig. 4.26 and 4.28: the only grounds on which they are regarded as hybrid rocks is the mottled appearance of the rocks at outcrop.

The lack of evidence for large - scale remelting of heterogenous hybrid rocks during M1 makes model (2) for the presence of a large ferrodioritc component in the hybrid rocks on the northern margin of the MBG rather implausible. It is not entirely excluded, because the hybrid rocks must have taken a finite time to cool from their stagnation temperature to their solidification temperature, and **if** the replenishment of the magma chamber with MgO - rich magma took place on a timescale that was short compared to this model (2) remains consistent with the field observations. However, the

uniform compositional range shown by the MBG rocks from the latter part of M1 through to mid - M2 argues against the rapid changes in the average composition of the magma chamber implied by such sudden replenishments. Model (1) appears to be more realistic, although this does not exclude the possibility of smaller rises (and falls) in the position of stratified layers in the magma chamber relative to the wall of the intrusion.

4.4.2. Mechanisms of formation of the hybrid magmas and implications for variations in the thermal regime at the margin of the intrusion.

An important feature of plots such as 4.26.1 – 4 is that hybrid rocks occur throughout the triangular field of compositions defined by the basic to intermediate and felsic endmembers involved in the mixing process, apart from the small field in the centre of the plot which was discussed in 4.4.1.2. Even when the heterogenous vein samples which plot close to the subalkaline granitoid samples are excluded, on the grounds that they largely postdate consolidation of the contact zone at the present level of exposure, it is apparent that the heterogenous hybrid rocks contain up to 60% of a felsic end - member component. Furthermore, the maximum observed proportion of this component does not vary with the MgO content (and, therefore, liquidus and rigidus temperatures) of the mafic component.

This feature of these rocks contrasts strongly with the patterns of magma mixing observed in mixed - magma ring dykes by Sparks & Marshall (1986). These workers noted that complete or near - complete mixing of small amounts of hot basic magmas, with high rigidus temperatures, with cooler felsic magmas can be inhibited by chilling (i.e. cooling to below their rigidus temperatures) of the basic magmas when the two are first brought into contact and before small - scale fluid mixing and diffusion can homogenise the mixture. The effects of this phenomenon on mixing between a mafic component with a range of compositions and temperatures and a felsic component with a restricted compositional range and uniform temperature are shown in Fig. 4.29, a schematic variation diagram for two elements which show a dog - leg tholeiitic fractionation trend, such as Ti and Mg. It should be noted that this is the case which applied to the MBG during M1, where the felsic component is the fusible material (subalkaline granitoids and siltstones (sensu lato)) present at the wall of the magma chamber and the mafic component is formed by the homogenous magmas in the interior of the chamber, which range from basaltic to intermediate compositions). In contrast to the ring -

Fig. 4.29. Schematic representation of hybrid compositions produced by mixing of cool felsic magma and a range of hotter intermediate to basic magmas which show an increase in rigidus temperature with rising MgO content
(modified after Sparks & Marshall 1986)

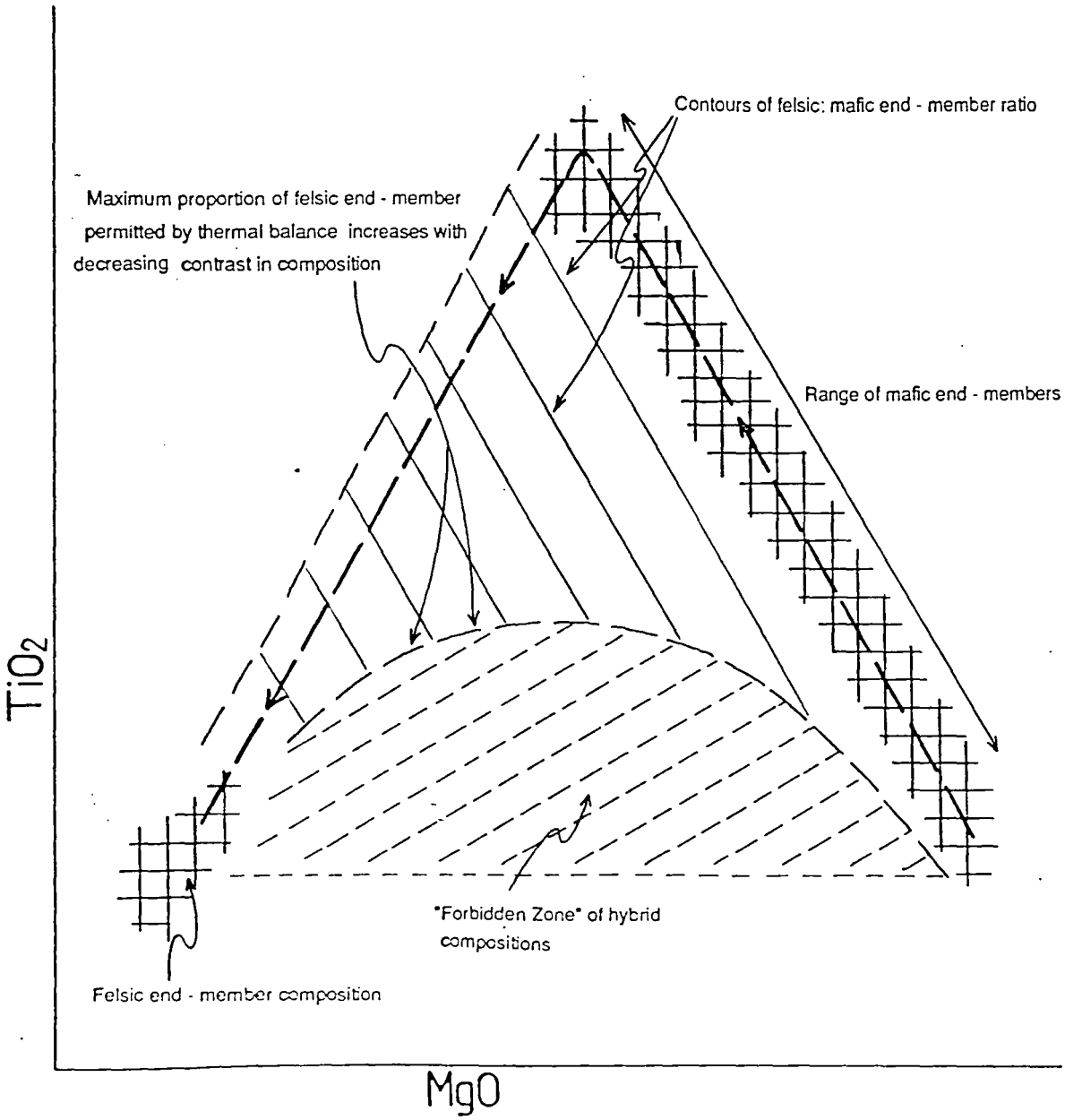

dyke suites investigated by Sparks & Marshall, there is no dependency of the maximum permitted proportion of the felsic component upon the MgO content of the mafic component: it is evident from Figs. 4.26.1 – 4 and 4.28 that the felsic rocks mixed just as freely with the basic magmas as with the high - Ti, Fe and P intermediate magmas. The presence of chilled mafic pillows and pillow fragments in the M1 microgranodiorites and the diopside microgranites at Duin Bhain in particular (sections 3.2.2 and 3.2.3) implies that a strong temperature contrast was present (at least initially; see below) between the felsic and basic magmas, as does the chilling at felsic magma – basic magma contacts, so the difference cannot be explained in terms of a smaller initial temperature difference between the two magmas.

A possible explanation for the two different styles of mixing lies in the different geological settings in which they occur. Hybrid and pillowed felsic - intermediate - basic ring dykes such as the Mullach Sgar and Sgurr nam Meann intrusions (Marshall 1984) and the Loch Ba felsite (Sparks 1988) are considered to form during short and violent volcanic eruptions (or equivalent intrusive events) triggered by magma - mixing events in an underlying magma chamber (Sparks et al. 1977; Thompson 1980). They will therefore have formed rapidly (preventing any significant conductive transfer of heat from adjacent magmas) and in a single - stage event. This contrasts strongly with the situation represented by the heterogenous hybrid rocks in the contact zone of the MBG, which is that of hybrid magma formation at the wall of a large magma chamber under rather more steady - state conditions and with multiple stages of mixing or multiple mixing events taking place (section 4.4.1.2).

Two lines of evidence are relevant to an understanding of felsic - basic magma mixing processes in the latter setting. The first of these is the geochemical evidence (section 4.4.1) that shows that the felsic magmas involved in mixing were mainly produced by melting and mobilisation of the most fusible rocks present in the wall of the intrusion. It was shown in section 4.2 that these magmas, which are represented at the present level of exposure by the subalkaline and anomalous granitoids, were generated, in the case of the anomalous granitoids at least, in discrete episodes. These were triggered by the formation of wedges of country rocks projecting into the magma chamber by movement on inward - dipping concentric normal faults (section 3.2; also Chapter 7). A corollary of this is that the heterogenous hybrid rocks must also have formed episodically, both around the melting tips of the downfaulted blocks (as in the case of the hybrid rocks around the Duin Bhain pseudoscreen; see

section 4.4.1.1) and around the bodies of low - density felsic magmas ascending the wall of the MBG magma chamber. This suggests that the hybrids could have formed in multiple episodes separated by periods in which the hybrid rocks could have been reheated by conduction from the main part of the magma chamber and thus enabled to participate in further hybridisation with cooler magmas. However, unless and until the time interval between episodes of concentric normal faulting, relative to the time taken for a rising body of felsic magma to pass a particular level in the wall of the intrusion (which will determine the duration of the hybrid - forming event in any one rock) and the time needed for conductive reheating can be established, this remains only a suggestion.

The second line of evidence which suggests a significant difference between the mechanisms of formation of the MBG heterogenous hybrids from those of ring - dyke hybrids comes from the nature of the pillowed and veined contacts between felsic and basic rocks, such as those which exposed at Glendrian Bay (section 3.2.2.1) and around the Duin Bhain pseudoscreen (section 3.2.3.1). The sequence of events in these rocks appears to have been as follows:

1) Mafic magma comes into contact with cooler felsic magma as the latter moves up the wall of the magma chamber or as an intervening layer of intermediate (in both composition and temperature) magma is stripped away by convection. A thin chilled zone is formed at the contact as the basic magma is rapidly cooled (Fig. 4.30.1). At the same time, the felsic magma to which it is losing heat must heat up (although not necessarily by the same amount as heat could be advected away from the contact by movement in the felsic magma body).

2). The chilled zone of mafic magma starts to fracture, either as a result of thermal contraction or of stresses imposed by magma movement on either or both sides of the chill zone. Felsic magma is injected up these fractures (Fig. 4.30.2). Examples of such veins preserved at outcrop are much longer (up to 1 - 2m) than they are wide (typically less than 10cm). Although the mechanism of formation of thermal contraction cracks (Lachenbruch 1962; Lister 1974) implies that they cannot cut all the way through the chill zone (see section 5.3 for further discussion of tensile thermal contraction crack formation in a related setting), thermal contraction cracking would concentrate other stresses into the narrow zone between the crack tips and the inner edge of the chill zone and thereby promote complete rupture of the chill zone.

Fig. 4.30. Schematic sequence of events leading to formation of hybrid magmas from felsic and basic end - member components initially separated by a basic chill zone around a rising pulse of felsic magma.

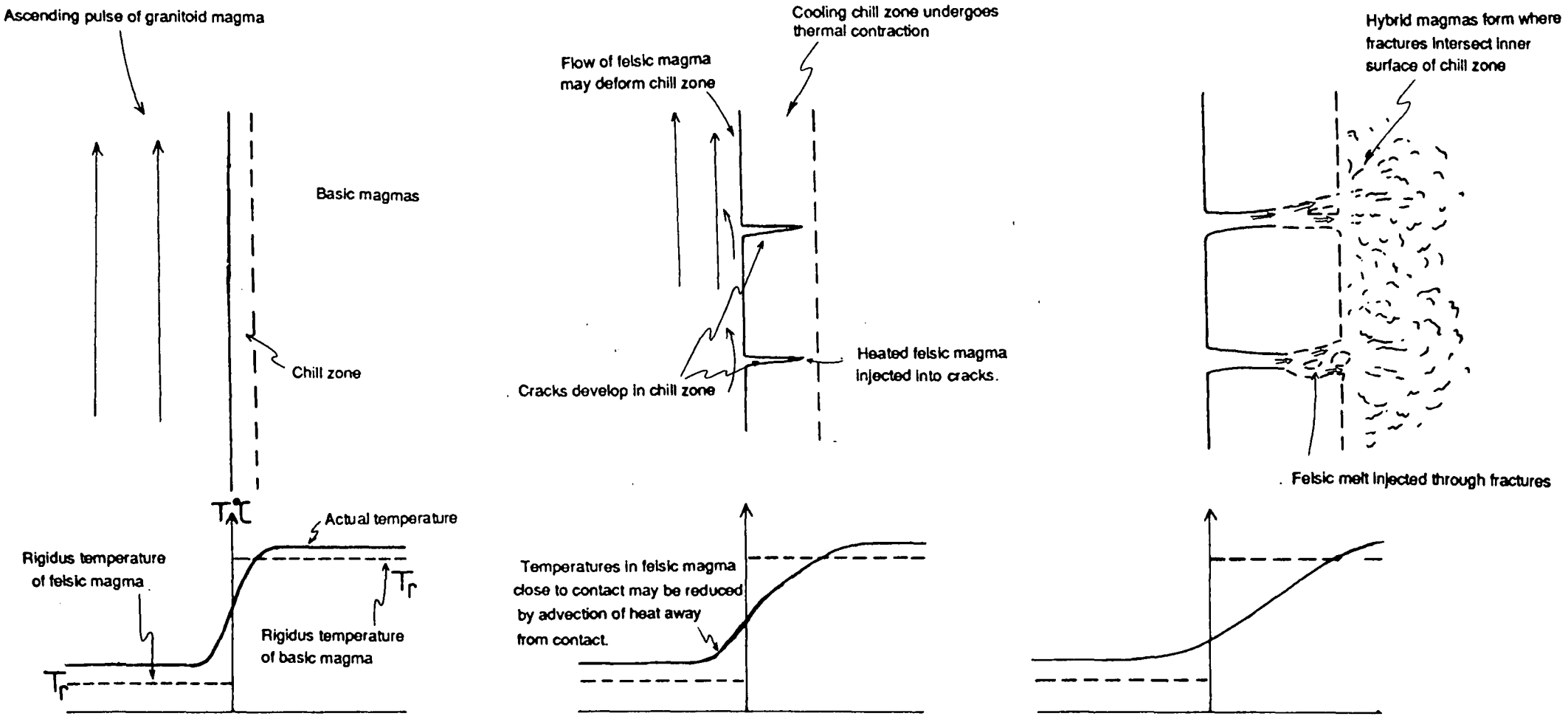

Plate 4.13. Diffuse region of mottled, relatively felsic hybrid rock at end of a vein cutting the chilled margin of the MBG microgabbros where this outcrops against partially fused metasdiments at the western end of the Duin Bhain pseudoscreeen. Field location 42A4, grid reference 44977023.

3). When the fracture reaches the the inner edge of the chilled margin, the felsic magma injected up it comes into contact with more mobile mafic magma. Having been pre - heated by heat lost from the chilled margin, it is able to mix with the mafic magma in a wide range of proportions, producing the diffuse patches of felsic rich hybrid rocks that occur around the inner end of the veins cutting the chill zone (Plate 4.13). These grade out into the more uniform mottled hybrid rocks which form most of the heterogenous hybrid outcrop and which have a smaller proportion of the felsic component. It would appear from the relative proportions of these rocks at outcrop that the effect of the chilling - and - backveining process on the volume of hybrids produced is minor, although it does seem to have produced a greater spread in hybrid compositions. For thermal balance reasons, the overall proportion of felsic material introduced into the basic magmas by this mechanism cannot be any greater than that permitted in the setting described by Sparks & Marshall (1986). However, the felsic material is unevenly distributed, with the greater proportion of felsic material in the hybrid rocks behind the chill zone being balanced by the complete lack of hybridisation in the chill zone itself, allowing the formation of some hybrid rocks with compositions that fall within the 'forbidden zones' of diagrams such as Fig. 4.29. Overall, the rate of hybrid magma formation between magmas of such strongly contrasted composition and temperatures will be limited by the rate at which the felsic magma flows into the veins cutting the chill zone.

Other contacts between contrasting rock types in the contact zone of the MBG do not show the chilling and veining phenomena described above. These are contacts between rock types with smaller differences in composition and hence temperature at the time of heterogenous hybrid magma formation, and are typically lobate or diffuse. Under these circumstances hybrid magma formation would be expected to be more efficient because it would not be limited by the rate of deformation of the chilled zone which separates the felsic and basic magmas in the previous case and/or by the rate of flow of the felsic magmas up the veins. The two types of contact, chilled - and - backveined and diffuse - and - unchilled, appear to correspond respectively to examples of the theoretical type 3 and type 2 boundary layers defined in section 4.1. However, granular - textured basic hornfels xenoliths are not common in the homogenous basic and intermediate rocks of the contact zone. This may indicate that complete disintegration of the veined chill zones was a relatively rare phenomenon.

The formation of chill zones at the contacts between the M1 felsic magmas and basic magmas raises

an important problem regarding the temperatures of the felsic magmas relative to those of the rest of the wall of the intrusion. There is no evidence to suggest that basic magmas chilled against the main wall of the intrusion during the latter part of M1 as represented by the peak of metamorphism: indeed the very high temperatures attained during this metamorphism demonstrate that there was no insulating zone of chilled magma between the wall rocks and the interior of the intrusion at this time, although this does not imply that such a zone could not have been present earlier in the history of the MBG magma chamber (see Chapter 5, however). This implies that the felsic magmas generated at the wall of the MBG magma chamber were actually **colder** than the bulk of the wall of the intrusion. The reason for this is the same as has been pointed in section 4.2.6: partial melting absorbs latent heat and reduces the rate of increase of temperature produced by a given heat flux into the rocks. The result of this is that the partially molten rocks may for a short period be significantly colder, as a result of the latent heat absorbtion associated with melting, than adjacent refractory rock units (such as pelitic or quartzitic beds, or entire sedimentary units such as the Middle Pabba Beds) in which latent heat absorbtion has not taken place during the same episode of melting. This is of course a transient phenomenon as eventually the thermal buffer represented by the melting reactions will be exhausted as the partially molten rocks reach thermal equilibrium or melt completely. However, two possible mechanisms for producing transient thermal conditions at the wall of the MBG magma chamber towards the end of M1 can be envisaged. Firstly, the entire wall of the intrusion may have still been heating up at the end of M1. This possibility is considered further in the next chapter. Secondly, the generation of melts in the downfaulted blocks after their formation by fault movements must occur under transient conditions (see section 4.2.6): there is no reason why a pulse of magma could not be generated **before** the wedge reached thermal equilibrium and had heated up to the temperature of the contact throughout, provided the rigidus temperature of the fusible rock involved was sufficiently less than the contact temperature. The chilling at the felsic - basic magma contacts and the lack of M1 chilling at the main wall of the intrusion clearly demonstrates that the rigidus temperature of the felsic rocks was indeed less than the contact temperature (see section 4.5 for estimates). The question of how this temperature difference could be maintained as the felsic magmas ascended the wall of the MBG magma chamber is deferred to section 4.5.2.

4.5. Summary: The behaviour of the Marginal Border Group Magma Chamber during the latter part of M1.

The work presented in this chapter has shown that the M1 age rocks of the Marginal Border Group correspond to magmas composed of a high percentage of liquid and a small percentage of (or no) suspended crystals. These magmas were present in the MBG magma chamber immediately prior to the period of quenching which ended the M1 phase of activity in the intrusion and provide information on the state of the magma chamber at that time.

4.5.1. Petrogenesis of the M1 - age components of the Marginal Border Group and associated minor intrusions and implications of each for the behaviour of the magma chamber.

The rocks within or associated with the MBG can be divided on petrogenetic grounds into three main groups: (i) anatectic rocks generated by melting and mobilisation of the fusible components of the wall rocks and xenolith swarms formed by disruption of more refractory units and their incorporation into the MBG magma chamber; (ii) homogenous basic and intermediate rocks which form the bulk of the MBG and represent the crustally - contaminated input to the magma chamber from the mantle; (iii) heterogenous hybrid rocks generated by mixing of magmas of the previous two groups in the contact zone of the magma chamber.

4.5.1.1. The Anatectic Rocks and Xenoliths.

All of the anatectic rocks sampled have granitoid compositions. However, they show wide compositional variation within this range, in addition to petrographic and structural differences, according to the particular fusible lithology within the wall rock sequence from which they were derived. They were produced by remelting and mobilisation of earlier Tertiary rocks or of pre - Tertiary sedimentary rocks. All of these parental lithologies can be shown to have been below the present level of exposure except for those granitoid rocks which occur within downfaulted blocks or pseudoscreens (the tips of downfaulted blocks). These appear to have been produced more - or - less in situ. This implies that the anatectic magmas flowed up the wall of the magma chamber or (in the case of the M2 felsites and most of the rheomorphic breccias) were intruded upwards as separate small

intrusions. The lithologies which have been identified as parental to granitoid rocks in or adjacent to the MBG are as follows:

Anatectic Rock:	Inferred parental lithology:
Subalkaline Granitoids	Pre - Hypersthene Gabbro Tertiary granitoid intrusions.
Diopside Microgranites	Scalpa Sandstone.
Peraluminous Microgranitoids	Lower Pabba Beds or hybrid of LPB and subalkaline granitoid material.
Rheomorphic Breccias	Most samples from Glendrian Bay: Triassic arkosic sandstones and siltstones ?
	Other samples: Liassic semi-pelites ??

The Moinian rocks, which were inferred to form most of the Pre - Tertiary succession above the Moine Thrust Zone in Chapter 2, are notable absentees from the above list despite containing numerous fusible semi - pelitic and meta - siltstone beds. This may indicate that the base of the MBG magma chamber was not only above the MTZ but also above the sub - Mesozoic unconformity. If this were the case, however, it seems unlikely that it would have been thick enough to have produced the observed early M1 dome structure, which extends for over a kilometre in a direction radial to the intrusion (see Chapter 7), unless the Triassic sequence to the west of the Glas Eilean fault is very much thicker than that exposed to the east. Large increases, of up to 2km, in the thicknesses of Triassic sequences across basin - margin faults do occur elsewhere in the Hebrides (Steel 1977) but the amount of Triassic movement (if any) on the Glas Eilean fault is unknown. Alternatively, concentric normal faults may not have intersected the wall of the magma chamber where it was formed by fusible Moinian lithologies (as might occur if the faults were largely confined to the upper part of the magma chamber), or any melts derived from Moinian lithologies might not have reached as far up the wall of the magma chamber as the present level of exposure.

The diopside microgranites and the peraluminous microgranitoids have been shown on the basis of geochemical and field data to have been produced by melting of fusible lithologies within the tips of downfaulted blocks displaced along concentric normal faults into the MBG magma chamber. The features of the other granitoid rocks which indicate that they too were formed in episodes of melting in downfaulted blocks can be summarised as follows:

1). They occur in a mumber of small, discrete bodies (this evidence applies to the M1 rocks with liquid - liquid contacts against other MBG rocks, not to those rocks in small discrete intrusions), rather than as a continuous sheath such as would be expected if they were produced uniformly around the intrusion.

2). Rocks produced by mixing of anatectic magmas from different parent lithologies are extremely rare, 183D1 being the only known example. Again, this is not what would be expected if melts were ascending the wall of the intrusion continuously, but is consistent with the production of melts in discrete batches in particular parts of the magma chamber wall.

3). All the anatectic rocks formed during M1 appear to have formed under conditions of strong thermal disequilibrium, being significantly (up to 100 - 150°C) colder than the magmas in the interior of the chamber and also colder than the main wall of the intrusion, as a result of latent heat absorbtion during melting. This thermal disequilibrium persisted as the magmas flowed up the wall of the chamber from their source regions to the present level of exposure, a distance of some hundreds of metres. The mechanisms by which this thermal disequilibrium was maintained between the ascending anatectic magmas and the rest of the chamber are discussed below.

A combination of geothermometry, phase assemblage arguments and geological arguments constrains the temperatures of formation of these rocks to between 1070 and 1120°C under dry conditions, or 990 - 1050°C if $P_{H_2O} = P_{total}$. The true value is more likely to lie towards the upper end of this range. Pressures of formation are 0.3 to 1.0 - 1.3kb in the former case, and 0.3 to 0.5 - 0.7kb in the latter.

The xenolith swarms consist of the most refractory lithogies from the country rock sequence. The occurence of most xenoliths, particularly near the wall of the intrusion, in swarms implies that these swarms also formed episodically, as is consistent with the field observation that brecciation of refractory rocks at the present level of exposure only occurs in the largely melted downfaulted block tips. Unlike the anatectic granitoids, the xenoliths appear to have tended to sink in the MBG magma chamber.

4.5.1.2. Homogenous Basic to Intermediate rocks.

These rocks, which include the groups 1 and 2 cone sheets of section 3.2 as well as rocks within the MBG, form a simgle, broadly tholeiitic suite of rocks with between 3 and 8% MgO. Many of them do not lie on a simple tholeiitic fractionation trend but are homogenous hybrid rocks formed by complete mixing of magmas lying at various points on the tholeiitic trend. All approximate closely to liquid compositions, indicating that residual melt segregation during the solidification of these rocks at the beginning of M2 did not have a significant effect on their bulk compositions. The M2 ferrogabbroic rocks which represent the products of this segregation appear to be volumetrically insignificant, suggesting that they have been concentrated in the inner part of the contact zone of the MBG after their initial segregation.

The preservation of major - element variation in these rocks and in particular the inheritance of varying incompatible element ratios resulting from contamination of the parental magmas to these rocks, prior to their entry into the MBG magma chamber, implies that the magma chamber (and even individual stratified layers within it) were not completely homogenised by the mixing. The contamination observed in these rocks is independent of crystal fractionation. It involved bulk assimilation of the mainly tonalitic to intermediate Lewisian gneiss complex by (probably) picritic or picrobasaltic parent magmas, rather than by selective assimilation of only the most fusible Lewisian lithologies by basaltic parent magmas as occurs in the Skye and Mull complexes (Thompson et al. 1982, 1986; Dickin et al. 1984). The amount of contamination within the MBG magma chamber, appears to have been very small.

Density calculations indicate that the interior of the MBG magma chamber was just stably stratified, with an upward decrease in MgO contents but an overall density decrease of as little as $0.05 gcm^{-3}$ between 8% and 3% MgO. On the northern and southern margins, MgO - poor rocks are confined to the contact zone, whilst on the western margin, which was probably higher up the chamber wall during M1, MgO - poor rocks are more common. This distribution suggests that MgO - poor magmas, cooled by less than 20 – 40°C, were flowing down the wall in the thermal and mechanical boundary layers. When these reached denser magmas in underlying layers, mixing would have occurred. This slow mixing process between otherwise stratified layers, controlled by heat flow out of the intrusion, would produce the incomplete homogenisation of the magma chamber apparent from

the compositions of these rocks (section 4.3.1). Mixing of magmas with different compositions may also have occurred as plumes of magma rose from feeder conduits on the floor of the chamber to the level of neutral buoyancy for their particular composition within the stratified magma column.

The calculated temperatures of these magmas when in the interior of the chamber range from 1050 to 1210°C, but at the present level of exposure on the northern and southern margins the dominant MgO - rich (6 - 8% MgO) magmas were at 1160 - 1210°C.

4.5.1.3. Heterogenous hybrid rocks.

These rocks formed around pulses of felsic magma ascending the wall of the magma chamber by incomplete mixing of various intermediate and basic magmas with the felsic magmas. The mixing may have been a multistage process: large - scale melt movements certainly took place after hybrid formation, as heterogenous hybrid rock with widely differing mafic and, probably, felsic end - member components are juxtaposed. The high content of intermediate end - member components in the hybrid rocks on the northern margin of the intrusion is in strong contrast to the almost complete absence of homogenous intermediate rocks at the present level of exposure in this sector of the MBG. This suggests that, like the homogenous intermediate rocks, the hybrid magmas were flowing down the wall of the MBG magma chamber when they were preserved in situ by the abrubt end - M1/earliest M2 quenching. The initial development of chill zones between basic and felsic rocks, prior to hybrid formation by injection of heated felsic magmas through fractures in the chill zone, suggests that the felsic magmas were much cooler than the basic magmas, and actually colder than refractory rocks in the main wall of the intrusion as a result of latent heat absorbtion during heating of the downfaulted blocks from which they were derived.

4.5.2. A model for the magma circulation within the MBG magma chamber and the effects of episodic wall rock melting.

4.5.2.1. Magma fluxes within the MBG magma chamber.

The distribution of rock types in the MBG suggests that, in the period towards the end of M1 which is represented by these rocks, magmas were flowing in two directions in the boundary layer close to

the contact at the present level of exposure. Discrete batches or pulses of compositionally buoyant anatectic magmas flowed up the wall of the chamber whilst cooled, dense intermediate (ferrogabbroic to ferrodioritic) magmas were flowing down the wall. These rocks occur more continuously along the contact of the MBG at the present day than do the felsic rocks, suggesting that the downflow was also more continuous. Both types of magma underwent mixing with more primitive magmas from the interior of the intrusion. At the same time, mixing as a result of release of buoyant plumes of magma at the floor of the chamber may have been going on in the interior of the chamber. These plumes may have been formed by the injection of new batches of buoyant magma into the chamber through conduits on its floor or by the release of buoyant residual melts from cumulate rocks on the floor of the chamber. This situation is shown schematically in Fig. 4.31.

The downflow of cooled intermediate and hybrid magmas is shown as being attached to the wall of the magma chamber in Fig. 4.31, as suggested by the experiments of Huppert et al. (1986a; see also Turner & Campbell 1986), but one effect of the sudden development of a saw - tooth profile in the magma chamber wall as a result of movement on the concentric normal faults could be to cause the boundary layer flow to become detached at the tip of the downfaulted blocks. This would bring hotter magmas from the interior of the chamber into direct contact with the downfaulted blocks and would be an additional mechanism for increasing the rate of heat input into the blocks.

The series of events envisaged to follow movement on an inward - dipping concentric normal fault and the creation of a downfaulted block are shown in the schematic cross - sections which form Fig. 4.32. The separation of the boundary layer flow from the wall of the chamber immediately after formation of the downfaulted block (Fig. 4.32B) might explain the increase in contact temperature implied by the absence of felsic magmas **not** produced at downfaulted block tips, of which the best example is the lack of magmas derived from the Lower Pabba Beds except in the sector of the contact where inward - dipping faults intersect the contact where it is inferred to be composed of LPB rocks. An alternative interpretation, however, is that such magmas were produced at depth over the whole of the sections of the wall formed by fusible lithologies but that only those produced by rapid melting of downfaulted blocks formed large enough bodies of magma to flow up the wall of the chamber to the present level of exposure, whilst the melts produced at lower rates of melting were assimilated into the interior of the chamber. This latter possibility cannot be excluded at the present level of understanding of the factors controlling rates of assimilation of rising felsic magmas

Fig. 4.31. Overall diagrammatic cross - section showing the inferred flows of magma within a magma chamber with "leaky" stratification of the interior of the chamber and episodic wall - rock melting triggered by faulting in the wall of the chamber. The MBG magma chamber seems to have been of this type towards the end of M1.

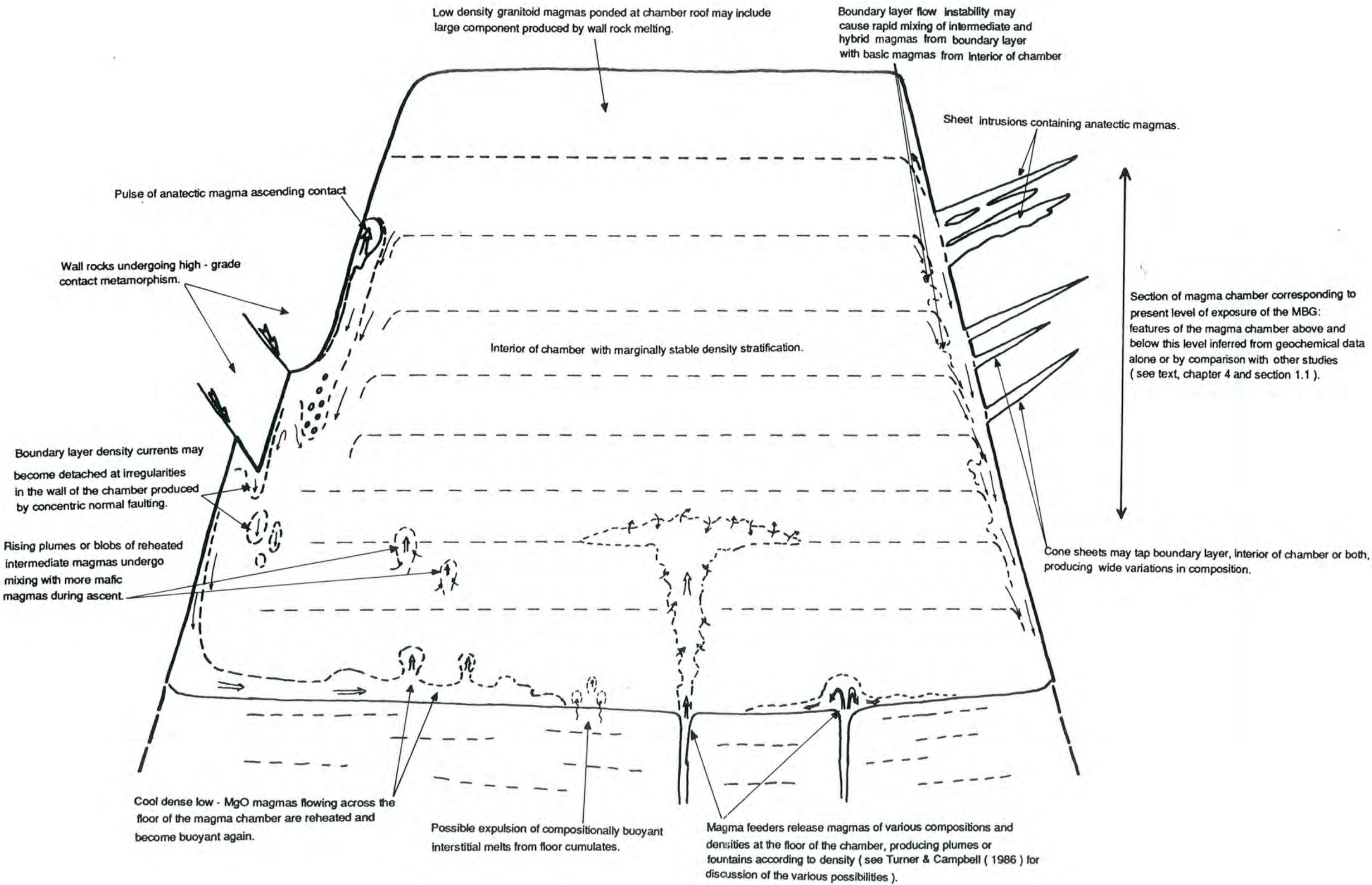

Fig. 4.32. Overall model for the generation of pulses of anatectic magmas at the wall of the MBG magma chamber by melting of projecting blocks of country rocks which are formed by movement on inward - dipping concentric normal faults.

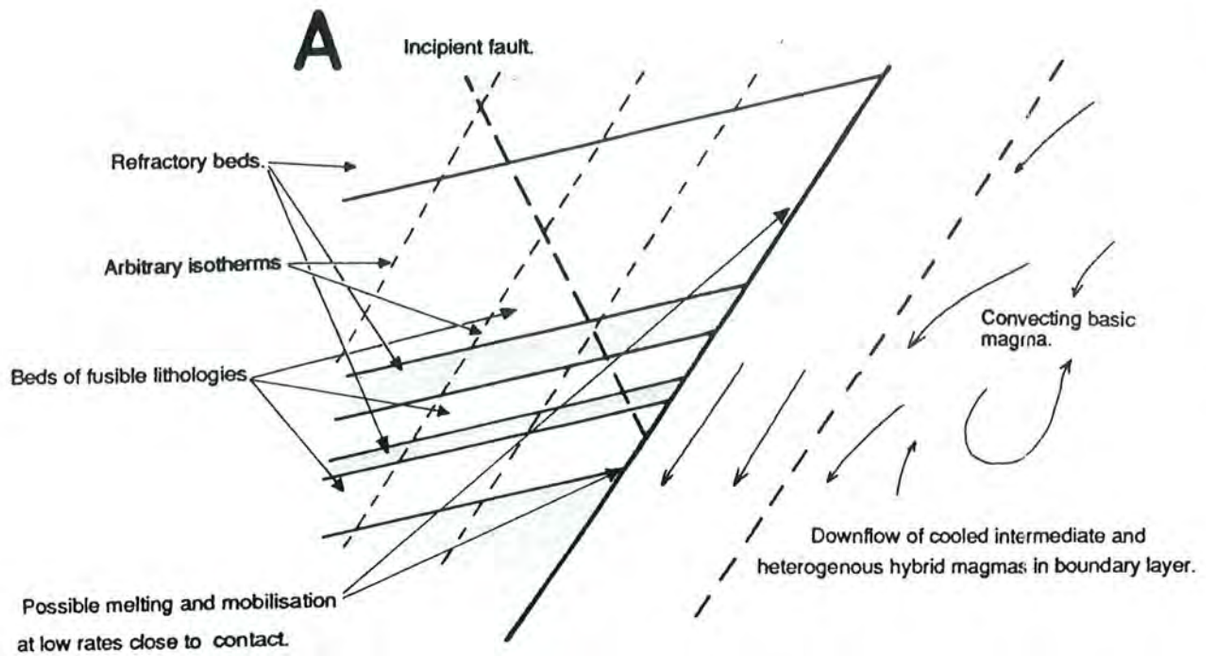

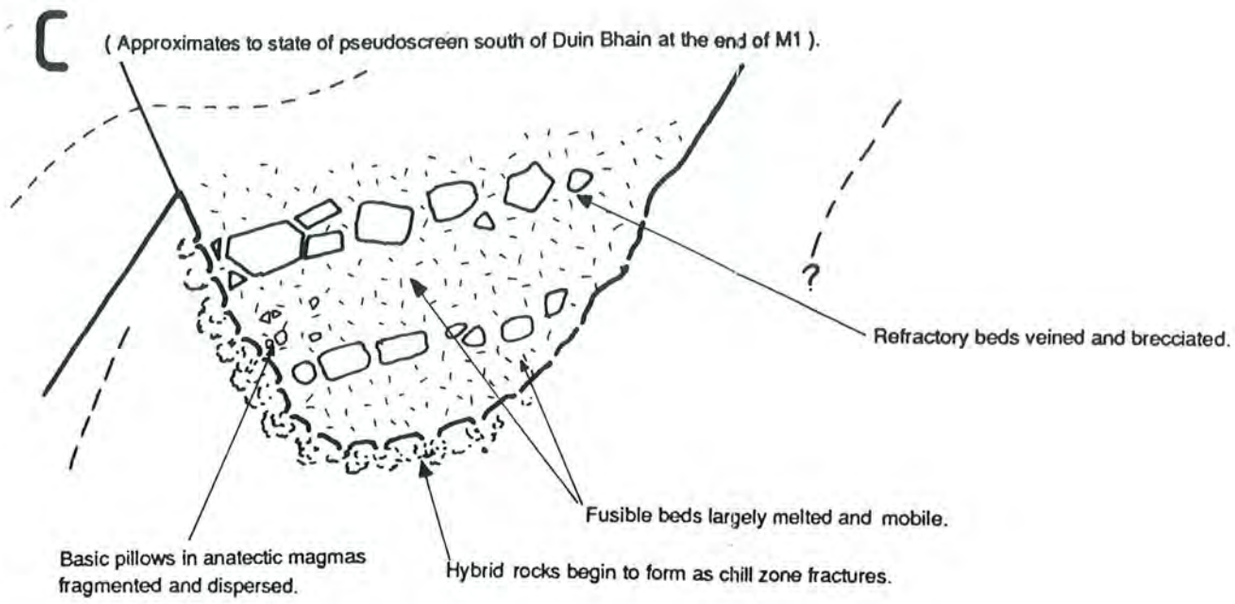

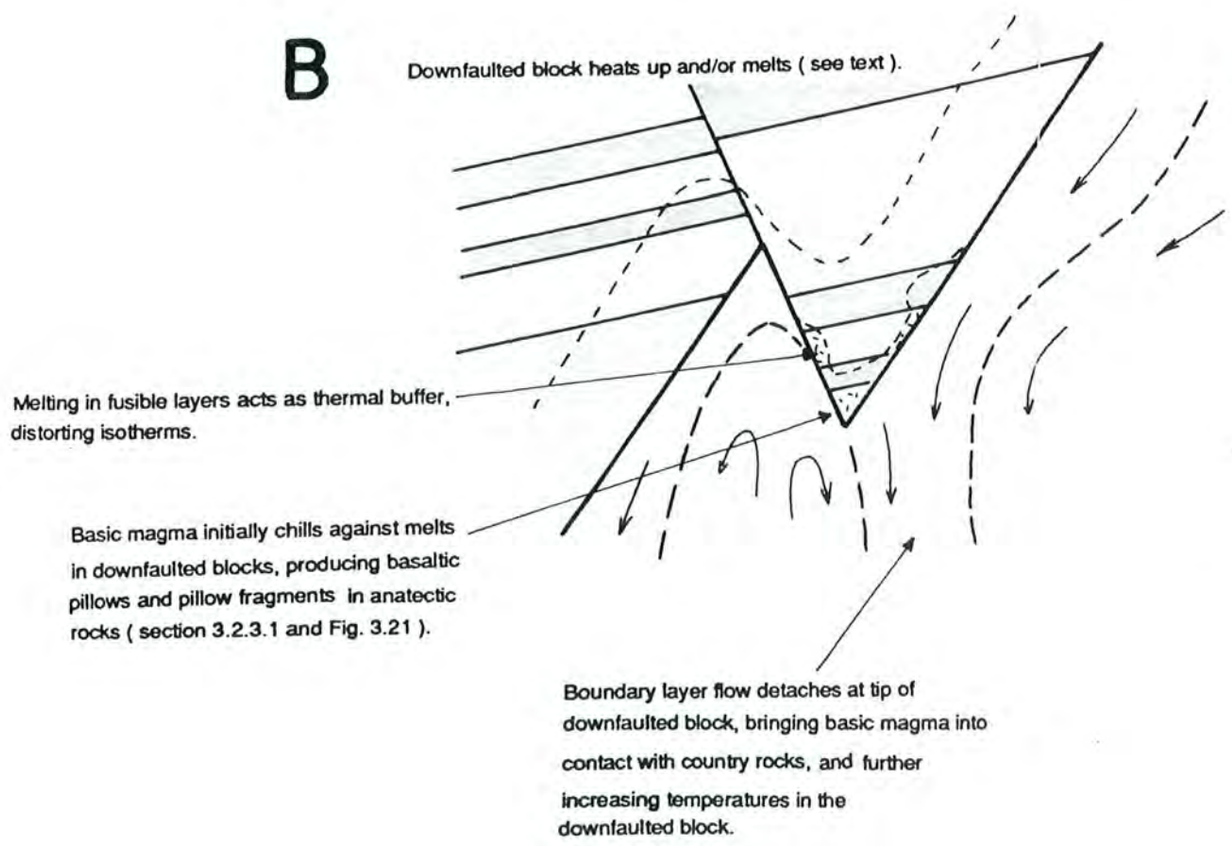

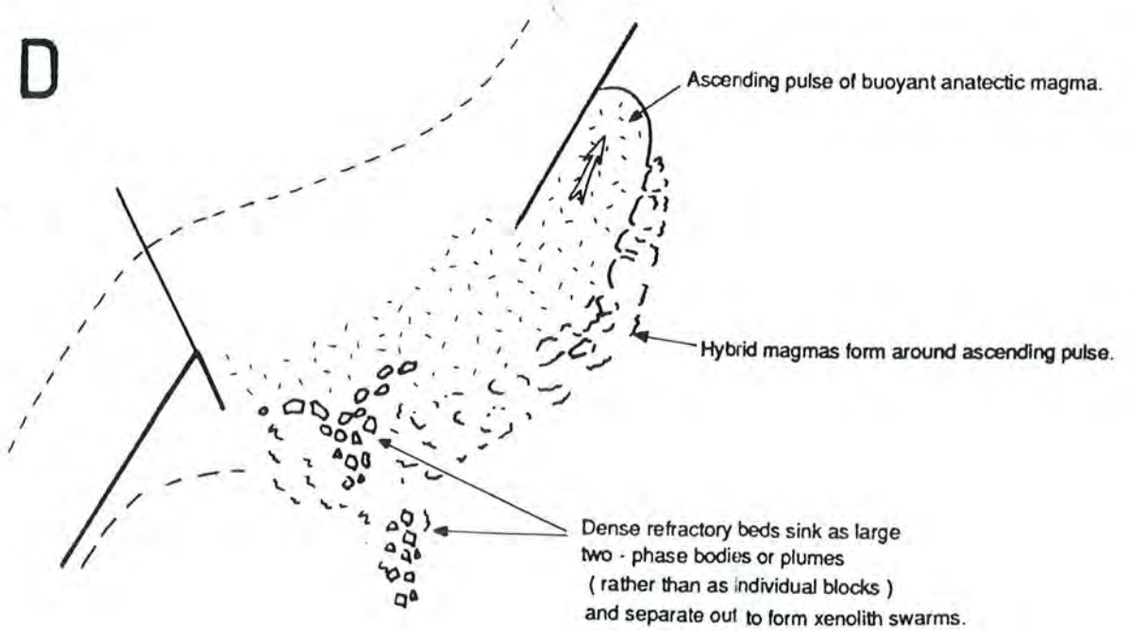

at the walls of basic magma chambers (see below).

Analogue experiments by Irvine (1980b) suggest that the pulses of magma would be expected to flow up the wall of the magma chamber at velocities of the order of kilometres per hour. It should be noted that although Irvine's experiments were on pulses of dense fluids flowing downwards, the results can be adapted to the case of low - density fluids flowing upwards by changing the sign of the gravity forces – or simply by turning the diagrams upside down, as was done in the opposite direction by Huppert et al. (1986b). It is extremely unlikely that the head of such a pulse of magma could be preserved in a recognisable form. However, Irvine's experiments also suggest that rising magma pulses would leave behind a thin, relatively stagnant 'tail' of magma from the pulse, attached to the wall of the magma chamber. Outcrops of M1 granitoids with liquid - liquid contacts against other MBG rocks, such as those at Glendrian Bay and south of Duin Bhain, are more likely to be preserved pulse 'tails' than actual magma pulse heads, and cannot be used to infer anything about the sizes of the pulses.

The mechanism of separation of dense refractory xenoliths from the anatectic melts, as large two - phase bodies rather than as single blocks, which is shown in Fig. 4.32D, is speculative but does provide a possible mechanism for creating the dense swarms of xenoliths observed. Such a process would be expected to occur more rapidly than separation of individual blocks, by analogy with the two - phase plumes studied by Brandeis & Jaupart (1986) and Morse (1986).

4.5.2.2. Effects of episodic wall - rock melting upon the compositional evolution of the MBG magma chamber.,

The pulses of melt produced by the proposed episodic melting process might either **(i)** rise to the top of the magma chamber to form a low - density stratified layer wholly or partly composed of such anatectic magmas; **(ii)** be diverted into minor intrusions during ascent, as may have happened to the rheomorphic breccias intruded during M1 in the Glendrian Bay area; **(iii)** be trapped under irregularities in wall, such as the tips of refractory downfaulted blocks (as seems to have happened at Loc. 183D); or **(iv)** be mixed with more mafic magmas to form hybrid rocks during their ascent up the wall of the magma chamber. The effects of any one episode of downfaulting upon the evolution of the magmas in the MBG magma chamber may therefore have varied unpredictably,

but some generalisations can be made regarding the effects of the processes depicted in Fig. 4.32 on the geochemical evolution of the MBG magma chamber, and of any other magma chambers in which they occur. The following discussion assumes, following Irvine (1970), Huppert (1989) and Huppert & Sparks (1989), that the heat flux from the wall of a magma chamber into its country rocks (Q_c, section 4.1) is initially high and declines monotonically as the country rocks heat up and thermal gradients in them decline. This assumes that heat transfer in the country rocks is largely conductive throughout. As will be seen in Chapter 5, this only holds for the M1 phase of metamorphism in the country rocks of the Marginal Border Group, but since this is the period in which the processes under discussion operated the assumption is valid for the purposes of this section.

The first of these effects is that high - degree partial melting and mobilisation of wall - rock lithologies may begin at lower overall contact temperatures than in the abscence of the formation of projecting bocks by downfaulting into the magma chamber, provided that a basic chill zone is not present at the contact, because the formation of the downfaulted block produces a section of wall rocks partly isolated from the rest of the country rocks (reducing the local heat flux out of the rocks in the downfaulted block) and may locally increase the heat flux out of the magma chamber (section 4.2.6). As was discussed in that section, if the downfaulted block has a refractory composition, this local increase in Q_m over Q_c will cause an increase in its temperature; if it is made up of fusible rocks, the excess heat will produce a greater degree of partial melting. In the case of the MBG the formation of a chill zone appears to have been inhibited, at least in part, by the flow of relatively evolved magmas (with a lower T_r) down the wall of the magma chamber. The mechanism of this is discussed further in section 4.5.3. Since a lower wall rock temperature is equivalent to a greater degree of thermal disequilibrium between the wall rocks and the magma chamber (i.e. to a greater value of Q_c) the combination of faulting in the wall rocks and the presence of a compositionally distinct boundary layer flow will permit wall rock melting and the formation of anatectic melts to begin earlier in the history of the magma chamber concerned. The length of this phase in the evolution of the magma chamber, on which, amongst other things, the overall importance of the melting of downfaulted blocks in its development, will depend on the length of the period for which $Q_c \approx Q_m$. This in turn depends on the variation of Q_c **relative** to Q_m with time: this is discussed in Chapter 5 for the case of the Marginal Border Group and in Chapter 8 for intrusions in general.

The second effect of the episodic formation of batches of anatectic magma by melting of downfaulted blocks concerns the subsequent fate of the melts. Apart from being injected into small intrusions at the side of the magma chamber, such as radial dykes, cone sheets or similar intrusions, and thereby lost from the system unless reworked as a result of later faulting, these melts can either be assimilated into the main body of the magma chamber, through the intermediate stage of hybrid formation, or ascend to the top of the chamber and accumulate in a low - density layer of granitoid magma, as is shown in Fig. 4.31. The release of mobile melts at the wall of the chamber in pulses rather than in a continuous thin film would be expected to either reduce or increase the ratio of assimilation relative to accumulation at the top of the chamber according to whether the first two or the third of the following effects dominated:

1). The pulses of magma, being generated intermittently but at greater rates during melting episodes (due to the high thermal gradients and heat fluxes in the downfaulted blocks, particularly near the section of the fault plane exposed to the magma chamber (see Fig. 4.32)), will tend to be thicker in a direction perpendicular to the chamber wall than would continuous flows produced by melting at the same overall rate. The greater ratio of volume to surface area will have two effects. Firstly, the greater ratio of buoyancy forces (proportional to the volume of low - density material) to viscous drag per unit of flow velocity (proportional to the surface area of the pulse) will cause the pulse of magma to ascend the wall at a greater velocity, as was found experimentally by Irvine (1980b) for density currents of different thicknesses. The thicknesses of the magma pulses were varied in Irvine's experiments by increasing the viscosity of the density currents, but increases in velocity were observed despite this, suggesting that the velocity increase due to increased rates of buoyant magma input into the pulse would be even greater. As a result the time available for assimilation to occur would be reduced, whilst the increased thickness of the magma pulse would reduce the surface area over which assimilation by magma - mixing could occur relative to the volume of the magma pulse.

2). The rate of assimilation could be further reduced by an increased temperature difference between the pulse of buoyant anatectic magma and the ambient magma. As noted in section 4.4.3, the ascending felsic magmas seem to have been colder than the rigidus temperature of the basic (MgO 6 – 8%) magmas in particular, producing the chilled and veined contacts seen at Glendrian Bay and south of Duin Bhain. The presence of this temperature difference

appears to have inhibited mixing between the two groups of magmas. Two factors could decrease the temperature of anatectic magmas at the contact between felsic and mafic magmas in pulses relative to continuous flows. The first of these is the reduction of temperature increases produced by latent heat absorbtion during melting (section 4.2.6). The effect of this is greater at higher melting rates and will tend to reduce the average temperature of the pulse relative to refractory wall rock temperatures. The second factor, which will be particularly important after the anatectic magmas have flowed up the wall of the chamber for some distance, involves circulation within the buoyant pulse of magma. Internal circulation within magmatic density currents was investigated (for very different purposes) by Irvine (1980b), who showed that drag on the surfaces of currents flowing down (or, in the present case, up) inclined surfaces produced circulation within the head of the current or pulse of 'magma' similar to that shown in Fig. 4.33. The form of this circulation is likely to differ in detail from those in Irvine's experiments, which were conducted using near - Newtonian fluids. Most subliquidus felsic magmas probably behave like Bingham bodies, with a small (compared to sub - rigidus materials) but finite yield strength (McBirney & Murase 1984), with the result that flow within the pulse would be concentrated near the margins, and the interior would be more stagnant. However, this would not change the overall flow pattern. The result of this flow is that cool magma from the interior of the pulse is constantly drawn forward to the head of the pulse, continuously regenerating the chilled skin or crust around it and continually protecting it from mixing until the entire pulse heats up to the rigidus temperature of the adjacent magma. In contrast, continuous laminar flows show no advection of material (and, hence, no cooling of the felsic / mafic magma interface) in a direction perpendicular to the overall transport direction. The experiments of Irvine (1980b) indicate a third effect which may increase the proportion of magma in the pulses which is assimilated. At high slope angles, Irvine found that his analogue magma pulses developed a turbulent tail in which much mixing took place (Irvine 1980b, p. 25). This would greatly increase the assimilation rate relative to that at the surfaces of laminar continuous flows in particular.

Further investigation of wall - rock melting in downfaulted blocks, using analogue and/or numerical methods, is needed to establish which of these effects would dominate, and hence what the geochemical effects of episodic, as opposed to continuous, wall rock melting would be. However, efficient transfer of wall rock melts to the top of the chamber in pulses of magma is one possible explanation

Fig. 4.33. Magma circulation within an ascending pulse of buoyant anatectic magma at the wall of a magma chamber (modified after Irvine 1980b). Flow velocity vectors drawn relative to the moving head of the pulse. Chill zone not to scale.

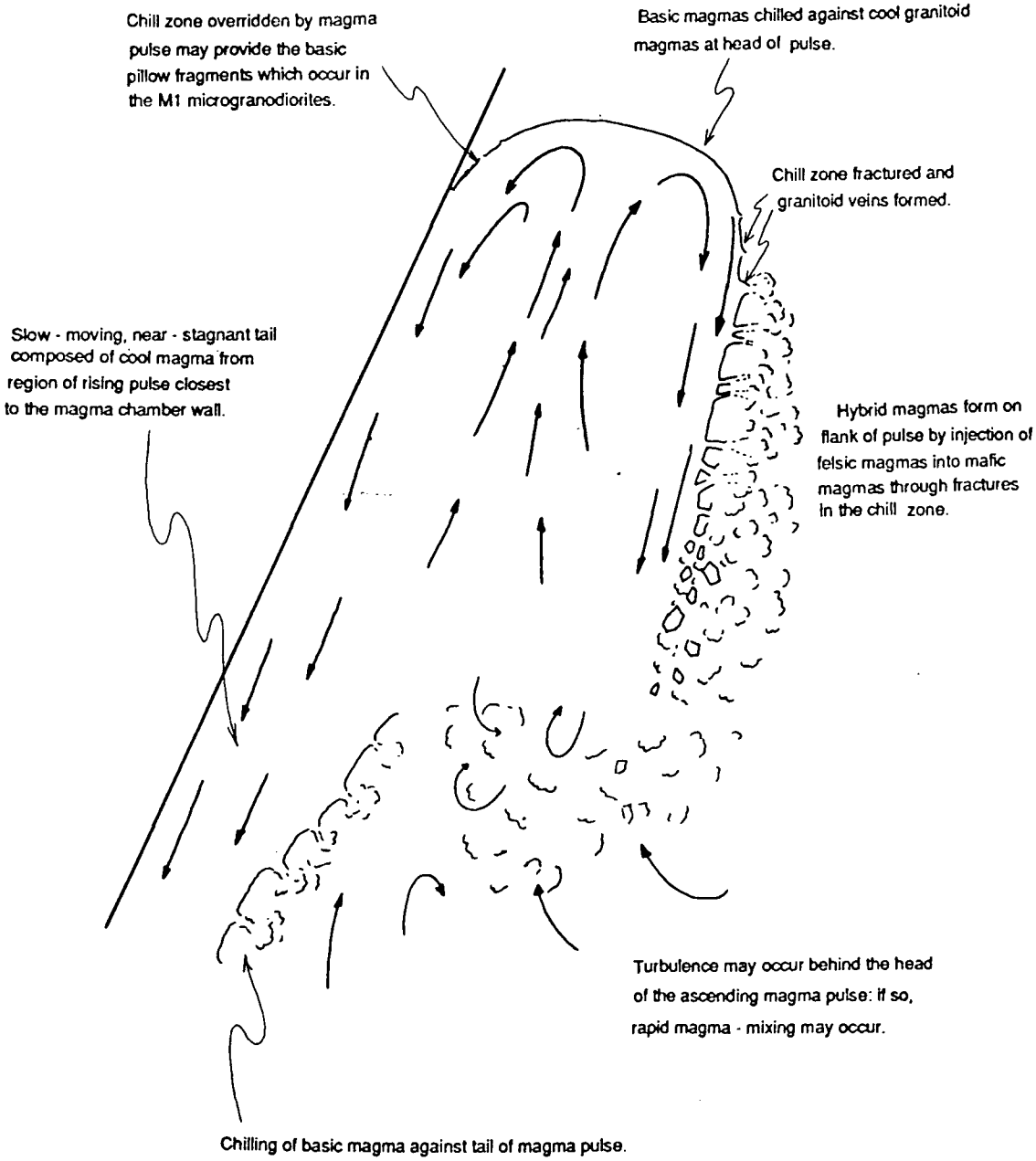

of the fact that although the contact zone of the MBG contains much evidence of wall - rock melting there is little evidence for contamination of the magmas in the interior of the chamber with the crustal lithologies present in the wall of the MBG. Alternatively, it may simply be a consequence of the volume of the interior of the MBG magma chamber being much greater than the volume of melts produced during the period of episodic wall - rock melting. This will be a function of both the length of this period (see Chapter 5) and the rate of anatectic melt production, which, as pointed out in section 4.2.6, will be controlled by the rate of deformation of the magma chamber walls.

4.5.2.3. To what extent has the MBG M1 boundary layer been preserved ?

As noted in section 3.2.7, there is much field evidence to suggest that a magma chamber boundary layer has been partly preserved in the contact zone of the MBG. The geochemical data presented in this chapter also suggests that the abrubt solidification of the contact zone at the end of M1 and in the earliest part of M2 has partly preserved part of the magma chamber. In view of the large magma flow velocities believed on the basis of numerical and analogue modelling to occur in magma chambers this seems rather surprising. It is therefore appropriate to consider the nature of what has been preserved in the contact zone of the MBG and place constraints on the actual requirements for its preservation. These constraints will be considered further in section 5.3.3, in which the ability of the observed quenching event at the M1 to M2 transition to preserve those parts of the M1 boundary layer which have been preserved will be examined.

The inference (section 4.5.2.2) that the granitoid rocks in the contact zone of the MBG represent the near - stagnant tails of felsic magma pulses means that nothing can be inferred about the thicknesses, velocities or volumes of these pulses from the outcrop data: none of the discussion above depends on being able to do so. The diopside microgranites south of Duin Bhain must have been preserved at their site of formation if the interpretation advanced in this chapter is correct, but at present not enough is known about the size to which a body of buoyant melt at the wall of a magma chamber can grow before it starts to flow up the wall of the chamber at the sorts of velocities estimated by Irvine: it should also be noted that the diopside microgranites contain a large number of refractory inclusions and until these had settled out the entire body, of diopside microgranite magma plus inclusions, may not have been buoyant. It is not, therefore, possible to determine on theoretical grounds whether or not such a body could be preserved by solidification, at any given value of a (

see equation (4.3)) of the boundary layer in which it was present.

Turning to the homogenous basic and intermediate rocks, one constraint which must be satisfied if the interpretation of these rocks put forward in this chapter is to be physically feasible is that the time taken for any one piece of rock to cool from its initial temperature to its solidus must be less than the characteristic time for separation of crystals and liquid to take place in it to any significant extent, because most of the rocks approximate to liquid compositions (section 4.3). However, the presence of the M2 ferrogabbros veins and pods does indicate that the solidification rate cannot have been so fast that late - stage melt segregation did not occur to a limited extent. This problem is considered further in section 5.3.3.

Paradoxically, the preservation of the zonation from intermediate to basic rocks away from the outer wall of the MBG magma chamber, which has been attributed in this section to flow of cooled magmas from higher in a stratified magma chamber down the wall of the chamber, actually requires the flow of intermediate magma to be halted. This is because solidification in a Type 1 boundary layer (Fig. 4.1) always occurs at the outer surface of the downflow at the wall. Thus, if the downflow of MgO - poor intermediate magma continued as solidification proceeded, a thick layer of solidified intermediate rock would build up, and the basic magmas in the interior of the chamber would not solidify on the wall at all. It is not necessary for the downward flow of cooled magma to stop altogether; the required effect could be achieved, for example, by accretion of intermediate magmas from higher in the stratified magma chamber onto the inward - migrating contact before they reached the present level of exposure (see section 5.3). Further consideration of this problem is deferred until after the pattern of cooling during the quenching event has been considered in more detail (section 5.3).

4.5.3. Implications of the magma circulation pattern proposed in section 4.5.1 for heat flow from the magma chamber and estimates of the temperature difference across the boundary layer.

4.5.3.1. Implications of compositional variation in boundary layers for boundary layer behaviour.

Although broadly of Type 2 (possibly with type 3 conditions developed around the rising pulses of anatectic magma) the M1 boundary layer of the MBG magma chamber cannot be adequately described by any of the three theoretical boundary layers depicted in Fig. 4.1. Two features distinguish it from any of these models. The first of these is the episodic melting of the wall rocks produced by concentric normal faulting and the consequent formation of hanging - wall blocks projecting into the magma chamber. The effect of this is to increase the rate of wall - rock melting at $Q_c \approx Q_m$ over that predicted by equation (4.3) provided that a chill zone is not present. The second feature of the M1 MBG magma chamber not allowed for in these models is the presence of compositionally distinct magmas in the thermal boundary layer. These are more evolved and would be expected to have a lower rigidus temperature than the hotter, more MgO - rich magmas in the interior of the chamber (see calculations below). The effect of this is to permit a greater temperature difference between the wall of the chamber and the interior (Fig. 4.34). Heat flow in this situation is given by a modified form of equation 4.2 (section 4.1.2):

$$Q_m = -h(T_{r_2} - T_{m_1}) \tag{4.10}$$

where the subscripts 1 and 2 denote the basic magma in the interior of the chamber and the intermediate magma in the boundary layer respectively. As noted in section 4.1 no completely satisfactory theoretical or experimental work has been done on the effect of varying viscosity in the boundary layer on heat transfer coefficients, so it is not possible to predict theoretically whether Q_m will be increased over its value in the absence of compositional differences. However, the lower effective rigidus temperature of the magma body will tend to inhibit formation of a chill zone, extending the range of values of Q_c over which boundary layers of Types 2 or 3 can exist.

4.5.3.2. Estimate of a value for the temperature difference across the thermal boundary layer.

As noted in section 4.1, one of the results of the work described in this chapter should be an estimate of the temperature difference across the thermal boundary layer (referred to below as ΔT_B). to be used in estimating the heat transfer coefficient h (see equation (4.9). T_m is given by the liquidus temperature of the magmas from the interior of the chamber (1160 - 1210°C in the case of the northern and southern margins of the MBG: see section 4.3.3). The contact temperature (the effective value of T_r) can be obtained in two ways:

Fig. 4.34. Diagrammatic velocity, temperature and density profiles through a boundary layer consisting of an outer zone of downflowing intermediate magma and an inner zone of basic magma.

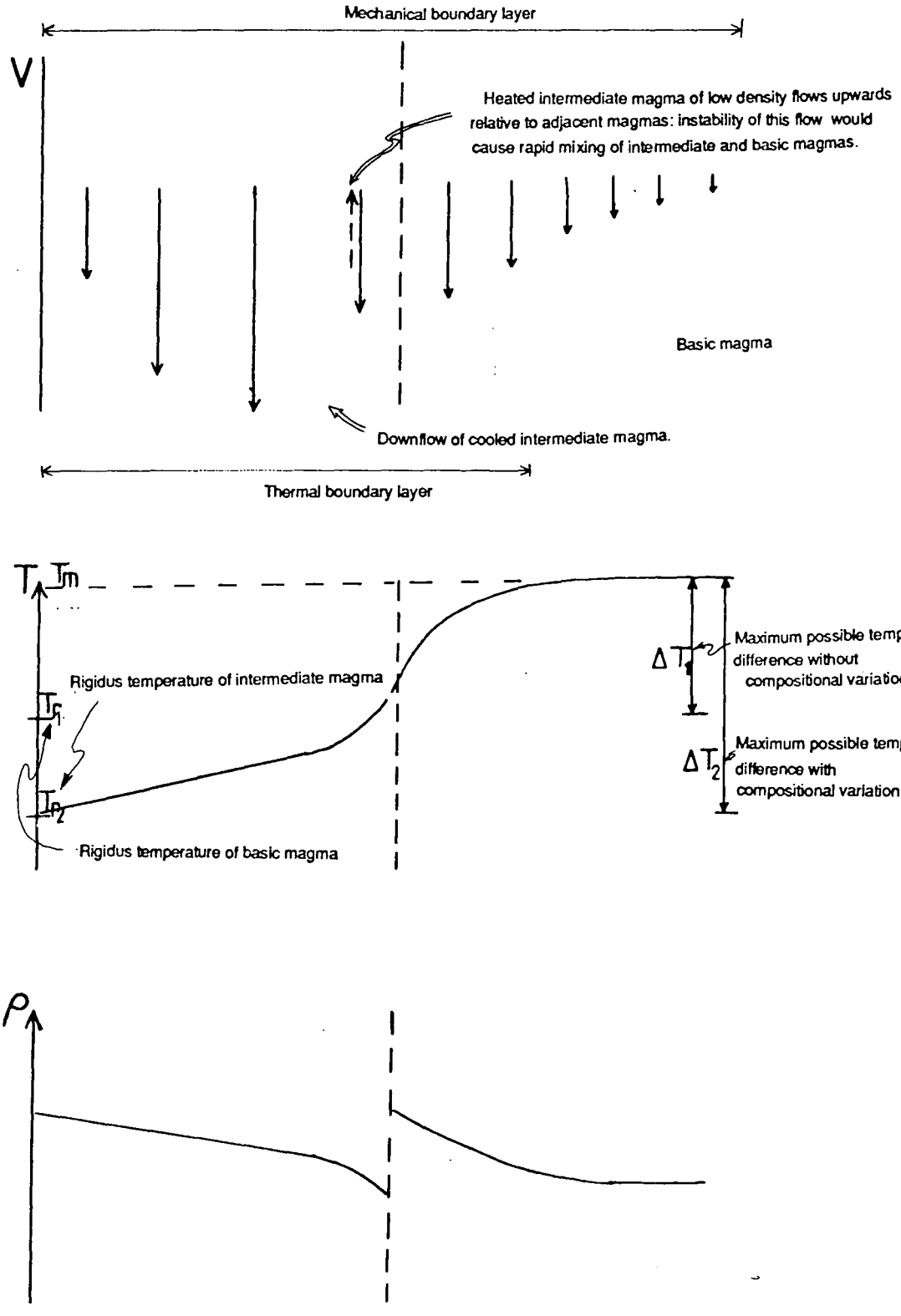

1). From the temperatures of the anatectic magmas . This gives a value of ΔT_B appropriate to contacts between rising pulses of anatectic magma and the remainder of the magma chamber, which will be greater than that at contacts against more refractory wall rocks. The actual value obtained depends on the value of P_{H_2O} assumed in the calculations of anatectic magma temperatures (section 4.2.5): at $P_{H_2O} = 0$, $\Delta T_B = 40-140°C$, whilst at $P_{H_2O} = P_{total}$, $\Delta T_B = 120 - 220°C$. The geological arguments in section 4.2.5 point to a low value of P_{H_2O}. whilst values of ΔT_B less than between 60°C and 100°C, depending on the amount of cooling necessary to cause chilling of basic magmas against the anatectic magmas (see below), are inconsistent with the chilling observed at such contacts. It is therefore concluded that the most likely range of ΔT_B adjacent to rising magma pulses or their stagnant tails is in the range 60 - 150°C.

2). Estimates based on calculated rigidus temperatures. The calculations of Wood (1978) on the relationship between percentages of liquid remaining and residual liquid compositions for a suite of Icelandic tholeiites broadly similar to the MBG tholeiites allow determination of the relationship between the crystal content of a partially crystallised magma (assuming closed - system crystallisation, in other words no crystal separation or accumulation) and its temperature, given its initial (liquidus) MgO content. If it is assumed that the rigidus temperature is a constant, in other words that the magma locks up at a constant rheological critical melt percentage (R.C.M.P.) independent of strain rate, crystal morphology and other factors discussed by Marsh (1988), then it is theoretically possible to calculate ΔT_B given a value for the R.C.M.P. and the range of magma compositions in the boundary layer. However, as noted in section 4.1 the R.C.M.P. is **not** a constant and the results of this method can only be considered to be rough estimates. The following table contains estimates for the temperatures of magmas with 8, 6 and 4% MgO at the liquidus at various crystal contents: the MgO contents are estimated from the best - fit curve through the data points from Wood (1978) of Sparks & Marshall (1986), and the temperatures are estimated using the empirical geothermometer of section 4.3.3. As noted in that section, this is not applicable below about 3% MgO: the bracketed values are likely to be underestimates.

MgO content of initial liquid	8%	6%	4%
Liquidus temperature °C	1200	1160	1096
MgO content of residual liquid after 20% crystallisation	6.8%	5.2%	3.5%
Temperature at 20% crystallisation	1181	1136	1078
MgO content of residual liquid after 40% crystallisation	5.7%	4.1%	2.8%
Temperature at 40% crystallisation	1151	1100	(1050)
MgO content of residual liquid after 60% crystallisation	4.2%	2.8%	1.7%
Temperature at 60% crystallisation	1103	(1050)	(1002)

As noted in section 4.1, the R.C.M.P is normally taken as 40% , equivalent to 60% crystallisation. This yields a rigidus temperature of 1050 – 1100°C for magmas with 6 – 8% MgO, which is clearly inconsistent with the observation that such magmas are chilled against M1 granitoid rocks (see temperature estimates above). However, R.C.M.P would be expected to rise with cooling rate because rapidly grown crystals are elongate and more likely to form interlocking networks at low crystal contents (Marsh 1988): an R.C.M.P of 70% would give temperatures of formation of the pillowed contacts of 1120 - 1165°C, which would be consistent with the estimated temperatures of the felsic and mafic magmas involved and is not unreasonably low. Within this range of R.C.M.P values, the **maximum possible** ΔT_B would be between 75 – 115°C (at an R.C.M.P of 30%) and perhaps 120 – 160°C (at an R.C.M.P of 60%) for a boundary layer consisting of magma with 4% MgO and a magma chamber interior with 6 – 8% MgO. These values of ΔT_B are two to three times greater than those possible in a constant - composition magma chamber. It should be noted that these ΔT_B values are not necessarily the actual values developed in the MBG contact zone, but only provide upper limits.

It is therefore concluded that the likely range of values for the temperature difference across the MBG boundary layer during M1 is 60 – 150°C. This corresponds to a probable contact temperature of 1050°C to 1150°C.

The inferred thermal and mechanical structure of the M1 MBG magma chamber boundary layer is shown schematically in Fig. 4.34. This diagram shows the simplest possible case, that in which the boundary layer is in a state of laminar flow. Turbulent flow involving mixing of the various layers may well have taken place, however. One of the interesting features of the boundary layer depicted

in Fig. 4.34 is that it is not of uniform composition and that compositional and thermal effects on density oppose each other: thus at any given temperature the intermediate magma would have been less dense that the basic magmas but because it is in general cooler it is mostly denser, except at the interface between basic and intermediate magmas. Heating of the intermediate magma at this interface would tend to produce a counterflow to the main downward flow of cooled magmas. The actual motions resulting from this would depend on the relative magnitudes of buoyancy and drag forces operating on the heated intermediate magma. However, it seems plausible to suppose that the density reversal at the interface would tend to cause mixing of the heated intermediate and the basic magmas, as is seen in simpler cases of buoyancy reversal in buoyant plumes (Goldman & Jaluria 1986). This would promote erosion of the down - going current of intermediate magma but the effect has not been modelled experimentally or theoretically so its precise effects are unknown.

5. METAMORPHISM ASSOCIATED WITH THE MARGINAL BORDER GROUP AND IMPLICATIONS FOR MASS AND HEAT FLUXES IN THE CONTACT AUREOLE AND IN THE BOUNDARY LAYER OF THE MBG MAGMA CHAMBER.

The primary subjects of this chapter are the heat fluxes in and around the MBG magma chamber during M1, M2 and the intervening episode or episodes (in different sectors of the contact aureole and contact zone) of rapid cooling and quenching, and the mechanisms by which heat flow occurred. In particular, the rapid changes in metamorphic conditions at the end of M1 imply a dramatic increase in heat transfer away from the contact and therefore a change in the mechanisms of heat transfer. As noted in section 3.2, the 'quenching event' is invariably associated with the development of a tensile fracture network and the circulation of hydrothermal fluids through those fractures. The mechanisms of fracture formation and possible causal relationships between the fractures and the 'quenching event' will be examined in this chapter. A further problem associated with the metamorphic aureole, that of the causes of the subsequent increase in metamorphic grade during the early part of M2 close to the contact, will also be considered in this chapter.

These problems are not only of interest with regard to the metamorphism of the country rocks because, as noted in section 4.1, the heat flux Q_c into the country rocks around a magma chamber exerts a controlling influence upon the behaviour of the magma chamber boundary layer and therefore upon the geochemical evolution of the magmas in the magma chamber. In particular, it was shown in section 4.2 that $Q_c \approx Q_m$ towards the end of M1 for the contact zone of the Marginal Border Group magma chamber. It follows from this that the value of Q_m for the MBG magma chamber, and therefore mass fluxes within the M1 boundary layer, can be estimated by study of the heat flow in the adjacent country rocks at the end of M1. A second problem connected with the MBG that will be studied in this chapter is that of the heat flux during the 'quenching event', on the northern margin of the intrusion in particular. Given a value for this it should be possible, using equation (4.3), to estimate the rate of solidification of the contact zone and thereby assess the physical plausibility of the interpretation of the contact zone as the more - or - less in situ remains of the M1 boundary layer.

A study of the conditions of metamorphism in the contact aureole of the MBG would ideally include

a detailed survey of mineral compositions, both for solid - solution - based geothermometry and oxygen activity measurements and to place more precise constraints on the stability limits of mineral assemblages. This was to a large extent impossible within the scope of the present work because of the small grain size (around 10 to 30 microns) of the majority of the minerals of interest, in M1 mineral assemblages in particular, relative to the diameter of the analytical 'spot' of the available electron microprobe, which was around 30 microns across. It should be possible in future to analyse these minerals with electron probes with a smaller analytical spot. The results presented here should therefore be regarded as initial estimates of metamorphic temperatures and therefore heat and mass fluxes, to be refined at a future date.

5.1. Conditions of metamorphism during M0.

Although the age relationships described in Chapter 3 indicate that this phase of metamorphism largely or wholly predates the emplacement of the MBG magma chamber at the present level of exposure, it is nevertheless of interest in the present context because of what it reveals about the temperatures, permeability and interstitial fluid compositions of the country rocks prior to the emplacement of the MBG magma chamber. The M0 mineral assemblages in the area north and west of the Glas Eilean fault can be summarised as follows:

1). Pelites: biotite + muscovite (no chlorite or clay minerals) + quartz, detrital feldspars, dark brown to black organic matter and opaques.

2). Vein and amygdale assemblages in metabasalts: clinozoisite/epidote + actinolite + sphene + albite and/or adularia ± prehnite ± chlorite.

3). Partially altered metabasalts and dolerites: chlorite + actinolitic amphibole + sodic feldspar + relict igneous phases.

4). Calc - silicate bearing, originally slightly calcareous, sandstones (also the Tertiary volcaniclastic sandstone, sample 190): epidote ± prehnite ± green actinolitic amphibole ± garnet, diopside (both very rare). These rocks also sometimes contain phases which could not be identified optically,

in some cases because of fine grain size. However, fibrous zeolites, wollastonite and idocrase are definitely absent.

5). Originally carbonate - rich calc - silicate rocks (principally the limestone unit in the Middle Jurassic sequence (section 2.3)): carbonate + actinolite + relict detrital feldspar ± epidote.

6). Felsic pre - Hypersthene Gabbro Tertiary rocks: chlorite + amphibole + albite + zeolites. The very earliest felsic rocks sometimes contain sericite and carbonate.

This is not an exhaustive list as the pelites and some calc - silicate rocks in particular contain much fine - grained material which could not be identified optically. This and the absence of mineral composition data makes rigourous mineralogical determination of the conditions of M0 impossible at present. This would in any case be made difficult by the compositions of the rocks, few if any of which correspond to simple systems which have been studied experimentally or theoretically; the lack of independent data on the compositions of coexisiting fluids (especially in respect of pH and dissolved cation contents); and the generally low pressure of metamorphism. This latter causes two problems: firstly, experimental data on low grade metamorphism at below 1kb are rare and, secondly, activities in the fluid phase are strongly fluid pressure - sensitive at low pressures. This means that reactions other than pure mineral - mineral exchange reactions are also highly pressure - sensitive under these conditions.

However, some idea of the conditions of M0 can be obtained by comparing the observed assemblages with those found during drilling operations in active hydrothermal systems where fluid compositions, pressures and temperatures can be determined directly. Calc - silicate minerals in active hydrothermal systems have been studied particularly intensively (see review in Bird et al. 1984) and show a well - defined and temperature - sensitive distribution in a wide range of host - rock lithologies. These range from basaltic to rhyolitic volcanic rocks to calcareous sandstones and metagreywackes in the geothermal fields studied, a range which covers all the rock types above except the pelites and limestones. Temperature constraints provided by the minerals discussed in Bird et al.'s review are as follows, with other limits on their occurrence noted in parentheses:

Prehnite: 250 – 350°C (only occurs in equilibrium with relatively Ca - rich, weakly acidic fluids)

Clinozoisite/epidote: > 200°C (Fe - free clinozoisite is restricted to more acid hydrothermal systems than those which contain prehnite but Fe^{3+} - bearing epidotes and prehnite will coexist). The upper limit of epidote stability is not constrained by observations of modern hydrothermal systems since all those investigated to date have maximum temperatures of only 300 – 350°C. The experimental data of Bird & Helgeson (1981) indicates that the upper stability limit of the mineral pair epidote + quartz is at about 400°C at 0.1kb P_{H_2O} and 450°C at 1kb P_{H_2O}; quartz is ubiquitous in all the M0 assemblages except for the metacarbonates.

Tremolite to actinolitic hornblendes: > 250°C.

Clinopyroxenes: ¿ 300°C; do not coexist stably with epidote below 350°C.

Wairakite: 200 – 300°C (only occurs in high Ca, high Ca/Al rocks coexisting with a silica - saturated fluid).

Grossular: > 300°C (only in equilibrium with Ca - rich, weakly acidic solutions, like prehnite).

Wollastonite: mainly > 200°C, but occurrence primarily controlled by the need for very high Ca^{2+}/H^{+} in the hydrothermal solution.

Clay minerals, sericite, pyrophyllite: Mainly at low temperatures, but occurrence mainly due to high fluid acidity.

The occurrence of prehnite, actinolitic amphibole and Fe^{3+} - poor epidotes and clinozoisites in the M0 assemblages, the rarity of clinopyroxene and garnet, and the general absence of zeolites and clay minerals therefore points to M0 temperatures between 250°C and 350°C in the area north and west of the Glas Eilean fault. This is consistent with the occurrence of biotite and muscovite in the pelitic rocks, as the upper limit of this mineral pair at $P_{H_2O} \leq 0.5$kb is 450 – 550°C (section 5.2.2, below), whilst the lower limit of biotite stability in pelites in the Cerro Prieto, California, hydrothermal field described by Bird et al. (1984) is at about 315°C. Bird et al. found that the assemblage chlorite + clay minerals was characteristic of pelites at lower temperatures.

Samples of Moinian rocks collected to the east of the Glas Eilean fault along the south coast of Ardnamurchan between Glas Eilean and Beinn Hiant are of distinctly lower grade than the rocks north and west of the fault: vein carbonate is commonly the main Ca - bearing mineral, M0 biotite is absent and the rocks contain much better preserved pre - M0 sedimentary and regional metamorphic textures. This suggests that the grade of M0 increases sharply towards the present - day site of the Hypersthene Gabbro and that the heat source for M0 metamorphism was either earlier Centre 2 intrusions or a magma body below the present level of exposure which was subsequently intruded upwards to form the MBG magma chamber. This would also explain the persistence of sericite, carbonate and zeolites in the early felsic intrusions furthest from the Hypersthene Gabbro, on the southern side of Maol Bhuidhe (section 3.2.5.5). However, field and petrographic evidence discussed in section 3.2.5.4 shows that the doming around the Hypersthene Gabbro which is associated with the initial emplacement of the MBG magma chamber postdates most of M0. This excludes the possibility that M0 may have been produced by the Marginal Border Group intrusion in its present position. It can therefore be assumed for the purposes of thermal modelling that the initial temperature of the host rocks at the time of emplacement of the MBG magma chamber was about 250 – 350°C.

The lack of mineral composition data means that fluid compositions during M0 are poorly constrained. However, the abundance of hydrous calc - silicates and the lack of carbonates, except in the lowest - grade rocks and in the initially most carbonate - rich rocks, suggests a high H_2O/CO_2 ratio. This is confirmed by the presence of sphene at the low temperatures inferred above, which implies very low X_{CO_2} indeed (perhaps less than 0.1 (Jacobs & Kerrick 1981)). The occurrence of prehnite and rare grossular, and the absence of aluminosilicates on the one hand and wollastonite on the other, suggests that the solutions had moderate acidities (Bird & Helgeson 1981). Although dark organic matter is common in thin sections of rocks affected by M0 alone, suggesting the presence of methane and possibly other hydrocarbons during M0, the low X_{CO_2} of the fluids also implies very low hydrocarbon contents (Ferry 1976). The preservation of this organic matter, together with the low Fe^{3+} of the epidote - group minerals present, the absence of haematite and the rarity of garnet, and the presence of prehnite (Bird & Helgeson 1981), implies low values of f_{O_2} in most of the M0 hydrothermal fluids. The experimental data of Bird & Helgeson (1981) indicate values of f_{O_2} between the haematite - magnetite and quartz - fayalite - magnetite buffers (log $f_{O_2} = -31$ to -36 at 300°C) for fluids in equilibrium with these assemblages.

Although precise constraints cannot be placed on fluid compositions during M0, it therefore appears that they were H_2O - rich, contained small amounts of CO_2 and hydrocarbons, and were relatively reduced.

5.2. Conditions of M1 Metamorphism.

5.2.1. The width of the M1 aureole and variations in the grade of metamorphism within it.

5.2.1.1. The relationship between the present - day width of the M1 contact aureole and its width perpendicular to the contact at the end of M1.

The available width of exposure of the country rocks in a direction normal to the outcrop of the contact is only great enough to expose the outer edge of the M1 aureole in two areas. The first of these is in the Glendrian Bay area, where the outer limit of recognisable M1 assemblages is only 300m, measured horizontally, from the contact (section 3.2.2.2). The second area is on the southern margin of the intrusion between the Dubh Chreag gorge and Glebe Hill. In this latter area, the outer limit of the M1 aureole is defined by the near - simultaneous disappearance of M0 biotite and muscovite in pelites and calc - pelites in outcrops some 600 – 700m from the outcrop of the contact. There is a factor - of - two difference between these widths and the first question which must be dealt with is which (if either) of these is close to the true width of the M1 contact aureole at the end of M1 or whether there is a genuine variation in the thickness of the M1 aureole, as measured normal to the contact, around the pluton.

Two factors in particular need to be considered. The first of these is the combined effect of the orientations of the contact and of the local topography on the apparent width of the aureole. This will tend to increase the apparent thickness, as measured on the ground, over the true thickness as measured perpendicular to the contact. In the case of the aureole in the Glendrian Bay area, the contact is more - or - less vertical whilst the width of the aureole was measured over the horizontal intertidal rock platform around the bay itself. This suggests that the apparent thickness of the aureole in this area will not have been greatly increased by topographic effects. On the southern margin, however, the contact dips outwards at 50 – 70° overall (section 3.2.5.1), and the outer edge of the aureole outcrops at elevations 100 to 150 metres below the contact itself. The combination of these factors suggests that the true thickness of the aureole on the southern margin of the intrusion is likely to be in the range 450 – 550 metres. This is nonetheless at least 50% greater than its thickness in the Glendrian Bay area.

The second factor which needs to be taken into consideration is the possibility of post - M1 dilation or compression of the aureole, by post - M1 intrusion and/or deformation. The average dilation direction in the post - M1 cone sheets and related intrusions appears to be near - parallel to the contact of the MBG, although individual intrusions and segments of intrusions show a greater variety of dilation directions (see Chapter 7). The overall effect of post - M1 dilation associated with cone sheet emplacement on the width of the aureole therefore appears to have been minor. The same is not true of the M2 concentric inward - and outward - dipping thrust faults which occur in large numbers in the Glendrian Bay sector of the contact (section 3.2.2.2). The effect of movements on these must have been to telescope the M1 aureole in the Glendrian Bay area. The actual amount of shortening cannot be determined because no suitably orientated marker horizons are present. However, the close spacing of the thrusts and the significant proportion of the outcrop which is formed by the intensely deformed rocks within them (Plate 3.18) suggests that the amount of post - M1 radial shortening in this area may have been large. In contrast, concentric thrusts are very rare on the southern margin of the MBG within the exposed part of the aureole. The effects of post - M1 movements on the widely spaced concentric normal faults in the area of interest, between the western end of Druim na Gearr Leacainn and Glebe Hill, on the width of the aureole in this area, have been allowed for in the above estimates of apparent and real thicknesses. The estimate of 450 – 550m for the real thickness of the M1 aureole on the southern margin of the MBG therefore appears to be close to its thickness at the end of M1, whilst the aureole in the Glendrian Bay area was much thicker at the end of M1 than its present - day thickness of 300m or so.

The unknown amount of post - M1 shortening in the Glendrian Bay area means that it cannot be established whether or not there was a genuine difference between the thicknesses of the M1 aureole at the end of M1 in the two areas. Furthermore, the presence of M1 intrusions (the rheomorphic breccias in particular), which form at least 20% of the aureole in the Glendrian Bay area, means that the development of the M1 aureole in that area cannot be modelled in terms of the simple models used in section 5.2.4. The following discussions will therefore concentrate upon the M1 aureole on the southern margin of the pluton where M1 intrusions are comparatively rare. However, the similar states of the contact zone in the two areas (with $Q_m \approx Q_c$) suggests that in fact the differences in the M1 aureole between the two areas were slight as far as investigations of the MBG magma chamber are concerned.

5.2.1.2. Metamorphic reactions and apparent isograds in the M1 aureole.

Fig. 5.1 shows the approximate positions of apparent isograds within the M1 aureole between Dubh Chreag and Glebe Hill. Of these the best - defined (because it occurs in both pelites and calc - pelites of the Middle and Upper Pabba Beds and is easily identified in the field by the disappearance of the M0 fissility) is that which forms the outer edge of the aureole, the breakdown of biotite and muscovite to form granular opaque ± cordierite ± aluminosilicate + K - feldspar pseudomorphs. The other apparent isograds are mainly developed in the Middle and Lower Pabba Beds, apart from the hornblende - out isograd in the plateau basalt suite metabasic and metapicritic rocks.

The reactions represented by the apparent isograds in the more - or - less pelitic rocks are discussed below in sequence proceeding from the outer edge of the aureole towards the contact reactions in the plateau basalt suite rocks are discussed seperately.

1). Biotite, muscovite - out; cordierite + aluminosilicate – in. Both micas disappear almost simultaneously as one proceeds toward the contact, although one sample from just outside the isograd as mapped (sample 305A, at Grid Ref. 46396305) contains pristine M0 muscovite and M0 biotite which has been partially replaced by opaques. Their disappearance coincides with the appearance of cordierite and probable very fine - grained aluminosilicate (presumably andalusite, although positive identification from the mineral optics was not possible). This suggests that this isograd corresponds to the reaction:

$$Muscovite + Biotite \pm Qtz \Leftrightarrow Cordierite + Magnetite + Al_2SiO_5 \mp Qtz + K \quad Feldspar + H_2O \quad [5.1]$$

(modified after Seifert (1976) and A.B.Thompson (1982). The ratio of cordierite to magnetite and aluminosilicate on the righthand side of reaction 5.1, and the amount of quartz consumed or produced will be controlled by the Fe^{3+}:Fe^{2+} + Mg ratio of the biotite (and the availibility of oxygen in the fluid phase if the reaction does not take place in a closed system). Excess muscovite in rocks such as 305A appears to have been consumed at only slightly higher grade by the reaction:

$$Muscovite + Quartz \Leftrightarrow Al_2SiO_5 + K \quad Feldspar \pm Cordierite + H_2O \quad [5.2]$$

(A.B.Thompson 1982)

305A is from the base of the Upper Pabba Beds. These are generally more calcareous and less clay mineral rich than the Lower Pabba Beds. The latter would therefore be expected to contain even

Fig 5.1 Zonation in the M1 aureole on the southern margin of the Marginal Border Group.

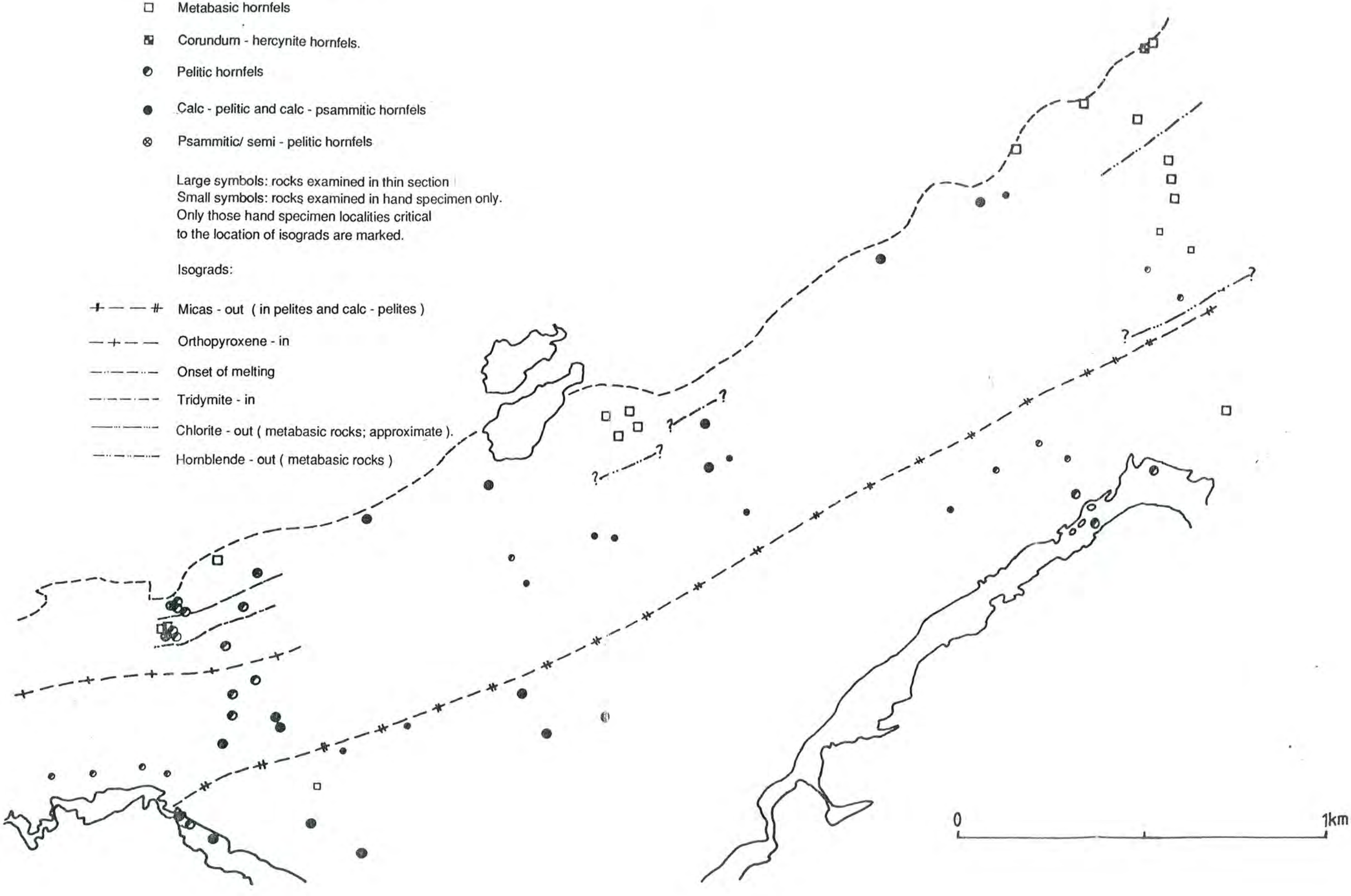

more aluminosilicate above the mica - out isograd, as is consistent with the observed abundance of the tentatively identified aluminosilicate phase in Middle Pabba Beds rocks from within this isograd.

Calc - silicate nodules which replace gryphaea and other thick - shelled fossils in rocks close to the mica - out isograd are dominated by diopside, which also points to higher grades of metamorphism than during M0.

2). Orthopyroxene - in. Orthopyroxene is normally produced during the prograde metamorphism of broadly pelitic rocks by dehydration reactions involving biotite remaining after the completion of reaction 5.1, such as

$$Biotite + Quartz \Leftrightarrow K\ Feldspar + Orthopyroxene + H_2O \qquad [5.3]$$

(Luth 1967).

In the case of the M1 aureole, however, biotite had already been consumed by reaction 5.1, above, before the development of orthopyroxene: furthermore, orthopyroxene does not normally coexist (except over a very narrow range of compositions and/or temperatures as a result of unequal partitioning of Mg and Fe between orthopyroxene and cordierite) with Al_2SiO_5 below the upper stability limit of the mineral pair cordierite + quartz (Pattison & Harte 1985). The appearance of orthopyroxene in the M1 aureole appears to coincide with the disappearance of the tentatively - identified aluminosilicate phase from the fine - grained pseudomorphs after micas; aluminosilicate polymorphs are certainly absent from the relatively coarse - grained rocks in the innermost M1 aureole. This implies an increase of the $\frac{Fe^{2+}+Mg}{Al}$ ratio of the pelitic rocks with increasing metamorphic grade. This change in bulk composition does not necessarily imply mobility of cations which are normally considered to be relatively immobile, as it may be produced simply by the reduction of magnetite:

$$4Al_2SiO_5 + 2Fe_3O_4 + 8SiO_2 \Leftrightarrow 2Fe_2Al_4Si_5O_{18} + 2FeSiO_3 + O_2 \qquad [5.4]$$

The assemblage ferrosilite – magnetite – quartz is, however, metastable with respect to fayalite – magnetite – quartz (see section 5.2.3) so the orthopyroxene in these rocks must be Mg - bearing. The only possible source of Mg in these rocks is cordierite, implying that the initial orthopyroxene - producing reaction must in reality be of the general form:

$$Cordierite_1 + Al_2SiO_5 + Magnetite + Quartz \Leftrightarrow Orthopyroxene + Cordierite_2 + O_2 \qquad [5.5]$$

where $Cordierite_2$ is more Fe - rich than $Cordierite_1$ and there is net production of cordierite as the reaction proceeds from left to right. It should be noted that this is a continuous reaction, due to unequal partitioning of Mg between cordierite and orthopyroxene (Pattison & Harte 1985). An obvious feature of both of these reactions is that they require the presence of a reducing vapour phase; the implications of this are discussed further in section 5.2.3. It is more realistic to interpret the observed mineralogical changes in terms of reduction reactions of this sort, rather than as the effects of large - scale metasomatic mass transfer, because of the preservation of primary textures and compositional heterogeneities in these rocks on scales of a millimetre or less, notably the persistence of clinopyroxene in nodules and pseudomorphs after fossils despite the overall peraluminous composition of the rocks.

Once the aluminosilicate had been exhausted, further orthopyroxene could have been produced in the reaction:

$$Cordierite_1 + Magnetite + Quartz \Leftrightarrow Orthopyroxene + Cordierite_2 + O_2 \qquad [5.6]$$

with no production of new cordierite. Although quantititive data are not available at present, orthopyroxene abundances in the metapelites appear to increase towards the contact: this may be due to reaction 5.6. Like reaction 5.5 this is a potential buffer reaction for oxygen activity in the coexisting fluid phase (see section 5.2.3).

3). Onset of low degree partial melting. This is most obvious in the Lower Pabba Beds but is also visible in the Middle Pabba Beds (section 3.2.5.5). The initial melting 'isograd' is, however, difficult to locate precisely because of the very small scale of melt segregation in the majority of the rocks in the contact aureole and the post - M1 recrystallisation which tends to obliterate evidence for the earlier presence of intergranular melt films. Microscopic melt veins and segregations in the pelitic and semipelitic rocks typically contain quartz + alkali felspar + minor opaques ± micropoikilitic or prismatic orthopyroxene. Later ferromagnesian alteration products (chlorite and uralitic amphibole) are also present in the veins, but cordierite (possibly masked by later alteration) and aluminosilicate are rare to absent. Within this isograd, relict cordierite occurs only in patches or bands of cordierite – quartz rock a few millimetres thick. In other areas of thin sections from rocks closer to the contact it, like alkali feldspar, only occurs as interstitial - poikilitic grains which appear to have crystallised from interstitial melts. These interstitial - poikilitic grains are ubiquitous except in areas composed of cordierite + quartz or orthopyroxene + magnetite +

quartz. The only relict feldspar grains are rare rounded equant grains of calcic plagioclase which occur in both Middle and Lower Pabba Beds rocks. The other apparently residual phases are quartz, opaques and orthopyroxene in most of these rocks; orthopyroxene and opaques (mainly or wholly magnetite) are only consumed completely in pelitic rocks in the downfaulted block on Hill 210, leaving excess quartz (inverted from tridymite: see below) as the only residual phase.

Possible reactions which could contribute to the melt phase in these rocks are, in order of occurrence proceeding upgrade (see Vielzeuf & Holloway 1988):

$$(Na, K) \qquad Feldspar + Quartz + H_2O \Leftrightarrow Melt \qquad [5.7]$$

(Tuttle & Bowen 1958)

$$Orthopyroxene + Cordierite + (K, Na) \qquad Feldspar + Quartz \pm H_2O \Leftrightarrow Melt \qquad [5.8]$$

(Vielzeuf & Holloway 1988)

$$Orthopyroxene + (K, Na) \qquad feldspar + Quartz \pm H_2O \Leftrightarrow Melt \qquad [5.9]$$

(Luth 1967)

H_2O in the above reactions (except for 5.7) may be in a distinct vapour phase or dissolved in the melt. Similarly, alkali feldspar may have disappeared at an early stage, the reactions being between ferromagnesian minerals, quartz, and an alkali - bearing melt instead. Reaction 5.8 must have been terminated by the disappearance of cordierite, as is consistent with the restricted occurrence of residual cordierite noted above, as otherwise reaction 5.9 would be replaced by the reaction:

$$Cordierite + Quartz + (K, Na) \qquad feldspar \pm H_2O \Leftrightarrow Melt + Al_2SiO_5 \qquad [5.10]$$

(Seifert 1976)

which would produce an aluminosilicate - bearing residuum rather than the orthopyroxene - bearing residuum which occurs in all but the most highly melted rocks. Melting reactions involving Fe^{3+} - bearing oxide phases in pelitic rocks have not been studied in detail: they could be analogous to the reactions involving orthopyroxene, above, with additional quartz in the solid reactants to balance the equations.

4). Tridymite - in. Like isograd (3) this isograd cannot be located precisely, because it is partially obscured by post - M1 inversion of tridymite to quartz. However, random internal straining of residual quartz grains (similar to that described in section 4.2.4) and poikiloblastic quartz pseudomorphs after possible tridymite needles in interstitial patches of quartz - feldspar intergrowth are common in pelitic to quartzitic rocks within 100m or so of the contact.

M1 assemblages in the rocks on the western margin of the intrusion are largely obscured by replacement with M2 assemblages, although relict orthopyroxene and interstitial quartz - feldspar intergrowths are recognisable in some sections (section 3.2.4) suggesting similar conditions of metamorphism. All of the reactions associated with the isograds identified above are identifiable in the Glendrian Bay area, except for the mica dehydration reactions, although pseudomorphs after micas are recognisable. This is simply because pelitic rocks are not exposed in the relevant part of the aureole in this area.

Graphical representation of these reactions on diagrams normally used to represent metamorphic reactions in metapelites (such as AKF, AFS and Thompson AFM plots) is complicated by the reduction of Fe^{3+} to Fe^{2+} implied by the appearance of orthopyroxene due to reactions 5.5 and 5.6. Orthopyroxene forms up to 5 – 10% of the mode of the highest - grade Lower and Middle Pabba Beds rocks, implying a large change in $\frac{Fe^{2+}+Mg}{Al}$ due to reduction of magnetite and therefore substantial movement of the position of the rocks in these diagrams.

The majority of the pre - M1 igneous rocks which outcrop on the southern margin of the intrusion either lie outside the M1 aureole altogether or occur within 200m of the contact. The latter contain anhydrous M1 assemblages (augite + calcic plagioclase + opaques ± olivine ± orthopyroxene, the last two phases being particularly common in patches of entirely recrystallised material which may correspond to the most altered, clay mineral rich parts of the original rock (Cann 1965)) in addition to the relict igneous phases which can be recognised in some of these rocks. At the southern end of Glebe Hill, however, the M1 metabasic to metapicritic hornfelses contain reddish - brown poikiloblastic pargasitic hornblende (section 3.2.6). This suggests that the quartz - absent hornblende - out reaction

$$Pargasitic \quad hornblende \Leftrightarrow Augite + Plagioclase + Olivine + Orthopyroxene \pm Ilmenite + H_2O \qquad [5.11]$$

(Spear 1981)

has only taken place within about 200m of the contact. The identification of this isograd is complicated by the extensive development of M2 reddish poikiloblastic hornblende, rimming and replacing corroded olivine and orthopyroxene grains, in higher - grade rocks. However, the red colour and replacive habit of this later hornblende distinguish it from the M1 hornblende present further from the contact.

5.2.2. A preliminary estimate of the temperature profile through the contact aureole at the end of M1.

The history of metamorphism during M1 and the subsequent rapid cooling or quenching (sensu lato) (section 3.5) implies that peak metamorphic conditions were attained almost simultaneously throughout the M1 aureole (in any one sector of the aureole at least). It follows from this that the peak metamorphic temperature profile through any one sector of the aureole corresponds closely to a true geotherm, which is developed at a particular moment in time, rather than to a normal metamorphic geotherm, which is in general markedly diachronous (Jaeger 1959). As noted in Chapter 4, this geotherm will correspond to the temperature profile through the contact aureole at the end of M1, immediately prior to the quenching event, and can therefore be used to estimate heat flow through the wall rocks at that time.

Temperatures of metamorphism can be deduced from the compositions of coexisting minerals using chemical exchange geothermometers, from the stable isotopic compositions of coexisting mineral pairs (reviewed in O'Neil (1986)) and characteristic mineral assemblages whose stability limits are bounded by temperature - dependent reactions. The reactions which define the pelitic isograds (1), (3) and (4), above, and the hornblende - out isograd in the plateau basalt suite rocks are of this type, although they also show pressure - dependence (see below). The orthopyroxene - in isograd in the pelites, however, involves a redox reaction dependent on f_{O_2} in the coexisting fluid phase and cannot, therefore, be used to infer metamorphic temperatures directly: its use in f_{O_2} determination is discussed in section 5.2.3.

The temperatures of occurrence of reactions 5.1 and 5.2, which together form the mica - out isograd,

depend on the Mg/Fe ratio of the micas and upon P_{H_2O}. However, neither is particularly sensitive to either of these factors: below P_{H_2O} = 1kb, both the Mg - mica and Fe - mica end - member reactions occur in the range 450 – 550°C (A.B.Thompson 1982). P_{H_2O} cannot be constrained more tightly than this although the lack of M1 fracture systems (which imply near - lithostatic water pressures throughout) and the presence of a free fluid phase and its likely composition (section 5.2.3) suggest that P_{H_2O} was probably in the range 0.3 – 1.0kb during M1, in which case the likely temperature of occurrence of reactions 5.1 and 5.2 is 500 – 550°C.

The onset of partial melting in quartz - and alkali feldspar - bearing systems (reaction 5.7) occurs at about 700 – 750°C at P_{H_2O} = 0.3 – 1kb (Tuttle & Bowen 1958). However, the position of isograd (3) in Fig. 5.1 is based on the occurrence of discrete quartzofeldspathic veins and segregations which generally contain accessory orthopyroxene and sometimes contain large amounts (up to 20% modal) of this mineral. Isograd (3) is therefore more likely to correspond to reactions 5.8 and/or 5.9. Vielzeuf & Holloway (1988) inferred that these reactions occur at 770 – 830°C under the same conditions in typical metapelites and semipelites, which have $X_{Mg} \approx 0.5$. The analyses of Lower and Middle Pabba Beds rocks in Appendix 2 suggest similar values of X_{Mg} as the mineralogy of these rocks suggests a low Fe^{3+} content. The melt - in isograd, as mapped, is therefore likely to correspond to a temperature of at least 770°C.

Isograd (4), the tridymite - in isograd, has already been discussed in the context of granitoid melt formation (section 4.2.5) where it was inferred to correspond to temperatures in the range 930 – 1100°C, according to P_{total}. Its occurrence at some distance from the contact (perhaps 100m or so) suggests that in fact it corresponds to a temperature of less than 1050°C or so, since the contact temperature itself was probably in the range 1050 – 1150°C (see Chapter 4, sections 4.2.5 and 4.5.3 in particular).

The decomposition of pargasitic hornblende in silica - free rocks was studied by Spear (1981). The experiments in this study were carried out upon an olivine tholeiite rather than alkaline basalts or picrobasalts, so the results must be applied to the Glebe Hill rocks with caution. In particular, the latter have higher Ti contents than tholeiitic rocks (see section 2.4.1), which may stabilise silica - deficient hornblendes to higher temperatures and/or lower P_{H_2O}, and also probably have slightly higher Mg/Fe^{2+} which would tend to have a similar effect. Spear (1981) found that the amphibole

dehydration reaction (5.11, section 5.2.1) was P_{H_2O} dependent, occurring at 890°C at 0.5kb and at 920°C at 1.0kb, but was insensitive to f_{O_2} in the range of oxygen activities in the M1 aureole (section 5.2.3, below). It therefore seems likely that the amphibole - out isograd corresponds to peak M1 temperatures in the range 850 – 950°C.

The available constraints on the end - M1 temperature profile through the M1 aureole on the southern side of the Hypersthene Gabbro are summarised in Fig. 5.2. It should be emphasised that, in the absence of mineral composition data, these can only be regarded as preliminary estimates. However, the profile in Fig. 5.2 is distinctly curved, with gradients of perhaps $-1.8°Cm^{-1}$ at the contact and of only -0.8 – $-1.0°Cm^{-1}$ around the mica - out isograd (the negative signs denote the decrease in temperature with increasing distance from the contact). The curved geometry of the contact means that the thermal profile would be concave - up even at conductive equilibrium (Carslaw & Jaeger 1959): however, the differences in thermal gradient produced by this effect are proportional to the ratio $\frac{r_i+r}{r_i}$ where r is the distance from the contact and r_i is the radius of the intrusion. The proportional difference in radial temperature gradient produced by this effect would therefore be 15% or less, an amount that would be barely noticeable given the uncertainty in the data. Other explanations of the positive $\frac{\partial^2 T}{\partial r^2}$ (second derivative of temperature T with respect to distance from the contact) shown by Fig. 5.2 must therefore be sought. Three distinct explanations are possible:

1). If heat transfer in the M1 aureole was purely by conduction and the position of the contact did not vary with time after the initial emplacement of the MBG magma chamber, Fourier's Law of heat transfer (see discussion in Hill & Dewynne (1987)) implies that the thermal profile in Fig. 5.2 must be a non - equilibrium one: in other words, that the M1 aureole was still heating up at the end of M1, just prior to the sudden cooling of the aureole.

2). If heat transfer in the M1 aureole was by a mixture of conduction and sluggish hydrothermal convection, a similar concave - up thermal profile could be produced at thermal equilibrium (Parmentier & Schedl 1981; Bickle & McKenzie 1987) if the relationship

$$\kappa_s \frac{\partial^2 T}{\partial r^2} = W_r \frac{\partial T}{\partial r} \qquad (5.1a)$$

(where W_r is the volumetric hydrothermal fluid flux towards the contact and κ_s is the overall thermal diffusivity of the host rock and stagnant interstitial fluid) is satisfied. Equation 5.1a

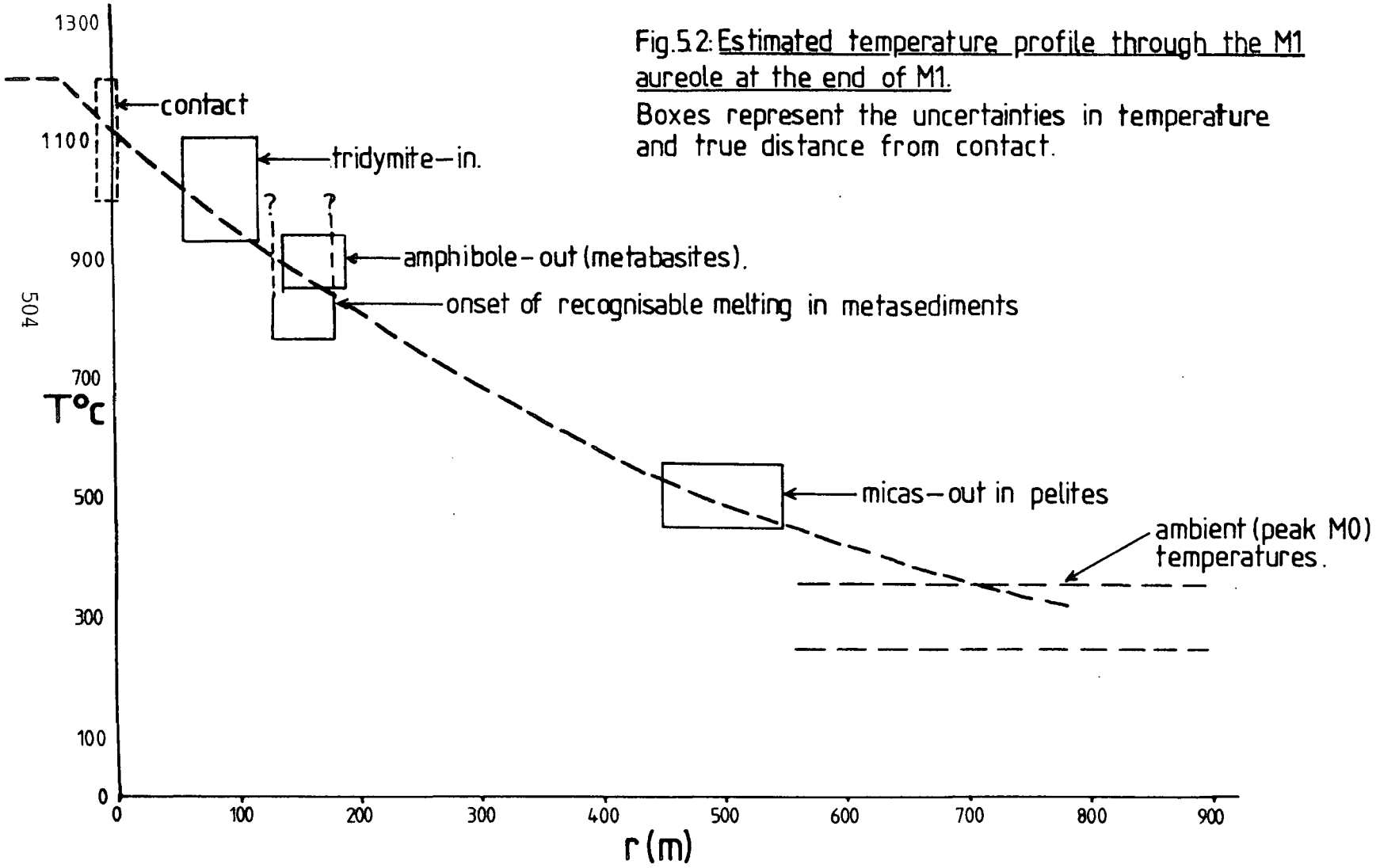

Fig.5.2: Estimated temperature profile through the M1 aureole at the end of M1.
Boxes represent the uncertainties in temperature and true distance from contact.

is derived from the more complex thermal balance relationship

$$Q = (\kappa_s \frac{\partial T}{\partial r}) \times \frac{\partial T}{\partial r} = \rho_{fluid} c_{fluid} \frac{\partial T}{\partial t} + W_r \rho_{fluid} c_{fluid} \frac{\partial T}{\partial r} \qquad (5.1b)$$

by setting the first term on the right hand side to zero (as it must be, by definition, at thermal equilibrium) and assuming that $\rho_{fluid} c_{fluid} = \rho_{rock} c_{rock}$, with the lower density of the fluid being cancelled out by its greater heat capacity (Norton 1984). This is only approximately true and in general a more complex relationship between T and W_r will produce a curved temperature profile at equilibrium (Brady 1988). However, the basic principle that weak hydrothermal circulation can produce thermal equilibrium at non - zero $\frac{\partial^2 T}{\partial r^2}$ remains true.

Interpretations (1) and (2) are not, of course, mutually exclusive if W_r is less than that required to maintain equilibrium. It is apparent, however, that interpretation of Fig. 5.2 is dependent upon an understanding of the hydrothermal fluid flux in the M1 aureole.

3). A third explanation of the thermal profile in Fig. 5.2 is that it represents the equilibrium thermal profile in front of an advancing heat source (Carslaw & Jaeger 1959). Although, as was shown in Chapter 4, $Q_m \approx Q_c$, so that wall - rock melting was concentrated in the downfaulted blocks, the amount of melting in these, averaged over the entire wall of the intrusion, may have been sufficient to cause the contact as a whole to advance outwards at an overall velocity a (equation 4.3, section 4.1).

In the absence of an independent estimate of a it is not possible to exclude this third possibility. Conversely, however, the thermal profile in Fig. 5.2 can be used to place an upper limit upon the value of a and therefore the difference between Q_m and Q_c (see section 5.2.4, below).

5.2.3. The oxidation state of rocks affected by M1 metamorphism and fluid flow in the M1 aureole.

As was shown in Chapter 3, there was no dense interconnected network of fractures in the M1 aureole such as is necessary for vigourous convection in hydrothermal systems (Norton 1984, 1988). This does not, however, preclude low rates of intergranular fluid movement, or fluid movement along M1 fault planes. Interpretation (2) of Fig. 5.2 therefore remains possible; indeed, the development of

redox reactions in the M1 aureole strongly suggests that some fluid movement did occur.

Fluid - rock reactions during contact metamorphism may involve fluids originally present within the rocks or generated within them by dehydration reactions and/or fluids which migrate into the rocks as a result of expulsion from underlying rocks or as a result of hydrothermal convection. The importance of the former sources are limited by the initial water content (as pore water or as water bound up in hydrous minerals) of the rocks. The previously metamorphosed (during M0) rocks of the M1 contact aureole can only have had an initial water content of 0.5 – 2% , mainly bound up in micas. Although the specific heat capacity of this water under the conditions of the dehydration reactions 5.1 and 5.2 would have been 4 – 6 times that of the host rocks under the same conditions (Norton 1984) the amount of heat removed from the aureole by **expulsion** of this water (as opposed to the latent heat absorbed by its generation) can only have been at most 10% of the heat input to heat the host rocks over the temperature interval in which dehydration and fluid expulsion took place. Although local thermal perturbations may be produced by channelisation of the flow of fluids released in dehydration reactions (as proposed on theoretical grounds by Brady (1988) in the context of dehydration of regional metamorphic terranes) the overall effects of heat transfer by fluids released on dehydration on the M1 aureole is likely to be slight.

This mass - balance argument does not apply to the case of circulation of externally - derived water moving through the M1 aureole, either as a result of true multi - pass hydrothermal circulation or expulsion of water from aquifers outside the M1 aureole driven by the decrease in density of heated fluids within the aureole. However, circulation of large volumes of externally - derived fluids through metamorphic rocks characteristically produces external buffering of the fluid phase in the rocks and hence of certain compositional features of the rocks themselves, although the effects of such circulation are critically dependent upon the activities of the species involved in any particular buffering reaction in the fluid phase (Wood & Walther 1986). In the case of the redox reactions considered in this section, however, Wood & Walther show that, at oxygen fugacities below the Nickel – Nickel Oxide (NNO) buffer, the activities of reduced species (mainly H_2 and CH_4) in hydrothermal fluids are relatively high and changes in the redox state of metamorphic rocks are a sensitive indicator of the circulation of hydrothermal fluids.

Constraints on the value of f_{O_2} at particular temperatures within the M1 aureole are provided by

the coexisting Fe oxide and ferromagnesian silicate assemblages present in the rocks affected by M1. The assemblages concerned and the constraints they provide can be summarised as follows:

1). (Mg,Fe)Orthopyroxene – Magnetite – Quartz in high - grade pelitic and semi - pelitic to psammitic hornfelses of the Middle and Lower Pabba Beds. This assemblage, the equivalent in moderate - to - high Mg/Fe^{2+}, Si - rich rocks of the Fayalite – Magnetite – Quartz (FMQ) buffer assemblage forms a 'continuous buffer', with the amount and Mg/Fe^{2+} ratio of the orthopyroxene varying over a divariant field in temperature – oxygen fugacity space. At any given $X^{opx}_{MgSiO_3}$, however, the assemblage defines a univariant curve in T – f_{O_2} space at some distance above the FMQ buffer itself (Nitsan 1974). However, at low temperatures and/or low Mg/Fe^{2+} ratios, the assemblage Opx_{ss}+ Qtz + Mt is unstable relative to the assemblage $Olivine_{ss}$ + Mt + Qtz (Nitsan 1974). The presence of Opx_{ss} + Mt + Qtz therefore not only implies f_{O_2} above FMQ but also above the stability conditions of the univariant (in the system Mg - Fe - Si - O) assemblage Opx_{ss} + Ol_{ss} + Mt + Qtz (Nitsan 1974; see Fig. 5.3, below). The presence of additional components in the orthopyroxene (mainly Ca and Al) will extend its stability range to slightly lower f_{O_2} and smear out the univariant reaction to form a narrow divariant field. However, the complete absence of olivine from the M1 assemblages implies that f_{O_2} was always above that of the univariant Mg - Fe - Si - O end - member assemblage.

This assemblage occurs from the apparent isograd (2) to the contact, implying that it was stable between 700 and 1100°C (see Fig. 5.2).

2. Cordierite – Magnetite – Aluminosilicate – Quartz. At lower grades than those of the apparent isograd (2) the Opx – Mt – Qtz continuous buffer assemblage is absent. However, the absence of both haematite and olivine (or some hydrous Mg,Fe - silicate (serpentine, talc or anthophyllite)), and the presence of magnetite and quartz constrains these rocks to have had f_{O_2} between the HM and FMQ buffers over a wide temperature range. The buffering of f_{O_2} within this range may have been caused by the reaction

$$Mg - Cordierite + Al_2SiO_5 + SiO_2 + Fe_3O_4 \Leftrightarrow Fe - Cordierite + O_2 \qquad [5.12]$$

with the reaction proceeding to the right with increasing temperature until the appearance of orthopyroxene and the final disappearance of Al_2SiO_5 in reaction 5.5: the position of reaction 5.5 would in fact be controlled by the change in bulk rock $\frac{Mg+Fe^{2+}}{Al}$ produced by reaction 5.12 under

these circumstances, with orthopyroxene appearing at lower temperatures in more reduced rocks. Offsetting of isograd (2) between different lithologies was not observed on the scale of sampling, however.

3). Olivine – Orthopyroxene – Magnetite in altered metabasic rocks. Previously altered (during weathering or M0) high - grade M1 hornfelses of the plateau basalt suite rocks, particularly picrobasaltic rocks such as samples 202 and 251 (see Appendix 2) commonly contain granular - textured patches with the assemblage orthopyroxene – olivine – magnetite. This is the silica - poor counterpart of the assemblage Opx_{ss} – Mt – Qtz and also only occurs at higher f_{O_2} (at any one temperature) than the four - phase assemblage Ol_{ss} – Opx_{ss} – Qtz – Mt. The assemblage occurs in rocks from just inside the hornblende - out isograd to close to the MBG contact, again implying that they lay between the HM buffer and the univariant line of the four - phase assemblage over a wide temperature range, perhaps 850 to 1050 – 1150°C.

4). Magnetite - free Hercynite – Corundum and metabasic hornfelses.

In strong contrast to the majority of the metamorphosed plateau basalt suite rocks the spinel – corundum hornfelses and adjacent metabasic rocks to the northeast of Glebe Hill (Field location 72; section 3.2.6) contain no magnetite at all, the only opaque oxide being minor ilmenite. The assemblage in the spinel hornfels is hercynite – plagioclase – ilmenite – corundum (sample 72/3; see mineral analyses in Appendix 3); Richey et al. (1930) considered that cordierite was also present but this was not found in the rock sampled. The hercynite – corundum pair is particularly significant because the Fe^{3+} content of hercynites coexisting with corundum can be used to estimate oxygen fugacity at the time of formation (Turnock & Eugster 1962). Hercynite Fe^{3+} contents, calculated from microprobe analyses by the method of Turnock & Eugster (1962), and inferred f_{O_2} values are as follows, although it should be noted that these values lie in a region where this oxygen geobarometer is relatively inaccurate:

Analysis Number	Wt% Fe_2O_3	$-\log f_{O_2}$ at 1100°C
53.03	6.46	-12 – -14
53.04	5.99	-14 – -19
53.05	7.13	-12 – -13
53.06	10.3	$\approx$ -12 ?
53.10	15.4	$\approx$ -7 ?

All analyses are of grain cores. The f_{O_2} estimates are extrapolated above the temperature range of Turnock & Eugster's data by 100°C and must be regarded as approximate values only. The reason for the discrepancy between the first three values (identical within the limits of error) and the last two is probably that, whilst the first three analyses are of grains in a patch of fine - grained (grain size $\leq$ 0.1mm) rock composed of all four phases present in the rock as a whole (Plate 5.1A) the last two are from patches of coarse - grained hercynite - ilmenite rock which lacks corundum (Plate 5.1B). The hercynite oxygen barometer is only valid in the presence of excess Al_2O_3 (Turnock & Eugster 1962) and the discrepancy in calculated f_{O_2} values may therefore indicate a lack of diffusional equilibration betwen Al - rich and Al - poor areas on a scale of a few millimetres or less. Some of the large hercynite grains, such as those represented by analyses 4 and 5 above, show optical zonation from dark (Fe^{3+} rich ?) cores to very thin paler green rims, suggesting that partial equilibration may have taken place, either during or after M1 metamorphism. The metabasic rocks adjacent to these hornfelses (sample 72/2) are unusual in being opaque - poor, the only opaque phase probably being ilmenite. 72/2 contains abundant orthopyroxene and olivine; the lack of magnetite implies f_{O_2} below the equilibrium $Olivine_{ss}$ + Magnetite $\Leftrightarrow$ $Orthopyroxene_{ss}$; in contrast to the majority of the M1 metabasic rocks (see above).

M1 temperature constraints from section 5.2.2 (in particular Fig. 5.2, which relates peak M1 temperatures to distance from the contact) and the f_{O_2} constraints from above are combined in Fig. 5.3. The buffer curves marked on this diagram are for P=1 Atm. and originate from Nitsan (1974) and Eugster & Wones (1962). No attempt is made to apply a pressure correction to the data presented in Fig. 5.3 because (a) the pressure of M1 metamorphism was low but its precise value is uncertain (b) the effect of pressure on the **relative** positions of the buffers shown is small, and it is these relative differences which are important in the present context. The position of the Al_2SiO_5 - out, orthopyroxene - in reaction on this diagram is diagrammatic only because the redox reactions

Plate 5.1A. Fine - grained area of hercynite - corundum hornfels, sample 72/3. Corundum forms small, very high relief colourless grains at corners of larger grains. Most of the opaque grains are hercynites (dark because of low illumination and abnormally thick section). Other minerals present: plagioclase, ilmenite, possibly cordierite. Plane - polarised light, field of view 1.5mm.

Plate 5.1B. Coarse - grained hercynite, ilmenite rich area of hercynite - corundum hornfels sample 72/3. Thin area of slide photographed under very strong illumination to show zonation in hercynites. Note magnetite exsolution lamellae in some grains. Plane - polarised light, field of view 1.5mm.

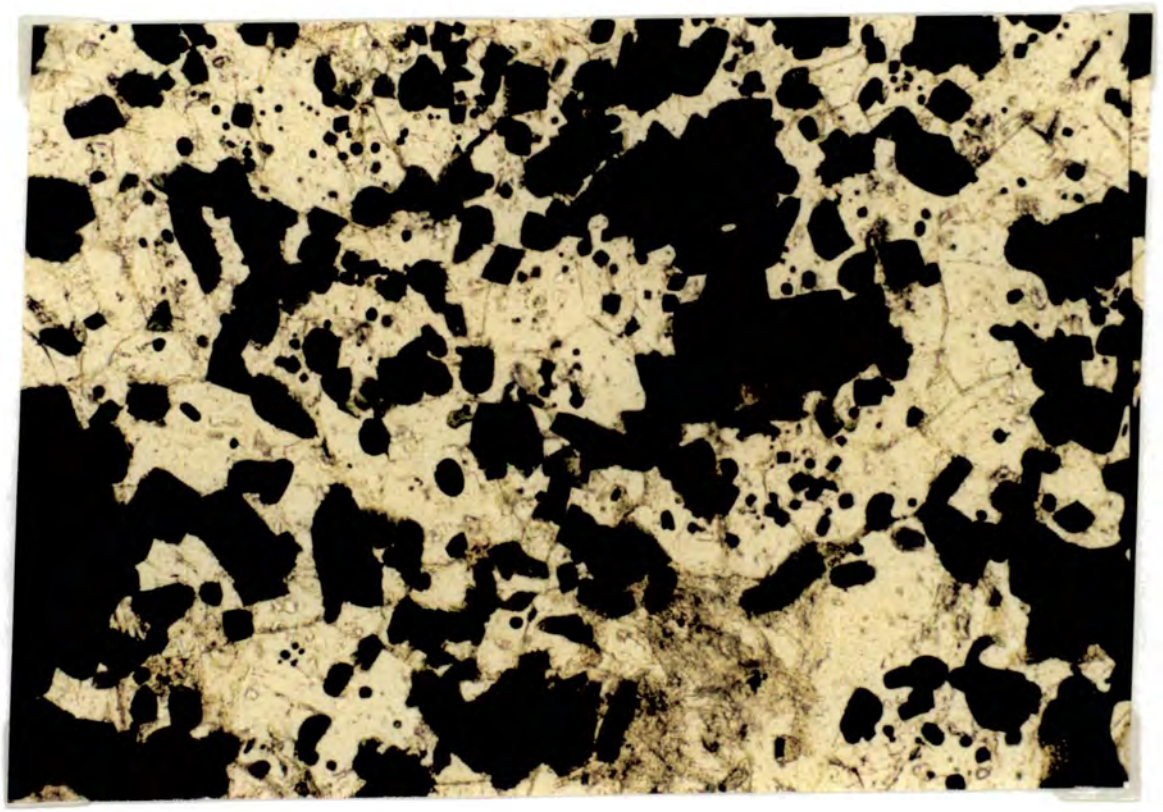

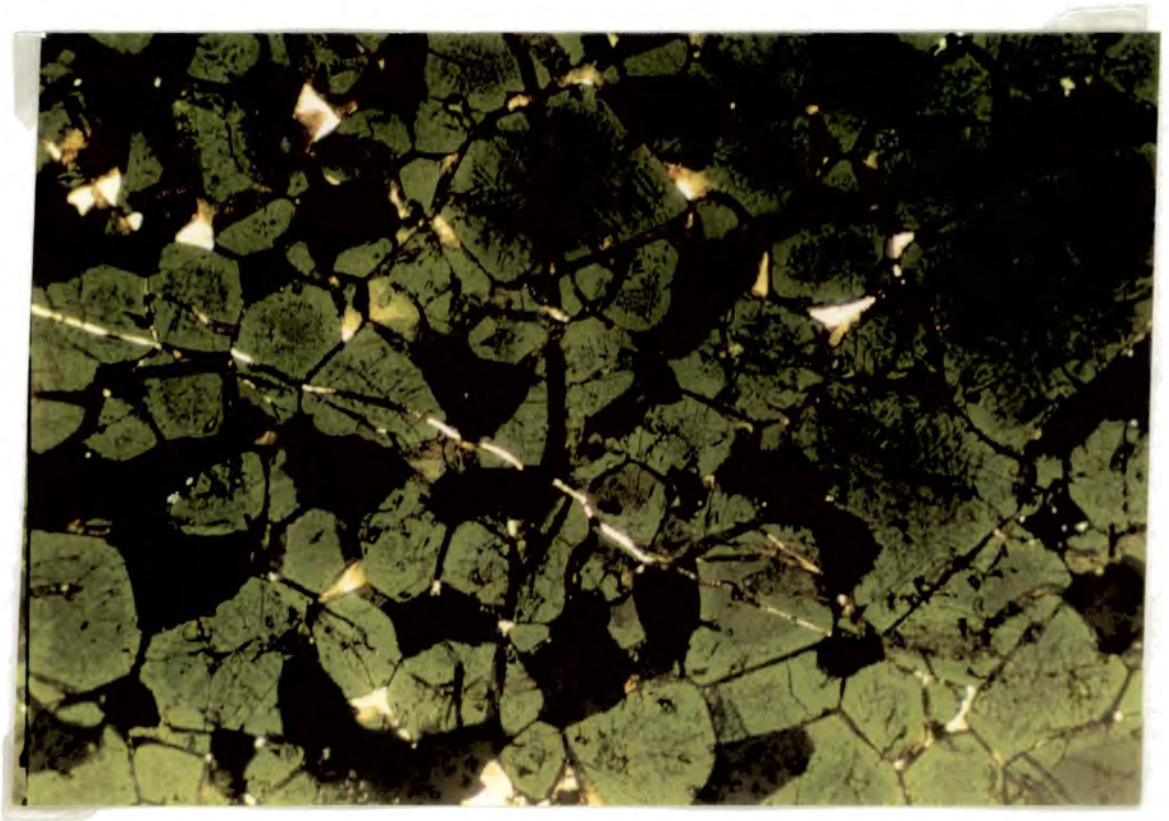

Fig. 5.3: Temperatures and Oxygen fugacities during M1.

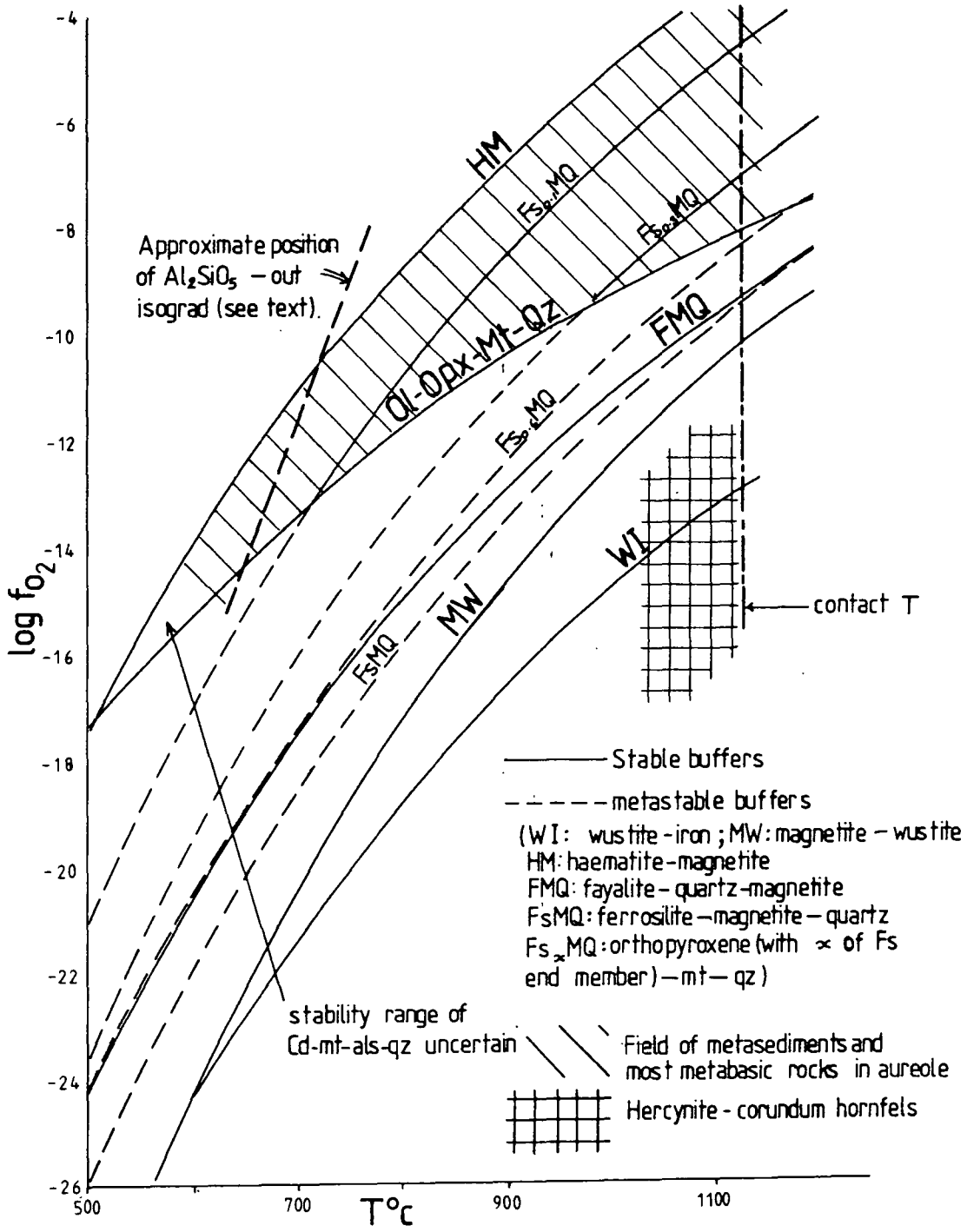

concerned, reactions 5.5 and 5.12, have not been studied experimentally.

Two conclusions can be drawn from Fig. 5.3. The first of these is that the majority of the rocks in the M1 aureole were buffered internally by redox reactions which maintained their oxygen fugacities between the HM and FMQ buffers throughout the wide range of temperature in the M1 aureole. It should be noted that the oxidation state of these rocks at the end of M1 seems to have been close to that at the beginning of M1, although some reduction did take place (see below), since the oxidation state of the M0 rocks outside the M1 aureole is also between the HM and FMQ buffers (section 5.1).

The second conclusion is that f_{O_2} varied by several orders of magnitude between rocks metamorphosed at similar peak metamorphic temperatures, with the hercynite - corundum bearing hornfelses having a late M1 f_{O_2} well below the magnetite - wustite buffer whilst most other rocks close to the contact record late M1 f_{O_2} values above that of the opx – ol – mt – qtz univariant assemblage. The hercynite - corundum hornfelses were also probably more reduced than the MBG magmas themselves, since the MBG rocks commonly contain the assemblage olivine - orthopyroxene - magnetite. The likeliest explanation for the very reduced state of the hercynite - bearing rocks is that they were originally adjacent to the Tertiary lignites and organic - rich mudstones which Richey et al. (1930) record from the base of the Tertiary plateau basalt lava pile elsewhere in Ardnamurchan, and were reduced by hydrocarbons released by them during M0 or the early part of M1. The preservation of the same oxidation state to the end of M1 therefore implies that the spinel hornfelses and adjacent rocks were also internally buffered during most of M1.

These two conclusions imply that fluid movements during M1 were not large enough, in terms of water – rock ratio, to impose an externally controlled f_{O_2} upon the hornfelses. However, the volume of fluid which migrated through the rocks **was** large enough to cause sufficient reduction of Fe^{3+} (in magnetite) to Fe^{2+} (in cordierite and/or orthopyroxene) to cause the disappearance of Al_2SiO_5 and produce perhaps 5 – 10% modal orthopyroxene in the high - grade hornfelsed Middle and Lower Pabba Beds rocks. Quantitiative determination of the fluid flux involved would require mineral composition data, modes and an estimate of the change in bulk - rock Fe^{3+}/Fe^{2+} during M1, as well as estimates of the temperature and composition of the fluids involved. However, comparison with the conclusions of Wood & Walther (1986) regarding reducing fluid fluxes in contact aureoles

suggests that the water - rock ratio in the M1 aureole must have been much less than 1. The absence of discrete flow channels through most if not all of the M1 aureole suggests that the flow was largely intergranular and that therefore the physical ratio of the mass of water which flowed through the M1 aureole to the mass of rocks was close to the ratio of water and rock which reacted with each other, as indicated by the occurrence of internal buffering of f_{O_2}. The question of whether this small fluid flux could maintain the thermal profile of Fig. 5.2 at equilibrium remains an open question, however. The qualitative implications of fluid flow through the M1 aureole for the controls on heat transfer aroung the MBG magma chamber will be returned to in subsequent sections.

5.2.4. Thermal modelling of the M1 metamorphic event.

5.2.4.1. An estimate of the heat fluxes Q_c and Q_m at the end of M1, and of the heat transfer coefficient h of the M1 boundary layer.

As noted at the beginning of this chapter, one of the main reasons for studying the M1 phase of contact metamorphism was to evaluate the heat fluxes at the wall of the M1 magma chamber at the end of M1. In the absence of convective heat transfer **at the contact itself** the heat flux Q_c into the wall rocks is given by a form of Fourier's law:

$$Q_c = -k\frac{\partial T}{\partial r}_{r=0} \tag{5.2}$$

where k is the thermal conductivity of the wall rocks at the contact and the negative sign denotes the fact that heat flows down the temperature gradient. The assumption that heat transfer at the contact itself is purely conductive is justified on the one hand by the definition of the contact as the surface at which magma changes to or from an immobile solid state (section 4.1), which precludes the transfer of heat through that surface by moving magma except at a very low rate by means of melt percolation, and on the other by the observation that hydrous fluid phases in partially molten rocks collect into discrete, disconnected bubbles (for example, Roedder (1984)), which implies that the contact was impermeable to the migration of discrete fluid phases.

Inspection of Fig. 5.2 yields an approximate best - fit value for $\frac{\partial T}{\partial r}$ at the contact ($r = 0$) of $-1.8^{o}\mathrm{Cm}^{-1}$, although the uncertainty in the data on which Fig. 5.2 is based is such as to permit values of $\frac{\partial T}{\partial r}$ at the contact of between -1 and $-3^{o}\mathrm{Cm}^{-1}$. Values of k at high temperatures for natural rocks are scarce. However, Murase & McBirney (1973) determined values of k at high

temperatures for a number of rock types and found that k varied little between an andesite and a rhyolite (which between them cover much of the compositional variation in the M1 aureole), values being in the range 8.4 - 12.6$Wm^{-1}K^{-1}$ at 1100°C. This yields a most - likely value of Q_c of 20Wm^{-2}, with a possible range of 8 - 38Wm^{-2}.

As was shown in Chapter 4, $Q_m \approx Q_c$ at the end of M1. It is however important to know by how much Q_m could have exceeded Q_c within the constraints provided by the available data. As noted in Chapter 4, the rate of anatectic magma production at the wall of the magma chamber is poorly constrained by observations made in the contact zone because of the uncertainty regarding how much of the melt produced has been preserved at the present level of exposure, as well as the uncertainty regarding the length of the period during which melt was produced. However, as noted in section 5.2.2, the outward velocity of the contact is limited by the width r_{I1} of the M1 aureole, according to the relationship between the velocity a of the boundary and the width of the conductive boundary layer in front of it:

$$r_{I1} \approx -\frac{\kappa}{a}\left(\ln\left(1-\frac{T_c - T_{I1}}{T_c - T_{M0}}\right)\right) \tag{5.3}$$

(modified after Carslaw & Jaeger 1959; Lister 1974) where r_{I1} is the true thickness of the M1 aureole from the contact to the first isograd defined in section 5.2.1, T_{I1} is the temperature corresponding to that isograd, T_{M0} is the ambient rock temperature (given by the temperature of M0 metamorphism) and T_c is the contact temperature.

(5.3) strictly only applies to a planar boundary (that is to say, to one - dimensional heat flow). However, the width of the M1 aureole is small compared to the size of the MBG and the departure from non - planar geometry could therefore only have a small effect upon the relationship: in any case, the effect would be to overestimate the maximum value of a compatible with the width of the aureole. Convective heat transfer in the aureole would also tend to reduce the maximum value of a compatible with the width of the M1 aureole. Fig. 5.2 indicates that the value of r_{I1} is of the order of 500m, which yields maximum values of a of the order of $2 \cdot 10^{-9}$ - $10^{-9}ms^{-1}$, using the values of thermal diffusivity (κ) from above. Values of the latent heat of melting of crustal rocks lie in the range 150 - 500$kJkg^{1}$ (Nicholls & Stout 1982). Rearrangement of equation 4.3 then yields **maximum** values of (Q_m - Q_c) in the range 1 to 3Wm^{-2}. It appears that Q_m was within 10% or so of Q_c at the end of M1.

Given the temperature difference of 60 – 150°C across the thermal boundary layer of the magma chamber which was deduced in Chapter 4, values of Q_m in the range 8 – 40Wm^{-2} yield estimates of the heat transfer coefficient h in the range 0.05 – 0.63$Wm^{-2}K^1$. The preferred value of about 20Wm^{-2} for Q_m gives values of h between 0.14 and 0.36$Wm^{-2}K^{-1}$. This estimate of h can clearly only be regarded as an order - of - magnitude estimate. However, equation 4.5 suggests that h may vary by a factor of the order of 10^5 between olivine basaltic and rhyolitic magmas at their liquidus temperatures, since liquidus viscosities vary by a factor of about 10^8 over this compositional range (Murase & McBirney 1973). It follows that, given the availability of suitable intrusions and contact aureoles, further studies of heat flow in contact aureoles should yield useful data on the variation in magma chamber behaviour with the composition of the magmas present.

The values of Q_m and h which have been determined in this section are very much lower than those predicted by constant - viscosity boundary layer theory: for example, Huppert & Sparks (1989) suggest values of Q_m of the order of 10^3Wm^{-2} for turbulently convecting basic magma chambers. However, as noted in section 4.1, the assumption that the magma in the thermal boundary layer is a constant - viscosity fluid with no yield strength is invalid: the discrepancy between the theoretical estimates and the value of Q_m deduced above for the MBG magma chamber can perhaps be taken as an indication of the magnitude of the error introduced by the assumptions of constant viscosity and Newtonian behaviour.

A check on the validity of this determination of Q_m is provided by a calculation of the thickness L_s of a stagnant conductive layer of magma which would insulate the wall of the magma chamber from convection in the interior to the same extent as the semi - stagnant thermal boundary layer. L_s is given by:

$$Q_m = h(T_m - T_{contact}) = k_m \frac{(T_m - T_{contact})}{L_s} \tag{5.4}$$

where k_m is the thermal conductivity of the magma. Hence:

$$L_s = \frac{k_m}{h} \tag{5.5}$$

Inserting the values of h obtained above and a value for k_m of 12$Wm^{-1}K^{-1}$ (thermal conductivity of a ferrobasaltic magma at 1200°C; Murase & McBirney (1973)) into (5.5) yields an estimate of L_s of between 19 and 240m, with a preferred value of between 33 and 86 metres, assuming that $Q_m = Q_c$

exactly. Since convective as well as conductive heat transfer will, by definition, occur in the thermal boundary layer, L_s must be regarded as a lower limit for the thickness of the thermal boundary layer. Conversely, since, again by definition, there must be significant temperature gradients in the thermal boundary layer, the true thickness is not going to be very much greater (perhaps by no more than a factor of 2 to 4). The estimated boundary layer thickness, like the value of Q_m at the end of M1, differs by 2 – 3 orders of magnitude from the thicknesses predicted by constant - viscosity boundary - layer theory for basaltic magma chambers with liquidus viscosity values used (e.g. Lister 1983a; Spera et al. 1982), but in the opposite direction. This is as would be expected because the two are inversely proportional to one another (equation 5.4).

The value of L_s for the MBG magma chamber obtained in this study is not so great, however, to be inconsistent with the model of the MBG magma chamber presented in Fig. 4.31. This has an interior with negligible horizontal temperature gradients and relatively narrow thermal and mechanical boundary layers; similarly, values of L_s calculated using the preferred values of $\frac{\partial T}{\partial \tau}$ and hence Q_m, are only 1 – 2.5% of the radius of the MBG magma chamber at the present level of exposure. The true thickness is therefore unlikely to have been more than 5 – 10% of the radius of the intrusion. The width of the mechanical boundary later separating the thermal boundary layer from the interior of the intrusion, in which neutrally buoyant magma at T_m is dragged down the wall of the chamber by the descending cooled magma can be described in terms of a constant - viscosity fluid (e.g. Spera et al. 1982) and is likely to be much thinner than the variable - viscosity thermal boundary layer whose thickness is deduced here. It follows that the majority of the chamber was not directly affected by the downflow at the chamber walls, as is independently implied by the evidence for stratification of the interior of the chamber.

5.2.4.2 Implications of the value of Q_m for mass fluxes in the boundary layer of the MBG magma chamber at the end of M1.

A central feature of boundary - layer theory as applied to magma chambers is that although heat is transferred out of the boundary layer to the wall of the intrusion by conduction, and heat may be transferred within the boundary layer partly by conduction, heat is introduced into it from the interior of the magma chamber purely by advection. Assuming the MBG boundary layer to be at or close to a steady state at the end of M1, with the heat flux into the boundary layer at its inner

surface being the same as the heat flux out of the wall of the chamber, this means that the estimate of Q_m made above can be used to make an approximate estimate of mass fluxes, and hence flow velocities, into and out of the boundary layer at the end of M1. Two quantities are of particular interest. The first of these is the mean velocity V_x with which magma at the liquidus temperature T_m flowed toward the boundary layer from the interior of the chamber, and the second is the mean velocity of the boundary layer flow down the wall of the chamber due to thermal contraction of the cooled magma in the boundary layer. The variation in flow velocities about these mean velocities cannot be constrained by the inferred value of Q_m. **It should be noted that V_x as defined here is NOT the average velocity of horizontal flow at the wall which, when density flows across the floor of the chamber (Fig. 4.31) are included, must be zero if the wall of the chamber is not moving, the flow of hot magma towards the wall of the chamber being balanced, volume for volume, by the volume of cooled magma flowing in the opposite direction.**

The simple thermal – balance model used here to model heat and mass flows in the M1 boundary layer is illustrated in Fig. 5.4. Lateral horizontal magma flows within the thermal boundary layer are ignored; these might have a significant effect on the pattern of heat flow if magma flowed into and out of the boundary region in distinct large regions which were stable over long periods, but there is no evidence to suggest this. The boundary layer is therefore divided into a large number of vertical elements of unit width parallel to the wall, height y_L equal to the depth of the magma chamber and thickness x_L equal to the thickness of the thermal boundary layer, each of which is considered in isolation. Although thermal boundary layers are normally considered to grow in thickness from the free leading or upstream edge of the cooled or heated surface (for example, a heat exchanger plate or turbine blade) (Eckert & Drake 1987), the concept of a free upstream edge is meaningless when applied to the wall of the MBG magma chamber because the boundary layer must have been attached, at its upstream end, to another, near - horizontal boundary layer, either at the roof of the chamber or at the base of the permanently buoyant layer of granitoid magma which may have been present at the roof of the chamber (Fig. 4.31). This horizontal boundary layer would itself have been undergoing cooling and may have released a certain amount of cooled melt into the wall boundary layer, although it cannot have been the sole source of cooled magma in the wall boundary layer because of the wide variety of magma compositions present in the latter. In the absence of precise information on any variation of x_L with height that may have occurred it is assumed here

Fig. 5.4 Diagrammatic element of the M1 thermal boundary layer showing mass fluxes into and out of the layer.

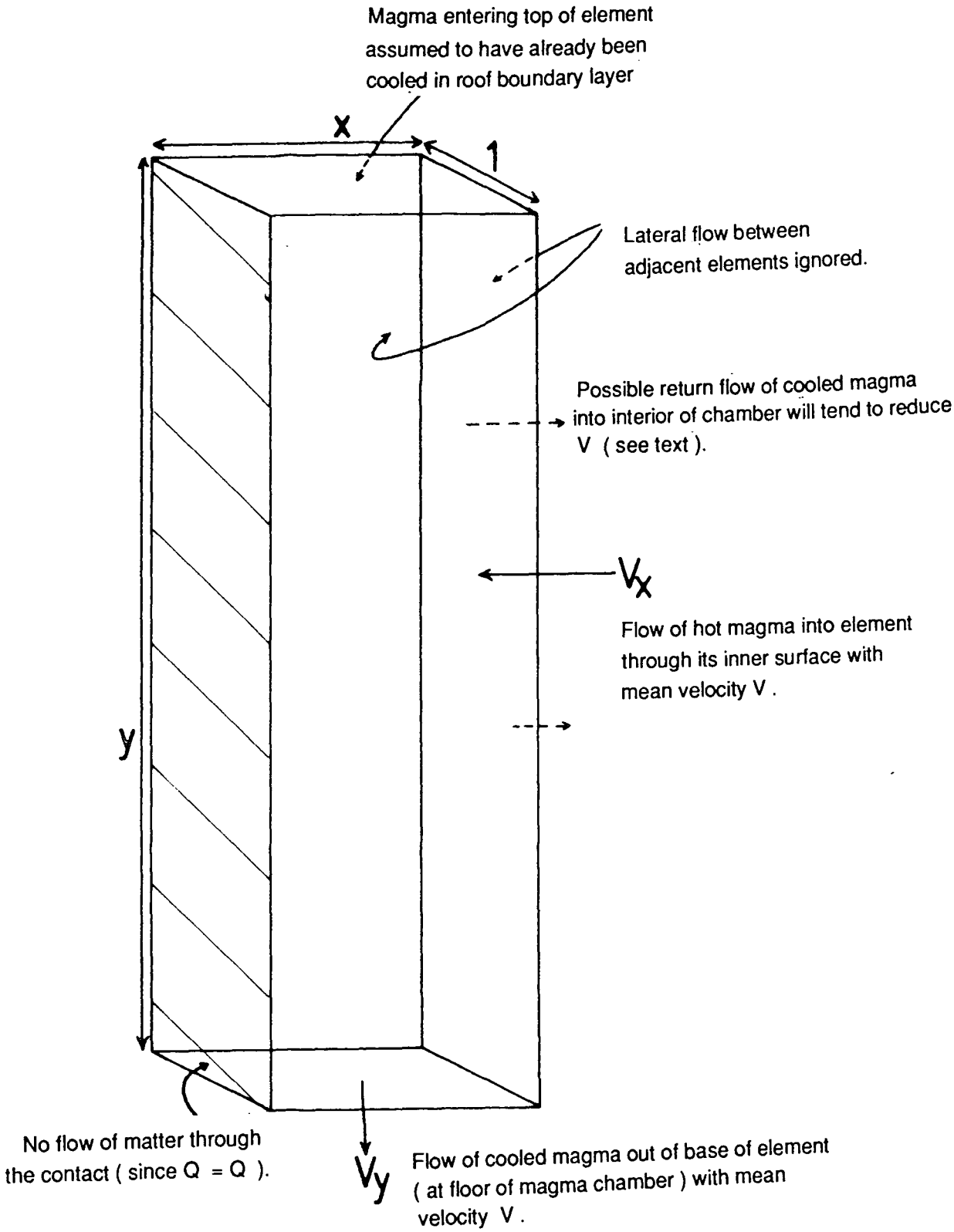

y = height of magma chamber

X = thickness of boundary layer

that x_L was a constant for the period under consideration; it is certainly the case that variations in x_L between the various sections of the M1 contact zone which have been examined was not so great as to cause formation of M1 sidewall cumulates or large scale melting and mobilisation of the main wall of the intrusion in different areas (as opposed to in the downfaulted blocks, around which x_L may have shown small - scale variation (Fig. 4.32)).

From the point of view of the thermal balance relationship, magma at the temperature of the interior of the magma chamber T_m is assumed to enter the element shown in Fig. 5.4 at its inner surface, be cooled by some average amount $\Delta T'$, and then flow out through the same surface or through the base of the element after flowing all the way down the wall of the chamber. Assuming that the change in density is small compared to its initial value (the Boussinesq approximation) it is then possible to write an expression for the mean velocity of flow of hot magma into the layer at its inner surface where the temperature gradient is small and heat transfer is largely convective:

$$V_x \approx \frac{Q_m}{\rho c_p \Delta T'} \tag{5.6}$$

where ρ and c_p are the density and specific heat (including a component for latent heat release on cooling) of the input magma. The discussion of values of $\Delta T'$ needed to reverse the density relationships of intermediate and basic magmas (section 4.3.3) suggests that it was at least 50°C, from the occurrence of significant downflows of compositionally contrasted magmas which were initially stably stratified. Any magma which entered the thermal boundary layer and was cooled by less than 50°C before leaving it again would be unlikely to contribute to this downward flow. However, $\Delta T'$ must have been significantly less than about 60°C because none of the magma in the boundary layer can have been cooled below its rigidus temperature during M1 (see section 4.5 for the argument on which this value of ($T_m - T_r$) is based). These two constraints are only marginally consistent with one another but given the assumptions and uncertainties involved in the density calculations in particular this may not be a significant problem. Assuming $\rho = 2800 \mathrm{kgm}^{-3}$ (section 4.3.3) and $c_p = 1100 \mathrm{Jkg}^{-1}\mathrm{K}^{-1}$ (Nicholls & Stout 1982), equation 5.6 yields values of V_x between $5.4 \cdot 10^{-8} \mathrm{ms}^{-1}$ and $6.5 \cdot 10^{-7} \mathrm{ms}^{-1}$ for the range of controlling variables given in Table 5.1, below, with a value of $1.6 \cdot 10^{-7} \mathrm{ms}^{-1}$, equivalent to only 5 metres per year, for the preferred value of Q_m and $\Delta T' = 40$°C. It should be noted that V_x is the **mean velocity** of the hot magma towards the wall of the chamber. If the magma was in a state of turbulent or chaotic convection in the interior of the chamber then the average speed (or root mean square velocity) of flow of the magma could be much greater in regions of the chamber away from the wall.

The mean vertical velocity V_y of the cooled magma descending the wall of the chamber in the thermal boundary layer is not as easily determined as V_x because it depends on the proportion of the magma which enters the boundary layer which leaves it at its base – in other words, the proportion of the magma in the boundary layer which flows all the way down to the floor of the chamber. The inference that boundary layer detachment may have taken place at the tips of downfaulted blocks (sections 4.2.6 and 4.5, especially Fig. 4.32), together with field observations which suggest mixing of basic and intermediate or hybrid magmas at the inner edge of the contact zone proper (section 3.2), implies that there was a return flow of cooled magma into the interior of the MBG magma chamber through the inner surface of the boundary layer shown diagrammatically in Fig. 5.4. It is therefore only possible to place an upper limit on the value of V_y at steady - state, which is given by:

$$V_y < \frac{y}{x} V_x \tag{5.7}$$

The actual value of y is poorly known, because the top of the MBG magma chamber has been eroded away and its subsurface structure is only constrained by the geophysical data for the thickness of the Ardnamurchan central complex as a whole. However, it can hardly have been outside the range 1 – 3km. The only available constraint on x is its minimum thickness, given by the thickness L_s of the equivalent stagnant layer (section 5.2.4.1). Again, however, inserting a minimum value for x into (5.7) yields a maximum value for V_y. Setting $y = 3000$m and $x = 30m$ and combining equations 5.6 and 5.7 yields a maximum value for V_y of between $5.4 \cdot 10^{-6} \mathrm{ms}^{-1}$ and $6.5 \cdot 10^{-5} \mathrm{ms}^{-1}$ (equivalent to 2000 metres per year at absolute maximum, and probably less than 1000m/yr). This is much less than estimates of the maximum velocities of downflowing currents deduced on the basis of the structure of igneous layering in the Skaergaard intrusion, a body comparable in size and composition to the MBG magma chamber (3000m/day: Shimazu 1959; Wager, 1968) and from scaling of analogue experiments to the properties of basaltic magmas (up to 5km/h; Irvine 1980b). However, both of these estimates are for the maximum velocities of intermittent currents and Wager in particular considered that the intermittent flows were superimposed on a much slower continuous 'background' flow with velocities somewhat less than the upper limit on V_y calculated above.

The heat fluxes and flow velocities at the wall of the MBG magma chamber at the end of M1 which have been estimated in this section are summarised in Table 5.1, below. The first column of data in this table contains values calculated using a value for the temperature gradient at the contact of

Table 5.1

Heat fluxes at the end of M1, the heat transfer coefficient h for the M1 MBG magma chamber boundary layer, and limits on the thickness of and flow velocities in this boundary layer

Method of calculation of these parameters discussed in text

Quantity	Best fit value or range	range permitted by data
$Q_c(Wm^{-2})$	21.6	8 - 38
$Q_m(Wm^{-2})$	21 - 24	8 - 41
$h(Wm^{-2}K^{-1})$	0.14 - 0.36	0.05 - 0.63
L_s(m)	33 - 86	19 - 240
$V_x(ms^{-1})$	$1.6{\cdot}10^{-7}$	$5.4{\cdot}10^{-8}$ - $6.5{\cdot}10^{-7}$
$V_y(ms^{-1})$	—	$<(\ 5.4{\cdot}10^{-6}$ - $6.5{\cdot}10^{-5}\ )$?

$-1.8°Cm^{-1}$, the best – fit value from Fig. 5.2, and the second contains the range of values associated with the permitted range of thermal gradients, from -1 to $-3°Cm^{-1}$. In both cases values for a range of temperature differences across the contact from 60 to 150°C are given as appropriate.

5.2.4.3. An estimate of the minimum duration of M1.

The end - M1 thermal profile in Fig. 5.2 can also be used to make an estimate of the minimum duration of M1, by assuming purely conductive heat transfer within the M1 aureole and applying a modified form of the conductive heat transfer equations for heat flow from a fixed boundary (see below). As noted in section 5.2.4.1, this assumption may be incorrect, for two reasons. Firstly, a limited amount of convective heat transfer may have taken place within the M1 aureole due to the movement of hydrous fluids (section 5.2.3). Secondly, melting at the margin of the intrusion could have caused a significant overall outward migration of the contact during M1. Both of these processes, however, would have the effect of slowing the approach to thermal equilibrium in the aureole and hence lengthening the time taken to achieve the thermal profile indicated in Fig. 5.2, to infinity if the thermal profile shown is in fact an equilibrium one and its curvature is caused solely by one or both of these effects.

Instead of attempting to model these effects, which is necessary if the true duration of M1 is to be determined by means of thermal modelling, and for which the necessary data are not available, the remainder of this section deals with the simpler problem of the minimum duration of M1. However, even this simpler problem involves a number of assumptions which have to be made as part of its solution. These are discussed below, together with plausible values of the variables to be used in the calculations.

1). Heat source characteristics. The heat source (the MBG magma chamber) is assumed here to approximate to a constant - temperature source fixed at the present - day position of the boundary. This is equivalent to saying that the MBG magma chamber was emplaced instantaneously with its final shape, had constant composition (and therefore temperature) throughout its history, and that no significant chill zone formed on the wall of the intrusion during the earliest part of its history when temperature gradients and therefore heat fluxes in the adjacent country rocks were highest. All of these assumptions are likely

to have been more or less incorrect. The growth of the magma chamber cannot have been instantaneous, although the period over which it was emplaced with a geometry close to its end – M1 form may have been short compared to the length of M1 (see Chapter 7 for further discussion of the mechanisms and rates of emplacement of the MBG). In the absence of substantial superheating or the presence of more than a few percent of suspended crystals, the temperature of the heat source is in this case governed by the composition of the magmas in the interior of the chamber. The inference that the interior of the chamber contained magmas ranging in composition from 3% MgO to 8% MgO (section 4.3) implies that source temperatures may have ranged from perhaps 1050°C to perhaps 1200°C. A constant temperature of 1200°C is assumed here and the thickness of the thermal boundary layer of the chamber is ignored; the effect of both of these will be to cause an underestimate of the length of M1. The assumption of no significant chill zone formation is also probably invalid: although Huppert & Sparks (1989) calculate that the lifetime of chilll zones at the wall of basic intrusions should be measured in days or hours, these lifetimes were calculated on the basis of values of Q_m which were estimated theoretically, using constant - viscosity boundary layer theory. These values of Q_m are two to three orders of magnitude greater than the value of Q_m that was estimated in section 5.2.4.1 for the MBG magma chamber during M1. The lifetime of a chill zone should be very sensitive to Q_m as this will determine both the length of the period during which Q_m is less than Q_c, during which the chill zone will be increasing in thickness, and the rate at which the chill zone is subsequently eroded by the convecting magma (Huppert & Sparks 1989). However, in the case of the MBG magma chamber any chill zone that did form early in M1 must have been entirely lost by its end, when Q_c was still approximately equal to Q_m. It follows that the period and rate of chill erosion must both have been small and that therefore the thickness of any chill zone present at the wall of the MBG magma chamber at any time after its initial emplacement must have been small. Possible reasons for this discrepancy between prediction and observation include preheating of the rocks which form the wall of the MBG at the present day by earlier intrusions with their contacts just inside its present position (although it is remarkable that no other evidence of these has been preserved) and mechanical spalling of the early chill zone by thermal or emplacement - related stresses (Furlong & Myers 1985). The effect of ignoring any thermo - mechanical erosion of the wall rocks upon the estimate of the duration of M1 will, like the effect of ignoring purely thermal erosion, be to underestimate its length.

2). Heat source geometry and the effects of proximity to the surface of the Earth. The geometry of the MBG magma cchamber at the present level of exposure is well constrained. An upper limit on its vertical extent below the present level of exposure of 3 to 5 kilometres is provided by the geophysical data reviewed in Chapter 2 (Bott & Tuson 1963; Barrett 1987; Harrison 1987; see also the discussion in Chapter 7). A lower limit on its buried vertical extent is provided by the presence of melts derived from wall rocks which must be some way below the present level of exposure (Chapter 4) and by the amplitude of the dome structure around the intrusion (at least 0.5 kilometres; see Chapter 7) which can only have been produced by a body whose base is at least at a similar depth below the surface. The principal uncertainties regarding the geometry of the MBG magma chamber as far as thermal modelling of the M1 aureole is concerned have to do with its shape above the present level of exposure and its depth below the palaeosurface. However, the sub - parallelism of the apparent isograds in the aureole with the contact, and the complete absence of roof contacts anywhere in the outcrop of the MBG suggest that the roof was at least a few hundred metres above the present level of exposure. Similarly, the pressure constraints discussed in section 4.2.5 and the coherent behaviour of the concentric fault system (section 4.2.5 and Chapter 7) suggest that the surface of the Earth was at least 1 kilometre above the present level of exposure, although probably no more than 4 kilometres. The M1 aureole is itself less than a kilometre wide in a direction perpendicular to the contact, from which it follows that the conductive thermal gradient at the surface of the Earth due to heat loss at the present level of exposure can only have been slight (a similar argument is used by Irvine (1970)). It follows that the proximity of the surface of the Earth, which can be regarded as a constant - temperature boundary, can only have had a slight effect upon heat flow at the present level of exposure.

It is therefore valid, as a first approximation, to treat the MBG magma chamber as being set in an infinite host for the purposes of thermal modelling of M1 metamorphism. In the absence of more precise data, the shape of the MBG magma chamber is taken to approximate to a sphere of radius 3500m. This is the closest approximation to the shape of the MBG magma chamber for which an analytical solution of the heat - flow equation is available. The true shape of the MBG magma chamber is likely to be closer to a section of this sphere bounded by horizontal planes above and below the present level of exposure (Fig. 5.5). However, the differences between this shape and

Fig. 5.5 The spherical approximation to the shape of the MBG magma chamber for the purposes of estimating the duration of M1 by thermal modelling.

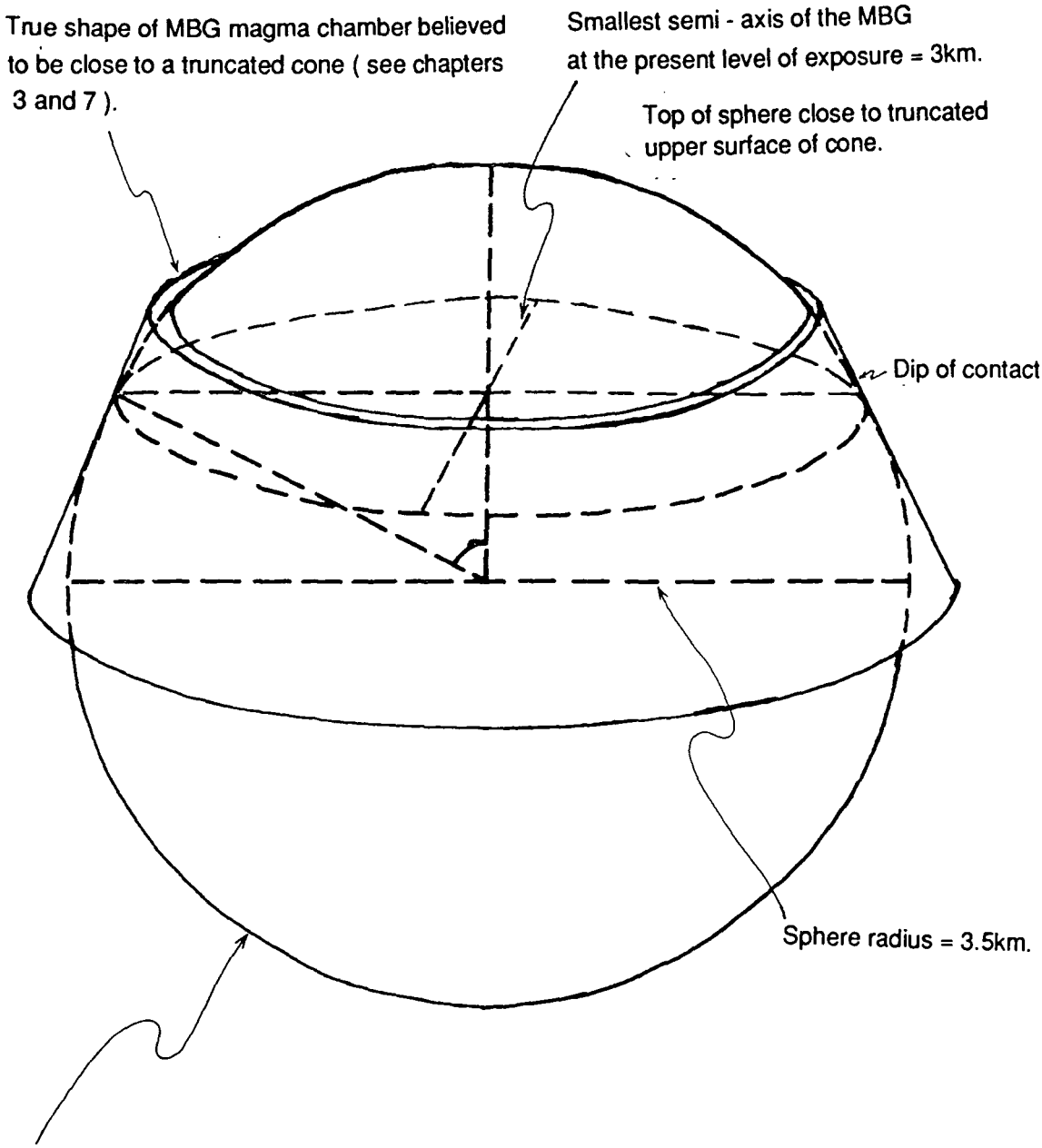

a complete sphere mainly occur well above and below the present level of exposure and will have relatively little effect on the results. Once again, the approximations made regarding the heat source made in this section will tend to cause underestimation of the length of M1.

3). Latent heat absorbtion by melting and metamorphic reactions in the M1 aureole. The effect of latent heat absorbtion by endothermic reactions such as melting and dehydration reactions can be modelled either as a decrease in effective thermal diffusivity, appropriate for continuous reactions, which take place over a finite temperature range, or as discrete heat sinks within the contact aureole (more appropriate for discontinuous reactions at specific temperatures). The latter approach was adopted by Irvine (1970). In the case of the M1 aureole, most of the reactions considered in section 5.2.1 are continuous and the former treatment is more appropriate. The data needed to precisely evaluate the variation in effective thermal diffusivity with temperature due to the occurrence of endothermic reactions (principally the temperatures at which reactions occur and the amounts of material involved in the reactions averaged over the various rock types in the aureole)are not available. However, given the other uncertainties discussed above, no great amount of additional error will be introduced by repeating the calculations below for two values of effective thermal diffusivity which bracket the likely range of values based on the data of Murase & McBirney (1973) and Nicholls & Stout (1982) ($10^{-6}m^2s^{-1}$, a value appropriate for unreactive rocks, and $0.5{\cdot}10^{-6}m^2s^{-1}$, appropriate for rocks which absorb about twice as much heat in dehydration and melting reactions as a typical granitoid).

To summarise, the MBG magma chamber is modelled here as an instantaneously - emplaced (at time $t = 0$) spherical body with a constant surface temperature T_1 of 1200°C and radius r_i = 3500m, emplaced into an infinite medium. This has an initial temperature T_0 of 300°C and thermal diffusivity κ of one or other of the two values given above. The temperature at any time t and distance r outside the surface of the sphere (equivalent to distance from the contact of the MBG if the approximations made are valid) is then given by a modified form of the error - function equation for the temperature distribution outside a sphere (Carslaw & Jaeger 1959):

$$T = \frac{r_i}{r + r_i}(T_1 - T_0)\mathrm{erfc}\frac{r}{2\sqrt{\kappa t}} + T_0 \qquad (5.8)$$

Solutions of equation 5.8 for different times in years after the initial emplacement of the model

Marginal Border Group magma chamber are presented graphically in Fig. 5.6.1 ($\kappa = 10^{-6}m^2s^{-1}$) and Fig. 5.6.2 ($\kappa = 0.5 \cdot 10^{-6}m^{-2}s^{-1}$). The best - fit curve through the constraints on temperatures at the end of M1 from Fig. 5.2 is also marked in these diagrams. Although the inferred temperatures in the inner part of the aureole are not sufficiently precise for them to provide useful constraints on the duration of M1, it is apparent that the biotite, muscovite - out isograd would have taken a minimum of perhaps three to ten thousand years to migrate out to its observed end - M1 position. M1 must therefore have lasted at least a few thousand years and may well have lasted longer, particularly if advective heat transport by hydrothermal fluids in the M1 aureole was significant. The true duration of M1 is, as noted above, uncertain, but can hardly have been more than a hundred thousand years or so, given that the entire Ardnamurchan central complex was emplaced in less than two million years (Dagley et al. 1984).

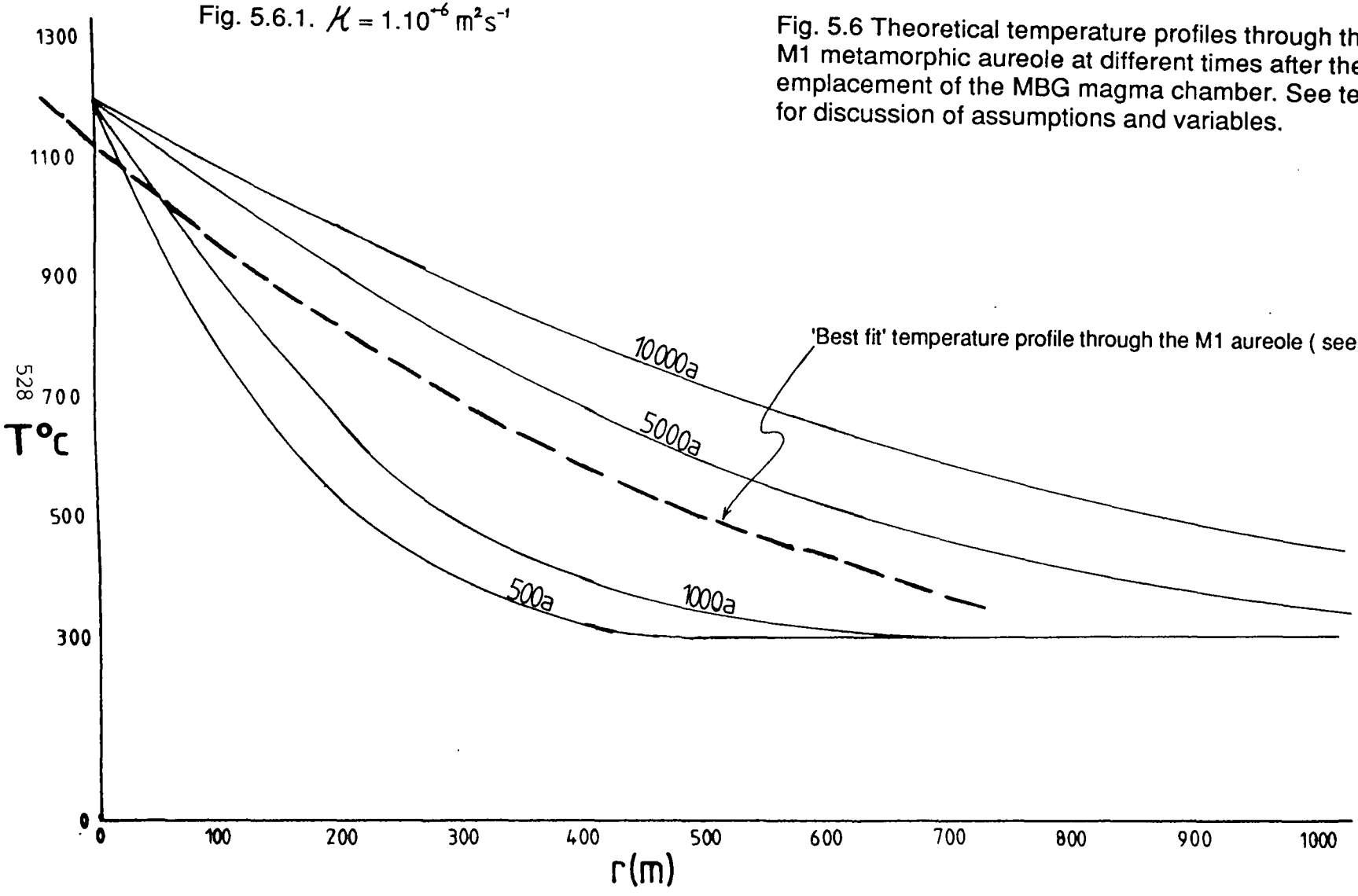

Fig. 5.6 Theoretical temperature profiles through the M1 metamorphic aureole at different times after the emplacement of the MBG magma chamber. See text for discussion of assumptions and variables.

Fig. 5.6.2. $\chi = 0.5.10^{-6}\ m^2 s^{-1}$

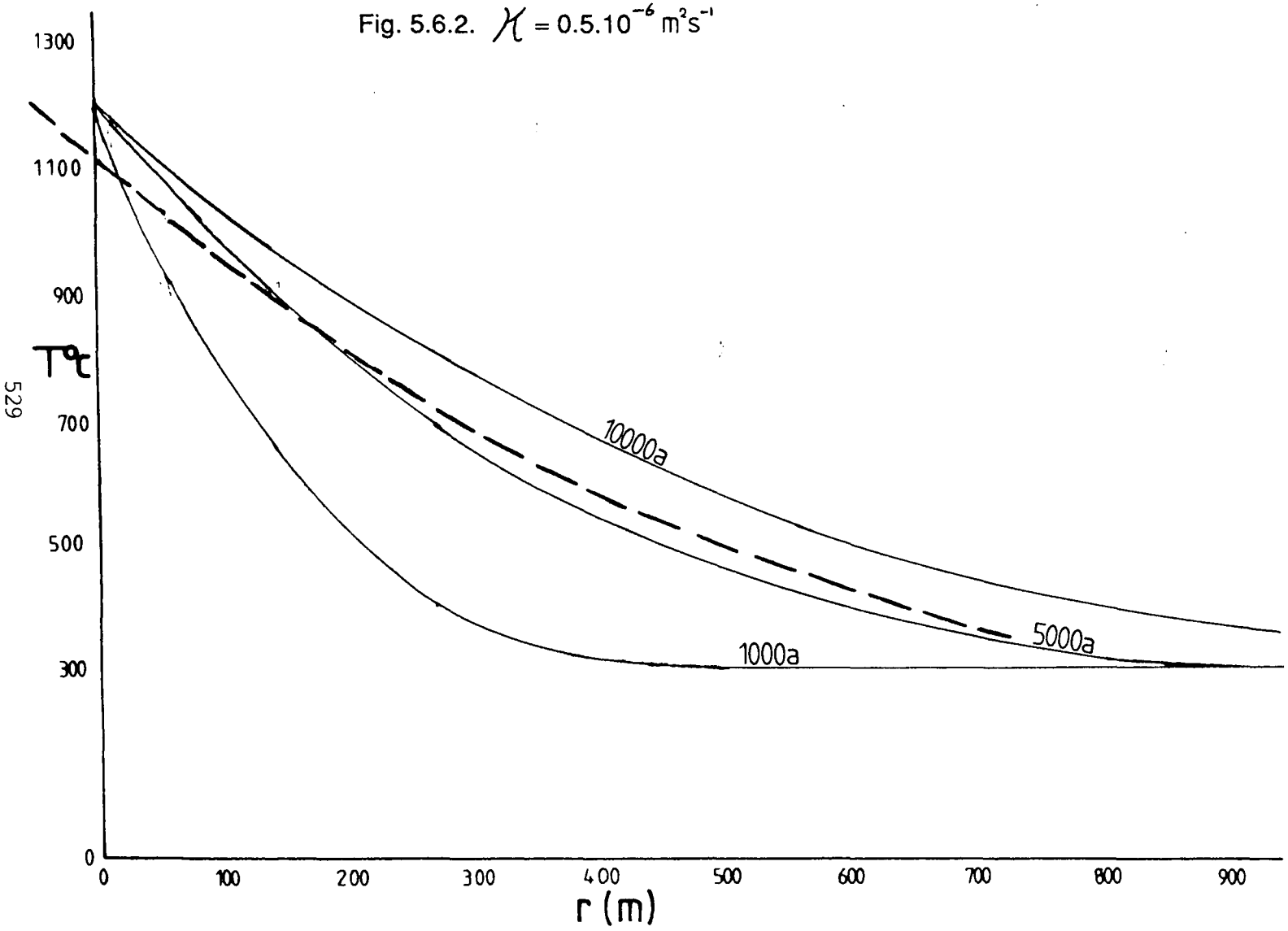

5.3. The quenching event(s) at the end of M1.

The subjects of this section are the abrubt cooling of the M1 aureole (and the associated partial quenching of anatectic melts in the aureole) and the subsequent rapid solidification of the Marginal Border Group of the Hypersthene Gabbro. Quench - textured and other rapidly cooled anatectic rocks have also been described from the contact aureoles of other large shallow intrusions. The include the southeast margin of the Cuillins complex in Skye (Wager et al. 1953), the aureole and marginal group of the Rhum ultrabasic complex (Dunham 1964; Greenwood 1987) and the contact aureole of the Skaergaard intrusion (Kays et al. 1981). The occurrence of these rocks is generally ascribed to sudden cooling associated with the development of a vigourous hydrothermal system after an earlier period of high - grade thermal metamorphism. However, the physics of the process or processes whereby vigourous hydrothermal circulation can suddenly develop around a subvolcanic or other upper crustal magma chamber has not been examined in detail in the context of intraplate central intrusive complexes. Rather more work, largely of a theoretical nature, has been done on the physics of hydrothermal systems at mid - oceanic ridges (see review by Lister (1983b)) and above subaerial lava lakes (Ryan & Sammis 1981). One of the main aims of this section will be to examine the application of the theoretical work of Lister and others to the interpretation of the end - M1/earliest M2 quenching event or events which occurred around and within the Marginal Border Group.

5.3.1. The tensile fracture network in the M1 contact aureole and in minor felsic intrusions of early M2 age.

The association of rapid cooling with hydrothermal activity in the rocks around the MBG is immediately suggested by the development, at the same time as the cooling (see section 3.2) of a dense network of thin joint - like veins filled with hydrothermal mineral assemblages (sections 3.2.2 and 3.2.5.5 in particular). Similar networks also occur in the quenched and devitrified M2 felsite intrusions (section 3.2, especially Plate 3.28). The general characterisitics of these veins can be summarised as follows:

1). Mechanism of formation. The vast majority of hydrothermal mineral - filled veins of this age appear to be tensile fractures with little or no offset of the margins parallel to the vein walls, no

Plate 5.2. Joint - like tensile fractures in M2 felsite, sample 42F2. Note lack of deformation around fractures, blocky quartz fill in the fractures. Plane - polarised light, field of view 14mm.

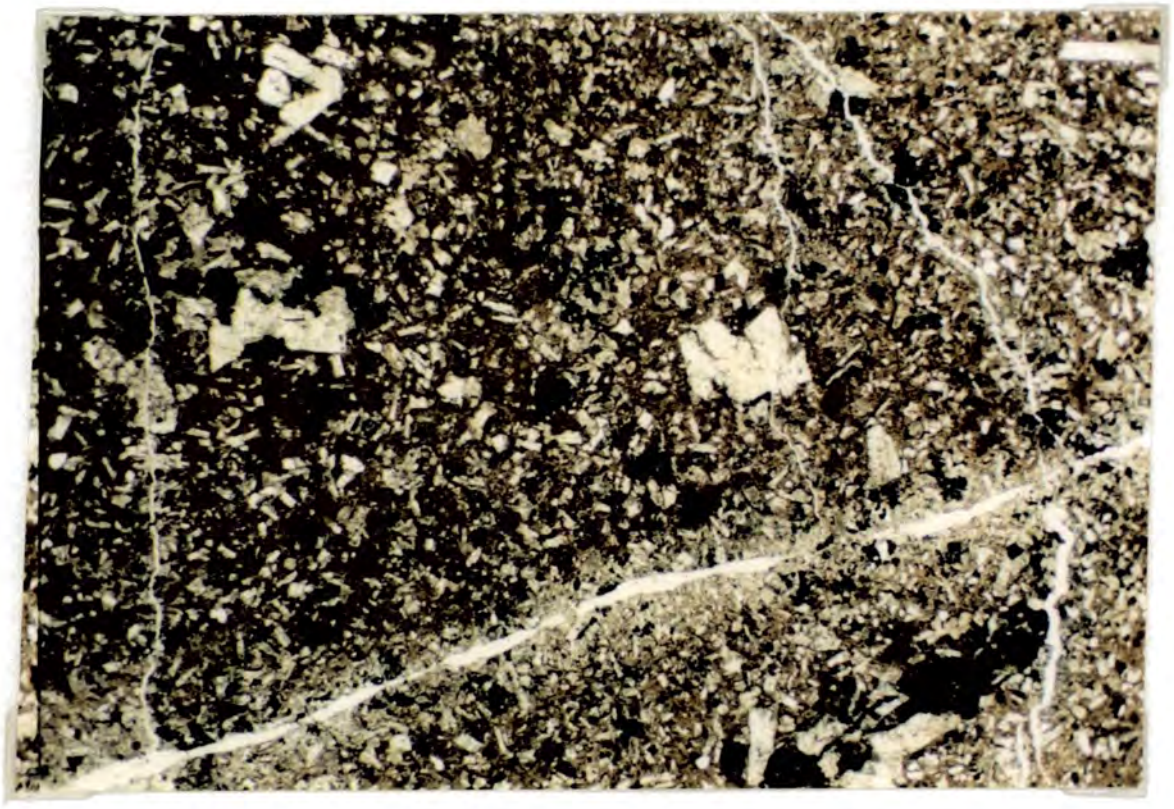

cataclastic deformation of the walls, and planar geometries. Lensoid and irregular veins and cavities filled with hydrothermal minerals which are associated with releasing bends in fault zones do occur in some outcrops, but are very distinct from the tensile fracture vein networks, both at outcrop and in thin section. They are particularly distinctive in thin section, as they are enclosed in much larger regions of fine - grained and banded cataclastically deformed rock.

2). Vein widths. The widths of the tensile fracture veins range from 0.1 to 0.2 millimetres downwards, with numerous smaller fractures branching off from the main fractures in some thin sections (Plate 5.2) and also occurring apparently independently in sections which do not contain larger fractures. The smallest fractures observed are only a few microns thick but there appears to be a definite lower size limit. The latter may be a result of later annealing rather than a primary feature, however. A few veins up to 1 to 2 millimetres thick were found in some sections but most of these are demonstrably associated with shear fractures, segments of thick dilational veins in the same slide being connected by cataclastic shear zones. This phenomenon may reflect exploitation of particularly large tensile fractures by shear stresses, however, rather than a primary shear origin.

It should be noted that the observed vein widths do not necessarily correspond to the widths of the open fractures at any one time because they may have opened gradually or incrementally, being largely closed by hydrothermal mineral deposits at most times. However, no evidence of incremental or multi - stage mineral deposition was observed in thin section (in strong contrast to the fracture vein networks in the Inner Series (section 3.4.6 and Chapter 6)). This is consistent with the theoretical model for fracture formation discussed below, which suggests that the tensile fractures should open in a single - stage process.

3). Tensile fracture vein spacings. The spacing of the larger tensile fracture type veins in particular is difficult to determine at many outcrops without very close examination because of the presence of numerous, much later joints (characterised by clayey alteration and iron oxyhydroxide staining of the joint surfaces) which may have followed veins or fractures associated with the quenching event in any particular outcrop. However, in certain outcrops (most notably that shown in Plate 3.21) the earliest generation of tensile fractures is readily identified at outcrop by the presence of hydrothermal minerals in the veins and by the advanced devitrification/alteration haloes which occur around the veins. In such outcrops, the largest tensile fracture veins show a fairly uniform

spacing, between 10 and 30 centimetres apart. Larger veins at more widely - spaced intervals were not observed in these outcrops; the larger, more - or - less sheared veins noted above have an irregular or sporadic distribution.

The spacing of the smaller tensile fracture veins appears to be roughly proportional to their size: around half of the thin sections (about 2cm by 3cm) of rocks from the inner part of the M1 aureole which were examined were found to contain at least one tensile fracture vein between 10 and 50 microns thick, suggesting that fractures of this size are spaced at intervals of the order of 2 – 5 cm. This is similar to the spacing of joints at outcrop. The smallest fractures identified occur at spacings of 5mm or less in some sections but are less common in others.

4). Vein orientations. Within any particular outcrop the tensile fracture veins mostly fall into a number of groups orientated at high angles to eachother. Veins which are roughly parallel and roughly perpendicular to the adjacent MBG contact are particularly common: the latter occur in roughly vertical and horizontal sets. When all of the joint - like structures (as noted above, it is often difficult to identify the earliest post M1 fracture sets) in most outcrops are considered together, vertical fractures radial to the pluton appear to be most common; however, the veins shown in Plate 3.21 show no strong preferred orientation out of the three near - perpendicular sets present.

5). Vein Lengths. The largest tensile - fracture veins observed can be traced across the whole of the outcrops (up to a few metres wide) in which they occur, and must therefore be at least this long. The smaller (below 50 microns thick) fractures tend to die out within distances of a few centimetres, however.

Many of the larger tensile fracture veins can be seen, either by close examination of the outcrops or in thin section, to be interrupted in two dimensions by asperities in the fracture walls at intervals of a few centimetres or so. The veins appear to be continuous in three dimensions, however, and the individual asperities are at most only a few millimetres across. They therefore approximate fairly closely to continuous planar fractures, with the vein walls being in contact over only a few percent of their areas.

There are no marked differences between the tensile fracture vein networks in the rocks of the M1

contact aureole and those which occur in the M2 felsites, although they must have formed in separate events. This suggests that their characteristics are controlled by a common formation mechanism operating under similar conditions.

5.3.2. Application of the theory of thermal contraction cracking and cracking front propagation to the quenching event.

5.3.2.1. Thermal contraction cracking and self - propagating hydrothermal systems.

The phenomenon of thermal contraction cracking arises from the positive coefficient of thermal expansion of all materials, including rocks. When an elastic body is cooled and not allowed to contract, a tensile stress is set up in it which is given by:

$$\sigma = \frac{E\alpha\Delta T}{(1-\nu)} \tag{5.9}$$

(Timoshenko & Goodier 1970)

where E = Young's modulus for the material concerned, α = linear coefficient of thermal expansion, ΔT = amount by which the body is cooled, ν = Poisson's ratio for the material concerned. In the context of the rocks of the M1 contact aureole and the MBG itself a complication is introduced by the partly viscous behaviour of rocks at high temperatures, which makes the thermal stress developed dependent upon the rate of cooling as well as the amount of cooling. Allowing for this latter phenomenon makes the equations discussed below very difficult to solve and the problem is simplified in the present work by changing the value of ΔT to allow for changes of state in the rocks (see below, especially equation 5.15) when this variation has to be allowed for.

When the stress σ produced by cooling reaches the tensile strength σ_t of the material it fails, with the development of tensile fractures. In the case of materials under a confining pressure P_L (lithostatic load pressure in the case of the MBG rocks) the failure condition, derived from equation 5.9 by setting the right - hand side equal to σ_t, has to be modified to allow for this:

$$\sigma_t + P_L = \frac{E\alpha\Delta T}{(1-\nu)} \tag{5.10}$$

The consequences of this phenomenon of tensile failure due to cooling for rocks cooled by hydrothermal fluids circulating through fractures were first examined by Lister (1974). Lister showed that,

provided that the temperature difference between the hydrothermal fluids and adjacent regions of hot rock lacking a fracture network is greater than the value of ΔT which satisfies (5.10), conductive heat loss from the rocks immediately adjacent to the hydrothermal system will cause tensile failure of these rocks by propagation of the fractures containing the hydrothermal system into the hot rocks. The hydrothermal system will therefore **automatically** propagate itself into the hot rocks, cooling them as it does so. The association of very rapid cooling and the formation of a tensile fracture network in the quenching event which ended M1 around the MBG, and also in the M2 felsites following their emplacement, suggests that both were associated with the self - propagation of a hydrothermal system through these rocks. The remainder of this section will deal with the characteristics of this system and the cooling which it produced.

Lister showed that all the fractures at the boundary of the hydrothermal system should propagate at the same average rate and that it is therefore possible to consider the propagation of the hydrothermal system in terms of the movement of a **cracking front** defined by the locus of the fracture tips (Fig. 5.7A). Lister also showed that thermal contraction stresses in the rocks between the fractures would regulate the spacing of the tensile fractures in such a way that the spacing of the fractures was less than the thickness of the conductively cooled and thermally stressed region in front of the cracking front (Fig. 5.7B,C).

Observations of microseismicity associated with propagating columnar joints produced by cooling aand contraction of lava lakes and studies of the fracture surfaces formed by the joints themselves (Ryan & Sammis 1981) show that although crack propagation occurs seismically the distance through which a crack propagates in any one event is strictly limited. Ryan & Sammis interpret the seismicity associated with columnar joint (or, more generally, thermal contraction crack propagation) formation as due to intermittent unstable propagation from the failure surface (at which $\sigma = \sigma_T + P_L$) into that part of the thermal boundary layer in front of the cracking front which is under tension ($\sigma > P_L$) until the surface at which $\sigma = P_L$ is reached. The overall stress state of the rock on the high - temperature side of this surface is compressive, preventing further unstable propagation (Sammis & Julian (1987)): creep deformation of the surrounding rocks is then thought to heal the crack tip (Ryan & Sammis 1981), preventing further propagation until further thermal contraction causes the failure criterion (equation 5.10) to be satisfied again. In the case of a relatively deep - seated propagating hydrothermal system in particular, the size of the individual crack increments

Fig. 5.7. Diagrammatic representation of the cracking front concept and temperature and thermal stress ( ) distributions in the hydrothermal - convective and conductive thermal boundary layers. Thicknesses of layers not to scale.

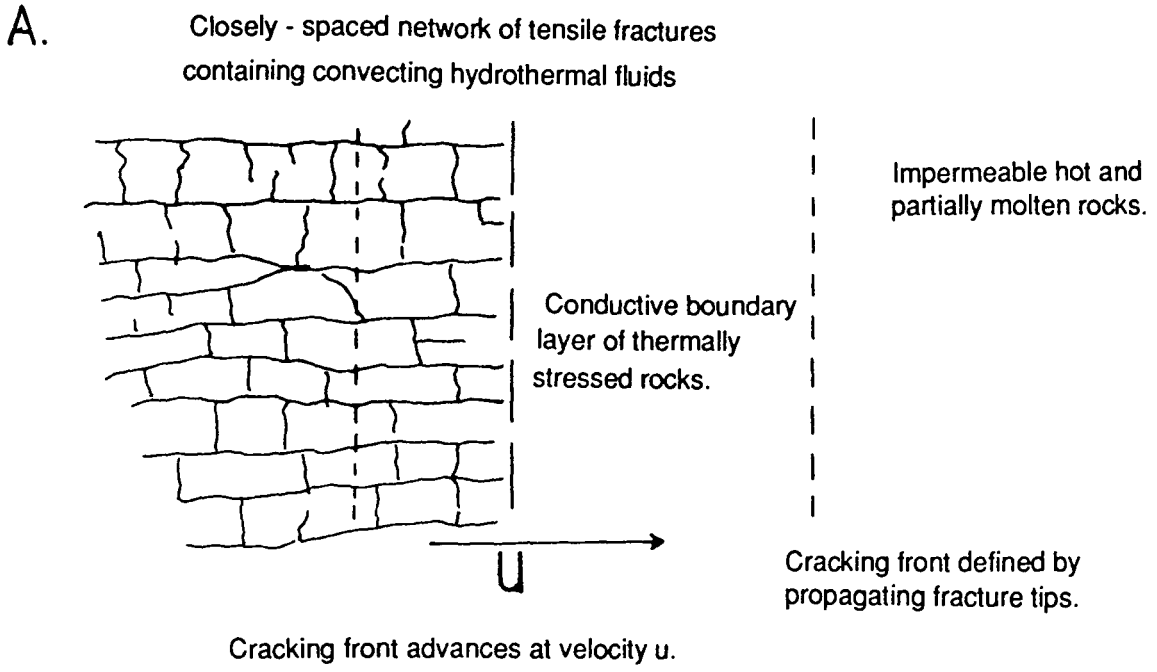

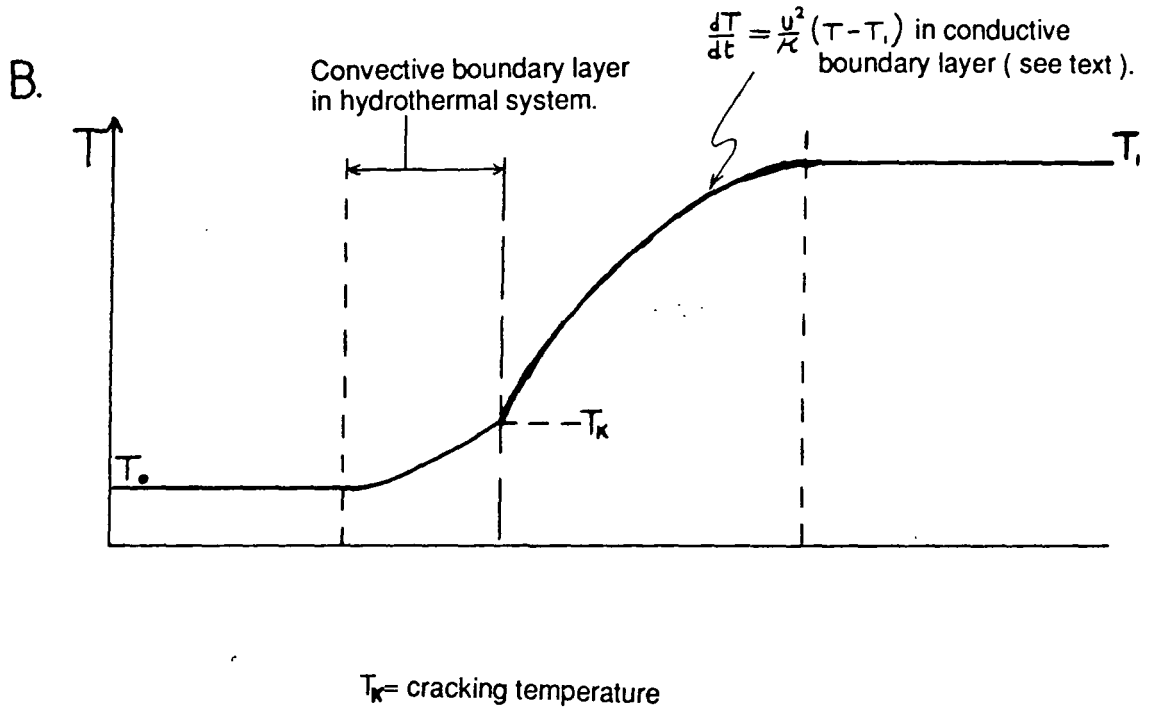

C.

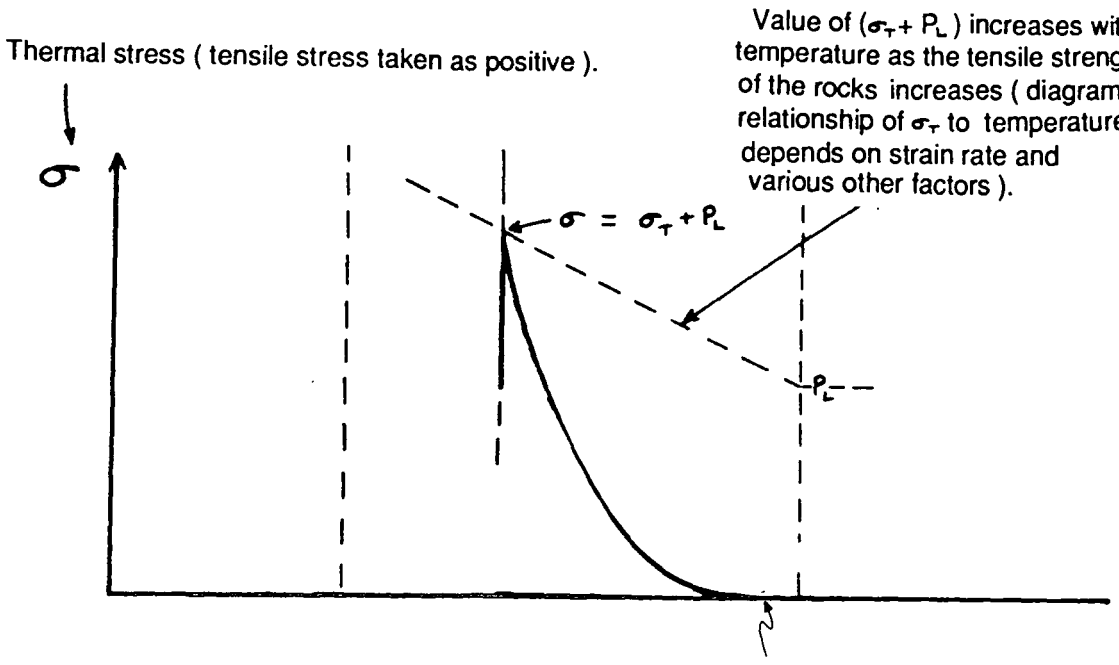

D.

Subdivision of the conductive thermal boundary layer based on the overall stress state.

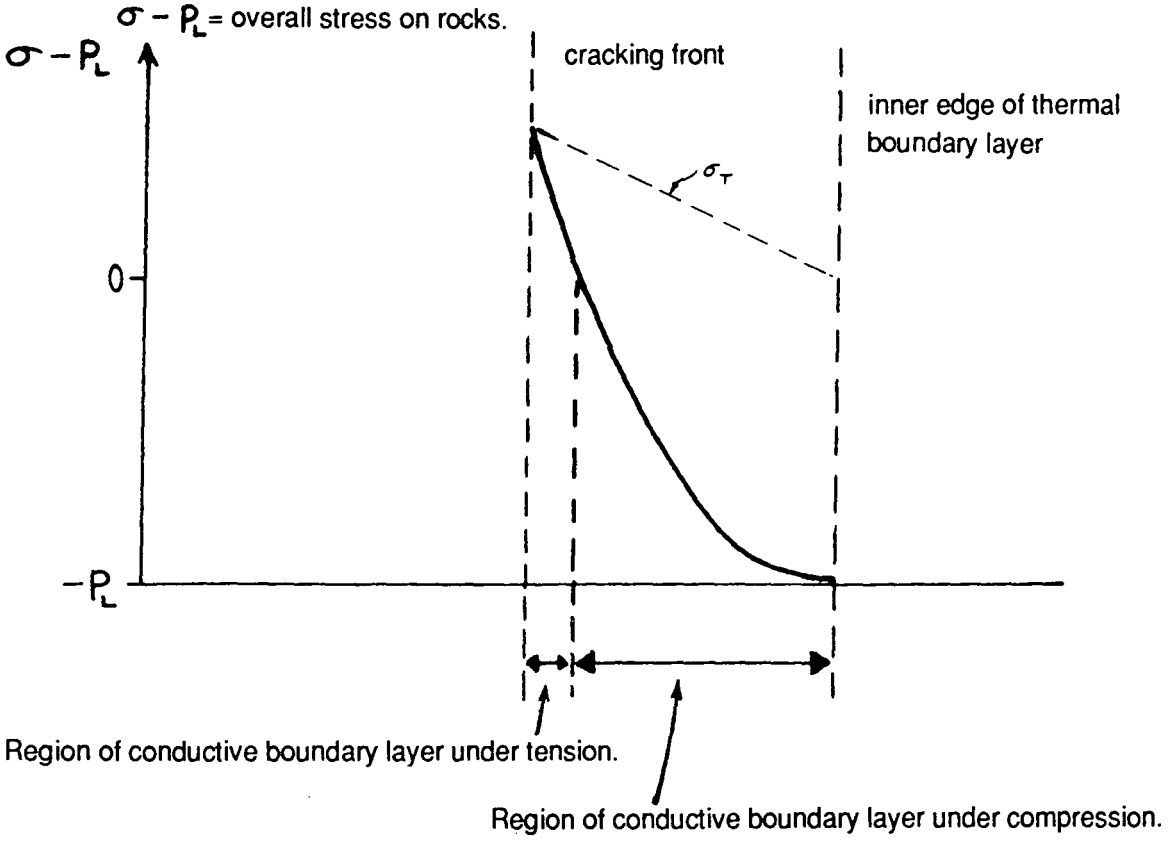

will therefore be small compared to the overall thickness of the conductive thermal boundary layer.

These three considerations show that it is possible to treat the cracking front as a constant - temperature moving boundary migrating through a region of hot rock with a conductively cooled moving boundary layer in front of it. The velocity u of the moving boundary and the temperature distribution within the conductively cooled boundary layer in front of it are related by:

$$T = T_1 - \Delta T \exp(\frac{u^2 t}{\kappa}) \tag{5.11}$$

and

$$\frac{\partial T}{\partial t} = -\frac{u^2}{\kappa} \Delta T \exp(\frac{u^2 t}{\kappa}) \tag{5.12}$$

where T is the temperature at a point within the layer, t is the time since it entered the moving layer, T_1 is the temperature of the hot rocks beyond the leading surface of the conductive boundary layer, κ is the thermal diffusivity of the rocks and the other quantities are as defined above.

Neither 5.11 nor 5.12 can be solved directly in the absence of direct measurements of any two of u, T and t. Lister (1974) therefore attempted to model the crack formation process, as governed by (5.9 and (5.10), in greater detail and thereby produce an equation for u in terms of the overall temperature changes in the system. The approach adopted by Lister (1974) assumes that the hydrothermal system produced by the fracturing is capable of removing heat at whatever rate it is supplied to it by cooling of the hot rocks at the cracking front and that the crack formation process itself is the rate - limiting step in the propagation process. Other models (notably that of Carrigan 1986) assume instead that the rate - limiting process is that of heat transfer within the hydrothermal system and model the migration of the cracking front in terms of buoyancy forces and permeabilities within the hydrothermal system. The problem with this is that the permeabilities of fracture - based hydrothermal systems are very poorly known indeed (Norton 1988) and the buoyancy forces developed are very sensitive to pressure, because of the compressible nature of hydrothermal fluids (Norton 1984). The quantities involved in Lister's equations are rather more easily determined in the case of deeply eroded ancient hydrothermal systems. Lister obtained values of u in the range 50 – 250m/year for an initial hot rock temperature of 1200°C, hydrothermal system temperatures in the range 200 – 300°C and a range of rock parameters appropriate to basic rocks, which Lister considered to show only relatively small differences from felsic crustal rocks in respect of their thermo - mechanical properties. Initial (end - M1) temperatures were close to 1200°C

Plate 5.3A. Quench plagioclase (note that most grains are hollow or swallow - tailed), orthopyroxene and inverted tridymite crystals in devitrified glass. Matrix of aluminous rheomorphic breccia, sample 184. Plane - polarised light, field of view 3.5mm.

Plate 5.3B. Quench plagioclase lath (hollow) in altered devitrified glass, M2 felsite. Sample 42F2. Plane - polarised light, field of view 0.75mm.

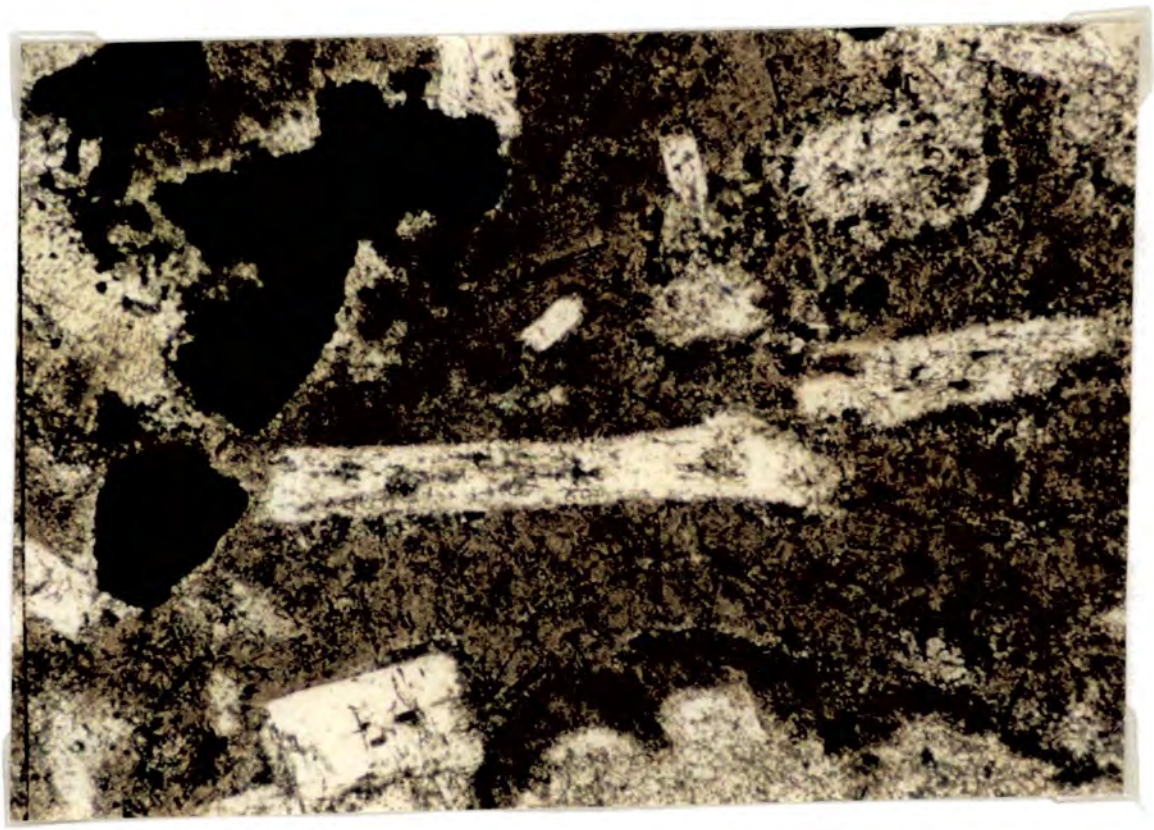

in the innermost parts of the M1 aureole and the presence of the assemblage quartz + epidote ± chlorite ± alkali feldspar ± actinolite in the tensile fractures and replacing un - devitrified patches of glass in the quenched rocks (section 3.2.2 and 3.2.3) suggests hydrothermal system temperatures during the quenching event in much the same range as the values in Lister (1974). However, given the assumptions made by Lister (1974) and the considerable uncertainties in many of the values used, an independent estimate of u during the quenching of the rocks in the M1 aureole is clearly desirable.

5.3.2.2. An alternative method of estimating the cracking front velocity u.

As was noted by Lister (1974), equations 5.11 and 5.12 can be combined to give:

$$\frac{\partial T}{\partial t} = \frac{u^2}{\kappa}(T - T_1) \tag{5.13}$$

where T is the temperature at some point within the moving conductive boundary layer at some particular time, and $\frac{\partial T}{\partial t}$ is the rate of cooling of the rock at that same point and time. 5.13 is an extremely simple equation; the problem is the evaluation of these two quantities for the rocks being investigated. A potential method of doing this for previously largely molten rocks which have been cooled and solidified by a propagating hydrothermal system is to use the composition of quench (sensu lato) crystals to determine the temperatures at which those crystals formed, and to compare the morphology of the same crystals with those produced in crystallisation experiments on similar melts at known cooling rates in order to estimate the cooling rate at the time of formation of the crystals in the natural rock.

This can be done using quench plagioclase crystals in rocks such as 184 (Plate 5.3). The advantages of using quench feldspar crystals are that plagioclase is the phase which has been studied most in cooling rate experiments to date and that plagioclase – melt geothermometry (see section 4.2.5) can be used to establish the temperatures at which the rims of the feldspar crystals grew. This temperature will be that at which the quench crystals ceased to grow and the remaining melt began to form much smaller crystallites. In the absence of valid feldspar - melt temperatures it can also be estimated, although with a reduced degree of accuracy, simply by considering the phase assemblages produced as the melt crystallised. The transition from crystallisation of skeletal crystals to formation of variolites or spherulites is relatively well - defined in these rocks, producing a pseudoporphyritic texture (see section 3.2.2). this is as would be expected because of the simultaneous decrease in

temperature (and therefore in diffusion and crystal growth rates) and increase in cooling rate (and therefore rates of crystallite nucleation) implied by equation 5.13. The actual value of the cooling rate should then be that at which the plagioclases produced in experiments on compositionally equivalent melts change from skeletal prisms to quench dendrites or spherulites. Although most of these experiments have been carried out on ternary feldspar melts (see review in Lofgren (1980)), whilst the natural rocks in the M1 aureole contain other components (notably Fe, Mg, Ti, Ca, excess Si (and Al in some)), the principal effect of these on feldspar crystal morphology – cooling rate relationships is generally considered to be that of a changed diffusion rate in the melt (Kirkpatrick 1981; Muncill & Lasaga 1987). The approximate validity of the Einstein – Stokes relationship between diffusivity and viscosity for silicate melts (Kirkpatrick 1981) therefore implies that the quenched melts in the M1 aureole are compositionally equivalent, as far as crystal growth is concerned, to pure - feldspar melts with the same viscosity (see below). However, extrapolating from experimental melts to natural magmas in this way is not a particularly reliable procedure because of other factors which may affect the textures produced in compositionally equivalent melts at any one cooling rate.

The controls on crystal morphology are reviewed in Lofgren (1980). The experiments discussed in that work, and subsequent experiments (notably Lofgren 1983), show that in addition to the controls exerted by cooling rate (or amount of supercooling) and melt composition (via its effect on diffusion rates), crystal morphologies may be strongly affected by the previous history of the melt, in particular the duration and temperature of the period of melting prior to the beginning of cooling. This affects the abundance of crystal nuclei or embryos in the melt and therefore the degree of supercooling at which crystallisation commences (Gibb 1974; Lofgren 1983). The precise effects are poorly understood but are likely to differ between experimental charges, which are kept molten for a few days at most prior to quenching (Lofgren 1981) and the rocks in the inner part of the M1 aureole which must have been partially molten for periods of years at least prior to the quenching event (see section 5.2.4.2). Conversely, however, the experimental charges are normally heated to higher temperatures, relative to their liquidus temperatures, than the natural rocks studied here. These typically contain at least a few percent of residual crystals and can never have been heated to above their liquidus temperatures.

It is assumed here for the purposes of calculations that the cooling rates at which particular crystal

Plate 5.4. Granular overgrowth on corroded plagioclase porphyrocryst, M2 felsite (sample 42F2). This material is believed to have formed by post - quench diffusion and nucleation of feldspars on a pre - existing feldspar substrate: see Table 5.2 for analyses. Plane - polarised light, field of view 3.5mm.

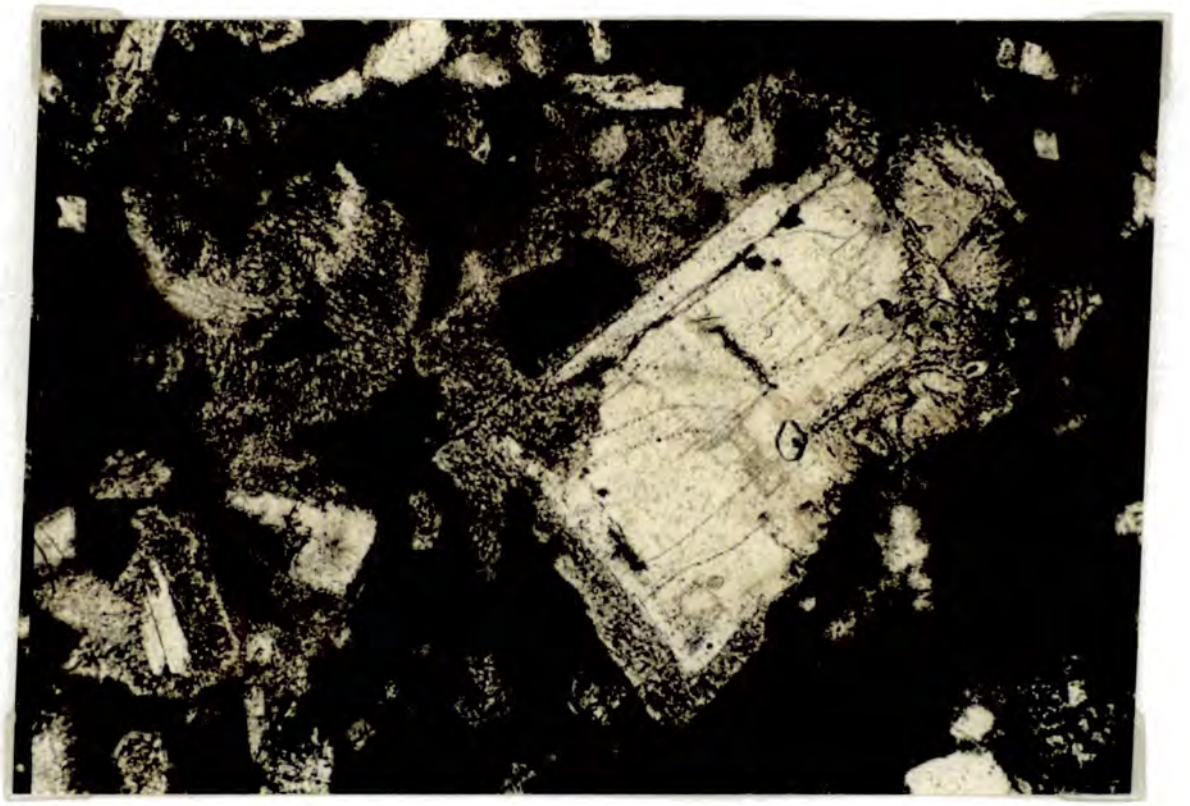

morphologies are or were produced do not differ by more than two orders of magnitude with the previous melting history of the materials concerned; this is the amount of variation with these factors observed by Lofgren (1983) in experiments on a basaltic rock which included runs with samples melted far above their liqidus temperatures. Since u is dependent upon the square root of the cooling rate this uncertainty will only produce an uncertainty of one order of magnitude in the estimated value of u.

The melt from which the rims of the skeletal feldspar crystals formed should, in the absence of sub - solidus recrystallisation or alteration, correspond to the interstitial devitrified glasses in rocks such as 184 and 42F2. Analyses of this material were obtained by rastered and defocussed - beam electron microprobe analysis (see Table 5.2 for details) and quench feldspar compositions were obtained by analysis of the rims of skeletal feldspars (see Appendix 3). It was found that plagioclase - melt temperatures in 42F2 were impossibly high (up to 1400°C). This may be attributed to two factors:

1). The large size of the focussed electron beam spot (about 30 microns across in the case of the instrument at Durham) relative to the scale of zonation in the skeletal feldspar crystals. This tends to raise the anorthite content of the analysed material above the true anorthite content of the rim material.

2). Subsolidus recrystallisation and alteration of the groundmass. This is manifested in many of the M2 felsites in particular by the development of granular overgrowths on relict and magmatic feldspar grains (Plate 5.4). Analyses of this material are also presented in Table 5.2. (42F2 OG1 and OG2). Compared to the remaining groundmass material in 42F2, represented by the devitrified glass analyses, this material is strongly enriched in Ca and Al. The devitrified material must therefore be depleted in these elements relative to the original quenched melt. The formation of hydrothermal epidote, which is commonly present in other devtrified subalkaline granitoid rocks of M1 and M2 age (sections 3.2.2 and 3.2.3) would also deplete the devitrified material in Ca and Al.

Both of these effects will tend to increase the apparent compositional difference between the quench crystals and the melt and thereby raise the temperatures of crystallisation as determined using the Kudo & Weill (1970) or Drake (1976) geothermometers (equation 4.6, section 4.2.5).

Table 5.2.

Devitrified glass analyses and analyses of rim overgrowths on feldspars in rocks quenched by propagating hydrothermal systems.

Sample	184	184	42F2	42F2	42F2	42F2
Analysis	Av. Glass	Variation(2σ)	Av. Glass	Variation2σ)	OG1	OG2
SiO_2	75.98	1.28	76.98	1.19	68.21	66.51
TiO_2	0.59	0.12	0.54	0.12	0.27	0.42
Al_2O_3	11.40	0.78	11.38	0.55	19.41	19.28
FeO	1.02	0.30	0.94	0.24	0.32	0.42
MnO	0.29	0.04	n.d	-	0.01	0.10
MgO	0.22	0.08	0.20	0.07	0.14	0.25
CaO	0.95	0.25	0.50	0.16	3.43	2.85
Na_2O	2.39	0.14	3.11	0.38	7.62	6.79
K_2O	5.47	0.43	5.45	0.57	0.93	2.84

Devitrified glass average analyses obtained by taking average of analyses of 4 areas in each case. Each area analysis is the average of between 3 and 6 rastered strips 60μm by 250μm. 42F2OG1 and 42F2OG2 are analyses of the granular material which fringes euhedral to skeletal plagioclase in 42F2 and several other sectioned M1 and M2 subalkaline granitoid rocks. See also discussion of plagioclase - melt geothermometry in section 4.2.5.

However, reasonable quench temperatures were obtained for the rheomorphic breccia sample 184 using this method. This sample appears to be less altered petrographically than 42F2. As noted in section 4.2.5, the temperatures obtained using the plagioclase - melt geothermometer are P_{H_2O} dependent; thus the quench temperatures for 184 are 1004 - 1050°C at 1Atm. and only 880 - 922°C at $P_{H_2O} = 0.5$kb. However, the estimate of the temperature of this rock during M1 (T_1 in equation 5.13) is also water pressure - dependent, being based on the estimated temperature of formation of the rheomorphic breccias and M1 microgranodiorites (section 4.2.5). Consequently, although both T and T_1 in equation 5.13 vary considerably with partial water presssure, the difference between them is relatively insensitive to P_{H_2O}, and has a value of about 100°C.

Although this value may be a slight underestimate of $(T - T_1)$ at the end of skeletal plagioclase growth in 184 (due to the instrumental and alteration effects noted above), phase equilibrium constraints indicate that the true value cannot have been much greater than this. Apart from residual quartz, 184 is composed of perhaps 10 - 20% skeletal crystals (including orthopyroxene and inverted tridymite as well as plagioclase) and 80% + devitrified groundmass. This implies that it was still well above its solidus when crystallisation of the large crystals in Plate 5.3, including the skeletal to acicular plagioclases, ceased. Similarly, although valid plagioclase – melt temperatures were not obtained for the M1 microgranodiorites and the M2 felsites, the combination of numerous plagioclase crystals and a significant proportion of residual devitrified glass which is present in almost all of them indicates a value of $(T - T_1)$ between -50 and -200°C at the end of skeletal plagioclase growth in all of them. This degree of uncertainty is acceptable in view of the order - of - magnitude uncertainties in the rate of cooling at the same temperature and the square - root dependence of u upon both (see equation 5.13). A number of the M2 felsites, however, contain very few magmatic or quench crystals (notably 43K1, 43Q and 250/1). This suggests that these rocks were quenched at such a high temperature that very little feldspar crystallisation took place prior to this, implying a locally higher value of u.

The actual values of cooling rates at the end of skeletal or acicular plagioclase crystal growth in these rocks can be estimated by comparison with constant cooling rate experiments (reviewed from unpublished or abstracted work in Lofgren 1980) on synthetic samples in the system An – Ab – (Or) – (Qz) – (H_2O). Viscosity calculations using the composition – viscosity relationships of Shaw (1972) suggest that the devitrified groundmass of 184 (Table 5.2) was equivalent to An – Ab melts of

composition $An_{10-15}Ab_{90-85}$, whilst the groundmasses of the subalkaline granitoids were probably equivalent to slightly more An - rich melts. Feldspar melts of these compositions typically show a transition from crystallisation of skeletal and acicular plagioclase to crystallisation of dendrites or spherulites at cooling rates of 1 – 2°C/hr (Lofgren 1980). Insertion of these values for cooling rate at $T - T_1 = -50$ to -200°C into equation 5.13 yields values of u in the range $0.83 \cdot 10^{-6} ms^{-1}$ to $2.61 \cdot 10^{-6} ms^{-1}$ (equal to 27 to 77 metres per year) for the case of the rocks at the inner edge of the M1 aureole. Even when a range of cooling rates between 0.1 and 10°C per hour is considered, equal to the two - orders - of - magnitude uncertainty in cooling rates suggested above, u still lies in the range $3.06 \cdot 10^{-7} - 6.1 \cdot 10^{-6} ms^{-1}$ (10 to 193 metres per year).

It should be noted that the rocks on which these calculations are based are the finest - grained rocks in the contact aureole to have crystallised during the quenching event. As noted in Chapter 3, many of the felsic MBG rocks and anatectic rocks in the M1 aureole have coarser textures. This may not necessarily indicate real variation in the value of u around the aureole or between different rock types, however. Possible alternative reasons are as follows:

1). In the case of those rocks which only ever contained low - degree partial melts (which are now visible as interstitial quartz - feldspar intergrowths), the temperatures of M1 metamorphism, although high in absolute terms, were low relative to the liquidus of these rocks. Lofgren (1983) found that heterogenous nucleation on pre - existing nuclei (either visible grains or submicroscopic embryos) caused holocrystalline textures to persist to much higher cooling rates in rocks heated at well below their liquidus temperatures: the same effect may account for the lack of interstitial glass in these rocks, even when they occur adjacent to more fusible rocks with large contents of devitrified glass.

2). As noted in Chapter 3, there is a broad correlation between the grade and intensity of post - quench M2 metamorphism and alteration, and the grain size and texture of rocks solidified at the end of M1. This correlation applies only to the groundmass material, however: rocks such as 183D1 and 65/3, which have granular and coarse granophyric groundmasses respectively and occur in areas of the southern margin of the intrusion where M2 is intense, have no greater contents of magmatic (euhedral to skeletal) crystals than the devitrified - groundmass rocks on the northern margin of the intrusion, as would be expected to be the case if they had cooled more slowly initially. This

supports the interpretation of these textures in terms of the subsolidus recrystallisation experiments of Lofgren (1971), who showed that a range of textures from spherulitic to microgranophyric could be produced by devitrification of rhyolitic glasses at different temperatures and in the presence of varying amounts of hydrous fluids of various compositions. Lofgren (1971) speculated that coarser granular or granophyric textures could be produced by recrystallisation over longer periods than were possible in the laboratory; it is certainly the case that M2 lasted orders of magnitude longer than the experiments described in Lofgren (1971).

5.3.2.3. Concluding remarks on the estimated value of u, and an estimate of the heat flux at the cracking front.

Although neither the estimate of u based on textural evidence nor the results of the theoretical calculations of Lister (1974) can be regarded as better than order - of - magnitude estimates, the degree of agreement between them suggests that neither value is far from the true value of the rate of propagation of the hydrothermal system or systems which caused the sudden cooling of the contact aureole, at least in those areas of the aureole in which devitrified glasses were found. A further check on the consistency of the two methods is provided by the relationship between u and the crack spacing y which was proposed by Lister (1974) as part of the derivation of the theoretical value of u:

$$y \approx \left(\frac{16\kappa^2}{u^2(T_1 - T_K)} \right)^{0.4} \tag{5.14}$$

where T_K is the temperature at which the rocks actually crack. If the two methods are truly consistent then insertion of the texturally - determined values of u into equation 5.14 should yield a value of y which is the same as the value observed in outcrops such as that shown in Plate 3.28 (Field location 42F, from which the sample 42F2 discussed above was collected). The value of T_K for the quenched anatectic granitoids and rheomorphic breccias in the inner part of the M1 aureole is given by a modified form of equation 5.8:

$$\sigma_t + P_L = \frac{E\alpha(T_{solidus} - T_K)}{(1 - \nu)} \tag{5.15}$$

The solidus temperature of these rocks is used in the calculation of T_K to allow for the change in Young's Modulus with a change in state: Van der Molen & Paterson (1979) demonstrated experimentally that the Young's modulus of a fine - grained granitic rock fell to less than 10% of its

subsolidus value when the melt percentage was still below 15% . It follows from this that thermal contraction of felsic, granitoid rocks such as contact aureole rocks and the M2 felsites above the solidus would be largely accomodated by viscous creep and that stress would only build up in them to a significant extent below the solidus.

The Young's Modulus and Poisson's ratio of glassy material of granitoid composition (note that the value of E relevant in the present case is that for the cooled anatectic rocks prior to devitrification and hydrothermal alteration) can be calculated from the data for compressional and shear wave seismic velocities for glassy materials determined by Murase & McBirney (1973). These workers found that for such materials $V_p \approx 6000 \mathrm{ms}^{-1}$ and $V_s \approx 2000 \mathrm{ms}^{-1}$ and that these values varied little with temperature in the high subsolidus range. Then, using rearranged forms of standard equations from Kearey & Brooks (1984) and Jaeger (1969):

$$\nu = \frac{(\frac{V_p}{V_s})^2 - 2}{2 \times ((\frac{V_p}{V_s})^2 - 1)} \approx 0.44 \tag{5.16}$$

and

$$K = \rho(V_p^2 - \frac{4}{3}V_s^2) \approx 8 \cdot 10^{10} Pa \tag{5.17}$$

(K = bulk modulus) hence:

$$E = 3K(1 - 2\nu) \approx 2.9 \cdot 10^{10} Pa = 290kb \tag{5.18}$$

Rearrangement of (5.15) with σ_t = 300b, P_L = 500b, $\alpha = 2 \cdot 10^{-5o}\mathrm{C}^{-1}$ (Murase & McBirney 1973) and $\mathrm{T}_{solidus}$ = 800 - 900°C (Tuttle & Bowen 1958) gives a value of T_K between 720 and 820°C according to the value of $\mathrm{T}_{solidus}$ and hence P_{H_2O}. Since the estimate of T_1 shows a similar dependence upon P_{H_2O} (although not exactly the same to that of the solidus and T_K) at low pressures, the value of $(T_1 - T_K)$ in equation 5.14 is approximately constant at about 280°C. Insertion of the values of u from section 5.3.2.2 into equation (5.14) gives values of the crack spacing y of between 0.55m (at u = 10 metres/year) and 0.05m (at u = 193 metres/year). This range of fracture spacings includes that of the larger tensile fracture veins observed in the field (section 5.3.1), again indicating that the two methods of calculating u are consistent with eachother. It follows from this that Lister's model (and in particular the assumption that the limiting step in the propagation of the fracture system is the buildup of stress in the conductively cooled rock in front of the cracking front, rather than heat transfer within the hydrothermal system) is valid for

the hydrothermal system(s) which produced these cracks. The presence of smaller fractures between the main fractures is also explained by this model (Lister (1974), p. 492 - 497), as the result of fatigue failure as the cooled blocks between the primary fracture set deformed under the lithostatic load during M2.

Given values of u the heat flux Q_H at the inner edge of the hydrothermal boundary layer, just behind the advancing cracking front, can be determined, from:

$$Q_H = u\rho_r c_r (T_1 - T_0) + Q_c \tag{5.19}$$

where c_r is the average specific heat capacity of the hot rocks over the cooling interval (about $1000 \mathrm{Jkg^{-1}K^{-1}}$; Nicholls & Stout (1982), although it should be noted that the effective heat capacity will be increased in the case of initially partially molten rocks by the release of latent heat), ρ_r is their density (assumed constant) and Q_c is the conductive heat flow in the hot rocks in front of the thermal boundary layer associated with the cracking front, due to any pre - existing temperature gradients. Q_c was assumed to be zero in Lister (1974) which dealt with the case of a constant hot rock temperature, but must have been finite in the M1 aureole as the cracking front swept through it. However, the range of values of Q_c deduced in section 5.2.4 for the innermost part of the aureole (where the pre - quenching temperature gradient was highest) is 10 - $40 \mathrm{Wm^2}$; these are very much smaller than the first term on the right - hand side of (5.19). Depending on u, the value of this ranges from about $670 \mathrm{Wm^{-2}}$ (at $u = 10$ metres per year) to as much as $13300 \mathrm{Wm^{-2}}$ (at $u = 193$m/a) for the hydrothermal system(s) which propagated through the inner part of the aureole. Values of Q_H further out, in cooler parts of the M1 aureole may in fact have been much the same, because although $(T_1 - T_0)$ would have been smaller Lister (1974) indicated that u should be inversely proportional to the difference between the initial temperature and the cracking temperature of the rocks raised to the power 0.7 and u would have therefore been greater in the outer part of the aureole (although it should be noted that Lister's equations break down at small values of $(T_1 - T_K)$, as u tends to infinity in the equations; given this it seems likely that the rate - limiting step in the propagation of the hydrothermal system through relatively cool rocks will be the rate of heat removal from the cracking front by the hydrothermal system). In general terms, however, it seems likely that the heat flux associated with the propagating hydrothermal systems which ended the high grade metamorphism was two to three orders of magnitude greater than the conductive heat flux at the end of M1.

5.3.3. Hydrothermal cooling and the solidification of the Marginal Border group.

5.3.3.1. A summary of the problems posed by the characteristics of the Marginal Border Group.

The occurrence of devitrified interstitial glasses and fine - grained interstitial granophyre in many of the more evolved (and therefore less refractory) rocks of the Marginal Border Group itself suggests that these rocks also underwent rapid cooling immediately after M1 ended in the country rocks. This rapidly cooled interstitial material is particularly prelevent on the northern margin of the intrusion in the Glendrian Bay and Duin Bhain areas, although not further west, around Field Location 39, where the contact zone rocks contain coarser - grained interstitial material. The occurrence of quench overgrowths on euhedral crystal cores (Plate 3.10) in the ferrogabbroic pods in the Glendrian Bay area suggests a history of initial slow cooling followed by more rapid cooling at lower temperatures (compare with photomicrographs in Lofgren 1980, p. 502) such as would be associated with the propagation of a hydrothermal system in a tensile fracture network through these rocks. As is the case with the contact aureole rocks, the rates of cooling implied by the presence of devitrified glasses in these rocks are such as to only be explicable in terms of cooling by propagation of a hydrothermal system through these rocks at high propagation rates. The basic aim of this section is to see whether such a process could explain a number of features of the MBG rocks in a consistent way. It follows that although some of the quantities involved in doing this are very poorly constrained, this is not particularly important as the aim of the section is to show whether or not a particular process is plausible, not to determine the precise rate at which it occurred.

The basic and intermediate rocks of the MBG are generally different from the quenched rocks in the aureole (and also some of the granitoid rocks in the contact zone itself, most notably the diopside microgranites at Duin Bhain) in that they are mainly holocrystalline, although typically with basaltic or doleritic textures. Furthermore, whilst the felsic and anatectic rocks in the contact aureole and within the MBG show no evidence for residual melt mobility during solidification, the ferrogabbroic veins and pods within the MBG basic rocks close to the contact form strong evidence for the operation of mesoscopic to macroscopic melt segregation during the solidification of their host rocks. As was noted in section 3.2.2, the columnar - joint geometry of the veins shown in Plate 3.11 indicates that they were formed by thermal contraction cracking of the host rocks in a

temperature gradient perpendicular to the contact, whilst the less regular geometries of the majority of the ferrogabbroic veins suggests the involvement of a more complex stress field in their formation, perhaps with superposition of thermal stresses and stresses related to wall - rock deformation and flow within the magma chamber.

It was shown in section 4.3 that segregation of these veins had a negligible effect upon the composition of the host rocks, which have compositions approximating to those of crustally contaminated basaltic liquids. This observation is consistent with the interpretation of the contact zone as the remnants of the boundary layer present at the wall of the MBG magma chamber in the latest stage of M1. The requirements for the preservation of this material in the form in which it occurs at outcrop were discussed in section 4.5, where it was concluded that the flow of intermediate magmas down the wall of the chamber to the present level of exposure, which was inferred to have taken place during M1 (section 4.3.3), had to cease as the MBG solidified during the earliest part of M2. The reason for this is that if it did not do so basic magmas from the interior of the chamber could not have solidified on the wall to form the homogenous basic rocks which make up the bulk of the MBG.

The problems which are to be addressed in this section can therefore be summarised as follows:

1). What are the causes of the textural differences between the felsic and basic rocks solidified during the period of rapid cooling, from the end of M1 through the earliest part of M2, in the contact aureole and the Marginal Border Group ?

2). What was the mechanism of formation of the segregation veins in the MBG basic rocks close to the contact ?

3). Was the velocity with which the hydrothermal system propagated through the Marginal Border Group sufficiently great to suppress mechanisms of interstitial melt segregation, other than those leading to formation of the ferrogabbroic veins ?

4). Was this velocity also large enough to suppress the downward flow of intermediate magmas in the thermal boundary layer of the magma chamber, from the level of occurrence of these magmas in the interior of the chamber to the present level of exposure ?

Plate 5.5. Partially altered (to carbonate + opaques) quench crystals of diopsidic - salitic clinopyroxene in groundmass of diopside microgranite from the Duin Bhain pseudoscreen. Sample 42D4. The other main quench crystal phase is tridymite, now inverted to quartz. Plane - polarised light, field of view 3.5mm.

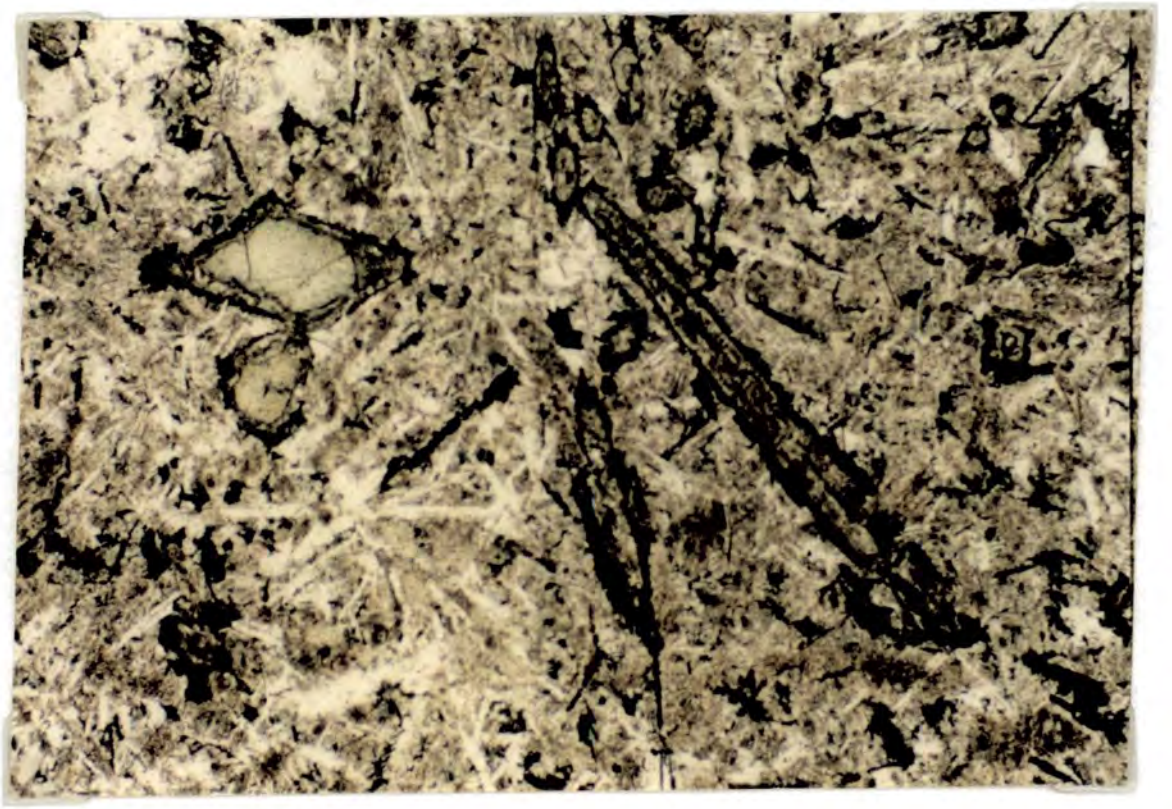

5.3.3.2. The propagation velocity u of the hydrothermal system in the Marginal Border Group.

The actual value of u, **in a direction perpendicular to the contact,** as the hydrothermal system penetrated the magma chamber is the principal controlling factor in all of these problems. When rocks of broadly similar composition (and therefore crystallisation behaviour; see section 5.3.2) to the wall rocks, such as the diopside microgranites and the interstitial material in the ferrogabbros on the northern margin of the pluton, are considered, it is apparent that there are few differences in texture. Devitrified quench glasses are as well developed in these rocks (Plates 3.10 and 5.5) as in the high - degree partially melted rocks in the contact aureole and minor intrusions. Although it was not possible to obtain microprobe analyses of the devitrified material the petrographic similarities in mineralogy and texture suggest similar cooling rates at similar temperatures in both groups of rocks. Since u varies with the square root of both cooling rate at quenching and the ΔT (see equation 5.13) at which quenching occured, this suggests that u was the same within the large uncertainties in its value (10m/year - 193m/year) in both the country rocks and within the MBG itself. This is consistent with the spacing of the tensile fracture veins shown in Plate 3.11, which also occur in the Glendrian Bay area. Although the spacing of these fractures is slightly greater than that of the 10 - 20cm interval typical of the fractures in the contact aureole (section 5.3.1) this is to be expected at constant u because of the higher temperature of formation of these fractures (see equation 5.14, section 5.3.2, and the discussion of the temperatures at which these fractures formed, below). This conclusion, that u was much the same in both the contact aureole and in the basic rocks of the MBG, is in accord with the prediction made by Lister (1974) to the effect that, with all other controlling variables held constant, the value of u should only vary by a factor of two for the entire range of silicate rock types.

Two lines of evidence indicate that the hydrothermal system was propagating in a direction perpendicular to the contact when it caused the solidification of the MBG. The first of these is the orientation of the columnar joint - like segregation veins shown in Plate 3.11. Analogous joints in lava flows (Ryan & Sammis 1981) and permafrost (Lachenbruch 1962) grow in a direction parallel to the temperature gradient under which they form. The joints shown in Plate 3.11 are orientated perpendicular to the outer contact of the MBG and therefore indicate that the temperature gradient during their formation was also perpendicular to the contact. Similarly, the rooted dolerite dykes in

the Glendrian Bay area (section 3.2.2.1) also indicate that temperatures increased towards the interior of the intrusion at the time of their emplacement (i.e. as the quenching event was in progress; see section 3.2.2.1).

The tentative conclusion that can be drawn from these observations, that the hydrothermal system was propagating directly towards the MBG magma chamber, at least by the time that it reached the contact in the Glendrian Bay area, is consistent with the theoretically - predicted temperature dependence of the cracking front propagation velocity, u (Lister 1974). As noted in section 5.2.4, Lister predicted that u should be greater in rocks at lower temperatures than in those at high temperatures, provided that the temperature contrast between the hot rocks and the hydrothermal system is sufficent to permit any cracking at all. Consequently, whatever the initial orientation of the cracking front, as it moved through the M1 aureole it would be expected to spread faster in the outer aureole than in the hotter rocks of the inner contact aureole and tend with time to form a cooling surface parallel to the wall of the MBG magma chamber.

There is, however, a problem associated with the scale of the pods and veins of ferrogabbroic rocks within the MBG relative to the scale of the thermal boundary layer in front of the advancing cracking front. Many of these bodies have maximum dimensions of a few metres or so. In the case of veins perpendicular to the margin it is possible that they grew progressively or incrementally, thereby attaining a greater thickness than that of the section of the thermal boundary layer betwen the solidus and the rigidus. This is given by a modified form of equation 5.3:

$$-\frac{\kappa}{u}(ln(1-\frac{T_R-T_K}{T_1-T_K})-ln(1-\frac{T_S-T_K}{T_1-T_K}))=x_r-x_s \qquad (5.20)$$

where T_1, T_R, T_S and T_K are, respectively, the initial, rigidus, solidus and subsolidus cracking temperatures of these rocks and x_r and x_s are the distances of the rigidus and solidus surfaces in front of the cracking front (the difference of these two is equal to the thickness of the region between solidus and rigidus where unchilled segregation and other igneous veins can form). The value of T_K in these rocks is likely to vary slightly with the amount of stress relaxed by interstitial melt movement (see below) and it is therefore difficult to evaluate 5.20 precisely; insertion of likely values of T_K yields an estimate for the thickness of the region of segregation vein formation of the order of 1 to 3 metres. Many of the ferrogabbroic and unchilled granitic veins and pods seem too large to have formed in a region of this thickness, particularly those near Sanna Point, at Ardnamurchan Point and at Corrachadh Mhor (sections 3.2.3 and 3.2.4). This may indicate a real variation in u around

the MBG as the textural constraints on the value of u discussed above strictly only apply to the rocks between Glendrian Bay and Duin Bhain. The intermediate rocks on the western margin of the intrusion typically contain interstitial microgranophyre rather than devitrified glasses but as noted in the previous section this may reflect the more intense alteration of these rocks than a slower rate of cooling. Although the model of Lister (1974) predicts that u should be more - or - less constant over large areas of a contact, lower values of u could have been produced in some sectors of the contact aureole than in others if the rate of circulation was not always sufficient to remove heat from the cracking front at a rate determined, instead, by the mechanics of crack formation (see above). Sectors of the contact where crack propagation appears to have been the rate - limiting step in propagation of the hydrothermal system include Glendrian Bay, Duin Bhain and possibly the area between Druim na Gearr Leacainn and Glebe Hill, where devitrified rocks of M1 or early M2 age occur (sections 3.2.5.3 and 3.2.6). In other areas where contact zone rocks are exposed, such as those just east of Sanna Point and at Ardnamurchan Point the rate of cooling of the M1 aureole may have been rather slower and in these areas the rate of hydrothermal circulation may have been the rate - limiting step. This could also result in greater temperatures within the hydrothermal system which could account for the greater intensity of alteration seen in these areas. However, there is no reason to believe that this is definitely the cause of the greater intensity of alteration because it could have been caused later on, in M2. Possible mechanisms for varying the rate of hydrothermal circulation during the quenching event are discussed below, in section 5.5.

5.3.3.3. Causes of the differences in the textures of the devitrified felsic and holocrystalline mafic rocks of the MBG.

Since u was probably constant to within an order of magnitude or so within particualar areas of the contact, the explanation for the variation in textures in the MBG within these areas, and even within small areas a few tens of metres across, has to be sought in the properties of rocks and magmas of the compositions present in the MBG. It is known both experimentally (for example Lofgren (1980, 1983)) and from theoretical considerations based on diffusion rates (Kirkpatrick 1981) that basic rocks will crystallise fully at higher cooling rates than felsic rocks. As an example, Lofgren (1983) found that a quartz - normative basalt (broadly comparable to the majority of MBG basic rocks) formed holocrystalline or intersertal textures at cooling rates of up to 10°C/hour. Although this argument would not apply to the crystallisation of the residual melts left after most of the rock had

crystallised, the crystallisation (or subsequent recrystallisation) of these would be promoted by the presence of surrounding crystals which would act as substrates for crystallisation of residual melts or glasses. Strongly zoned rims are features of many plagioclase grains in these rocks and these may represent much of the residual material.

In conclusion, there seems to be no good reason to interpret the doleritic to coarse basaltic, holocrystalline textures of the basic rocks of the MBG as evidence of slower cooling rates than those of the felsic rocks of the aureole and minor intrusions outside the MBG, whilst the occurrence of interstitial devitrified glasses in ferrogabbroic pods enclosed within the basic rocks and in the MBG microgranitoids points to similar rates of cooling at similar temperatures, and therefore values of u in the same range.

5.3.3.4. Cracking and interstitial melt migration in the Marginal Border Group.

The formation of ferrogabbroic segregation veins, such as those forming the columnar joint network in Plate 3.11, in the basic rocks of the MBG implies that the basic rocks were undergoing brittle fracture above the solidus. The occurence of this melt segregation process in these rocks and not in the felsic rocks can therefore be explained in terms of the different rheologies of these rocks above the solidus.

Basic rocks, being more strongly non - eutectic than felsic rocks, will form a two - phase material composed of an interlocking crystal network and an interstitial melt over a wider temperature interval than the latter. An alternative method of stating this is to say that the temperature interval between the rigidus and the solidus is greater in basic rocks than in felsic rocks. Furthermore, the interstitial melt in the former will be an intermediate or ferrobasaltic melt, less viscous than interstitial melts in most felsic rocks due to the lower abundance of network - forming cations and also its higher temperature (Shaw 1972). It will therefore segregate from the host crystalline framework at greater rates under any given pressure gradient (McKenzie 1984). The presence of significant pressure gradients due to non - gravitational stresses (principally thermal contraction stresses in the present context) is made possible by the presence of the relatively rigid crystal network, which gives basic rocks a significant short - term Young's Modulus (as much as $4 \cdot 10^{10}$Pa; Ryan & Sammis 1981) at temperatures above the solidus but below the rigidus. The presence of an interstitial melt

phase will however tend to cause increased relaxation of thermal and other stresses over timescales on which recrystallisation and diffusional creep of the crystal lattice are possible, thereby reducing the long - term Young's modulus of the partially molten rock. These creep processes are, however, only effective at low strain rates and will not prevent stress accumulation at the cooling and thermal contraction rates associated with the propagation of the hydrothermal system through the MBG (see equation 5.21, below).

It is therefore possible, at high enough cooling rates, for materials with a sufficiently large average supersolidus value of Young's Modulus and a large enough rigidus – solidus temperature interval (see equation 5.10) to undergo tensile failure above the solidus. Tensile failure above the solidus will be promoted by the presence of an interstitial melt phase, which will reduce the effective confining pressure from the lithostatic load pressure to a pressure $P_L - P_F$ where P_F is the interstitial melt pressure (note that P_F will not necessarily be identical to P_L because of the greater thermal expansivity of the melt phase, which causes it to undergo a greater amount of thermal contraction on cooling). This raises the possibility that an initially molten rock may undergo two episodes of thermal contraction cracking during solidification as it cools and solidifies.

Possible variations in thermal contraction stress with temperature for basic rocks, assuming a rate of cooling which varies with temperature according to equation 5.13, are shown in Fig. 5.8 for high and low values of u. At low u the relaxation of thermal stresses by viscous creep of the partially molten rock may be sufficient to suppress tensile failure above the solidus altogether (Fig. 5.8A), in which case the rock will undergo tensile failure only at the hydrothermal cracking front, well below the solidus. At high u, however, the rate of thermal contraction may be sufficient to cause cracking above the solidus, in which case the thermal stresses in the partially molten rocks will fall to a value governed by the rate at which interstitial melt can leak out of the contracting matrix and into the cracks (Sleep 1988). This rate falls with temperature and the increasing viscosity and falling abundance of the remaining interstitial melt, permitting thermal stresses to build up again. The subsequent behaviour of the rocks will be similar to those in which tensile failure only occurs below the solidus, although the temperature at which the second cracking, that which admits the hydrothermal system, takes place may be rather different (it could be higher or lower according to whether the effect of the greater value of u or the effect of the stress release by above - solidus cracking dominates).

Fig. 5.8. Qualitative variation in tensile stress σ due to thermal contraction in the conductive boundary layer during propagation of the hydrothermal system through the MBG basic rocks.

5.8.1: Low value of **u** ; low strain rate.

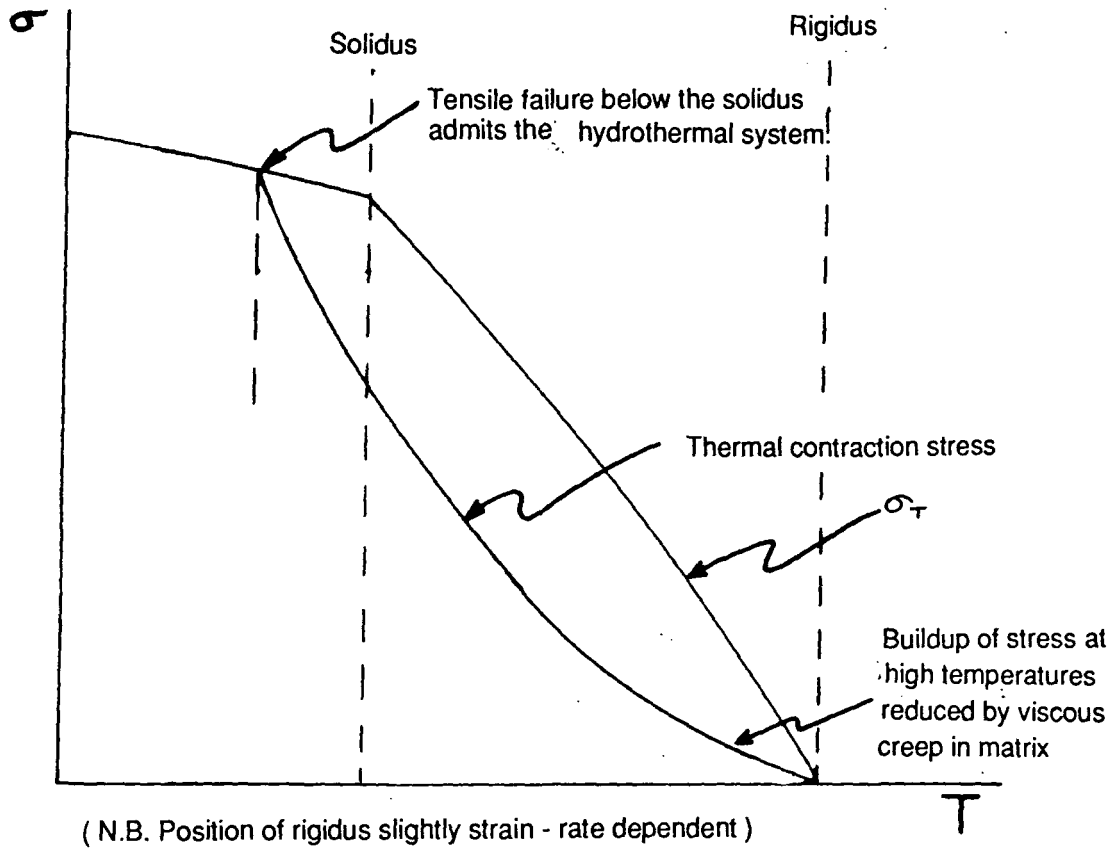

(N.B. Position of rigidus slightly strain - rate dependent)

5.8.2: High **u** ; high strain rate.

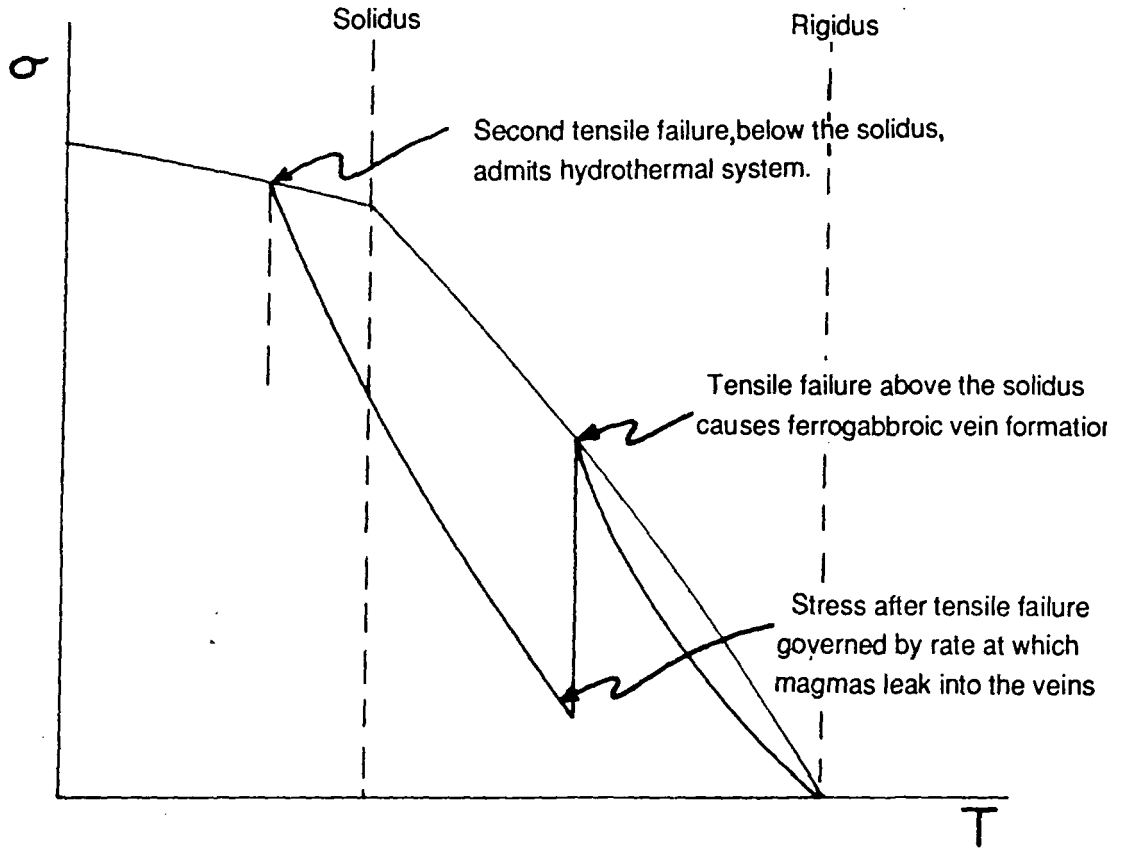

The rates of melt migration into cracks or veins is at present incompletely understood (Sleep 1988) and quantitative values cannot as yet be placed upon the temperature – thermal contraction stress curves in Fig. 5.8. However, the columnar jointing defined by the veins in Plate 3.11 implies that the basic rocks at the locality shown in this plate exhibited the type of behaviour depicted in Fig. 5.8B. As was noted in Chapter 3, the majority of the ferrogabbro pods and veins in the inner part of the contact zone of the MBG have a less regular arrangement than the columnar structure visible in Plate 3.11. The stresses which produced them may have been a complex mixture of thermal contraction stresses and volcanotectonic stresses associated with deformation around the magma chamber. Consequently it is not clear whether the concentration of these veins in the inner part of the contact zone, and their absence further into the MBG, indicates a real change in u (and hence the thermal stresses) or a change in the volcano - tectonic stress field in the rocks around the Hypersthene Gabbro.

One other implication follows from the buildup of thermal and other stresses in partially molten rocks which is implied by the occurrence of veins in these rocks. The finite strength of the crystalline matrix which this implies would have allowed pressure gradients to form as a result of thermal contraction of the matrix, at least in the short term (that is to say, at high strain rates resulting from high values of u). The fall in temperature would be accompanied by a fall in interstitial melt pressure, as noted above in the context of the effective confining pressure which operated on the host matrix, in addition to the pressure gradients produced by opening of the segregation veins (Sleep 1988). This would lead to an overall migration of interstitial melts down the temperature gradient from the unstressed high - temperature part of the boundary layer. This flow would be focussed in the veins (where pressures would be lowest and permeabilities highest). Melt - producing reactions between the warmer melts from the interior of the conductive boundary layer and the vein walls could account for the non - dilational, partly replacive character of some of these veins (section 3.2.4), along with disaggregation of the vein walls by melts leaking into the veins. It should be noted that such melting reactions could only occur in the veins because thermal equilibration of migrating melts and the host crystal matrix would occur very rapidly relative to fluid motion during intergranular percolation (McKenzie 1984). Continuous migration of interstitial melts from the high temperature part of the conductive boundary layer toward the low temperature part would tend to buffer the composition of the rocks close to their original liquid composition despite the extraction of the evolved melts represented by the contents of the segregation veins, in a manner analogous to the compensated

crystal settling model of Krishnamurthy & Cox (1977) except that in this case it is the melt phase which is moving in an absolute frame of reference, rather than settling crystals. Whether or not this process is capable of accounting for the observed discrepancy between the high proportion of certain outcrops (particularly those along the west coast of Ardnamurchan (section 3.2.4)) made up of ferrogabbroic segregations and the inference, made on the basis of geochemical analysis, that their hosts approximate to liquid compositions (section 4.3.1) awaits a more complete understanding of the vein segregation process.

5.3.3.5. Rates of solidification and rates of crystal fractionation during the solidification of the MBG basic rocks.

In the general discussion of types of magma chamber boundary layer, in section 4.1, Type 1 boundary layers such as the conductive boundary layer in front of the cracking front as it penetrated the Marginal Border Group were divided into two types. One of these occurs when the rate of solidification is low relative to rates of crystal fractionation in the partially molten region between rigidus and solidus, and is characterised by the formation of sidewall or congelation cumulates. In the second type, in contrast, solidification is rapid relative to crystal fractionation and rocks corresponding to magma compositions solidify directly on the wall of the chamber. It was shown in section 4.3.1 that the MBG basic rocks at least approximate to liquid compositions, from which it follows that the velocity of the rigidus surface a (see equation 4.3) should be much greater than the characteristic velocities of processes such as buoyancy - driven crystal matrix compaction and thermogravitational melt segregation (Lesher & Walker 1988).

The first of these processes, buoyancy - driven melt segregation, although occurring by a similar mechanism to the thermal contraction - driven segregation process discussed above, differs in that it will drive melts parallel to or away from the advancing cracking front, and in the very much smaller pressure gradients that drive it. The occurrence of supersolidus tensile failure in the partially solidified crystal matrix implies pressure differences, over the width of the rigid part of the conductive thermal boundary layer, of the same size as the tensile failure strengths of the matrix (of the order 10^7 Pa; Ryan & Sammis 1981) and therefore pressure gradients in the interstitial melt of the order of 10^6 – 10^7 Pa per metre in the absence of melt migration. In contrast, static pressure gradients in interstitial melts due to buoyancy effects are of the order 10^3 Pa m^{-1} (McKenzie 1984). It will

therefore be a very much slower process. Under pressure gradients of this size, the matrix is only likely to deform by the mechanism of diffusional or solution - reprecipitation creep (McKenzie 1987; Hunter 1987). Strain rates in partially molten basic rocks deforming by this mechanism are of the order $10^{-15}s^{-1}$ or less in fine - grained rocks (McBirney & Murase 1984). In contrast, strain rates associated with the propagation of the hydrothermal system(s) through the MBG are given by:

$$\frac{d\epsilon}{dt} = \alpha\frac{dT}{dt} = \alpha\frac{u^2}{\kappa}(T - T_1) \tag{5.21}$$

where α is the linear coefficient of thermal expansion (about $2{\cdot}10^{-5o}C^{-1}$ (Murase & McBirney 1984). They will exceed $10^{-12}s^{-1}$ at values of $(T - T_1)$ of only 0.003°C (at u = 190m/year) to 0.3°C (at u = 10m/year), although this rises by a factor of 100 for every ten - fold decrease in u. Nevertheless, it seems unlikely that buoyancy - driven compaction could be an effective process of melt segregation as the MBG solidified.

Thermogravitational diffusion processes, including both Soret diffusion in the melt and compositional diffusion driven by solubility variations with temperature, in basaltic material in an externally - maintained temperature gradient were studied experimentally by Lesher & Walker (1988). These workers found that neither process was characterised by a Lewis number (ratio of thermal diffusivity to chemical diffusivity) of less than 10^4. It follows that in a non - equilibrium thermal gradient, such as that within the thermal boundary layer in front of a moving cracking front, thermogravitational diffusion will have a negligible effect on the compositions of the rocks solidifying in that boundary layer.

In conclusion, self - propagation of a tensile crack - based hydrothermal system is a viable mechanism for preserving basic rocks within the MBG which correspond to basaltic liquids from the interior of the MBG magma chamber, **provided that these magmas gain access to the thermal boundary layer in front of the advancing cracking front.** As noted above, the preservation of the basic MBG rocks also requires that the Type 1 magma chamber boundary layer (see definition in section 4.1) associated with the cracking front, or some other process, inhibited the flow of cooled intermediate and hybrid magmas down the wall of the magma chamber to the present level of exposure from whaterver level above the present surface they occurred at within the interior of the magma chamber.

5.3.3.6. The relationship between the cracking front velocity u and the maximum

distance Δy magmas were able to flow down the wall of the MBG magma chamber as it solidified, and implications for the interpretation of the magmatic structure of the MBG.

The process which limits the distance any one packet of magma can flow down the wall of a magma chamber, such as the MBG magma chamber as the hydrothermal system propagated into it, can be described in the following terms. Consider a particle entering a downward - flowing boundary layer current which is of thickness x and has an average downward velocity, averaged across that area, of V_y. If the boundary layer is of Type 1, every particle within it also has a velocity component towards the wall of the chamber, equal to the velocity a (equation 4.3) with which the wall of the magma chamber is migrating into the interior of the original chamber. At quasi - steady state, this velocity is equal to that of the cracking front of the hydrothermal system that, in the case of the MBG, is removing heat from the chamber (as was argued in the theroetical model described by Carrigan (1986)). It is therefore possible to write an equation for the distance Δy which the particle travels down the wall of the magma chamber before being accreted onto it:

$$\Delta y = \frac{V_y}{a} x = \frac{V_y}{u} x \tag{5.22}$$

One way of satisfying the requirement for the preservation of the observed structure of the MBG can now be stated as follows: if u, and hence a, is sufficiently large relative to V_y, magmas flowing down the wall of the chamber from the intermediate layers higher in the interior of the MBG magma chamber (see section 4.3.3 and Fig. 4.31) will congeal on the wall of the chamber before reaching the present level of exposure. Those magmas already descending in the boundary layer, and therefore below their original position, will accrete on the wall of the chamber forming the observed zone of hybrid and intermediate magmas in the contact zone but once these are exhausted accretion of basic magmas from the interior of the chamber onto the wall will occur. If this is to be a viable mechanism for allowing accretion of basic magmas onto the wall of the MBG magma chamber, Δy must be less than 100 – 1000m. This upper limit is provided by the pressure constraints from section 4.2.5, which imply that the intermediate magma layers in the interior of the chamber cannot have been more than a kilometre above the present level of exposure and were probably at a lesser height above the present land surface.

The terms on the right - hand side of 5.22, other than u, whose value has been determined above, are

poorly known. Both V_y and x are dependent on the fluid dynamical structure of the boundary layer, which is poorly known because of the complex compositional, temperature and viscosity variations in it, particularly in that part of the boundary layer where intermediate magmas are still present and the structure is similar to that described in Chapter 4. However, as was shown in section 5.2.4.2, the **maximum** value of V_y is inversely proportional to x (equation 5.7) and it is therefore possible to rewrite 5.22 to eliminate both, using equations 5.6 to express Δy in terms of the factos controlling V_x:

$$\Delta y = \frac{yQ_m}{u\rho c\Delta T} \tag{5.23}$$

The value of Q_m in 5.23 should in general be that for the boundary layer present during solidification of the MBG, which is poorly known, although probably higher than that associated with the M1 boundary layer because a greater proportion of it is made up of less - viscous basic magmas. However, the present application of 5.23 is to determine whether or not a boundary layer with the structure described in section 4.5 could have persisted into the period of solidification of the MBG magma chamber, early in M2. It is therefore permissible to use the value of Q_m determined in section 5.2.4 in equation 5.23. It should be noted also that if the heat flux through the hydrothermal system is the rate limiting step in its propagation an increase in Q_m could also significantly reduce u. This does not apply, however, to those parts of the contact zone and MBG where Q_H is limited only by the rate of heat transfer in the thermal boundary layer in front of the cracking front (see section 5.3.2): in this case an increase in Q_m would simply increase thermal gradients in the conductive boundary layer (make it thinner, in other words) and thereby cause an increase in Q_H without changing u. l.

Maximum values of Δy for u between 10 and 193 metres/year and the values of ΔT, ρ, c and y used in section 5.2.4.2 are between 6000m ($Q_m = 40\mathrm{Wm}^{-2}$, $u = 10$m/year) and 810m ($Q_m = 8\mathrm{Wm}^{-2}$, $u =$ 193m/year). If Δy was close to these maximum values (that is to say, there was very little return flow of cooled magma into the interior of the chamber through the inner surface of the boundary layer (see Fig. 5.4, section 5.2.4.2) then it is most unlikely that this mechanism could account for the observed solidified structure of the MBG. Several alternative explanations are possible:

1). The actual value of Δy could have been less than its maximum value because of a finite return flow of magma by mixing at the inner surface of the boundary layer. The occurrence of this is entirely

consistent with the geochemical data in Chapter 4 which suggests extensive mixing of intermediate and basic magmas somewhere in the chamber, and with field observations in the contact zone (summarised in section 3.2.7) which suggest mixing at the inner edge of the hybrid - intermediate part of the contact zone with basic magmas.

This explanation also accounts for an observed correlation between the occurrence of wide zones of hybrid and intermediate rocks close to the outer contact (notably at Ardnamurchan Point (Fig. 3.8) and just east of Sanna Point (Map 3) and occurrences of particularly large unchilled granitoid and ferrogabbroic veins, which suggest lower - than - normal values of u (section 5.3.3.2). In such sections of the wall of the magma chamber Δy would be greater than normal and hence the thickness of intermediate and hybrid rocks accumulated at the moving wall of the chamber would also be grater than average.

2). The occurrence of M2 felsites formed by wall - rock melting below the present level of exposure (section 4.2.2) shows that the M1 to M2 transition and consequent solidification of the wall of the MBG magma chamber began at higher levels in the chamber and proceeded downwards with time. It is therefore possible that the intermediate magmas at high levels in the chamber were removed by cooling and mixing with underlying layers or by accretion onto the wall of the chamber as solid rocks before solidification of the lower, basic levels of the MBG magma chamber had proceeded very far. Eruption of the intermediate magmas at the surface, or emplacement into higher level intrusions would also have the same effect. Both of these mechanisms, however, imply a change in the average composition of the chamber from M1 to M2 which would somehow have to be reversed, by replenishment with the right proportions of magmas, before the emplacement of the M2 minor intrusions. This seems unlikely.

It was noted in Chapter 4 that downflows of magma in the thermal boundary layer could have become detached from the wall of the chamber at the tips of downfaulted blocks. The downward flow of intermediate and hybrid magmas could therefore have been interrupted by intense concentric normal fault activity at the chamber walls. The coincidence of faulting with the M1 to M2 transition is not necessarily fortuitous; see section 5.5, below.

These effects are not mutually exclusive and it seems likely that a combination of (1) and (3) could

explain the observed distribution of intermediate and basic rocks within the MBG, together with the differences in the level of exposure, due to faulting, which were inferred in section 4.3.3.

5.3.3.7. Summary and Conclusions.

The results of this section can therefore be summarised as follows.

1). The tensile fracture based hydrothermal system or systems (in different sectors of the contact zone) which propagated through the adjacent contact aureole with velocities of up to 10 – 190m/year appears or appear to have propagated through the MBG itself at similar velocities. There may have been a reduction in propagation rates in some areas due to restrictions on the rate of hydrothermal convective heat transfer away from the cracking front.

2). The differences in texture between felsic and basic rocks, and the development of tensile fractures above the solidus in the latter, appear to be mainly due to, respectively, greater crystallisation rates in the basic rocks and the development of a finite yield strength and Young's Modulus in the basic rocks at a greater temperature above their solidus temperature.

3). Solidification of the MBG magma chamber by a propagating hydrothermal system is a viable mechanism for preserving rocks corresponding to liquid compositions present in the magma chamber. This is definitely the case for propagation velocities in the range 10 to 190 metres per year and is also probably largely true at propagation velocities of as little as 0.1 – 1m/year, from equation 5.21.

4). The rate of solidification of material at the wall of the magma chamber may have been just sufficent to suppress downflow of intermediate magmas from higher levels in the chamber to the present level of exposure. The coincidence of areas where u may have been lower than normal with wide tracts of intermediate and hybrid rocks close to the contact suggests some control of the occurrence of the corresponding magmas in the boundary layer at the present level of exposure by the propagation velocity of the hydrothermal system. It may however be necessary to invoke other processes, especially disruption of the boundary layer flow by concentric normal faulting, to account for the preservation of wide tracts of basic rock close to the MBG contact.

With regard to the physical plausibility of the interpretation of the contact zone as a partly preserved magma chamber boundary layer, the results of this section suggest that, as proposed in Chapter 4, the compositions of the rocks present and some of the structures close to the contact itself (for example, the downfaulted blocks and pillow structures) correspond closely to those present in the M1 boundary layer, but that the overall width of the contact zone and the distribution of the intermediate rocks in particular are products of the solidification of the MBG and cannot be used to infer anything about the width of the M1 boundary layer or the distribution of downflows in it. The best constraints on the former are provided by the scale of structures within it, such as mafic pillows, which provide an absolute lower limit, and the thermal arguments concerning the thickness of the equivalent stagnant layer (section 5.2.4.1).

5.4. M2 metamorphism in the contact aureole and within the MBG.

Unlike M1, M2 metamorphism around the Hypersthene Gabbro and within the MBG was not ended by a sudden quenching or cooling event, with the possible exception of localised events in the Glebe Hill area (section 3.2.6). M2 metamorphic assemblages cannot, therefore, be used to infer an instantaneous geotherm even within a single sector of the contact. Furthermore, the distribution of M2 assemblages is complicated by the fact that it is essentially a rehydration, under varying conditions, of rocks affected by M1, or a first hydration in the case of intrusive rocks emplaced during M1 or M2. The abundances and to a lesser extent the distribution of M2 minerals are therefore controlled by the local flux of hydrothermal fluids and the activities of soluble species in the fluid phase as much as by temperature and rock composition. Nevertheless there is a marked zonation of the M2 aureole which is defined by the highest - grade mineral assemblages present in the rocks. This is particularly well developed on the southern margin of the MBG where the width of exposure is greatest and marked reheating of the aureole and the MBG contact zone appears to have taken place early in M2, after the end - M1 to earliest M2 quenching event (section 3.2.5.5). Interpretation of these assemblages was made easier by the relatively coarse grain size of the M2 assemblages in some of these relatively high grade M2 rocks, which made microprobe analysis with the instrument at Durham practicable.

5.4.1. Conditions of M2 metamorphism at the peak of metamorphism and towards the end of M2.

The best constraints on conditions of M2 metamorphism at the highest grades attained are provided by the following assemblages (other assemblages are discussed in Chapter 3):

1). In pelites within about 200m of the contact on the southern margin of the intrusion: biotite + cordierite + K - feldspar + quartz + intermediate plagioclase + opaques. A similar assemblage is commonly present in the Lower Pabba Beds semipelitic to psammitic hornfelses within a similar distance of the contact and in the anomalous granitoids on Hill 210 (sections 3.2.5.5 and 3.2.5.2 respectively). Certain laminae within the Lower Pabba beds hornfelses contain granular green hornblende believed to be of the same age as the rest of the peak M2 assemblage in the rocks on

the basis of their textural similarity, and contain only a little biotite and cordierite. Relict M1 orthopyroxene is commonly present in these rocks, although badly corroded, and biotite commonly rims Ti - magnetite grains believed to be of M1 age. This may reflect stabilisation of biotite by titianium released on cooling of these opaque grains. Microprobe analyses of biotites in samples 121/3 (a Middle Pabba beds pelite) and 183D1 (the orthopyroxene - bearing hybrid microgranitoid discussed in section 4.2.3) reveal the presence of up to 5 wt% Ti in biotites in 121/3 which rim opaque grains; those in 183D1 are less Ti - rich (c. 1.5 wt%), and rim orthopyroxenes rather than opaques. They are also much more Mg - rich (molecular $\frac{Mg}{Mg+Fe^{2+}} \approx 0.70$, in contrast to values of 0.45 to 0.50 in 121/3; Fe^{2+} calculated on the basis of stoichiometry and charge - balance constraints).

The presence of biotite + cordierite + K - Feldspar + Quartz in these rocks places the conditions of highest - grade M2 metamorphism between the reactions:

$$2Chlorite + 3Muscovite + 6Quartz \Leftrightarrow Biotite + 3Cordierite + 12H_2O \qquad [5.13]$$

(Seifert 1976) and

$$Biotite + 3Quartz \Leftrightarrow 3Orthopyroxene + K \quad Feldspar + H_2O \qquad [5.14]$$

(Luth 1967; Hoffer & Grant 1980)

Reaction 5.13 is preferred as the lower limit on cordierite stability in these rocks, rather than the reactions for Al - rich rocks proposed for the lower limit of cordierite stability in the Ballachulish aureole by Pattison & Harte (1985). These have muscovite and biotite in the products of cordierite breakdown. In contrast, biotite and cordierite both disappear at lower grades or on retrogression in the M2 aureole, to be replaced by chlorite - rich, relatively muscovite poor assemblages. The lower abundance of muscovite in low - grade M2 assemblages, as compared to its prominence in the M0 assemblages (section 5.1), reflects the higher $Mg + Fe^{2+}/Al$ of the rocks in the contact aureole after reduction during M1.

Both of these reactions are hydration/dehydration reactions and are therefore extremely sensitive to P_{H_2O} at the low pressures likely in the M2 aureole. Hoffer & Grant (1980) consider that the right - hand side assemblage in 5.14 is stable above 600°C at $P_{H_2O} = 0.5$kb in Ti - free assemblages with biotite $X_{Mg} \approx 0.5$. The presence of Ti in the biotite would tend to stabilise it to higher temperatures

and/or lower water pressures, as would higher Mg contents (Luth 1967). The high Ti contents of the biotites in 121/3 may therefore reflect temperatures close to the upper stability limit of biotite as the rock itself is not unusually biotite - rich (see analysis in Appendix 2). Seifert (1970) studied reaction 5.13 in the Mg - endmember haplopelitic system KMASH and found that it took place at about 400°C at 0.5kb P_{H_2O}. In natural rocks the reaction would occur at rather lower temperatures (or higher water pressures).

The same assemblage is ubiquitous in pelitic rocks exposed on the western margin of the intrusion but pelites on the northern margin show direct replacement of M1 orthopyroxene by chlorite (although small amounts of biotite do occur in a few laminae). Cordierite - biotite bearing rocks only occur on the northern margin close to the contact of the later Great Eucrite intrusion and are believed to form part of its aureole rather than being M2 in age (section 3.2.2).

2). Metabasic rocks, particularly the Group 2 cone sheets of section 3.2.5.4 and other cone sheets intruded during the early part of M2 and the rocks of the plateau basalt suite. Samples of these rocks from within 100 – 200m of the contact on the southern margin of the intrusion also contain M2 biotite, particularly in and around veins forming part of the tensile fracture network of these rocks. This suggests that the introduction of K into the rocks by hydrothermal fluids flowing along these fractures exerted an important control on its formation.

The tholeiitic, usually quartz - saturated or oversaturated rocks of the MBG suite are characterised by the replacement of olivine (if present) by talc and of orthopyroxene by uralitic amphibole, and recrystallisation of augites with exsolution lamellae of Ca - poor pyroxene or opaques to clear clinopyroxene with granular opaque inclusions. A few basic rocks close to the contact (mainly in the Glebe Hill area) lack hornblende and contain granular cpx + mt + plag + quartz assemblages of M2 age (sections 3.2.5.5 and 3.2.6). Granular interstitial orthopyroxene in one of these rocks may be of M2 age (section 3.2.5.5). This could have been produced by oxidation of, or addition of silica to, earlier olivine by the hydrothermal fluids (Bird et al. 1988). The absence of amphibole from these few rocks implies conditions at the peak of M2 metamorphism which were around the upper stability limit of hornblende in quartz - saturated rocks. The precise temperatures of the hornblende - out equilibrium in quartz - sturated rocks at low pressures and moderate f_{O_2} is poorly known, however.

With regard to the plateau basalt suite rocks, magmatic or M1 olivine and of M1 orthopyroxene, (but not clinopyroxene which generally remains fresh in most), is often replaced by an unusual weakly pleochroic but strongly coloured red amphibole, possibly an oxyhornblende or Ti - rich hornblende. The lack of normal hornblendes and the continued stability of clinopyroxene suggests that the highest - grade M2 metamorphism in these rocks took place above the lower limit of cpx + amphibole stability but below the lower limits of stability of olivine and orthopyroxene in equilibrium with amphibole. These equilibria were studied in quartz - deficient tholeiites by Spear (1981) but the results of that study are probably not applicable to alkaline basic rocks due to the greater abundance of cations such as Ti which may extend the stability range of hornblendes. Replacement of olivine by talc occurs close to biotite - lined veins in some of these rocks, but replacement of olivine by orthopyroxene or Ca - poor amphibole does not occur, due perhaps to reduced silica activities (Bird et al. 1988).

The lack of compositional data and the poor constraints on P_{H_2O} during M2 (other than that it was less than 1kb, and probably much less) means that it is difficult to place precise constraints on the maximum temperatures of M2 in these rocks. However, comparison with the higher - grade rocks of the Inner Series, for which exchange geothermometric data is available (Chapter 6), suggests that the maximum possible temperature for the peak of M2 in these rocks is around 700°C. The formation of biotite and aluminous hornblendes, and the absence of actinolite and chlorite from the peak M2 assemblages (although they are common as later overprinting phases; see below), together with comparison of the assemblages developed with those from other shallowly buried central intrusive complexes in East Greenland (Bird et al. 1988) and Skye (Ferry 1985; Ferry et al. 1987) suggests minimum peak M2 temperatures in these rocks in the range 400 – 500°C.

M2 assemblages in MBG basic rocks and M2 cone sheets on the western margin of the intrusion are similar to the high - grade assemblages described above but with the exception of the outcrops on the western side of Hill 90 (section 3.2.2.2) those on the northern margin of the intrusion are of lower grade. Chlorite and green hornblende are the characteristic M2 phases, biotite being more or less absent. In contrast the occurence of augite + orthopyroxene + opaques ± quartz assemblages in veins in basic rocks at field location 185, on the western side of Hill 90, implies the occurence of much higher grade conditions, above the amphibole stability range, during M2. This suggests that although temperatures of M2 were rather lower overall on the northern margin of the intrusion,

thermal gradients were locally very much higher.

3). Calc - silicate assemblages, principally in impure calc - silicate hornfelses of the Middle Jurassic sequence exposed on the northern side of Druim na Gearr Leacainn within 100m or so of the contact with the MBG. (Fig. 3.11 and Map 1). These contain a variety of assemblages, mainly clinopyroxene + pink (Fe - bearing ?) garnet + sphene ± wollastonite ± idocrase ± quartz. However, an outcrop of almost pure idocrase rock with accessory grossular occurs at 46786384. Using the generalised sequence of calc - silicate minerals in active geothermal fields (Bird et al. 1984), the presence of garnet, clinopyroxene and wollastonite in these rocks, together with the absence of epidote and prehnite, suggests rather higher temperature (by 100°C or more ?) conditions than are recorded by M2 calc - silicate assemblages further from the contact. However, as emphasised by these workers and also by Bird & Helgeson (1981) the stability ranges of all of these phases is dependent on fluid compositions and it is not therefore possible to be more precise about the temperatures at which these assemblages formed.

The later M2 assemblages throughout the M2 aureole and the M2 assemblages found further from the contact are very similar overall to the M0 assemblages described in section 5.1 and will not be dealt with in detail here. They suggest that the temperatures of metamorphism later in M2 were no more than 300°C or so. Perhaps the principal difference between the M0 and low - grade M2 assemblages is that carbonate is more widespread in the latter, occuring as replacements of calc - silicate minerals including diopside in the diopside microgranites at Duin Bhain and as miarolitic cavity fills in some of the MBG rocks, and in the very intensely altered, very low grade (sericite - bearing) rocks at An Acairseid. This may reflect higher X_{CO_2} in some of the hydrothermal fluids, although the calc - silicate assemblage epidote ± actinolite ± prehnite ± quartz ± albite ± adularia, indicative of high fluid X_{H_2O}, also occurs in late M2 vugs and veins (section 3.2.5.5). The replacement of carbonate by very fine - grained dark aggregates, probably wairakite or another zeolite phase, which took place in the Middle Jurassic limestone unit on Duin Bhain, probably during M2 (section 3.2.5.5) also suggests low dissolved carbonate contents in the fluid phase.

The mineral assemblages formed during M2 suggest that the composition of the M2 hydrothermal fluids was generally similar to the fluid compositions present during M0. As noted above, X_{CO_2} in the fluid phase may have been slightly higher but was still low. The growth of M2 biotite in

originally K - poor rocks suggests that K was present at sufficiently high concentrations in the fluid for large - scale redistribution of potassium to occur, although no other cations appear to have been mobile on a similar scale in the M2 hydrothermal system. This is consistent with the inference made on the basis of O - isotope studies by Taylor & Forester (1971) that the hydrothermal fluids were meteoric in origin (see Chapter 1).

The oxygen fugacity of the hydrothermal solutions is indicated by the following assemblages:

1). Haematite occurs in some of the lowest - grade rocks, and also in association with albite and actinolite in certain retrogressed meta - amygdales in plateau basalt suite metabasic rocks. This indicates that the rocks were above the Haematite - Magnetite buffer during the latest stages of M2.

2). Apart from the above, the mineral pair magnetite - quartz is ubiquitous in rocks of the appropriate composition, up to and including magnetite - quartz veins in the two - pyroxene hornfelses on the western side of Hill 90. Orthopyroxene - magnetite veins occur in the same rocks, implying f_{O_2} above that of the four phase univariant assemblage olivine - orthopyroxene - quartz - magnetite (section 5.2.3). This suggests that the rocks were buffered to lie between HM and FMQ over a very wide temperature range, from perhaps 200 – 300°C to over 600°C, implying internal buffering of the rocks during M2. However, the extensive oxidation of M2 basic rocks observed in thin section (most notably the lamellar and granular oxidative exsolution of iron from augite to form magnetite) implies significant fluid movements through the rocks, consistent with the large - scale fluid ciculation deduced from stable isotope studies by Taylor & Forester (1971).

5.4.2. Implications of the variation in peak metamorphic temperatures for hydrothermal circulation during M2.

Although the maximum temperatures of M2 metamorphism are not well constrained, it is apparent that there are wide differences in these in a direction radial to the likely heat sources, the Inner Series and/or other intrusions emplaced within the MBG (see section 3.5), particularly on the southern margin of the pluton. In that area, between Dubh Chreag and Glebe Hill, temperature differences of perhaps 200 – 400°C occurred **within the M2 hydrothermal system** over distances of a few hundred metres. Temperature differences of a similar or even greater size occurred within

the M2 aureole at Glendrian Bay, assuming the identification of the two - pyroxene assemblages in the metadolerite at loc. 185 as being M2 in age to be correct.

The significance of such large temperature variations within hydrothermal systems close to their hot boundaries has been examined by Bickle & McKenzie (1987). Bickle & McKenzie showed that the occurence of substantial temperauture gradients through a significant proportion of a hydrothermal system is indicative of relatively slow convection which does not transport heat between the boundaries of the system (in this case, the contact of the M2 intrusions which drove the convection and the surface of the earth) many times faster than would conduction alone. In the case of the M2 hydrothermal system, the two ends of the hydrothermal system are unlikely, therefore, to have been more than a few kilometres apart. It follows that the convective boundary layer represented by the variation in peak M2 metamorphic conditions formed a significant part of the M2 hydrothermal system and that fluid flow in it was much slower than that during the preceding quenching event.

5.5. Possible causes of the changes in heat flow mechanisms during metamorphism in and around the Marginal Border Group.

The two periods of metamorphism and the quenching event(s) recognised in and around the Marginal Border Group have been shown in this chapter to be characterised by very different heat flow rates, mechanisms of heat loss and rates of hydrothermal circulation. These can be summarised as follows:

M1: Largely conductive heat flow, falling with time to as little as 8 - 40Wm^{-2} at the contact at the end of M1. Hydrothermal fluid movements occurred (from the significant amount of reduction of the rocks that took place during M1) but were very slow. This movement took place largely by pervasive intergranular percolation rather than by circulation through a discrete fracture or vein network. This period of metamorphism lasted at least a few thousand years.

Quenching event (or events, one in each sector of the MBG and contact aureole: Very rapid cooling and heat loss associated with the propagation of a tensile fracture network, or a series of similar networks, through the M1 aureole and into the MBG itself. Each fracture network contained a very vigourous hydrothermal convection system which caused the fracture network to propagate by thermal contraction cracking resulting from cooling of the hot rocks within a thermal boundary layer adjacent to the cracking front. Cooling at any one time was concentrated in this boundary layer, allowing very high cooling rates (around 1°C per hour). The quenching event was, therefore, diachronous even within individual sectors of the MBG and its contact aureole. Age relationships (Chapter 3), inferred variations in the temperature of the host rocks of syn - quenching event dykes at the time of their emplacement (section 3.2.2.1) and the orientation of the thermal stress field associated with formation of supersolidus columnar jointing suggest that the cracking front and associated rapid cooling propagated inwards and downwards with time. Heat fluxes at the cracking front were in the range 670 - 13300Wm^{-2}, up to two to three orders of magnitude greater than those at the peak of M1 metamorphism, immediately prior to the quenching event.

M2: Relatively slow heat loss from the successor intrusions to the MBG (chiefly the many small intrusions making up the Inner Series; see section 3.5). This took place by a mixture of

conduction and weak hydrothermal convective flow. This hydrothermal circulation took place within the fracture network created in the quenching event(s) and in fractures created by syn - M2 faulting (see sections 3.2.5.5 and 3.4.6 in particular).

The most surprising feature of this history of variation in heat loss rates is that, although hydrothermal fluids were present in the contact aureole of the MBG in all three stages of activity, the rate and pattern of fluid circulation appears to have varied greatly. This variation in fluid circulation rate appears to have been the dominant cause of changes in the temperature distribution in the aureole, at least during M1 and the quenching event, since the other factor involved – the geometry and heat output (Q_m) of the heat source – changed little between M1 and the quenching event, at least until the cracking front penetrated into the MBG itself. The cause of the increases in temperature implied by the overprinting relationships observed for the earlier part of M2 metamorphism (Chapter 3) is more complex, since the Inner Series was emplaced during M2 and would have provided an additional heat source. However, the fact that the Inner Series rocks did heat up the country rocks at some distance from them and were not themselves immediately quenched implies much - reduced hydrothermal circulation rates resulting from a reduction in the permeability of the country rocks after the quenching event (see below). This is consistent with the development of large temperature gradients through a large part of the M2 hydrothermal system.

There is therefore a clear distinction to be made between the hydrothermal system(s) associated with the quenching event(s) and those present during M1 and M2. The origins of this difference seem to lie in the ability of the former to create regions of high permeability by thermal contraction cracking of the rocks, whilst the latter were confined to pre - existing pores and fractures, or to fractures created by syn - metamorphic faulting.

The explanation for this contrasting behaviour is implicit in equation 5.10 (section 5.3.2.1). This equation implies that a hydrothermal system can only create its own permeability, and thereby self - propagate, when there is a large degree of thermal disequilibrium between it and the rocks around it, corresponding to a temperature difference between the two of the order of 100 – 200°C, in the range of confining pressures believed to have been present in the MBG and its contact aureole at the time of quenching (around 0.5kb; section 4.2.5). This degree of disequilibrium is necessary both to initiate the propagating hydrothermal system and to allow it to continue to propagate. This implies

that such a hydrothermal system can only be initiated by the very rapid flow of fluid from a cool reservoir into rocks which are hotter than that reservoir by at least this critical amount, at such a rate that when the fluid enters the hot rocks there is still a sufficent temperature difference between it and them for thermal contraction cracking to occur, despite heating by the rocks between the reservoir and the very hot rocks. Once the hydrothermal system has been in existence for some time it will approach thermal equilibrium with the rocks within it and the fluid flow requirement is then only that it be sufficient to maintain the necessary temperature difference at the cracking front.

The key prerequisites for the development of a self - propagating hydrothermal system and the associated thermal contraction crack network are therefore the formation of a large open fracture connecting the hot rocks and a cool fluid reservoir, and a high fluid (in the form of water or steam) flux from the reservoir into the fracture and down the fracture into the hot rocks. This latter requirement suggests that the reservoir must either be a highly permeable pressurised aquifer or a large body of surface water. In the case of the MBG, the latter, if present, is most likely to have been a lake of some sort: caldera lakes are known from the British Tertiary Volcanic Province (Bailey et al. 1924), and as far as is known the province was entirely subaerial (Richey 1961). The rapidity with which the propagating hydrothermal system(s), once initiated, cooled the contact aureole and solidified the MBG magma chamber suggests that the delay in their development (and consequently the occurence of M1 at all) was caused solely by the fact that the requirements for the initiation and propagation of the hydrothermal system(s) were only satisfied some time after the emplacement of the MBG magma chamber. Once it was active, however, any small intrusions emplaced into it (notably the M2 felsites and the radial dykes at Glendrian Bay (section 3.2.2.)) were also rapidly solidified by propagation of the crack network into them. It is not necessary to postulate seperate fracture network initiation events for each of these later intrusions.

The relatively low temperature gradients (less than 1°C/metre) in the outer parts of the M1 aureole (see Fig. 5.2) place a lower limit on the length of the fracture or fractures from which the tensile fracture network(s) originated. In order to produce a temperature difference of 100 to 200°C between fluids in the fracture and the wall rocks these initial fractures must have been at least a few hundred metres long or deep. Conversely, the low pressure of emplacement of the MBG indicates that the fractures could not have been more than a few kilometres deep. These large fractures will subsequently be referred to as **master** fractures, since their formation appears to have triggered the

quenching event(s). Furthermore, the rate of hydrothermal circulation up and down the fractures, between the reservoirs and the regions of thermally fractured rocks, through its effect on circulation and hence convective heat transfer within the fractured regions, may have been an additional rate - controlling step in the propagation of the fracture network(s).

Fractures of these dimensions are most likely to be tectonic in origin (where tectonic is taken to include both the effects of regional stresses and of stresses produced by input or removal of magmas from magma chambers, that is to say, emplacement - related stresses). Most large tectonic fractures are faults – in other words, they are associated with displacements in the plane of the fracture – and are often unsuitable as conduits for rapid, sustained convective circulation. The reason for this is that when the absolute stress across the fault surface is compressive, deformation at the fault surface typically produces a layer of fine - grained material which varies from clay - rich fault gouge through mechanical cataclasites and ultracataclasites (which seem to be the commonest types of fault rock in the MBG contact aureole (see Chapter 3)) to pseudotachylites. Whilst all of these types of fault rock except the last may be highly permeable during active faulting (Sibson 1981), they become highly impermeable soon after movement ceases (G.P.Roberts pers comm.). Although fault zones of this type may have high porosities, due to the presence of cavities at extensional bends and jogs, these cavities are isolated from eachother by intervening segments of sheared rocks and the overall permeablities are low. Faults with coarse fault breccias at the contact may be permeable for long periods but such faults were not found in the MBG aureole.

The master fractures must therefore have been dilatant fractures, which may be either purely dilational or else faults with a dilational component of displacement. In either case, the stress across the fault plane must be tensile. There are three main mechanisms by which such a stress field may be produced at constant temperature. The most widely applicable is the presence of a high interstitial fluid pressure at the site of the fault, which cancels out the lithostatic pressure. This could apply in the situation under consideration if the reservoir intersected by the master fracture was a highly permeable aquifer at lithostatic pressure, but not if it was a surface body of water, as one of the requirements for the initiation of a quenching event is a high fluid flux from the cool reservoir into the master fracture. This can only occur if the pressure in the water reservoir, be it an aquifer or a surface body of water, is greater than the pressure in the fracture (Sibson 1981).

A second mechanism by which dilatant fractures may develop in magmatically active areas is by injection of magmas into part of the fracture. Interpretation of the seismic source characteristics of earthquakes in the Long Valley caldera (California, U.S.A.) by Sammis & Julian (1987) suggests that unstable (i.e. seismogenic) propagation of near - surface dilational cracks partly filled by magma may occur over distances which are comparable with the dimensions of the pressure source, which is the magma chamber from which the fractures originated. In the case of the MBG magma chamber, if such fractures formed around it they could be up to a few kilometres long and would form in periods of the order of seconds, and fill up with magma at a much lower rate governed by the flow rate of magma down the crack. A fracture a few kilometres long which happened to intersect a suitable reservoir could clearly satisfy the requirements for a master fracture: whether it would fill with magma before it was flooded with water would depend on the flow rates of water and magma in the crack, and hence on the relative viscosities and driving pressures of the two fluids. These would vary from case to case.

Finally, at very low pressures and at low temperatures, the short - term strength of the rocks may permit absolute tensile stresses to develop in rocks affected by rapidly - applied regional or emplacement - related stresses.

A number of dilational fracture sets are visible at outcrop in Western Ardnamurchan, although none can be definitely associated with end - M1 quenching events. These include a large (up to 0.5m wide) carbonate - filled vein which runs along the foreshore at Ormsaigbeg, west of Kilchoan (Grid Ref. 475633) for some 200m in a northeast - southwest direction (strike $\approx 070°$), parallel to the contact of the pluton inland (section 3.2.5.4). This vein may well be of M2 age but lies outside the M1 aureole and the region of tensile fracture development. A much later set of tensile fractures are developed in radial faults at An Acairseid, where they cut Inner Series rocks (Map 4 and Plate 3.72). As noted in Chapter 3, many of the less well - exposed radial faults around the pluton are associated with haloes of intense hydrothermal alteration, suggesting that they acted as fluid flow conduits for considerable periods and therefore must have contained dilational fracture networks. The association of intense alteration with the radial faults, and the occurence of dilational fractures in the fault zones where these are exposed, suggests that they are the most likely candidates for possible master fractures. In contrast the concentric normal and thrust faults are not associated with hydrothermal alteration haloes and typically contain thick cataclastic zones (sections 3.2.2 and

3.2.5.4). Steeply - dipping syn- to post- Inner Series concentric reverse faults at An Acairseid and to the north and west (sections 3.3.2 and 3.4.7) are associated with hydrothermal vein networks; the large carbonate - filled vein at 475633 also appears to be associated with a reverse fault, although probably one which was mainly active at an earlier time (section 3.2.5.4).

The presence of fine - grained impermeable cataclastic fault zones within the M1 and M2 aureoles may account for the possible variation in the propagation velocity u of the hydrothermal system(s) in different sectors of the contact aureole and Marginal Border Group which was proposed in sections 5.2 and 5.3 as a possible explanation of the variation in quench and crystallisation textures between sectors. This interpretation requires that the different sectors were isolated from each other by barriers which not only stopped fluid flow but also prevented thermal contraction crack propagation below some critical temperature difference across the fault zone. Being both impermeable and structurally weak (and therefore unable to transmit thermal contraction stresses) cataclastic fault zones could have both of these properties.

It therefore seems likely that the transition from M1 to M2, and the associated quenching of anatectic melts and solidification of the MBG was triggered by the formation of radial tensile fractures by tectonic stress release. Sudden cooling of the walls of these fractures by cool fluids flowing along them from a reservoir or reservoirs outside the M1 aureole initiated the self - propagating tensile fracture network or networks. As noted in Chapter 3, there is no direct geological evidence to confirm or exclude the alternative possibilities, that the quenching events recorded in different sectors of the aureole and MBG correspond to a single diachronous event, triggered by a single phase of master fracture formation, or that they correspond to distinct events separated in time. If the end - M1 temperature profile in Fig. 5.2 records thermal disequilibrium then the similar state of the contact zone in different sectors of the MBG, which implies a similar heat flux Q_c into the wall rocks and therefore a similar temperature profile, implies that the period over which quenching occurred was short compared to the time - scale of variation in Q_c. However, as noted in section 5.2.2, there is at present no way of proving that this interpretation of the end - M1 thermal profile is the correct one.

Two indirect arguments do however suggest that the transition from M1 to M2 occurred in a single event or in a small number of events each of which affected a large part of the contact. Firstly, the inferred pattern of downward (from the occurrence of the M2 felsites) and inward (from

the inferred temperature gradients during the emplacement of the rooted dykes at Glendrian bay) propagation of the tensile fracture networks is at right angles to the propagation direction expected if these fractures had originated from nearby radial master fractures. As noted in section 5.3.2, the temperature - dependence of the propagation velocity u means that with time (and hence distance from the master fracture) the cracking front will move round into an orientation perpendicular to the pre - existing temperature gradient, suggesting that the quenching observed at the present level of exposure occurred at some distance from the master fractures (either horizontally or vertically). This implies a few widely spaced master fractures and therefore a relatively small number of quenching events, each in a different sector of the contact aureole. Secondly, the inference made above that the master fractures are associated with tectonic stresses implies that they should develop under the same stress conditions all around the pluton (in the case of stresses produced by input or removal of magma from the chamber, since the latter will produce a radially symmetric stress field) or at least on opposite, sub - parallel sides of the pluton (in the case of regional stresses). This suggests that the master fractures may have developed more - or - less simultaneously all around the pluton. The stress field around the MBG magma chamber is considered further in Chapter 7.

The very much reduced rate of convective heat transfer associated with the post - quenching phase of metamorphism, M2, implies that the permeability of the contact aureole during M2 was very much lower than it was during the propagation of the tensile fracture networks. This implies both that the permeability produced by the latter was reduced early in M2, by mechanisms considered below, and that temperature differences between the host rocks and the M2 hydrothermal fluids were never great enough at any one point to initiate new thermal contraction crack networks.

Evidence for the operation of four mechanisms of permeability reduction and/or limited amounts of creation of new permeability during M2 is present in the country rocks and the MBG itself. These are as follows:

1). Deposition of M2 mineral assemblages in tensile fractures. These are commonly peak - M2 assemblages, implying either that the increases in temperature were not produced by the effects of mineral deposition in fractures or that earlier M2 assemblages were redissolved or replaced at the peak of M2: metamorphosed early M2 assemblages are rare whilst late - M2 vein assemblages mainly occur in shear fractures.

2). Permeability reduction by ductile creep (at high temperatures) or static fatigue failure (at low temperatures) in the blocks between the tensile fractures (Lister 1974). The occurrence of fatigue failure may be recorded by the presence of very small irregular fractures between the main fractures of the tensile fracture network (section 5.3.1).

3). Dissection of the fracture network by M2 cataclastic fault zones. The low permeability of these fault zones would cause blocking of the fluid flow paths. However, in the areas where low - angle cataclastic thrust faults are most common (Glendrian Bay and Duin Bhain) M2 temperatures were generally low and permeabilities are considered to have remained high during M2 (section 5.4.2). This may have been due to the formation of radial fractures with dilations perpendicular to the thrust direction, which is also radial (see section 3.2.2). Radial vertical fractures of M2 age (or younger) are common in both areas. In other areas both thrusts and radial fractures are less common but M2 movements on concentric normal faults (sections 3.3.5.1 and 3.2.5.4) produced cataclastic rocks which may have partly blocked hydrothermal circulation. It appears that the effects of tectonic deformation upon permeabilities at a particular locality during M2 were critically dependent on the orientation of the M2 stress field at that locality.

M2 cone sheets and other minor intrusions, even those emplaced late in M2, are characterised by well - developed vein and joint networks perpendicular to their margins. These would be expected to develop as bodies of this size cooled and contracted, even in the absence of hydrothermal circulation, and mean that such intrusions would only be temporary barriers to circulation. Subsequently, however, basic minor intrusions would tend to become more impermeable than their host rocks because of reaction of ferromagnesian minerals to lower - density hydrous phases, producing a volume increase which would be accomodated by partial closure of the fractures.

The involvement of large - scale tectonic deformation of the wall rocks of the MBG magma chamber in the initiation or triggering of propagating thermal contraction crack networks carries a very important corollary. It has been shown in this chapter (sections 5.2 and 5.3) that, as a result of the rapid hydrothermal cooling associated with the propagating cracking front(s) the boundary layer of the MBG magma chamber changed from one in which heat flow from the interior of the magma chamber was just sufficient to melt the walls of the chamber at a very low rate (by the episodic meting process described in Chapter 4) to one in which rapid solidification of magmas from

the interior of the chamber took place. To use the theoretical classification described in section 4.1, the boundary layer changed from a Type 2 boundary layer, with the wall of the magma chamber migrating outwards (although only at a very low rate) to a Type 1 boundary layer, with very rapid inward migration of the wall of the chamber. Indeed, if the hydrothermal system continued to propagate into the interior of the MBG magma chamber with the same value of u as was inferred for its migration through the aureole and contact zone, the entire MBG magma chamber could have been solidified in as little as a few tens of years. This is perhaps an unlikely extreme case but it illustrates the point that the structural evolution of the Marginal Border Group magma chamber, and in particular the pattern of brittle deformation in its host rocks, exerted a controlling influence on its overall evolution as well as upon the behaviour of the M1 boundary layer (through the downfaulted block melting phenomenon described in Chapter 4). Other intrusions, emplaced at subvolcanic depths in brittle rocks and therefore potentially accessible to circulating hydrothermal fluids might also be expected to show similar phenomena: the occurrence of fine - grained to quenched anatectic rocks around such intrusions, as noted at the beginning of this chapter, suggests that the Hypersthene Gabbro is not unique in this respect.

6. MAGMATIC AND METAMORPHIC PROCESSES IN THE INNER SERIES OF THE HYPERSTHENE GABBRO.

6.1. Differences between petrological and geophysical models of basic magma chambers in the upper crust: does the Inner Series correspond to a 'geophysicist's magma chamber' ?

As was noted in Chapter 1, there is a discrepancy between geophysical data on the melt percentage present in most subvolcanic basic magma bodies and the normal petrological model used to interpret geochemical and mineralogical variations in suites of basic to ultrabasic rocks affected by low - pressure fractionation. The former suggest that most, although by no means all (Detrick et al. 1987) magma chambers at shallow depths in the crust are mostly made up of low - melt - percentage material, although they may contain ramifying networks of small, sill and/or dyke - like intrusions with higher melt percentages (Ryan 1988). In contrast, petrological models for the evolution of low - pressure suites are normally based upon the concept of fractionation in large, high - melt - percentage magma bodies, although some recent petrological (Bedard et al. 1987), theoretical - geochemical (Langmuir 1989) and fluid dynamic (Sparks et al. 1985) studies have emphasised the importance of intercumulus crystallisation and the exchange of melts between regions of high melt percentage and cooler regions of low melt percentage by compositionally - driven intercumulus convection. Such processes were examined by these authors in the context of crystallisation of cumulates on the walls and floor of large, high - melt - percentage magma chambers but there seems to be no good reason to suppose that similar processes could not go on in large, slowly - crystallising low - melt - percentage magma bodies, particularly if these contain a network of high - melt - percentage magma conduits capable of acting as melt sources and sinks.

A crucial problem in the interpretation of rocks affected by shallow - level magmatic processes is, therefore, whether there are significant differences between the products of fractionation in high- and low - melt - percentage magma bodies, as the answer to this question will determine whether there is any good petrological reason for preferring one type of magma body over the other in the interpretation of the petrogenesis of suites of rocks affected by low - pressure fractionation processes. Another way of stating the same problem is that it concerns whether or not petrological data can

be used to infer whether the magma chamber(s) that produced a particular suite of rocks were high- or low - melt - percentage magma bodies.

Field and petrographic evidence discussed in sections 3.3 and 3.4 suggest that the gabbronorites and later related rocks of the Inner Series represent the solidified remains of a large, mainly low - melt - percentage magma body, made up of many small intrusions, analogous to the bodies of magma believed to occur beneath many active volcanoes on the basis of geophysical data (Iyer 1984; Ryan 1987). It was shown in sections 3.4.1 to 3.4.3 that these rocks (in contrast to some of the pre - gabbronorite banded and laminated rocks present in the Inner Series) lack unambiguous evidence for the operation of **cumulus** (in the terminology of Wager et al. (1960)) processes, such as graded layering and cross - layering, which would indicate crystallisation at the margins of a large high - melt - percentage magma body. Settling of plagioclase porphyrocrysts and some differentiation may have taken place within a few sheet intrusions at Sanna (section 3.4.1; especially Fig. 3.23) but that is all. In contrast, there is much evidence for the operation of a variety of processes which would mormally be considered to be post - cumulus in age although in this case this is something of a misnomer because there was no phase of cumulus crystallisation as such. These 'post - cumulus' processes include the formation of a generally weak, but intermittently well - developed, plagioclase lamination, textural equilibration of olivine poikilocrysts and internal straining of olivine, all of which reflect compaction and melt expulsion, and the formation of metasomatic pyroxenite bodies.

The gabbronorites and related rocks of the Inner Series therefore have considerable potential for the study of the effects of these processes upon the compositions of the intrusions in which they operated. Provided the composition of the rocks prior to the operation of these processes is well constrained, the compositions of the complementary interstitial melts can be deduced. Given the interpretation of the Inner Series as a low - melt - percentage magma chamber the distinctive features (if any) of these melts could be used to identify the products of such a chamber amongst volcanic rock suites.

6.2. Sub - rigidus and other magmatic processes and their compositional effects in the gabbronorites and related rocks of the Inner Series.

The group of rocks to be discussed in this section is formed by the generally porphyritic gabbronorites (both those which can clearly be shown on field evidence to form discrete sheet intrusions and those for which the field evidence is less clear), the slightly later metasomatic pyroxenites and the still later porphyroblastic granular - textured dolerite and microgabbronorite sheets. The single isotropic ferrogabbro sample from An Acairseid is also considered in this section as its age relationships indicate that it is broadly coeval with the gabbronorites, although probably slightly earlier (section 3.4.2). The pre - gabbronorite laminated gabbros (although not the more exotic granular banded rocks) are also relevant to this section because although they are demonstrably older that the gabbronorite suite proper, they appear to provide extreme examples of rocks affected by the post - cumulus processes which produced igneous lamination in the gabbronorite suite rocks (sections 3.4.1 and 3.4.2). In addition, the metasomatic pyroxenites in the Sanna area replace both rock types in much the same way.

6.2.1. Other causes of compositional variation in the gabbronorite suite.

Before the effects of sub - rigidus or 'postcumulus' processes on the compositions of the gabbronorite suite rocks can be considered it is necessary to examine the effects of other causes of variation within the suite. These are as follows:

1). Accumulation of phenocryst phases suspended in the magmas when they were emplaced, especially the bytownitic feldspar porphyrocrysts present in the majority of the gabbronorites themselves, but possibly other phases as well.

2). Varying degrees of differentiation in the parental magmas from which individual intrusions or groups of intrusions were derived (or, in the conventional terminology of basic plutonic rocks, cryptic variation).

3). Variation in the parental magmas reflecting different degrees of partial melting in the mantle source of the magmas, or variation in mantle source composition, or differing degrees or types of crustal contamination.

6.2.1.1. Were the rocks of the gabbronorite suite derived from cogenetic magmas ?

The third of these factors is perhaps more relevant to the discussion (section 6.3) of differences between the gabbronorite suite rocks and other groups of rocks within the Hypersthene Gabbro (notably the pre - gabbronorite rocks in the Inner Series, the basic rocks of the Marginal Border Group (section 4.3), and the various late - M2 and post - Inner Series dolerites and quartz gabbros). The uniform mafic mineral composition of the gabbronorite suite rocks (two pyroxenes ± olivine) suggests that all were derived from tholeiitic magmas. However, the later, finer - grained granular dolerites tend to have lower contents of orthopyroxene relative to augite than the gabbronorites proper, suggesting perhaps that they were derived from less extreme tholeiitic magmas.

The extremely low abundances of most incompatible elements in these rocks, coupled with the errors in XRF major and trace - element analyses (see Appendix 1) and the need to allow for other causes of variation in those elements for which accurate analyses are available, make it difficult to quantify any variations in the parental magmas of the gabbronorite suite. Such variations do appear to occur within some basic and ultrabasic intrusions, both outside the British Tertiary Province (e.g. Lambert & Simmons 1987) and within it, for example within the Cuillins complex (Dickin et al. 1984) and possibly within the marginal border group of the Rhum complex (data of Greenwood 1987). However, several lines of evidence suggest that the parental magmas of the gabbronorite suite were relatively uniform except in degree of differentiation and varying amounts of porphyrocryst accumulation.

Fig. 6.1 is a plot of TiO_2/MgO vs. $Fe_2O_3^T/MgO$ (all values being calculated using weight percent data in this case). The gabbronorite suite rocks form a well - defined, linear or slightly curved array in this diagram. In part, this reflects the coincidence of the array defined by the non - cumulate granular dolerites (which must correspond to a liquid line of descent) with a mixing line between such magmas and typical high - temperature Ti-magnetites, which contain around 10 – 20% TiO_2 (such as would be produced by late - stage accumulation of Ti - magnetite, which appears to have

Fig. 6.1. Plot of TiO2/MgO vs. Fe2O3T/MgO for the gabbronorite suite rocks.

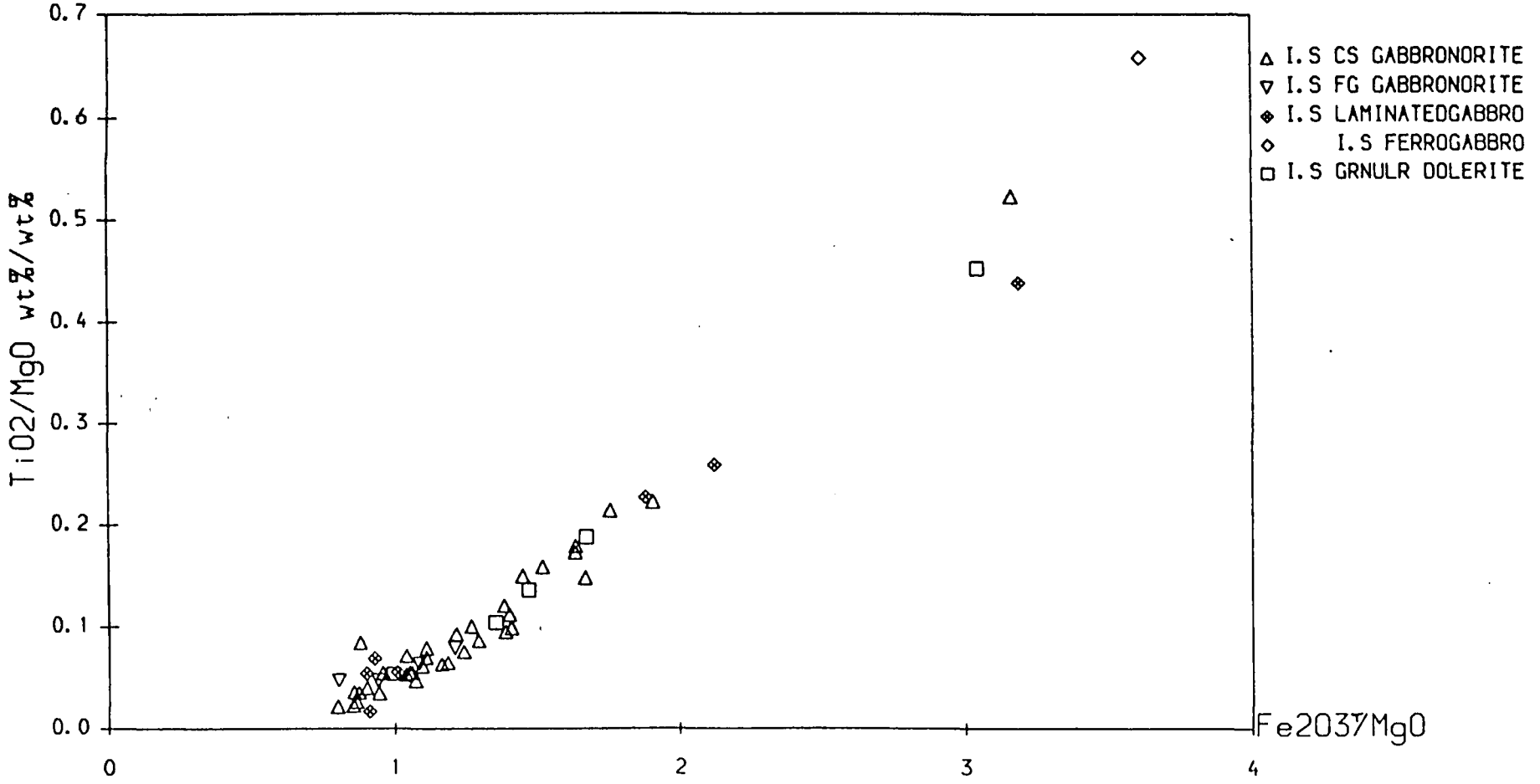

taken place in some of the more evolved laminated rocks (section 6.2.2.1)). However, the well - defined array in Fig. 6.1 would also not be present if the parental magmas had shown a significant variation in Ti contents at a given degree of differentiation, for example due to differences in the amount of partial melting in the mantle source region: Ti is a sensitive although rather imprecise indicator of such variations (Klein & Langmuir 1987). The narrowness of the array in Fig. 6.1 therefore implies a fairly uniform parental magma composition.

The observed variation in modal orthopyroxene abundances between the orthopyroxene - rich gabbronorites and the relatively opx - poor granular dolerites suggests that normative orthopyroxene contents would be a still more precise indicator of variation in the parental magmas than the other quantities discussed here. However, the errors in SiO_2 analysis by XRF, the method used to analyse most of the gabbronorites and all of the granular dolerite samples, are as much as $\pm 2\%$ (2σ confidence limits; see Appendix 1). This corresponds to a 20% (absolute) variation in normative orthopyroxene contents in olivine and orthopyroxene normative rocks and implies that normative orthopyroxene contents derived from the present data set would be far too imprecise to distinguish the granular dolerites from the gabbronorites, quite apart from the problems introduced by the alteration of the Fe^{3+}/Fe^{2+} ratios of the rocks by the observed oxidative metamorphism (section 6.4.2).

Fig. 6.2 plots Ce_N/Yb_N (see Appendix 1 for chondrite - normalisation factors) against a variety of other parameters. Considerable amounts of scatter are present in these diagrams, a significant part of which may be due to the errors in REE analysis, especially at the very lowest abundances ($\pm \geq 20\%$ relative at Ce $\leq$ 5ppm; an approximate error bar at these abundances is marked). However, some overall trends are apparent in these plots.

The ratio Ce/Yb would be expected to vary as a result of a number of processes:

1). Expulsion of REE - rich residual melts from clinopyroxene and/or plagioclase - rich crystal mushes. Heavy rare earth elements (HREEs) such as Yb are only moderately incompatible in clinopyroxenes in equilibrium with basaltic magmas (K_D cpx/melt $\approx$ 0.5 - 1.0) whilst light rare earth elements (LREEs) are more strongly incompatible ($K_D \leq 0.2$; both values from compilation of Henderson (1982)). LREEs show limited substitution into

Fig. 6.2. Variation in the ratio Ce /Yb with other compositional variables in the gabbronorite suite rocks.

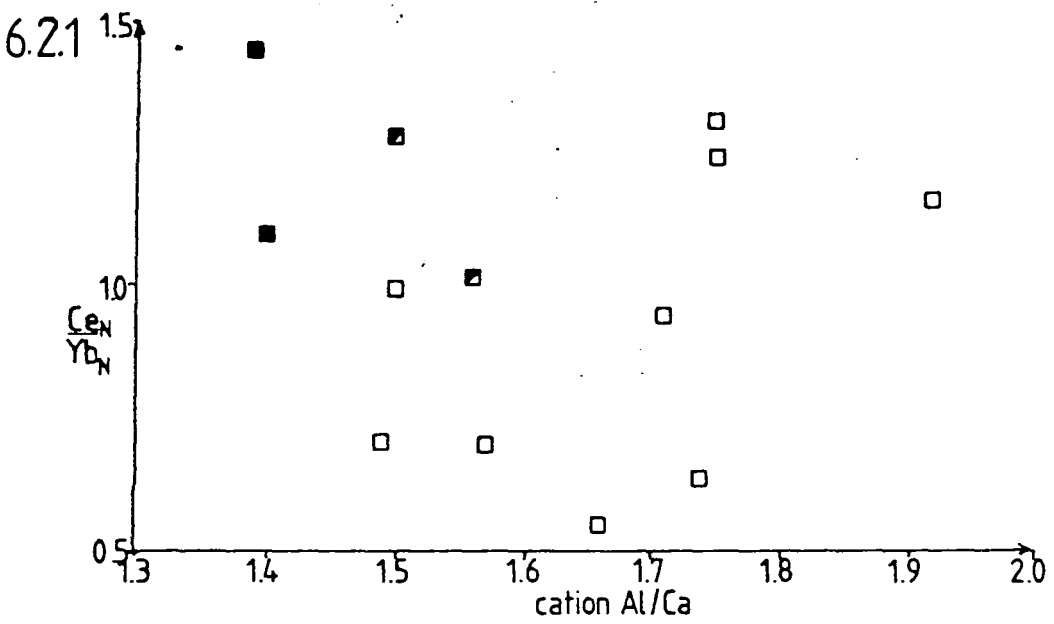

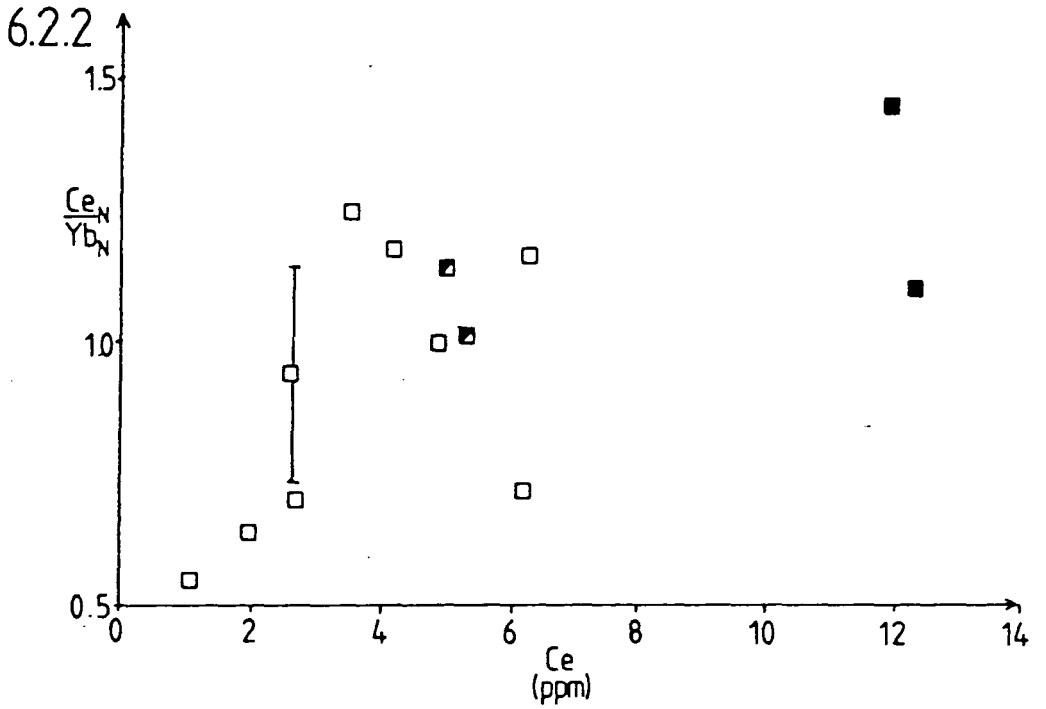

■ Granular dolerites

◪ Fine - grained gabbronorites

□ Coarse - grained gabbronorites

6.2.3

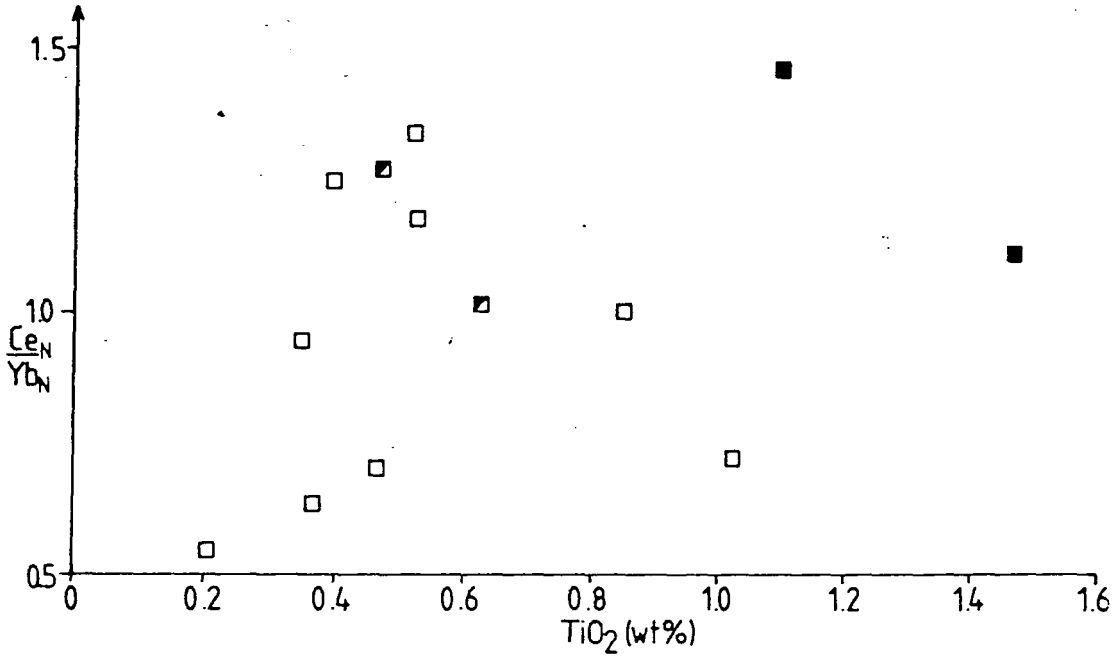
1.5
1.0
0.5
$\frac{Ce_N}{Yb_N}$
0
0.2
0.4
0.6
0.8
1.0
1.2
1.4
1.6
TiO_2 (wt%)

6.2.4

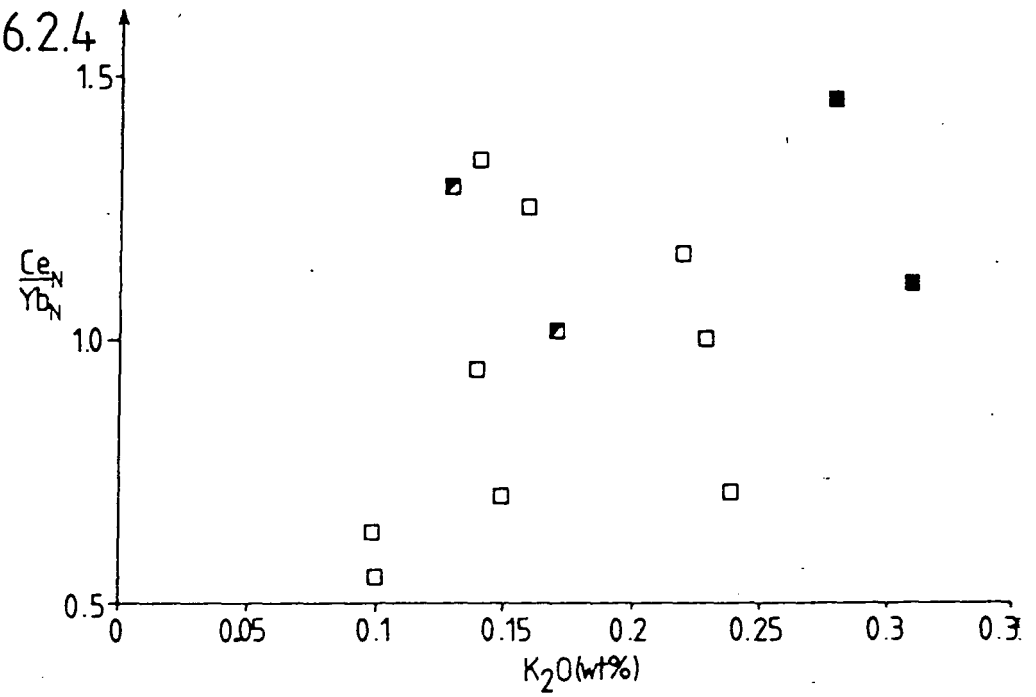
1.5
1.0
0.5
$\frac{Ce_N}{Yb_N}$
0
0.05
0.1
0.15
0.2
0.25
0.3
K_2O(wt%)

even very calcic plagioclase (Lambert & Simmons 1987) whilst HREEs do not. The lack of positive correlation of Ce/Yb with Al/Ca (which increases with plagioclase accumulation) in Fig. 6.2.1 suggests that this latter substitution does not significantly affect the REE content of the gabbronorite suite rocks. The lower Ce/Yb in most of the coarser - grained rocks in the suite which is apparent in these plots suggests instead that some of the variation in Ce/Yb is due to preferential retention of HREEs relative to LREEs in interstitial clinopyroxene as melt expulsion took place. However, Ce/Yb only correlates with Ce content (Fig. 6.2.2) and not with the abundances of other incompatible elements (Figs. 6.2.3 and 6.2.4).

2). Degree of differentiation. This would be expected to produce a correlation with the abundances of incompatible elements in the fine - grained rocks in Fig. 6.2, which is not observed except in the case of Ce itself.

3). Crustal contamination of the magmas prior to their entry into the low - melt - percentage Inner Series magma chamber. Tholeiitic magmas such as those parental to the gabbronorite suite rocks have very low REE contents and their LREE/HREE ratios are therefore strongly sensitive to crustal contamination with high LREE/HREE rocks such as those of north west Scotland (see Chapter 2). The variation in Ce/Yb in these rocks could therefore be produced by relatively small differences in the amount and/or composition of any crustal contaminants present. Conversely, the generally low Ce/Yb suggsts that the average amount of crustal contamination was small and that the high modal orthopyroxene content of the majority of the gabbronorite suite rocks reflects the extremely tholeiitic character of the original, uncontaminated parental magmas.

Whatever the cause of the variation in Ce/Yb, the key point to be drawn from Fig. 6.2 is that Ce/Yb is in fact very uniform within the gabbronorite suite rocks, with little variation over and above the limits of analytical error. It follows that the parental magmas must have been nearly uniform with respect to REEs, again implying that they shared a common primary parent magma.

Such evidence as is available therefore suggests that the parental magmas of the gabbronorite suite rocks were uniform, weakly crustally contaminated tholeiitic rocks. In the following discussion it is assumed as a first approximation that all the gabbronorite suite rocks were derived from cogenetic

magmas and that any variations not due to post - cumulus processes are due to variations in the amounts of porphyrocryst accumulation or in the degree of previous fractionation. The variations in modal orthopyroxene abundances in rocks showing similar degrees of fractionation suggests that this assumption is only approximately true but the lack of systematic variation in other compositional quantities implies that it can be taken as valid for present purposes. This assumption is in any case irrelevant when the effects of 'postcumulus' or sub - rigidus processes on different parts of the same small intrusion are under consideration, but it does affect the interpretation of the overall variations within the gabbronorite suite.

6.2.1.2. Cryptic variation in the gabbronorite suite.

Wells (1954) concluded, on the basis of optical determinations of mineral compositions in rocks which are here considered to form part of the gabbronorite suite, that there was relatively little cryptic variation within the Hypersthene Gabbro, and certainly no consistent pattern of variation. Microprobe analyses of mineral compositions and bulk rock analyses carried out as part of the present work confirm this conclusion, at least as a first approximation. Fig. 6.3 shows plots of magmatic (as opposed to later symplectite and vein minerals) plagioclase, olivine and pyroxene grains in those gabbronorites (senso stricto) analysed by microprobe (see Appendix 3), and whole - rock cationic $Fe_{total}/(Fe_{total} + Mg)$ vs. normative (An/An + Ab) for all the gabbronorite suite rocks analysed. A significant spread of data is apparent in all of these plots but much of this is due to factors other than cryptic variation, particularly in the case of the mineral data.

The plagioclase data show a well - defined trimodality, with dense clusters of analyses between An_{82} and An_{85}, An_{78} and An_{80}, and An_{60} to An_{70}. To a very large extent, these correspond to the petrographically identified porphyrocryst cores, outer cores or 'mantles', and porphyrocryst rims and groundmass feldspars respectively (Table 6.1). A few samples from each petrographically defined group lie in other groups as far as their composition is concerned: in some cases this may be because of petrographic misidentifications resulting from the fact that identification has to be made on the basis of single two - dimensional sections. The presence of this trimodal distribution in almost all of the gabbronorites analysed indicates a common three - stage crystallisation history and, again, suggests that the gabbronorites are very closely related rocks. In contrast, the two granular dolerites analysed using the microprobe show a bimodal distribution of feldspar compositions. In

Fig. 6.3. Analyses of magmatic plagioclases, olivines and pyroxenes in the gabbronorites (senso stricto) and granular dolerites, and of Mg' vs. An - number for all gabbronorite suite rocks.

6.3.1
PLAGIOCLASES

AB - AN - OR

COARSE AND FINE GRAINED GABBRONORITES

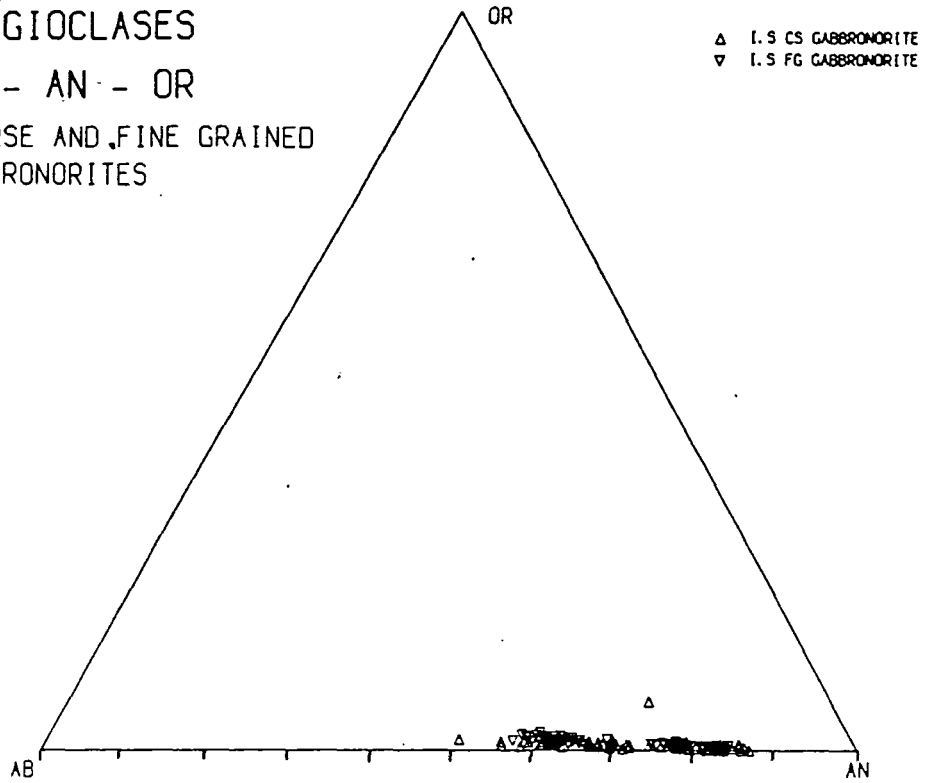

6.3.2
PLAGIOCLASES

AB - AN - OR

GRANULAR DOLERITES

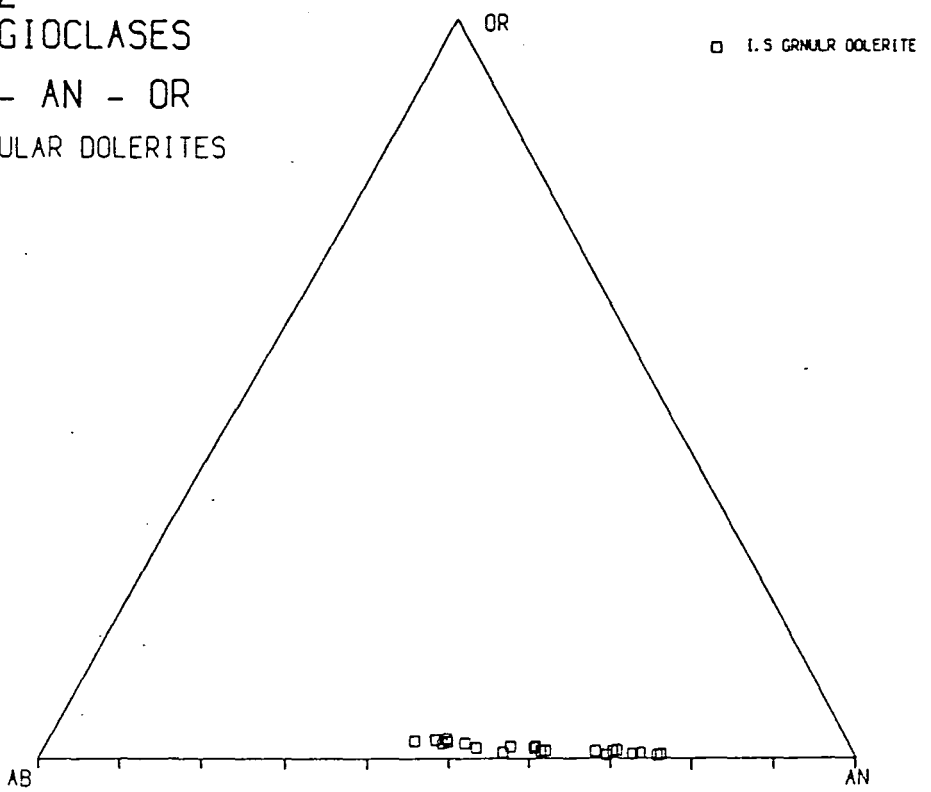

6.3.3 PYROXENE

EN - FS - WO

COARSE AND FINE - GRAINED GABBRONORITES

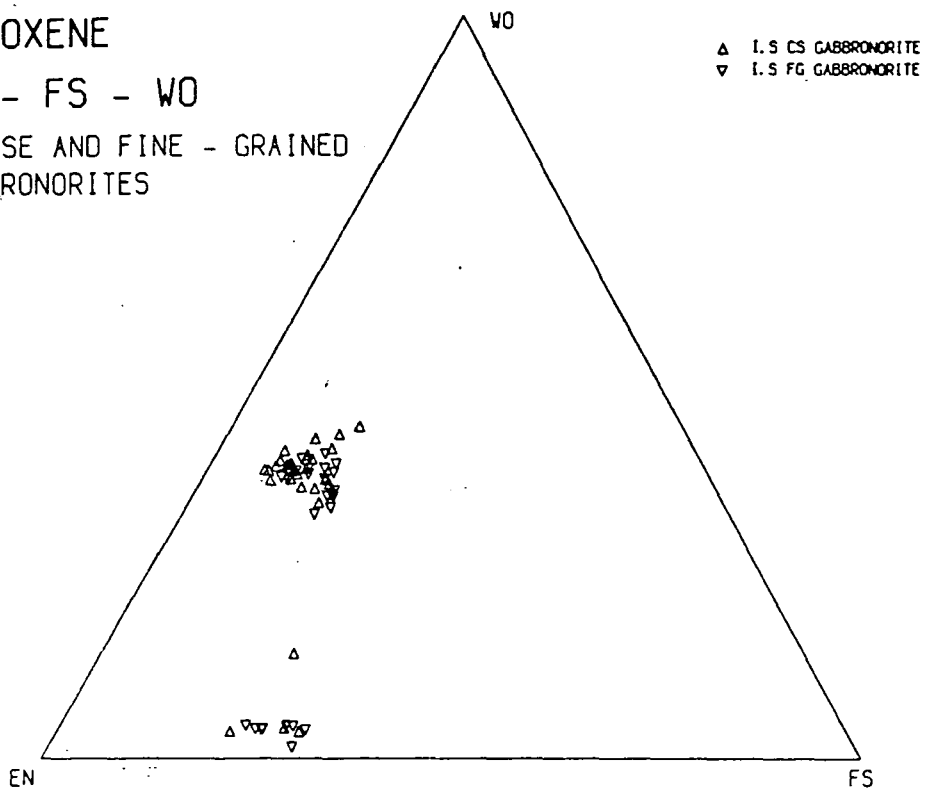

6.3.4 PYROXENES

EN - FS - WO

INNER SERIES GRANULAR DOLERITES (2 ROCKS ONLY)

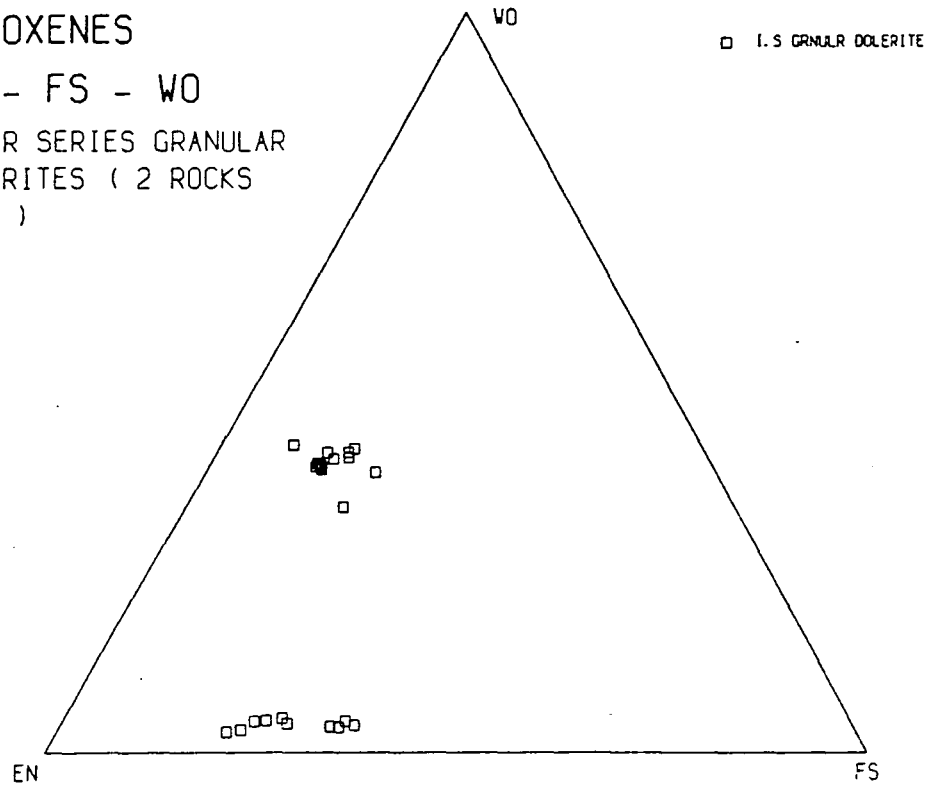

6.3.5 OLIVINES.

FO - FA - MN

GABBRONORITES

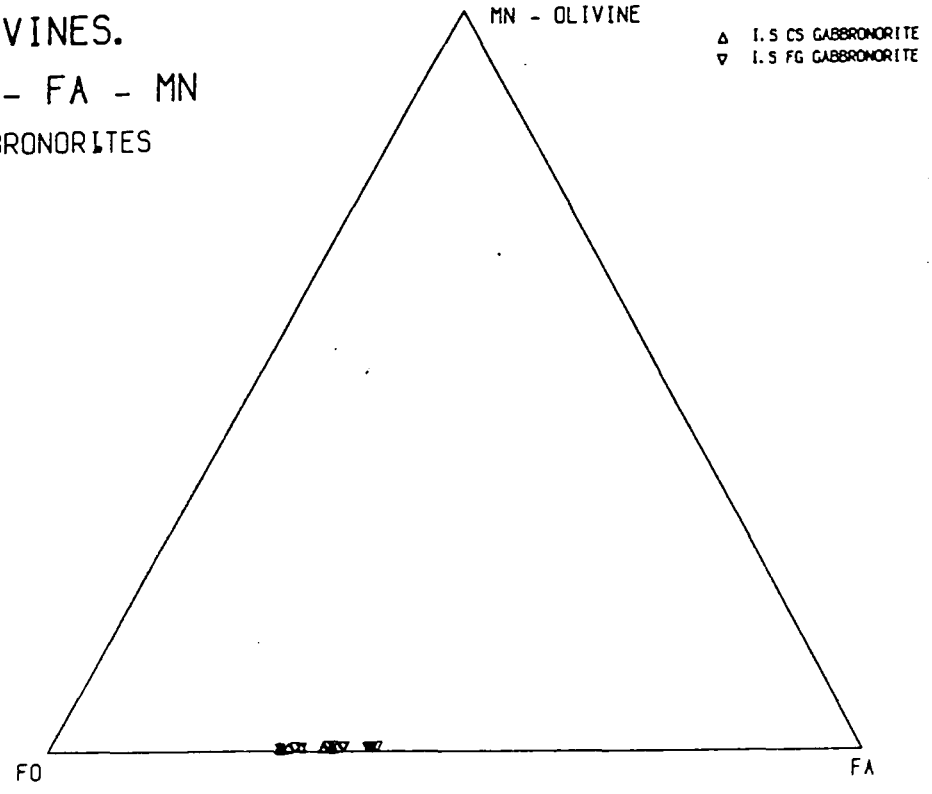

6.3.6

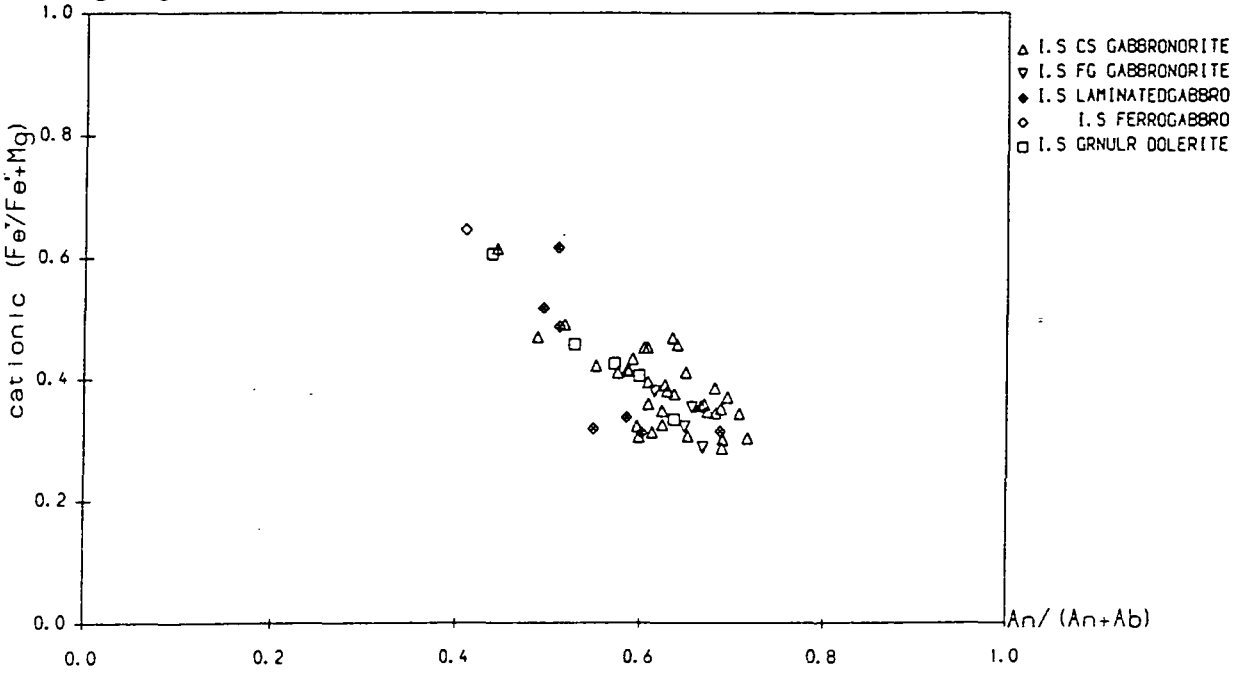

Table 6.1

Compositions of porphyrocryst and groundmass plagioclases from gabbronorite suite rocks.

Column 1 lists sample analysed, column 2 lists whether the sample is a coarse - grained or fine - grained gabbronorite, or a granular dolerite. Columns 3 to 6 list the compositions of feldspar types from each sample expressed as An - numbers; the number **n** of analyses of crystals or parts of crystals of each type analysed in the sample concerned are listed in the second row of each entry. The two sets of values for groundmass feldspars in samples 296 and 275/6 are for rims and cores respectively.

Table 6.1 (continued)

Sample	Rock Type	Porphyrocryst Inner Core	Porphyrocryst Outer Core	Porphyrocryst Rim or replaced area of core	Groundmass
275/1	Fine	77 – 84	–	61 – 69	60 – 65
n		10	0	5	5
315C	Coarse	79 – 83	68, 70	59, 62	56 – 71
n		3	2	2	6
25	Coarse	78 – 86	78, 72	56 – 71	50 – 71
n		11	2	4	3
296	Fine	82 – 84	76 – 78	58 – 65	60-66, 66-79
n		14	10	16	11
2	Coarse	83 – 87	76 – 82	77	69
n		7	5	1	1
315D1	Coarse	65	–	–	58 – 61
n		1(?)	0	0	3
6A	Fine	–	–	–	57 – 61
n		0	0	0	3
5	Coarse	82 – 86	–	60 – 63	61, 62
n		3	0	5	2
35	Coarse	81	74	66 – 70	67 – 69
n		1	1	4	5
275/6	Granular	70 – 73	70 – 76	69	44-49, 47-60
n	dolerite	3	3	1	5, 5
286/5	Granular	68	–	56	61, 61
n	dolerite	1	0	1	2

sample 275/6, which is very fine grained and contains relicts of variolitic texture, the feldspar compositional range also extends to distinctly more sodic compositions. This may, however, simply reflect greater zonation of groundmass feldspars under conditions of more rapid cooling.

The three - stage crystallisation history implied by the trimodal distribution of feldspar compositions, together with the corroded, xenomorphic habit of many of the feldspar cores, suggests that the gabbronorite magmas were the products of a complex cooling history and compositional evolution. This may have included mixing of compostionally contrasted basic (or possibly basic and ultrabasic) magmas, one of which contained the bytownitic feldspars. Alternatively, the calcic plagioclase porphyrocrysts may have been derived from pre - existing cumulates of uniform composition (see core analyses in Table 6.1). The development of intracrystalline deformation in these feldspars does not, however, constitute proof of this (in contrast to the situation in the undeformed M2 felsites (section 4.2)) because the groundmass in which the porphyrocrysts occur also shows intracrystalline deformation, indicating that the rocks were deformed in situ (section 3.4.1). For present purposes, however, a key feature of the data in Table 6.1 is that most of the variation in plagioclase compositions occurs within individual thin sections and there is relatively little systematic variation between samples.

The ferromagnesian minerals plotted in Figs. 6.3.3 to 6.3.5 also show a restricted range of compositions. All the grains in these plots were identified on petrographic grounds as being of magmatic origin (ophitic pyroxenes and ophitic or equant olivines). Nevertheless, the low *Wo* contents of the orthopyroxenes and the variable but often very high *Wo* contents of the clinopyroxenes point to relatively low - temperature (i.e. near - solidus or high - grade metamorphic) compositional re - equilibration of these minerals (see section 6.4). Furthermore, since much of this re - equilibration has involved oxy - exsolution or oxidation reactions (sections 3.4.6 and 6.4) the Fe/Mg ratios of these minerals are likely to have been reset to greater or lesser extents, and are not reliable indicators of cryptic variation.

A plot of whole - rock $Fe_{total}/(Fe_{total}+Mg)$ against normative An/(An + Ab) for the gabbronorite suite (Fig. 6.3.6) shows considerable scatter around an overall fractionation (or cryptic variation) trend or trends defined by the fine - grained gabbronorites and granular dolerites. Although some of the metamorphic reactions to be discussed in section 6.4 imply significant mobility of many elements,

including Fe, Mg and Si, during the high - grade hydrothermal metamorphism of the Inner Series, much of this may have been on a small scale and would therefore affect bulk - rock compositions less than mineral compositions. Whole rock parameters such as those plotted in Fig. 6.3.6 will probably therefore be a better indicator of cryptic variation in such rocks than mineral data.

The scatter about the overall fractionation trends in Fig. 6.3.6 probably has a number of causes:

1). **Accumulation of An - rich plagioclase porphyrocrysts** in the gabbronorite magmas, either by crystal settling in situ (visible in only a few cases, however) or in magma chambers at depth through which the magmas passed before being emplaced at the present level of exposure. Most of the gabbronorites are An - enriched relative to fine - grained rocks with the same Fe/Mg ratio, implying that this effect is an important one in these rocks.

2). **Accumulation of Mg - rich ferromagnesian minerals in the magmas.** This could either be by accumulation of ferromagnesian primocrysts in the magmas prior to consolidation (that is to say, above the rigidus temperature of these magmas), or by preferential growth of ferromagnesian minerals below the rigidus, during compaction and the development of lamination (section 6.2.2.1, below). Primocrysts of ferromagnesian phases, particularly olivine, have in the past been assumed to be more - or - less euhedral (e.g. Wager et al. 1960): there is little petrographic evidence to suggest that large - scale accumulation of such crystals has taken place in the gabbronorite magmas. However, it has recently been suggested that the true form of some olivine primocrysts in basic magmas is dendritic or poikilitic (R.H.Hunter pers comm.). Poikilitic olivine crystals occur in the finer - grained gabbronorites in particular, and can be shown to pre - date post - consolidation deformation of the host rocks (section 3.4.1, especially Plate 3.74). Geochemical evidence (section 6.2.1.3) suggests that accumulation of such olivine crystals may indeed have occurred in many of the gabbronorites, the petrographic evidence having been obscured by subsequent recrystallisation.

3.) **Accumulation of Fe - rich oxide minerals.** These minerals invariably occur as late -stage, largely post - compaction interstitial grains and can only have accumulated by 'post-cumulus' growth of oxide phases in the interstices of the crystal mush.

4.) Bulk compositional changes during hydrothermal metamorphism (see section 6.4).

These various possibilities are discussed further below. Whatever the cause of the scatter, it is apparent from the plots in Fig. 6.3 that there is a small but detectable amount of cryptic variation within the gabbronorite suite rocks. This suggests a test of the interpretation (see sections 1.2, 3.3.2 and 3.4.1) of the whole of the gabbronorite suite as a series of confluent intrusions, rather than a layered sequence intruded by the relatively small proportion of gabbronorite suite rocks which can be shown unequivocally, on the basis of field evidence, to form sheet intrusions (sections 3.4.1 and 3.4.4). Regular upward cryptic variation within a mafic pluton is a very strong indication that it formed by the progressive crystallisation of a single large magma body. The opposite case, however, is not as good an indicator of the geometry of the original magma bodies because irregular or cyclic cryptic variation may be produced either by intermittent or periodic replenishment of a single magma body or by the presence of multiple intrusions.

In the case of the Inner Series, even if a regular pattern of cryptic variation had originally been present it would have been disrupted by vertical movements on syn- to post- Inner Series faults (section 3.4.7). However, a number of relatively large fault - bounded blocks are present within the Inner Series (Fig. 3.29 and Map 1). If systematic cryptic variations are present within these blocks then it should be apparent in radial traverses across them, given that all interpretations of the Hypersthene Gabbro as a single layered intrusion (Wells 1954; Skelhorn & Elwell 1971) indicate that the 'layering' dips inwards. Conversely, if within these blocks the known intrusive sheets of gabbronorite have the same composition (in terms of cryptic variation) as the rest of the gabbronorite in those blocks, whilst cryptic variation occurs **between** fault blocks then the variation will support the confluent sheet intrusions model.

A number of such radial traverses, with known faults marked, are presented in Fig. 6.4. With the possible exception of the Druim na Gearr Leacainn – Beinn Hiant traverse (and even in this case a fault could be present, in the poorly exposed ground between Druim na Gearr Leacainn and the foot of Beinn na Seilg), there is no strong evidence for systematic cryptic variation within the fault - bounded blocks comparable to that between them. The first sample traverse, that in the Sanna Bay area, is particularly significant because it includes a number of sheet intrusions identifiable as such

Fig. 6.4. Radial sample traverses through the Inner Series, showing changes in cryptic variation indices with distances from the contact (corrected for the effects of topography).

1. Sanna Bay.

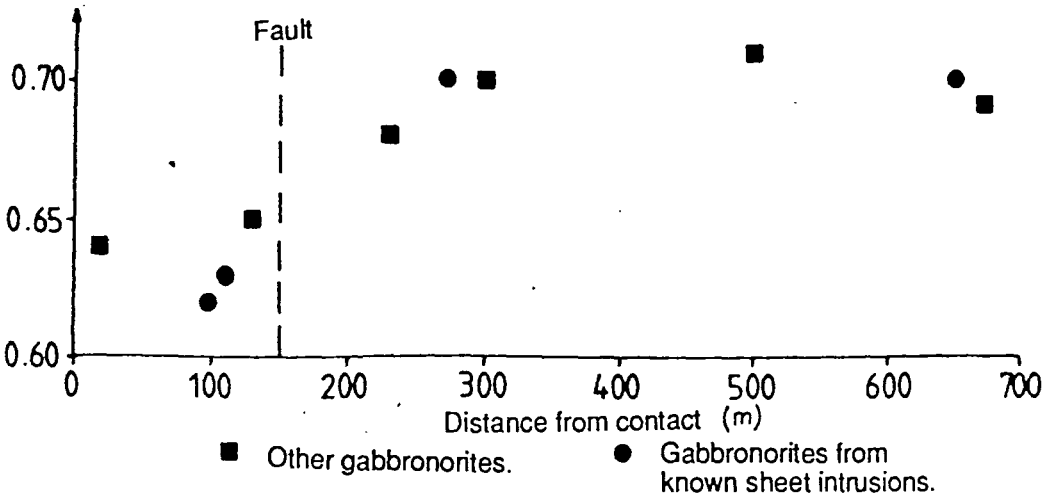

2. Ardnamurchan Point and East of Gharblach Mhor.

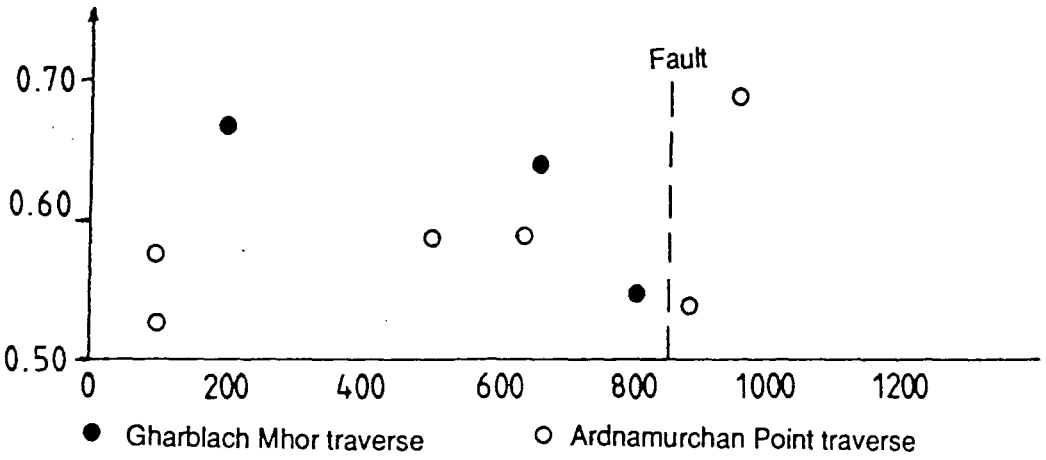

3. South of Beinn na Seilg (distances corrected for topography assuming an average dip of 30°).

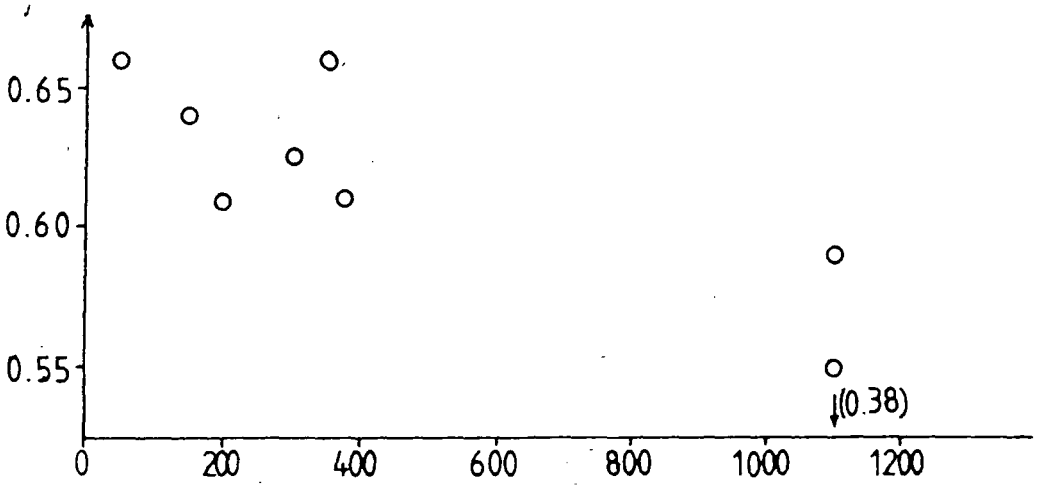

on the basis of field evidence, as well as rocks which cannot be shown unequivocally to form part of sheet intrusions at outcrop. The known intrusive gabbronorites and the other gabbronorites show the same change in Fe/Mg ratio across the concentric fault which separates the two groups of rocks (that immediately to the south of the northernmost group of laminated rocks shown in Fig. 3.25). This suggests that the two blocks are each composed of a compositionally distinct group of intrusive gabbronorite sheets, each with a uniform composition, which were juxtaposed after emplacement by movement on the faults.

The data on cryptic variation is therefore at least consistent with the interpretation of the gabbronorite suite rocks, and perhaps the Inner Series as a whole, as being made up of a large number of intrusive sheets. Furthermore, this interpretation is confirmed by the parallel variations in the compositions of known intrusive sheets and other gabbronorites in the Sanna area.

6.2.1.3. Compositional variations due to super - rigidus processes in the gabbronorite suite rocks.

This section is primarily concerned with the overall variation in Ca, Al and Mg contents of the gabbronorite suite rocks. These three elements are good indicators of low - pressure fractionation and crystal accumulation in tholeiitic basalt magmas, which are usually dominated by the effects of crystallisation of olivine, plagioclase and, in the more evolved magmas, augite (with or without orthopyroxene).

The first three plots in Fig. 6.5 show variation in these elements for the gabbronorite suite rocks and for the pre - gabbronorite laminated gabbros (including the laminated microgabbronorite in the xenolithic screen at the southern end of the Sanna Bay section (Fig. 3.26)). The samples marked individually on these diagrams are as follows:

315C, 197/1, 133/2, 281/2: gabbronorites with relatively well - developed plagioclase lamination. This lamination dies out, gradually within the outcrops from which the samples were taken, into ordinary near - isotropic gabbronorites. This implies that these rocks were originally ordinary gabbronorites, within which lamination has developed after initial consolidation of the parent magma.

Fig. 6.5. Variations in the abundances of Ca, Mg, Al, K and Ti in the gabbronorite suite rocks and the pre - gabbronorite laminated gabbros. See text for discussion of named samples.

Mixing lines between various minerals and assemblages and magmas, with weight percentages of the former marked at intervals.

Generalised fractionation trend.

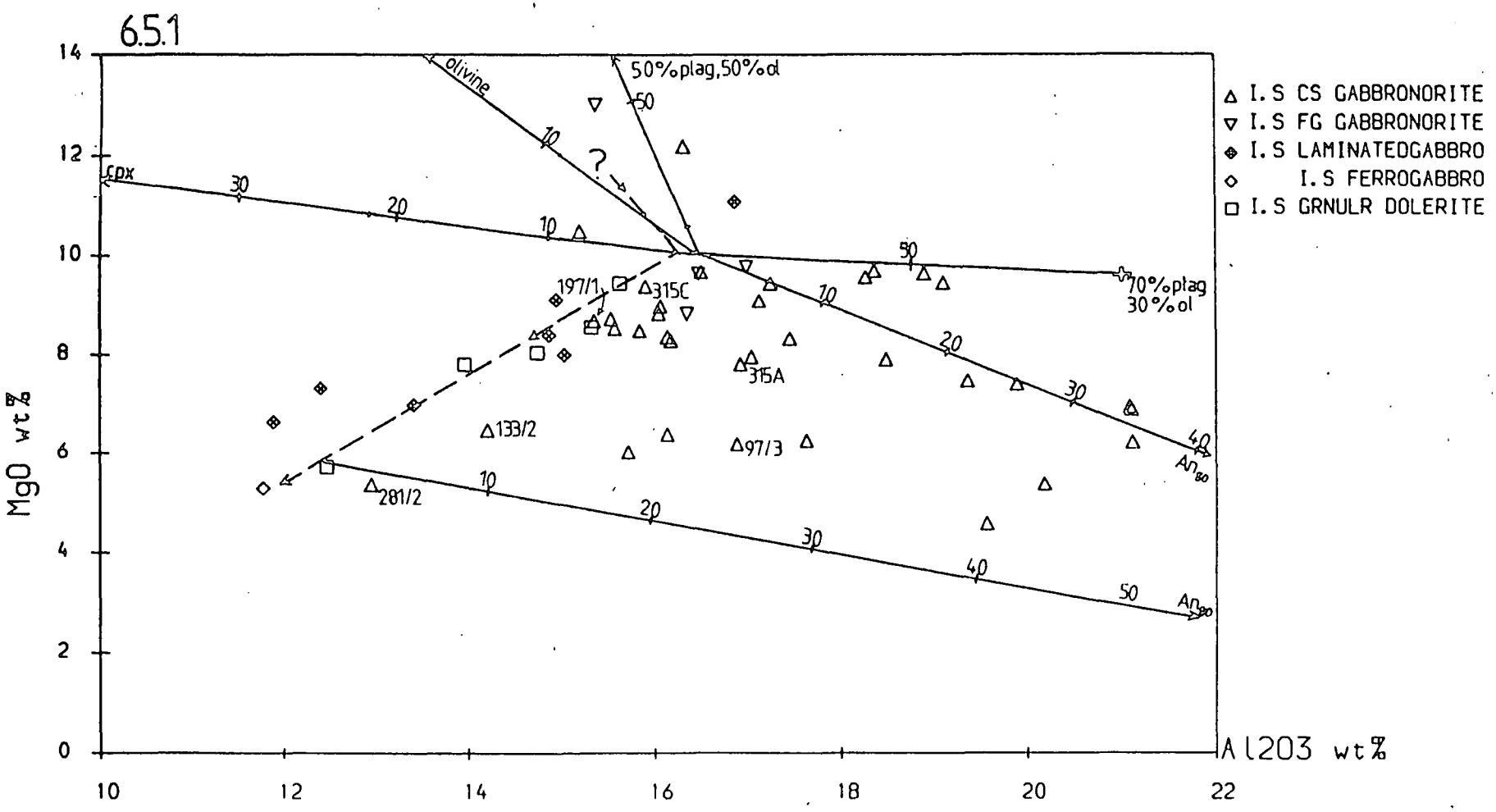

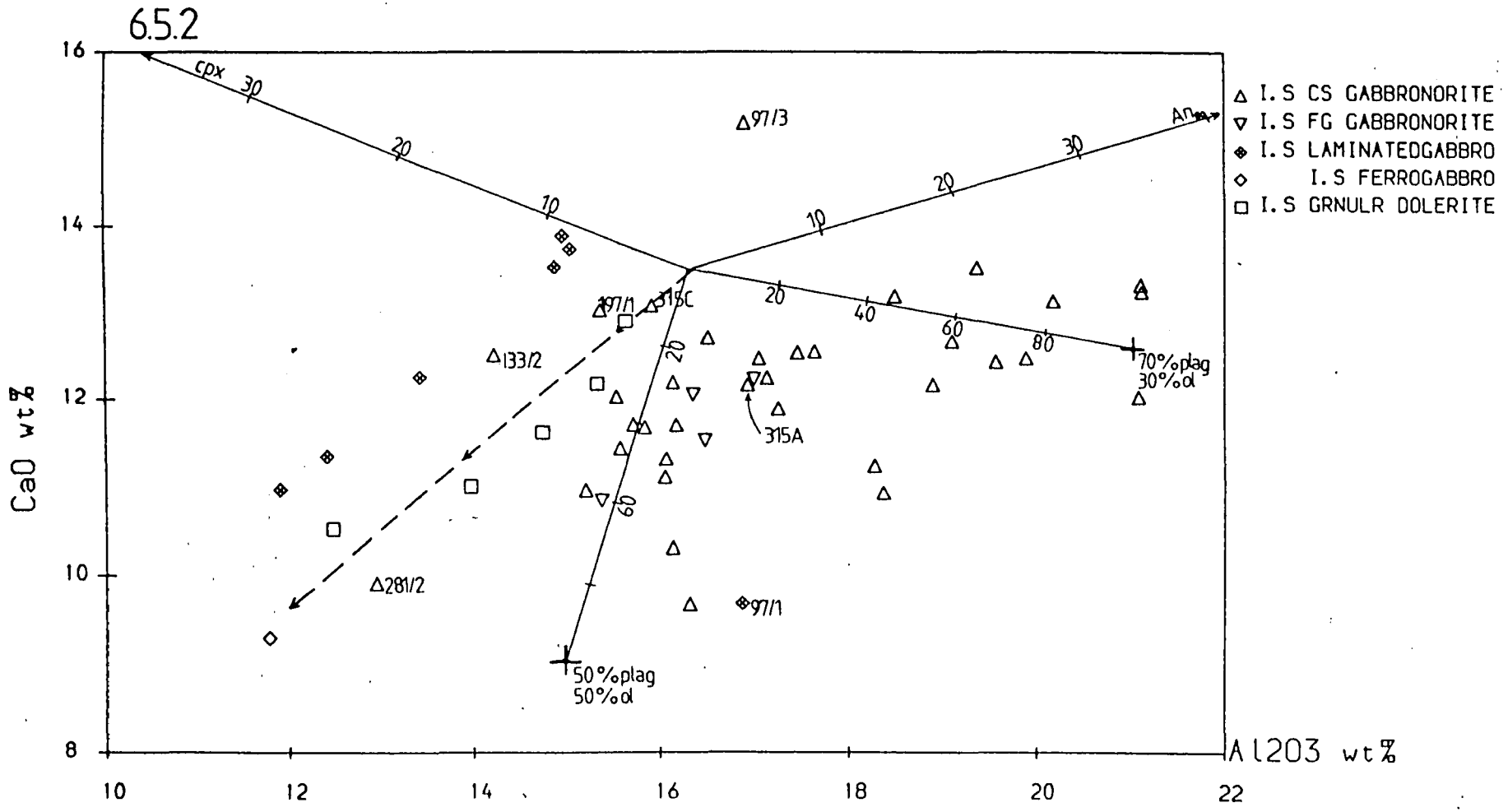
6.5.2
cpx
An
△ I.S CS GABBRONORITE
▽ I.S FG GABBRONORITE
◈ I.S LAMINATEDGABBRO
◇ I.S FERROGABBRO
□ I.S GRNULR DOLERITE
△97/3
△97/1
315C
△133/2
△281/2
315A
◈97/1
70%plag
30%ol
50%plag
50%ol
CaO wt%
Al2O3 wt%
16
14
12
10
8
10
12
14
16
18
20
22

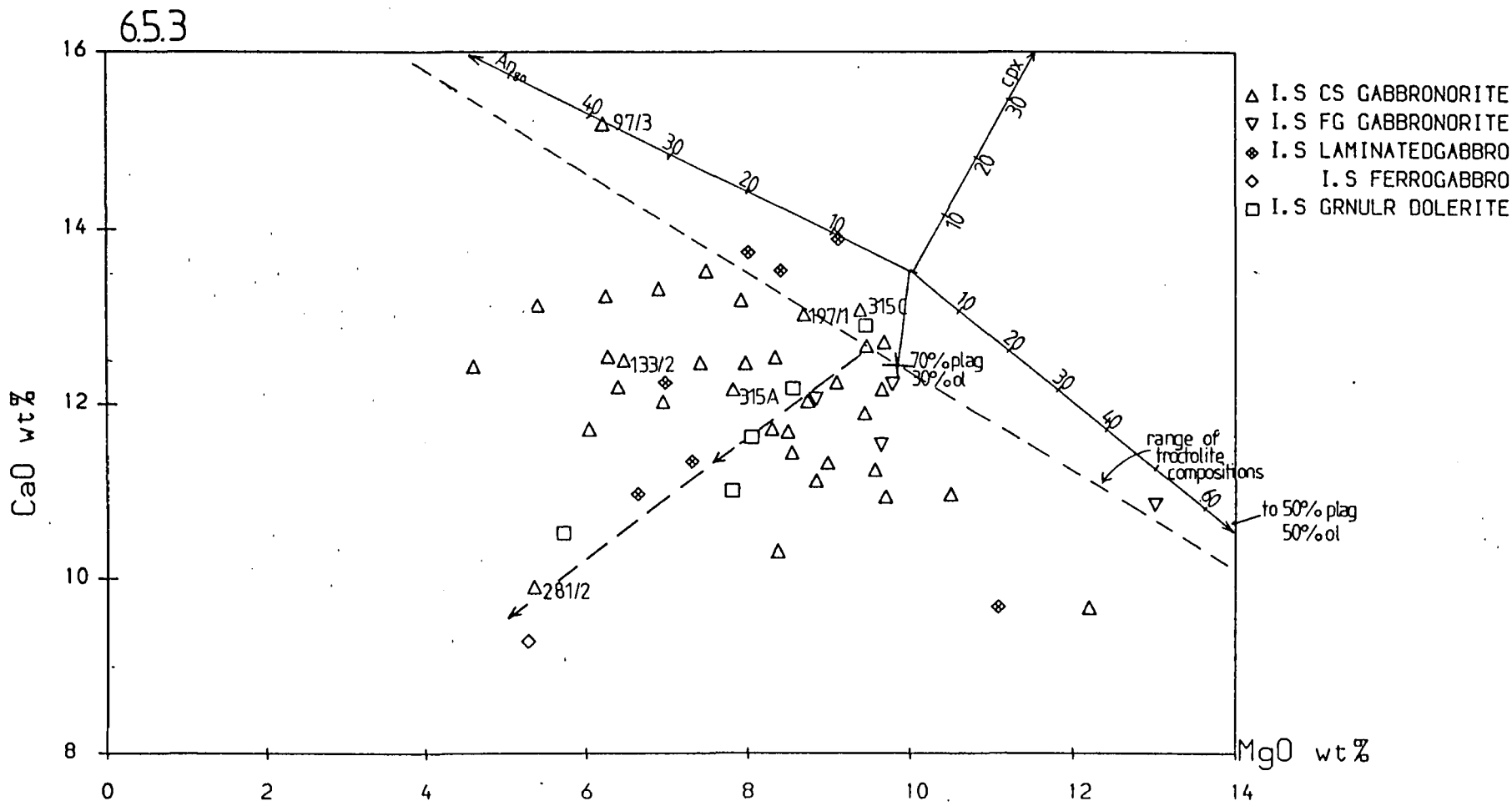
6.5.3
16
14
12
10
8
0
2
4
6
8
10
12
14
CaO wt%
MgO wt%
An
40
30
20
10
cpx
97/3
197/1
315C
133/2
315A
281/2
70% plag
30% ol
range of
fractolite
compositions
to 50% plag
50% ol
I.S CS GABBRONORITE
I.S FG GABBRONORITE
I.S LAMINATEDGABBRO
I.S FERROGABBRO
I.S GRNULR DOLERITE

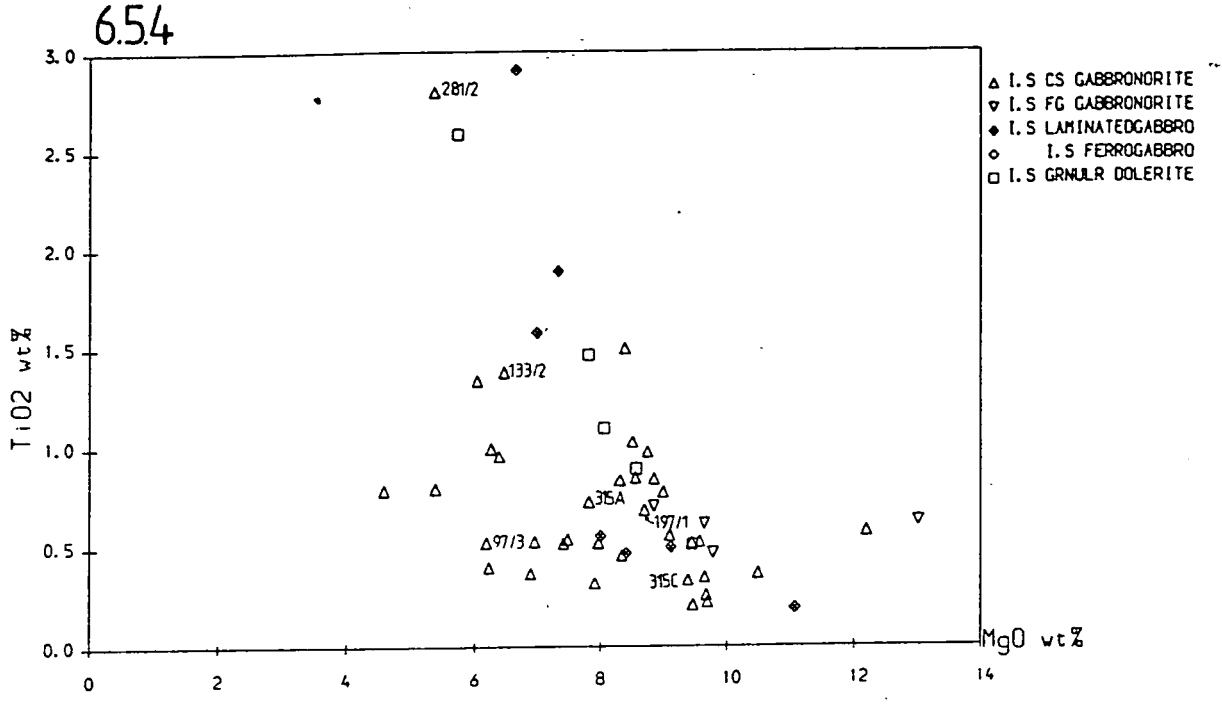
6.5.4
TiO2 wt%
MgO wt%
281/2
133/2
315A
197/1
97/3
315C
I.S CS GABBRONORITE
I.S FG GABBRONORITE
I.S LAMINATEDGABBRO
I.S FERROGABBRO
I.S GRNULR DOLERITE

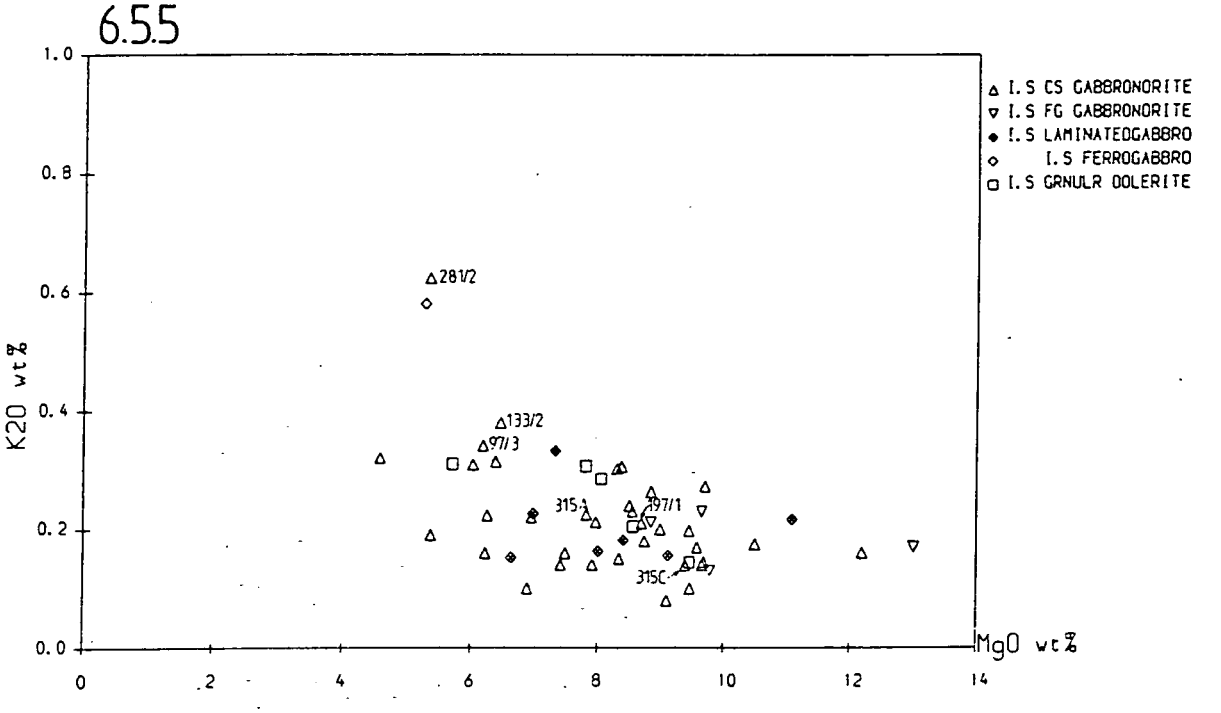
6.5.5
K2O wt%
MgO wt%
281/2
133/2
97/3
315A
197/1
315C
I.S CS GABBRONORITE
I.S FG GABBRONORITE
I.S LAMINATEDGABBRO
I.S FERROGABBRO
I.S GRNULR DOLERITE

315A: the host near - isotropic gabbronorite to to 315C. There is a particularly clear gradational transition between 315C and 315A, shown in Fig. 3.24A. 315C originates from the top of the lower laminated unit in this diagram, whilst 315A comes from about 50cm below this.

97/3: an anomalous near - isotropic gabbronorite. This is a rather weathered sample, which contains abundant epidote, carbonate and a fibrous brown zeolite. All of these phases replace plagioclase and the first two at least have a higher Ca/Al ratio than this mineral, suggesting that the low Ca/Al and high Ca of this rock may be due to alteration rather than being a primary feature.

In addition to the analysed samples, mixing lines (which, in this case, would be produced by porphyrocryst accumulation) between a hypothetical primitive gabbronorite magma (10wt% MgO, 16.5wt% Al_2O_3, 13.5wt% CaO) and plagioclase (of composition An_{80}, corresponding to the gabbronorite porphyrocrysts), olivine and augite are plotted in Fig. 6.5. The last two phases are assigned average Inner Series compositions for the purposes of these calculations: there is relatively little variation in compositions of ferromagnesian minerals within the Inner Series (Fig. 6.3, above), but, as noted in the previous section, considerable resetting of ferromagnesian mineral compositions may have taken place during high - grade metamorphism. However, the results discussed below are not greatly changed by changing ferromagnesian mineral compositions within the ranges in equilibrium with basaltic magmas. Mixing lines between the model primitive magma and troctolites with different proportions of olivine and calcic plagioclase are also plotted, as is an approximate liquid variation path which drawn to lie through the field of the fine - grained granular dolerites. The isotropic Inner Series ferrogabbro sample also lies close to this trend and appears to approximate to a liquid composition.

The deduction, made in section 6.2.1.1, that the gabbronorite magmas and the granular dolerite magmas are broadly cogenetic, suggests that the liquid components of the gabbronorite magmas must also have shown a similar compositional trend to the granular dolerites. The offsets from olivine - plagioclase mixing lines towards less Ca - rich compositions apparent in the gabbronorites from their positions in Fig. 6.5.2 and 6.5.3 are consistent with this, although as will be seen below the causes of the similar trends in the two groups of rocks could be rather different.

Fig. 6.5.1 indicates that, with a few exceptions, the gabbronorites are enriched in Al_2O_3 relative to the inferred liquid trend. This is consistent with the presence of calcic plagioclase porphyrocrysts in these rocks and suggests that these feldspars are accumulative in origin. Up to 30% of the most feldspar - rich samples are composed of such porphyrocrysts, consistent with the maximum amount of Al_2O_3 enrichment observed. The wide field occupied by the gabbronorites in this diagram can be interpreted in terms of accumulation of lesser amounts of olivine as well as plagioclase in magmas of different compositions within the range of granular dolerite compositions. To illustrate this point, an additional mixing line is drawn on Fig. 6.5.1 between the most evolved granular dolerite and the nominal An_{80} plagioclase porphyrocryst. In contrast to the near - isotropic gabbronorites, however, the well - laminated gabbronorites, along with the pre - gabbronorite laminated gabbros, lie close to the granular dolerite trend in this diagram. This is consistent with the almost complete absence of feldspar porphyrocrysts from the rocks and points to compositional changes during the formation of the lamination in the well - laminated gabbronorites (see section 6.2.2, below).

One apparent problem with the interpretation of Fig. 6.5.1 in terms of fractionation and accumulation of feldspar **and** olivine is the apparent lack of equant, euhedral to subhedral olivines which would generally be regarded as cumulus olivines. The characteristic primary olivine morphology in the gabbronorites is, instead, sub - poikilitic to poikilitic (section 3.4.1). However, as noted in section 6.2.1.2, such crystals may in fact be early - formed primocrysts and could therefore be accumulative, as is implied by the bulk compositional evidence.

Much more serious problems with an interpretation of the gabbronorites and granular dolerites in terms of fractionation and accumulation of olivine and plagioclase alone are apparent in Figs. 6.5.2 and 6.5.3. With the exception of the most evolved samples, which have c. 6% MgO, the granular dolerites are too primitive and MgO - rich to have been in equilibrium with clinopyroxene close to their liquidii at low pressures. Similarly, augite is a late (generally post - deformational) interstitial phase in the gabbronorites, indicating that they too were derived from augite - undersaturated magmas. Nevertheless, Ca behaves as a strongly compatible element in these diagrams, with a similar bulk distribution coefficient to those of Mg and Al, whereas it should be a weakly incompatible element in magmas in equilibrium with a troctolitic crystal assemblage.

In purely geochemical terms, the trends in Fig. 6.5.2 and Fig. 6.5.3 can of course be explained

in terms of the presence of a relatively small proportion (perhaps 20% at most) of augite in the fractionating assemblage. However, as noted above, augite appears to have been a late - crystallising 'sub - rigidus' phase in the gabbronorites and was certainly not present in the liquidus assemblage of the granular dolerites. The strongly compatible behaviour of Ca in Figs. 6.5.2 and 6.5.3 therefore seems to represent an example of 'cryptic fractionation' of augite, such as has been described from Mid - Ocean - Ridge basalt suites (see review by Thompson (1987)) and certain other suites of rocks (Langmuir 1989).

This may be interpreted in various ways. Firstly, the 'liquid composition trend' defined by the granular dolerites could represent a mixing line between primitive magmas (with around 10% MgO) and evolved, augite - saturated magmas. This could have occurred by mixing of two high - melt - percentage magmas or by mixing of primitive magmas with magmas which had circulated through a cooler cumulate pile and equilibrated with intercumulus pyroxene. Simple mixing processes can normally be identified geochemically be the occurrence of linear mixing lines between the end - member components on plots of an incompatible element against a compatible element (for example, TiO_2 or K_2O vs. MgO, Figs. 6.5.4 and 6.5.5) although Langmuir (1989) shows that continuous mixing of primitive magmas with expelled intercumulus melts is more subtle in its effects and may closely resemble simple fractiontion in many ways. A simple mixing trend may be present in Fig. 6.5.4, although the range of granular dolerite compositions is not large and a normal fractionation trend in this diagram would not be strongly curved. Any fractionation or mixing trend in Fig. 6.5.5 is obscured by variations due to other causes, such as crustal contamination (see section 6.2.1.1). Alternatively, the rocks could represent magmas which had last equilibrated at moderately high pressures (c. 10kb; O'Hara 1968) where the clinopyroxene stability field is greatly expanded but plagioclase crystallisation is not completely suppressed, and which were emplaced at high crustal levels without further fractionation.

Low - temperature, low - pressure clinopyroxene fractionation would also also account for the correlation between high Ca and, especially, high Ca/Mg and Ca/Al, and the development of lamination in the coarser gabbronorites. This is particularly apparent from the relative positions of sample 315C and its near - isotropic counterpart, 315A. A similar association of enrichment in Ca relative to Mg and Al and the presence of lamination is present in the majority of the pre - gabbronorite laminated gabbros. This correlation indicates that extensive fractionation of clinopyroxene took

place during the formation of the lamination. Since it was shown in sections 3.4.1 and 3.4.2 that the lamination and the clinopyroxene in these rocks are both 'post-cumulus' in age it follows that sub - rigidus clinopyroxene fractionation, such as would produce 'cryptic fractionation' of clinopyroxene in primitive magmas mixed with residual melts expelled from these rocks, has taken place in them. This process is discussed further in section 6.2.2.

6.2.2. Late magmatic ('post - cumulus' or sub - rigidus) processes in the gabbronorite suite rocks.

The age relationships discussed in sections 3.4.1 and 3.4.3 indicate that two distinct processes operated during the 'post - cumulus' stage of evolution of the Inner Series rocks in the Sanna area, and to a lesser extent in other parts of the Inner Series. These are the formation of lamination, defined by aligned plagioclase crystals, in the gabbronorites, and the metasomatic replacement of laminated gabbros and gabbronorites by pyroxenite. In at least one case, that of the gabbronorite sheet logged in Fig. 3.24A, the two processes show a close spatial association: thin pyroxenite veins or selvedges occur at the top of each of the laminated bands within this rock. On the other hand, there is no secondary lamination associated with the Upper Main Pyroxenite where it cuts the same sheet and pyroxenite formation in the underlying laminated gabbros appears to be associated with the destruction of an earlier feldspar lamination.

6.2.2.1. The formation of 'post - cumulus' lamination in the gabbronorites, and associated mineralogical and bulk compositional changes.

The occurrence of laminated units with gradational bases within the porphyritic gabbronorite sheet intruded into laminated gabbros around Grid. Ref. 44057000 (Figs. 3.23, 3.24A and 3.25) provides an opportunity to study mineralogical and bulk geochemical changes associated with the formation of the lamination. Petrographic evidence discussed in section 3.4.1 indicates that the well - laminated rocks formed from the feldspar - porphyrocrystic, near - isotropic gabbronorite at a time when the latter was composed of an interlocking network of plagioclase, olivine (and possibly some augite crystals) together with an interstitial melt phase. A number of changes appear to have occurred more - or - less simultaneously as the lamination developed progressively:

1). Loss of plagioclase porphyrocrysts by reaction or dissolution.

2). Development of the feldspar lamination, by some combination of preferential dissolution of feldspars with near vertical z-axes, preferential growth of feldspars with z-axes close to the plane of lamination, growth of new feldspars in this orientation, and mechanical rotation and intracrystalline deformation (see section 3.4.1).

3). Reduction in the grain size of mafic minerals, particularly olivine, by the breakdown of poikilocrysts into granular clusters of equant grains.

4). Subsequent to most of the deformation of mafic phases, small subpoikilitic grains of augites and opaques formed.

Differences in the compositions of minerals from the well - laminated and near - isotropic parts of 315C, a sample which cuts the top of the lower laminated unit in Fig. 3.24A at a point where pyroxenite selvedges are not present, are shown in Fig. 6.6. These differences may be associated with the development of the lamination or with later metamorphism but since the field and petrographic evidence implies that the laminated rock was originally similar to the near - isotropic rock they cannot have formed any earlier than the lamination.

The much narrower range of feldspar compositions apparent in Fig. 6.6.1, and in particular the loss of the refractory calcic cores characteristic of the porphyrocrysts in the near - isotropic gabbronorites, is consistent with the suggestion that the development of lamination under 'post - cumulus' or sub - rigidus conditions involves wholesale recrystallisation and re - equilibration of the rock (Maaloe 1976; Mathison 1987). The pyroxenes, on the other hand, show a rather wider range of compositions. The very low temperatures obtained from some of these pyroxenes (section 6.4, Table 6.5a) implies that they have been partially re - equilibrated under sub - solidus conditions and are not indicative of the conditions of formation of the lamination.

The bulk compositions of samples 315C and 315A (the near - isotropic gabbronorite which grades up into the laminated sample 315C) are summarised in Table 6.2, together with the differences between them. Both samples were analysed by XRF methods and were always analysed in the

Fig. 6.6. Comparison of mineral compositions in the laminated and near - isotropic parts of the intrusive gabbronorite sheet at loc. 315.

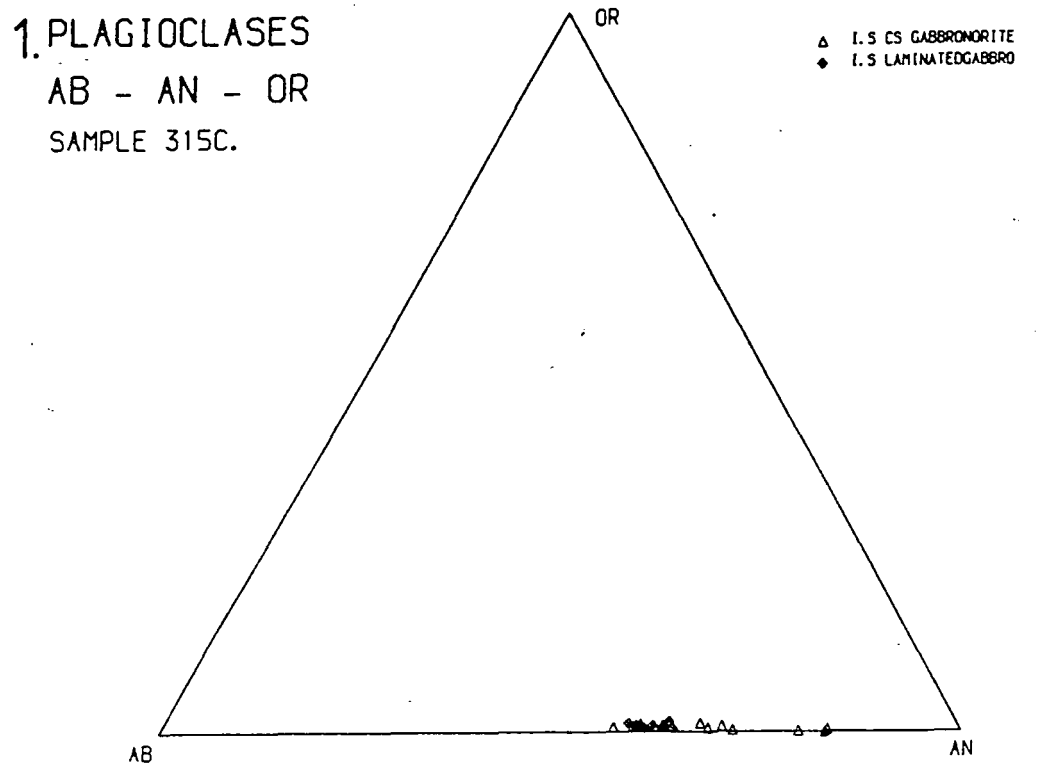

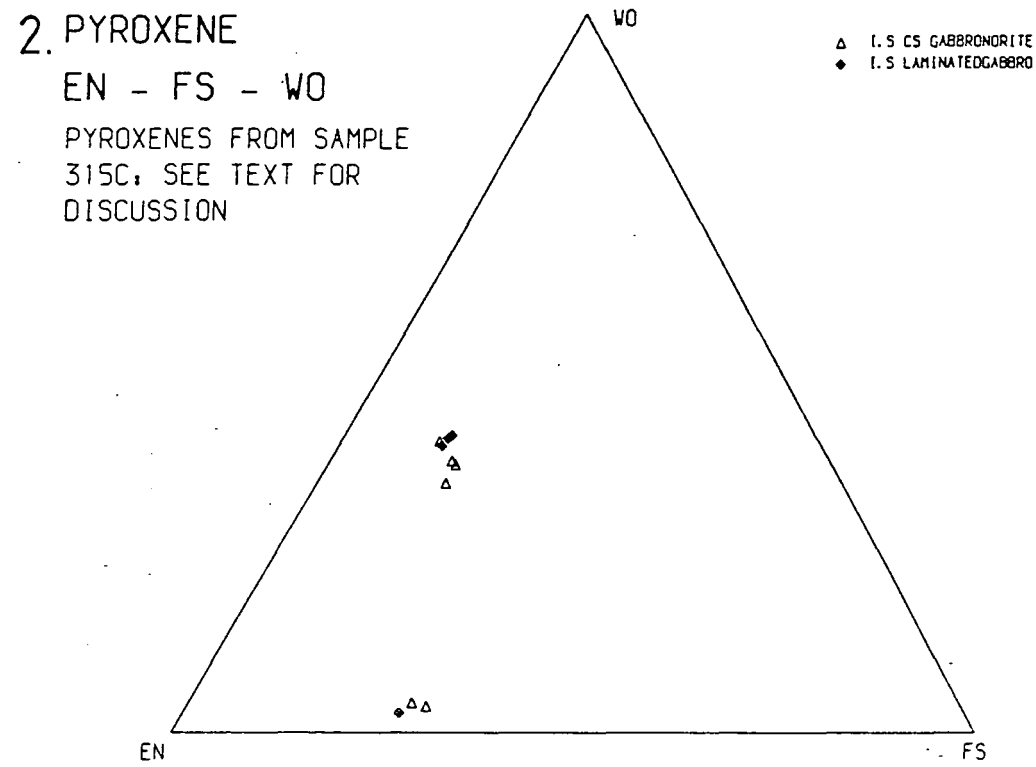

same batch of samples. The differences between them are therefore unlikely to have been greatly affected by systematic errors in the analysis procedures (this is particularly important with respect to Na and Al, as there are systematic differences between XRF and ICP - AES data for these two elements in the internal reference material, 35; see Appendix 1). However, the differences in the concentrations of certain elements between the two samples, Si in particular (also Ca and Na) are not much larger than the 1σ uncertainties in the XRF analyses of gabbroic rocks (again, see analysis of replicate data for sample 35, Appendix 1) and cannot be regarded as significant. Furthermore, the systematic errors in analyses for many trace elements (Ba, Zr, V in particular amongst those listed) are so large relative to their absolute abundances as to make the calculated proportional changes in composition unreliable).

The development of igneous lamination under sub - rigidus conditions has parallels in the development of fissility due to mica and clay mineral growth and alignment during the compaction and diagenesis of argillaceous sediments. One plausible interpretation of the compositional differences between 315A and 315C, which can be summarised as enrichment of compatible elements (notably Mg, Cr and Ni) and depletion of incompatible elements (notably Ti, K, P, Zr and V) in the latter relative to the former, is that they result from partial expulsion of an interstitial melt and compaction of the host crystal mush. The insignificant difference in the SiO_2 contents of the two rocks and the incompatible behaviour of Ti and P suggest that the expelled melt was of broadly basaltic composition. This presents problems for mass - balance calculations designed to constrain the average compositions of the expelled melt and the crystalline component of the residuum during compaction, as it means that Mg cannot be regarded as perfectly compatible, whilst the analyses of the other two compatible elements, Cr and Ni, are unreliable at the level of precision of interest (see Appendix 1). It is assumed for the purposes of the calculations below that perfectly compatible elements are enriched in the residual mush, composed of crystals + remaining interstitial liquid, by 50% relative to their initial values, whilst perfectly incompatible elements are depleted by the same amounts. It should be noted that whilst both Ti and P are depleted by approximately this amount, K, Ba and Zr are not. This may be due to later alteration in the case of K (see section 6.4.2), whilst the Ba and Zr data are affected by positive residual blanks which would tend to reduce the apparent depletions in these elements (see Appendix 1).

Given these assumptions, average compositions of the expelled melt and crystalline residuum can be

Table 6.2.

Changes in bulk composition during formation of laminated gabbronorite 315C from porphyritic isotropic gabbronorite 315A.

Compositions of both samples and the difference ΔC expressed as weight percent oxides or parts per million (major and trace elements respectively), except in column 4 (percentage change relative to composition of 315A).

	315A	315C	ΔC (absolute)	ΔC (relative) %
SiO_2	49.02	50.13	+1.11	+2.26
Al_2O_3	16.92	15.90	−1.02	−6.0
$Fe_2O_3^T$	9.49	8.17	−1.32	−13.9
MgO	7.81	9.38	+1.57	+20.1
CaO	12.17	13.09	+0.92	+7.6
Na_2O	2.31	2.41	+0.10	+4.3
K_2O	0.22	0.14	−0.06	−27
P_2O_5	0.07	0.03	−0.04	−57
TiO_2	0.73	0.34	−0.39	−53
MnO	0.16	0.15	−0.01	−6
Ba	202	179	−23	−11
Cr	240	430	+190	+79
Cu	106	114	+8	+7.5
Ni	112	141	+29	+26
Pb	19	22	+3	+16
Sr	386	333	−53	−14
V	208	134	−74	−35
Zn	54	43	−11	−20
Zr	49	32	−17	−35

obtained by mass - balance calculations, the results of which are presented in Table 6.3. Although the assumptions made will affect the precise compositions of these materials the qualitiative inferences made below do not depend on these precise compositions, only on the general features of the two hypothetical materials. It should also be noted that these are average compositions and may have changed with time as compaction proceeded. The expelled melt is a Mg - poor ferrobasalt, but has higher Al and Sr contents than most such magmas and could be described as a high - alumina tholeiite. The corresponding crystalline residuum has elevated Ca/Al and Mg/Fe ratios, reflecting the increased abundance of augite and reduced abundances of plagioclase and interstitial opaques in 315C, relative to 315A, which are apparent in thin section.

As noted in the previous section, the same pattern of enrichment in Ca and Mg relative to Al is apparent in Fig. 6.5.1 and 6.5.2, where the strongly laminated gabbronorites plot to the left of and above the near - isotropic gabbronorites (i.e. at higher Mg/Al and Ca/Al ratios). The same feature is shared by the pre - gabbronorite laminated gabbros, although not by the laminated gabbronorite 97/1 which is much more primitive in its composition and is apparently unrelated to the other laminated rocks (sections 3.4.2 and 6.3). This general pattern suggests that the recrystallisation associated with the development of lamination involves a net loss of plagioclase and a net gain of augite, implying a relative reduction in the stability of the former. Possible causes of this change in mineral stability and the consequent high Al and Sr contents of the expelled material are discussed at the end of this chapter (section 6.5).

A second implication which follows from the composition of the extracted melt in Table 6.3 is that melt extraction from the partially molten rocks corresponding to 315A and 315C must have largely ended at relatively high temperatures, when Ti and P were still incompatible overall and the residual melt composition was still relatively primitive. In the gabbronorite suite as a whole, however, the pattern of residual melt extraction may have been more complex. This is indicated by the series of plots which make up Fig. 6.7. In each of these, two elements which are partitioned into basaltic melts in equilibrium with gabbroic assemblages are plotted against each other. As would be expected, overall positive correlations are present in all of these diagrams, although this may be due more to the variation in degree of fractionation than to variation in the amount of crystallised trapped melt present in the samples. There is, however, considerable variation about the overall trend, particularly in the case of those element pairs which become compatible at widely different

Table 6.3. Calculated compositions of average residuum and extracted melt during formation of laminated gabbronorite

Compositions calculated assuming 50% relative depletion of incompatible elements overall and that the solid component of the residuum (solid + remaining melt) contained no incompatible elements.

	Major - element composition of solid residuum	Composition of extracted melt
SiO_2	51.24	46.80
Al_2O_3	14.88	18.96
$Fe_2O_3^T$	6.85	12.13
MgO	10.95	4.67
CaO	13.99	10.33
Na_2O	2.50	2.11
K_2O	0.08	0.34
P_2O_5	0.00	0.15
TiO_2	0.00	1.51
MnO	0.14	0.18
Ba		248
Cr		(−140)
Cu		90
Ni		54
Pb		13
Sr		492
V		356
Zn		76
Zr		73

Trace element data in column 2 are unreliable (except for Sr, Cu, possibly V and Zn) because of magnification of analytical errors in calculation procedure; see text for dicussion.

Fig. 6.7. Variations in incompatible and compatible minor and trace elements in the gabbronorite suite rocks indicative of sub - rigidus interstitial melt expulsion processes. ICP - AES and spectrophotometric data only plotted in Figs. 6.7.2 - 6.7.4.

6.7.1

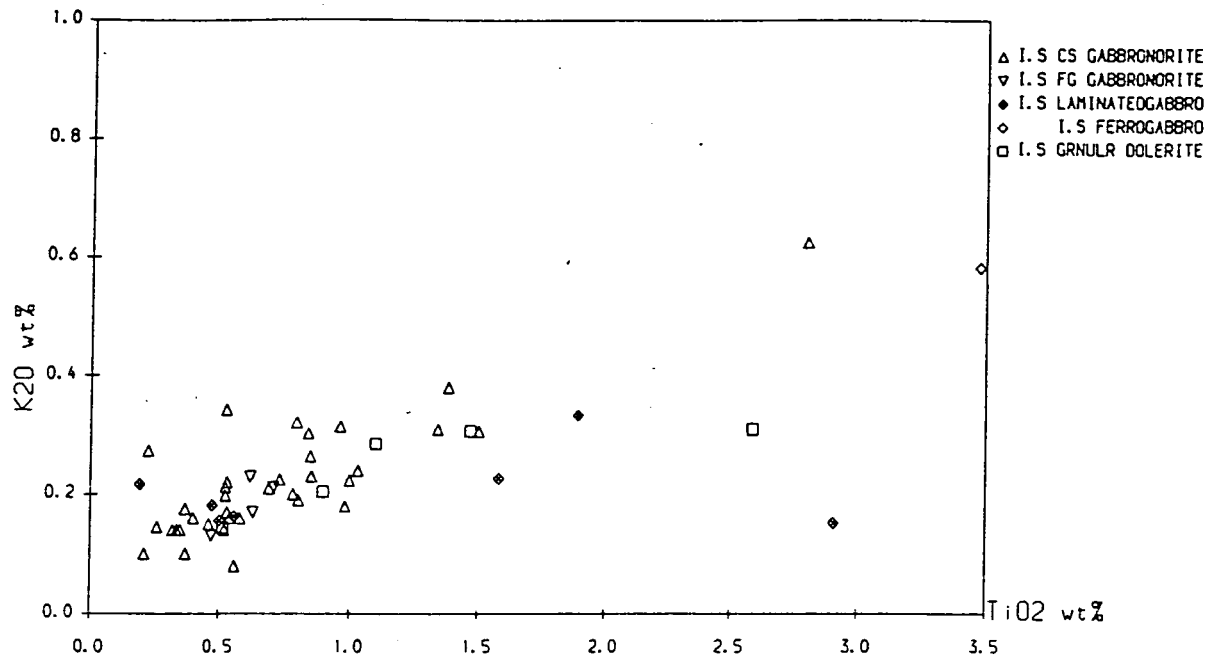

6.7.2

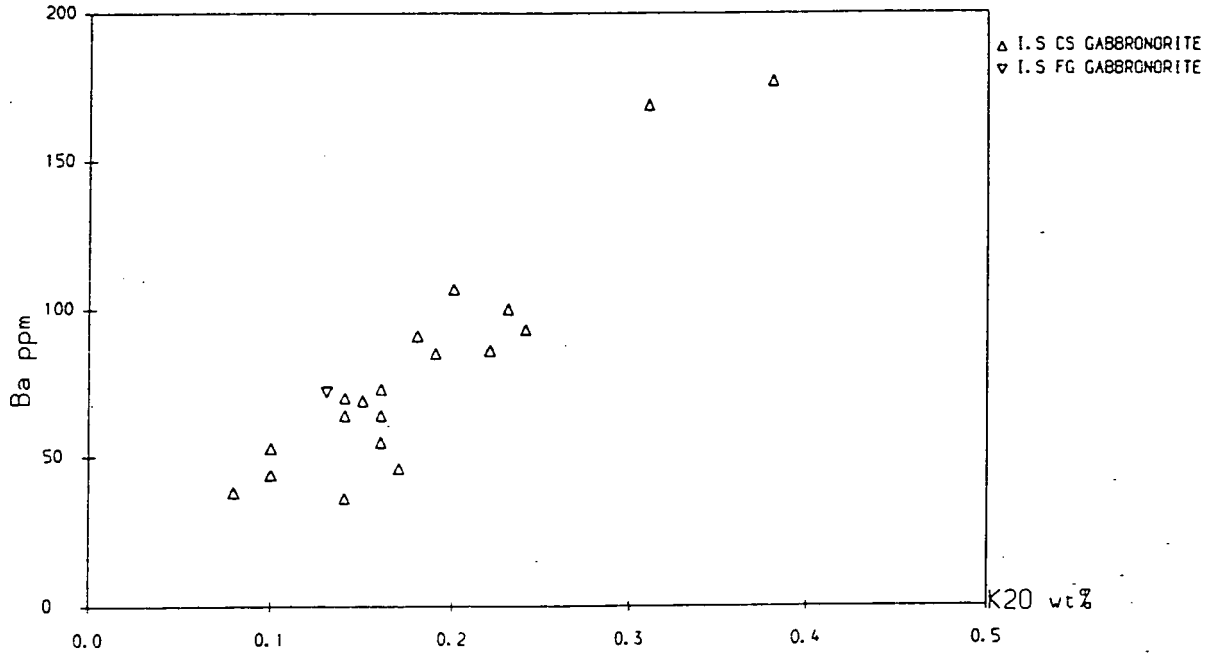

6.7.3

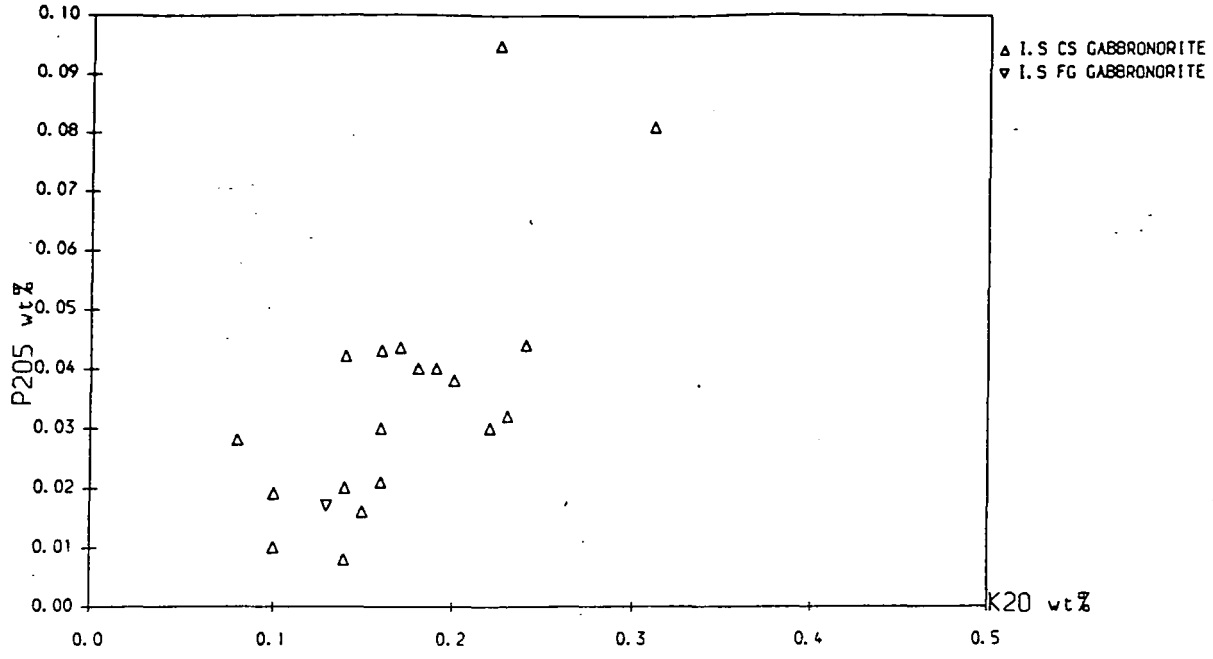
I.S CS GABBRONORITE
I.S FG GABBRONORITE
P205 wt%
K20 wt%
0.00
0.01
0.02
0.03
0.04
0.05
0.06
0.07
0.08
0.09
0.10
0.0
0.1
0.2
0.3
0.4
0.5

6.7.4

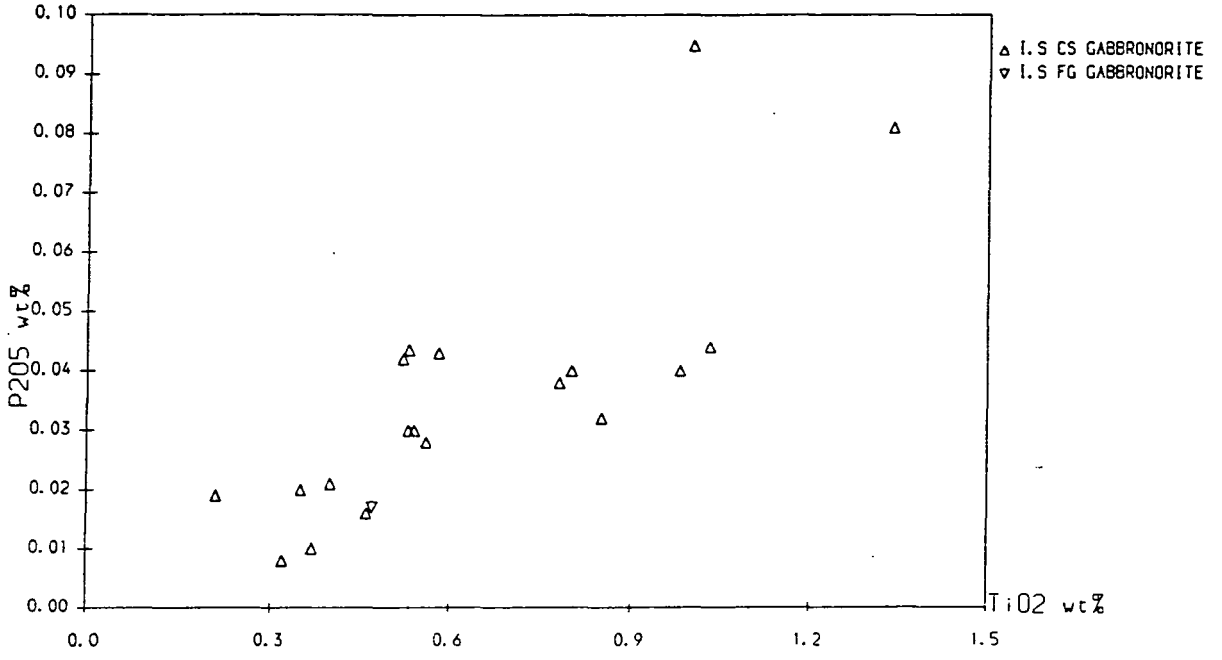
I.S CS GABBRONORITE
I.S FG GABBRONORITE
P205 wt%
TiO2 wt%
0.00
0.01
0.02
0.03
0.04
0.05
0.06
0.07
0.08
0.09
0.10
0.0
0.3
0.6
0.9
1.2
1.5

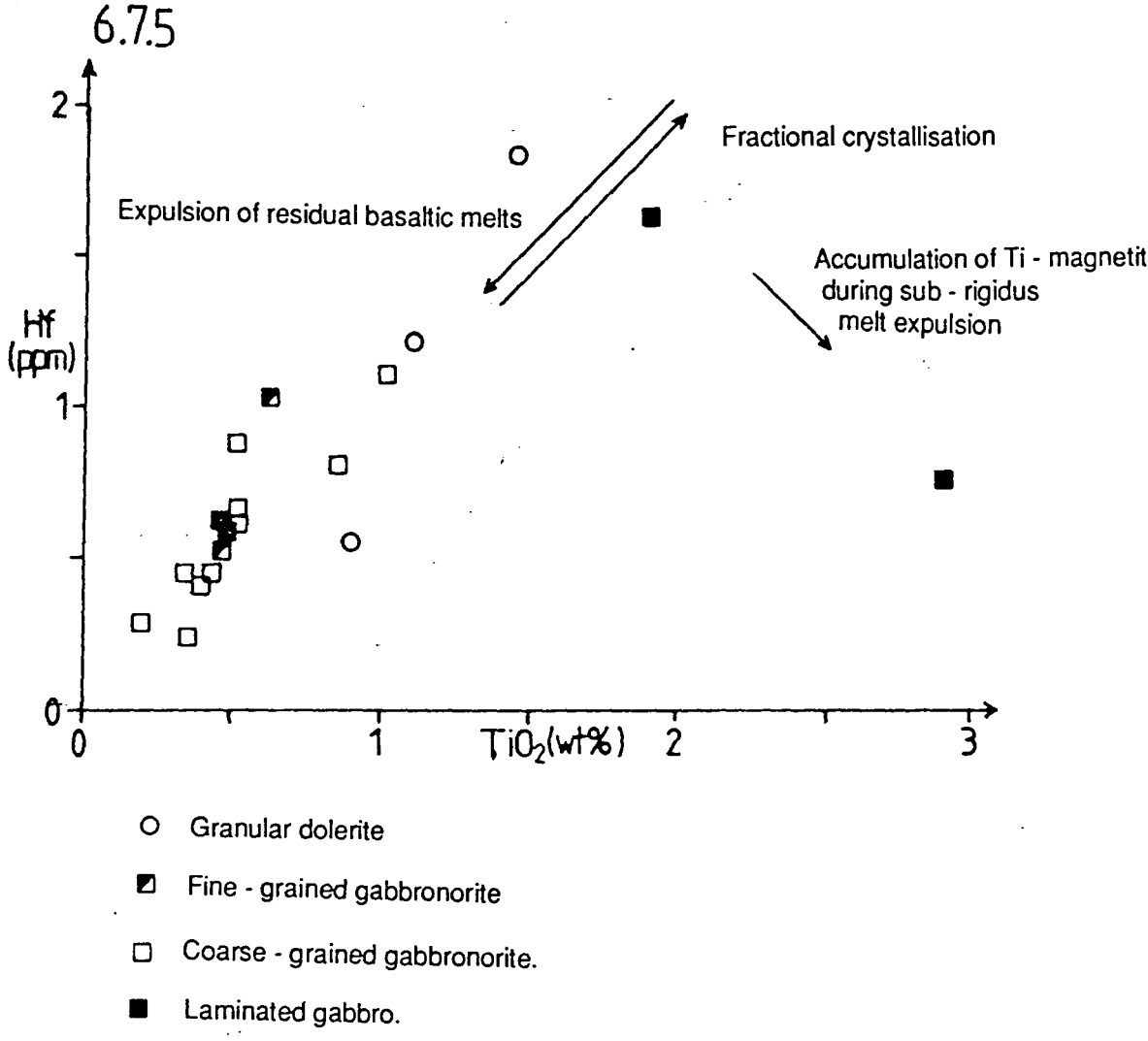
6.7.5
Hf (ppm)
2
1
0
0
1
TiO2(wt%)
2
3
Expulsion of residual basaltic melts
Fractional crystallisation
Accumulation of Ti - magnetit during sub - rigidus melt expulsion
Granular dolerite
Fine - grained gabbronorite
Coarse - grained gabbronorite.
Laminated gabbro.

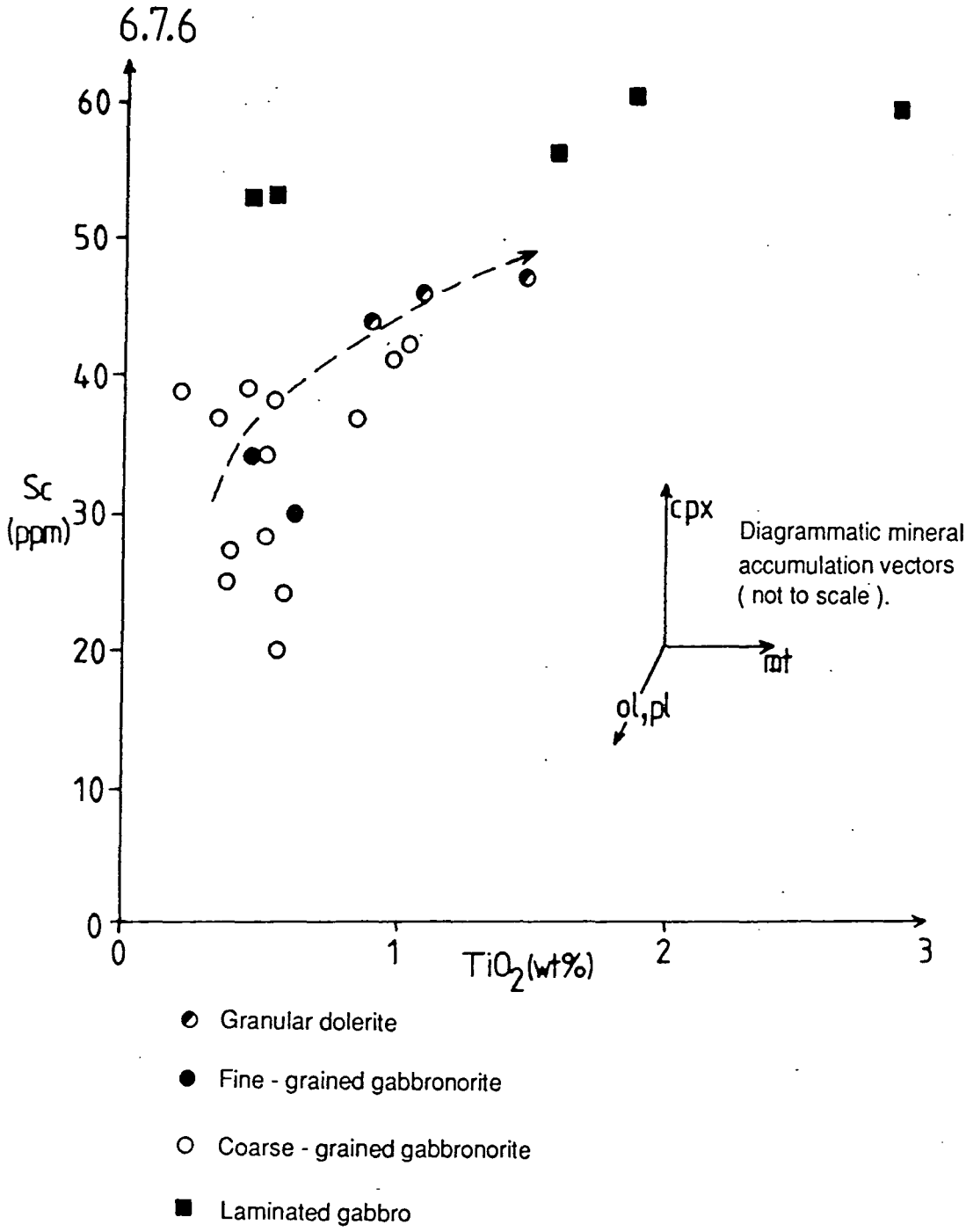
6.7.6
60
50
40
30
20
10
0
Sc
(ppm)
0
1
2
3
TiO2(wt%)
cpx
mt
ol,pl
Diagrammatic mineral accumulation vectors (not to scale).
Granular dolerite
Fine - grained gabbronorite
Coarse - grained gabbronorite
Laminated gabbro

degrees of fractionation (for example, in plots of Ti (which becomes compatible in ferrobasaltic melts) vs. K or Hf (which are only compatible during fractionation of granitic melts)). This scatter may be due to slight differences in the composition of the primary mantle - derived melt or, more plausibly, differences in the amount and composition of crustal contaminants, but could also be due to differences in the average composition of the expelled melts due to differences in the temperature (and therefore final expelled melt composition) at which melt expulsion ceased. It is, however, impossible to make a definitive choice between these various alternatives without more precise trace element data, and isotopic data to provide an independent constraint on crustal contamination.

The roles of differing amounts and temperatures of melt expulsion during the formation of lamination are more clearly apparent in Fig. 6.7.6, a plot of Sc (which substitutes almost exclusively into augite) against Ti (which only partitions into Ti - magnetite in tholeiitic rocks). The laminated gabbros in this diagram all have exceptionally high Sc contents, consistent with the conclusion made previously that the development of lamination is associated with the preferential growth of augite. However, their Ti contents vary widely, suggesting that in some magnetite is accumulative whilst in others the development of the lamination and melt expulsion mainly took place above the upper temperature limit of magnetite saturation in the magmas. The other rocks in this diagram show the effects of a variety of processes involving addition and removal of various combinations of plagioclase, olivine and, to a lesser extent, augite.

In principle, it should be possible to determine the the total amount of melt expulsion from the coarse - grained gabbronorite suite rocks by considering the depletions of incompatible elements such as Ti and P with respect to an element with a distribution coefficient close to unity during fractionation and other processes which have affected the gabbronorite suite rocks. Sr appears to be the closest approximation to such an element for which reliable data is available (c.f. Fig. 6.8.1, which indicates that Sr increases only slightly with increasing Al (and, by inference, plagioclase accumulation) in the gabbronorite suite rocks: plagioclase accumulation or dissolution is the process which would be expected to affect Sr concentrations most in these rocks). Ti and P are particularly suitable incompatible elements to use in conjunction with Sr because all three show similar behaviour during mantle melting in the BTVP and similar tholeiitic provinces (Thompson et al. 1984), removing an additional possible cause of variation in Ti/Sr and P/Sr. These ratios are, however, sensitive to crustal contamination. Unfortunately, Figs. 6.8.2 – 4 indicate that Ti/Sr in particular, and P/Sr to

Fig. 6.8. Plots indicating that variations in incompatible element abundances due to sub - rigidus melt expulsion are small compared to the effects of other processes.

6.8.1. Plot of Sr vs. Al, showing that the K_D of Sr in the gabbronorites is close to unity and that it is a suitable element for use in Figs. 6.8.2 - 6.8.4.

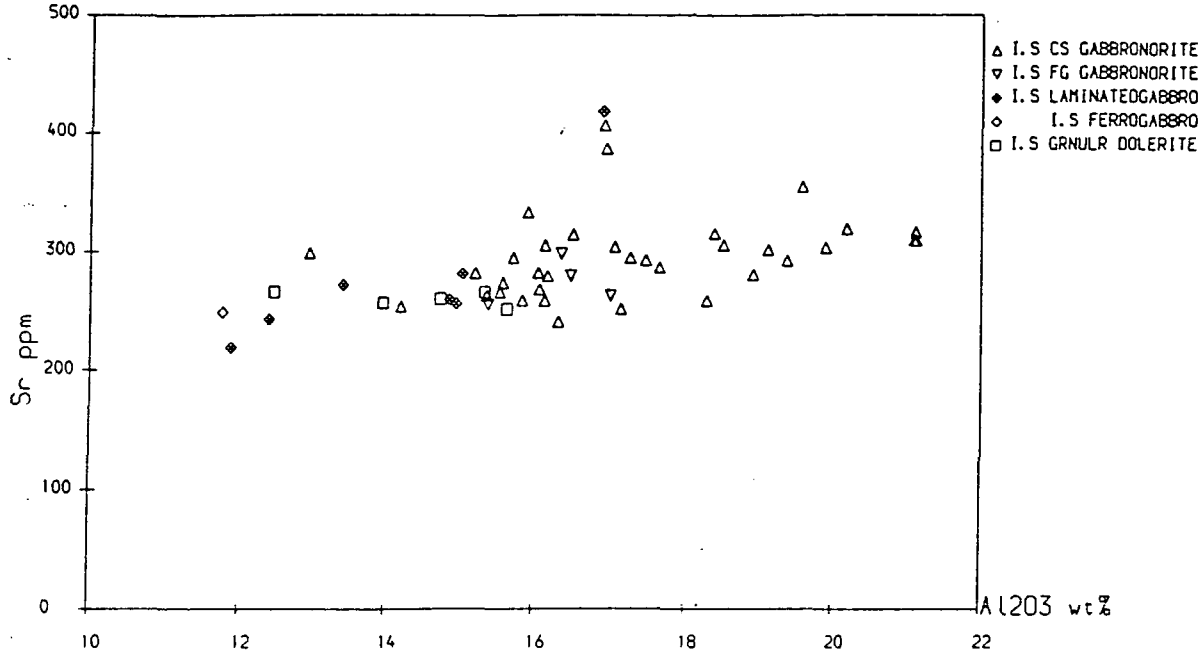

Figs. 6.8.2 - 6.8.4. Plots of Ti/Sr and P/Sr against $Fe^T/(Fe^T + Mg)$ and Al2O3, indicating that the abundances of Ti and P are mainly controlled by the composition of the parental magma rather than by sub - rigidus melt expulsion.

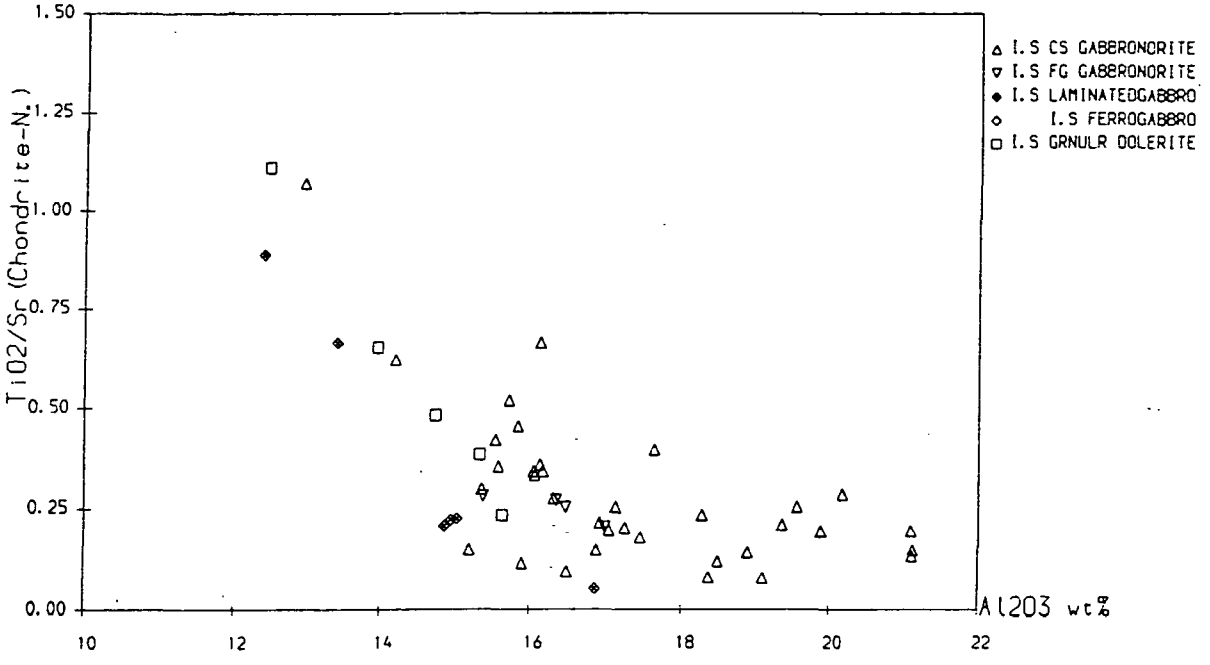

6.8.3

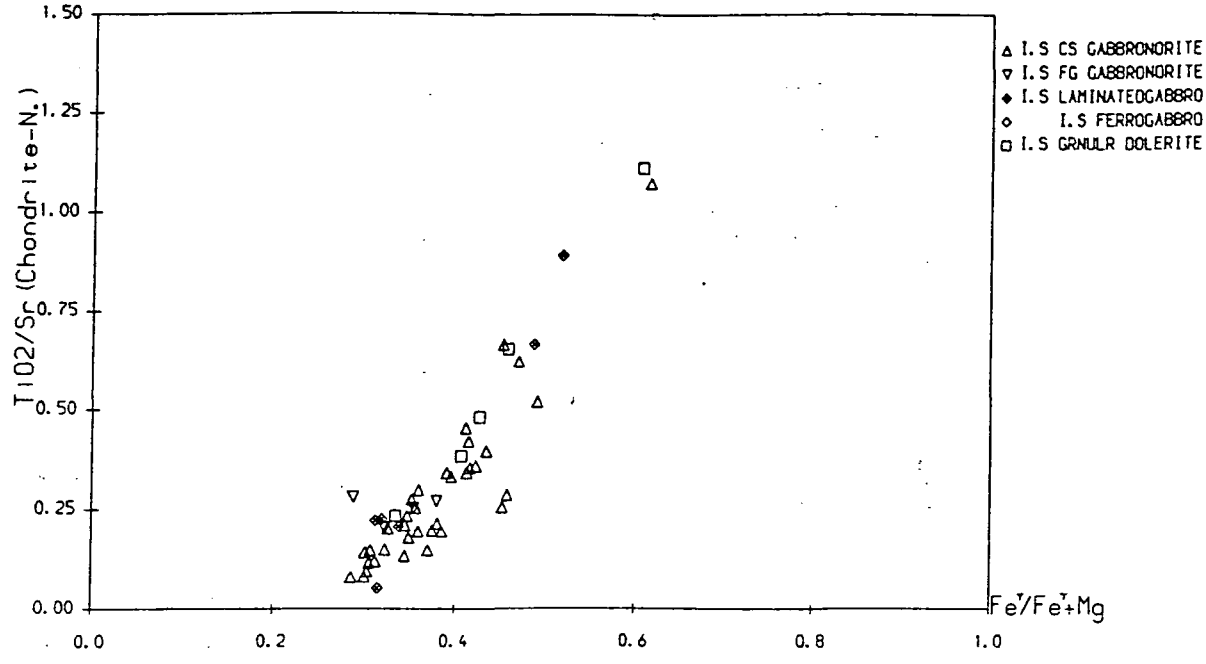
1.50
1.25
1.00
0.75
0.50
0.25
0.00
TiO2/Sr (Chondrite-N.)
0.0
0.2
0.4
0.6
0.8
1.0
Fe^T/Fe^T+Mg
I.S CS GABBRONORITE
I.S FG GABBRONORITE
I.S LAMINATEDGABBRO
I.S FERROGABBRO
I.S GRNULR DOLERITE

6.8.4

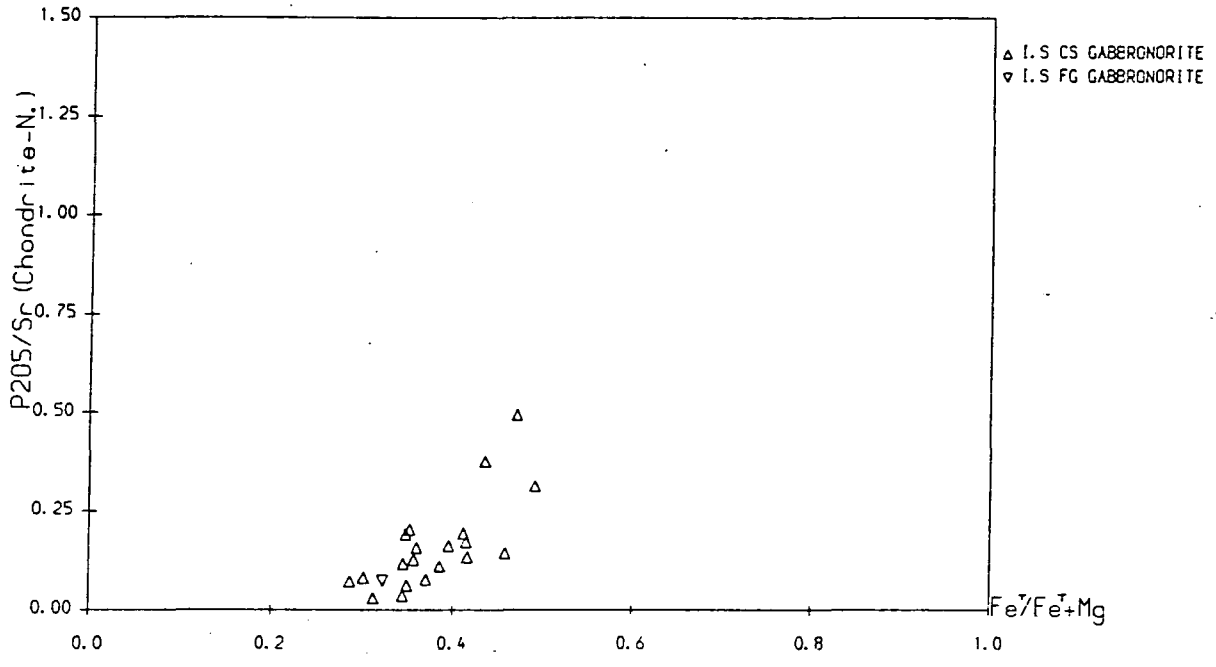
1.50
1.25
1.00
0.75
0.50
0.25
0.00
P2O5/Sr (Chondrite-N.)
0.0
0.2
0.4
0.6
0.8
1.0
Fe^T/Fe^T+Mg
I.S CS GABBRONORITE
I.S FG GABBRONORITE

a lesser extent, are more sensitive to fractional crystallisation (particularly cryptic fractionation), magma mixing, and whatever other super - rigidus processes produced the liquid composition trend represented by the granular dolerite compositions, than to sub - rigidus melt expulsion.

Two conclusions follow from these plots. Firstly, although in situ sub - rigidus melt expulsion associated with the formation of lamination appears to have been capable of producing significant compositional changes in specific outcrops, the process seems to have been less important in the majority of Inner Series rocks than the previous history of super - rigidus fractionation of the various batches of magma in high - melt - percentage magma bodies, either elsewhere in the Inner Series magma reservoir or in separate magma bodies at greater depths. Secondly, future studies of the mechanisms of in situ, sub - rigidus fractionation need to concentrate on those relatively rare cases, such as those at field location 315, where the 'before' and 'after' states of rocks affected by a particular process are visible in a single small intrusive body which can be assumed to be of constant initial composition.

6.2.2.2. Pyroxenite formation.

It was argued in section 3.4.3, on the basis of the field relationships and petrographic features of these rocks, that they formed by approximatley constant - volume replacement of earlier porphyritic gabbronorites or laminated gabbros (or both, in the case of the Upper Main Pyroxenite at Sanna, which cuts across a gabbronorite/laminated gabbro contact). This conclusion is confirmed by microprobe analyses of the relict feldspar cores (Plate 3.100) which occur in the thin pyroxenite selvedges and near - concordant veins which cut the gabbronorite at Loc. 315 (Fig. 3.23 and 3.24A) and in the Upper Main Pyroxenite band where it cuts gabbronorites around 44087003, but not in outcrops of the same body where it occurs within laminated gabbros. The control on the distribution of these crystals according to the host lithology strongly implies that the host rocks rather than the pyroxenites are the source of these feldspar cores. Analyses of the corroded cores are presented in Fig. 6.9, from which it is apparent that these relict feldspars lie within the compositional field of the bytownitic porphyrocrysts in the gabbronorites. This suggests that these corroded crystals are the refractory remnants left after the remainder of the original gabbronorite has been dissolved away and replaced by pyroxenite.

Fig. 6.9. Analyses of plagioclases from the metasomatic pyroxenites and their host rocks, showing that the corroded feldspar cores in the pyroxenites have the same compositional range as the porphyrocrysts in the host gabbronorites. Fields of gabbronorite plagioclase compositions enclosed by dotted lines.

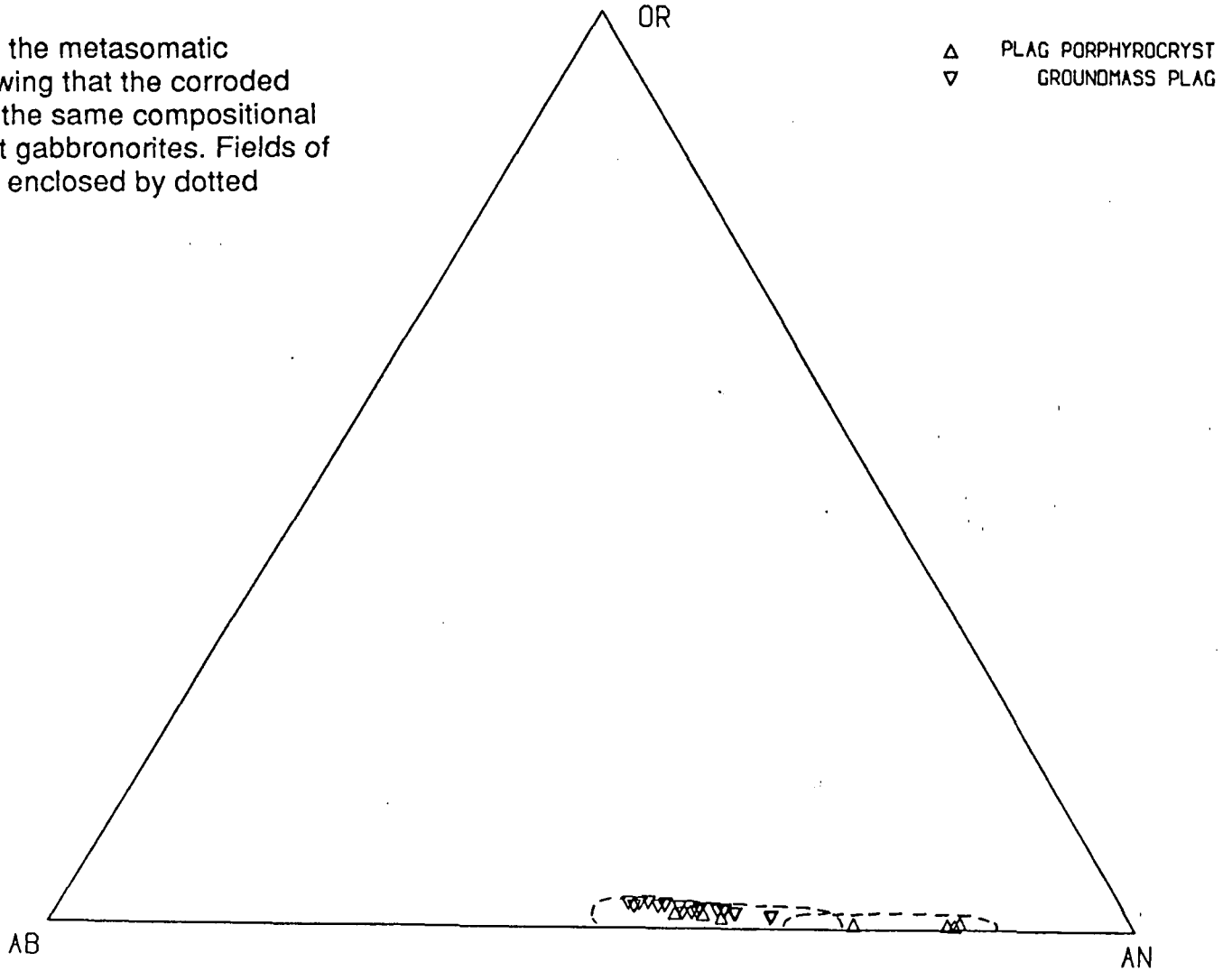

A sample of the Upper main pyroxenite for bulk analysis was collected from a locality where it replaces pre - gabbronorite laminated gabbro (sample 314). The differences in the compositions of these two rocks (Table 6.4) suggests even greater compositional changes during pyroxenite formation than during the formation of laminated gabbronorite at the adjacent Location 315. The metasomatic nature of the pyroxenite implies that these changes cannot simply be modelled in terms of expulsion of material as this would imply massive volume reductions, for which there is no evidence. However, there is a general trend apparent in Table 6.4, which is that the components of ferromagnesian minerals (especially olivine and orthopyroxene) have been added to the rock at the same time as large - scale removal of Si, Al and various Group 1 and 2 elements (Na, Ca, Sr and Ba), although not potassium. This anomaly is reflected in the presence of a few grains of interstitial poikiloblastic biotite in the pyroxenite, and is probably due to addition of small (in absolute terms) amounts of K during metamorphism (section 6.4.2).

The compositional changes determined by XRF analysis are consistent with the differences in modal abundances of ferromagnesian minerals and plagioclase between the pyroxenite and its host rock. The euhedral shape of many of the pyroxenes and the poikilitic habit of the groundmass feldspar (Plate 3.100B) in the pyroxenites suggests that pyroxenite formation involve the passage of a melt phase through the rock. The composition of this melt and the changes in its composition cannot be determined from the compositional changes listed in Table 6.4 because both are also dependent on the total flux of melt through the rock, which is unknown. The case which involves the smallest melt to rock ratio and the largest change in the composition of the melt phase requires the addition of mafic melt to the rock, dissolution of feldspar and precipitation of ferromagnesian minerals, and the expulsion of a relatively Si - rich, high - Al melt of dioritic to plagiogranitic composition. However, the widespread occurence of olivine in the pyroxenites implies that the expelled melt must have been in equilibrium with this phase and therefore still broadly basaltic in character, although enriched in Al and alkalis relative to the input melt. This is consistent with the absence of any trapped granitic residua in the vicinity of the pyroxenites. The pyroxenites must, therefore, have reacted with a proportionally large volume of melt whose composition changed only by a small amount relative to the change in composition of the solid component during pyroxenite formation.

Table 6.4 nevertheless implies that pyroxenite formation was accompanied by a considerable decrease in feldspar stability and a relative increase in the stability of pyroxenes. This is consistent with the

Table 6.4.

Bulk compositional changes during the replacement of laminated gabbro 314 by metasomatic pyroxenite 316A.

Format of table as for Table 6.2. See text for discussion of replacement process. Abundance of K probably affected by alteration in 316A.

	314	316A	ΔC (absolute)	ΔC (relative)
SiO_2	49.96	42.66	−7.30	−14.6
Al_2O_3	15.03	5.54	−9.49	−63
$Fe_2O_3^T$	7.41	19.40	+11.99	−162
MgO	8.00	21.35	+13.35	−167
CaO	13.74	7.10	−6.64	−48
Na_2O	2.64	0.50	−2.14	−81
K_2O	0.16	0.18	+0.02	+13
P_2O_5	n.d.	n.d.	–	–
TiO_2	0.56	0.40	−0.16	−29
MnO	0.14	0.30	+0.16	+114
Ba	195	144	−51	−26
Cr	148	353	+205	+138
Cu	130	400	+270	+208
Ni	74	302	+248	+335
Pb	18	8	−10	−56
Sr	281	85	−196	−70
V	192	134	−58	−30
Zn	43	93	+50	+116
Zr	–	–	–	–

petrographic evidence for the corrosion and dissolution of even the most calcic feldspars in the parent rock. Possible reasons for this are discussed at the end of this chapter, in the context of the evidence for volatile activities in the Inner Series which is discussed in section 6.4, below.

6.3. Compositional relationships of the different groups of rocks within the Inner Series and their relationships to the other rocks of the Hypersthene Gabbro.

6.3.1. Pre - gabbronorite Inner Series rocks.

Features of the mineralogy and geochemistry of these rocks are summarised in Figs. 6.10 and 6.11 respectively. As noted in chapter 3, these rocks form a number of distinct rock types. It is, therefore, convenient to consider each group in turn. Reference is also made to the analyses of individual samples in Appendices 2 and 3.

6.3.1.1. Augite - anorthite/bytownite gabbros or eucrites (samples X1 and 97/5 (bulk rock analyses) and 312B3, and 97/5 (mineral analyses)).

These very unusual rocks are characterised by a combination of extremely calcic plagioclases, in the range An_{80} to An_{94}, and relatively iron - rich pyroxenes. These features are shared by the apatite - rich anothositic granular rock, 36/2. The pyroxenes are also very unusual in having very high Ca contents ($X_{Wo} \geq 0.45$; see Fig. 6.10.2), implying that the rocks are extremely undersaturated in low - Ca pyroxene. This is consistent with the high Ca and Ca/Al of the bulk - rock analyses.

The adcumulate to heteradcumulate textures of these rocks, coupled with the fine - scale banding present in the southernmost outcrops of these rocks in the Sanna Bay area (samples X1 and 97/5; see Figs. 3.25 and 3.26) suggests that they are extreme cumulate rocks, with only a small percentage of crystallised trapped residual melt. This makes it difficult to deduce the composition of the parental magma from which they were derived. It is clear that this cannot have been the same as the magmas from which any of the other rocks of the Inner Series were derived, from the implied high Ca/Al of the parent magmas and the unusual combination of very high An contents in the feldspars and relatively low bulk - rock X_{Mg} (Fig. 6.11.4). One possible interpretation of these features is that the rocks represent cumulates derived from a basic magma contaminated with Ca - rich, high Ca/Al calc - silicate metasediments, such as the hybrid rock 200/1 (section 4.4 and Appendix 2). This is consistent with the relatively high Ce/Yb of sample X1 (Fig. 6.11.6), particularly since the high clinopyroxene content of this rock would tend to reduce its Ce/Yb ratios relative to that of its

Fig. 6.10. Mineral compositions in the pre - gabbronorite Inner Series rocks.

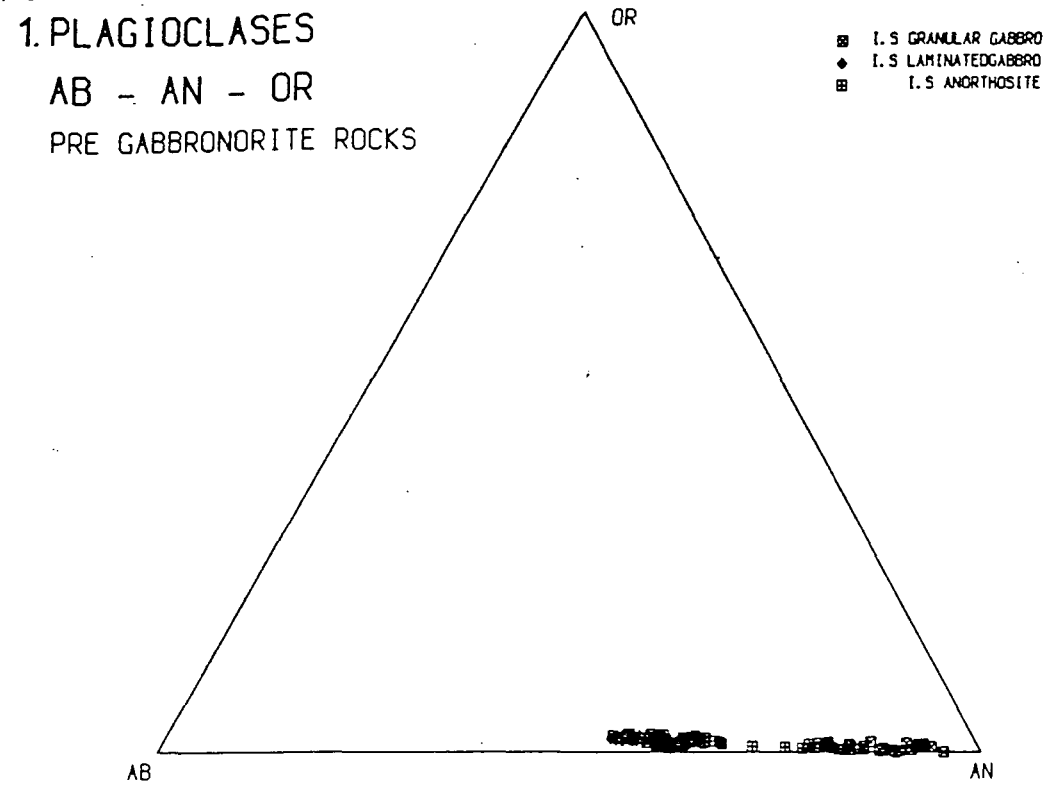

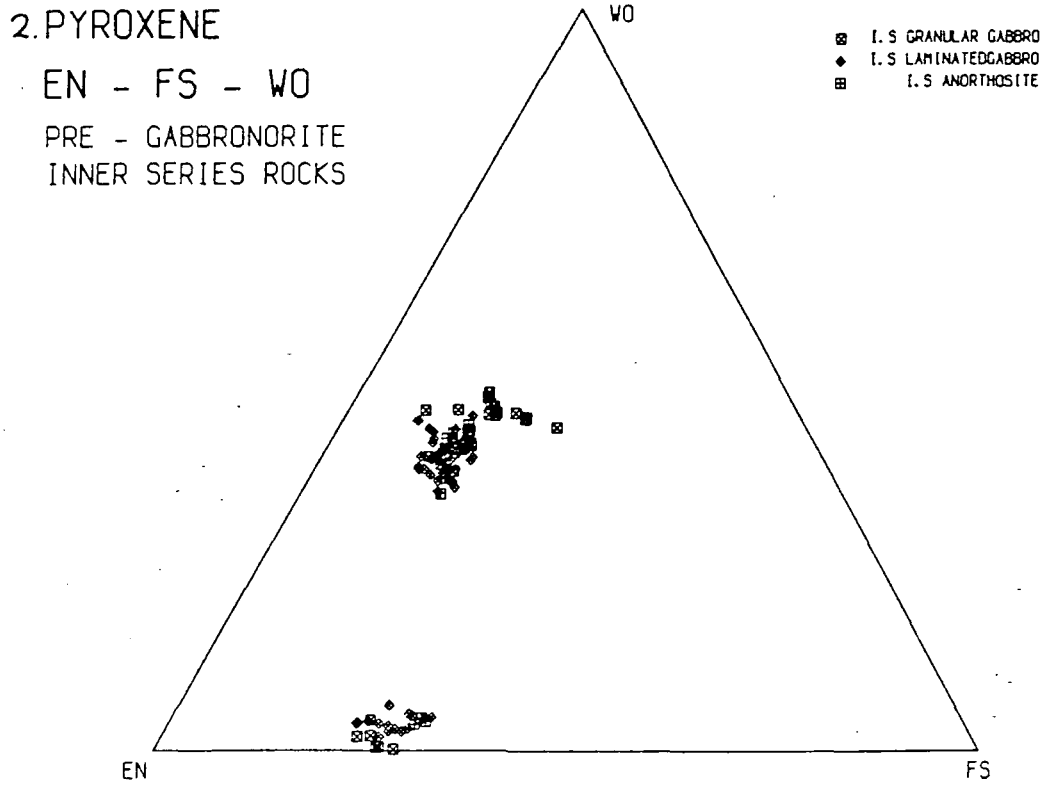

3. OLIVINES

FO - FA - MN OLIVINE

PRE - GABBRONORITE ROCKS

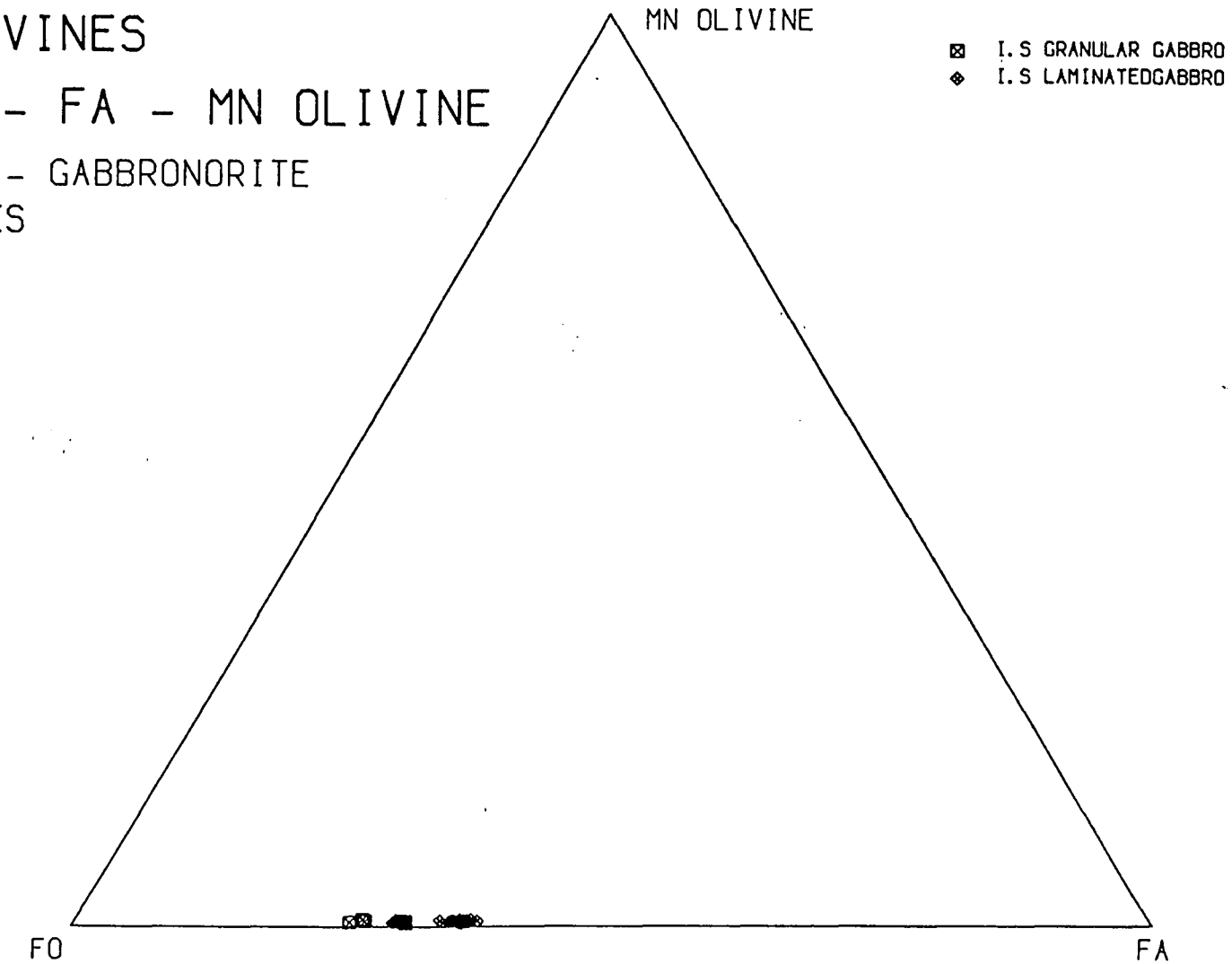

Fig. 6.11. Bulk compositional data for the pre - gabbronorite Inner Series rocks. See text for discussion of the named samples. Gabbronorite suite rocks plotted for purposes of comparison.

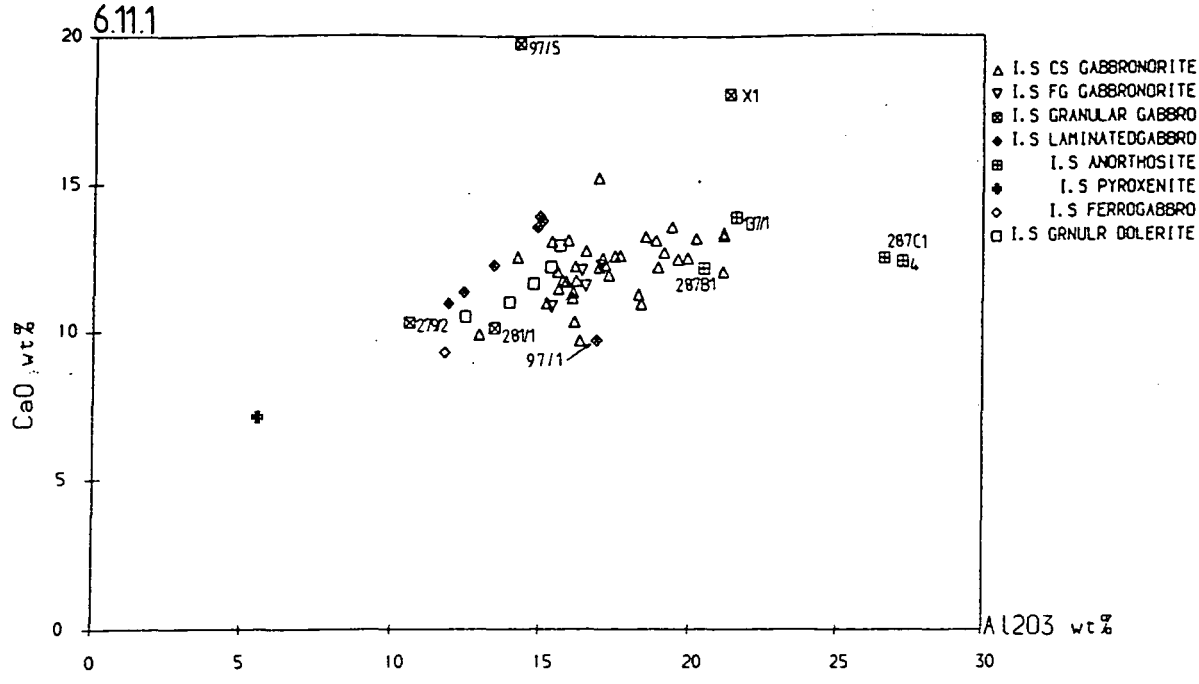

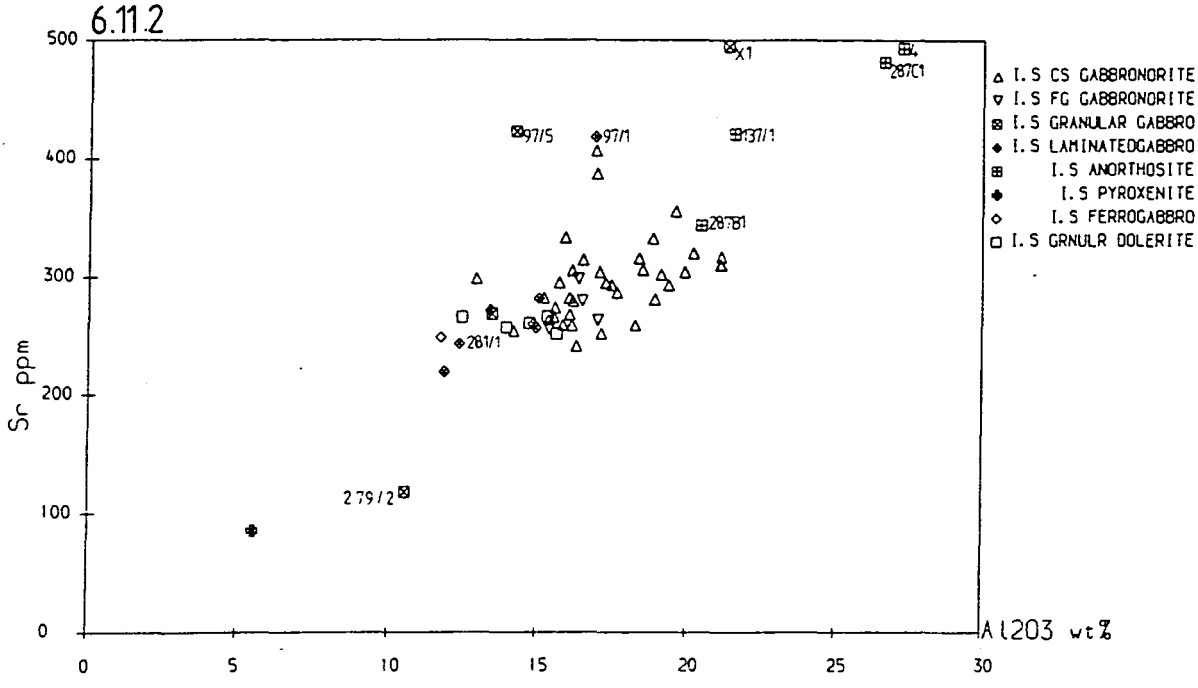

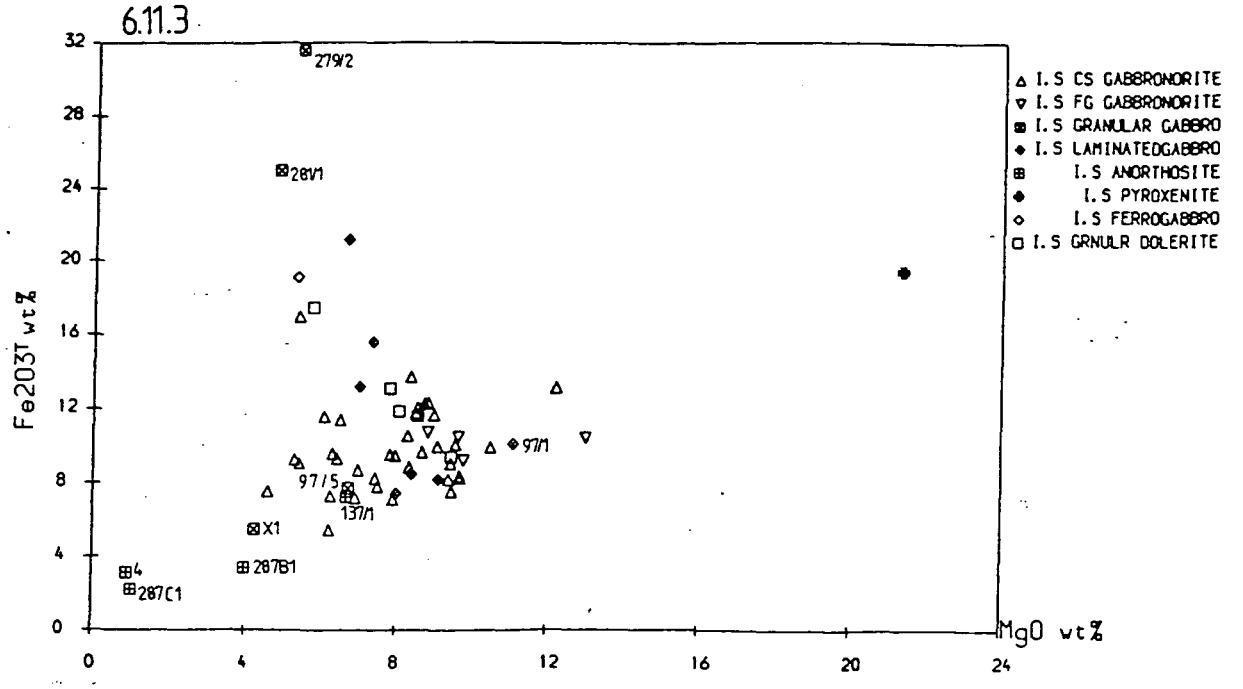
6.11.3
Fe2O3T wt%
MgO wt%
279/2
281/1
97/1
97/5
137/1
X1
287B1
4
287C1
I.S CS GABBRONORITE
I.S FG GABBRONORITE
I.S GRANULAR GABBRO
I.S LAMINATEDGABBRO
I.S ANORTHOSITE
I.S PYROXENITE
I.S FERROGABBRO
I.S GRNULR DOLERITE

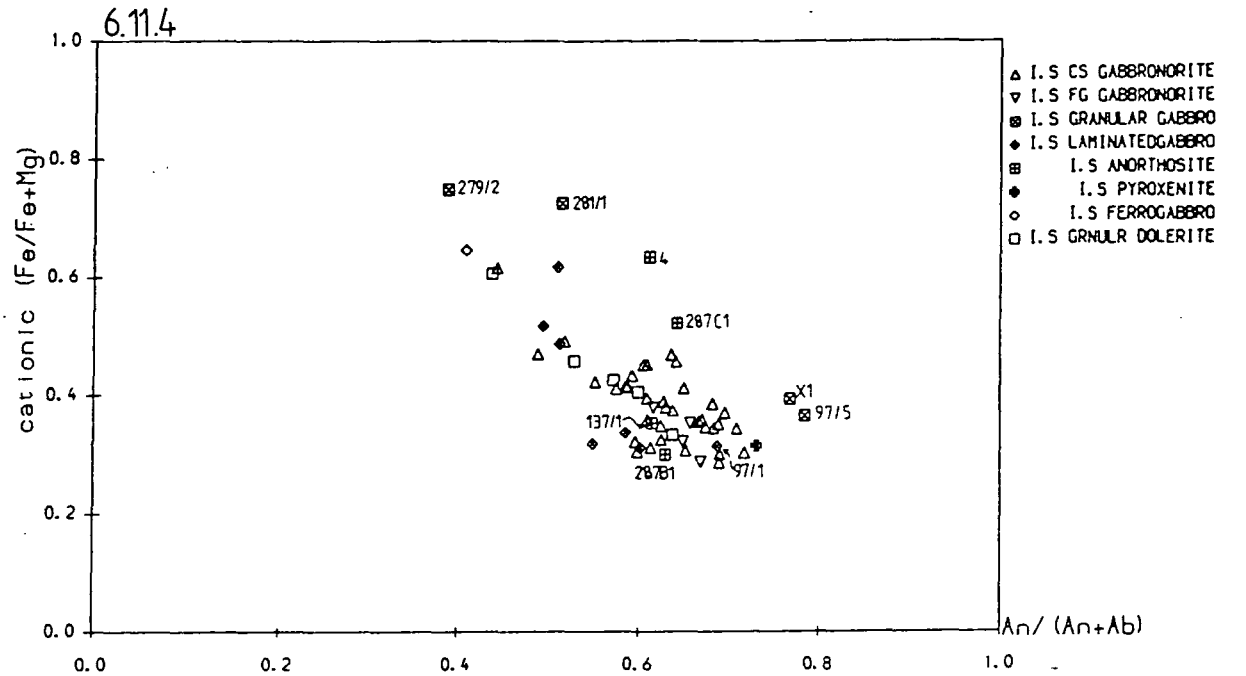
6.11.4
cationic (Fe/Fe+Mg)
An/ (An+Ab)
279/2
281/1
4
287C1
X1
97/5
137/1
287B1
97/1
I.S CS GABBRONORITE
I.S FG GABBRONORITE
I.S GRANULAR GABBRO
I.S LAMINATEDGABBRO
I.S ANORTHOSITE
I.S PYROXENITE
I.S FERROGABBRO
I.S GRNULR DOLERITE

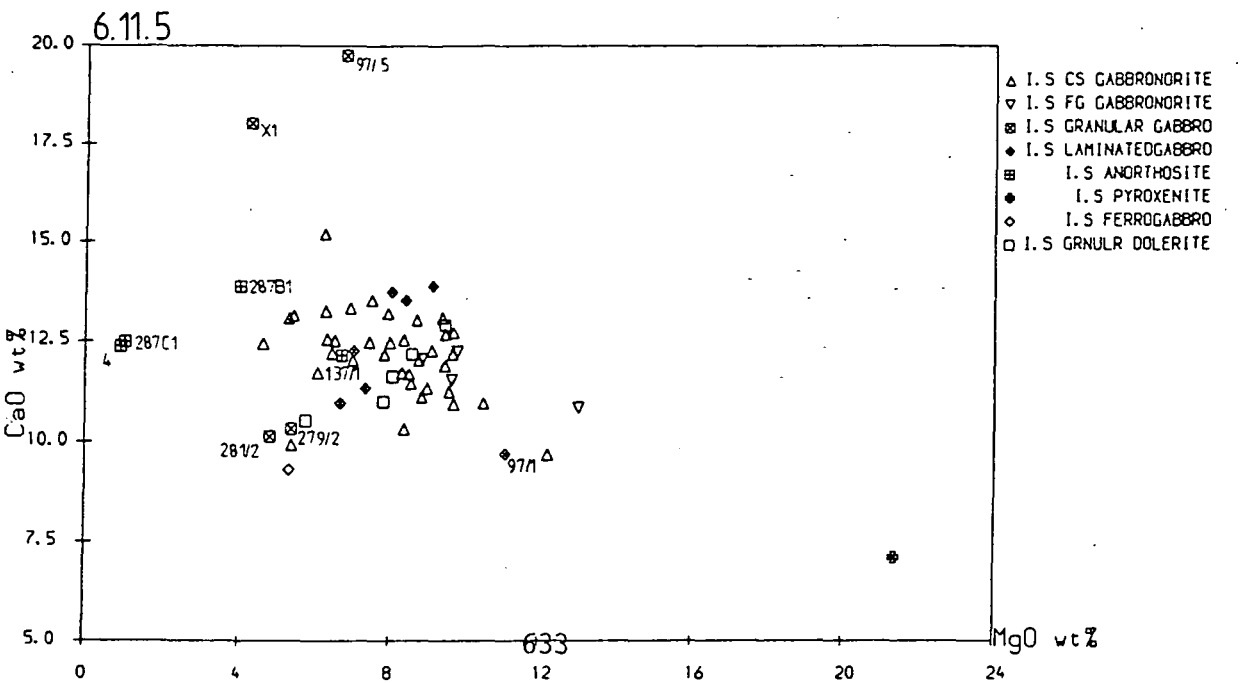
6.11.5
CaO wt%
MgO wt%
97/5
X1
287B1
287C1
4
137/1
281/2
279/2
97/1
I.S CS GABBRONORITE
I.S FG GABBRONORITE
I.S GRANULAR GABBRO
I.S LAMINATEDGABBRO
I.S ANORTHOSITE
I.S PYROXENITE
I.S FERROGABBRO
I.S GRNULR DOLERITE

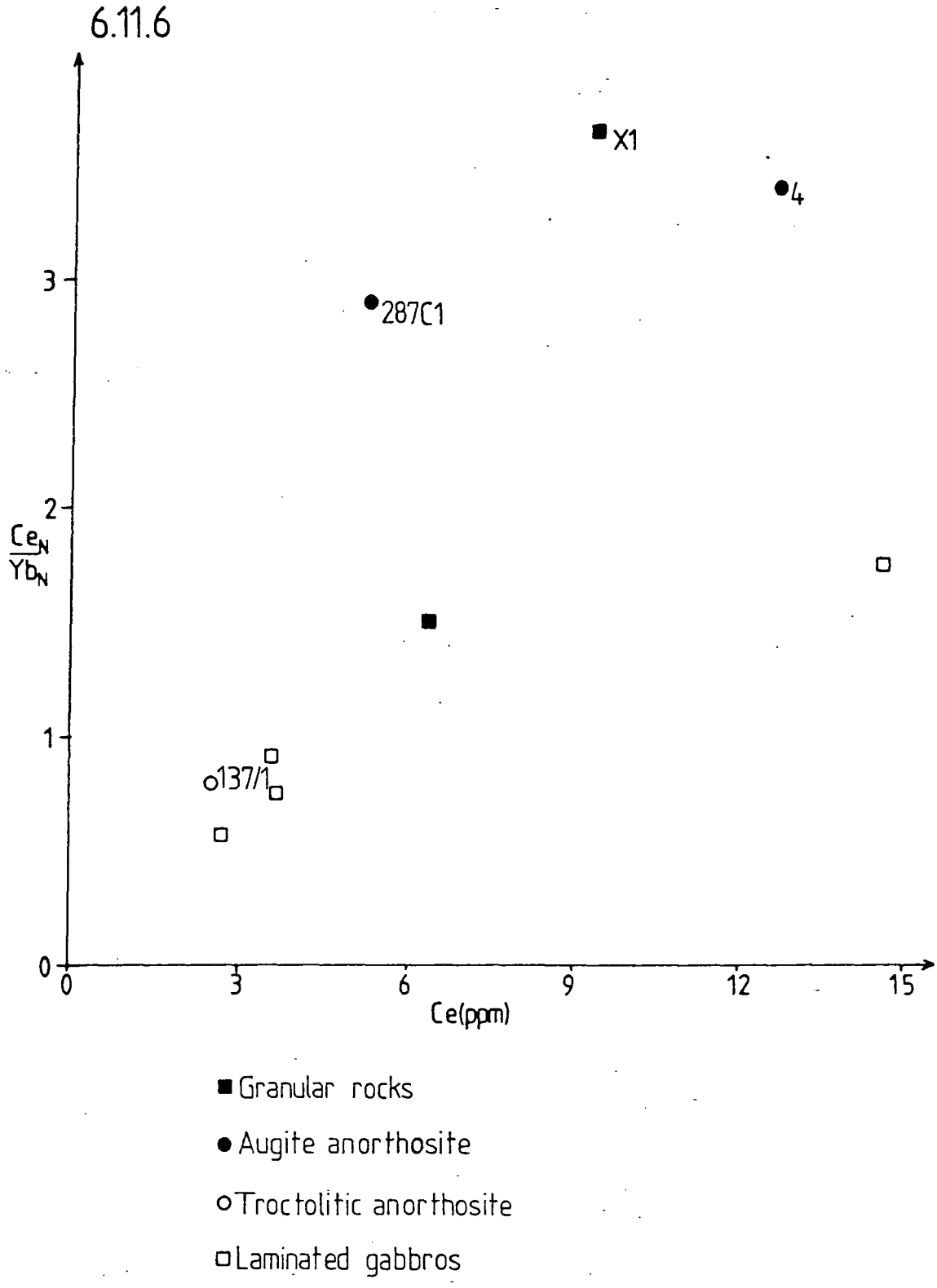
6.11.6
X1
4
287C1
137/1
3
2
1
0
$\frac{Ce_N}{Yb_N}$
0
3
6
9
12
15
Ce(ppm)
Granular rocks
Augite anorthosite
Troctolitic anorthosite
Laminated gabbros

parent magmas. The reasons for the occurrence of apatite in 36/2 are not clear, however: the high Ca content of the parent magma may have increased the stability field of this phase sufficiently to cause its early precipitation.

6.3.1.2. Granular magnetite - anorthosites and magnetite - troctolites (samples 284, 166A2 and 108 (microprobe analyses) and 279/2 and 281/1 (whole - rock analyses)).

The bulk compositions of these rocks reflect their modal mineralogies: high Fe and Ti, and low Si, due to the presence of iron oxides; relatively high Al, Ca and Na due to the presence of plagioclase; low Mg and Ca/Al due to low abundances of olivine and clinopyroxene. The relatively low *An* content of the analysed feldspars (An_{54} to An_{63}) and the abundance of magnetite suggest crystallisation from a relatively evolved, iron - rich magma. If this interpretation is correct this magma must also have been characterised by low Ca/Al (in contrast to normal tholeiitic magmas) and Si contents, as otherwise the dominant ferromagnesian phase(s) would be one or more pyroxenes, rather than the observed olivine. However, the analysed olivines in these rocks are amongst the most Mg - rich examples analysed from any of the Inner Series rocks (up to Fo_{72} in sample 284; see Fig. 6.10.3 and analyses in Appendix 3). This discrepancy between plagioclase and olivine compositions is shown in section 6.4.2.2, below, to be related to oxidation of these rocks during high - grade metamorphism prior to their incorporation into the gabbronorite suite rocks in which they now occur. Their present - day mineralogy and compostion may therefore not, therefore, be that which they originally posessed.

One of these rocks (166A2), which originates from the southern margin of the Inner Series, contains coarse anorthositic veins which are characterised by much more calcic feldspar compositions (around An_{80}) than their host rocks. Feldspars of the same composition occur in the coarse - grained anorthosites in the northern and western sectors of the Inner Series, suggesting that this latter rock type may have originally been more widespread within the Inner Series, and as porphyrocrysts in the gabbronorites (section 6.2.1). This suggests that these veins may also be related to the source rocks of the latter, if they are xenocrystic in origin.

6.3.1.3. Coarse - grained anorthosites.

The four samples of this rock type form two distinct pairs. One of these is formed by samples (4 and 287C1) from the series of anorthosite outcrops on the northern side of Sanna Bay (see Fig. 3.25). These are characterised by very high contents of large feldspar crystals most of which are more sodic than the gabbronorite porphyrocrysts, although a few contain calcic cores in the same compositional range as the latter. Furthermore, the dominant mafic phase in these two rocks is clinopyroxene, only small amounts of both olivine and orthopyroxene being present. Chemically, the two rocks are also distinctive in having much higher Ce/Yb (chondrite - normalised ratio about 3) than the gabbronorite suite rocks. In principle this could be due to partitioning of light rare earth elements into plagioclase, and accumulation of the latter, from a magma with a flat REE distribution pattern like that of the gabbronorite suite rocks. However, this would also produce a large increase in Eu relative to the other rare earths as a result of the substitution of Eu^{2+} into plagioclase. The actual chondrite - normalised abundances of Ce, Eu and Yb in these rocks are as follows:

	Ce_N	Eu_N	Yb_N
287C1	6.1	5.8	2.1
4	14.7	11.4	4.3

These data indicate that if the high Ce/Yb ratios were due simply to plagioclase accumulation, trivalent LREEs would have to have been more compatible in the feldspars than Eu. This is inconsistent with the normal tholeiitic oxidation state of the parent magmas, implied by the presence of interstitial - poikilitic olivine and orthopyroxene in these rocks, and published REE distribution coefficients between feldspars and normal, low - f_{O_2} magmas (Henderson 1982; Lambert & Simmons 1987). The high Ce/Yb of these rocks must therefore have been inherited from the magmas from which they crystallised. Whether this feature of the latter was caused by crustal contamination or by lower degrees of partial melting in the mantle source region, it implies that these anorthositic rocks crystallised from a distinct magma to the low Ce/Yb magma parental to the gabbronorite suite rocks.

In contrast, the second pair of anorthositic rocks (137/1, from an area east of Ardnamurchan Point, and 287B1, also from the outcrops on the northern side of Sanna Bay) are less distinct in their compositions from gabbronorite suite rocks (although still very distinctive petrographically and distinctly older). They are characterised by higher modal olivine contents than the high Ce/Yb

anorthosites and plot close to the more troctolitic gabbronorites in Fig. 6.11.1 – 4. Sample 137/1 also has low Ce/Yb, in the same range as Ce/Yb in the gabbronorite suite rocks, and cannot have been derived from the same magmas as samples 4 and 287C1. At least two separate magma batches are therefore represented in the anorthositic rocks.

6.3.1.4. Laminated gabbros and olivine gabbronorite.

As is apparent from Figs. 6.5 and 6.7 as well as 6.10, these rocks are similar to the well - laminated members of the gabbronorite suite in many respects. Although they show a wide range of degrees of fractionation there is no reason to suppose that they could not have formed from a single cogenetic suite of magmas, except in the case of the olivine microgabbronorite sample 97/1. This is both markedly more primitive (olivines of composition Fo_{65-70}, rather than about Fo_{60}) and contains a much larger amount of modal orthopyroxene than any of the other pre - gabbronorite laminated rocks.

Although similar geochemically to some of the gabbronorite suite rocks, the low abundance of orthopyroxene in the majority of the pre - gabbronorite laminated rocks argues against their derivation from the same extremely tholeiitic magma suite. The present geochemical data set is however an insufficient basis for deciding whether these rocks were derived from a less extreme tholeiitic magma or whether they were produced from early members of the gabbronorite suite by the same sub - rigidus processes which produced the well - laminated members of the gabbronorite suite (section 6.2.2.1).

6.3.2.1. The Inner Series and the Marginal Border Group.

These two groups of rocks are not easily compared because the MBG basic and intermediate rocks correspond fairly closely to liquid compositions whereas the IS rocks have been affected by a variety of crystal accumulation and 'post - cumulus' or sub - rigidus processes. This problem is particularly severe in the case of the exotic pre - gabbronorite rocks. However, the principal problem in the relationship between the MBG and the Inner Series is that of the relationship, if any, of the gabbronorite suite magmas to some of the later MBG rocks, particularly the M2 porphyritic dolerites (see section 3.2.7). These rocks can be compared by plotting ratios of elements which do not

substitute into calcic plagioclase, the main accumulative porphyrocryst phase in the gabbronorites, to any significant extent.

The colinearity of the two groups of rocks in Fig. 6.12.1, a plot of TiO_2/MgO vs. cationic $Fe_{total}/(Fe_{total}+Mg)$, indicates that both groups of rocks were derived from incompatible element - poor primary tholeiitic magmas. In general the MBG rocks have higher Ti/Mg and Fe/Mg than most of the IS rocks. In part, this reflects the accumulative nature of many of the IS rocks but it is notable that even the fine - grained, doleritic - textured gabbronorites and the granular dolerites of the gabbronorite suite have lower values of these ratios than the majority of analysed MBG rocks. This implies that most of the gabbronorite suite magmas were less fractionated than the majority of the MBG magmas and that although conditions in the mantle source region may not have changed greatly between the emplacement of the two groups of rocks they are nevertheless two distinct suites of rocks.

Although the primary magmas appear to have been broadly similar, a plot of K_2O/MgO vs. cationic $Fe_{total}/(Fe_{total}+ Mg)$ for the two groups of rocks (Fig. 6.12.2) indicates that the MBG magmas were in general more contaminated by K - rich crustal material than the IS magmas, although caution must be exercised in the interpretation of this diagram because of the possibility of alteration of K contents during hydrothermal metamorphism. The various ratios used to investigate crustal contamination of MBG rocks in section 4.3 are less sensitive to alteration but the abundances of Th, La and to a lesser extent Ta and Hf, in the Inner Series rocks are usually too close to detection limits to be known with sufficient precision to constrain crustal contamination reliably; ratios involving La and Th or Ta are also affected by late - stage melt expulsion.

Fig. 6.12 also indicates that the M2 porphyritic dolerites which cut the MBG rocks, along the western margin of the pluton in particular, are probably more closely related to the MBG rocks than to the gabbronorite suite rocks. Most are more evolved than the latter (Fig. 6.12.1) and some at least appear to show a greater degree of crustal contamination, although this may be an artefact, produced by the addition of K during growth of M2 biotite in these rocks.

6.3.2.2. The gabbronorite suite rocks and late - M2 and younger rocks.

Fig. 6.12. Comparison of the compositions of the Inner Series rocks with those of the basic and intermediate rocks of the Marginal Border Group.

6.12.1

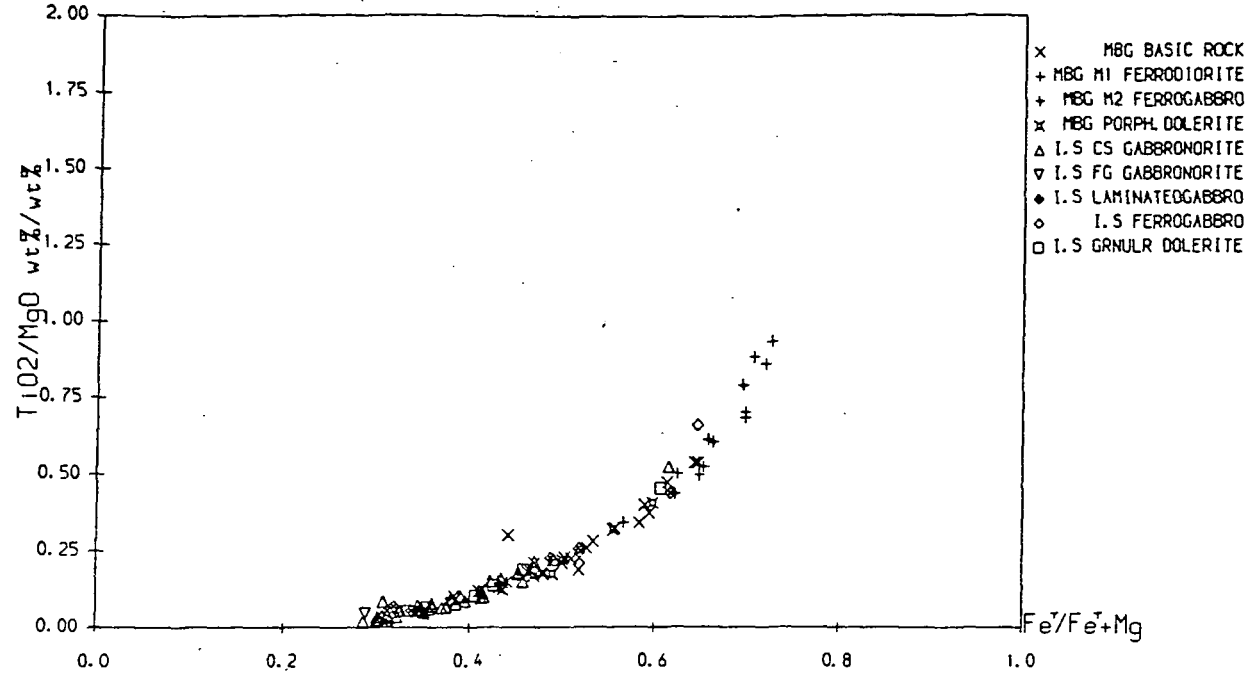

6.12.2

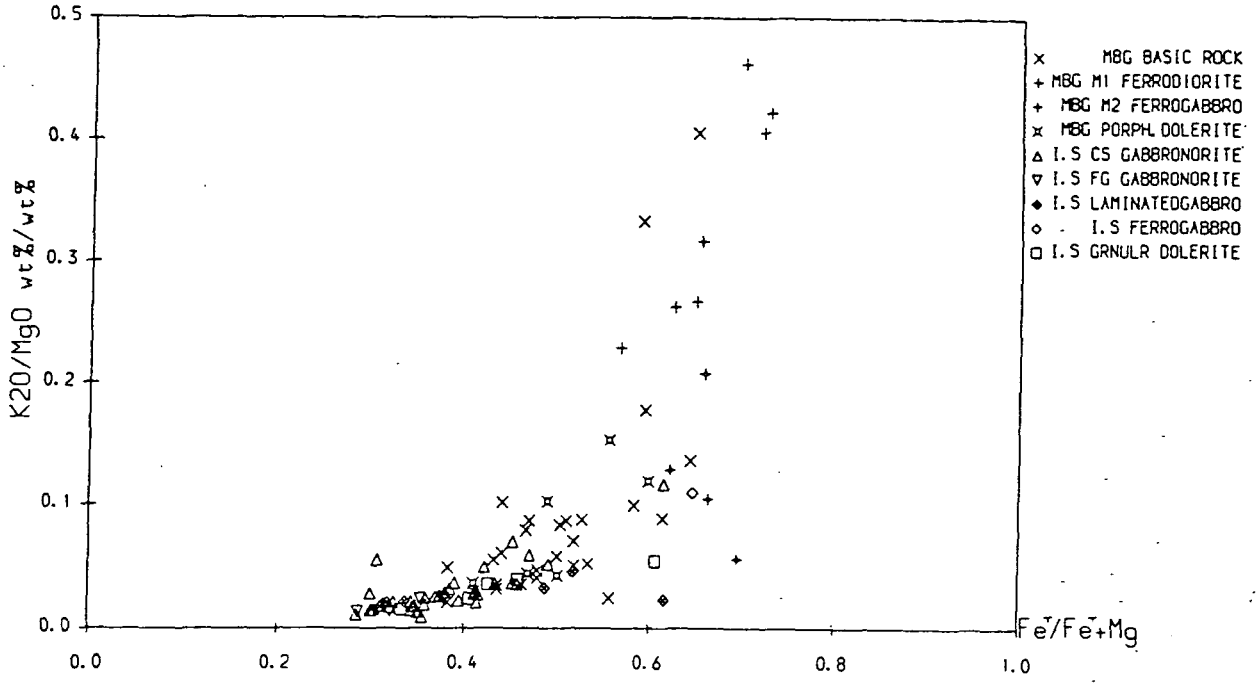

The same problems which affect comparisons of IS rocks with MBG rocks also affect comparison of the gabbronorite suite rocks with late M2 rocks (the Group 3 cone sheets and Group 4 minor intrusions to the south of the pluton (sections 3.2.5 and 3.2.6), and rocks of the same age within the Inner Series), the Glebe Hill gabbros (section 3.2.6) and later intrusions of Centre 2 of the Ardnamurchan central complex (see Figs. 1.2 and 1.3). As in previous cases involving strongly porphyritic rocks ratio/ratio plots can be used to reduce or eliminate the effects of porphyrocryst accumulation. Figs. 6.13.1 and 6.13.2 indicate that all the gabbronorite suite and later rocks lie on similar fractionation trends which, as with all the other rocks associated with the Hypersthene Gabbro, are broadly tholeiitic in character. As was noted in Chapter 3, orthopyroxene is a much less prominent phase in these later rocks but this does not seem to correlate strongly with the rest of their geochemistry.

Fig. 6.13.3, on the other hand, indicates that the later rocks do differ from the gabbronorite suite rocks with respect to their history of crustal contamination. Although some show the same low K contents as the gabbronorite suite rocks others show much greater K/Mg ratios at the same degree of differentiation, pointing to more crustal contamination of these later rocks with high - K crustal material. This suggests that the magmas from which these later rocks were derived ascended to the present level of exposure through a separate system of magma conduits to that which fed the gabbronorite suite magma bodies. The apparent lack of crustal contamination in the latter, which is implied both by their low K contents and by their low Ce/Yb ratio (Fig. 6.2) indicates that they ascended through the crust in a conduit system with relatively refractory walls. These walls could either be formed by cumulates from earlier Tertiary magma batches or by highly refractory crustal rocks remaining after melting out of all the fusible components by the earlier magmas.

One final conclusion which can be drawn from Fig. 6.13 is that the sampled Group 3 cone sheets and post - metamorphic Inner Series dolerites form a vary homogenous and presumably cogenetic suite of rocks. In contrast, the other post - metamorphic rocks sampled are spread over wide compositional ranges in these diagrams. In particular, there is no geochemical evidence to support the suggestion, made in section 3.2.6 on the basis of age relationships, of a link between the ultraporphyritic Group 3 cone sheets and the similarly feldspar - rich Glebe Hill gabbros. It appears that, during the time interval bounded by the available constraints on the relative ages of these rocks, a number of separate magma batches reached the present level of exposure and formed discrete groups of intrusions.

Fig. 6.13. Comparison of the gabbronorite suite rocks and laminated gabbros with post - M2 rocks associated with the Hypersthene Gabbro and with later Centre 2 intrusions.

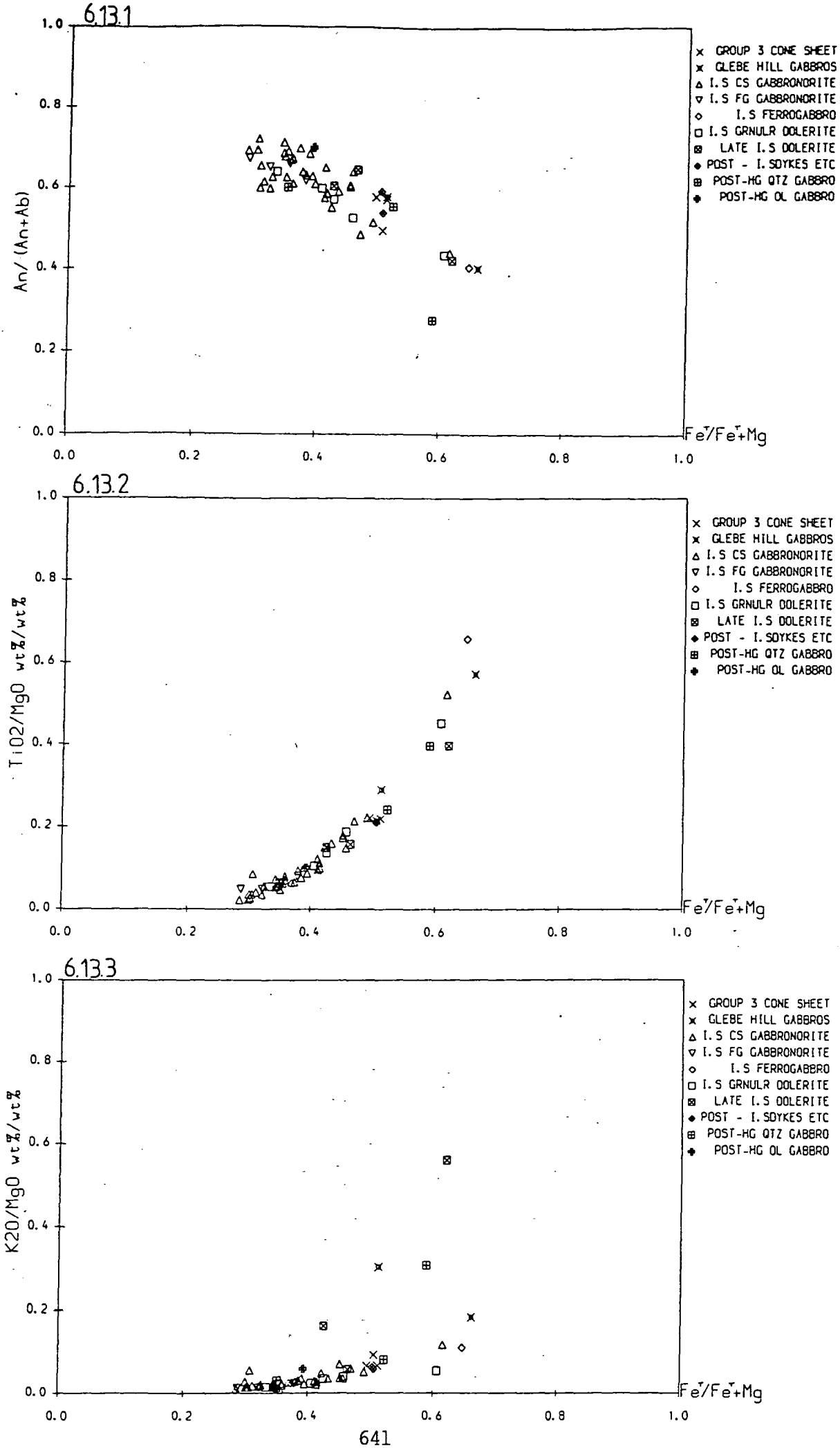

6.3.3. Conclusions regarding the magma supply to the Hypersthene Gabbro during its evolution.

The discussion of the basic, intermediate and accumulative rocks of the Hypersthene Gabbro in the preceding subsections indicates with a fair degree of certainty that a number of discrete magma batches were present at different stages in its evolution. These include the crustally contaminated tholeiitic rocks of the Marginal Border Group, with mainly Lewisian contaminants; the granular anorthite - gabbros or eucrites of the Inner Series, which may represent cumulates derived from magmas contaminated with calc - pelitic or calc - silicate metasediments of the sequence above the Moine thrust; the high - Ce/Yb pre - gabbronorite suite anorthosites; the weakly contaminated, strongly tholeiitic rocks of the gabbronorite suite; and the crustally contaminated post - gabbronorite suite rocks. The differing intensities of crustal contamination, and the differences (between at least some of these groups of rocks) in the source of the contaminant implies that the form of the conduit system through the crust which fed the pluton changed with time, producing differences in the composition of the wall rocks and in wall rock temperatures and thereby changing the pattern of contamination. In part because of this variation in crustal contamination, however, it is less clear as to whether the composition of the mantle source of the magmas, or the degree of partial melting within that source, changed with time. The variation in abundance of modal orthopyroxene at similar degrees of differentiation, which is either independent of crustal contamination or may even show (perhaps coincidentally) a negative correlation with the latter, implies differences in the mantle melting regime. This could involve differences in the final depth of equilibration of the magmas, or different average degrees of partial melting, or (which is most likely) both (McKenzie & Bickle (1988)). Changes in the composition and/or degree of partial melting within the mantle source during the lifetime of single plutons in the British Tertiary Volcanic Province were identified by Dickin et al. (1984) in the case of the Cuillins complex of Skye and are also indicated by the data of Greenwood (1987) for rocks of the marginal suite of the Rhum complex. In the case of the Hypersthene Gabbro, however, the available compositional data are not sufficiently precise for evaluation of geochemical evidence for or against such variations in primary magma composition.

6.4. Ultra - High Grade Hydrothermal Metamorphism of the Inner Series rocks.

Very high grade (broadly speaking, two - pyroxene hornfels facies) metamorphic mineral assemblages occur in the majority of rocks in the interior of the Inner Series (section 3.4.6). These were related in that section to the formation of a tensile fracture network through which hydrothermal fluids circulated at temperatures above, and water partial pressures below, the upper stability limits of high - grade metamorphic hydrous phases such as pargasitic hornblende and Ti - rich biotite or phlogopite.

Fluid circulation at very high temperatures (700 – 1000°C) through basic and ultrabasic plutonic rocks has been identified in a number of plutons in the BTVP (Taylor & Forester 1971; Forester & Harmon 1983; Ferry 1985; Greenwood 1987) and elsewhere (see review in Taylor 1987). The evidence for this, however, has primarily involved the presence of isotopically light oxygen compositions (i.e. ^{18}O depletions), in apparently pristine and certainly anhydrous gabbroic and ultrabasic rocks, which are interpreted as the result of reaction of the rocks with isotopically light fluids derived from meteoric groundwaters at conditions within the stability ranges of those primary minerals. This conclusion has been supported by study of the temperature - dependent isotopic fractionations between minerals present in these rocks: the small size of these fractionations imply isotopic exchange at high temperatures. As was noted in section 1.2, the rocks studied by Taylor & Forester (1971) include two samples from the Hypersthene Gabbro which were shown by them to have strong ^{18}O depletions, indicating intense high - temperature meteoric - hydrothermal fluid circulation in the pluton. The sample location descriptions given by Taylor & Forester (1971) indicate that these samples originate from Inner Series rocks.

Despite the abundance of isotopic evidence for ultra - high - grade hydrothermal circulation in mafic plutonic rocks, definite mineralogical and petrographic evidence for hydrothermal circulation under these conditions, in the form of demonstrably open - system reactions and two - pyroxene - hornfels facies mineral assemblages in veins, has not previously been described from ^{18}O - depleted rocks. Several studies have, however, described high - temperature hydrous assemblages from such rocks, notably that on the East Greenland gabbros by Bird et al. (1988). Bird et al. describe pyroxene (clinopyroxene **or** orthopyroxene, but not both) + hornblende assemblages from these plutons.

Pyroxene - hornblende exchange equilibria on these rocks indicate temperatures of up to around 900°C.

A number of unrelated studies on the oxidation of basaltic rocks (Muir et al. 1957; Haggerty & Baker 1967) and plutonic nodules (Johnston & Stout 1984) have revealed the presence of orthopyroxene - FeTi oxide symplectitic intergrowths, replacing olivine, similar to those which occur in the Inner Series rocks (section 3.4.6, especially Plates 3.108 – 3.110). Similar intergrowths in deep crustal plutonic rocks of the south Norway anorthosite complex have been described by Barton & Van Gaans (1988), although in this case the association of symplectitic intergrowth formation with alteration of olivine is not as close. Barton & Van Gaans show, however, that the formation of the intergrowths occurred in association with an increase in the f_{O_2} of the rocks, relative to solid - state internal buffers, which they attribute to circulation of oxidising hydrous fluids.

None of these studies have investigated the oxygen isotopic compositions of the rocks in which the intergrowths occur although in many cases this would not be a profitable exercise because the fluids will only be isotopically light if there is a high - latitude meteoric component in the source of the fluids. Examination of samples of the Skaergaard intrusion layered series rocks in the Durham University undergraduate teaching collection (collected by A.R.McBirney) has revealed the presence of symplectitic intergrowths identical to those from the Inner Series of the Hypersthene Gabbro described in section 3.4.6. These have not been described in the literature but it is noteworthy that seperate splits of the same rocks were analysed by Norton & Taylor (1979) and shown by those workers to have undergone ^{18}O depletion at very high temperatures.

Four petrographically distinctive anhydrous metamorphic mineral assemblages are present in the Inner Series rocks (see section 3.4.6). These are all believed to have been produced by reactions between Inner Series rocks and a coexisting hydrous fluid phase under subsolidus conditions. The primary evidence which indicates that these assemblages are subsolidus in origin is textural (see section 3.4.6); additional evidence in support of this interpretation is presented in this section, principally in the form of geothermometric data which indicate that temperatures of formation were mainly in the range 700 – 900°C. The four assemblages can be summarised as follows:

1). Symplectitic intergrowths of orthopyroxene and FeTi oxides (usually Ti - magnetite, but

occasionally with ilmenite as well), or granular intergrowths of opaques with small amounts of orthopyroxene, or opaques alone, replacing olivine. The opaque - rich intergrowths only occur in FeTi oxide - rich granular pre - gabbronorite rocks.

2). Vein assemblages filling tensile fractures: orthopyroxene ± clinopyroxene ± opaques, or opaque oxides alone. The latter are especially common as granules occuring in trails along very small (originally $< 10\mu$m wide ?) annealed fractures in both ferromagnesian minerals and in plagioclase crystals. Rare thick (up to more than a millimetre wide) clinopyroxene - rich veins are also present.

3). Recrystallised ophitic (originally magmatic) clinopyroxenes containing opaque exsolution lamellae or granular opaque inclusions, and lacking orthopyroxene exsolution lamellae, although these are typically present in adjacent grains or even in unrecrystallised parts of the same grain. Clinopyroxenes with opaque oxy - exsolution lamellae are also present within the Inner Series but are less common than in the high - grade M2 assemblages in basic rocks of the Marginal Border Group and cone sheets close to the MBG contact (section 5.4).

4). Plagioclase + olivine or clinopyroxene symplectitic or myrmekite - like intergrowths rimming or replacing opaque grains. These were only found in one pre - gabbronorite granular magnetite - plagioclase rock.

In addition to these anhydrous assemblages, brown pargasitic hornblende (associated in one sample, 137/1, with orthopyroxene, opaques and Ti - rich biotite) occurs as inclusions in primary olivine (137/1) or in orthopyroxenes in the metasomatic pyroxenites (samples 316A and 6A). These hornblendes may be of similar age to the above assemblages: all other hydrous minerals – principally green hornblende, biotite, talc and chlorite – in Inner Series rocks are distinctly younger in age.

Of the four anhydrous assemblages, the most important for present purposes are those containing one or more pyroxenes as these can be used to constrain the temperatures of formation of the assemblages using the pyroxene geothermometer of Lindsley (1983). Pyroxene geothermometry on these assemblages and the implications of the results for the timing of deformation and fluid flow through the rocks are discussed in section 6.4.1. The reactions involved in the production of

the assemblages and inferences regarding the activites of various components in the fluid phase, especially oxygen, are considered in section 6.4.2. It should be noted that since no stable isotope data is available for these particular rocks the fluid phase cannot definitely be shown to be mainly meteoric in origin, although this is implied by the evidence for high - temperature ^{18}O depletion of the Hypersthene Gabbro found by Taylor & Forester (1971).

6.4.1. Two - pyroxene geothermometry of metamorphic assemblages in Inner Series rocks: temperatures of formation of the metamorphic assemblages and of very high grade hydrothermal fluid circulation in the Inner Series.

6.4.1.1. Errors in two - pyroxene geothermometry and the nature of the temperatures obtained.

Two - pyroxene geothermometry is based on the degree of solid solution, in the form of substitution of Ca into the M2 site in Ca - poor pyroxenes (orthopyroxene and pigeonite) and of Mg and Fe into the M2 site in Ca - rich clinopyroxenes, between coexisting Ca - rich and Ca - poor pyroxenes. Lindsley (1983) identified three causes of error in temperatures obtained by this method. These are uncertainty in pressure (because the amount of solid solution increases slightly with pressure), the presence of components (principally Al, Fe^{3+}, Ti and Na) which displace the composition of the pyroxenes out of the Wo - En - Fs compositional plane in which they are plotted for the purposes of the geothermometer, and analytical error.

Experiments summarised in Lindsley (1983) show that the pressure - dependence of temperatures obtained from pyroxene compositions is about 8°C per kilobar of pressure. Given the low pressure of emplacement of the rest of Hypersthene Gabbro and of the Ardnamurchan complex as a whole, probably no more than 1kb, the use of the one atmosphere temperature - pyroxene composition relationships of Lindsley (1983) will cause errors due to this effect of no more than 10°C or so. This is small in comparison with other errors (see below). The effects of pressure may in part account for an apparent anomaly in the data discussed, that many of the more Ca - rich orthopyroxenes actually plot within the two - phase orthopyroxene - pigeonite field at one atmosphere. Lindsley (1983) showed that the position of the position of the three - phase equilibrium point orthopyroxene - augite - pigeonite is strongly pressure - dependent, moving to more iron - rich compositions at

higher pressures and the same temperature. The orthopyroxene - pigeonite field therefore contracts with increasing pressure and some at least of the analysed points would then plot in the field of orthopyroxenes in equilibrium with augite alone, as is consistent with the absence of recognisable inverted pigeonite from all of the rocks analysed using the electron microprobe.

The effects of 'non - quadrilateral' components (i.e. cations other than Ca, Fe^{2+}, Mg and Si) on equilibria between ortho - and clino - pyroxenes have not been investigated thermodynamically. However, Lindsley (1983) presented an empirical scheme for recalculating pyroxene compositions to allow for the effects of the main non - quadrilateral components. This procedure has been followed in calculating the temperatures presented below. It is not entirely satisfactory, particularly in the form used, which depends on an assumption of perfect stoichiometry in calculation of Fe^{3+} abundances from microprobe data, leading to propagation of errors from the rest of the analysis into the estimates of the abundance of Fe^{3+} bearing components. Lindsley (1983) considered that the correction procedure, and hence the geothermometer as a whole, is only reliable when the concentration of 'non - quadrilateral' components is less than 10% . All the pyroxenes analysed in the course of the present work contain less than about 5% (by molecular abundance) of such components, suggesting that the geothermometer can be legitimately applied to them. Lindsley & Andersen (1983) estimated that errors in the correction procedure produced additional uncertainty in the final temperature estimates of $\pm 5^{\circ}C$ per percentage point of non - quadilateral components present above a lower limit of 2% of such components, below which the error produced was insignificant.

The presence of these components in pyroxenes also has the effect of reducing the stability field of pigeonite as they substitute much less readily into this phase than into augite or orthopyroxene (Lindsley 1983). Their presence in the analysed pyroxenes therefore also helps to account for the apparent metastability of some of the most Ca - rich orthopyroxenes with respect to pigeonite + orthopyroxene when projected into the Wo - En - Fs plane. This anomaly is not, therefore, considered to indicate systematic errors in analyses for Ca in pyroxenes, for which no other evidence was found, for example in errors in stoichiometry, although a relatively high - Ca orthopyroxene reference material was not available to check the analyses.

Analytical errors in the two - pyroxene geothermometer include both those in the analyses used to set up the original calibration ($\pm 20^{\circ}C$; Lindsley & Andersen (1983)) and those in the analyses

of the Inner Series pyroxenes made during the course of the present work. The latter are likely to be at least as large as the former, given the extra care used in the construction of the original geothermometer calibration (Lindsley & Andersen 1983).

It therefore seems likely that the errors in the temperatures of metamorphism of Inner Series rocks obtained by pyroxene geothermometry are likely to have associated uncertainties of at least ±50°C, and perhaps as much as ±100°C. A large part of this, possibly as much as fifty degrees, is likely to be systematic error produced by the effects of pressure, errors in the original geothermometer calibration and in the calibration of the Durham microprobe, and the effects of non - quadrilateral components (note that these are present in broadly similar amounts in all the crystals of each mineral analysed formed in any one temperature range). Thus, as will be seen, texturally distinct groups of pyroxenes separated by differences in their calculated equilibration temperatures of only 50°C or so can be resolved according to the latter as well as by textures. It should be borne in mind, however, that absolute temperature estimates for any one pyroxene grain may be in error by as much as 100°C, particularly in the case of the orthopyroxene analyses. Orthopyroxene compositions are much less temperature - sensitive than clinopyroxenes in the range of interest of the present work and the corresponding temperatures are therefore more sensitive to analytical errors. For this reason the orthopyroxenes are grouped in 100°C brackets in Table 6.5 whilst the clinopyroxene data are grouped in 50°C brackets.

In the form in which it is presented by Lindsley (1983) the two - pyroxene geothermometer is, strictly speaking, two geothermometers (an orthopyroxene geothermometer and a clinopyroxene geothermometer) neither of which is fully valid unless the other pyroxene is present and equilibrated with the analysed pyroxene at the temperature at which it ceased re - equilibration. One pyroxene on its own only gives an indication of the minimum possible temperature of final equilibration. The assumption of two - pyroxene equilibrium appears to be valid for the majority of pyroxenes for which temperatures of equilibration were obtained for the following reasons. Firstly, most of the sections for which temperatures were obtained contain pyroxenes which appear to have equilibrated in the same temperature ranges. Since the equilibration involved reaction with a fluid phase (melt in the case of relict magmatic pyroxenes, hydrothermal fluid in the case of metamorphic pyroxenes) it follows that the pyroxenes must also have been in equilibrium with each other. Furthermore, where it was possible to analyse several grains of the same textural type (for example, symplectitic orthopyroxenes or

opaque granule - bearing clinopyroxene), some of which had grain - grain contacts with pyroxenes of the other species and others of which did not, no systematic compositional differences were apparent between the former amd the latter.

The principal exceptions to the rule that the analysed pyroxenes formed in equilibrium with the other pyroxene species are formed by (1) the (apparently) lowest - temperature vein ortho- and clinopyroxenes in rocks which lack examples of the other pyroxene recording the same temperature; (2) orthopyroxenes formed by oxidation of olivines in clinopyroxene - free rocks (principally sample 166B2).

Although it appears that individual pyroxene grains equilibrated with the other pyroxene during final equilibration (rather than with an ortho - or clinopyroxene undersaturated fluid phase) the preservation of texturally distinct groups recording different equilibration temperatures in the same rock, and of variations in recorded equilibration temperatures within those groups, implies a substantial degree of disequilibrium within the rocks. This can be explained as the result of slow intracrystalline diffusion rates as compared to the overall cooling rate of the system. Compositional re - equilibration between pyroxenes seems to have only occurred during constitutive recrystallisation (for example during oxidation of primary augites) or during initial growth (for example during growth of sympletitic orthopyroxenes) but not at other times. These reactions appear to have required a considerable degree of supercooling for nucleation to occur, from the patchy distribution of the products, which is particularly apparent in the case of the symplectitic intergrowths, and also from the nature of these intergrowths, which are believed to form only under supercooled, non - equilibrium conditions (Barton & Van Gaans 1988). It is assumed during the calculation of the pyroxene temperatures that the composition of the products of the reactions are not affected by this supercooling: there is no way to evaluate the validity of this assumption from the available data. It follows that, with one exception which is discussed below, the temperatures obtained from the metamorphic pyroxenes record the temperatures of formation of the various textures observed, although the situation in the relict magmatic pyroxenes may be slightly more complex (see following section).

6.4.1.2. Temperatures obtained from different textural types of pyroxene.

Table 6.5.

Pyroxene Temperatures obtained

from Inner Series rocks.

All temperatures presented in degrees centigrade. See text for discussion of the significance of these temperatures. Distribution of temperatures presented as number of analyses falling within particular indicated temperature intervals (50°C intervals for clinopyroxenes, 100°C intervals for orthopyroxenes: the narrower temperature intervals for the former reflects the greater sensitivity of cpx compositions in equilibrium with opx to temperature).

Table 6.5a. Gabbronorites

Sample	Clinopyroxenes with exsolution lamellae	Clinopyroxenes with granular opaques	Poikilitic Orthopyroxenes
275/1	1150 – 1200: 1	1000 – 1050: 1	1100 – 1200: 1
	1100 – 1150: 3	950 – 1000: 1	700 – 800: 1
	1050 – 1100: 2		
296	1100 – 1150: 1	1100 – 1150: 1	1100 – 1200: 4
		1050 – 1100: 2	
		950 – 1000: 1	
35	1100 – 1150: 2	1100 – 1150: 1	1100 – 1200: 1
	1050 – 1100: 2	1050 – 1100: 2	
	1000 – 1050: 2	1000 – 1050: 3	
	950 – 1000: 1	950 – 1000: 1	
$315C_1$		950 – 1000: 1	900 – 1000: 1
		900 – 950: 3	
$315C_2$	1100 – 1150: 1	950 – 1000: 1	1100 – 1200: 1
	1050 – 1100: 2		1000 – 1100: 1
315D1	1100 – 1150: 1	1000 – 1050: 1	1100 – 1200: 2
	1000 – 1050: 1	900 – 950: 1	

$315C_1$: laminated component; $315C_2$: near - isotropic component.

Table 6.5b: Laminated gabbros and microgabbronorite

Sample	Clinopyroxenes with exsolution lamellae	Clinopyroxenes with granular opaques	Poikilitic Orthopyroxenes
314	1050 – 1100: 3	c. 850: 1	900 – 1000: 6
	1000 – 1050: 3	c. 650: 1	800 – 900: 1
	950 – 1000: 1		700 – 800: 1
318	1100 – 1150: 2	1000 – 1050: 1	1000 – 1100: 2
	1050 – 1100: 2	950 – 1000: 1	900 – 1000: 2
		950 – 1000: 1	
		c. 800: 1	
316A (host)	1100 – 1150: 1		
	1100 – 1150: 3		
97/1	1000 – 1050: 1	c. 800: 1	1100 – 1200: 3
			1000 – 1100: 1

Table 6.5c.

Vein clinopyroxenes and

vein and symplectitic

intergrowth orthopyroxenes.

Sample	Vein Clinopyroxene	Vein Orthopyroxene	Symplectitic Opx
314	750 – 800: 2		1000 – 1100: 1
	600 – 650: 1		800 – 900: 2
318			1000 – 1100: 1
			900 – 1000: 2
			800 – 900: 3
			700 – 800: 2
97/1	950 – 1000: 3	1100 – 1200: 3	
	900 – 950: 1	1000 – 1100: 6	
		900 – 1000: 1	
286/5	950 – 1000: 1		$\geq$ 1100: 1
			1000 – 1100: 2
284		1100 – 1200: 1	
		900 – 1000: 1	
		800 – 900: 2	
		700 – 800: 3	
		600 – 700: 3	
166A2	c.700: 1	1000 – 1100: 1	700 – 800: 1[1]
		900 – 1000: 1	600 – 700: 1[1]
		800 – 900: 2	
		700 – 800: 1	

([1]) Orthopyroxenes in sample 166A2 have poikiloblastic rather that symplectitic texture.

Clinopyroxenes (columns 1 & 2, Tables 6.5a, 6.5b and column 1 of Table 6.5c).

Three types of clinopyroxene were identified during the course of the present work in Inner Series rocks: magmatic (poikilitic or ophitic) augites with fine - scale orthopyroxene exsolution lamellae (typically only 1 to 3 microns thick and spaced at intervals of less than 10 to 15 microns); clinopyroxenes with opaque exsolution lamellae and recrystallised poikilitic clinopyroxenes (high Ca augites and salites) with granular opaque inclusions; and vein clinopyroxenes (also of high Ca augite or salite, and containing opaque inclusions). The exsolved pyroxenes containing orthopyroxene were analysed with defocussed (60 × 30 microns spot) or defocussed and rastered (by hand, over areas up to sixty microns wide and two hundred microns long) microprobe electron beams as necessary to obtain re - integrated clinopyroxene compositions. It was not possible to obtain satisfactory analyses for pyroxenes containing opaque exsolution lamellae: post - exsolution compositions could not be obtained because of the close spacing of the lamellae whilst area - integrated analyses are not representative of the initial composition in this case because the reaction involved is an open - system one (section 6.4.2.3).

In most samples from which a sufficient number of poikilitic to sub - poikilitic clinopyroxene analyses were obtained to give some idea of the spread of temperatures (a minimum of 5 or 6), a sharp division into a high temperature group (900 – 1150°C) of analyses from augites with exsolved opx lamellae and a low temperature (650 – 1100°C) group of high - Ca augites and salites with opaque inclusions is apparent. The clinopyroxene temperature of the boundary between the two groups varies between as much as 1100°C (sample 296) and as little as 900°C (sample 314) but is usually in the range 1000 – 1050°C. The exception to the rule of division into two groups is formed by a coarse - grained gabbronorite, sample 35, in which both types of pyroxene give temperatures in the range 950 – 1150°C.

The vein clinopyroxenes typically give lower temperatures than either of these two groups (600 – 1000°C, usually below 800°C), even when occurring with vein orthopyroxene or when in host rocks containing orthopyroxenes that give similar temperatures.

Orthopyroxenes (column 3, Tables 6.5a and 6.5b, and columns 2 & 3, Table 6.5c).

The analysed orthopyroxenes can also be divided according to texture into three groups. The first of these is formed by poikilitic magmatic orthopyroxenes and thick, opaque - free rims on olivine grains such as are normally interpreted as having formed by the peritectic reaction of tholeiitic melts with early - formed olivine. These mainly give pyroxene temperatures in the range 1100 – 1200°C, with a few in the range 1000 – 1100°C and a small number giving values as low as 800°C. These last occur in rocks containing relatively abundant orthopyroxene – FeTi oxide intergrowths and give the same temperatures as the latter when in optical continuity with them. This suggests that re - equilibration of early, high - temperature orthopyroxenes is associated in some way with growth of neomorphic orthopyroxene during the formation of the symplectitic intergrowths.

These intergrowths include the second group of orthopyroxenes, which are characteritically intergrown with opaque oxides and replace olivine. The analysed orthopyroxenes in sample 166A2, however, occur as poikiloblasts filled with, and rendered completely opaque by, minute magnetite grains. These also appear to replace olivine. All the orthopyroxenes in this group, whether symplectitic or poikiloblastic, give temperatures in the range 600 – 1100°C, with most between 800 and 900°C. The occurrence of ilmenite and magnetite in a few of the symplectitic intergrowths allows the determination of FeTi oxide temperatures as well; these are discussed in section 6.4.2.

The third group of orthopyroxenes are those which occur in discrete veins. Analysable orthopyroxenes were only found in three of the probe sections, although orthopyroxene - bearing veins are rather more common than this suggests. Vein orthopyroxenes from two of these samples, 166A2 and 284, give temperatures in the range 600 – 1100°C, with most below 900°C. the third sample, 97/1, contains a recrystallised and annealed orthopyroxene vein (Plates 3.91 and 3.113). All but one of the ten orthopyroxenes analysed from this vein give temperatures above 1000°C. These, however, most be regarded as the temperatures at which the recrystallisation and annealing took place, rather than the temperatures at which the vein pyroxenes were initially deposited.

6.4.1.3. The evolution of pyroxene compositions and textures with time during metamorphism of the Inner Series rocks and the ending of diffusive re - equilibration of compositions and textures.

The correlation of particular pyroxene temperatures with particular textures in the majority of the

rocks from the Inner Series analysed using the electron microprobe indicates the following sequence of stages of pyroxene crystallisation or compositional re - equilibration as the rocks cooled after their emplacement (or the emplacement of the enclosing gabbronorites in the case of the pre - gabbronorite rocks):

1). Crystallisation of late magmatic pyroxenes from an interstitial melt during, and perhaps after, residual melt expulsion. This occurred at temperatures of 1100 – 1200°C. This stage is mainly recorded by the highest - temperature, most Ca - rich orthopyroxenes, although the re - integrted compositions of some augite grains yield similar temperature estimates.

2). Re - equilibration of some magmatic augites under non - oxidising conditions. The evidence for occurrence of this phase comes from the re - integrated compositions of most of the augites which retain orthopyroxene lamellae and were not re - equilibrated subsequently ((3) below). These grains, on re - integration of the exsolved orthopyroxene lamellae by defocussed or rastered microprobe analysis (see above), mainly yield temperatures in the range 1000 – 1100°C. Since they were obtained from re - integrated analyses these temperatures record the lowest temperatures at which the augites underwent re - equilibration by diffusive transfer of Mg and Fe out of the crystal and into adjacent orthopyroxenes, rather than by in situ orthopyroxene exsolution. The other clinopyroxenes, which underwent further Fe and Mg loss at lower temperatures, may also have undergone this stage of re - equilibration but do not record it.

3). Recrystallisation of augites under oxidising conditions, producing opaque inclusion bearing, Ca - rich clinopyroxenes, oxidation of olivines producing orthopyroxene + FeTi oxide symplectitic intergrowths and formation of pyroxene - bearing vein assemblages. All of these pyroxene - forming reactions took place at 700 – 1000°C, with the vein assemblages tending to have formed at the lower end of this temperature range.

4). In 97/1 alone amongst the probed samples, reheating and recrystallisation of an earlier vein assemblage to give orthopyroxene temperatures in excess of 1000°C. The coarse orthopyroxene - FeTi oxide intergrowths and equant granular opaque inclusions in orthopyroxenes noted in section 3.4.6 may have formed as a result of reheating of earlier symplectitic intergrowths. They should record high orthopyroxene temperatures, although it was not possible to analyse any of

them within the scope of the present work.

As was noted in section 3.4.6, a clear textural distinction can be made between texturally - equilibrated, coarse - grained minerals which are believed to have formed in equilibrium with a melt phase and the fine - scale textures, principally the symplectitic intergrowths but also the fine - grained veins and the exsolution lamellae in the clinopyroxenes, which post - date the end of effective textural re - equilibration in these rocks. The above data suggest that the latter process ended at temperatures between 1000 and 1100 degrees centigrade in the rocks of the Inner Series, although it should be noted that the timing of the end of textural equilibration may be as much a function of variation in the cooling rate of the rocks as of the absolute temperature at which it occurs. The oxidation reactions involving pyroxenes and the deposition of pyroxenes in the tensile - fracture vein networks appear to have begun at temperatures as much as 100°C below the temperatures at which textural and bulk compositional diffusive equilibration ceased. This implies that brittle tensile fracture and the formation of a hydrothermal circulation system in the rocks only occurred at a significantly lower temperature than the temperature at which textural equilibration, diffusional re - equilibration and diffusive or solution / re - precipitation creep ended in these rocks.

One possible interpretation of this observation is that the brittle fracture was caused by thermal contraction due to propagation of a hydrothermal system filled with very high temperature (although still at least a few hundred degrees cooler than the rigidus temperature of the gabbronorites) hydrothermal fluids. As was discussed in sections 5.2 and 5.3, rocks under a few to several hundred bars of overburden pressure have to be cooled to a temperature at least 100 degrees or so below the temperature at which they acquire a significant Young's modulus for thermal stresses to cancel out the lithostatic load pressure and begin to place the rocks under tension. Since textural re - equilibration is an effective process for producing creep at very low stresses (McKenzie 1984) it has to stop before thermal (or any other) stresses can build up to any significant extent.

The absence of quench textures like those seen in the contact zone of the marginal border group indicates that the rates of tensile crack propagation would have to be very much lower than those in the MBG and its contact aureole (sections 5.2 and 5.3). This could be due to the very much higher temperature of the fluids in the Inner Series (implied by the extremely high temperatures of hydrothermal alteration and the preservation of magmatic olivine and pyroxene grains) and low

rates of convective heat transfer within the hydrothermal system (Carrigan 1986). Possible reasons for these contrasts in behaviour between the tensile fracture - forming hydrothermal systems in the MBG and the Inner Series are considered in section 6.5.

A major problem in connection with the above sequence of events is the explanation of the clinopyroxene temperatures in the coarse - grained gabbronorite sample 35, in which both lamella - bearing and opaque inclusion - bearing clinopyroxenes give temperatures of between 900 and 1100 degrees centigrade. One possibility is that the coarse grain size of this sample has prevented complete compositional re - equilibration at both stages (2) and (3) of the above sequence of events; another is that the sample has undergone brief periods of reheating leading to partial recrystallisation of different parts of the various grains analysed.

6.4.2. Metamorphic reactions in the Inner Series rocks and implications for f_{O_2}, P_{H_2O} and dissolved cation concentrations in the coexisting fluid phase.

6.4.2.1. The formation of symplectitic intergrowths of orthopyroxene and oxide phases and the oxidation of olivine in the Inner Series rocks.

Although characterised by a lamellar or plate - like intergrowth texture in the best - preserved and favourably orientated examples (e.g. Plate 3.108) these intergrowths should not be regarded as true symplectites, which are exsolved lamellae **within** earlier mineral grains and are considered to have formed by decomposition of high - temperature solid solutions on cooling, without the addition of any components except oxygen (Putnis 1979; Moseley 1984). It should be noted that Barton & Van Gaans (1988), amongst others, use the term symplectite to describe a variety of two - phase lamellar intergrowths similar to those described here. In the examples from the Inner Series under consideration here, although the orthopyroxene - FeTi oxide intergrowths clearly replace olivine in many cases (e.g. Plates 3.108 and 3.110) they contain a number of components (principally Ca and Al in the orthopyroxene and Ti in the Ti - magnetites and ilmenites) which would not have been present in the original olivine. Furthermore, the difference in the Mg/Fe ratio of the relict olivines and the symplectitic orthopyroxenes which replace them is small, the former typically being around Fo_{65} in composition and the latter around En_{70}. This means that it is not even possible to write a balanced equation for the (Ca, Al, Ti) free reaction of olivine to orthopyroxene (En - Fs

solid solution) and Ti - free magnetite without invoking a fluid phase to, at the very least, either add Si or remove Mg in solution. Various intergrowth - forming reactions can be written according to which components it is proposed to consider as conserved:

(1) Conserving MgO and Fe:

$$0.05O^{2-}_{fluid} + 0.84SiO_{2(fluid)} + Fe_{0.7}Mg_{1}.3SiO_4 \Leftrightarrow 0.92Fe_{0.6}Mg_{1.4}Si_2O_6 + 0.05Fe_3O_4 \quad [6.1]$$

(2) Conserving SiO_2 and Fe:

$$0.13O^{2-}_{fluid} + Fe_{0.7}Mg_{1.3}SiO_4 \Leftrightarrow 0.5Fe_{0.6}Mg_{1.4}Si_2O_6 + 0.13Fe_3O_4 + 0.6MgO_{fluid} \quad [6.2]$$

Reaction [6.2] involves a considerable reduction in the volume of the solid components, whilst [6.1] is closer to a constant - volume reaction. The textural evidence suggests that the true reaction should be a constant - volume reaction and therefore closer to [6.1]. However, as noted by Barton & Van Gaans (1988), there is no reason to suppose that **any** component is immobile during the formation of these intergrowths. The occurrence of pyroxenes and magnetite in the coeval vein assemblages indicates that Fe, Mg and Si were all significantly soluble in the coexisting fluids. It is not, therefore, possible to write a fully - balanced reaction for the formation of the orthopyroxene - FeTi oxide intergrowths without precise data on the modal abundances of these phases in the intergrowths. Examination of such intergrowths in polished thin sections under reflected light indicates that the volumetric orthopyroxene/opaque ratio is around 4:1, suggesting a molecular ratio of around 3:1 in the original reaction although it is possible that subsequent recrystallisation may have distorted these ratios through net transfer of orthopyroxene into enclosing orthopyroxene rims on the primary olivine (c.f. Plate 3.110). This suggests that a modified version of [6.2], with addition of silica and iron to maintain constant volume, may be closest to the true reaction:

$$O^{2-}_{fluid} + (CaFeAlTiSi)_{fluid} + Olivine \Leftrightarrow 0.7Orthopyroxene + 0.3FeTi - oxide + Mg_{fluid} \quad [6.3]$$

The Ca, Al and Si in the solution on the left - hand side of the above reaction could have originated from oxidation of augite (section 6.4.2.3, below) whilst the most likely source for the titanium is the exsolution of titanium from earlier, higher - temperature FeTi oxide grains on cooling and oxidation (Buddington & Lindsley 1964).

All of the above model reactions emphasise the importance of the fluid composition in the symplectite - forming reaction as they require that the fluid phase be in equilibrium with both orthopyroxene and FeTi oxides. Undersaturation of the fluid in orthopyroxene may account for the oxide - only olivine replacement reactions observed in initially opaque - rich rocks, particularly the pre - gabbronorite banded magnetite - anorthosites and magnetite - troctolites (sections 3.4.2 and 6.3.1.2). The absence of orthopyroxene in the product assemblage of much of the oxidation of olivine in these rocks may be due to one or both of two factors. Firstly, reduced SiO_2 and MgO activities in the fluid phase, owing to the low abundances of both in the rocks (see section 6.3.1.2 and analyses in Appendix 2), may lead directly to undersaturation in orthopyoxene. Secondly, if the oxygen fugacity in the fluid falls below that of the quartz - undersaturated equivalent of the univariant assemblage Qz - Ol - Opx - Mt (Nitsan 1974), Ol - Opx - Mt - $SiO_{2(fluid)}$, the olivine will no longer oxidise to orthopyroxene + FeTi oxide but to FeTi oxide + dissolved silica; note that the preservation of Mg - rich olivine, except for oxidative replacement, requires that the fluid phase be significantly undersaturated in silica, as otherwise non - oxidative replacement of olivine by orthopyroxene alone would be observed.

The oxide - rich rocks do, however, contain vein orthopyroxene in the largest and most widely - spaced fractures, and one (sample 166A2) also contains the rare poikiloblastic orthopyroxenes noted above. These contrasted assemblages can be explained in two ways. Firstly, the orthopyroxenes may have formed in a distinct, probably later, period of fluid flow when the fluid had higher dissolved Mg and Si activities and/or higher f_{O_2}. Secondly, activities in the fluid may have varied spatially during a single phase of fluid circulation, with Mg and Si activities and/or f_{O_2} being higher in the largest fluid - filled fractures than in the bulk of the rock.

Consideration of the setting of these rocks suggests that the latter alternative is the more likely one. The magnetite - rich rocks occur within a sequence of more Mg and Si rich rocks (the host gabbronorites) and as a result would be expected to be out of equilibrium with fluids entering them from these rocks with respect to these elements. Where fluid - rock ratios were high the result would be reaction to produce assemblages in equilibrium with the fluid phase (i.e. external buffering of the fluid composition to that in equilibrium with the enclosing gabbronorites), as in the main fractures. On the other hand, although numerous fractures are present in the bulk of the rock, they are very much narrower. This would greatly reduce fluid fluxes through them (since fluid fluxes through

Plate 6.1. Myrmekite - like intergrowth of plagioclase and a ferromagnesian phase (olivine or augite) rimming and partially replacing earlier magnetite. Granular magnetite - anorthosite, sample 166B2. Plane - polarised light, field of view 0.75mm.

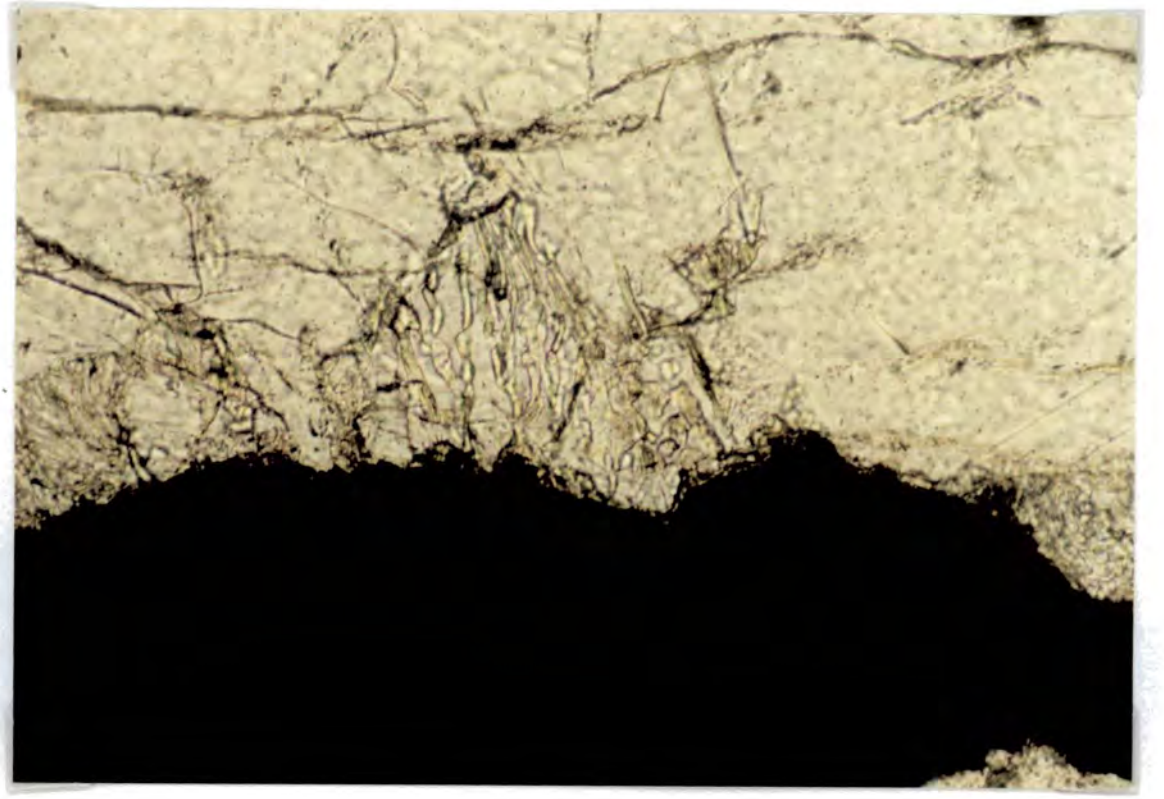

fracture networks are proportional to the cube of the fracture widths but only linearly dependent on the fracture spacing (Lister 1974)) and therefore also reduce the fluid - rock ratio over the period of metamorphism. Internal buffering of the fluid and coexisting metamorphic mineral assemblage, at lower Mg and Si activities, would therefore have occurred away from the main fractures and thereby produced the observed distribution of metamorphic orthopyroxene in these rocks.

6.4.2.2. Magnetite reduction.

Evidence for the reversal of oxidation reactions such as [6.3] in rocks of the Inner Series only occurs in one, and possibly a few more, of the pre - gabbronorite granular banded magnetite anorthosite and magnetite troctolite xenolithic sheets. Sample 166B2 contains a small number of symplectitic or myrmekite - like intergrowths of plagioclase and a ferromagnesian mineral. These occur as discontinuous rims around magnetite grains, partly replacing the magnetite and partly replacing the adjacent plagioclase grains (Plate 6.1). The extremely fine scale of the intergrowth (individual rods are less than 10 microns thick and are spaced at intervals of 10 – 20μm) makes it difficult to identify the ferromagnesian phase: it may be olivine or clinopyroxene (C.H.Emeleus pers comm.). Either is possible, as different reactions involving a fluid phase can be written for the formation of this texture, depending on whether the plagioclase in the intergrowth is more or less Ca - rich than the feldspar which it has replaced:

$$Na-plagioclase + magnetite + Mg_{fluid} \Leftrightarrow olivine + Na^{+}_{fluid} + Al^{3+}_{fluid} + O^{2-}_{fluid} \qquad [6.4]$$

$$Ca-plagioclase + magnetite + Mg_{fluid} \Leftrightarrow clinopyroxene + Al^{3+}_{fluid} + O^{2-}_{fluid} \qquad [6.5]$$

Both [6.4] and [6.5] are reduction reactions. Their occurrence indicates that the fluids which produced them were reduced relative to the initial redox state of the rocks, in contrast to all other fluids identified from high grade metamorphic redox reactions in the Inner series rocks.

This apparent contrast in fluid oxygen fugacities may be due in part to a difference in the redox state of the rocks rather than of the fluids. Analysed 'primary' olivines (i.e. those forming part of the main granular texture) in the magnetite - rich rocks are amongst the most magnesian found in the Inner Series (section 6.3.1, especially Fig. 6.10.3). As noted in section 6.3.1, this is anomalous because the analysed feldspars in the same rocks are relatively Na - rich, which suggests that the

original rocks were relatively evolved. Since the forsterite content of olivine in equilibrium with magnetite increases sharply with f_{O_2} (Nitsan 1974), this can be interpreted as an indication that, prior to the development of the granular, texturally equilibrated 'primary' texture in these rocks (and hence possibly prior to their inclusion in the host gabbronorites), they were strongly oxidised by circulating fluids with higher f_{O_2} values than those of some of the fluids which caused oxidation in the gabbronorites. When these later fluids entered the magnetite - rich rocks they would then behave as reducing, rather than oxidising fluids. Nevertheless, the occurrence of both oxidation and reduction in the magnetite - rich rocks implies real variation in the oxidation state of the circulating fluids relative to the various mineralogical buffers.

6.4.2.3. Augite oxidation.

The development of opaque exsolution lamellae or granular inclusions in place of orthopyroxene exsolution lamellae in most of those clinopyroxenes which record clinopyroxene temperatures of less than around 1000°C implies oxidation of these augites via a reaction which in its simplest form can be written as:

$$augite_{ss} + O^{2-}_{fluid} \Leftrightarrow Ca-rich \quad augite + Fe_3O_4 + Mg^{2+}_{fluid} + Si^{4+}_{fluid} \qquad [6.6]$$

It should be noted that oxidation of clinopyroxene in this way implies either an increase in the Mg/Fe ratio of the clinopyroxene or else release of Mg and Si to the fluid phase. The reaction is written in the latter form because although some of the low - temperature clinopyroxenes have higher Mg/Fe ratios than some of the high - temperature clinopyroxenes in the same rocks, many others do not.

A more serious problem posed by clinopyroxene oxidation in this way is that although it appears to have taken place at the same time as the development of orthopyroxene - bearing symplectitic intergrowths and the re - equilibration of some older pyroxenes, reaction [6.6] implies that the fluid phase was undersaturated in orthopyroxene if it is assumed that it took place at equilibrium. This apparent inconsistency in phase stabilities during the metamorphism can be explained instead as a result of reaction under disequilibrium conditions. The fact that it does not occur at all in rapidly cooled rocks implies that the orthopyroxene exsolution reaction has a large activation energy at low temperatures. If this activation energy is sufficient to cause a significant amount of supercooling under the conditions of formation of the Inner series metamorphic assemblages, the occurrence of metamorphic grains of orthopyroxene would be controlled by the occurrence of suitable nucleation

sites. As a result, orthopyroxene components released by the decomposing high - temperature pyroxene solid solution would, rather than appearing as exsolution lamellae, be released to the fluid phase and precipitated on pre - existing separate orthopyroxene grains or at sites of olivine oxidation. The true form of the clinopyroxene oxidation reaction would then be:

$$Augite + O^{2-}_{fluid} \Leftrightarrow Ca-rich \quad augite + Fe_3O_4 + orthopyroxene + Si^{4+}_{fluid} \qquad [6.7]$$

It is not clear why this reaction should in some cases produce exsolution lamellae of opaque oxide and in others lead to complete recrystallisation and the formation of granular inclusions. Similar nucleation effects, coupled to transport of ions in the fluid phase to suitable nucleation sites, have long been recognised in regional metamorphic reactions involving aluminosilicate phases (Carmichael 1969). The occurrence of analogous phenomena involving pyroxenes (which are normally considered to react at rates sufficient to maintain near - equilibrium) in the Inner Series of the Hypersthene Gabbro presumably reflects greater rates of change in ambient conditions of temperature and f_{O_2} in the latter.

6.4.2.4. Stability relationships of high - temperature hydrous phases in the Inner Series rocks.

This section is concerned with the small number of occurrences of high temperature hydrous metamorphic phases, such as Ti - rich phlogopitic or Mg - rich biotite mica ($X_{Mg} \approx 0.70$; see analyses in Appendix 1) and brown pargasitic hornblende, which appear to be of much the same age as two - pyroxene assemblages in the Inner Series rocks, rather than with the much more abundant lower - temperature hydrous assemblages which are distinctly younger (section 3.4.6). Although they are confined to a few olivine and/or orthopyroxene - rich rocks these early hydrous minerals are nonetheless of considerable interest as indicators of P_{H_2O} during the high - grade metamorphism. Their interpretation in this way requires an understanding of the conditions leading to their formation, which are discussed here, whilst consideration of the overall partial pressure of water during the very high grade hydrothermal alteration is deferred to section 6.4.3.

Both the biotite and pargasitic hornblende under consideration here occur mainly as inclusions in large grains of olivine or orthopyroxene or as interstitial phases in olivine and/or orthopyroxene - rich rocks. In one example (Plate 3.115) both phases occur together with orthopyroxene and magnetite

Plate 6.2. Orthopyroxene - rich vein cutting strained olivine poikilocryst, sample 137/1. The vein post - dates the internal straining and subgrain development in the olivine, which itself appears to post - date recrystallisation of the olivine around orthopyroxene - hornblende - biotite inclusions (Plate 3.115). Plane - polarised light, field of view 3.5mm.

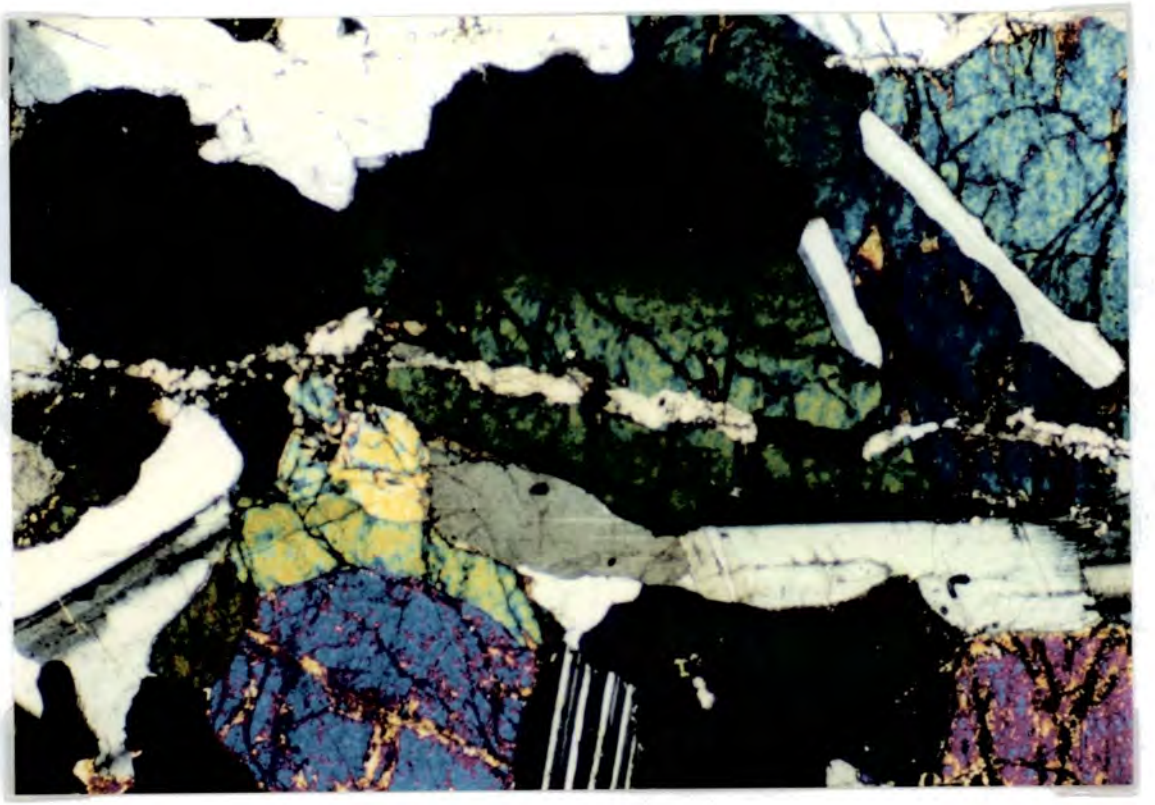

in a composite inclusion within olivine. This particular sample is critical to the interpretation of the age relationships of these assemblages as the enclosing olivine grain is cut by an anhydrous, orthopyroxene - bearing vein (Plate 6.2), implying formation of the inclusion prior to the end of the very - high - grade hydrothermal metamorphism. In no case does either phase occur in association with clinopyroxene. Furthermore, neither hornblende nor biotite of any composition occur in the main hydrothermal veins, except as later and lower - grade assemblages which partly replace earlier two - pyroxene assemblages where these are present.

The high temperature stability relationships of hornblende in olivine - bearing, quartz - absent tholeiitic basic rocks at low to moderate P_{H_2O} (0.5 to 3kb) were studied by Spear (1981). The composition of the sample used by Spear is close to that of the Inner Series gabbronorites (particularly with respect to Ti, which can greatly affect the upper stability limit of hornblendes) except for the higher Al content of many of the latter. However, since both the experimental samples and the gabbronorites are saturated in an Al - rich phase (plagioclase) this is unlikely to affect the application of Spear's results to the ferromagnesian minerals of Inner Series rocks for present purposes. It was shown in Spear (1981) that hornblende breaks down with increasing temperature and/or decreasing P_{H_2O} in a series of reactions. These produce clinopyroxene alone in the initial stages of decomposition, then clinopyroxene + orthopyroxene and finally cpx + opx + olivine, over a temperature interval of between 50 and 100°C.

A corollary of these experimental results is that the stability range of hornblendes must extend to higher grades in the absence of clinopyroxene. Spear (1981) also showed that the hornblende stability field expands with increasing Mg/Fe ratio. This suggests that the association of pargasitic hornblende with orthopyroxene and olivine, and its complete absence from vein assemblages is due to very local buffering of the fluid phase to Ca - poor and high Mg/Fe ratio compositions by the enclosing ferromagnesian minerals. The stability field of biotite/phlogopite is also strongly dependent upon its Mg/Fe ratio (Luth 1967; Hoffer & Grant 1980) so a similar localised buffer effect may also account for its restricted occurrence amongst the very high - grade assemblages.

This model implies that at least during the later, lower - grade stages of very high grade hydrothermal metamorphism in the rocks where these high - grade hydrous minerals occur, the conditions of metamorphism lay between the clinopyroxene - in and orthopyroxene - in hornblende decomposition

reactions of Spear (1981).

6.4.2.5. Metasomatism and the scale of internal buffering of fluid compositions in the Inner Series rocks.

The oxidation - replacement reactions discussed in sections 6.4.2.1 and 6.4.2.3 clearly demonstrate that many components, including some which are not normally considered to be mobile during hydrothermal metamorphism such as Ti and Al, were mobile on at least a small scale, of the order of a few millimetres to perhaps a few centimetres. If such cation mobility occurred on a larger scale, of the order of the size of the Inner Series (as was demonstrated for certain components during lower - grade metamorphism of the Cuillins gabbros, Skye, by Ferry (1985)) then it would have serious implications for the interpretations of the bulk compositions of the Inner Series rocks, as these could then be more a product of hydrothermal processes than of the magmatic processes considered in sections 6.2 and 6.3.

Quantitative estimates of the scale of transport of cations and any resulting bulk compositional changes in the Inner Series rocks requires a measure of the fluid flux through the rocks, with which any compositional changes due to hydrothermal alteration would be correlated, such as oxygen isotope ratios for the rocks (assuming that the fluid was meteoric in origin). These data are not available, but a number of observations suggest that the compositions of the rocks were buffered internally with respect to most components on a small scale.

1). The magnetite - rich granular anorthosites and troctolites, although occurring in bands only a few metres thick at most, appear to have largely retained the effects of earlier, higher - f_{O_2} alteration throughout the very - high - temperature alteration of the surrounding gabbronorites (section 6.4.2.2) except in the immediate vicinity of the larger hydrothermal veins which cut them. With the possible exception of potassium (see below) oxygen and hydrogen would be expected to be the elements with the highest concentrations in the fluid phase relative to their abundances in the host rock. Oxygen fugacities would therefore be expected to be much more sensitive to hydrothermal alteration than the abundances of most elements in the rocks, at least in relatively reduced systems (below the haematite - magnetite buffer or thereabouts), in which reduced species concentrations in the fluid can be high (Wood & Walther 1986). The

preservation of variations in initial f_{O_2} during the hydrothermal alteration implies that, to a large degree, the Inner Series was internally buffered with respect to oxygen activities,although the fact that the internal buffers were continuous buffers involving Mg - bearing silicate phases may have allowed some variation in f_{O_2} (Fig. 6.14 and section 6.2.4.6, below).

2). The restriction of orthopyroxene to veins in most of the magnetite - rich rocks (section 6.4.2.1) and the localised stability of hydrous phases discussed in section 6.4.2.4 imply that, away from the main fractures, significant variations in the dissolved cation content of the fluid may have been present on a very small scale. This suggests that although rapid fluid circulation through the main fractures of the hydrothermal fracture network may have produced high fluid - rock ratios and significant cation transport in those fractures, the fluid in the bulk of the rocks was near - stagnant and buffered on a very small scale indeed (c.f. Norton 1984). Thus even if large compositional changes occurred in the vicinity of the fratures the bulk of the rock (and hence its bulk composition) could be largely unaffected. The presence of radically different assemblages in the veins (for example, the occurrence of pyroxene - rich assemblages in the initially pyroxene - poor magnetite anorthosites and troctolites) does not, therefore, necessarily indicate major changes in the bulk of the rock. In this the very high temperature alteration in the Inner Series appears to resemble the lower - temperature alteration studied by Dickin et al. (1980) around the Cuillins complex. Dickin et al. showed that bulk compositional and isotopic changes are confined to the immediate vicinity of the main hydrothermal veins in these rocks, with the exception of oxygen isotopic compositions which are more pervasively altered.

3) One definite exception to the tentative conclusion drawn from these observations, that large - scale cation transport in the hydrothermal system represented by the alteration of the Inner Series rocks was not an important process, is formed by potassium. The widespread occurrence of metamorphic biotite in the Inner Series rocks, particularly in veins, suggests that net transport of K into the pluton from the surrounding K - rich sediments took place once the system had cooled sufficiently for biotite to become stable. As with oxygen and hydrogen, the concentrations of potassium in the hydrothermal fluids are likely to have been relatively high, and its abundance in the initially K - poor rocks of the Inner Series would therefore be more prone to alteration by the hydrothermal system than other cations. However, the coherent trend formed by the gabbronorite suite rocks in Fig. 6.12.2 indicates that K contents in these rocks were not greatly

affected by hydrothermal alteration. It therefore appears unlikely that the bulk compositions of the rocks were affected to any great extent with respect to other elements.

Although qualitative in nature the arguments presented in this section strongly suggest that the very high grade hydrothermal alteration apparent in the Inner Series of the Hypersthene Gabbro resembles the lower - temperature hydrothermal systems studied in other intrusins in that although it produced considerable changes in mineral compositions and much small - scale elemental mobility its effects upon bulk rock compositions were relatively slight.

6.4.2.6. Quantitative estimates of P_{H_2O} and f_{O_2} during very high grade hydrothermal alteration of the Inner series rocks.

Partial water pressure. The apparent stability of two - pyroxene assemblages down to temperatures at least as low as 800°C, and possibly as low as 600 – 700°C (athough as noted in section 6.4.1.2, many of the lowest temperatures obtained by pyroxene geothermometry should be regarded as lower limits rather than as true temperature determinations), implies, by comparison with the amphibole stability limits established by Spear (1981), partial water pressures less than 0.5 – 1.0kb. Conversely, the sporadic occurrence of pargasitic hornblende and Mg, Ti - rich biotite/phlogopite of the same age as some of the pyroxenes implies that P_{H_2O} was significant (perhaps a few hundred bars ?), as would be expected given the geological setting of the metamorphism, in a large plutonic complex.

Oxygen fugacity. The absence of quartz from the Inner series metamorphic assemblages, even those in which FeTi oxide is the only oxidation product of olivine, implies that the hydrothermal fluid was undersaturated in SiO_2. This complicates the interpretation of the oxidised assemblages in terms of the f_{O_2} of the coexisting metamorphic fluid. Instead of being bounded at low f_{O_2} by the univariant assemblage Ol - Opx - Qz - Mt, the assemblage Ol - Opx - Mt is instead replaced at low f_{O_2} by the 'assemblage' Olivine + Magnetite + $SiO_{2(fluid)}$. The stability field of the latter in T - f_{O_2} space must be greater than that of Ol - Mt - Qz (note that in silica - undersaturated fluid - present systems dissolution of orthopyroxene or its decomposition to olivine will tend to raise silica activities in the fluid) and will increase with decreasing a_{SiO_2} in the fluid (Fig. 6.14). As noted in section 6.4.2.1, this means that the replacement of olivine by magnetite alone in

Fig. 6.14. Temperatures and oxygen fugacities during very high - grade hydrothermal metamorphism of the Inner Series rocks.

Buffers: see Fig. 5.3 for abbreviations.

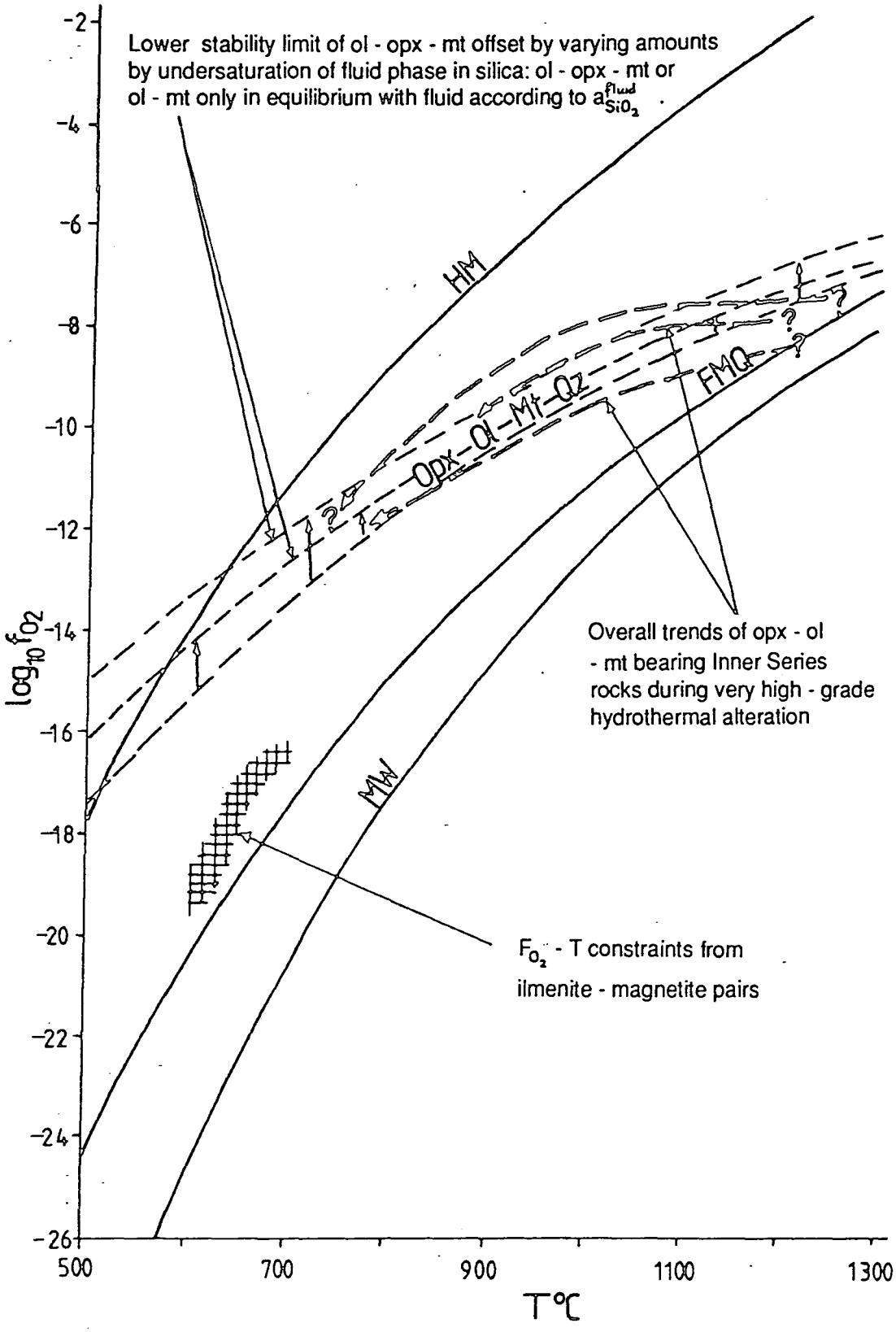

the silica - poor pre - gabbronorite magnetite - rich rocks may have occurred at the same f_{O_2} as formation of orthopyroxene - magnetite inter growths in the adjacent rocks, the difference in the assemblages produced being the effect of the lower silica activity (and also lower X_{Mg}) in the magnetite - rich rocks.

Although it is therefore not possible to constrain absolute f_{O_2} values from the olivine oxidation reactions, the variations in X_{Mg}^{opx} with temperature which are apparent in Fig. 6.15 can nevertheless be used to gain some idea of the variation in f_{O_2}. Fig. 6.15 indicates that the content of the enstatite ($MgSiO_3$) end - member varies from around En_{70} to as much as En_{80} in different rocks, the variation in any one sample being less than 5% Enstatite component. Most of these samples, except for the granular magnetite anorthosites (166A2 and 284) contain evidence for only one phase of hydrothermal alteration. It follows that the variation in enstatite contents indicates buffering of f_{O_2} to different values in different rocks, consistent with the small scale of buffering inferred above. Some samples (notably 286/5, 314 and 166A2) show a systematic increase in En contents with decreasing temperature, suggesting that fluid flow in these rocks was sufficient to change the position of the continuous internal buffers as temperatures fell from 1000°C to 800°C or so. The change in composition corresponds to an increase in f_{O_2}, relative to a buffer such as FMQ, of 1 to 2 log units as temperatures decreased through this range. As noted in the context of reduction of the contact aureole rocks under similar conditions during M1 metamorphism (section 5.2.3), however, this need only have involved a few rock volumes of fluid at most.

An independent constraint upon the path of the Inner Series rocks through T - f_{O_2} space during the very high grade hydrothermal metamorphism is provided by the rare occurrence of separate symplectitic grains of ilmenite and magnetite (as opposed to exsolution - oxidation lamellar intergrowths of the two phases, which also occur) in orthopyroxene - FeTi oxide intergrowths. These allow determination of both f_{O_2} and temperature at the end of equilibration between the ilmenite and magnetite using the geothermometer - oxygen geobarometer of Buddington & Lindsley (1964). The results, from samples 314 and 318 (two pre - gabbronorite laminated gabbros in the outcrops at the northern end of Sanna bay), are as follows: 700°C and $\log f_{O_2} = -16.4$; 670°C and $\log f_{O_2} = -18$; and 630°C and $\log f_{O_2} = -19$. The temperatures are lower than those recorded by the orthopyroxenes in the same symplectitic intergrowths, while the oxygen fugacities are lower than is consistent with the inferred position of the lower limit of orthopyroxene stablity at the same

Fig. 6.15. Compositions of Inner Series metamorphic pyroxenes plotted in segments of the Di - Hd - Fs - En quadrilateral, with temperature contours from Lindsley (1983).

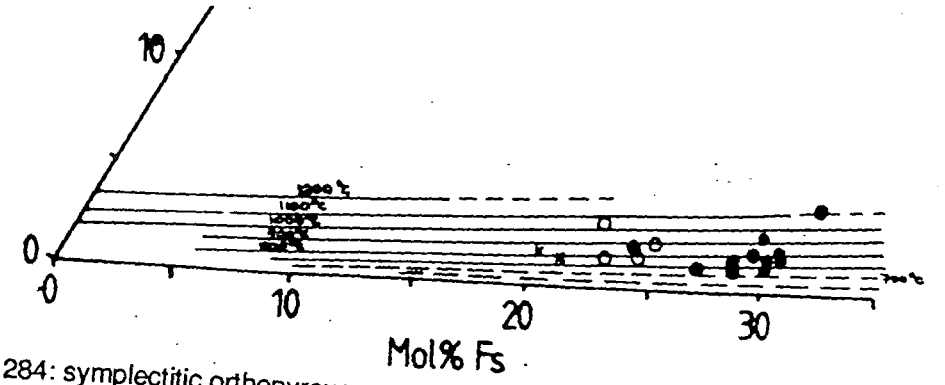

284: symplectitic orthopyroxene ×
vein orthopyroxene ○

166A2: vein orthopyroxene ●

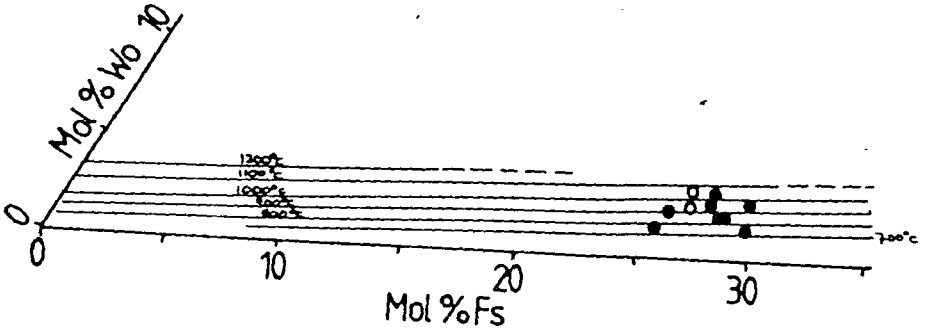

318:
rim orthopyroxene ○
symplectitic orthopyroxene ●

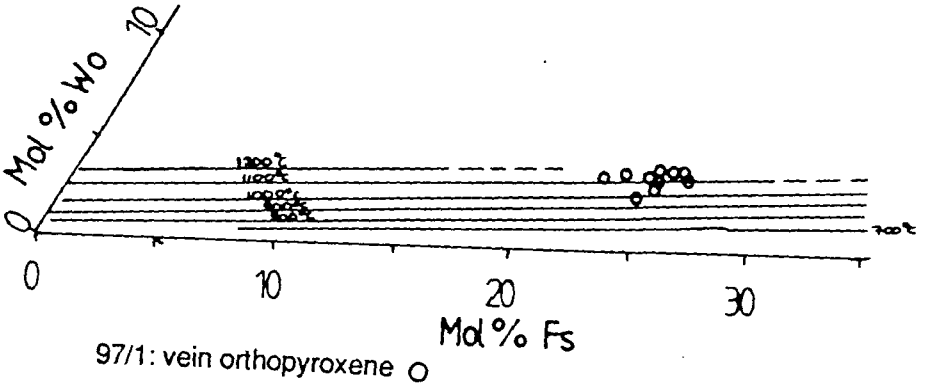

97/1: vein orthopyroxene ○

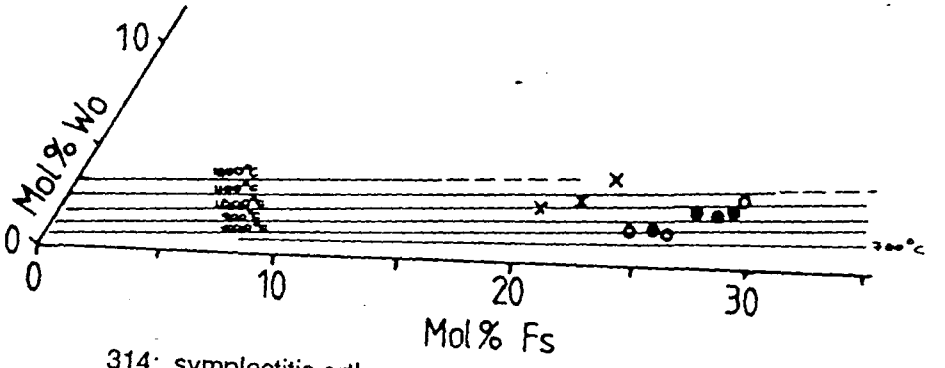

314: symplectitic orthopyroxene ●
rim orthopyroxene ○

286/5: symplectitic orthopyroxene ×

temperature. Both of these observations may be due to continued re - equilibration of the oxide phases after the end of re - equilibration of the orthopyroxene with the fluid, although the apparent metastability of the orthopyroxene may also have been produced by the stabilising effect of minor components (such as Ca and Al) within it.

6.4.2.7. Conclusions on the mineralogical and compositional effects of hydrothermal fluid circulation at very high temperatures through the Inner Series.

The varied lines of evidence discussed in the above sections indicate that the circulation of hydrothermal fluids through the Inner Series of the Hypersthene Gabbro at temperatures exceeding the upper stability limits of hydrous phases such as hornblende and biotite in equilibrium with most of the fluid compositions present had a variety of effects upon the mineralogy of the rocks but had relatively little effect upon the bulk composition of the rocks. This latter point needs to be confirmed by a combined stable isotopic / geochemical study, however. The mineral reactions, primarily oxidation reactions, took place under conditions of strong undercooling. Nucleation and perhaps other kinetic effects appear to have caused bypassing of some simple exsolution reactions in favour of solution - reprecipitation reactions as a result. Although different reactions appear to have taken place in different lithologies which at first sight appear to be due to variation in the oxygen fugacity of the fluid phase these are more likely to be due to differences in the activities of components, such as Si and Mg, which are more likely to have been buffered by the host rock compositions. Other variations in the metamorphic assemblage, between veins and the bulk of the same rocks, may be attributed to very high fluid/rock ratios in the veins alone. This caused external buffering of the fluid composition in the largest veins in rocks which form small compositionally distinct bodies, such as xenolithic sheets.

In general the fluids and rocks appear to have been buffered by the latter with respect to most components. The abundance of the symplectitic intergrowths and secondary magnetite (perhaps as much as a few percent of the rocks as a whole; the patchy distribution of the symplectites precludes more precise estimates) and possible changes in the compositions of the ferromagnesian minerals coexisting with opaque phases (section 6.4.2.6) suggest that a significant amount of oxidation of the rocks occurred. This implies that there was a significant flux of relatively oxidised fluids into the Inner Series from outside the intrusion as it is unlikely that the volume of fluid involved (perhaps

equivalent to a water/rock ratio of about 1 (Wood & Walther 1986)) could have been of magmatic origin, given the very low water contents of tholeiitic magmas (Michael 1988).

6.4.3. A history of late stage crystallisation and high - temperature hydrothermal metamorphism in the Inner Series.

The textural evidence from section 3.4.6, the geothermometric data from section 6.4.1 and the reactions deduced in section 6.4.2 can be combined to give an overall history of late stage crystallisation and metamorphism in the Inner Series rocks. As noted in section 3.4, the different stages of this history may have been developed at the same time in different regions of the Inner Series but in any one rock the following sequence of events is followed closely.

1). Late - stage magmatic crystallisation, of pyroxenes and other phases (plagioclase and opaque oxides) at temperatures of 1100 – 1200°C, towards the end of the period of compaction of the partially molten rocks but at a time at which textural and compositional re - equilibration was still going on.

2). Between the end of pervasive textural re - equilibration between grains but before the onset of hydrothermal alteration. Exsolution of orthopyroxene from augites without oxidation. There is no evidence for the presence of a fluid phase during this phase. Temperatures were generally in the range 1000 – 1100°C.

3). Formation of a tensile fracture network, possibly by thermal contraction resulting from cooling of recently - emplaced rocks by very hot hydrothermal fluids circulating through older Inner Series rocks. Oxidation reactions produced by the fluid phase and the by - passing of exsolution reactions in favour of solution - reprecipitation reactions, as a result of kinetic effects, are characteristic of this stage. Temperatures of metamorphism during this stage were generally in the range 700 – 1000°C, the maximum temperatures in any one rock ranging from 900°C to over 1000°C. As noted in section 3.4.6, this stage of activity appears to have overlapped with the peak of M2 metamorphism in the country rocks and in the Marginal Border Group and also with lower - grade metamorphism, similar to M2, in those Inner Series rocks close to the contacts with the MBG. Reheating of rocks affected by this stage of metamorphism on emplacement of

later gabbronorite and granular dolerite sheet intrusions may have been common (see sections 3.4.1 and 3.4.4).

4). Later hydrous metamorphism. This has not been discussed in detail here (see section 3.4.6 for a general summary of the assemblages produced) because it is generally similar to hydrothermal metamorphism described from numerous other mafic plutons (e.g. Bird et al. 1988; Ferry 1985).

Two general points concerning the above history of metamorphism are worthy of note. Firstly, each stage of metamorphism is very incomplete in its effects in most samples sectioned, with the later stages in particular only being well - developed around the large and small veins present in the rocks. This is consistent with the involvement of a fracture - based hydrothermal system in the latter stages of metamorphism and suggests that the occurrence of many of the reactions was controlled by the availability of a fluid phase, to participate in the reactions and/or transport cations to suitable nucleation sites. Textural evidence in the form of the patchy nature of the alteration and the development of symplectitic intergrowths (Barton & Van Gaans 1988) points to the reactions having occurred under conditions of strong supercooling, in which case nucleation effects would be important in determining the amount of reactants consumed.

The second point concerns the supposed cryptic nature of the very highest temperature oxygen isotope depletion in mafic plutonic rocks, which is considered to leave no mineralogical record in the rocks (Norton & Taylor 1979; Taylor 1987). The above metamorphic history indicates that in the Inner Series hydrothermal circulation only took place at temperatures below those at which diffusive recrystallisation was capable of re - equilibrating textures and thereby eliminating mineralogical and textural evidence of fracture - based circulation. Even in the case of Inner Series rocks which have subsequently been reheated to temperatures in excess of 1000°C earlier veins are still recognisable (Plate 3.112, which is of the pre - gabbronorite sample discussed in section 6.4.1 in the context of resetting of orthopyroxene compositions by reheating and recrystallisation).

Norton (1984, 1988) points out that large - scale hydrothermal circulation, of an intensity sufficient to cause noticeable oxygen isotopic changes or other metasomatic effects, is only likely to occur on short timescales if a tensile fracture network is present to provide the necessary high permeabil-

ity. Norton considere that these timescales were similar to the lifetimes of hydrothermal systems associated with large subvolcanic mafic intrusions. Given this, it follows that such hydrothermal circulation must normally only occur in other upper crustal basic and ultrabasic intrusions under distinctly cooler conditions than the lower temperature limit of large - scale textural equilibration. This is because it is only when the latter process has ceased, either through decreasing temperature or an increasing cooling rate, that the rocks acquire a significant long - term Young's modulus and can build up thermal contraction stresses sufficient to cancel the effects of overburden stress and thereby make tensile crack formation possible (see section 5.3). It should be noted that this argument only applies to the case of hydrothermal fluid - filled fractures in a convecting hydrothermal system and not to magma - filled fractures since the pressure of interstitial magma will itself cancel the overburden pressure (see section 5.3.3). It is not, therefore, inconsistent with observations indicating formation of dilatant dykes in texturally - equilibrated rocks showing evidence of syn - emplacement ductile deformation, such as the tectonitised harzburgite unit of most ophiolites (e.g. Rabinowicz et al. 1987)

It is therefore surprising that very high grade, anhydrous hydrothermal metamorphic vein assemblages, similar to those described here, have not been described from other plutons in which very high temperature hydrothermal circulation has been inferred from oxygen isotopic evidence. In part this could be because of lower oxygen fugacities in the fluids in many intrusions than in those which affected the Inner Series of the Hypersthene Gabbro, which would reduce the amount of oxidation produced. However, because of the steep slopes of fluid buffers, relative to partially solid - state buffers such as fayalite - magnetite - quartz, in T - f_{O_2} space, it is unlikely that hydrothermal fluids would not cause oxidation or reduction at some temperature within the 700 – 1000°C range of very high temperature hydrothermal circulation. An additional factor could be that the high - grade metamorphism observed in the Inner Series of the Hypersthene Gabbro developed in a much shorter period than the oxygen isotope depletions observed in other mafic plutons. This would have two effects:

1). Permeabilities in the cumulate sequences could be lower for a given total fluid flux, and result from the presence of a much less dense fracture network. As noted in section 3.4.6 the majority of fractures formed at very high temperatures in the Inner Series of the Hypersthene Gabbro appear to be tensile in origin. Such fractures would be expected to be more common

in a sheet complex than in a layered series of cumulates because local cooling rates, following emplacement of sheet intrusions, would be much greater than the low cooling rates characteristic of cumulate sequences derived from much larger magma bodies. Strain rates due to thermal contraction would therefore be much greater and less of the strain would be taken up by ductile creep of the rocks in confluent sheet complexes. The latter would therefore be expected to have greater permeabilities at high temperatures.

2). The longer timescale of metamorphism would allow more time for annealing of fracture networks by solid - state creep of the host rocks. As noted above, however, recognisable orthopyroxene - opaque symplectitic intergrowths replacing olivine are present in samples of the layered series of the Skaergaard intrusion in the Durham University collection, as are myrmekite - like feldspar - olivine/clinopyroxene intergrowths rimming magnetite (C.H.Emeleus pers comm.) similar to those described in section 6.4.2.2. This indicates that some of the products of very high - grade hydrothermal circulation have been preserved in this intrusion and that therefore the lack (or at least, low abundance) of very high temperature hydrothermal veins in the Skaergaard layered series is a primary feature.

6.5. Conclusions: magmatic processes in a low - melt - percentage magma body and their relationship to very high temperature hydrothermal circulation.

6.5.1. The problems of interpreting overall compositional trends in the gabbronorite suite of the Inner Series.

The pincipal aim of the work described in this chapter was to investigate magmatic processes in the low - melt - percentage magma body represented by the Inner Series of the Hypersthene Gabbro, and in particular by the gabbronorites and related rocks which make up the bulk of the Inner Series. The compositional evolution of these rocks appears to have been much the same as those produced in high - melt - percentage magma bodies, although this is perhaps not surprising if one accepts the view that the geochemical features of the products of the latter are largely the product of processes operating in the low - melt - percentage regions at their margins (Langmuir 1989). It is however difficult to be certain about this as the patterns of major element variation are largely the same in both coarse- and fine- grained gabbronorite suite rocks, except for those elements affected by super - rigidus porphyrocryst accumulation. The gabbronorite suite rocks also seem to show some slight heterogeneity in the effects of crustal contamination. This implies that much of the geochemical variation in the rocks has been inherited from the residence of their parental magmas in other magma chambers, perhaps at deeper levels within the crust or elsewhere in the Ardnamurchan central complex. Melt percentages within these bodies are of course unknown, which means that study of the Inner Series rocks in general reveals little about processes in low - melt - percentage magma bodies, except that crystallisation and other processes in this particular example have in general had little effect upon rock compositions.

The gabbronorite suite rocks are, nonetheless, of some interest as they show an overall fractionation trend, from weakly crustally contaminated tholeiitic basic magmas, involving the fractionation of augite as well as plagioclase and olivine. This is despite the fact that most of the fine - grained, near - liquid composition rocks are too primitive to have been in equilibrium with augite at the liquidus and that the coarser - grained rocks show clear textural evidence to suggest that augite was a late - crystallising interstitial phase in most of these rocks. The gabbronorite suite of the Inner

Series therefore seem to represent an example of a suite of rocks showing 'cryptic fractionation' of clinopyroxene. This may have been produced by mixing of various primitive and more evolved high melt percentage magmas, which would accunt for the complex zoning patterns observed in the plagioclase porphyrocrysts if these were suspended in some of these magmas, or by mixing of primitive melts form the interior of magma bodies with various more evolved melts released from low - melt - percentage rocks at their margins. In this latter case the porphyrocrysts are more likely to be xenocrystic in origin and to have been derived from pre - existing cumulates. The coarser - grained rocks show considerable scatter about the main fractionation trend in plots involving Ca, Mg and Al. This appears to have been produced by plagioclase and olivine accumulation, mainly above the rigidus, and growth of augite during the formation of lamination below the rigidus, which produces a characteristic association of the development of lamination with increases in modal augite contents and is one of the few cases where a compositional trend can be identified as due to in situ sub - rigidus (or low melt percentage) processes.

6.5.2. A possible relationship between very high temperature hydrothermal circulation and sub - rigidus feldspar dissolution during the formation of lamination and metasomatic pyroxenites.

Detailed examination of sub - rigidus magmatic processes was found to be possible only where the 'before' and 'after' states of rocks affected by them could be identified, in single small intrusions (single gabbronorite sheets, for example) or initially uniform outcrops which had only been affected by the processes in some parts. In these cases it can be assumed that the body was of approximately uniform composition prior to the operation of the sub - rigidus process, be it the formation of lamination or the formation of a metasomatic pyroxenite body. Mineralogical evidence and calculated bulk compositional changes indicate that both of these processes involved the dissolution of feldspars and the growth of augite. In the case of the formation of sub - rigidus or 'post - cumulus' lamination this appears to have been associated with the expulsion of a high - Al ferrobasaltic melt from the rocks. The mineralogy of the pyroxenites and the constant - volume character of the replacement process are inconsistent with a simple melt expulsion model. They appear to have formed at the sites of interstitial melt migration conduits and to have involved reaction of the rocks with many times their own volume of migrating melts. The reactions involved seem to have been generally similar, although in the case of the pyroxenites olivine and orthopyroxene were precipitated as well

as augite and dissolution of feldspars proceeded to a much more advanced stage.

Whilst the dissolution of olivine (and also chrome spinel) and its replacement by pyroxenes, as is seen in metasomatic rocks in the Rhum complex (Bedard et al. 1988) can be explained in terms of the peritectic reaction between olivine and melt as the latter fractionates at low pressures, feldspar dissolution and its replacement by pyroxenes cannot be explained in terms of fractionation under constant conditions as there are no peritectic reactions involving plagioclase and basaltic melts at low pressure. Dissolution of plagioclase on reheating is a possible mechanism for producing the initial dissolution but the only phases which would replace it under these conditions are olivine and/or chrome spinel, both of which appear on the liquidus at higher temperatures than plagioclase in tholeiitic magmas. Some mechanism for reducing the liquidus field of feldspar in the basalt phase diagram has to be invoked in order to explain its replacement by pyroxenes and the very late - stage crystallisation of feldspar implied by its poikilitic habit in the main pyroxenite bands (Plate 3.100).

One possible explanation is that the high - Al melts which must have coexisted with these rocks were hydrous, which would have the effect of reducing plagioclase stability even at relatively low total pressures (Spulber & Rutherford 1983; Whitney 1975). Flushing - through of a crystal mush whose interstices were initially occupied by anhydrous melts by hydrous melts would cause preferential feldspar dissolution. Reheating of originally anhydrous rocks containing a hydrothermal fluid phase could have a similar effect (note that on the small scales of reheated aureoles around newly - emplaced gabbronorite sheets diffusion of water into the region of melting could be an effective way of increasing the water content of the melt over the amount contributed by that originally present in the parent rocks; see Lesher & Walker (1989) for estimates of effective diffusion distances within large mafic intrusions).

Penetration of H_2O into regions containing partial melts in basic intrusions has been proposed by a number of workers to account for transgressive pegmatitic or granophyric pods and veins interpreted as the products of remelting of earlier accumulative rocks (notably Irvine 1987), although the residua of such remelting processes have not been explicitly identified nor have detailed investigations of the pods and veins themselves, to identify the source of the supposed water, been carried out. The inference made in section 6.4.3, that hydrothermal circulation in the Inner Series of the Hypersthene

Gabbro only took place at temperatures below the lower limit of primary crystallisation implies that direct penetration of water along fractures into regions of partial melting would be unlikely to occur: the formation of hydrous melts must therefore have involved diffusion of water into localised regions of partially molten rock or reheating of water - saturated rocks. Both of these processes are more likely to occur to a significant extent in an intrusive complex composed of many small confluent intrusions emplaced in sucession than around a single large magma body.

Changing the phase relationships of partially molten rocks by a change in water activities requires an addition of water to the rocks or redistribution of water within them by crystallisation and segregation of residual hydrous melts. The former case is perhaps more significant since the initial water contents of tholeiitic magmas are small (Michael 1988) and the amount of remelting that could be produced in a closed system correspondingly limited. In contrast, if the water is externally supplied, as in the case of rocks showing ^{18}O depletions due to interaction with meteoric water, the amount of hydrous remelting, relative to the overall size of the pluton under consideration, is limited only by the thermal constraint that the fluids and the rocks they affect have to be reheated to magmatic temperatures. The proposed mechanism for the formation of the of the pyroxenites and augite - enriched laminated gabbros in the Inner Series therefore implies that the occurrence of low - ^{18}O basaltic magmas or mafic cumulates is not necessarily indicative of assimilation of hydrothermally altered wall rocks by a large, vigourously convecting magma body with a Type 1 boundary layer (as defined in section 4.1), although the occurrence of isotopically light mafic xenoliths (Norton & Taylor 1979; Irvine 1987) is. As noted above, confluent sheet intrusion complexes may be more prone to produce such magmas than large compact high - melt - percentage magma bodies.

6.5.3. Controls on the occurrence of very - high - temperature hydrothermal circulation in mafic rocks.

The very high temperature hydrothermal circulation in the Inner Series, although identified on purely mineralogical grounds rather than by the use of stable isotopes, appears to have been similar to the fossil hydrothermal systems identified in cumulates formed on the floors of basic and ultrabasic magma chambers. These are characteristic of a very distinctive hydrothermal environment which is only found in basic to ultrabasic plutons (Taylor 1987).

Taylor (1987) attributed the development of these unusual hydrothermal systems to the partial trapping of circulating meteoric water beneath the magma chamber and associated partially molten cumulates, which acted as an impermeable cap, preventing upward flow of the fluids. Buoyant upward flow of heated, low - density fluids is the driving force of thermal convection and if it is blocked the fluids will stagnate and heat up to very high temperatures indeed. A sheet intrusion complex such as the Inner Series, containing a series of partially molten sheets around which fluids would have to circulate in order to migrate upwards would also be expected to contain near - stagnant hydrothermal fluids. Both large high melt percentage magma bodies and mainly low melt percentage magma bodies would therefore be expected to have such hydrothermal systems associated with them, although as noted in the previous section the effects of the presence of this system upon the compositions of the magmas produced would tend to be greater in confluent intrusive sheet complexes like to the Inner Series than around large single magma bodies. This represents the only possible difference in the products of high - and low - melt - percentage magma bodies identified in the course of this work.

7. EMPLACEMENT MECHANISMS OF THE VARIOUS COMPONENTS OF THE HYPERSTHENE GABBRO AND OF THE ASSOCIATED MINOR INTRUSIONS.

The division of the Hypersthene Gabbro into two main components, the Marginal Border Group and the Inner Series (see Chapter 3), resolves the problem posed by the contradictory interpretations of the geometry of the pluton which were proposed by Richey et al. (1930) and Skelhorn & Elwell (1971), on the one hand, and by Wells (1978) and Walker (1975) on the other (section 1.2). Field evidence discussed in Chapter 3 indicates that the former interpretation (in terms of a single, steep - sided intrusion) applies most closely to the Marginal Border Group, whilst the Wells/Walker model is a more plausible interpretation of the Inner Series of the pluton. It should be emphasised, however, that although the Inner Series is largely composed of shallowly - inclined confluent intrusive sheets, its margins are **not** conformable to the surrounding rocks, as was proposed by Wells (1954, 1978) and Walker (1975) for the Hypersthene Gabbro as a whole. Instead, these contacts are largely formed by steep syn - emplacement reverse faults. This division of the pluton into two components of strongly contrasted geometries means that the emplacement mechanisms of the two components must be considered independently.

Field and petrographic evidence also shows that, contrary to previous interpretations of their age relationships, the cone sheet intrusions around the Hypersthene Gabbro mainly post - date its initial emplacement and must have formed at its sides rather than above the apex of a more deeply buried intrusion (Anderson 1936). This means that the emplacement mechanisms of the cone sheets need to be re - investigated and also that they, along with other minor intrusions such as the rheomorphic breccia bodies and M2 felsites, can be used to investigate the stress fields around the MBG magma chamber during the later stages of its evolution. Deduction of these stress fields should in principle make it possible to assess the contributions of different types of stress (due to magma pressure in the chamber, thermal contraction or expansion, or externally - imposed tectonic or regional stresses) to the structural evolution of the pluton and thereby relate its structural history to its magmatic history.

7.1. The overall geometry and initial emplacement of the MBG magma chamber.

7.1.1. Constraints on the geometry of the MBG magma chamber above and below the present level of exposure.

The geometry of the Hypersthene Gabbro above and below the present - day surface is one of the most important unknowns with respect to its structure and emplacement mechanisms as well as with respect to the thermal models used to estimate the duration of M1 and flow velocities in the M1 boundary layer of the magma chamber (Chapter 5). The model for the internal stratification of the MBG magma chamber (Chapter 4, especially Fig. 4.31) and the interpretation of structures around the intrusion presented below require that the MBG magma chamber have been at least this thick (and probably more than a kilometre thick).

7.1.1.1. Geophysical models for the sub - surface structure of the Ardnamurchan central complex.

A number of studies of gravity and magnetic anomalies associated with the Ardnamuchan central complex have provided constraints on the subsurface extent of the complex as a whole (Bott & Tuson 1973; Barrett 1987; Harrison 1987). It is not possible to interpret these anomalies directly in terms of the subsurface geometry of the MBG because of the presence of numerous later basic intrusions (troctolites to quartz gabbros; see Fig. 1.2). However, the Marginal Border Group of the Hypersthene Gabbro does form the outermost large intrusion in most of the western part of the complex and it is therefore likely that the outer contact of the complex determined from geophysical data corresponds fairly closely to the outer contact of the MBG, at least within one or two kilometres of the surface. The geophysical data also provides the best constraint on the maximum possible depth to the base of the MBG, when combined with constraints on the composition of the rocks in the subsurface.

These compositional constraints are important because the interpretation of gravity and magnetic anomalies requires some knowledge of the densities and magnetic susceptibilities of the rocks causing the anomalies. In general, it is not possible to obtain a unique solution, but only to produce

alternative interpretations consistent with the available compositional data. In the case of the central complexes of the British Tertiary province the anomalies associated with them can be interpreted in terms of two models for the composition of the complexes (e.g. Bott & Tantrigoda 1987):

1). Gabbroic bulk composition. This assumes that the entire thicknesses of the complexes (except Rhum, which has to be interpreted in terms of high density ultrabasic rocks (Coppin 1982)) is composed of gabbroic rocks similar to those which dominate the basic component of the central complexes at the surface. This is the lowest - density composition which satisfies the gravity data and yields the greatest depths to the bases of the gravity anomalies associated with the central complexes, around 5 to 6 kilometres in the case of the Ardnamurchan complex (Barrett 1987; Bott & Tuson 1973).

2). Picritic lower layer. This model divides the complexes into a gabbroic upper layer and a higher - density (typically close to 3000kg m^{-3}) lower layer of ultrabasic rocks with a picritic bulk composition. Interpretation of the Ardnamurchan complex in terms of this model yields inferred depths to the base of the density anomaly of as little as 3 kilometres (Barrett 1987).

There is a large degree of uncertainty in the depths to the bases of the complexes (as opposed to the depths to the bases of the anomalies) obtained using these models. One reason for this is uncertainty in the regional gravitational and magnetic fields, which introduces an uncertainty of the order of a kilometre in the depths to the base of the anomalies (Barrett 1987). A further and more important problem in the interpretation of the geophysical anomalies in terms of inferred sub - surface geology arises from uncertainties in the compositions (and therefore densities and magnetism) of the country rocks at depth. If these are silica - rich and of low density and magnetic susceptibility, then the base of the observed anomaly will coincide with the actual base of the main part of the complex, although small feeder intrusions must be present below this level. However, the complexes could extend to greater depths than the anomalies if emplaced in rocks of similar properties below the base of the anomalies, in which case the latter would reflect earlier crustal structure rather than the geometry of the complexes. This latter interpretation is unlikely if the complex concerned contains large amounts of ultrabasic rocks, because none of the volumetrically significant pre - Tertiary rocks near the surface in north west Scotland are sufficiently dense, except

in the cases of those complexes (notably Rhum, Skye and Blackstones) which are associated with anomalies extending to the lowermost crust (Bott & Tuson 1973; Coppin 1982). On the other hand, the density of the granulite - facies basic to intermediate rocks which may form much of the lower crust of north - west Scotland (see Chapter 2, especially section 2.1, for discussion of work on the lower crust in this area) is similar (Bamford et al. 1977, 1978) to that of gabbroic rocks. The interpretation of the base of the geophysical anomaly associated with a central complex is therefore much more ambiguous if the complex has a gabbroic bulk composition.

The interpretation of magnetic data in terms of distributions of rock types is even more problematic than the interpretation of gravity data because the magnetic properties of rocks are dependent on the abundances and distribution of a minor mineral component, magnetite. Thus an accumulative rock with a generally basaltic composition could be much less magnetic than its fine - grained equivalents because of expulsion of a ferrobasaltic residual melt, whilst its properties would change again if it was affected by oxidising hydrothermal fluids. The results obtained from the magnetic data for the Ardnamurchan complex as a whole are similar to those obtained from the gravity data, although the Hypersthene Gabbro itself has very little effect upon the magnetic field in the area (Harrison 1987).

The gravity and magnetic anomalies associated with the Ardnamurchan complex can be interpreted in three main ways, corresponding to the models discussed in general terms above, which are summarised below and in the three diagrammatic cross - sections in Fig. 7.1:

1). Gabbroic bulk composition in a felsic to intermediate crust, depth to base of complex about 5km.

2). Picritic lower layer (1 – 1.5km thick); depth to base of complex as little as 3km. Also emplaced in a felsic to intermediate crust.

3). Deep - rooted gabbroic complex, emplaced in a layered crust which has high - density intermediate to basic granulite - facies Lewisian rocks occurring as little as 5km below the surface. This latter model seems rather implausible on the grounds that high - density pre - Tertiary rocks occurring within a few kilometres of the surface in the Ardnamurchan area

Fig. 7.1. Interpretations of the geophysical anomalies associated with the Ardnamurchan Central Complex as a whole: Based on Bott & Tuson 1973, Barrett 1987 & Harrison 1987.

1. Shallow - rooted gabbroic complex in low - density crust.

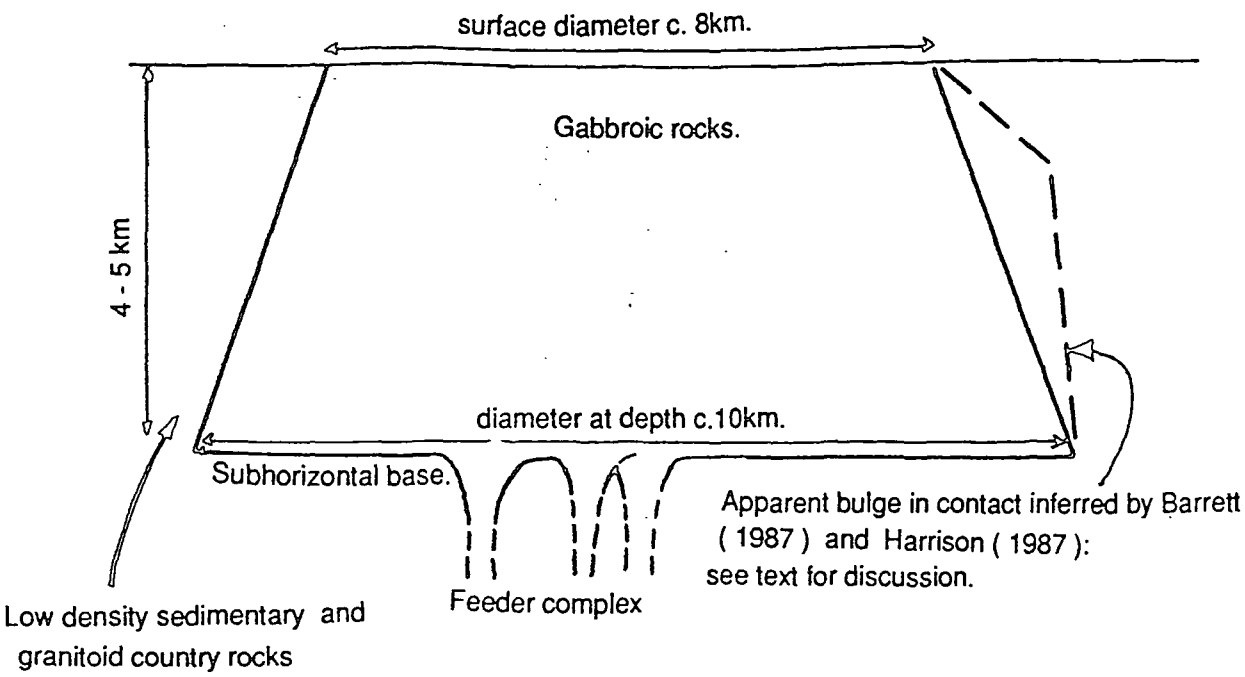

2. Shallow two - layer complex in low - density crust.

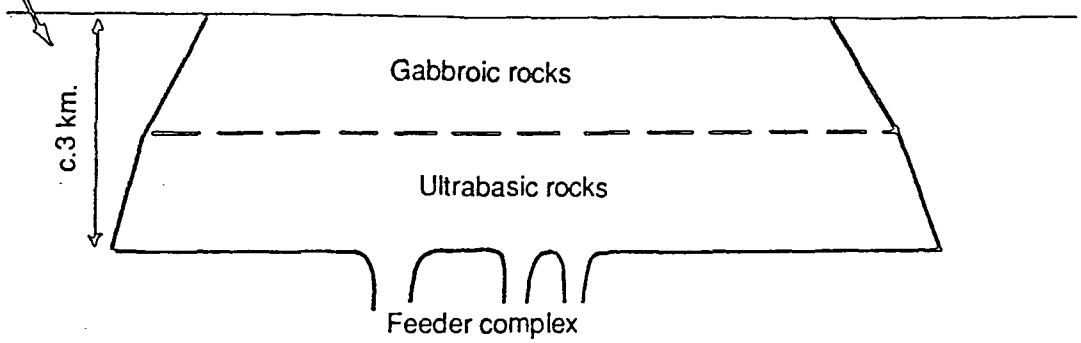

3. Deep - rooted gabbroic complex with root hidden in high - density middle and lower crustal granulite facies rocks.

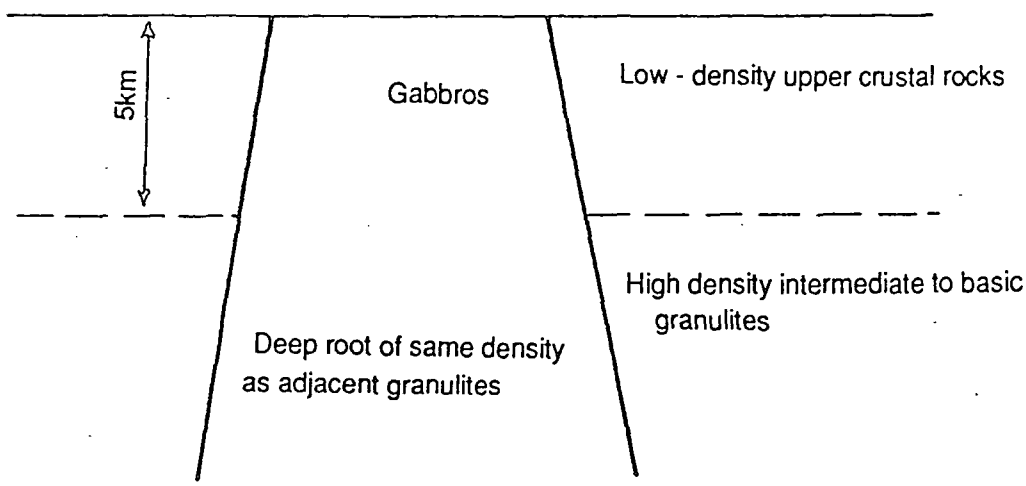

would produce a broader positive gravity anomaly on which that due to the complex itself would be superimposed. This wider anomaly does not occur.

These cross - sections are based on the work of Barrett (1987) and Harrison (1987), with one important modification. This concerns the form of the outer contact of the plutonic complex, which both of these workers considered to be shallowly - dipping (30° outwards or less) near the surface and to steepen with depth. The presence of a shallowly - dipping outer contact is inconsistent with the surface geology of the Marginal Border Group (see section 3.2.5.2 in particular) and is considered here to be an artefact of the model used by both Barrett and Harrison. This neglects the presence of cone sheets and other doleritic intrusions outside the main contact of the central complex. These would tend to increase the density of the country rocks within a few kilometres of the contact and, being magnetite - rich, would have an even stronger effect on their magnetic properties: it is noticeable that the outward curvature of the contact as inferred from magnetic data (Harrison 1987) is stronger than that obtained from the gravity data (Barrett 1987).

7.1.1.2. Evaluation of the alternative geophysical models using geochemical data.

The three alternative interpretations of the geophysical data listed above all imply different Tertiary magma and country rock compositions. Each implies different patterns of contamination of the Tertiary rocks: it is therefore possible to discriminate between them according to whether or not they are likely to be associated with the observed pattern of crustal contamination, in the MBG rocks (section 4.3.2) in particular.

The occurrence of contamination with high La/Ta, high Th/Hf and low Hf/Sm intermediate to tonalitic igneous rocks (most probably amphibolite - facies orthogneisses) in the homogenous MBG rocks implies the presence of a significant thickness of low - density amphibolite - facies Lewisian (?) rocks beneath the Moine Thrust zone below Ardnamurchan. The constraints on the pre - Tertiary crustal structure in the area (Chapter 2, especially Fig. 2.9) make it unlikely that all this material occupies only the uppermost five kilometres or so of the crust. This excludes 'deep - rooted' models of the Ardnamurchan complex and indicates that the depth to the base of the geophysical anomaly corresponds to the true depth to the base of the central complex.

The inference that crustal contamination of the parent magmas of the MBG homogenous basic rocks involved bulk assimilation of a range of Lewisian lithologies (including relatively refractory tonalitic and dioritic rocks) by high - temperature, low - viscosity picrobasaltic or picritic magmas, rather than selective assimilation of fusible lithologies by basaltic magmas, implies that picritic magmas entered the crust beneath Ardnamurchan during the lifetime of the MBG magma chamber. If a layered model (e.g. that of Bamford et al. 1977, 1978) is applicable to the Lewisian basement complex beneath Ardnamurchan then the occurrence of amphibolite - facies tonalitic/dioritic contaminants in the MBG magmas and the basaltic composition of the latter imply that fractionation of large volumes of contaminated high - MgO magmas to basaltic magmas took place in the upper half of the crust in the area. This implies the presence of large volumes of ultrabasic, high - density cumulate rocks in the middle to upper crust. These cumulates would be expected to produce a large gravity anomaly and it therefore seems likely that they should occur within a few kilometres of the surface, in the lower half of the two - layer intrusive complex shown in Fig. 7.1.2. Formation of these cumulates could either have taken place in the subsurface part of the MBG magma chamber, if it had a stratified internal structure similar to that envisaged by Young et al. (1988) for the Rhum complex, or in sills beneath the main magma chamber. The preservation of heterogenous contamination (section 4.3.2) during this extended period of fractionation suggests that the latter alternative is more likely, as convection in thin picritic layers at the floors of mainly basaltic magma chambers is thought to be unusually vigourous (Huppert & Sparks 1980; Marsh 1989). Unless fractionation of the ultrabasic magmas to produce basaltic residual melts took place in separate magma chambers the heterogeneity due to previous crustal contamination is unlikely to have been preserved.

The interpretation of the geophysical data in the light of these geochemical constraints therefore suggests that the Ardnamurchan complex as a whole consists of a series of gabbroic intrusions (with a few small intermediate to felsic bodies; see Fig. 1.2, also Barrett (1987) for an estimate of their subsurface extent) above a lower layer of ultrabasic cumulates which pass down into a volumetrically small feeder complex (Fig. 7.1.2 above). This implies that the base of the MBG magma chamber was no more than 3 km below the present level of exposure and may have been rather less, because earlier and later intrusions, as well as the inferred ultrabasic sill complex, have to be fitted into this depth range as well. Although this argument is not secure because it depends upon the precise crustal structure of the area as well as upon the precise behaviour of stratified

magma bodies, the discussion below, concerning the emplacement of the MBG magma chamber, would not be greatly affected if its base was five kilometres below the present surface rather than only three kilometres.

7.1.1.3. A summary of geological constraints on the original extent of the MBG magma chamber above the present level of exposure and of its overall geometry.

The geological constraints on the geometry of the MBG magma chamber and in particular upon the height of the roof of the chamber above the present level of exposure have all been derived in previous chapters (see especially section 4.2.5 and section 4.5). They can be summarised as follows:

– The occurrence of anatectic melts derived from rocks not exposed at the present level of exposure close to the contact (probable Triassic sediments and earlier Tertiary granitoids; sections 4.2.4 and 4.2.2 respectively) suggests that the magma chamber extended at least several hundred metres below the present level of exposure.

– The steepness of the isograds in the contact metamorphic aureole, particularly on the southern margin of the intrusion (Fig. 5.1) and their approximate parallelism to the contact at the present level of exposure suggests that the same contact orientation was maintained for some hundreds of metres both above and below the present level of exposure, and therefore that large areas of relatively flat - lying roof and floor contacts were at least this far from the present - day surface.

– The low pressures at which wall rocks melting took place (section 4.2.5) imply that the magma chamber was emplaced at a depth of no more than 3 – 4km. The presence of wall - rock deformation and a coherent system of concentric and radial faults imply that the roof of the intrusion was a relatively rigid body. These two constraints, taken together, suggest that the roof of the MBG magma chamber was at most around two kilometres above the present level of exposure and must therefore have been a fairly broad flat - lying surface; the intrusion must have been a truncated cone shape rather than tapering to an apex (see Fig. 5.5.).

– The absence of an exposed roof facies, including the layers of intermediate magmas inferred

to overlie the basic MBG magmas in section 4.3.3 as well as buoyant layers of granitoid magmas (if present) and actual roof rocks, implies that the roof of the chamber was at least a few hundred metres above the present level of exposure.

When all of these constraints are considered together, it appears most likely that the MBG magma chamber was a tabular body with an elliptical cross - section (about 6km by 8km), steep outward - dipping walls (see section 3.2), and a flat - lying roof and floor. It may have been as much as 6km thick (but only if it occupied the whole of the region now formed by the rest of the complex and the tentative inference of an ultrabasic lower layer is incorrect) but is more likely to have been less than 3 – 4km thick and may have been as thin as 1 – 2km, corresponding to an aspect (height/width) ratio of between 2 and 6.

7.1.2. Initial emplacement of the MBG magma chamber: evidence from early structures.

The main early, late M0 to early M1 structure associated with the initial emplacement of the MBG is the dome structure first noted by Judd (1874). This can be divided into three concentric zones, which are best seen on the southern margin of the intrusion (section 3.2.5.4):

– Inner zone, characterised by relatively shallow outward dips (20 – 25° overall) and the development of inward - facing monoclines with inward - dipping fold axes (Fig. 3.14). The larger area of inward - dipping rocks close to the contact in the Glendrian Bay area may be part of a similar structure.

– Central zone, with steeper outward dips (35° or so). This is best developed on the southern margin of the intrusion, where it is up to 0.5km wide. Most of the corresponding uplift on the northeastern margin of the intrusion, where the zone of steeply outward - dipping sediments is much narrower, may have been taken up on concentric outward - dipping faults (Fig. 3.4). It should be noted that these faults cut out much more of the succession (including the whole of the plateau basalt sequence in this area) than the corresponding fault (the Kilchoan Bay fault) on the southern margin of the intrusion, although whether this actually indicates a greater throw is in doubt because it is not possible to assume a perfect 'layer -

cake' stratigraphy in the pre - Hypersthene Gabbro rocks (see Chapter 2).

– Outer zone, in which dips decrease outwards from 35°.to less than 15 – 20°. Minor folding is more common in this zone than in the central zone of the dome structure, at least to the south of the pluton. The outer zone is cut by a number of broadly concentric faults on both the north eastern and southern margins of the intrusion. The fault system at Maol Bhuidhe (Fig. 3.17.) may have developed at this time and be associated with this zone of the dome structure but is more likely to pre - date it (section 3.2.5.4).

The development of the dome structure was interpreted by Walker (1975) in terms of deformation around an early granitic diapir. However, deformation around a diapir (Marsh 1982) or around an expanding plug - like intrusion (Jackson & Pollard 1988) involves radial compression of the country rocks (and downward motion in the case of rocks around a diapir) which is characteristically accomodated by the development of an annular rim syncline. No such structure is present in western Ardnamurchan: although a fault - bounded trough is present this is bounded by subvertical or normal faults, at least where the orientation of these faults can be identified. The trough is therefore extensional rather than compressional and cannot have been produced by the upward passage of a diapir through the present level of exposure. Furthermore, all the small early structures around the Hypersthene Gabbro (in contrast to late M1 and M2 structures dealt with in section 7.2, below) are associated with radial extension rather than radial compression in those cases where the sense of motion can be shown to involve a horizontal component.

It is therefore more appropriate to consider the evolution of the dome and the initial emplacement of the MBG magma chamber in terms of the field and model studies of laccolith development (Gilbert 1877; Pollard & Johnson 1973; Johnson & Pollard 1973; Koch et al. 1981; Dixon & Simpson 1987; Jackson & Pollard 1988). These studies consider the evolution of a growing sill emplaced close to the surface in a series of well - layered rocks (for example, a sequence of bedded sediments). They differ in detail but the conclusions of the more recent field and experimental studies all point to a three - stage sequence of development:

1). Initial emplacement of a sill within a bedded sequence by symmetric deformation of the rocks above and below the sill. Growth of the sill to a critical radius or width at a constant low aspect

ratio. This critical radius is governed by the effective thickness (thickness of a single layer with the same resistance to bending as the actual bedded sequence) of the overlying rocks. The eefective thickness is generally much less than the true overburden thickness (around 0.15 to 0.7 of the true thickness in the case of the laccoliths in the Henry Mountains, Utah, U.S.A., interpreted in these terms by Pollard and Johnson (1973)).

2). Once the sill has grown to the critical size, the roof of the intrusion bends upwards and its aspect ratio increases sharply. Deformation is initially distributed over the whole of the roof of the intrusion but becomes concentrated at its periphery with time (Dixon & Simpson 1988), producing an annular monocline around the edge of a steep - sided but still conformable body.

3). Eventually, brittle failure of the rim monocline and development of a through - going annular outward - dipping normal fault occur. Further uplift of the roof of the intrusion produces a steep - sided, cross - cutting intrusion with a flat conformable roof and floor. The stage at which this faulting develops depends upon the rheology of the country rocks and has not been sucessfully predicted by any of the experimental or theoretical studies referred to above. In the case of the Henry Mountains intrusions it can occur at aspect ratios as high as 5 (Johnson & Pollard 1973) although in other cases it appears to have been unimportant in the formation of intrusions with aspect ratios as low as 1 (Jackson & Pollard 1988). This type of laccolith was termed a 'bysmalith' by Iddings (1898) and although this term is now considered obsolete it is useful in the present context as it emphasises the distinction between conformable laccoliths and those with steep margins which cross - cut the surrounding up - domed rocks.

The latter stages at least of this sequence of events is consistent with almost all of what is known of the early history of the MBG magma chamber. In this case, the precursor sill complex would have grown to a diameter of around 8km before updoming began and further lateral growth ceased. This yields an effective overburden thickness of 1 – 1.5km (from the critical diameter – effective overburden thickness relationship of Pollard & Johnson (1973)), perhaps 20 – 50% of the true overburden thickness in Ardnamurchan. This is within the range of ratios of effective to true overburden thicknesses proposed by these workers. Updoming of the roof of the developing laccolith by 500m or more appears to have followed; although the inner shallowly - dipping segment of the dome is not well - developed its presence suggests that a peripheral monocline may have formed at this stage.

Final central uplift along outward - dipping normal faults, as indicated by the occurrence of such faults in the country rocks, would be an efficient mechanism for creating the observed steep - sided contacts. This interpretation implies that the wall of the magma chamber was initially formed by a fault surface. No evidence for the presence of this fault has been found, in the form of fault rocks at the contact, but thermo - mechanical erosion of these rocks due to thermal stresses set up in the country rocks immediately after the emplacement of the magma chamber (see discussion of such stresses in Furlong & Myers (1985)) could account for their absence. The uplift on these faults appears to have been of the order of a few hundred metres at least; there is considerable uncertainty in the actual amount of uplift because the thickness of the Tertiary plateau basalt sequence west of the Glas Eilean fault is unknown. The minimum total amount of uplift associated with the faulting and doming is therefore close to a kilometre. For all of this to be associated with the MBG magma chamber, this must have been a kilometre or more thick by the end of concentric outward - down-throwing normal fault movements, consistent with the constraints on its overall shape discussed in the previous section.

The interpretation of the early development of the MBG magma chamber in terms of the growth of a very large fault - bounded laccolith implies that the precursor sill complex was emplaced into a sequence of bedded rocks. A thick sequence of such rocks is present in the area, in the shape of the Moinian and Mesozoic successions above the Moine thrust zone (sections 2.2, 2.3 and 2.5). The implication that the whole of the intrusion must therefore lie above the Moine thrust zone is consistent with what is known of the position of this thrust (section 2.2 and Fig. 2.9) and the overall shape of the complex (particularly the maximum depth to the base of the MBG magma chamber inferred in section 7.1).

7.2. Deformation around the MBG magma chamber after its initial emplacement.

Ever since the pioneering study by Anderson (1936) investigations of the stress fields and mechanisms of emplacement of minor intrusions around near - surface magma chambers have tended to approach the problem by theoretical, experimental or numerical analyses of the stress fields expected around pressurised cavities of more - or - less simplified shapes in idealised host materials (see review in Chevallier & Verwoerd 1988). In recent years, however, advances in the interpretation of irregularities and minor or parasitic structures in fault zones (Gamond 1987; Petit 1987) and of offsets across dykes and other sheet intrusions (Delaney & Pollard 1981; Pollard et al. 1982; Pollard & Nicholson 1985) have made it possible to deduce the sense of movement and/or dilation directions associated with these structures and thereby empirically determine the stress field at the time of their formation. The approach followed in this section is therefore to attempt to use these sense - of - movement criteria to deduce the stress field around the MBG magma chamber at various times and investigate the mechanisms of emplacement of the minor intrusions associated with it, particularly the cone sheets.

7.2.1. M1 and M2 faulting associated with the MBG magma chamber.

Theoretical studies of the pattern of faulting around cylindrical or ellipsoidal magma chambers (e.g. Anderson 1936; Robson & Barr 1964; Roberts 1970; Phillips 1974) have all emphasised that two different sets of structures will commonly be present. Each of these sets is associated with a characteritic value of the hydrostatic pressure of magma within the chamber (due to the difference between the average densities of the magma column beneath the chamber, down to the magma source region and of the wall rocks of this column), relative to the lithostatic load on the chamber. If the pressure in the chamber is greater than the load pressure ($P_{excess} > 0$, where $P_{excess} = P_{magma} - P_{load}$) the chamber will tend to inflate, producing tangential stretching and radial compression in the chamber walls, whilst if it is less ($P_{excess} < 0$) the chamber will tend to contract, causing tangential shortening of the chamber walls. The true situation is likely to be rather more complex as none of these studies consider changes in the patterns of deformation as finite amounts of strain occur, but the division is useful nonetheless as it provides a relationship between instantaneous stress fields and magma chamber pressures. Further complications are likely to be produced by stresses

due to thermal expansion in the wall rocks as they heat up (Furlong & Myers 1985).

It should be noted that this division into inflationary and deflationary structures is not the same as the conventional division of faults and folds into extensional and compressional structures. For example, stretching of a near - vertical intrusion wall may be accomplished by movement on low - angle thrust faults and inward - dipping caldera faults are normally associated with chamber deflation (Walker 1984), although this view has been challenged by Gudmundsson (1988).

In general, periods of chamber deflation and inflation alternate beneath active and recently active volcanoes, on timescales of months to hundreds or even thousands of years (Ryan 1988; Walker 1984; Wallmann et al. 1988). It is therefore to be expected that both inflationary and deflationary patterns of wall - rock deformation will be found around ancient magma bodies emplaced at shallow depths and that these will show no systematic age relationships to each other, as the timescale of inflation and deflation cycles may be very short relative to the lifetime of the intrusion. Such a pattern of deformation is apparent around the MBG, as periods of movement on opposing sets of structures cannot be separated (Chapter 3, section 3.2.5.5 in particular). Nevertheless, a number of groups of faults can be distinguished, which are considered here in turn together with the stress fields that produced them.

7.2.1.1. The concentric inward - dipping normal fault system.

This series of faults, together with the radial compartmental faults which transfer displacements between them, are the largest structures associated with the post - initial - emplacement history of the MBG magma chamber. Although some examples are believed to have been present just above the present level of exposure, or out to sea, on the northern and western margins of the intrusion (sections 3.2.2 to 3.2.4 and section 4.2) concentric normal faults are best exposed on the southern margin of the intrusion (Fig. 7.2) between Glebe Hill and the Lochan na Cloiche fault (Fig. 3.10). Different faults in this system have been shown (sections 3.2.5, 3.2.6 and 4.2.3) to have been active at various times between the latter part of M1 and the latter part of M2, after the MBG magma chamber itself solidified, whilst the largest fault of all in this system, the Glas Eilean fault, appears to be a reactivated pre - Tertiary structure (sections 2.5 and 3.2.6).

Fig. 7.2. Concentric Normal and Radial Compartmental faults active during M1 and the earlier part of M2 on the southern margin of the Hypersthene Gabbro. Earlier and later faults omitted.

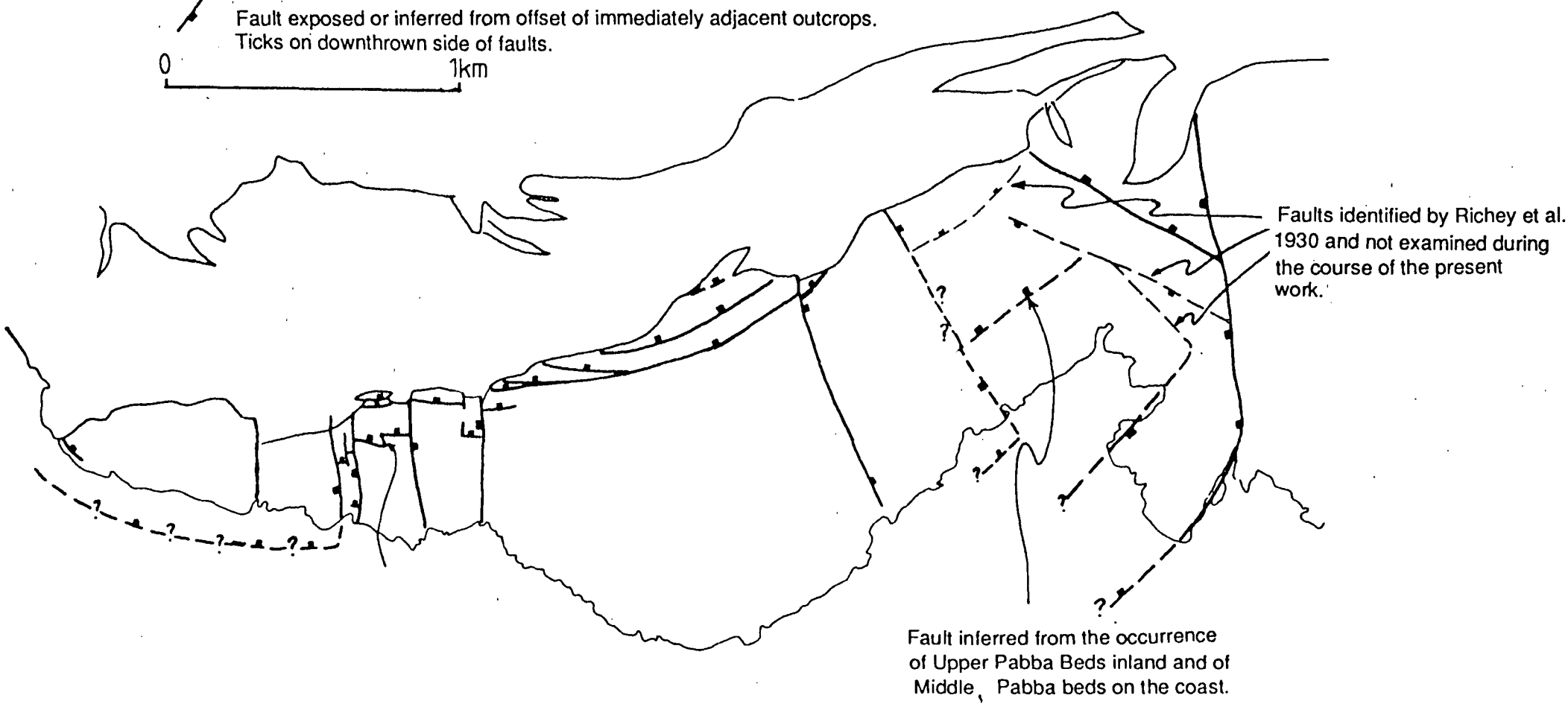

The amount of exposure of the fault system shown in Fig. 7.2 varies from adequate around Hill 210 and Druim na Gearr Leacainn to very poor between Tom na Moine and the western side of Glebe Hill. The faults in this area are taken from Richey et al. (1930), apart from one fault whose presence is inferred solely from the presence of Lower and Middle Pabba Beds rocks on the coast at the head of Kilchoan Bay and of Upper Pabba Beds inland: its geometry and age are unknown but its strike and the sense of movement on it are consistent with it being part of the concentric normal fault system.

The concentric normal faults shown in Fig. 7.2 fall into two main groups, an inner and an outer set. The former run from Tom na Moine to Hill 210, and may also include the faults on the eastern side of Tom na Moine (around Grid Ref. 475643) identified by Richey et al. (1930). The total amount of displacement on these faults is of the order of 200m (section 3.2.5.1). The outer set of faults mainly occur offshore or are very poorly exposed, apart from the southern end of the Glas Eilean fault. The total displacement on these is at least 300m (from the offset of the base of the Tertiary lavas across the Glas Eilean fault between Glebe Hill and Glas Bheinn (Fig. 1.2 & Map 1)) but the age of this movement is poorly constrained.

The total amount of post - emplacement, syn - MBG vertical movement on these faults is therefore likely to have been at least a few hundred metres and may well have been more than 500m, quite apart from any movements on faults which rooted out into the MBG magma chamber above the present level of exposure and have not been preserved. This movement could therefore have been as much as 25% of the thickness of country rocks above the MBG magma chamber, although it may have been little more than 5% . It seems very possible that the expression of the MBG magma chamber at the Tertiary surface may have included a caldera some hundreds of metres deep (although possibly partly or wholly filled in by extrusive rocks) and more than 8km wide, in the centre of the dome structure formed by the initial emplacement of the MBG magma chamber.

Although it has been described here as a concentric fault system, the system of faults shown in Fig. 7.2 shows one striking departure from radial symmetry. This is at its eastern end, where it runs into the north - south to NNW - SSE striking Glas Eilean fault, which is definitely not concentric to the Hypersthene Gabbro as a whole (Map 1). This asymmetry can be interpreted in two ways. Firstly, the fault is known to pre - date the MBG magma chamber and may be as old as the early Jurassic (

section 2.3). It may therefore have been reactivated, despite being oblique to the minimum principal stress direction associated with the other normal faults in Fig. 7.2. Alternatively, the stress field associated with the MBG may have been slightly asymmetric due to interaction of emplacement - related and regional stresses (section 7.4).

Since these faults dip inwards they must be associated with radial extension or stretching of the roof of the MBG magma chamber and tangential stretching of the footwalls in the horizontal plane. The actual amount of extension involved is difficult to estimate because of its sensitivity to the precise dip of the faults, being a cosine function of the dip angle (it decreases by a factor of two between an average dip of 60° and an average dip of 75°). Assuming a total downthrow on the faults of 500m, the radial extension can be estimated as between 500m and 250m across the entire width of the roof of the chamber, whilst the corresponding tangential extension around the circumference of the chamber is of the order of 1600 – 800m. In both cases this corresponds to an average strain of between 6% and 3% .

The tangential horizontal extension of the footwalls implied by movements on these concentric faults may have been accomodated in a variety of ways (the extension in the hanging wall is taken up by the downward movement of the tapered, upward - broadening central block). These include dilation of radial fractures, particularly the compartmental faults and also M1/early M2 radial dykes where these are present (principally in the Glendrian Bay area); normal faulting on those radial faults which are not quite perfectly vertical; dilation of the oblique segments present in certain cone sheets (Fig. 3.15A); and strike - slip motions on concentric faults in the footwall, both normal faults and the anastamosing thrust faults such as those at Glendrian Bay (section 3.2.2 and section 7.2.1.2. below)).

The stress field associated with the concentric normal fault system is relatively easily deduced: it has the minumum principal stress (σ_3) radial and sub - horizontal (or possibly dipping shallowly outwards in some cases), the intermediate stress σ_2 tangential to the intrusion and the maximum compressional stress σ_1 subvertical. The relationship of this stress field to processes in the MBG magma chamber is discussed in section 7.2.3.

7.2.1.2. Low angle concentric faults.

The faults considered in this section are the relatively common minor faults and fault zones on the northern margin of the MBG which dip inwards or outwards relative to the MBG at angles of less than 40° or so: conjugate sets of inward - and outward - dipping faults are generally present in any one area of outcrop. Displacements on these faults are individually much smaller (although very poorly constrained below an upper limit because they rarely offset recognisable lithological boundaries) than those on the concentric inward - dipping normal faults. However, they are much more numerous and commonly occur within broader zones of more - or - less cataclastically deformed rocks (Plates 7.1 and 7.2); average strains in regions such as the rock platform south east of Glendrian Bay may therefore be high but are again poorly known because of the lack of recognisable markers.

This lack of recognisable markers also makes it difficult to determine the sense of movement on these fault zones, particularly since the style of deformation is cataclastic and the sense of shear criteria used to determine motions in ductile shear zones are not present. However, large numbers of parasitic and anastamosing microfaults are visible in thin section which root down or up into the larger, through-going fault zones (Plates 7.3 and 7.4, both of thin sections cut in a vertical plane radial to the pluton). The vast majority of these microfaults show a thrust geometry and indicate radial shortening of the wall rocks. A few microfaults with apparently normal geometries are also visible in some thin sections, suggesting that periods of radial shortening may have alternated with periods of radial extension. However, the sections are not precisely orientated with respect to the margin of the pluton and it is possible that these rare extensional faults may represent oblique sections through extensional microfaults with transport directions tangential to the pluton: it should be noted that such concentric extension would be expected to be associated with radial thrusting because of the radially symmetric geometry of the fault system. The anastamosing geometries of the macroscopic fault zones also suggest that some movement tangential to the MBG magma chamber may have occurred on these faults.

Although it was possible to section only a few of these fault zones the available data, together with the data from the rare examples on the southern margin of the intrusion where it is possible to determine sense of motion from offsets, suggest that they are mainly associated with horizontal compression and vertical extension. Since the adjacent contact of the MBG magma chamber is steeply inclined or near - vertical this corresponds to radial compression and vertical extension of the chamber wall, implying the following orientations of the principal stresses:

Plate 7.1. Ultracataclastic fault zone in M2 felsite, south of Duin Bhain. Note that the host felsite is itself deformed, with a variety of brittle and more ductile deformation textures present. Sample 43L3. Crossed polars, field of view 14mm.

Plate 7.2. Recrystallised cataclastic fault zone (possibly with some ductile deformation) in matrix of rheomorphic breccia, Glendrian Bay. Fault zone dips outwards at c. 40°: section cut in vertical plane radial to contact with north - east to the left of the plate. Note small - scale thrusts with southwestward displacement of the hanging walls. Sample 47T3. Plane - polarised light, field of view 14mm.

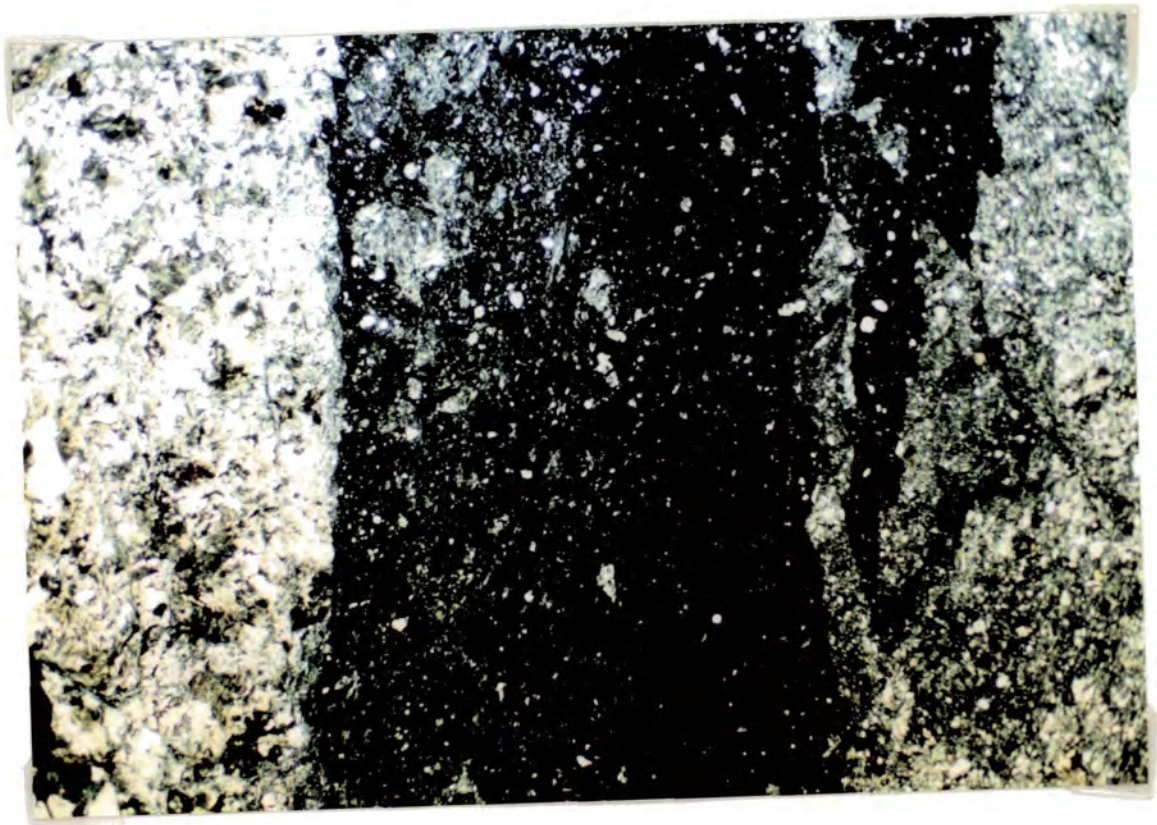

Plate 7.3. Microthrusts cutting banded cataclastic/ductile fault rock and merging into the main fault zones at their lower ends. South - dipping fault zone in M2 felsite, south of Duin Bhain. Section cut in vertical plane radial to the contact: north - south compression and thrusting of the hanging wall of the main fault to the north is indicated by the orientation of the microthrusts. Sample 43L3. Plane - polarised light, field of view 3.5mm.

Plate 7.4. South - west directed microthrusts in the hanging wall of the fault zone shown in Plate 7.2: note merging of these thrusts into the main fault zone, which acted as a sole thrust to the deformation in the hanging wall. Sample 47T3. Plane - polarised light, field of view 3.5mm.

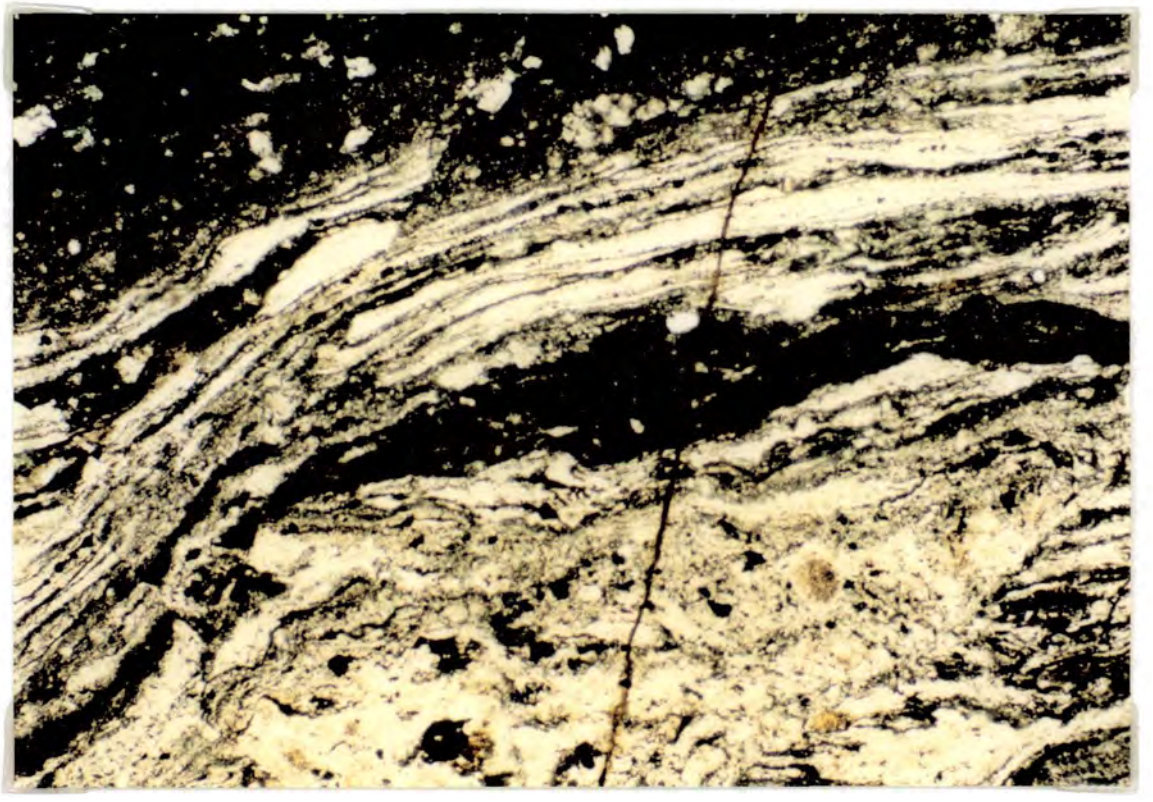

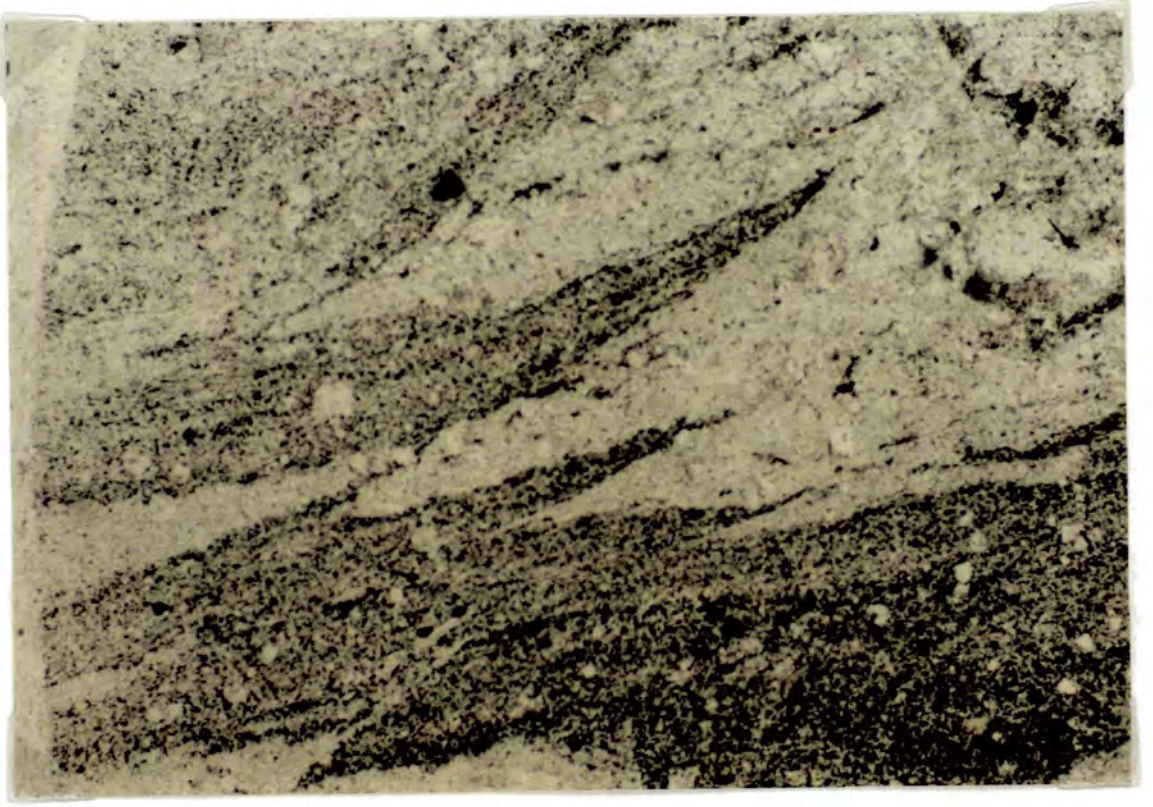

σ_1 Radial, near - horizontal

σ_2 Horizontal, tangential to contact

σ_3 Vertical, tangential to contact

All three of these stresses must have been compressive because otherwise pervasive dilation of the fractures would have taken place (see section 7.2.2). Instead, dilation of low - angle faults is only observed at releasing bends or jogs in the faults and is immediately obvious because the fractures are filled with basic magmas or with blocky - textured or drusiform hydrothermal mineral deposits where dilation has occurred.

7.2.1.3. Concentric high - angle reverse faults.

Faults with this orientation are very rarely associated with the MBG magma chamber, being much more common as bounding faults enclosing the Inner Series (section 3.3). Some examples which are definitely of M1 or early M2, pre - Group 2 cone sheet age do occur at the lower end of the Dubh Chreag gorge, however (section 3.2.5.4). The sense of movement on them apparently indicates that they are associated with a similar stress field to that associated with the low - angle reverse faults noted above, which raises the question of why faults with this orientation are developed at all around the MBG magma chamber. Two possible interpretations exist. Firstly, that they are concentric normal faults reactivated by the stress field associated with the low angle thrust faults. Alternatively, they may have been produced by deformation at the tips of large, unexposed cone sheets. Pollard & Johnson (1973) showed that the large stress fields around the propagating tip of an ellipsoidal cross - section pressurised crack (the closest tractable mathematical analogue to a blunt - headed sill) will tend to produce reverse faults at 30 to 60 degrees to the axial plane of the crack: steep reverse faults would be produced if the crack was itself inclined at 30° or so to the horizontal.

7.2.2. The emplacement mechanisms and associated stress fields of cone sheets and other minor intrusions related to the MBG magma chamber.

7.2.2.1 Cone sheets and other concentric minor intrusions.

The swarms of cone sheets around the Hypersthene gabbro have long been regarded as among the best examples of cone sheets known. However, field and petrographic data presented in section 3.2 (especially section 3.2.5.4) indicate that there are two major discrepancies between the generally - accepted model for these cone sheets and what is actually seen at outcrop:

1). The age relationships of the vast majority of the cone sheets indicate that they formed at the side of a steep - sided magma chamber, rather than above the apex of a deep - seated magma body, as proposed by Bailey et al. (1924) and Anderson (1936).

2). Rather than forming a single confocal set of near - planar sheets corresponding to tensile fractures (Anderson 1936), the cone sheets are the dominant set of a conjugate pair of sets of structures, the other half being the relatively rare outward - dipping sheet intrusions. These sometimes occur as different segments of the same intrusion (for example, that shown in Fig. 3.15B). The angle between the two sets was found to be in the range 50 – 70°. The cone sheets were also found to be markedly less regular and laterally continuous than is commonly supposed, apart from the rare post - Hypersthene Gabbro Group 3 cone sheet intrusions on the southern margin of the pluton. These later cone sheets can be traced laterally for over a kilometre in some cases (section 3.2.5.4). The tendency of the cone sheets, particularly those belonging to Group 2 as defined on the southern margin of the pluton and its equivalents elsewhere, to occur in dense, laterally discontinuous swarms (see Map 1 for their overall distribution) is also not a feature of the classical model for cone sheets.

Theoretically - based alternatives to the original interpretation of cone sheets as simple tensile fractures have been proposed by Robson & Barr (1964), Roberts (1970) and Phillips (1974). The models proposed by these workers differ in detail but all consider cone sheets to have formed by injection of magmas into shear fractures associated with radial compression of the wall rocks around a magma chamber rather than by injection of magma into tensile fractures. These models are supported by the occurence of conjugate intrusions to the cone sheets, and can be tested further by considering the orientation of the cone sheets and the outward - dipping sheet intrusions relative to the contact of the MBG in detail, and also by studies of the offsets and dilation directions of both

groups of intrusions.

Orientation. The vast majority of the cone sheets dip inwards at angles in the range 35° to 60°, whilst the outward - dipping sheets typically have slightly shallower dips. Obliquely - dipping segments occur in some of the intrusions (Fig. 3.15A) and the intersection of inward - and outward - dipping segments of the same intrusion in the one example where it can be measured accurately (Fig. 3.15B) also implies that the intrusion concerned is not perfectly concentric to the MBG magma chamber. However, as a first approximation it is apparent that these cone sheets are in much the same orientation as the low - angle thrust faults described in section 7.2.1.2. A number of cone sheets of various ages show much steeper dip, however, similar to those of the inward - dipping normal and reverse faults described in sections 7.2.1.1 and 7.2.1.3 (see Fig. 7.3, below; also Fig. 3.14).

Dilation directions. Methods of determining the direction of opening of dilatant fractures have been decribed by Delaney & Pollard (1981), Pollard et al. (1982) and Pollard & Nicholson (1985). All employ the offsets of markers on opposing surfaces of the sheet (such as intersections of contacts with bedding or the contacts of older intrusions and matching irregularities in the contacts) to give the dilation direction, which is parallel to the local σ_3 direction at the time of intrusion.

The sheet intrusions under consideration here can be divided into four groups, of which the first is by far the most common, all of which show distinctive dilation directions relative to the MBG contact and/or to their own margins:

1). Sheets with moderate inward or outward dips and dilation directions which are near - vertical (for example, the intrusion shown in Fig. 3.15B) to steeply outward - dipping (Fig. 7.3.1). These dilations are sub - parallel to the adjacent contact of the MBG and bisect the obtuse angle between conjugate pairs of sheets or segments of the same intrusion, supporting the interpretation that cone sheets occupy shear fractures associated with radial compression (see references above).

2). Irregular sheets and veins occupying dilatational segments of low - angle fault zones. Where senses of dilation and offset can be determined, these are associated with inward -

Fig. 7.3.1. Irregular cone sheet at Grid Ref. 45356309 (W. side of Dubh Chreag gorge) showing dilation in a steeply outward - dipping direction. Note slight variation in dilation direction across the outcrop: average plunge of the dilation direction is 64 south, parallel to the MBG contact to the north.

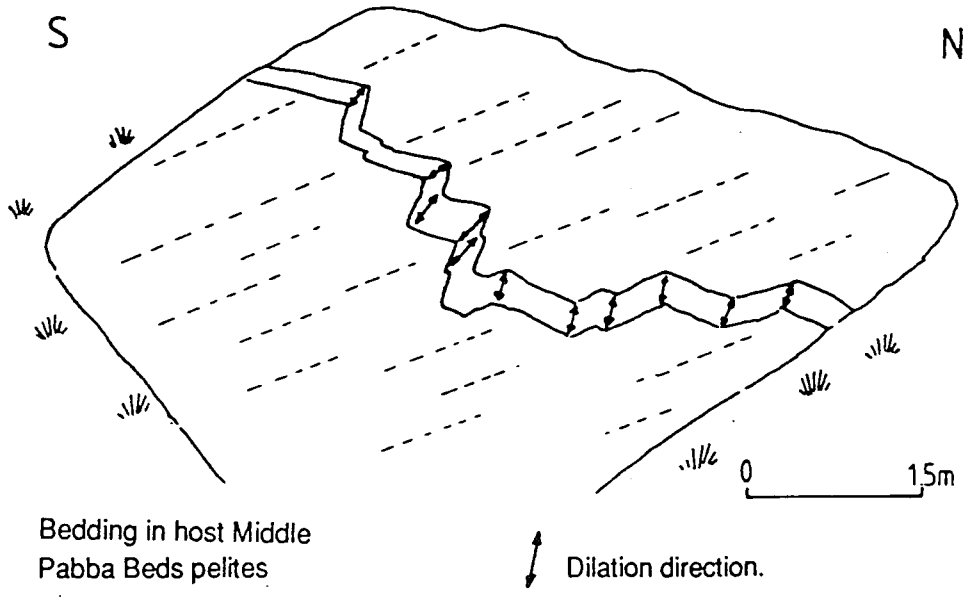

Fig. 7.3.2. Irregular cone sheets showing thrust displacements, west side of Maol Bhuidhe (Grid Ref. 45536267). The outcrop is slightly oblique to the likely transport direction.

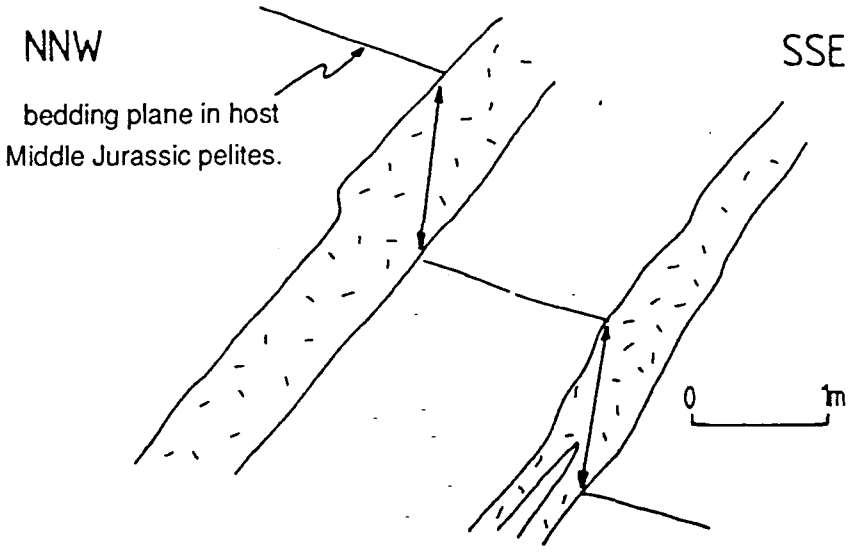

Fig. 7.3.3. Steeply - dipping cone sheets with near - horizontal dilations exposed in north - south trending crag, south of the Hypersthene Gabbro (Grid square 451631, S.E. of Hill 210).

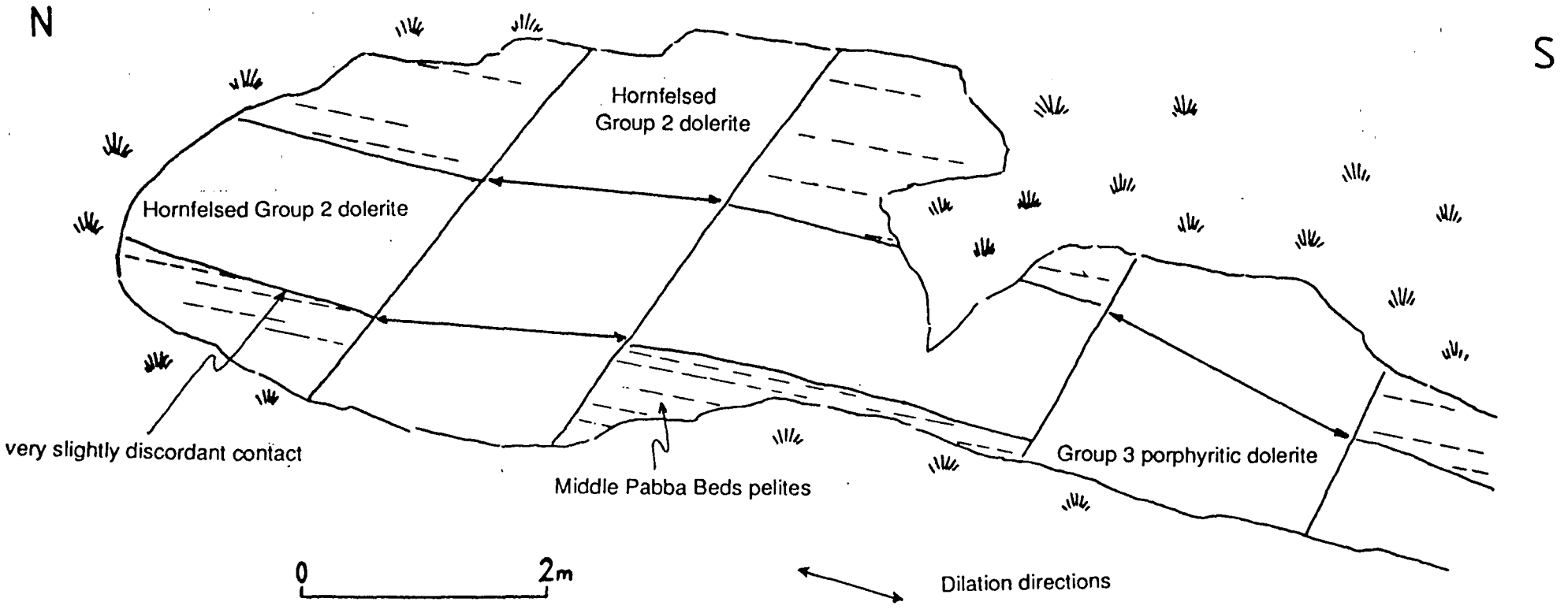

dipping dilations associated with thrust displacements of the wall rocks (Fig. 7.3.2).

3). The steeply - dipping cone sheets found show near - horizontal or shallowly inward - dipping dilation directions (Fig. 7.3.3), implying that σ_3 was almost radial to the contact at the time of their formation. The larger M2 felsite intrusions along the northern margin of the MBG, south and wet of Duin Bhain (Map 3) may also be of this type.

4). Obliquely - dipping segments of sheet intrusions appear to show the same near - vertical dilation direction as concentric segments of the same intrusions (Fig. 3.15A).

With only a few exceptions, therefore, the cone sheets do not seem to be associated with large shear displacements, offsets across them being mainly dilational. With the exception of the steeply - inclined sheets, the inferred stress field associated with their emplacement is:

σ_1 Radial, subhorizontal

σ_2 Tangential, subhorizontal

σ_3 Tangential to subvertical, always in the vertical plane

As noted by Richey et al. (1930), the emplacement of the cone sheets implies a total uplift of the centre of the complex, relative to its margins, of several hundred metres: the age relationships discussed in Chapter 3 show that much of this displacement was associated with vertical expansion of the MBG magma chamber. Given that the chamber was no more than a few kilometres deep, this implies a relative dilation of the order of 20% . However, the fact that the cone sheet swarms die out laterally (Map 1) implies that the uplift was not always uniform around the pluton. This is confirmed by the geometry of a number of cone sheets examined in radial cliff sections (Fig. 7.4.1 and 7.4.2). These show stepwise offsets and fractured bridge structures which indicate that the intrusions initially formed as a series of offset en echelon fractures which subsequently expanded, causing fracture of the bridge structures and formation of a continuous but irregular sheet intrusion. It should be noted that the margins of the sheet shown on the right of Fig. 7.4.1 do not match up: this could be due to stoping of the dyke walls but could alternatively be interpreted as evidence for shear displacement across the intrusion in a direction oblique to the cliff face (and also oblique to the wall of the pluton). Similar structures have been studied in dyke swarms by Delaney & Pollard (1981), Pollard et al. (1982) and Pollard & Nicholson (1985) (see also the discussion of

Fig. 7.4.1. Detail of bridge structures in cone sheets exposed in western side of Dubh Chreag gorge around 455628 (see Fig. 3.16).

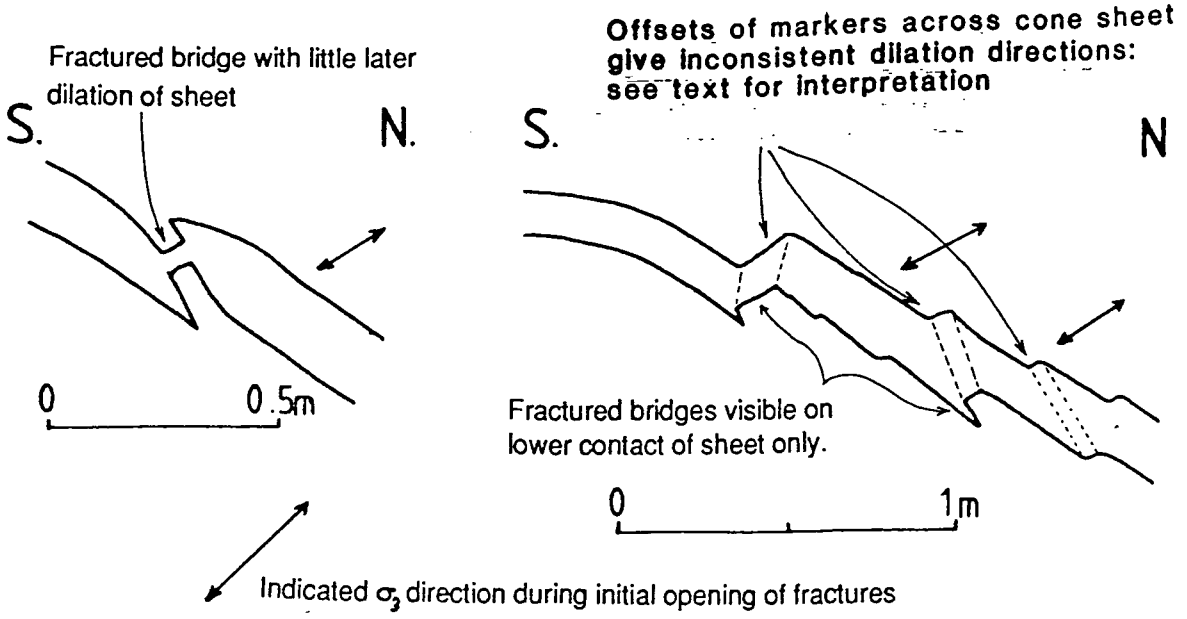

Fig. 7.4.2. Details of poorly preserved fractured bridge structures in cliff at S.W. end of Maol Bhuidhe, Grid ref. 460624 approx.

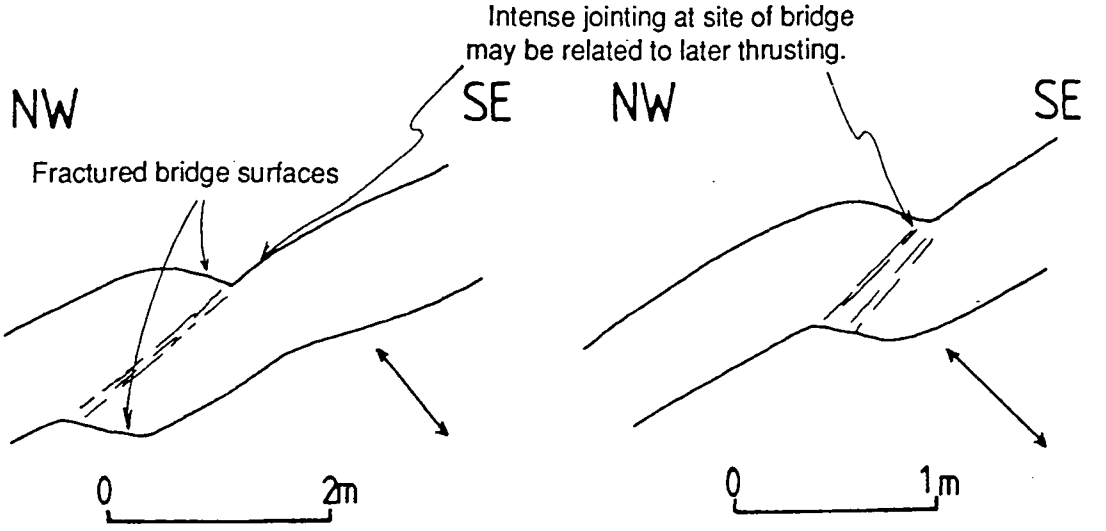

bridge structures in general by Gamond 1987). All of these workers concluded that **straight** bridge structures in dyke swarms formed as an initially planar sheet intrusion propagated into a region where the local stress field was oblique to that associated with the sheet intrusion itself and broke up into a series of en echelon intrusions with elliptical cross - sections and long axes parallel to the local σ_3 and perpendicular to the propagation direction (Fig. 7.5, modified after Delaney & Pollard 1981). The occurrence of such structures in cliffs which are approximately radial to the contact of the MBG has two implications. Firstly, the cone sheets shown in Fig. 7.4 must have propagated in a direction oblique to the contact of the MBG. Secondly, the inward - verging offset of the en echelon fracture surfaces implies in both cases that the sheets propagated into a region where the wall rocks were contracting tangential to the contact (i.e. the chamber was deflating). Although inconsistent with theoretical models based on instantanous stress fields which do not allow for the effects of finite strain, this is perhaps as would be expected given that the cone sheets were fed from the MBG magma chamber (section 4.3): as magma entered the cone sheet fractures, the volume of the chamber would decrease slightly unless the resistance to flow of magma from its source region was no greater than that associated with the flow of magma into the cone sheets. Studies of the time scales of magma replenishment in active magma reservoir systems (Tryggvason 1977; Ryan 1988) suggests that this is unlikely, and that the immediate impetus for injection of magma into minor intrusions around large magma bodies comes from release of elastic strain energy stored in the country rocks around the magma body. This elastic strain is considered to have been built up by magma input from depth over a relatively long period of time prior to the intrusion event.

A tentative interpretation of the formation of the majority of cone sheets and other concentric intrusions which show vertical dilations is therefore as follows. Input of magma from depth into the MBG magma chamber caused the chamber to expand, storing elastic strain in the wall rocks and producing a network of incipient shear fractures in a stress field as noted above, with σ_3 consistently vertical because of the proximity of the magma chamber to the surface, which would tend to weaken the resistance of the wall rocks to vertical dilation or extension. Once the excess of magma pressure in the chamber had risen to the point where σ_3 became tensile, the incipient shear fractures would tend to dilate, allowing magma to enter them under pressure. Once magma was present in the crack its further evolution would be dominated by the pressure of that magma and it would tend to dilate rather than undergo shear displacements (see Julian & Sammis 1987; Hill 1977). The complex, non - symmetric stress field implied by the occurence of oblique propagation of cone sheets

Fig. 7.5. Segmentation of a cone sheet intrusion (viewed from above and to one side) caused by changes in the stress field as the sheet propagated laterally. Modified after Delaney & Pollard 1981.

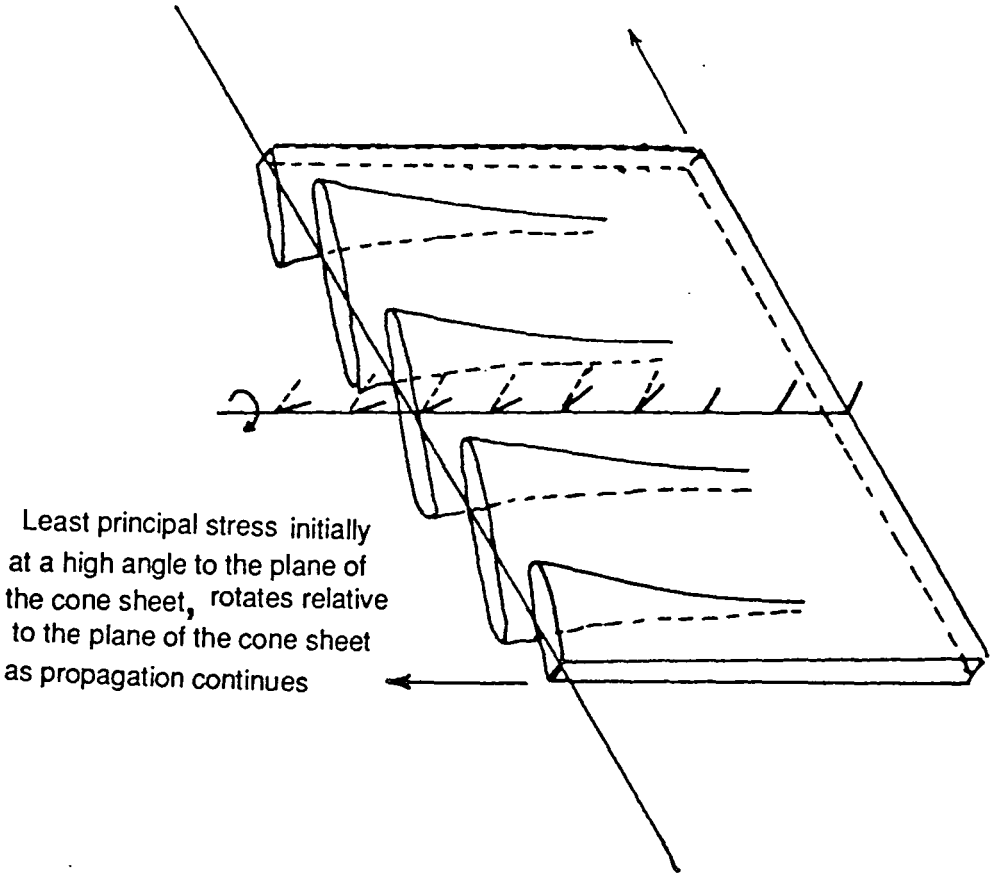

← Propagation direction.

and the effects of fluctuating P_{excess} in the MBG magma chamber as the cone sheets grew would complicate this picture but would not alter the overall conclusion that the majority of cone sheets occupy fractures initially produced as incipient shear fractures with the same orientation as the low - angle faults present in some areas of the contact.

The inference that σ_3 was vertical and tensile during the emplacement of the cone sheets when magma was present in the fractures may help to account for the curious lack of compressive deformation associated with M2 cone sheet emplacement in the Marginal Border Group itself in many areas, especially in the Glendrian Bay sector of the MBG where numerous thrust faults are present in addition to the cone sheets. M2 deformation in these rocks is limited to the development of subhorizontal unchilled veins of ferrogabbroic to granitic composition (sections 3.2.2 and 3.2.3). The orientation of these is consistent with vertical dilation of rocks containing an interstitial melt phase, which would cancel out the load pressure on the rocks and thereby promote tensile rather than shear failure. Unless it is supposed that the distribution of strain in the contact zone rocks is very heterogenous, however, and that the exposed outcrops happen to be areas of low strain, the contact zone rocks are remarkably undeformed, given the large amount of early M2 deformation in the country rocks. One possible explanation of this may be that much of this deformation occurred very early in M2, before solidification of the MBG contact zone but after quenching of the country rocks.

The steeply - inclined, near - horizontally dilated concentric intrusions may bear a similar relationship to the steeply dipping concentric normal faults to that shown by the more shallowly dipping cone sheets and faults. It should, however, be noted that in contrast to the common occurrence of dolerite veins and lenses in the thrust faults and occasional evidence for shearing at the margins of dolerites (Plate 3.30) evidence for magma injection up these faults is very rare, the only certain example being in the M2 faults on the southern side of Druim na Gearr Leacainn, which contain strongly chilled porphyritic basalt veins around Grid Ref. 46526368.

7.2.2.2. Radial dykes.

Although the concentric geometry of the faults described in the previous sections implies that extension in the horizontal plane in a direction tangential to the margin of the MBG magma chamber

must have taken place, in the footwalls of the faults at least, the radial dykes which are a common feature of many central intrusive complexes in the British Tertiary province and elsewhere are almost entirely absent from the rocks around the Hypersthene Gabbro. As was shown in section 3.2, the only radial dykes of M1 or early M2 age are the rooted dykes at Glendrian Bay (section 3.2.2), although later radial dykes are quite common in that area (Map 2) and also occur at An Acairseid, on the opposite side of the pluton (Map 4). The stress field associated with these dykes is quite distinctive:

σ_1 Radial; orientation in the radial vertical plane unknown

σ_2 Radial; orientation in the radial plane unknown

σ_3 Tangential to the MBG magma chamber; **Horizontal**

and is only developed in the Glendrian Bay area. Possible reasons for this are discussed in the following section. A similar stress field may have produced the radial master fractures (section 5.3) which admitted the hydrothermal system(s) which subsequently self - propagated to produce the sudden cooling of the M1 aureole and the solidification of (at least) the contact zone of the MBG magma chamber.

7.2.3. Causes of variation in the stress field around the MBG magma chamber during M1 and the early part of M2 and the relationship between magma pressure in the magma chamber and episodic melting at the walls of the chamber during the latter part of M1.

The wide variety of fault and minor intrusion orientations and senses of displacement discussed in the preceding sections implies that the stress field around the MBG magma chamber after its emplacement showed marked variations over short periods of time (particularly in the orientation of σ_1 and σ_3 in the vertical radial plane). In addition, whilst σ_2 was consistently horizontal and tangential to the magma chamber around much of its circumference, σ_3 appears to have had this orientation at times in the Glendrian Bay area. This latter area is also anomalous in that low - angle thrust faults associated with radial shortening are much more common there than elsewhere around the pluton.

Both of these latter features may be accounted for by supposing that the principal stresses in a plane

tangential to the contact of the MBG magma chamber were both lower in the Glendrian Bay area than elsewhere around the pluton, and in particular that the horizontal tangential stress was much lower than σ_1 (radial) and lower than the vertical tangential stress at times. As a result, compressive shear failure of the rocks along low - angle faults would occur at lower P_{excess} in the magma chamber, and therefore under compressive vertical σ_3 (note that shear failure of rocks occurs when some critical **deviatoric** stress, proportional to the differences between principal stresses, is exceeded: see discussion of shear failure criteria in Hobbs et al. 1976). In normal fault zones it is only the deviatoric stress in the plane of the transport direction which is important in this respect, but because radial compression around the MBG magma chamber must have involved horizontal tangential extension, perpendicular to the main transport direction, a reduction in σ_2 relative to σ_1 would also tend to promote shear failure. Elsewhere around the magma chamber, shear failure appears to have only taken place when the excess pressure in the magma chamber was so high that dilation of the shear fractures and cone sheet emplacement, rather than thrust faulting, was produced.

One possible reason for the differences in the stress field around the MBG magma chamber between the Glendrian Bay area (and, to a lesser extent, the Duin Bhain area where thrust faults are relatively common, although radial dykes are not present) and the rest of the contact is that the curvature of the contact in the horizontal plane (and therefore the horizontal stress produced by a given P_{excess}) is greater in the Glendrian Bay area. This does not, however, account for the numerous occurrences of thrust faults south and west of Duin Bhain and is inconsistent with the lack of radial dykes in the Glebe Hill area, where the outer contact of the MBG takes another sharp turn. It appears more likely that the occurrence of dykes and thrust faults in the Glendrian Bay and Duin Bhain areas reflects an externally - applied regional tectonic extension in a north - west to south - east direction. Further discussion of the origin of this extension is deferred to section 7.4 as it also appears to have affected the Inner Series (section 7.3, below).

Although the results of the present work confirm the causal relationship between cone - sheet formation and high excess magma pressure in the chamber around which the cone sheets form in the case of those cone sheets which show vertical dilations, the case of those sheets associated with the MBG magma chamber which show horizontal dilations (for example, the older of the two steeply inclined sheets shown in Fig. 7.3.3) is less clear. The dilations imply that σ_3 was almost radial to the contact, suggesting that the magma chamber was contracting, and yet the inward dip of the

sheets still imply that extension of the roof was taking place as the sheets dilated.

A similar problem concerning the relationship of deformation to magma pressure applies in the case of the inward - dipping normal faults (section 7.2.1.1). The relationship between the latter and pressure in the magma chamber is particularly important because of the control which the concentric normal faulting exerts upon the episodic wall rock melting process (sections 3.2 and 4.2). The interpretation of the concentric normal fault system as the lower termination of a caldera fault system suggests, by analogy with active basaltic caldera volcanoes, particularly those in the Galapagos (Simkin & Howard 1970; McBirney & Williams 1969), that episodes of concentric normal faulting (expressed at the surface by caldera collapse) are associated with the draining or deflation of an overpressured magma chamber by lateral or flank intrusions or eruptions. The following sequence of events is envisaged as leading to an episode of concentric normal faulting or intrusion of steeply - dipping, horizontally - dilating concentric intrusions:

1). Magma input to the chamber during a period of high magma pressure in the source region at depth produces inflation of the magma chamber which is accomodated by elastic strain in the wall rocks, together with thrust faulting and cone sheet emplacement.

2). Drainage of magmas into cone sheets, other intrusions or surface lava flows reduces magma pressure in the chamber and a reduction in chamber volume occurs. This is accomodated by subsidence of the roof of the chamber along concentric normal faults.

3). Subsequent re - inflation of the chamber may have exploited the lines of weakness represented by concentric normal fractures, leading to injection of horizontally - dilating cone sheets into these fractures.

This last point is not fully satisfactory as there is no evidence of previous normal faulting along the observed steep - sided intrusions. A possible alternative explanation for those emplaced immediately after the end - M1 quenching event, such as the M2 felsite intrusions at Duin Bhain, is that they were produced by the differential stresses set up as the upper parts of the chamber walls and the roof cooled and contracted whilst at the same time the rocks lower down the wall of the chamber were still undergoing melting (section 4.2.2). Thus the apparent paradox of radial dilation at a

time when P_{excess} was negative may have been produced by greater amounts of contraction of the wall rocks than of the chamber. This would result in tensile stresses being set up in the wall and roof of the chamber even if the chamber was itself contracting.

Of greater significance, however, is the implication of the above model that **episodes of wall rock melting were triggered by fluctuations in P_{excess} in the magma chamber**, specifically periods of low magma pressure following partial drainage of the chamber as the wall rocks deformed in response to an influx of magma from depth.

7.3. The emplacement of the gabbronorite sheets of the Inner Series.

The gabbronorite sheet intrusions and granular dolerites of the Inner Series were considered by Walker (1975) and Wells (1978) to be fundamentally similar to other cone sheets, albeit rather larger and more closely spaced, both in time of emplacement and spatially. However, the present work has shown that there are some fundamental differences in the geometry and mode of emplacement of the gabbronorite sheets in the Inner Series and of the cone sheets outside the intrusion, as follows:

1). All the gabbronorite sheets and most of the granular dolerite sheets have only shallow inward dips, of between 10 and 30 degrees. More steeply dipping granular dolerites are confined to the inner edge of the Inner Series outcrop on the southern margin of the intrusion between Beinn na Seilg and Stacan Dubha (see Map 1).

2). There are no conjugates to intrusions in the Inner Series, either with steep inward or steep outward dips, except perhaps for the syn - gabbronorite faults which form most of the periphery of the Inner Series and are inclined at an angle of 60^{o} or so to the intrusions. These may, however, have been produced by other mechanisms (see below).

3). There are very few low - angle faults associated with the Inner series rocks (the best examples occur close to the contact with the Marginal Border Group at Ardnamurchan Point, at 41776738, where a north - south striking conjugate pair of granular fault zones is present); most outcrops contain none at all.

The Inner Series sheet intrusions do however share one feature of the older cone sheets outside the intrusion, which is that they characteristically occur in swarms. This is most easily seen in the case of the granular dolerites, particularly dense swarms of which occur at the western end of Beinn na Seilg (Grid Ref. 456642) and on Stacan Dubha, around Grid Ref. 464643.

The association of the gabbronorites with inward - dipping pyroxene hornfels facies shear zones with reverse senses of movement (see Map 4 and Fig. 3.22, section 3.3.2) implies that their emplacement was accomplished by uplift of the roof rocks of these intrusions relative to the rocks outside the Inner

Series, coupled with radial compression. Stoping (Plate 3.80) and host - rock assimilation may also have contributed to the emplacement of the gabbronorite sheets. The minimum total amount of uplift involved is given by the sum of the known throw on the peripheral fault system and the thickness of the exposed sequence inside these faults (width of gabbronorite outcrop divided by average dip) and is of the order of 400 – 500m. The true amount of uplift may have been greater, particularly since a number of reverse faults occur entirely within the Inner Series (Fig. 3.29).

The stress field associated with the emplacement of the gabbronorite sheets can, as with the cone sheets, be deduced from the geometry of the intrusions and the peripheral faults:

σ_1 Radial, subhorizontal to shallowly outward - plunging.

σ_2 Tangential, parallel to strike of faults.

σ_3 Approximately vertical.

This is similar to the stress field associated with emplacement of cone sheets around the MBG magma chamber and suggests that a large axial magma body, perhaps with a less steeply - dipping outer contact, may have been present during the emplacement of the Inner Series, in the region now occupied by later and unrelated (section 6.3.2) intrusions of Centre 2 of the Ardnamurchan complex (Figs. 1.2 and 1.3). This stress field could also explain the consistent orientation of the laminated bands in the gabbronorites and of the metasomatic pyroxenites at Sanna, as interstitial melts would be expected to migrate along subhorizontal fractures if these were present. It should be noted that the stress field noted above refers only to the rigid matrix of the partially molten gabbronorites and is not inconsistent with the occurrence of vertical compaction of the gabbronorites due to residual melt expulsion, although it might influence the precise path taken by the residual melt (c.f. Spiegelman & McKenzie 1987; this study refers to melt migration in the mantle under the influence of a deviatoric stress field but the governing equations are the same whether the matrix is mantle material or compacting plutonic rocks (McKenzie 1984)).

The radial dykes at An Acairseid (Map 4) suggest that σ_3 was at times tangential to the Inner Series in this area, and orientated north - west – south - east, mirroring the situation at earlier and later times in the Glendrian Bay area on the opposite side of the intrusion. The Inner Series shows a number of other departures from perfect radial symmetry, although its horizontal cross - section is approximately equidimensional. These are the development of faulted contacts on the northern

and southern margins of the pluton in particular, the restriction of Inner Series gabbronorite sheet intrusions in the MBG to the western and south - western sectors of the Hypersthene Gabbro, and the occurrence regional - trend faults striking 140° – 150° along the western sector of the Inner Series (section 3.4.7). As with the asymmetry of the Marginal Border Group and the deformation around it, the asymmetry of the Inner Series may be explicable in terms of the addition of a regional stress field to that assoicated with magma inputs to the pluton. The occurrence of northeast – southwest striking dykes at An Acairseid also suggests northwest – southeast extension. However, extension in this direction appears to be inconsistent with the observed and inferred reverse faulting on the northern and southern margins of the intrusion, suggesting that the regional stress field may have varied with time (see section 7.4). The reasons for the development of reverse faulting rather than emplacement of sheet intrusions into the adjacent MBG rocks on the northern and southern margins is not clear but may reflect reactivation of pre - existing normal faults, produced by earlier north - south extension (see section 7.5, below), and/or shear failure at lower P_{excess} in tha magma chamber (and therefore compressive vertical stress) due to the addition of north - south regional compression to the radial compression produced by input of magma into the Inner Series.

The exposed part of the Inner Series occurs entirely within the earlier inward - dipping normal fault system. This implies that uplift of the Tertiary land surface associated with the emplacement of the Inner Series gabbronorites would have taken place within the caldera structure postulated in section 7.2.1.1. The surface expression of the emplacement of the Inner Series would therefore have been resurgence of the postulated caldera, analogous to that deduced for the Rhum complex by Emeleus et al. (1985) and Smith (1987).

7.4. The regional stress field of the British Tertiary Volcanic Province and the asymmetry of the Hypersthene Gabbro.

The discussion of the stress fields around the various components of the Hypersthene Gabbro in the preceding sections of this chapter have shown that it departs from the ideal radial or cylindrical symmetry assumed in most theoretical studies of deformation around shallow magma chambers (Robson & Barr (1964), which explicitly considers regional stress fields around pressurised cavities, being the most notable exception). Specifically, the tangential stress in the horizontal plane appears to have been least, on average, on the northeastern and southwestern margins of the pluton at many stages in its history. The clearest expressions of this are the radial dyke swarms which indicate that this was commonly the least principal stress direction in these areas of the contact and was at times tensile.

This is best interpreted as indicating that there was externally - imposed extension across the site of the pluton during its evolution, in a northwest to southeast direction. The dominant extension direction in the BTVP, as inferred from the orientation of the dyke swarms, is however WSW – ENE, almost at right angles to the inferred extension across the Hypersthene Gabbro (Speight et al. 1982; England 1988b).

In addition to the main WSW – ESE dilation produced by the dyke swarms, however, both Speight et al. (1982) and England (1988b) identified smaller swarms with north - south to NNE – SSW trends. These were used by England (1988b) to infer dextral strike - slip motions across the BTVP in addition to the dominant extension. Strike - slip motions (both dextral and sinistral, on different faults or even on the same fault at different times) are certainly present on regional - trend faults around the Hypersthene Gabbro (sections 3.2.5.4 and 3.2.6) although all the definite examples are either earlier or later than the pluton. The pyroxene - hornfels facies granular shear zones cutting the Inner Series along the western edge of Ardnamurchan link into known strike - slip faults to the south east but it is not known if these faults were active as strike - slip faults during emplacement of the Inner Series.

Given the presence of a dextral strike - slip component of movement across the province as a whole,

the site of the Hypersthene gabbro can be plausibly interpreted as a releasing jog or pull - apart in the regional fault system, with dextral movement on the Glas Eilean fault on its eastern side being transferred west to hypothetical faults offshore from the western tip of Ardnamurchan (although it should be noted that the NW - SE trending faults in western Ardnamurchan could be part of this swarm). The rhombohedral shape of the Inner Series, the distribution of radial dykes and of syn - MBG thrust faults are all consistent with this (Fig. 7.6). However, the occurrence of NW – SE to NNW – SSE trending faults with sinistral offsets, the obliquely dipping sheet intrusions with north - west or south -east dips if the dilations on these are vertical like those of the other low - angle sheet intrusions (sections 3.2.5.4 and 7.2.2), and the inference from the distributions of faulting and intrusion around the Inner Series (section 7.3) that north - south compression may have occurred across the site of the pluton. This suggests that the regional stress field may have been reversed, producing sinistral motion, at certain times during the period in which the pluton was emplaced..

The inference that the site of emplacement of the Hypersthene Gabbro was influenced by the occurrence of a releasing offset in the regional fault system does not imply that the intrusion can be considered to be have been passively emplaced: the structures discussed in this chapter clearly imply that this is not so. Furthermore, there is no evidence for large - scale (of the order of several kilometres) strike - slip displacements along the strike of the regional dyke and fault trend, either in Mull to the south - east, or in the Sea of the Hebrides to the north - west (Binns et al. 1974). The Hypersthene Gabbro appears to have made almost all of the space it now occupies by actively deforming the rocks around it (by doming, central uplift along concentric faults, and dilation of the wall rocks by cone - sheet emplacement; radial expansion by thrust faulting appears to havebeen a minor process by comparison with the preceding). Hutton (1988) pointed out that any intrusion must be regarded as forcefully emplaced if the rate of magma input, expressed as a dilational strain rate, is greater than the externally imposed tectonic dilational strain rate, whether the latter is positive or negative. However, the presence of extensional stresses in the walls of the Hypersthene Gabbro magma chambers means that the magma in the chambers would have to do less work (in the physical sense) in producing a given expansion of the chambers than in similar chambers emplaced in a compressive offset or in unstressed rocks. This effect would be expected to produce a tendency for large, long - lived magma bodies to occupy releasing offsets and other sites of localised extension as magmas ascending through the crust would tend to be diverted preferentially into such bodies.

Fig. 7.6. Interpretation of the asymmetry of the Hypersthene Gabbro in terms of emplacement at a releasing offset in a regional strike - slip fault system.

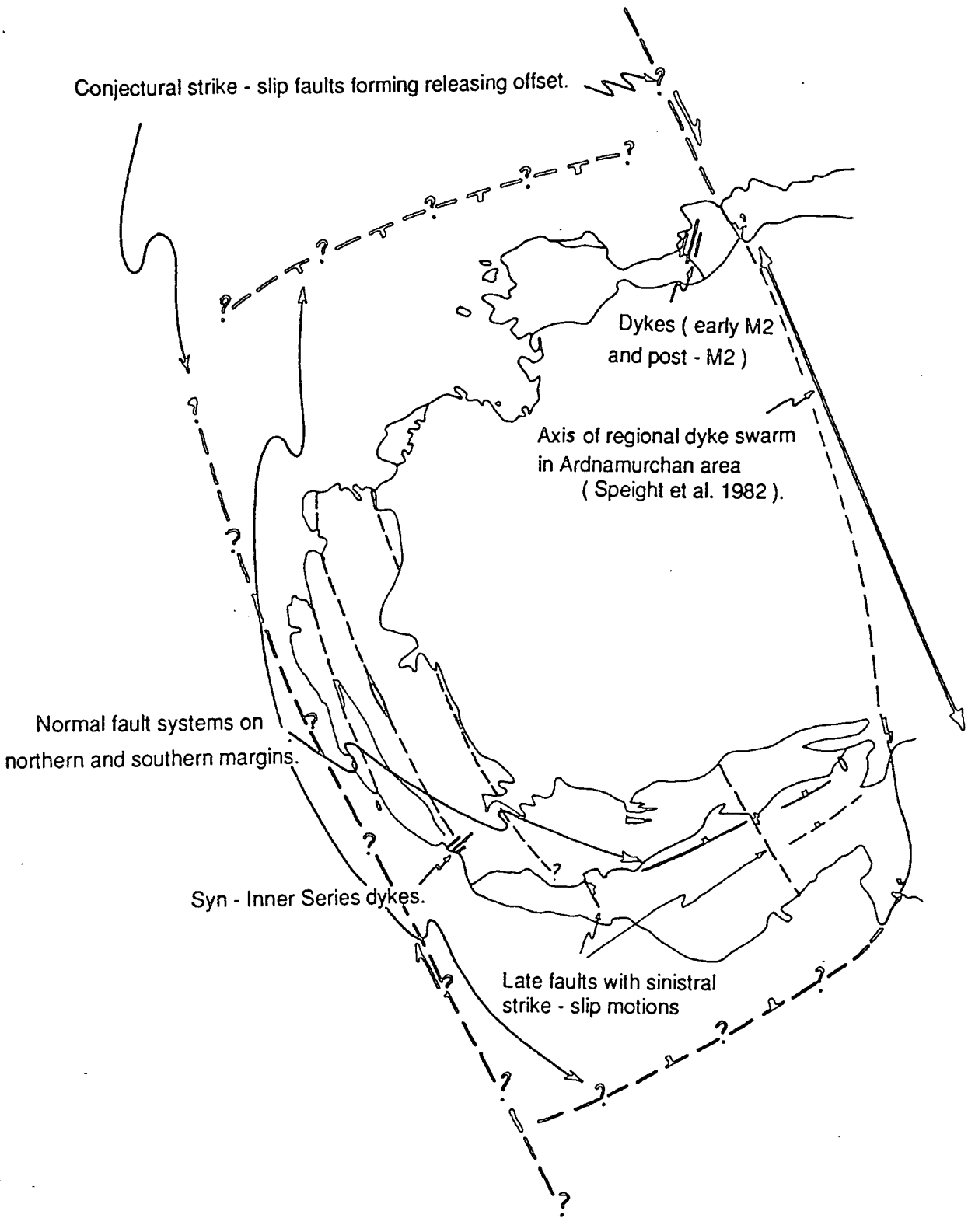

7.5. The structural development of the Hypersthene Gabbro.

The inferred stress fields and emplacement mechanisms discussed in this chapter can be combined with the age relationships discussed in Chapter 3 to produce an overall structural history of the Hypersthene Gabbro which can be divided into five stages:

1). Initial emplacement of a large sill complex. This probably formed in the stratified and/or tectonised rocks at or above the Moine Thrust zone, where the presence of mechanically contrasted layers may have promoted sill formation through concentration of compressive stresses in competent horizons (Gudmundsson 1988). The subsequent development of these sills certainly implies that they were emplaced into well - stratified rocks capable of bending as a series of layers separated by planes of weakness (Pollard & Johnson 1973). The development of a sill complex would also be favoured by a high magma input rate relative to the rate of crustal dilation, as otherwise the magma would be diverted into regional dyke swarm intrusions. The initial formation of the sill complex may therefore have been triggered by an increase in magma input rate or by a decrease in crustal extension rates; the latter is implied by the dominance of strike - slip in the externally - imposed stress field, whilst the change to extreme tholeiitic magma compositions with the development of the MBG (and. by implication, an increase in the rate of melt release from the underlying mantle (McKenzie & Bickle 1988)) suggests that increased magma fluxes may also have been important in producing sills.

2). Growth of the sill complex to the critical limit, (Pollard & Johnson 1973) followed by doming of the roof of the largest sill(s). This produced a dome structure some ten kilometres across, with an amplitude of at least several hundred metres and dips of up to 35^{o} towards its periphery. It is likely that this dome developed a flat top as the underlying magma body grew. This laccolithic intrusion may have provided the heat source for the latter stages of M0.

3). Failure of the roof of the laccolith along concentric outward - dipping normal faults. Uplift of the central block by as much as a kilometre followed, emplacing the MBG magma chamber more or less in its present position. Although smaller outward - dipping

normal faults are present around the MBG the intrusion itself is not now bounded by fault zones. These may have been removed by subsequent thermal or, more likely, thermo - mechanical (Furlong & Myers 1985) erosion of the wall of the intrusion early in M1 (note that it was shown in Chapter 5 that the wall of the magma chamber must have been essentially fixed in position for most of M1).

4). Alternating expansion and contraction of the MBG magma chamber through M1 and the early part of M2. This was accomodated primarily by emplacement of cone sheets, which may have produced a vertical dilation of the wall of the chamber of as much as 700m – 1000m, and by subsidence of the roof and upper walls of the chamber along concentric normal faults by several hundred metres. Subsidence of the roof of the chamber may well have produced a caldera structure in the centre of the dome on the surface above the intrusion. Radial compression of the walls of the chamber appears to have been limited (strains of 3 – 6%), except where thrust faulting took place as a result of reduction of the smaller principal stresses by regional transtension in a direction tangential tothe contact. The assumption that the M1 aureole was not subsequently compressed, made during the course of the thermal modelling in section 5.2, is therefore justified except in the Glendrian Bay area, which is of course the area in which later compression of the M1 aureole was invoked to explain its markedly smaller thickness. Episodic partial melting during M1 appears to have been triggered by falling magma pressure in the chamber after periods of inflation, which led to concentric normal faulting and the formation of wedges of country rocks projecting into the magma chamber, whilst the tangential extension which most probably led to master fracture formation and hydrothermal quenching was associated with simple chamber expansion.

5). Emplacement of the Inner Series. This appears to have occurred by incremental central uplift as gabbronorite sheet intrusions or intrusion swarms, truncated at their outer edges by reverse faults, were emplaced into the Inner Series and the surrounding rocks. The regional stress field appears to have varied considerably during this period, with both sinistral and dextral motions and therefore alternating compression and extension across the Inner Series.

8. CONCLUSIONS: INTERRELATIONSHIPS BETWEEN STRUCTURAL, THERMAL AND MAGMATIC ASPECTS OF THE EVOLUTION OF THE HYPERSTHENE GABBRO AND THEIR IMPLICATIONS FOR MAGMATIC PROCESSES IN OTHER UPPER CRUSTAL MAGMA CHAMBERS.

The present work has involved the study of examples of two distinct types of upper crustal (and almost certainly subvolcanic) magma chamber: a large high - melt - percentage magma body, the Marginal Border Group, and a low - melt - percentage magma body composed of a large number of confluent sheet intrusions, the Inner Series. The conclusion that the two are distinct entities makes the inclusion of both in a single pluton, the Hypersthene Gabbro of Ardnamurchan Point, somewhat doubtful. The original nomenclature of Richey et al. (1930) has been retained, however, for the following reasons:

- Compatability with previous work

- In recognition of the unusual (for the British Tertiary Volcanic Province) high orthopyroxene content of both suites of rocks (although orthopyroxene contents are distinctly higher, on average, in the Inner Series) which is not due simply to crustal contamination and implies a distinct mantle melting regime beneath the area.

- The general lack of strong chilling of the Inner Series rocks at exposed intrusive contacts between the two groups of rocks. It should, however, be borne in mind that this is probably more an indication of the multiply - intrusive nature of the Inner Series rocks, which appears to have resulted in reheating of the MBG rocks before intrusion of the particular gabbronorite sheets which form these contacts, than of a short time interval between the emplacement of the two groups of rocks. If the latter were the case, then M2 would be an entirely retrogressive phase of metamorphism whereas in reality there is evidence for a period of prograde metamorphism early in M2.

The main aim of the present study was to use the Hypersthene Gabbro and its country rocks as a 'natural laboratory' in which to investigate processes in and around magma chambers by a number

of methods not normally use in conjunction with eachother. It has proved easier to do this in the case of the Marginal Border Group than for the Inner Series because of certain features of the evolution of the former and section 8.1 of this chapter in particular mainly deals with the Marginal Border Group magma chamber.

8.1. The importance of the Marginal Border Group for theoretical and analogue experimental studies of magma chamber processes.

A combination of field, igneous and metamorphic mineralogical, and geochemical studies, coupled with interpretation of the results in terms of heat transfer processes, has shown that magmatic processes in the MBG magma chamber were controlled by a variety of processes – particularly those resulting from expansion and contraction of the magma chamber in response to inputs and outputs of magma – which have not previously been taken into consideration in the construction of analogue and theoretical models of magma chamber behaviour. In addition to demonstrating the qualitative importance of these processes for magma chamber evolution, the results of the present work are also of particular significance for the **quantitative** study of magma chamber physics. This is because of two particular features of the evolution of the MBG magma chamber which have allowed the estimation of certain important parameters in the MBG magma chamber during the early (M1) part of its history:

The sudden cooling of the contact aureole and the rapid solidification of at least the outer parts of the MBG magma chamber which resulted from the abrubt development of a propagating, tensile fracture - based hydrothermal system or systems. This preserved the metamorphic zonation present in the high grade M1 contact metamorphic aureole immediately prior to the quenching. It is therefore possible to estimate an **instantaneous** thermal gradient in the M1 aureole, (rather than the diachronous (Jaeger 1957, 1959) maximum temperature profile which is all that is normally recorded by contact metamorphic aureoles), and therefore the heat flux Q_c into the country rocks from the contact in the period immediately prior to the onset of hydrothermal cooling.

The rapid solidification of the contact zone of the MBG magma chamber, besides preserving evidence for marginally stable stratification of the interior of the magma chamber and thermally - driven downflows at the chamber walls, preserved evidence for **the episodic melting of the wall rocks.** This pattern of melting indicates that the rate of melting of the wall rocks, expressed in terms of the outward migration velocity of the contact a (Chapters 4 & 5) was small. The same conclusion follows from a calculation of the upper limit on a, based on

the width of the aureole when this is treated as a moving boundary layer (Chapter 5), which implies that Q_m can have been no more than 10 - 20% greater than Q_c. **A preliminary estimate of Q_m is that it was in the range 8 to 40Wm^{-2}.**

Although only an order of magnitude estimate this **measurement** of the heat flux from the interior of an ancient basic magma chamber is of value in testing alternative theoretical predictions of boundary layer heat fluxes in basic magma chambers, since these produce estimates of Q_m for basaltic magma bodies which vary from as little as a few watts per square metre (Marsh 1988, 1989) to in excess of 10^3Wm^{-2} (e.g. Huppert & Sparks 1988a, b). Most of these estimates relate to heat fluxes at horizontal boundaries, whereas the measurement made in this work is of heat flux at a near - vertical contact. However, since convection is generally considered to be more rapid at steeply - inclined boundaries than at horizontal magma chamber boundaries, the low Q_m measured in this work clearly favours those theoretical models which predict very low values of Q_m.

To date this is the only empirical estimate of the heat flux at the margin of a large magma body at depth. The only similar measurements of instantaneous temperature profiles and heat flows around magma bodies of any sort have been on Hawaiian lava lakes (Peck et al. 1977; Peck 1978; Wright & Okamura 1977). These subaerial magma bodies largely solidify from the top down (Helz 1989) and are therefore atypical of most large subterranean magma chambers, in which floor accumulation of crystals dominates solidification. Since it is the only large intrusion for which the relevant data is available at present, it is not certain if the MBG magma chamber is (or was) typical of large basaltic to intermediate magma chambers. Evidence from other plutons which suggests that they may have behaved in a similar fashion is considered in section 8.3.

8.2. A summary of the evolution of the Hypersthene Gabbro.

Before the results of this study are extended to other plutons it is appropriate to summarise the structural, thermal and magmatic history of the MBG magma chamber, and of the Hypersthene Gabbro as a whole in terms of the physical processes which operated and the geological controls on their occurrence. In addition to summarising the conclusions of previous chapters, this section also considers some possible additional feedbacks between strcutural, thermal and magmatic processes.

1). **Emplacement of a sill complex** in the bedded sedimentary/metasedimentary sequence above the Moine thrust, but below the present level of exposure. Growth of one (or more ?) of these sills to the critical size (c. 10km diameter) at which doming of the overlying rocks began. The late - M0 dome structure in the rocks around the Hypersthene Gabbro was produced by this process, which may have been triggered either by an increase in rates of magma input or by a decrease in regional extension rates.

2). **Failure of the roof of this conformable laccolithic intrusion along outward - dipping normal faults** and emplacement of the MBG magma chamber at the present level of exposure. Initially rapid heat loss to the walls of the chamber, while thermal gradients in the wall rocks were still high, would have been expected to produce a chill zone of solidified magma. This would then have insulated the wall rocks until it was eroded away, which Huppert & Sparks (1989) and Huppert (1989) suggest would not have occurred until $Q_m \gg Q_c$, assuming erosion of the chill zone to have been purely thermal. This is clearly not the case. One explanation is that emplacement of the intrusion was not instantaneous, but occurred at a sufficiently low rate for pre - heating of the future wall rocks by conduction or hydrothermal convection in the active concentric fault zones to prevent chill zones from forming. Alternatively, erosion of any chill zone which did initially form may have involved thermo - mechanical erosion (Furlong & Myers 1985) of the chill zone. It should be noted that thermal stresses in the chill zone would be tensile, whilst those in the heated wall rocks would tend to be compressive (and therefore less likely to produce pervasive brecciation of the wall rocks and consequent stoping) and would in any case die away as temperature gradients in the wall rocks decreased. The assumption of a fixed boundary made in calculating the

minimum duration of M1 (section 5.2.4) may therefore still be realistic, and the low value of a later in M1 is not inconsistent with the suggestion that thermo - mechanical erosion may have been an efficient means of removing any early M1 chill zone.

3a). Following initial emplacement of the MBG magma chamber, heating of the wall rocks produced a high - grade contact aureole. Heat transfer in this was primarily conductive, although small amounts of hydrothermal circulation through existing and grain - boundary permeability also occurred and resulted in reduction of many of the rocks in the aureole, although this was limited by continuous internal buffer reactions. As this aureole broadened and Q_c fell, the region close to the contact approached a quasi - steady state at which Q_c was only a little less than Q_m. Under these conditions wall rock melting was only significant when Q_c was locally reduced, and Q_m probably locally increased, in the wedge - shaped protrusions formed by the downfaulted hanging - wall blocks of concentric normal faults. **Wall rock melting was an episodic process due to concentric normal faulting which was in turn triggered by deflation of the magma chamber** after periods of inflation due to input of basic magma into the chamber. Pulses of compositionally buoyant anatectic melt were thereby produced which flowed up the walls of the chamber and may have collected as a layer of anatectic granitoid magma beneath its roof.

3b.) During the same period (the latter part of M1) **the bulk of the interior of the MBG magma chamber was probably stratified**, with intermediate magmas at the top overlying a series of progressively more basic layers. The total density difference associated with the observed range in in MgO contents, from 3% to 8%, was no more than 0.05g cm^{-3} or so, and the chamber was only just stably stratified. **Cooling at the walls of the magma chamber produced thermal downflows of more evolved magmas** which mixed with both the ascending anatectic magmas and the more basic magmas in the interior of the chamber to produce a complex, partly hybrid boundary layer. The temperature difference across this boundary layer was at least 60°C and may have been as much as 150°C, yielding estimates of its heat transfer coefficient h, $(0.05 - 0.63 Wm^{-2}K{-}1)$ and minimum possible (equivalent stagnant layer) thickness L_s (20 - 240m). The most likely values of these quantities are given in Table 5.1 (p.521). Stable stratification of tholeiitic magma chambers is not normally expected to develop: its probable occurrence in the MBG magma chamber

may reflect previous crustal contamination, which increased the proportion of low - partial - molar - density components in the incompatible fraction of the melt.

3c). There appears to have been no great change in the range of magma compositions present in the MBG magma chamber during the period from the latter part of M1 to the early part of M2, for which samples of the magma chamber are available. The samples from the MBG itself, which date from the period of solidification of the MBG magma chamber after development of the hydrothermal system(s), show as much (or more) variation in composition (both with respect to major elements and crustal contamination indices) as the older and younger samples. Crustal contamination in the homogeneous intermediate and basic MBG rocks appears to have mainly occurred by bulk assimilation of the Lewisian basement complex by picritic or picrobasaltic parent magmas and to have preceded the period of crystal fractionation which produced the observed range of basic to intermediate magma compositions. The preservation of heterogeneity in the amount and/or composition of crustal contaminants which must have been assimilated before the magmas entered the MBG magma chamber has been used to show that **convection in the MBG magma chamber was insufficiently vigorous to homogenise the magmas which entered the chamber.**

3d). The geochemical evidence implies the frequent input of distinct batches of basic to intermediate magma into the MBG magma chamber. This is consistent with structural evidence for inflation and deflation of the magma chamber. Inflation of the chamber was mainly by uplift of the chamber roof through the emplacement of cone sheets along incipient shear fractures produced by failure of the chamber walls after elastic stretching. Horizontal radial compression of the chamber walls was of minor importance. The cone sheets mainly occupy the inward - dipping set of a network of conjugate shear fractures, in accordance with recent theoretical models, but in detail their emplacement was a complex process involving lateral as well as radial propagation and magma flow.

4a). Some several thousand years (at least) after the initial emplacement of the MBG magma chamber and the onset of M1, **master fractures** (probably radial vertical tensile fractures) **began to form around the MBG magma chamber.** These admitted large volumes of cold water or hydrothermal fluid into the M1 aureole, at such a high rate that

a temperature difference of more than perhaps 100 – 200°C was maintained between the fluids and the wall rocks. This was sufficient for the wall rocks to undergo tensile failure as a result of thermal contraction, and thereby initiate self - propagating tensile fracture networks containing vigorously convecting hydrothermal fluids.These rapidly cooled the M1 aureole and solidified the preserved part of the MBG magma chamber as they propagated at rates of up to 250m/year. The agreement between the cooling rates in the conductive boundary layer in front of the fracture systems, as inferred from quench textures, and those predicted by the thermo - mechanical theory of Lister (1974) suggests that the latter was applicable to at least some parts of the rapidly cooling aureole and MBG contact zone. In other, more slowly cooled areas, the rate of hydrothermal system propagation may have been limited by heat transport rates within the hydrothermal system.

Initiation of hydrothermal cooling in this way requires:

a). The formation of master fractures, which appear to have been related to extension in a tensile stress field produced by high excess pressure in the MBG magma chamber, perhaps aided by regional stresses.

b). The presence of a large surface water reservoir, or an even larger high - permeability subsurface aquifer, able to sustain the high water input rates implied by the estimated heat fluxes at the cracking fronts, of up to 700 – 13000 Wm^{-2}.

This latter requirement suggests that the delay in onset of hydrothermal cooling after the emplecement of the MBG magma chamber may reflect the time needed to develop a suitable water reservoir above the MBG magma chamber, in the form of a caldera lake. The structural history of the intrusion implies that the surface above is likely to have been domed initially (quite apart from the effects of acumulation of eruptive products) but that a caldera structure developed later which may have provided a suitable site for a caldera lake: deposits formed in such lakes occur in the Mull central complex (Judd 1874; Bailey et al. 1924). If the formation of a caldera lake made the MBG magma chamber prone to hydrothermal quenching, this implies a feedback between chamber growth and hydrothermal quenching which would limit the ability of sub - caldera magma chambers to grow much beyond their initial size.

4b). Solidification of the preserved part of the MBG magma chamber occurred rapidly enough to preserve the compositions of the magmas previously present in the chamber: melt segregation during solidification was limited to local migration of interstitial melts into tensile fractures produced in part by thermal contraction of the host crystalline matrix. Solidification was not, however, sufficiently rapid to freeze low - viscosity magmas in situ and the observed distribution of hybrid, intermediate and basic magmas (in particular the widths of the zones formed by each) was strongly affected by magma flow down the wall of the chamber during its progressive solidification.

5). Following solidification of the preserved part of the MBG magma chamber the intensity of the hydrothermal circulation appears to have died away and later intrusions were not quenched in the same way. The decline in hydrothermal circulation reflects in part the closing up of the existing fracture network by mineral deposition and creep and/or static failure. In addition, however, catastrophic cooling caused by the self - propagation of hydrothermal systems appears to have been limited to only the one period in the history of the Hypersthene Gabbro. One possible reason for this, **if** the source of water for the hydrothermal system(s) which ended M1 was a caldera lake, is infilling of the postulated caldera or uplift of its floor by the emplacement of the Inner Series. The decline in hydrothermal activity and the emplacement of new intrusions appears to have been the cause of prograde M2 metamorphism and a general increase in temperatures in and around the Hypersthene Gabbro, to perhaps as much as 600 – 700°C.

6. The confluent gabbronorite sheets which make up the bulk of the Inner Series of the Hypersthene Gabbro **were emplaced in continuous successsion, possibly in localised swarms, to form a large, low - melt - percentage magma body**. This may have been analogous to the low - melt - percentage magma chambers inferred, on the basis of geophysical evidence, to underlie many active basaltic volcanoes. The pre - gabbronorite rocks which form a variety of xenoliths and screens within the gabbronorite sequence originate from a number of unrelated intrusions. Classical cumulus processes do not seem to have operated to any significant extent within the gabbronorite sheets but sub - rigidus melt expulsion, associated with the formation of a weak to, locally, strong feldspar lamination, appears to have been pervasive. Other late magmatic and high - grade metamorphic processes in the Inner Series

were associated with infiltration of hydrothermal fluids along a tensile fracture network. The formation of this network was not associated with sudden cooling to low temperatures: it may have been produced by the emplacement of the relatively small (and therefore rapidly cooled) gabbronorite sheets into rocks which already contained hydrothermal fluids. Two processes in particular have been identified as related to this very high temperature fluid circulation:

a). The circulating fluids caused oxidation of ferromagnesian minerals at temperatures of 800 – 1000°C, although the reactions were controlled for the most part by continuous internal buffer reactions, implying low water - rock ratios in most cases.

b). Infiltration or diffusion of water into hotter regions of the Inner Series, or reheating of older rocks by later intrusive sheets, may have resulted in remelting under hydrous conditions. This may account for the high - Al character of the expelled interstitial melt where it was possible to calculate its composition, and also for the formation of the rare metasomatic pyroxenites.

The high fluid temperatures may reflect the lack of clear upward flow paths along which heated fluids could escape: this suggests either that the Inner Series sheet complex was capped by a relatively large high - melt - percentage magma chamber or that sufficient impermeable, relatively hot partially molten sheets were present within the Inner Series at any one time to have had a similar effect. In general, however, the effects of sub - rigidus processes upon the compositions of the Inner Series rocks were slight in comparison to the pre - existing variation in the magmas fed into the Inner Series: it appears to have acted more as a site of magma storage than of magma differentiation.

7). Following the end of the high - grade metamorphism associated with the Inner Series, a large number of unrelated intrusions were emplaced. Some of these, particularly in the Glebe Hill area, were not previously recognised as separate intrusions and account for some of the anomalies in previous interpretations of the structure of the Hypersthene Gabbro.

8.3. To what extent are the results of the present study applicable to other upper crustal magma bodies ?

The three most important respects in which the present study has produced unexpected results can be summarised as follows:

- The very low heat flux Q_m from the interior of the MBG magma chamber to its contact.

- The suddenness of the transition from slow conductive to very fast convective cooling of the MBG magma chamber as a result of the self - propagation of the tensile fracture networks.

- The importance of the structural evolution of the pluton in controlling magma evolution, through the episodic melting process and the triggering of the fracture networks by formation of master fractures.

This section seeks to address the question of whether these results are applicable to other large mafic plutons. Whilst a definitive answer can only be obtained by similar integrated studies of the petrology, structure and contact metamorphic effects of a large number of such plutons, some indications can be gained from the existing literature.

8.3.1. Constraints from contact metamorphism, crustal contamination and the compositions of granites in central complexes upon values of Q_m in other mafic plutons.

It was shown in Chapter 5 that the development of a broad high temperature aureole around the Marginal Border Group implied that the contact itself had been near - stationary for a long period prior to the end of M1. If it had been moving outwards at a velocity of more than a few centimetres per year, the conductive boundary layer (equivalent to the metamorphic aureole) in front of the moving contact would never have attained a thickness of more than a few tens of metres. The occurrence of very high temperatures (up to over 1000°C), which can only be produced by heating by a constant - temperature heat source such as a convecting magma body, in aureoles wider than this (for example, around the Cuillins complex of Skye (Almond 1964; Ferry 1985a) and the

Monteregian plutons (Philpotts 1970)) implies that values of the contact velocity a, and therefore of Q_m, around these bodies were low, of the same order as those estimated for the MBG in section 5.2.4, when these aureoles formed. This conclusion needs to be treated with caution because it is conceivable that Q_m, and therefore a, could have been much higher for most of the history of these complexes and have decreased gradually as crystallisation proceeded, thereby producing a relatively broad aureole at a relatively late stage. However, the generally - accepted relationship between Q_m and magma composition means that this could only occur in plutons which show a well - defined fractionation trend, such as Skaergaard (Wager & Deer 1939). Neither the Cuillins complex (Dickin et al. 1984) nor the Monteregian plutons (Philpotts 1970), the examples cited above, show such a systematic trend.

Another piece of evidence which suggests that low values of Q_m may be the norm originates from the point that, if Q_m is as high as has often been suggested or implied, most of the heat lost by a large basic or ultrabasic magma body would be expected to be converted into wall rock melts (Huppert & Sparks 1989) except in the presence of very vigorous hydrothermal convection. Depending on the subsequent fate of these melts, either the mafic magmas should be very strongly contaminated or else the ratio of anatectic granitoids to those produced by extended crystal fractionation of mafic magmas (limited to around 10% of the volume of original mafic melt; see, for example, Wood (1978)) should be very high, of the order 10:1. Again, if one takes the British Tertiary Volcanic Province central complexes as examples, it is clear that neither of these alternatives occurs. Dickin et al. (1984) showed that, although the Cuillins gabbroic complex has a broad high - temperature aureole similar to the M1 aureole of the Hypersthene Gabbro, it shows very little in situ crustal contamination. Greenwood (1987) showed that the Rhum complex also showed little in situ contamination although in this case the interpretation of his results is more equivocal because the contact aureole appears to have been convectively cooled for most of its history and the precise heat flow regime is not well understood: Greenwood (1987) and Robinson & McLelland (1987) reach contradictory conclusions on this. Extensive studies of the BTVP granitic rocks (summarised in Thompson (1982); Dickin et al. (1984)) have shown that they contain a high percentage of material produced by fractionation of basic magmas (typically over 50%). This suggests that Q_m was on average no more than about 20% greater than Q_c during the residence period of the parental basic magmas in the crust. Whilst this argument is open to the criticism that the size, geometry, location and heat transfer mechanisms in and around the parent magma reservoirs are unknown (

although it should be noted in particular that much of the contamination may have taken place in magma conduits (e.g. Thompson et al. 1986) and that therefore Q_m may have been elevated by forced convection during the contamination process) it does at least suggest that low values of Q_m are not unique to the Marginal Border Group of the Hypersthene Gabbro.

8.3.2. The frequency of occurrence of sudden or catastrophic cooling events associated with the development of tensile fracture network - based hydrothermal systems around upper crustal plutons.

Quenched anatectic melts have been described from the contact aureoles of a number of upper crustal and subvolcanic basic and ultrabasic plutons (see Chapter 5), implying that sudden cooling, possibly at rates of up to degrees per hour, is a common feature of these contact aureoles. Cooling rates of this magnitude can only be plausibly be produced in the narrow boundary layers in front of fast - moving thermal tensile cracking fronts. Ryan & Sammis (1981) suggest that the cracking process is likely to be an episodic, seismogenic process (see section 5.3.2). Earthquakes with apparently dilational source characteristics which occur in the vicinity of central volcanoes have been interpreted as resulting from propagation of tensile fracture - based hydrothermal systems (Foulger 1988) although the small size of the region of failure (section 5.3.2) means that the earthquakes produced are likely to be always at or below the limit of detection unless generated very close to the surface (R.Westaway, pers. comm.): the larger and much less frequent earthquakes recorded by Foulger and co - workers could result from the catastrophic failure of tough thermally stressed bands within the hydrothermal systems (Sammis & Julian 1987). Sudden bursts of hydrothermal activity, lasting for periods of several years or more, such as would be associated with large - scale propagation of hydrothermal systems into large plutons, have not, however, been recorded from active subaerial volcanoes. Such events might in any case be very rare: there is only evidence for one such period of activity in the case of the Hypersthene Gabbro.

8.3.3. The importance of episodic melting in the formation of anatectic magmas in upper crustal magma chambers.

Of all the effects examined in this work, that of the formation of downfaulted blocks upon wall rock melt production rates and patterns of magma evolution is the most difficult to evaluate with

respect to its wider importance. In general terms, it can only have significant effects if the following requirements are satisfied:

- that $Q_m \approx Q_c$, so that neither melting nor solidification occur over the whole of the wall of the intrusion concerned at rates which would, respectively, swamp the contribution from melting of downfaulted blocks or insulate the wall of the intrusion with refractory cumulates.

- that there is a high rate of formation of downfaulted blocks, which implies a high rate of fluctuation in magma chamber pressure to produce the necessary fault movements (see Chapter 7).

- that decreases in magma chamber pressure (due, for example, to failure of the wall of the main magma chamber and emplacement of a minor intrusion) and consequent fault movements are intermittent or episodic.

With regard to the first requirement, it was shown in section 5.2.4 that $Q_m \approx Q_c$ for the MBG magma chamber at a nominal time of several thousand years after the initial emplacement of the chamber. The studies by Irvine (1970) indicate that by several thousand years after its initial emplacement the value of Q_c at the contact of a convecting sheet intrusion will only be varying slowly, even if a quasi - steady state has not been reached as a result of slow hydrothermal convection or proximity to the surface. Similar results are likely in the cases of intrusions with other shapes. It follows that most large magma chambers in the same basic to intermediate compositional range as the MBG magma chamber would be expected to have $Q_m \approx Q_c$ for long periods provided that they were mainly cooled by conduction.

A second situation in which $Q_m \approx Q_c$ for long periods may arise in tha case of ultrabasic magma chambers cooled by vigourous hydrothermal systems. Greenwood (1987) demonstrated that the marginal zone of the Rhum complex was characterised by neither significant growth of sidewall cumulates on the one hand nor by a high rate of host rock melting, and that the Rhum magma chamber was surrounded by a vigorous hydrothermal system at the time. In such a situation concentric normal faulting would have a particularly strong effect upon wall rock melting because the tip of the downfaulted block would be isolated from the hydorthermal system and would only

be cooled by conduction: it would be expected to melt very rapidly.

The other two conditions are likely to be satisfied in some cases but not in others, according to the geometry of the magma chamber, the rheology of the country rocks and the actual variations in magma pressure within the chamber concerned. The predicted surface expression of magma chambers similar to the M1 MBG magma chamber is a steep - sided dome with a deep summit caldera: such structures are very rare. Perhaps the best examples are the steep - sided shield volcanoes of Albemarle and Narborough islands in the Galapagos archipelago (McBirney & Williams 1969). The structure of these has been modelled in terms of deformation above a shallow, lensoid (or laccolithic ?) magma chamber by Cullen et al. (1987) and the resemblance to the Ardnamurchan central complex is heightened by the presence of arcuate or concentric chains of vents around the volcanoes which may be the surface expression of cone sheets. The rarity of such volcanoes suggests that in fact large, shallowly - buried magma chambers analogous to the MBG magma chamber are relatively unusual, in which case the specific mechanism of episodic melting proposed in the present work may be unimportant in terms of the actual volumes of magma produced on a world - wide basis.

8.4. Future Work.

8.4.1. Further work on the Hypersthene Gabbro.

Aspects of the geology of the Hypersthene Gabbro which particularly merit further investigation, beyond that which has been possible within the scope of the present work, may be summarised as follows:

1). More precise determinations of the temperature gradients in the country rocks during the latter part of M1, using mineral composition data, are necessary to reduce the uncertainties in the estimates of Q_c and the boundary layer parameters Q_m, V_x, h and L_s.

2). The actual duration of M1 needs to be more precisely constrained, and the role of slow hydrothermal circulation in the M1 aureole needs to be better defined. The latter requires evaluation of the fluid - rock ratio during M1, using mineralogical and bulk compositional data, and numerical thermal modelling to investigate the effects of the temperature dependence of thermal capacities and fluid properties. An independent estimate of the duration of M1, perhaps using crystal size distributions in the highest grade contact metamorphic rocks (Cashman & Ferry 1988) would be most useful.

3). The duration and rates of melt production during the melting events associated with the formation of the downfaulted blocks has not yet been well constrained: numerical heat flow modelling appears to be the best way to investigate the extremely complex thermal problem which these events represent.

4). This study has shown that cone sheet emplacement mechanisms are much more complex than was previously thought. Systematic structural studies are necessary, in order to investigate cone sheet propagation and the relationship between changes in the stress fields during cone sheet emplacement and faulting and finite inflations and deflations of the MBG magma chamber.

5). Many more precise estimates of the compositions and amounts of interstitial melts expelled

from particular Inner Series rocks are needed. It would be useful to compare the results with estimates of the amount of sub - rigidus strain recorded in the rocks made using textural indicators such as the degree of development of preferred crystal orientations.

6). The relationship between the ultra - high - temperature metamorphism of the Inner Series rocks and mechanisms and amounts of oxygen isotope exchange needs to be investigated. Detailed studies of the oxygen isotope compositions of the various pyroxene species would be particularly interesting as a means of constraining the amount of diffusive isotopic exchange not related to recrystallisation.

7). Oxygen isotope studies are also needed to investigate any oxygen isotope depletions associated with the formation of igneous sub - rigidus laminations and especially the development of metasomatic pyroxenites, to evaluate the idea that these may be associated with, respectively, the expulsion of low - ^{18}O hydrous melts and the migration through the rocks of large volumes of such melts.

8.4.2. Implications of the present study for research into magma chamber processes.

Perhaps the most important conclusion of all to be drawn from the present study is that, under favourable circumstances, it is possible to make empirical measurements of heat flow rates around and within ancient magma chambers with a degree of accuracy which is sufficient to discriminate between competing theories of magma chamber behaviour and is very precise relative to the amount of variation in Q_m to be expected over the compositional range of terrestrial magmas. Further progress in the application of such measurements will involve advances in the following fields:

– Integrated metamorphic, structural and petrological/ geochemical studies to obtain estimates of Q_m and the parameters derived from it for suitable plutons with as wide a range of geometries and compositions as possible, in order to investigate the range of values of Q_m and possible causes of variation in it.

– Improvements in low - pressure geothermometry, and better calibration of the relationship between cooling rates and crystallisation textures, in order to improve the accuracy of the

measurements needed to obtain estimates of heat fluxes in the various situations described.

– Numerical and analogue modelling of specific boundary layers, especially steeply - inclined boundary layers and those within which marked compositional variation occurs, for which Q_m and other parameters have been measured, in order to improve understanding of the relationship between these parameters and the theoretical models of overall magma chamber behaviour.

REFERENCES.

ALMOND, D.C. (1964). Metamorphism of Tertiary lavas in Strathaird, Skye. TRANS ROY SOC EDINB **65** 413-434.

ANDERSON, E.M. (1936). Dynamics of Formation of Cone-Sheets, Ring-Dykes and Cauldron Subsidences. PROC ROY SOC EDINB **56** 128-157.

ANDERTON, R., BRIDGES, P.H., LEEDER, M.R. & SELLWOOD, B.W. (1979). A dynamic stratigraphy of the British Isles. Publ. George, Allen & Unwin.

ARZI, A.A. (1978). Critical phenomena in the rheology of partially melted rocks. TECTONOPHYSICS **44** 173-184.

BAILEY, E.B., CLOUGH, C.T., WRIGHT, W.B., RICHEY, J.E. & WILSON, G.V. (1924). The Tertiary and Post-Tertiary Geology of Mull, Loch Aline and Oban. MEM. GEOL. SURV. SCOTLAND.

BAMFORD, D., NUNN, K., PRODEHL, C. & JACOB, B. (1977). LISPB - III. Upper Crustal Structure of Northern Britain J GEOL SOC LOND **133** 481-488.

BAMFORD, D., NUNN, K., PRODEHL, C. & JACOB, B. (1978). LISPB -IV. Crustal structure of N. Britain. GEOPHYS J ROY ASTR SOC **54** 43-60.

BARRETT, M.J.C. (1987). Interpretation of a Bouguer anomaly profile across the Tertiary Igneous Complex of Ardnamuchan, Argyllshire. Unpubl. BSc Dissertation, Univ. Durham.

BARTON, M. & VAN GAANS, C. (1988). Formation of orthopyroxene - FeTi oxide symplectites in Precambrian intrusives, Rogaland, Southwestern Norway. AMER MINERALOGIST **73** 1046-1059.

BEDARD, J.H., SPARKS, R.S.J., RENNER, R., CHEADLE, M.J., & HALLWORTH, M.A. (1988). Peridotite Sills and Metasomatic Gabbros in the Eastern Layered Series of the Rhum Complex. J

GEOL SOC LOND **145** 207-224.

BICKLE, M.J. & McKENZIE, D.P.(1987). The transport of heat and matter by fluids during metamorphism. CONTRIB MINERAL PETROL **95** 384-392.

BINNS, P.E., McQUILLIN, R. & KENOLTY, N. (1974). The geology of the sea of the Hebrides. REP. INST. GEOL. SCI. 73/14.

BIRD, D.K. & HELGESON, H.C. (1981). Chemical interaction of aqueous solutions with epidote - feldspar mineral assemblages in geologic systems. II. Equilibrium constraints in metamorphic/geothermal processes. AM J SCI **281** 576-614.

BIRD, D.K., SCHIFFMAN, P., ELDERS, W.A., WILLIAMS, A.E. & McDOWELL, S.D. (1984). Cale silicate Mineralisation in Active Geothermal Systems. ECON GEOL **79** 671-695.

BIRD, D.K., MANNING, C.E. & ROSE, N.M. (1988). Hydrothermal alteration of Tertiary layered gabbros, East Greenland. AM J SCI **288** 405-457.

BLAKE, D.H., ELWELL, R.W.D., GIBSON, I.L., SKELHORN, R.R. & WALKER, G.P.L. (1965). Some relationships resulting from the intimate association of acid and basic magmas. Q J GEOL SOC LOND **121** 31-49.

BLUNDELL, D.J., HURICH, C.A & SMITHSON, S.B., (1985). A model for the MOIST seismic reflection profile, N. Scotland. J GEOL SOC LOND **142** 245-258.

BOTT, M.H.P. & TUSON, J. (1973). Deep structure beneath the Tertiary volcanic regions of Skye, Mull & Ardnamurchan. NATURE (PHYS SCI) **242** 114-116.

BOTT, M.H.P. & TANTRIGODA, D.A. (1987). Interpretation of the gravity and magnetic anomalies over the Mull Tertiary intrusive complex, N.W. Scotland. J GEOL SOC LOND **144** 17-28.

BOTTINGA, Y. & WEILL, D.F. (1970). Densities of Liquid Silicate Systems Calculated from

Partial Molar Volumes of Oxide Components. AM J SCI **269** 169-182.

BOWEN, N.L. (1917). The problem of the anorthosites. J GEOL **25** 209-243.

BOWEN, N.L. (1927). The origin of ultrabasic and related rocks. AM J SCI **14** 89-108.

BOWEN, N.L. (1928). The Evolution of the Igneous Rocks. Publ. Princeton University Press.

BOWEN, N.L. (1948). The granite problem and the method of multiple prejudices. MEM GEOL SOC AMER **28** 79-90.

BRADY, J.B. (1988). The role of Volatiles in the Thermal History of Metamorphic Terranes. J PETROL **29** 1187-1213.

BRANDEIS, G. & JAUPART, C. (1986). On the interaction between convection and crystallization in cooling magna chambers. EARTH PLANET SCI LETT **77** 345-361.

BRATT, S.R. & SOLOMON, S.C. (1984). Compressional and shear wave structure of the East Pacific Rise at 11° 20' N: constraints from three component ocean bottom seismometer data. J GEOPHYS RES **89** 6095-6110.

BROOK, M., POWELL, D. & BREWER, M.S. (1977). Grenville events in Moine rocks of the Northern Highlands, Scotland. J GEOL SOC LOND **133** 489-496.

BROWN, G.M. (1954). A suggested igneous origin for the banded granular hornfelses within the hypersthene - gabbro of Ardnamurchan, Argyllshire. MINERAL MAG **30** 529-533.

BROWN, G.M. (1956). The layered ultrabasic rocks of Rhum, Inner Hebrides. PHIL TRANS ROY SOC LOND **A240** 1-53.

BUDDINGTON, A.F. & LINDSLEY, D.H. (1964). Iron-titanium oxide minerals and synthetic equivalents. J PETROL **5** 310-357.

BUTCHER, A.R., YOUNG, I.M. & FAITHFULL, J.W. (1985). Finger structures in the Rhum Complex. GEOL MAG **122** 491-502.

CAMPBELL, I.H., ROEDER, P.L. & DIXON, J.M. (1978). Plagioclase buoyancy in basaltic liquids as determined with a centrifuge furnace. CONTRIB MINERAL PETROL **67** 369-377.

CAMPBELL, I.H. & TURNER, J.S. (1987). A laboratory investigation of assimiliation at the top of a basaltic magma chamber. J GEOL **95** 155-172.

CANN, J.R. (1965). The metamorphism of amygdales at 'S Airde Beinn, Northern Mull. MINERAL MAG **34** 92-106.

CARMICHAEL, D.M. (1969). On the mechanism of prograde metamorphic reactions in quartz - bearing pelitic rocks. CONTRIB MINERAL PETROL **20** 244-267.

CARRIGAN, C.R. (1986). A two - phase hydrothermal cooling model for shallow intrusions. J VOLCANOL GEOTHERM RES **28** 175-192.

CARRIGAN, C.R. & CYGAN, R.T. (1986). Implications of Magna Chamber Dynamics for Soret-Related Fractionation. J GEOPHYS RES **91** 11451-11461.

CARRIGAN, C.R. (1987). The magmatic Rayleigh number and time-dependent convection in cooling lava lakes. GEOPHYS RES LETT **14** 915-918.

CARRIGAN, C.R. (1988). Biot number and thermos bottle effect: implications for magma-chamber convection. GEOLOGY **16** 771-774.

CARSLAW, H. & JAEGER, J. (1959). Conduction of heat in solids 2nd ed. Publ. Clarendon Press, Oxford.

CASHMAN, K.V. & FERRY, J.M. (1988). Crystal size distribution (CSD) in rocks and the kinetics and dynamics of crystallisation. III. Metamorphic crystallisation. CONTRIB MINERAL PETROL

99 401-415.

CHEVALLIER, L. & VERWOERD, W.J. (1988). A Numerical Model for the Mechanical Behaviour of Intraplate Volcanoes. J GEOPHYS RES **93** 4182-4199.

CLOUGH, C.T., MAUFE, H.B. & BAILEY, E.B. (1909). The cauldron - subsidence of Glencoe, and the associated igneous phenomena. Q J GEOL SOC LOND **65** 611-678.

CONDOMINES, M., GRONVOLD, K., HOOKER, P.J., MUEHLENBACHS, K., O'NIONS, R.K., OSKARSSON, N. & OXBURGH, E.R. (1983). Helium, oxygen, strontium and neodymium isotopic relationships in Icelandic Volcanics. EARTH PLANET SCI LETT **66** 125-136.

COPPIN, R. (1982). A geophysical investigation of the Tertiary Igneous Complex of Rhum, Inner Hebrides. Unpubl. MSc. thesis, Univ. of Durham.

COX, K.G. & MITCHELL, C. (1988). The Differentiation of Basaltic Magmas: Crystal Settling vs. Convective Fractionation. NATURE **333** 447-449.

COWARD, M.P. (1983). The thrust and shear zones of the Moine thrust zone and the NW Scottish Caledonides. J GEOL SOC LOND **140** 795-811.

CULLEN, A.B., McBIRNEY, A.R. & ROGERS, R.D. (1987). Structural controls on the morphology of Galapages Shields. J VOLCANOL GEOTHERM RES **34** 143-151.

DAGLEY, P., MUSSETT, A.E. & SHELHORN, R.R. (1984) The palaeomagnetism of the Tertiary igneous complex of Ardnamurchan. GEOPHYS J ROY ASTR SOC **79** 911-922.

DAY, S.J. (1985) The Geology of North West Ardnamurchan. Unpubl. B.A. dissertation, Univ. of Oxford.

DEER, W.A., HOWIE, R.A., ZUSSMAN, J. (1966). An introduction to the rock-forming minerals. Publ. Longman.

DELANEY, P.T. & POLLARD, D.D. (1981). Deformation of host rocks and flow of magma during growth of minette dykes and breccia - bearing intrusions near Ship Rock, New Mexico. U.S. GEOL SURV PROF PAP **1202.**

DePAOLO, D.J. (1985). Isotopic studies of processes in Mafic Magma Chambers. I: The Kiglapait Intrusion, Labrador. J PETROL **26** 925-952.

DETRICK, R.S., BUHL, P., VERA, E., MUTTER, J., ORCUTT, J., MADSEN, J. & BROCHER, T. (1987). Multi-channel seismic imaging of a crustal magma chamber along the East Pacific Rise. NATURE **326** 35-41.

DICKIN, A.P., EXLEY, R.A. & SMITH, B.M. (1980). Isotopic measurements of Sr and O exchange between meteoric - hydrothermal fluid and the Coire Uaigneich Granophyre, Isle of Skye, N.W. Scotland. EARTH PLANET SCI LETT **51** 58-70.

DICKIN, A.P. (1981). Isotope geochemistry of Tertiary igneous rocks from the Isle of Skye, NW Scotland. J PETROL **22** 159-189.

DICKIN, A.P., MOORBATH, S. WELKE, H.J. (1981) Isotope, trace element & major element geochemistry of Tertiary igneous rocks, Isle of Arran, Scotland. TRANS ROY SOC EDINB: EARTH SCI **72** 159-170.

DICKIN, A.P., BROWN, J.L., THOMPSON, R.N., HALLIDAY, A.N., MORRISON, M.A. (1984). Crustal contamination and the granite problem in the British Tertiary Volcanic Province. PHIL TRANS ROY SOC LOND **A310** 755-780.

DIXON, J.M. & SIMPSON, D.G. (1987). Centrifuge modelling of laccolith intrusion. J STRUCT GEOL **9** 87-103.

DONALDSON, C.H. (1985a). The rates of dissolution of oluine, plagioclase and quartz in a basalt melt. MINERAL MAG **49** 683-694.

DONALDSON, C.H. (1985b). A comment on crystal shapes resulting from dissolution in magmas. MINERAL MAG **49** 129-132.

DRAKE, M.J. (1976). Plagioclase - melt equilibria. GEOCHEM COSMOCHIM ACTA **40** 457-465.

DRAKE, M.J. & WEILL, D.F. 1975. Partition of Sr, Ba, Ca, Y, Eu^{2+}, Eu^{3+} and other REE between plagioclase feldspar and magmatic liquid; an experimental study. GEOCHEM COSMOCHIM ACTA **39** 689-712.

DRUITT, T.H. & BACON, C.R. 1988. Compositional zonation and cumulus processes in the Mount Mazama magma chamber, Crater Lake, Oregon. TRANS ROY SOC EDINB: EARTH SCI **79** 289-298.

DRURY, S.A. (1972) The chemistry of some granitic veins from the Lewisian of Coll and Tiree. CHEM GEOL **9** 175-194.

DRURY, S.A. (1974). Chemical changes during retrogressive metamorphism of Lewisian granulite facies rocks from Coll & Tiree. SCOTT J GEOL **10** 237-256.

DRURY, S.A. (1978). REE distributions in a high grade Archaean greiss complex in Scotland: implications for the genesis of ancient sialic crust. PRE CAMB RES **7** 237-257.

DUNHAM, A.C. (1964). A petrographic and geochemical study of back-veining and hybridisation at a gabbro-felsite contact in Coire Dubh, Rhum, Inverness-shire. MINERAL MAG **33** 887-902.

DUNN, T. (1987). Partitioning of Hf, Lu, Ti & Mn between olivine, clinopyroxene and basaltic liquid. CONTRIB MINERAL PETROL **96** 476-484.

ECKERT, E.R.G., & DRAKE, R.M. (1987). Analysis of Heat and Mass Transfer (2nd Edn.) Publ. Hemisphere Publ. Corp.

ELLIS, D.J. & THOMPSON, A.B. (1986). Subsolidus and Partial Melting Reactions in the Qtz

- excess CaO + MgO + Al_2O_3 + SiO_2 + H_2O system under H_2O - excess and H_2O - deficient conditions to 10kb: Some implications for the origin of peraluminous melts from mafic rocks. J PETROL **27** 91-122.

EMELEUS, C.H., WADSWORTH, W.J. & SMITH, N.J. (1985). The early igneous and tectonic history of the Rhum Tertiary Volcanic Centre. GEOL MAG **122** 451-457.

ENGLAND, R.W. (1988a). The Ascent and Emplacement of Granitic Magma: the Northern Arran Granite. Unpubl. Ph.D. thesis, Univ. of Durham.

ENGLAND, R.W. (1988b). The early Tertiary stress regime in NW Britain: evidence from the patterns of volcanic activity. **in** A.C. Morton & L.M. Parson (eds) Early Tertiary Volcanism and the opening of the NE Atlantic. GEOL SOC SPEC PUBL **39** (381-389).

EUGSTER, H.P. & WONES, D.R. (1962). Stability Relations of the Ferriginous Biotite, Annite. J PETROL **3** 82-125.

FERRY, J.M. (1976). P,T, f_{CO_2} and f_{H_2O} during metamorphism of calcareous sediments in the Waterville - Vassalboro area, south-central Maine. CONTRIB MINERAL PETROL **57** 119-143.

FERRY, J.M. (1985). Hydrothermal alteration of Tertiary Igneous rocks from the Isle of Skye, NW Scotland, Part 1: Gabbros. CONTRIB MINERAL PETROL **91** 264-282.

FERRY, J.M. (1985). Hydrothermal alteration of Tertiary Igneous Rocks from the Isle of Skye, NW Scotland, Part II: Granites. CONTRIB MINERAL PETROL **91** 283-307.

FERRY, J.M., MUTTI, L.J. & ZUCCALA, G.J. (1987). Contact metamorphism/hydrothermal alteration of Tertiary basalts from the Isle of Skye, Northwest Scotland. CONTRIB MINERAL PETROL **95** 166-181.

FOLK, R.L. (1974). Petrology of Sedimentary Rocks. Publ. Hemphill Publ. Co. Austin, Texas.

FORESTER, R.W. & HARMON, R.S. (1983). Stable isotope evidence for deep meteoric / hydrothermal circulation: Island of Rhum, Inner Hebrides, Scotland. Abstract, 4th. International Symposium on Water/Rock Interaction, Misasa, Japan.

FOULGER, G.R. (1988). Hengill Triple Junction, SW Iceland. 2. Anomalous Earthquake Focal Mechanisms and Implications for Processes within the Geothermal Reservoir and at Accretionary Plate Boundaries. J GEOPHYS RES **93** 13507 -13523.

FUJII, T. & KUSHIRO, J. (1977). Density, viscosity and compressibility of basaltic liquid at high pressure. YB. CARNEGIE INSTN. WASH. **76** 419-424.

FURLONG, K.P. & MYERS, J.D. (1985). Thermal-mechanical modeling of the role of thermal stresses and stoping in magma contamination. J VOLCANOL GEOTHERM RES **24** 179-192.

GAMOND, J.F. (1987). Bridge structures as sense of displacement criteria in brittle fault zones. J STRUCT GEOL **9** 609-620.

GIBB, F.G.F. (1974). Supercooling and the crystallization of plagioclase from a basaltic magma. MINERAL MAG **39** 641-653.

GILBERT, G.K. (1877). Report on the geology of the Henry Mountains. U.S GEOG GEOL SURV ROCKY MOUNTAINS REGION.

GOLDMAN, D., & JALURIA, Y. (1986). Effect of opposing buoyancy on the flow in free and wall jets. J FLUID MECH **166** 41-56.

GREENWOOD, R.C. (1987). Geology and Petrology of the Margin of the Rhum Ultrabasic Intrusion, Inner Hebrides, Scotland. Unpubl. PhD. Thesis, University of St. Andrews.

GRIBBLE, C.D. & O'HARA, M.J. (1967). Interaction of basic magna with pelitic materials. NATURE **214** 1198-1201.

GROUT, F.F. (1918). Internal structures of igneous rocks. J GEOL **26** 439-458.

GUDMUNDSSON, A. (1988). Formation of collapse calderas. GEOLOGY **16** 808-810.

HAGGERTY, S.E. & BAKER, I. (1967). The alteration of olivine in basaltic and associated lavas. 1. High temperature alteration. CONTRIB MINERAL PETROL **16** 233-257.

HARKER, A. (1904). The Tertiary Igneous Rocks of Skye. MEM. GEOL. SURV. SCOTL.

HARRISON, P.V. (1987). A geophysical study of the deep structure of the Tertiary Igneous centre of Ardnamurchan. Unpubl. BSc dissertation, Univ. Durham.

HAWKES, L. (1929). On a partially fused quartz-felspar rock and on glomerogranular texture MINERAL MAG **22** 163-172.

HELZ, R.T., KIRSCHENBAUM, H. & MARINENKO, J.W. (1989). Diapiric transfer of melt in Kilauea Iki Lava Lake, Hawaii: A quick, efficient process of igneous differentiation. GEOL SOC AMER BULL **101** 578-594.

HENDERSON, P. (1982). Inorganic Geochemistry. Publ. Pergamon Press.

HILDRETH, W. (1981). Gradients in silicic magma chambers: implications for silicic magmatism. J GEOPHYS RES **86** 10153-10192.

HILL, D.P. (1977). A model for earthquake swarms. J GEOPHYS RES **82** 1347-1352.

HILL, J.M. & DEWYNNE, J.N. (1987). Heat Conduction. Publ. Blackwell Scientific Publications, Oxford.

HOBBS, B.E., MEANS, W.D. & WILLIAMS, P.F. (1976). An outline of structural geology. Publ. Wiley.

HOFFER, E. & GRANT, J.A. (1980). Experimental investigation of the formation of cordierite - orthopyroxene parageneses in pelitic rocks. CONTRIB MINERAL PETROL **73** 15-22.

HOWARD, L.N. (1966). Convection at high Rayleigh number. Proc 11th Int. Congr. Appl. Mechanics, Munich 1964 (p.1109 - 1115), ed. H. Girtler, publ. Springer Verlag.

HUDSON, J.D. (1964). The petrology of the sandstones of the Great Estuarine Series and the Jurassic palaeogeography of Scotland. PROC GEOL ASSOC **75** 499-528.

HUDSON, J.D. (1983). Mesezoic sedimentation and sedimentary rocks in the Inner Hebrides. PROC ROY SOC EDINB **83B** 47-63.

HUNTER, R.H. (1987). Textural Equilibrium in Layered Igneous Rocks. **in** I.Parsons (ed) Origins of Igneous Layering. Publ. Riedel, Dordrecht. p. 473-504.

HUNTER, R.H. & SPARKS, R.S.J. (1987) The differentiation of the Skaergaard Intrusion. CONTRIB MINERAL PETROL **95** 451-461.

HUPPERT, H.E. & SPARKS, R.S.J. (1980). The fluid dynamics of a basaltic magma chamber replenished by an influx of hot, dense ultrabasic magma. CONTRIB MINERAL PETROL **75** 279-289.

HUPPERT, H.E. & SPARKS, R.S.J. (1984) Double-diffusive convection due to crystallization in magmas. ANN REV EARTH PLANET SCI **12** 11-39.

HUPPERT, H.E. & SPARKS, R.S.J. (1985). Cooling and contamination of mafic and ultramafic magmas during ascent through continental crust. EARTH PLANET SCI LETT **74** 371-386.

HUPPERT, H.E., SPARKS. R.S.J., WILSON, J.R. & HALLWORTH, M.A. (1986a) Cooling & crystallization at an inclined plane. EARTH PLANET SCI LETT **79** 319-328.

HUPPERT, H.E., TURNER, J.S., CAREY. S.N., SPARKS, R.S.J. & HALLWORTH, M.A. (1986b).

A Laboratory simulation of pyroclastic flows down slopes. J VOLCANOL GEOTHERM RES **30** 179-199.

HUPPERT, H.E. & SPARKS, R.S.J. (1988a). Melting the roof of a chamber containing a hot, turbulently convecting fluid. J FLUID MECH **188** 107-131.

HUPPERT, H.E. & SPARKS, R.S.J. (1988b). The Generation of Granitic Magmas by Intrusion of Basalt into Continental Crust. J PETROL **29** 599-624.

HUPPERT, H.E. (1989). Phase changes following the initiation of a hot turbulent flow over a cold solid surface. J FLUID MECH **198** 293-319.

HUPPERT, H.E. & SPARKS, R.S.J. (1989). Chilled margins in igneous rocks. EARTH PLANET SCI LETT **92** 397-405.

HUTTON, D.H.W. (1988). Igneous Emplacement in a shear-zone termination: The biotite granite at Strontian, Scotland. GEOL SOC AMER BULL **100** 1392-1399.

IDDINGS, J.P. (1898). Bysmaliths. J GEOL **6** 704-710.

IRVINE, T.N. (1970) Heat transfer during solidification of layered intrusions I : sheets & sills. CAN J EARTH SCI **7** 1031-1061.

IRVINE, T.N. (1980a). Magmatic infiltration metasomatism, double-diffusive fractional crystallisation, and adcumulus growth in the Muskox intrusion and other layered intrusions. **In** R.B. Hargraves (ed). Physics of Magmatic Processes, publ. Princeton University Press, p. 325-383.

IRVINE, T.N. (1980b). Magmatic density currents and cumulus processes. AM J SCI **280A** 1-58.

IRVINE, T.N. (1987). Layering and related structures in the Duke Island and Skaergaard Intrusions: similarities, differences and origins. **In** I. Parsons (ed) Origins of Igneous Layering (publ Riedel) p. 185-245.

IYER, H.M. (1984). Geophysical evidence for the locations, shapes and sizes, and internal structure of magma chambers beneath regions of Quaternary volcanism. PHIL TRANS ROY SOC LOND **A310** 473-510.

JACKSON, M.D. & POLLARD, D.D. (1988). The laccolith - stock controversy: New results from the southern Henry mountains, Utah. GEOL SOC AMER BULL **100** 117-139.

JACOBS, G.K. & KERRICK. D.M. (1981). Devolatilisation equilibria in H_2O - CO_2 and H_2O - CO_2 - NaCl fluids: an experimental and thermodynamic evaluation at elevated pressures and temperatures. AM MINERAL **66** 1135-1153.

JAEGER, J.C. (1957). The temperature in the neighbourhood of a cooling intrusive sheet. AM J SCI **255** 306-318.

JAEGER, J.C. (1959). Temperatures outside a cooling intrusive sheet AM J SCI **257** 44-54.

JAEGER, J.C. (1969). Elasticity, fracture and flow with engineering and geological applications. Publ. Methuen, London.

JOHANNES, W. (1983). Metastable melting in granite and related systems. **In:** Migmatites, Melting and Metamorphism. eds. M.P. Atherton & C.D. Gribble, publ. Shiva. p.27-36.

JOHNSON, A.M. & POLLARD, D.D. (1973). Mechanisms of growth of some laccolithic intrusions in the Henry Mountains, Utah. I: Field observations, Gilbert's model, physical properties and flow of the magma. TECTONOPHYSICS **18** 261-310.

JOHNSTON, A.D. & STOUT, J.H. (1984). Development of orthopyroxene - Fe/Mg ferrite symplectites by continuous olivine oxidation. CONTRIB MINERAL PETROL **88** 196-202.

JOHNSTONE, G.S., SMITH, D.I., HARRIS, A.L. (1969). Moinian assemblage of Scotland. MEM AMER ASS PETROL GEOL **12** 159-180.

JUDD, J.W. (1874). The secondary rocks of Scotland. Second paper. On the ancient volcanoes of the Highlands and the Relations of their products to the Mesozoic strata. Q J GEOL SOC LOND **30** 220-302.

KAYS, M.A. McBIRNEY, A.R. & GOLES, G.G. (1981). Xenoliths of Gneisses and the conformable, clot-like Granophyres in the Marginal Border Group, Skaergaard Intrusion, E. Greenland. CONTRIB MINERAL PETROL **76** 265-284.

KEAREY, P. & BROOKS, M. (1984). An Introduction to Geophysical Exploration. Publ. Blackwell, Oxford.

KERR, R.C. & TAIT, S.R. (1986). Crystallization and compositional convection in a porous medium with application to layered igneous intrusions. J GEOPHYS RES **91** 3591-3608.

KILLE, I.C. (1987). The Minor Tertiary Intrusions around Loch Scridain, Isle of Mull. Unpubl. Ph.D. thesis, University of London.

KIRKPATRICK, R.J. (1981). Kinetics of Crystallization of Igneous Rocks. **In** A.C. Lasaga & R.J. Kirkpatrick (eds) Kinetics of Geochemical Processes MIN SOC AMER REV IN MINERAL **8** 321-398.

KLEIN, E.M. & LANGMUIR, C.H. (1987). Global correlations of Ocean Ridge Basalt Chemistry with Axial Depth and Crustal Thickness. J GEOPHYS RES **92** 8089-8115.

KOCH, F.G., JOHNSON, A.M. & POLLARD, D.D. (1981). Monoclinal bending of strata over laccolithic intrusions. TECTONOPHYSICS **74** T21-T31.

KRETZ, R. (1966). Interpretation of the shape of mineral grains in metamorphic rocks. J PETROL **7** 68-94.

KRISHNAMURTHY, P. & COX, K.G. (1977). Picrite basalts and related lavas from the Deccan traps of Western India. CONTRIB MINERAL PETROL **62** 53-75.

KUDO, A.M. & WEILL, D.F. (1970) An igneous plagioclase thermometer. CONTRIB MINERAL PETROL **25** 52-65.

LACHENBRUCH, A.H. (1962). Mechanics of thermal contraction cracks and ice-wedge polygons in permafrost. GEOL SOC AMER SPEC PAP **70**.

LAMBERT, D.D. & SIMMONS, E.C. (1987). Magma evolution in the Stillwater Complex, Montana: 1. Rare earth element evidence for the formation of the Ultramafic Series. AM J SCI **287** 1-33.

LANGMUIR, C.H. (1989). Geochemical consequences of in situ crystallisation. NATURE **340** 199-205.

LE MAITRE, R.W. (1982). Numerical Petrology: statistical interpretation of geochemical data. Publ. Elsevier.

LEE, G.W. & BAILEY, E.B. (1925). The Pre-Tertiary Geology of Mull, Loch Aline and Oban. MEM. GEOL. SURV. GREAT BRITAIN.

LESHER, C.E. & WALKER, D. (1988). Cumulate Maturation and Melt Migration in a Temperature Gradient. J GEOPHYS RES **93** 10295-10311.

LINDSLEY, D.H. (1983). Pyroxene Thermometry. AM MINERAL **68** 477-493.

LINDSLEY, D.H. & ANDERSEN, D.J. (1983). A two - pyroxene thermometer. Proc. 13th Lunar and Planetary Science Conference, Part 2. J GEOPHYS RES **88** Supplement A887 - A906.

LISTER, C.R.B. (1974). On the penetration of water into hot rock. GEOPHYS J ROY ASTR SOC **39** 465-509.

LISTER, C.R.B. (1983a). On the intermittency and crystallization mechanisms of sub-seafloor magma chambers. GEOPHYS J ROY ASTR SOC **73** 351-365.

LISTER, C.R.B. (1983b). The Basic Physics of Water Penetration into Hot Rock. **In:** P.A. Rona, K. Bostrom & L. Laubier (eds). Hydrothermal Processes at Seafloor Spreading Centers. Publ. Plenum Press, NY. (NATO conference series. IV: Marine Sciences Vol. 12).

LOFGREN, G. (1971). Experimentally produced dentification textures in natural rhyolitic glass: GEOL SOC AMER BULL **82** 111-124.

LOFGREN, G. (1974). An experimental study of plagioclase crystal morphology: Isothermal Crystallization. AM J SCI **274** 243-273.

LOFGREN, G. & DONALDSON, C.H. (1975). Curved Branching Crystals and Differentiation in Comb-Layered Rocks. CONTRIB MINERAL PETROL **49** 309-319.

LOFGREN, G. (1980). Experimental studies on the dynamic crystallization of silicate melts. **In:** R. Hargraves (ed) Physics of Magmatic Processes, publ. Princeton University Press.

LOFGREN, G.E. (1983). Effect of Heterogenous Nucleation on Basaltic Textures: A Dynamic Crystallization Study. J PETROL **24** 229-255.

LOWELL, R.P. (1985). Double-difusive convection in partially molten silicate systems - its role during magma production and in magma chambers. J VOLCANOL GEOTHERM RES **26** 1-24.

LUTH, W.C. (1967). Studies in the System $KAlSiO_4$ - Mg_2SiO_4 - SiO_2 - H_2O: I, Inferred Phase Relations and Petrologic Applications. J PETROL **8** 372-416.

MAALOE, S. 1976. The zoned plagioclase of the Skaergaard Intrusion, East Greenland. J PETROL **17** 398-419.

MACDONALD, R., SPARKS, R.S.J., SIGURDSSON, H., MATTEY, D.P., McGARVIE, D.W., & SMITH, R.L. (1987). The 1875 eruption of Askja volcano, Iceland: combined fractional crystallization and selective contamination in the generation of rhyolitic magma. MINERAL MAG **51** 183-202.

MARSH, B.D. (1981). On the crystallinity, probability of occurrence, and rheology of lava and magma. CONTRIB MINERAL PETROL **78** 85-98.

MARSH, B.D. (1982). On the Mechanisms of Igneous Diapirism, Stoping and Zone Melting. AM J SCI **282** 808-855.

MARSH, B.D. (1988). Crystal capture, sorting, and retention in convecting magma. BULL GEOL SOC AMER **100** 1720-1737.

MARSH, B.D. (1989). On Convective Style and Vigor in Sheet - like Magma Chambers. J PETROL **30** 479-530.

MARSHALL, L.A. (1984). Origin of net-veined and mixed magma ring intrusions. Unpubl. PhD Thesis, Univ. of Cambridge, U.K.

MARTIN, D., GRIFFITHS, R.W. & CAMPBELL, I.H. (1987). Compositional and thermal convection in magma chambers. CONTRIB MINERAL PETROL **96** 465-475.

MATHISON, C.I. (1987). Pyroxene oikocrysts in troctolitic cumulates: evidence for supercooled crystallization and postcumulus crystallization. CONTRIB MINERAL PETROL **97** 228-236.

MAXWELL, D.T. & HOWER, J. (1967). High-grade diagenesis and low grade metamorphism of illite in the PreCambrian Belt Series, AM MINERAL **52** 843-857.

McBIRNEY, A.R., & WILLIAMS, H. (1969). Geology and petrology of the Galapagos Islands. MEM GEOL SOC AMER **118**.

McBIRNEY, A.R., & NOYES, R.M. (1979). Crystallisation and layering of the Skaergaard Intrusion. J PETROL **20** 487-554.

McBIRNEY, A.R. (1980). Mixing and Unmixing of magmas. J VOLCANOL GEOTHERM RES **7** 357-371.

McBIRNEY, A.R. & MURASE, T. (1984). Rheological properties of magmas. ANN REV EARTH PLANET SCI **12** 337-357.

McBIRNEY, A.R. (1985) Further considerations of Double-Diffusive Stratification and Layering in the Skaergaard Intrusion. J PETROL **26** 993-1001.

McBIRNEY, A.R., BAKER, B.H. & NILSON, R.H. (1985). Liquid fractionation. Part 1: basic principles and experimental simulations. J VOLCANOL GEOTHERM RES **24** 1-24.

McKENZIE, D.P. (1984). The generation and compaction of Partially Molten Rock. J PETROL **25** 713-765.

McKENZIE, D.P. (1985). The extraction of magma from the crust and mantle. EARTH PLANET SCI LETT **74** 81-91.

McKENZIE, D.P. (1987). The compaction of igneous and sedimentary rocks. J GEOL SOC LOND **144** 299-307.

McKENZIE, D.P. & BICKLE, M.J. (1988). The volume and composition of Melt Generated by Extension of the Lithosphere. J PETROL **29** 625-679.

MEIGHAN, I.G., JAMISON, D.D., GAFFIKIN, P.J. & HEWITT, A.S. (1988). An Interlaboratory Major and Trace Element Study of 11 Queen's University In - House Standards for X - Ray Fluorescence Analysis. Int. Rept. The Queen's University of Belfast.

MEHNERT, K.R. (1971) Migmatites and the origin of granitic rocks (2nd. ed.). publ. Elsevier, Amsterdam.

MICHAEL, P.J. (1988). The concentration, behaviour and storage of H_2O in the suboceanic upper mantle: implications for mantle metasomatism. GEOCHIM COSMOCHIM ACTA **52** 555-566.

MORRISON, M.A., THOMPSON, R.N., GIBSON, I.L. & MARRINER, G.F. (1980). Lateral chem-

ical heterogeneity in the Palaeocene upper mantle beneath the Scottish Hebrides. PHIL TRANS R SOC LOND **A297** 229-244.

MORSE, S.A. (1981). Kiglapait Geochemistry IV: the major elements. GEOCHIM COSMOCHIM ACTA **45** 461-479.

MORSE, S.A. (1986). Thermal structure of crystallizing magma with 2-phase convection. GEOL MAG **123** 205-214.

MUIR, I.D., TILLEY, C.E. & SCOON, J.H. (1957). Contributions to the petrology of Hawaiian basalts. 1. The picrite basalts of Kilauea. AM J SCI **255** 241-253.

MURASE, T. & McBIRNEY, A.R. (1973). Properties of some common igneous rocks and their melts at high temperatures. GEOL SOC AMER BULL **84** 3563-3592.

NELSON, S.A. & CARMICHAEL, I.S.E. (1979). Partial Molar Volumes of Oxide Components in Silicate Liquids. CONTRIB MINERAL PETROL **71** 117-124.

NICHOLLS, J. & STOUT, M.Z. (1982). Heat Effects of Assimilation, Crystallization and Vesiculation in Magmas. CONTRIB MINERAL PETROL **81** 328-339.

NILSON, R.H. McBIRNEY, A. R. & BAKER, B.H. (1985). Liquid Fraeticriation. Part II: Fluid dynamics and quantitative implications for magmatic systems. J VOLCANOL GEOTHERM RES **24** 25-54.

NITSAN, U. (1974). Stability field of olivine with respect to oxidation and reduction. J GEOPHYS RES **79** 706-711.

NORTON, D.L. & TAYLOR, H.P. (1979). Quantitative simulation of the hydrothermal systems of crystallizing magmas on the basis of transport theory and oxygen isotope data: an analysis of the Skaergaard intrusion. J PETROL **20** 421-486.

NORTON, D.L. (1984). Theory of Hydrothermal Systems. ANN REV EARTH PLANET SCI **12** 155-177.

NORTON, D.L. (1988). Metasomatism and Permeability. AM J SCI **288** 604-618.

O'HARA, M.J. (1968). The bearing of phase equilibria studies on the origin and evolution of basic and ultrabasic rocks. EARTH SCI REV **4** 69-133.

O'HARA, M.J. & MATHEWS, R.E. (1981). Geochemical evolution in an advancing, periodically replenished, periodically tapped, continuously fractionated magma chamber. J GEOL SOC LOND **138** 237-277.

OKAKA, H. WATANABE, H. YAMASHITA, H. & YOKOYAMA, I. (1981). Seismological significance of the 1977-1978 eruptions and the magma intrusion process of Usu volcano, Hokkaido. J VOLCANOL GEOTHERM RES **9** 311-334.

O'NEIL, J.R. (1986). Theoretical and experimental aspects of isotopic fractionation. In: J.W. Valley, H.P. Taylor & J.R. O'Neil (eds) Stable Isotopes in High Temperature Geological Processes. MIN SOC AMER REV IN MINERALOGY **16** 1-40.

PALACZ, Z.A. & TAIT, S.R. (1985). Isotopic and geochemical investigations of unit 10 from the Eastern Layered Series of the Rhum Intrusion, Northwest Scotland. GEOL MAG **122** 485-490.

PARMENTIER, E.M. & SCHEDL, A. (1981). Thermal aureoles of igneous intrusions: some possible indications of hydrothermal convective cooling. J GEOL **89** 1-22.

PATCHETT, P.J. (1981). Thermal effects of basalt on continental crust and crustal contamination of magmas. NATURE **283** 559-561.

PATTISON, D. & HARTE, B. (1985). A petrogenetic grid for pelites in the Ballachulish and other Scottish thermal aureoles. J GEOL SOC LOND **142** 7-28.

PECK, D.L., HAMILTON, M.S. & SHAW, H.R. (1977). Numerical analysis of lava lake cooling models: Part II, application to Alae lava lake, Hawaii. AM J SCI **277** 415-437.

PECK, D.L. (1978). Cooling and vesiculation of Alae lava lake, Hawaii. U.S. GEOL SURV PROF PAP **935B**

PEDERSEN, R.B. (1986). The nature and significance of magma chamber margins in ophiolites: examples from the Norwegian Caledonides. EARTH PLANET SCI LETT **77** 100-112.

PETIT, J.P. (1987). Criteria for the sense of movement on fault surfaces in brittle rocks. J STRUCT GEOL **9** 597-608.

PETTIJOHN, F.J., POTTER, P.E. & SIEVER, R. (1973). Sand and Sandstone. Publ. Springer-Verlag, Berlin.

PHILLIPS, E.R. (1969). On the rock name Beerbachite. GEOL MAG **106** 281-283.

PHILLIPS, W.J. (1974). The dynamic emplacement of cone sheets. TECTONOPHYSICS **24** 69-84.

PHILPOTTS, A.R. (1970). Mechanism of emplacement of the Monteregian Intrusions. CAN MINERAL **10** 395-410.

POLLARD, D.D. & JOHNSON, A.M. (1973). Mechanics of growth of some laccolituic intrusions in the Henry Mountains, Utah. II: Bending and failure of overburden layers and sill formation. TECTONOPHYSICS **18** 311-354.

POLLARD, D.D., SEGALL, P. & DELANEY, P.T. (1982). Formation and interpretation of dilatant echelon cracks. GEOL SOC AMER BULL **93** 1291-1303.

POLLARD, D.D. & NICHOLSON, R. (1985). Dilation and linkage of echelon cracks. J STRUCT GEOL **7** 583-590.

POTTS, P.J. (1987). A Handbook of Silicate Rock Analysis. Publ. Blackie, Glasgow.

POWELL, D. (1974). Stratigraphy and structure of the western Moine and the problem of Moine orogenesis. J GEOL SOC LOND **130** 575-593.

RABINOWICZ, M., CEULENEER, G. & NICOLAS, A. (1987). Melt segregation and flow in mantle diapirs below spreading centres: evidence from the Oman ophiolite. J GEOPHYS RES **92** 3475-3486.

RICHEY, J.E., THOMAS, H.H., BAILEY, E.B., SIMPSON, J.B., EYLES, V.A. & LEE, G.W. (1930). The Geology of Ardnamurchan, North-west Mull and Coll. MEM. GEOL. SURV. SCOTLAND.

RICHEY, J.E. (1932). Tertiary ring structures in Britain. TRANS GEOL SOC GLASG **19** 42-140.

RICHEY, J.E. (1961). Scotland: the Tertiary Volcanic Districts. Regional Geology of Great Britain Series. Publ. HMSO.

RICHTER, F.M., NATAF, H.-C. & DALY,S.F. (1983). Heat transfer and horizontally averaged temperature of convection with large viscosity variations. J FLUID MECH **129** 172-192.

RINEHART, E.J., SANFORD, A.R. & WARD, E.R. (1979). Geographic extent and shape of an extensive magma body at mid crustal depths in the Rio Grande Rift near Socorro, New Mexico. In R E Riecker (ed) Rio Grande Rift: Tectonics and Magmatism. Publ. Am. Geophys. U.

ROBERTS, J.L. (1970). The intrusion of magma into brittle rocks. **In** G Newall & N Rast (eds.) Mechanisms of Igneous Intrusion, p.287-338. Publ. Gallery Press, Liverpool.

ROBINS, B. (1982). Finger Structures in the Lille Kufjord Layered Intrustion, Finnmark, Northern Norway. CONTRIB MINERAL PETROL **81** 290-295.

ROBINS, B., HAUKVIK, L. & JANSEN, S. (1987). The Organisation and Internal Structure of

Cyclic Units in the Honningsvag Intrusive Suite, North Norway: Implications for Intrusive Mechanisms, Double-Diffusive Connection and Pore-Magma Infiltration. In I. Parsons (ed) Origins of Igneous Layering (publ Riedel). 287-312.

ROBINSON, M.A. & McLELLAND, E.A. (1987). Palaeomagnetism of the Torridonian of Rhum, Scotland: evidence for limited uplift of the Central Intrusive Complex. EARTH PLANET SCI LETT **85** 473-487.

ROBSON, G.R. & BARR, K.G. (1964). The effect of stress on faulting and minor intrusions in the vicinity of a magma body. BULL VOLCANOLOGIQUE **27** 315-329.

RYAN, M.P. & SAMMIS, C.G. (1981). The Glass Transition in Basalt. J GEOPHYS RES **86** 9519-9535.

RYAN, M.P. (1987). Neutral buoyancy and the mechanical evolution of magmatic systems. In: B.O. Mysen (ed.) Magmatic Processes: Physicochemical Principles. GEOCHEM SOC AMER SPEC PUBL **1** 259-288.

RYAN, M.P. (1988). The Mechanics and Three-Dimensional Internal Structure of Active Magmatic Systems: Kilauea Volcano, Hawaii, J GEOPHYS RES **93** 4213-4248.

SAMMIS, C.G. & JULIAN, B.R. (1987). Fracture Instabilites Accompanying Dike Intrusion. J GEOPHYS RES **92** 2597-2605.

SANDERS, I.S. van CALSTEREN, P.W.C. & HAWKESWORTH, C.J. (1984). A Grenville Sm-Nd age for the Glenelg eclogite in northwest Scotland. NATURE **312** 439-440.

SEIFERT, F. (1970) Low-temperature compatibility relations of cordierite in haplopelites of the system K2O-MgO-Al2O3-SiO2-H2O. J PETROL **11** 73-99.

SEIFERT, F. 1976. Stability of the asemblage cordierite + K-Feldspar + quartz CONTRIB MINERAL PETROL **57** 179-185.

SHIMAZU, Y. (1959). A Physical interpretation of crystallization differentiation of the Skaergaard Intrusion J EARTH SCI NAGOYA UNIV **7** 35-48.

SIBSON, R.H. (1981). Fluid flow accompanying faulting: field evidence and models. **In** D.W. SIMPSON & P.G.RICHARDS (eds), Earthquake Prediction: an International Review. Am. Geophys. U. Maurice Ewing Series **4** 593-603.

SIBSON, R.H. (1989). Earthquake faulting as a structural process. J STRUCT GEOL **11** 1-14.

SIGURDSSON, H. & SPARKS. R.S.J. (1981). Petrology of rhyolitic and mixed-magma ejecta from the 1875 eruption of Askja, Iceland. J PETROL **22** 41-84.

SIMKIN, T. & HOWARD, K.A. (1970). Caldera collapse in the Galapagos Islands, 1968. SCIENCE **169** 429-437.

SKELHORN, R.R. & ELWELL, R.W.D. (1966). The structure and form of the Granophyric Quartz Dolerite Intrusion, Centre 2, Arnamurchan. PHIL TRANS ROY SOC EDINB **66** 285-306.

SKELHORN, R.R. & ELWELL, R.W.D. (1971). Central subsidence in the layered hypersthene - gabbro of Centre II, Ardamurchan, Argyllshire. J GEOL SOC LOND **127** 535-551.

SLEEP, N.H. (1988). Tapping of Melt by Veins and Dikes. J GEOPHYS RES **93** 10255-10272.

SMITH, M.K. (1988). Thermal convection during the directional solidification of a pure liquid with variable viscosity. J FLUID MECH **188** 547-570.

SMITH, N.J. (1987). The age and structural setting of limestone and basalt on the Main Ring Fault of South - East Rhum, Inner Hebrides, Scotland. Unpubl. MSc. thesis, Univ. of Durham.

SMITH, P.J. & BOTT, M.H.P. (1975). Structure of the crust beneath the Caledonian Foreland and Caledonian Belt of the North Scottish Shelf Region GEOPHYS J ROY ASTR SOC **42** 187-205.

SMYTHE, D.K., DOBINSON, A., McQUILLIN, R., BREWER, J., MATTHEWS, D.H., BLUNDELL, D.T. & KELK, B. (1982). Deep structure of the Scottish Caledonides revealed by the MOIST reflection profile. NATURE **299** 338-340.

SOPER, N.J. & BARBER, A.J. (1982). A model for the deep structure of the Moine thrust zone. J GEOL SOC LOND **139** 127-138.

SPARKS, R.S.J., SIGURDSSON, H. & WILSON, L. (1977). Magma mixing: a mechanism for triggering acid explosive eruptions. NATURE **267** 315-318.

SPARKS, R.S.J., HUPPERT, H.E., KERR, R.C., McKENZIE, D.P. & TAIT, S.R. (1985). Postcumulus processes in layered intrusions. GEOL MAG **122** 533-568.

SPARKS, R.S.J. & MARSHALL, L.A. (1986). Thermal and mechanical constraints on mixing between mafic and silicic magmas. J VOLCANOL GEOTHERM RES **29** 99-124.

SPARKS, R.S.J. (1988). Petrology and geochemistry of the Loch Ba ring-dyke, Mull (N.W. Scotland): an example of the extreme differentiation of tholeiitic magmas. CONTRIB MINERAL PETROL **100** 446-461.

SPEAR, F.S. (1981). An Experimental Study of Hornblende Stability and Compositional Vanability in Amphibolite. AM J SCI **281** 697-734.

SPEIGHT, J.M., SKELHORN, R.R., SLOAN, T. & KNAPP, R.J. (1982). The dyke swarms of Scotland. **In** D.S. SUTHERLAND (ed.) Igneous rocks of the British Isles. Publ. J.Wiley & Son. p.449-459.

SPERA, F.J., YUEN, D.A. & KIRSCHIVINK, S.J. (1982). Thermal Boundary Layer Convection in Silicic Magma Chambers: Effects of Temperature - Dependent Rheology and Implications for Thermogravitational Chemical Fractionation. J GEOPHYS RES **87** 8755-8767.

SPIEGELMAN, M. & McKENZIE, D.P. (1987). Simple two - dimensional models for melt extraction

at midocean ridges and island arcs. EARTH PLANET SCI LETT **83** 137-152.

SPULBER, S.D. & RUTHERFORD, M.J. (1983). The origin of rhyolite and plagiogranite in oceanic crust: an experimental study. J PETROL **24** 1-25.

STEEL, R.J. (1977). Triassic rift basins of north-west Scotland - their configuration, infilling and development. MNNSS-7. In: Proceedings, Mesozoic Northern North Sea Symposium ed. K.G. Finstad & R.C Selley. Publ. Norsk Petroleum Forening.

STRENS, M.R. & CANN, J.R. (1986). A fracture-loop thermal balance model of black smoker circulation. TECTONOPHYSIGS **122** 307-325.

SWEATMAN, T.R. & LONG, J.V.P. (1969). Quantitative Electron - Probe Microanalysis of rock - forming minerals. J PETROL **10** 331-380.

TAIT, S.R. (1988). Samples from the crystallizing boundary layer of a zoned magma chamber. CONTRIB MINERAL PETROL **100** 470-483.

TAMMENAGI, H. (1976). Radioelement concentration in British Tertiary granites. GEOL MAG **113** 271-276.

TARNEY, J. WEAVER, B.L. & DRURY, S.A. (1979). Geochemistry of Archaean trondhjeimitic and tonalitic gneisses from Scotland and East Greenland. **In:** Trondhjemites, Dacites and Related Rocks. Ed. F. Baker, publ Elsevier 275-299.

TAYLOR, H.P. & FORESTER, R.W. (1971). Low - O^{18} igneous rocks from the intrusive complexes of Skye, Mull and Ardnamurchan, W. Scotland. J PETROL **12** 465-497.

TAYLOR, H.P. (1987). Comparison of hydrothermal systems in layered gabbros and granites, and the origin of low - O^{18} magmas. **In** B.O.Mysen (ed.), Magmatic Processes: Physicochemical Principles. GEOCHEM SOC SPEC PUBL **1**, 337-357.

TAYLOR, H.P. (1988). Oxygen, Hydrogen and Strontium Isotope constraints on the origin of granites. TRANS ROY SOC EDINB EARTH SCI **79** 317-338.

THOMPSON, A.B. (1982). Dehydration Melting of Pelitic Rocks and the Generation of H_2O - undersaturated granitic liquids. AM J SCI **282** 1567-1595.

THOMPSON, R.N. (1973). One-atmosphere melting behaviour and nomenclature of terrestrial lavas. CONTRIB MINERAL PETROL **41** 197-204.

THOMPSON, R.N. (1980). Askja 1875, Skye 56Ma: basalt-triggered Plinian mixed-magma eruptions during the emplacement of the Western Redhills granites, Isle of Skye, Scotland. GEOL RUNDSCH **69** 245-262.

THOMPSON, R.N. MORRISON, M.A. MATTEY, D.P., DICKIN, A.P. & MOORBATH, S. (1980). An assessment of the Th-Hf-Ta diagram as a discriminant for tectonomagmatic classification and in the detection of crustal contamination of magmas. EARTH PLANET SCI LETT **50** 1-10.

THOMPSON, R.N. (1981). Thermal aspects of the origin of Hebridean acid megmas I: An experimental study of partial fusion of Lewisian gneisses and Torridonian sediments. MINERAL MAG **44** 161-170.

THOMPSON, R.N. (1982). Magmatism of the British Tertiary Volcanic Province. SCOTT J GEOL **18** 49-108.

THOMPSON, R.N. DICKIN. A.P. GIBSON, I.L. & MORRISON, M.A. (1982) Elemental Fingerprints of Isotopic contamination of Hebridean Palaeocene Mantle-derived magmas by Archaean Sial. CONTRIB MINERAL PETROL **79** 159-169.

THOMPSON, R.N. (1983). Thermal aspects of the origin of Hebridean Tertiary acid magmas II: Experimental melting behaviour of the granites at 1kb P_{H_2O} MINERAL MAG **47** 111-122.

THOMPSON, R.N., MORRISON, M.A., HENDRY, G.L. & PARRY, S.J. (1984). An assessment

of the relative roles of crust and mantle in magma genesis: an elemental approach. PHIL TRANS ROY SOC LOND **A310** 549-590.

THOMPSON, R.N., MORRISON, M.A., DICKIN, A.P., GIBSON, I.L. & HARMON, R.S. (1986). Two contrasting styles of interaction between basic magmas and continental crust in the British Tertiary Volcanic Province J GEOPHYS RES **91** 5985-5997.

THOMPSON, R.N. (1987). Phase - equilibria constraints on the genesis and magmatic evolution of oceanic basalts. EARTH SCI REV **24** 161-210.

THOMPSON, R.N. & MORRISON, M.A. (1988). Asthenospheric and lower - lithospheric mantle contributions to Continental Extensional Magmatism: an example from the British Tertiary Province. CHEM GEOL **68** 1-15.

THORPE, R.S., POTTS, P.J. & SARRE, M.B. (1977). Rare earth evidence concerning the origins of granites of the Isle of Skye, northwest Scotland. EARTH PLANET SCI LETT **36** 111-120.

TIMOSHENKO, S.P. & GOODIER, J.N. (1970). Theory of Elasticity (3rd Edn) Publ. McGraw-Hill.

TRYGGVASON, E. (1986). Multiple magma reservoirs in a rift zone volcano: ground deformation and magma transport during the September 1984 eruption of Krafla, Iceland. J VOLCANOL GEOTHERM RES **28** 1-44.

TURNER, J.S. & GUSTAVSON, L.B. (1981). Fluid motions and compositional gradients produced by crystallization or melting at vertical boundaries. J VOLCANOL GEOTHERM RES **11** 93-125.

TURNER, J.S., HUPPERT, H.E. & SPARKS, R.S.J. (1983). Experimental investigations of volatile exsolution in evolving magma chambers. J VOCANOL GEOTHERM RES **16** 263-277.

TURNER, J.S. & CAMPBELL, I.H. (1986). Convection and mixing in magma chambers. EARTH SCIENCE REV **23** 255-352.

TURNOCK, A.C. & EUGSTER, H.P. (1962). Fe-Al oxides: phase relationships below 1000°C. J PETROL **3** 533-565.

TUTTLE, O.F. & BOWEN, N.L. (1958). Origin of granite in the light of experimental studies in the system $NaAlSi_3O_8$ - $KAlSi_3O_8$ - SiO_2 - H_2O MEM GEOL SOC AMER **74**.

VAN der MOLEN, I. & PATERSON, M.S. (1979). Experimental deformation of Partially-Melted Granite. CONTRIB MINERAL PETROL **70** 299-318.

VERNON, R.H. (1970). Comparative grain-boundary studies of some basic and ultrabasic granulites, nodules and cumulates. SCOTT J GEOL **6** 337-351.

VIELZEUF, D. & HOLLOWAY, J.R. (1988). Experimental determination of the fluid absent melting relations in the pelitic system: consequences for crustal differentation. CONTRIB MINERAL PETROL **98** 257-276.

WAGER, L.R. & DEER, W.A. (1939). Geological Investigations in East Greenland III. The Petrology of the Skaergaard Intrusion. MEDD OM GRONLAND **105** 1-352.

WAGER, L.R. & BAILEY, E.B. (1953). Basic magma chilled against acid magma. NATURE **172** 68-70.

WAGER, L.R., WEEDON, D.S. & VINCENT E.A. (1953). A granophyne from Coire Uaigneich, Isle of Skye, containing quartz paramorphs after tridymite. MINERAL MAG. **30** 263-276.

WAGER, L.R. BROWN, G.M. & WADSWORTH, W.J. (1960). Types of igneous cumulates. J PETROL **1** 73-85.

WAGER, L.R. (1968). Rhythmic and Cryptic layering in Mafic and Ultramafic plutons. **in** H.H. Hess & A. Poldervaart (eds) Basalts: The Poldervaart Treatise on Rocks of Basaltic composition vol. 2, p. 573-622. Publ. Wiley.

WAGER, L.R. & BROWN, G.M. (1968). Layered Igneous Rocks. Publ. Oliver & Boyd, Edinburgh & London.

WALKER, D., JUREWICZ, S., & WATSON, E.B. (1988). Adcumulus dunite growth in a laboratory thermal gradient. CONTRIB MINERAL PETROL **99** 306-319.

WALKER, G.P.L. (1975). A new concept of the evolution of the British Tertiary intrusive centres. J GEOL SOC LOND **131** 121-141.

WALKER, G.P.L. (1984). Downsag calderas, ring faults, caldera sizes and incremental caldera growth. J GEOPHYS RES **89** 8407-8416.

WALLMANN, P.C., MAHOOD, G.A. & POLLARD, D.D. (1988). Mechanical models for correlation of ring - fracture eruptions at Pantelleria, Strait of Sicily, with glacial sea-level drawdown. BULL VOLCANOL **50** 327-339.

WALSH, J.N., BECKINSALE, R.D., SHELHERN, R.R. & THORPE, R.S. (1979). Geochemistry and petrogenesis of Tertiary granitic rocks from the Island of Mull, Northwest Scotland. CONTRIB MINERAL PETROL **71** 99-116.

WARD, S.G. & WHITMENE, R.L. (1950). The viscosity and sedimentation of suspensions of rough powders. BRITISH JOURNAL OF APPLIED PHYSICS **1** 325-328.

WATSON, E.B. (1979). Apatite saturation in basic and intermediate magmas. GEOPHYS RES LETT **6** 937-940.

WATSON, E.B., OTHMAN, D.B., LUCK, J.M. & HOFMANN, A.W., (1987). Partitioning of U, Pb, Cs, Yb, Hf, Re, & Os between diopsidic pyroxene and haplobasaltic liquid. CHEM GEOL **62** 191-208.

WATSON, J.V. (1963). Some problems concerning the evolution of the Scottish Caledonides. PROC GEOL ASSOC **74** 213-258.

WATSON, J.V. (1985). Nothern Scotland as an Atlantic-North Sea divide. J GEOL SOC LOND **142** 221-243.

WEAVER, B.L. & TARNEY, J. (1980). Rare Earth Geochemsitry of Lewisian Granulite - Facies gneisses, Northwest Scotland: Implications for the petrogenesis of the Archaean Lower Continental Crust. EARTH PLANET SCI LETT **51** 279-296.

WEAVER, B.L. & TARNEY, J. (1981). Levisian gneiss geochemistry and Archaean crustal development models. EARTH PLANET SCI LETT **55** 171-180.

WEINSTEIN, S.A., YUEN, D.A. & OLSON, P.L. (1988). Evolution of crystal settling in magma-chamber convection. EARTH PLANET SCI LETT **87** 237-248.

WELLS, M.K. (1951). Sedimentary inclusions in the hypersthene-gabbro, Ardnamurchan, Argyllshire. MIN MAG **29** 715-736.

WELLS, M.K. (1954). The structure and petrology of the hypersthene-gabbro intrusion, Ardnamurchan, Argyllshire. Q J GEOL SOC LOND **109** 367-395.

WELLS, M.K. & McRAE, D.G. (1969). Palaemagnetism of the Hypersthene-gabbro intrusion, Arnamúrchan, Scotland. NATURE **223** 608-609.

WELLS, M.K. (1978). A contribution to the study of cone sheets and related intrusions of Centre 2, Ardnamurchan, Scotland. (abstract in conference report, 'Emplacement and crystallization of Miner Intrusions'). J GEOL SOC LOND **135** 350.

WHITE, A.J.R. & CHAPPELL B.W. (1977). Ultrametamorphism and granitoid genesis. TECTONOPHYSICS **43** 7-22.

WHITNEY, J.A. (1975). The effects of presure, temperature and X_{H_2O} on phase assemblage in four synthetic rock compositions. J GEOL **83** 1-31.

WICKHAM, S.M. (1987). The segregation and emplacement of granitic magmas. J GEOL SOC LOND **144** 281-298.

WIEBE, R.A. (1988). Structural and Magmatic Evolution of a Magma Chamber: The Newark Island Layered Intrustion, Nain, Labrador. J PETROL **29** 383-411.

WILLIAMS, H. (1942). Geology of Crater Lake National Park, with a reconnaissance of the Cascade Range southward of Mount Shasta. Carneigie Instn. Wash. Publ. 540.

WILSON, J.R. & LARSEN, S.B. (1985). Two-dimensional study of a layered intrusion - the Hyllingen Series, Norway. GEOL MAG **122** 97-124.

WILSON, J.R. & ENGELL-SORENSON, O. (1986). Basal reversals in layered intrusions are evidence for emplacement of compositionally stratified magma. NATURE **323** 616-618.

WOOD. B.J. & WALTHER, J.V. (1986). Fluid flow during metamorphism and its implications for fluid-rock ratios. In: Fluid-rock interactions during metamorphism (ed. J.V. Walker & B.J. Wood) ADVANCES IN PHYSICAL GEOCHEMISTRY **5** 89-108.

WOOD, D.A., GIBSON, I.L., & THOMPSON, R.N. (1976). Elemental mobility during zeolite facies metamorphism of the Tertiary basalts of eastern Iceland. CONTRIB MINERAL PETROL **55** 241-254.

WRIGHT, T.L. & OKAMURA, R.T. (1977). Cooling and crystallisation of tholeiitic basalt, 1965 Makaopuhi lava lake, Hawaii. U.S. GEOL SURV PROF PAP **1004.**

WYLLIE, P.J., HUANG, W.L., STERN, C.R. & MAALOE, S. (1976). Granitic magmas: possible and impossible sources, water contents, and crystallization sequences. CAN J EARTH SCI **13** 1007-1079.

YOUNG, I.M., GREENWOOD, R.C. & DONALDSON, C.H. (1988). Formation of the Eastern Layered Series of the Rhum Complex, Northwest Scotland. CAN MINERAL **26** 225-234.

ZEN, E-AN (1988). Thermal modelling of stepwise anatexis in a thrust-thickened sialic crust. TRANS ROY SOC EDINBURGH EARTH SCI **79** 223-235.

ADDENDA.

GOVINDARAJU, K. (1984). Compilation of Working Values and Sample Description for 170 international reference samples of mainly silicate rocks and minerals. SPEC ISS GEOSTANDARDS NEWSLETTER **8.**

GOVINDARAJU, K. (1989). 1989 Compilation of Working Values and Sample Description for 272 geostandards. SPEC ISS GEOSTANDARDS NEWSLETTER **13.**